Electron and Scanning Probe Microscopies

2012 Principal Investigators' Meeting

Gaithersburg Marriott Washingtonian Center
Gaithersburg, Maryland
September 9 - 12, 2012

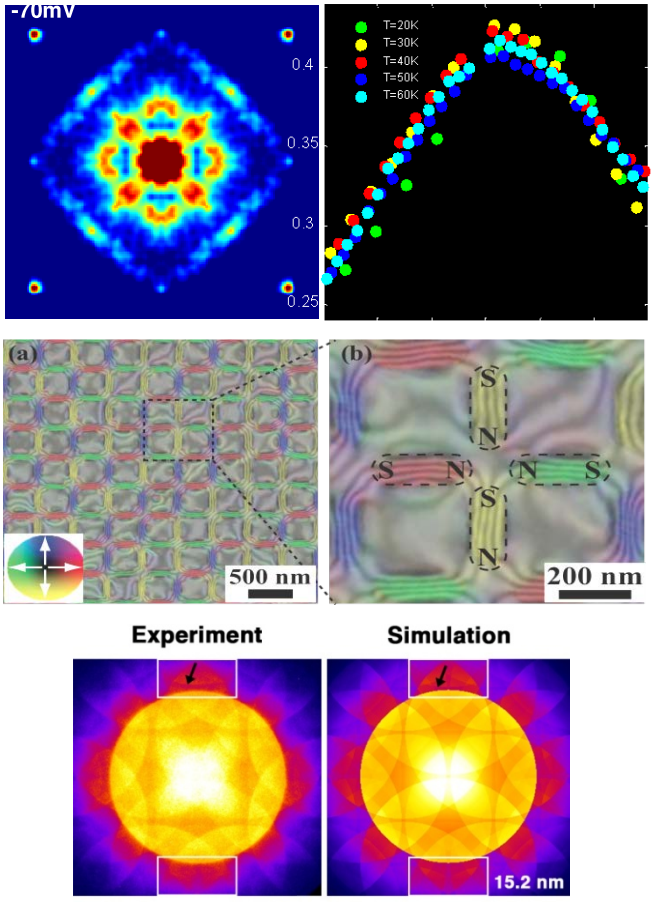

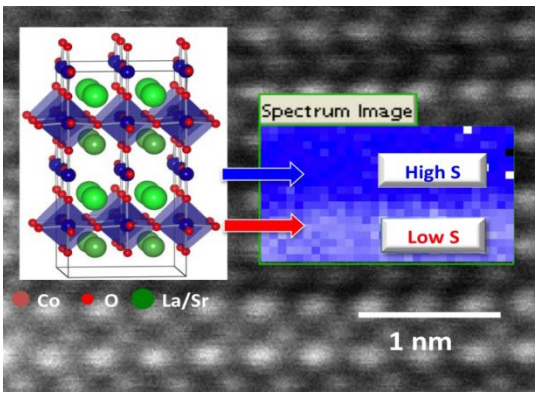

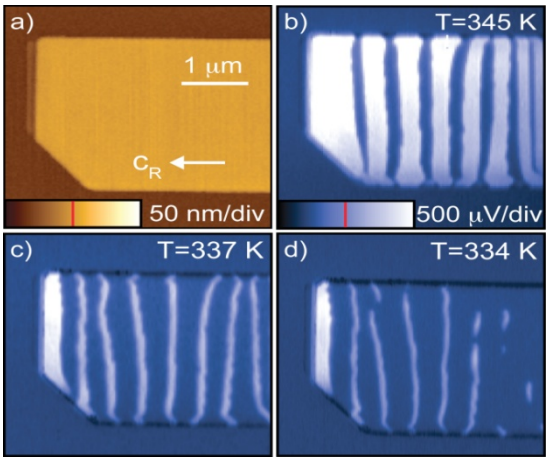

Office of Basic Energy Sciences
Division of Materials Sciences and Engineering

U.S. DEPARTMENT OF ENERGY | Office of Science

On the Cover

Top Left: *Scanning tunneling microscopy study of the emergence of heavy electrons & their quantum critical properties.* (Left) Two-dimensional Fourier transform of scanning tunneling conductance maps is used to probe the momentum structure of heavy fermions and to directly probe their emergence as temperature is reduced. (Right) Spectroscopy of the heavy fermion states show energy momentum scaling, indicating the proximity of this system to quantum criticality. The conductance (y-axis) plotted as function of energy/k_BT (x-axis) collapses data measured for tunneling into heavy fermions at different temperatures. Work published in *Nature* **486**, 201 (2012).
***Courtesy**: Ali Yazdani, Princeton University*

Top Right: *Real-space, atomic-resolution mapping of a spin state superlattice in $La_{0.5}Sr_{0.5}CoO_{3-\delta}$.* Insets (on a matching scale): crystal structure along with the map of the O *K* edge normalized pre-peak intensity, which for this compound correlates with the spin state of Co atoms. Work published in *Nano Letters* **11**, 973 (2011).
***Courtesy**: M. Varela and S. Pennycook, Oak Ridge National Laboratory*

Left Middle: *Imaging exotic properties of nanoscale magnetic lattices*. (a) Nanoscale experimental magnetic induction map of patterned NiFe islands on a square lattice. The color indicates the direction of magnetization in each island, and black/white lines indicate the magnetic field lines; (b) The magnetic induction associated with an "emergent magnetic monopole defect" at the center of four islands (indicated by dashed lines). Work published in *Phys. Rev. B* **83**, 1 (2011).
***Courtesy**: C. Phatak and A. Petford-Long, Argonne National Laboratory*

Bottom Left: *Development of characterization methods that can analyze the direction of the ferroelectric polarization in areas of a few unit cells*. The pattern shown on the left was obtained by a scanning transmission electron microscopy-based convergent beam electron diffraction method (PACBED) from a 4×4 unit cell area of a ferroelectric $BaTiO_3$ film. Comparison with the simulation allows for identifying the direction of the local ferroelectric polarization in this area. The arrows indicate features due to a 4 pm off-centering of Ti atoms. Work published in *Appl. Phys. Lett*. **98**, 052904 (2011).
***Courtesy**: Susanne Stemmer, University of California, Santa Barbara*

Bottom Right: *Metal-to-insulator transition in VO_2.* Depicted are topography (a) and scattering scanning near-field microscopy images (b-d) of the metal insulator transition (MIT) for VO_2 showing gradual growth of insulating (dark) domains, with remaining metallic phase islands persisting well below the nominal T_{MIT}.
***Courtesy**: Markus Raschke, University of Colorado*

This document was produced under contract number DE-AC05-06OR23100 between the U.S. Department of Energy and Oak Ridge Associated Universities.

The research grants and contracts described in this document are supported by the U.S. DOE Office of Science, Office of Basic Energy Sciences, Materials Sciences and Engineering Division.

Foreword

This volume comprises the scientific content of the 2012 Electron and Scanning Probe Microscopies (ESPM) Principal Investigators' (PIs) Meeting sponsored by the Materials Sciences and Engineering Division (MSED) in the Office of Basic Energy Sciences (BES) of the U. S. Department of Energy (DOE). The meeting, held on September 9-12, 2012 in Gaithersburg, Maryland, is the fourth biennial PIs' meeting in the ESPM area and is one among a series of research theme-based PIs' meetings conducted by MSED. The meeting highlights materials research using advanced electron and scanning probe microscopy and spectroscopy techniques, and it also features research that cuts across other BES program areas where appropriate and relevant.

The Electron and Scanning Probe Microscopies Core Research Activity supports basic research in materials sciences using advanced electron and scanning probe microscopy and spectroscopy techniques to understand the atomic, electronic, and magnetic structures and properties of materials. This activity also supports the development of new instrumentation and techniques to advance basic science and materials characterizations for energy applications. Topical areas highlighted in this year's meeting include advanced microscopy techniques, ferroelectrics & multiferroics, superconductivity, magnetism, nanoscale science and phenomena, plamonics, carbon-based materials, and materials for clean energy.

The purpose of the biennial PIs' meetings is to bring together researchers funded by BES in the ESPM area to facilitate the exchange of new results and research highlights, to foster new ideas and collaborations among the participants, and to discuss how to advance electron and scanning probe microscopy and spectroscopy, as well as the associated theoretical tools, in order to address forefront scientific challenges. The meeting will also help MSED in assessing the state of the program and in charting future programmatic directions.

I thank all the meeting participants for their active contributions in sharing their ideas and latest research results. The assistance of the Meeting Chairs, Art Smith and Susanne Stemmer, in organizing this meeting is greatly appreciated. Sincere thanks also go to Teresa Crockett in MSED and Lee-Ann Kiser and her colleagues at the Oak Ridge Institute for Science and Education for their excellent work providing all the logistical support for the meeting.

Jane G. Zhu
Program Manager, Electron and Scanning Probe Microscopies
Division of Materials Sciences and Engineering
Office of Basic Energy Sciences
U. S. Department of Energy

AGENDA

2012 Electron and Scanning Probe Microscopies Principal Investigators' Meeting

SUNDAY, SEPTEMBER 9, 2012

6:00 – 8:00 pm	**Registration**
	*****Dinner on Your Own*****

MONDAY, SEPTEMBER 10

7:00 – 8:00 am	***** Breakfast *****
8:00 – 8:30 am	*Introductory Remarks* **Linda Horton** Director, Materials Sciences and Engineering Division, Basic Energy Sciences
8:30 – 8:50 am	**Jane Zhu** Program Manager, Electron and Scanning Probe Microscopies Meeting Chairs: **Art Smith** and **Susanne Stemmer** Ohio University/University of California – Santa Barbara
Session I	**Transmission Electron Microscopy: Advanced Techniques** Chair: **Laurence Marks**, Northwestern University
8:50 – 8:55 am	*Chair's Introduction*
8:55 – 9:20 am	**Maria Varela**, Oak Ridge National Laboratory *An Atomic Resolution View at Magnetic Oxides*
9:20 – 9:45 am	**Chong-Yu Ruan**, Michigan State University *Dynamical Nanoscale Electron Crystallography*
9:45 – 10:10 am	**Mike Treacy**, Arizona State University *Medium-Range Order in Amorphous Materials Studied by Fluctuation Electron Microscopy*
10:10 – 10:25 am	*Chair-Led Discussion*
10:25 – 10:55 am	***** Break *****
Session II	**Transmission Electron Microscopy: Advanced Applications** Chair: **Amanda Petford-Long**, Argonne National Laboratory
10:55 – 11:00 am	*Chair's Introduction*

11:00 – 11:25 am	**Yimei Zhu**, Brookhaven National Laboratory *Direct Observations of Magnetic Monopoles and Vortex-Core Precession Orbit with Electrons*
11:25 – 11:50 am	**Paul Voyles**, University of Wisconsin – Madison *Imaging Point Defects with Quantitative STEM*
11:50 – 12:15 pm	**Jian-Min (Jim) Zuo**, University of Illinois, Urbana-Champaign *Local to Macroscopic Symmetry for Piezoelectric (1-x)Pb($Mg_{1/3}Nb_{2/3}$) O_3-x$PbTiO_3$ Single Crystal in the Morphotropic Phase Boundary*
12:15 – 12:30 pm	*Chair-Led Discussion*
12:30 – 1:30 pm	Working Lunch *Overview of Poster Session I: Presenters with Highlights*
1:30 – 3:00 pm	***Poster Session I***
3:00 – 3:30 pm	Coffee Break
Session III	**Ferroelectrics, Dielectrics and Multiferroics** Chair: **Susanne Stemmer**, University of California – Santa Barbara
3:30 – 3:35 pm	*Chair's Introduction*
3:35 – 4:00 pm	**R. Ramesh (Invited)**, LBNL/UC Berkeley *Coupling Magnetism to Electricity in Multiferroic Heterostructures: The Role of Imaging and Spectroscopy*
4:00 – 4:25 pm	**A. Gruverman**, University of Nebraska – Lincoln *Resistive Switching Behavior in Ferroelectric Tunnel Junctions Studied at Nanoscale*
4:25 – 4:50 pm	**Sergei Kalinin**, Oak Ridge National Laboratory *Probing Coupled Metal-Insulator and Ferroic Transitions from the Atomistic to Mesoscopic Scales*
4:50 – 5:15 pm	**Xiaoqing Pan**, University of Michigan *Structure and Dynamics of Domains in Ferroelectric Nanostructures – In Situ TEM Studies*
5:15 – 5:30 pm	*Chair-Led Discussion*
5:30 – 7:00 pm	**Working Dinner**
	Jim Schuck, Lawrence Berkeley National Laboratory *Pushing the Frontiers of Nano-characterization: Recent Highlights and New Capabilities at the Molecular Foundry*

Session IV	**Superconductivity & Magnetism** Chair: **Aharon Kapitulnik**, SLAC/Stanford
7:00 – 7:05 pm	*Chair's Introduction*
7:05 – 7:30 pm	**Maria Iavarone**, Temple University *Vortex Matter in Confined Superconductors and Mesoscopic Hybrid Heterostructures*
7:30 – 7:55 pm	**Kathryn Moler**, SLAC National Laboratory/Stanford University *Scanning SQUID Microscopy of Novel Materials*
7:55 – 8:20 pm	**Ian Fisher**, SLAC National Laboratory/Stanford University *Nematicity in Fe-pnictide and Chalcogenide Superconductors*
8:20 – 8:45 pm	**Séamus Davis**, Brookhaven National Laboratory *Spectroscopic Imaging STM for Complex Electronic Matter*
8:45 – 9:00 pm	*Chair-Led Discussion*

TUESDAY, SEPTEMBER 11

7:00 – 8:00 am	***** Breakfast *****
Session V	**Nanoscale Science** Chair: **Ward Plummer**, Louisiana State University
8:00 – 8:05 am	*Chair's Introduction*
8:05 – 8:35 am	**S.-W. Hla (Invited)**, Ohio U/Argonne National Laboratory *Frontiers of STM Manipulations: Imaging Atomic Spin to Operating Nanomachines*
8:35 – 9:00 am	**Markus Raschke**, University of Colorado *Nano-imaging and -spectroscopy of Correlated Electron Materials*
9:00 – 9:25 am	**Minghu Pan**, Oak Ridge National Laboratory *From Graphene to Molecular Assembly: Probing at Atomic/Single Molecular Scale*
9:25 – 9:50 am	**Dawn A. Bonnell**, University of Pennsylvania *Local Properties at Nanosized Interfaces: Metal-Semiconductor and Ionic Conductor-Electrode Systems*
9:50 – 10:05 am	*Chair-Led Discussion*
10:05 – 10:30 am	***** Break *****

Session VI	**Magnetism and Spintronics** Chair: **Chris Hammel**, Ohio State University
10:30 – 10:35 am	*Chair's Introduction*
10:35 – 11:05 am	**Andreas Heinrich (Invited)**, IBM *The Quantum and Classical Properties of Spins on Surfaces*
11:05 – 11:30 am	**David Goldhaber-Gordon**, SLAC/Stanford University *Spin Physics and Nanoscale Probes of Quantum Materials*
11:30 – 11:55 am	**Andreas Schmid**, Lawrence Berkeley National Laboratory *Imaging Magnetism by Spin-Polarized Low-Energy Electron Microscopy*
11:55 – 12:20 pm	**Art Smith**, Ohio University *Spin-Polarized Scanning Tunneling Microscopy Studies of Nanoscale Magnetic and Spintronic Nitride Systems*
12:20 – 12:35 pm	*Chair-Led Discussion*
12:40 – 2:00 pm	Working Lunch *Overview of Poster Session II: Presenters with Highlights*
2:00 – 3:30 pm	***Poster Session II***
3:30 – 4:00 pm	Coffee Break
Session VII	**Nano Materials Growth and Phase Transformations** Chair: **John Spence**, Arizona State University
4:00 – 4:05 pm	*Chair's Introduction*
4:05 – 4:30 pm	**Norman Bartelt**, Sandia National Laboratories *Nanometer-Scale Surface and Interface Phenomena*
4:30 – 4:55 pm	**Geoffrey Campbell**, Lawrence Livermore National Laboratory *Complex Fundamental Mechanisms of Transient States in Materials Quantified by DTEM*
4:55 – 5:20 pm	**Haimei Zheng**, Lawrence Berkeley National Laboratory *Real Time TEM Imaging of Materials Transformations in Liquid or Gas Environments*
5:20 – 5:45 pm	**Charudatta Phatak**, Argonne National Laboratory *3D Visualization of Emergent Behavior in Nanoscale Functional Heterostructures*
5:45 – 6:00 pm	*Chair-Led Discussion*

6:00 – 7:30 pm	**Working Dinner** *Scientific Highlights: Discussion and Input from Attendees*
Session VIII	**Energy Materials and Energy Transport** Chair: **Ian Robertson**, University of Illinois
7:30 – 7:35 pm	*Chair's Introduction*
7:35 – 8:00 pm	**Nitash Balsara**, Lawrence Berkeley National Laboratory *Soft Matter Electron Microscopy*
8:00 – 8:25 pm	**Shen Dillon**, University of Illinois *In Situ TEM Observations of Degradation Mechanisms in Next-Generation High-Energy Density Lithium-Ion Battery Systems*
8:25 – 8:50 pm	**James Morris**, Oak Ridge National Laboratory *Atomistic Mechanisms of Metal-Assisted Hydrogen Storage in Nanostructured Carbons*
8:50 – 9:15 pm	**Pramod Sangi Reddy**, University of Michigan *Study of Energy Transport at the Nanoscale*
9:15 – 9:30 pm	*Chair-Led Discussion*

WEDNESDAY, SEPTEMBER 12

7:00 – 8:00 am	***** Breakfast *****
Session IX	**Carbon-Based Materials** Chair: **Sokrates Pantelides**, Vanderbilt University
8:00 – 8:05 am	*Chair's Introduction*
8:05 – 8:30 am	**Amir Yacoby**, Harvard University *Transport and Imaging of Mesoscopic Phenomena in Single and Few Layer Graphene*
8:30 – 8:55 am	**Lian Li**, University of Wisconsin – Milwaukee *Tailoring Electronic Properties of Graphene via Defect Engineering and Doping*
8:55 – 9:20 am	**John Cumings**, University of Maryland *Interfacial Thermal Resistance of Carbon Nanotubes*
9:20 – 9:35 am	*Chair-Led Discussion*
9:35 - 10:00 am	***** Break *****

Session X	**Plasmonics and Coupled Phenomena** Chair: **Steve Pennycook**, Oak Ridge National Laboratory
10:00 – 10:05 am	*Chair's Introduction*
10:05 – 10:30 am	**P.E. Batson**, Rutgers University *Discovery of Dielectric Response and Forces in Nanoscale Objects*
10:30 – 10:55 am	**Jon Camden**, University of Tennessee *Applications of STEM/EELS to Plasmon-Related Effects in Optical Spectroscopy*
10:55 – 11:20 am	**R. Könenkamp**, Portland State University *High Resolution Photoemission Electron Microscopy*
11:20 – 11:35 pm	*Chair-Led Discussion*
11:35 – 12:05 pm	*Remarks* **Art Smith** and **Susanne Stemmer**, Meeting Chairs **Jane Zhu**, Program Manager, Electron and Scanning Probe Microscopies
12:05 – 1:30 pm	**Working Lunch**
	Meeting Feedback, Suggestions for Future Meetings
	*****Adjourn*****

POSTER SESSIONS

2012 Electron and Scanning Probe Microscopies Principal Investigators' Meeting

Poster Session 1: Monday, Sept. 10, 2012, 1:30 – 3:30 pm

P-I.1 Encased Cantilevers and Spiral Scanning for High Spatial and Temporal Resolution In-Situ Atomic Force Microscopy
Paul Ashby, Dominik Ziegler, Babak Sanii, Alex Chen, Travis Meyer, Rodrigo Farnham, Nen Huynh, Jim DeYoreo, Jen-Mei Chang, and Andrea Bertozzi, Lawrence Berkeley National Laboratory and University of California – Los Angeles and California State University – Long Beach

P-I.2 Electronic States and Transport in Semiconductor Nanostructures
Rachel S. Goldman and Harley T. Johnson, University of Michigan and University of Illinois

P-I.3 Probing Phase Transitions, Chemical Reactions, and Energy Transfer at the Atomic Scale: Multifunctional Imaging with Combined Electron and Scanning Probe Microscopy
Albina Borisevich and Minghu Pan, Oak Ridge National Laboratory

P-I.4 Oxide Surfaces: New Tools and Approaches
Laurence D. Marks, Northwestern University

P-I.5 Properties of $LaAlO_3/SrTiO_3$ Interface Structures
Venkat Chandrasekhar and Chang-Beom Eom, Northwestern University and University of Wisconsin – Madison

P-I.6 Combined Microscopy Studies of Complex Electronic Materials
David H. Cobden, University of Washington

P-I.7 In Situ Light Illumination of Photocatalytic Materials in an Environmental Transmission Electron Microscope
Peter A. Crozier, Ben Miller, and Liuxian Zhang, Arizona State University

P-I.8 Quantum Control of Spins in Diamond for Nanoscale Magnetic Sensing and Imaging
Gurudev Dutt, University of Pittsburgh

P-I.9 Advances in Imaging Delicate Ice Films with Scanning Probe Microscopy
Konrad Thuermer, Sandia National Laboratories

P-I.10 Nano-scale Optical Spectroscopy in Correlated Electron Systems
Adrian Gozar, Brookhaven National Laboratory

P-I.11 Current Trends in Scanning Probe Microscopy at the Center for Nanoscale Materials: Low-Dimensional Materials at the Atomic Scale
Nathan P. Guisinger, Argonne National Laboratory

Poster Session 2: Tuesday, Sept. 11, 2012, 2:00 – 4:00 pm

P-II.1 Materials Properties at Interfaces in Nanostructured Materials: Fundamental Atomic Scale Issues
Nigel D. Browning, Pacific Northwest National Laboratory and University of California – Davis

P-II.2 Mapping Interactions in Hybrid Systems with Active Scanning Probes
Jesse Berezovsky, Case Western Reserve University

P-II.3 Materials Applications of Aberration-Corrected Lorentz Microscopy
Marc De Graef, Carnegie Mellon University

P-II.4 In Situ Analytical Electron Microscopy for Probing Electrochemistry at NanoScale
Shirley Meng, Feng Wang, Jason Graetz, and Nancy Dudney, University of California – San Diego, Brookhaven National Laboratory, and Oak Ridge National Laboratory

P-II.5 Physics of Complex Materials Systems through Theory and Microscopy/EELS
Sokrates T. Pantelides, Mark Oxley, and Kalman Varga, Vanderbilt University

P-II.6 Single Atom Imaging and Spectroscopy of Defects in Graphene
Stephen J. Pennycook, Andrew R. Lupini, Matthew F. Chisholm, Sokrates T. Pantelides, Wu Zhou, and Juan-Carlos Idrobo, Oak Ridge National Laboratory and Vanderbilt University

P-II.7 Emerging Functionality in Transition-Metal Oxides Driven by Spatial Confinement
E. Ward Plummer, Jiandi Zhang, Zac Ward, and Jian Shen, Louisiana State University, Oak Ridge National Laboratory, and The University of Tennessee

P-II.8 A Reactive Regime of Electron Transport
Petro Maksymovych, Oak Ridge National Laboratory

P-II.9 Visualization and Quantification of Deformation Processes Controlling the Mechanical Response of Alloys in Aggressive Environments
Ian M. Robertson, University of Illinois, Urbana-Champaign

P-II.10 Trimodal Tapping Mode Atomic Force Microscopy: Simultaneous 4D Mapping of Conservative and Dissipative Probe-Sample Interactions of Energy-Relevant Materials
Santiago D. Solares, University of Maryland

P-II.11 Electron Nanodiffraction - Seeing Bonds, STEM Lithography, Oxide Superlattices
John H. Spence and Collaborators, Arizona State University

P-II.12 Phonons and Electrons in Thin Complex Oxides
Susanne Stemmer, University of California – Santa Barbara

P-II.13 Direct Observation of Ferromagnetic Nanoclusters and Their Role in Colossal Magnetoresistance
Jing Tao, L. Wu, V. V. Volkov, and Y. Zhu, Brookhaven National Laboratory

Table of Contents

Table of Contents

University Grant Projects

Invited Talks

LABORATORY PROJECTS

Encased Cantilevers and Spiral Scanning for High Spatial and Temporal Resolution in-situ Atomic force Microscopy

Paul Ashby[*+], Dominik Ziegler*, Babak Sanii[*], Alex Chen[#], Travis Meyer[#], Rodrigo Farnham[†], Nen Huynh[†], Jim DeYoreo[*], Jen-Mei Chang[†], Andrea Bertozzi[#]

[*]Imaging and Manipulation Facility, Molecular Foundry, Lawrence Berkeley National Laboratory, 67-2228, 1 Cyclotron Rd, Berkeley, California, USA, 94720.
[#] Department of Mathematics, University California Los Angeles, Los Angeles, California, USA, 90095.
[†]Department of Mathematics, California State University Long Beach, Long Beach, California, USA, 90840.
[+]pdashby@lbl.gov

Research Scope

Spatial and Temporal resolution in Atomic Force Microscopy is fundamentally limited by the force noise, $F_n = \sqrt{4k_B Tb}$, or thermal noise of the cantilever. It is a function of damping, b, and temperature, T, and has the units of N/√Hz. Thus experiments at cryogenic temperature in vacuum (low damping) and sampled slowly have exquisite force resolution. The electron densities of single bonds or spin state of individual electrons have been measured. Measurements in aqueous environments pose substantial challenges for high resolution Atomic Force Microscopy because high temperatures and high damping, due to the viscosity of the fluid, increase force noise by many orders of magnitude. Furthermore, observation of dynamic processes in ambient conditions requires faster scanning and sampling. In-situ microscopy achieves lattice resolution on crystal surfaces and single domain resolution of proteins supported by hard substrates. We have developed encased cantilevers that lower cantilever damping in solution by a factor of 300 for similar

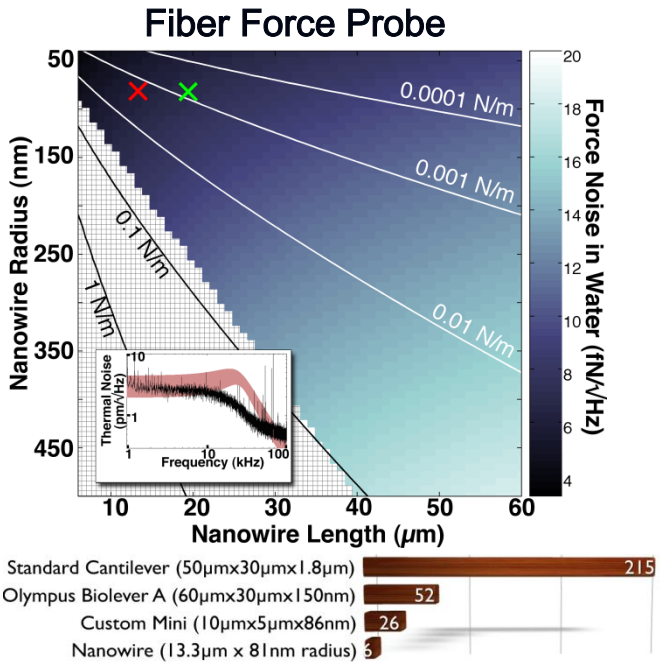

Figure 1 - The calculated force noises of nanowires as a function of their radii and lengths, in water. Contour lines denote cantilever stiffnesses, and the hashed region corresponds to thermal fluctuations that are too small to be detected with our system. Inset is the measured thermal noise spectrum of the 2±1 mN/m stiff nanowire marked with a red × (force noise of 6±3 fN/√Hz), as well as a theoretical prediction, red curve, based on its dimensions and material properties. The bar chart shows Fiber Force Probe force noise relative to other AFM cantilevers. The Fiber Force Probe has record low force noise in solution.

geometries. We also have developed spiral scanning capabilities which substantially increase frame rates enabling the capture of sample dynamics.

Recent Progress

Although quite fashionable, attempts to use feedback methods such as Q-control and frequency modulation have failed to improve the image quality when in solution. Q-control amplifies weak tip-sample interactions and the thermal noise equally providing no overall advantage.[1] Frequency modulation also amplifies weak tip-sample interactions but controls the amplitude noise. However, the feedback shifts the amplitude noise to the time domain precluding a precise measurement of frequency providing no overall advantage either.[2] Instead, the thermal force-noise of the cantilever is the principal limitation to reducing sample deformation. Minimizing a cantilever's cross- section reduces its noise significantly and the minimum size of the cantilever is currently limited by a conventional deflection detection scheme, which requires a large surface area for laser specular reflection. A forward scattering optical deflection detection technique enables the use of nanowires as cantilevers. We achieved a force noise in water of 6 fN/√Hz that is orders of magnitude gentler than conventional AFM using the Fiber Force Probe AFM (figure 1).[3] The Fiber Force Probe has a number of significant limitations such as slow scan speed, difficult sample geometry, and lack of robustness. To mitigate these challenges we reduced force noise by reducing the fluid viscosity with a protective encasement for the cantilever (figure 2). The cantilever operates in air but the probe protrudes from the encasement through the solution to the sample. Encased cantilevers have exceptionally high resonance frequency, Quality factor,

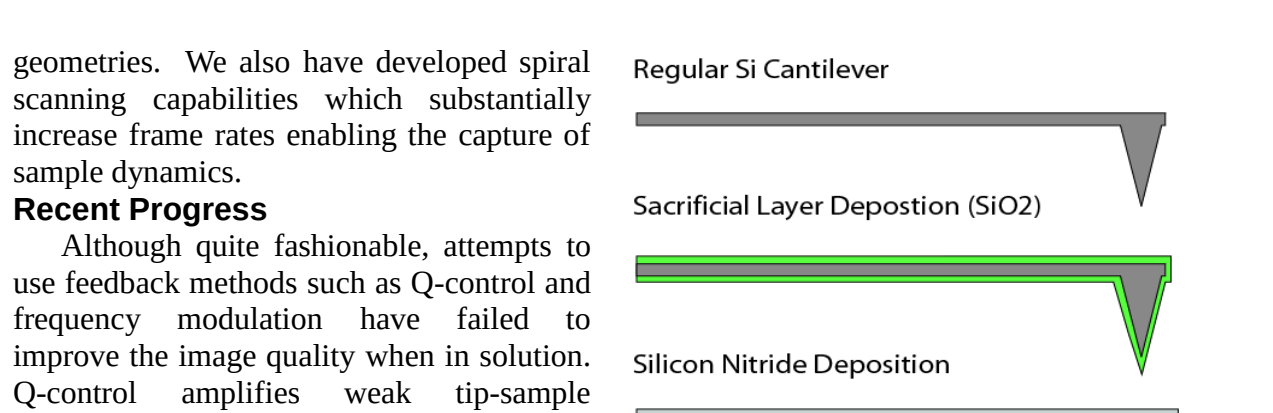

Figure 2 - Cartoon of encased cantilevers fabrication process. PE CVD is used to deposit a sacrificial layer and the encasement. The sacrificial layer is etched back from an opening at the probe apex. Surface tension prevents water from entering the encasement.

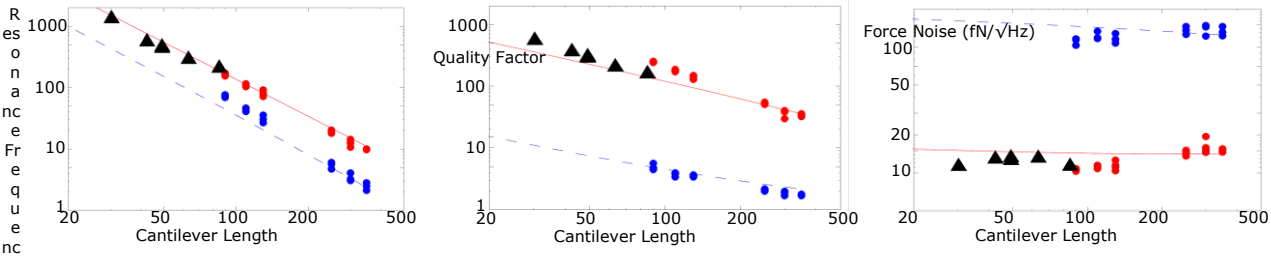

Figure 3 - Resonance frequency, quality factor, and force noise as a function of cantilever length for normal cantilevers in air (●) and in water (●). The encased cantilevers (▲) in water have the same high-performance as normal cantilevers in air.

and detection sensitivity and low force noise (figure 3) enabling gentle high resolution imaging.[4] They also work in all commercial AFM systems without modification.

Present raster scan techniques are poorly matched to the instrument limitations of Atomic Force Microscopy. Raster scanning persists as the convention because images are displayed as pixels on a square grid and the instrument is expected to fill a pixel with each sample leading to constant tip velocities along a row or column of data. Since the instrument is required to be at each point in space during the sample, feedback and feed forward schemes are required to compensate for piezo nonlinearity and creep. However, these techniques slow the instrument for accuracy and do not fully compensate the errors such that it is still required to display only the trace or retrace but not interlace the collected data. Effectively half of the scan time is wasted during each image. We have regained the lost scan time by using advance image processing algorithms, such as inpainting, to display the date directly from the X and Y sensor signals. Also, inpainting allows the recovery of high-resolution images from sparse quickly collected data to improve temporal resolution without applying more force or increasing bandwidth (figure 4).[5] Furthermore, We are also using non-raster scan algorithms such as spiral scanning to increase temporal resolution. Spiral scanning better matches the mechanical limitations of the AFM scanner and allows higher tip velocities without distortion. Inpainting or interpolation is used to quickly create images from the nongrided data.[6]

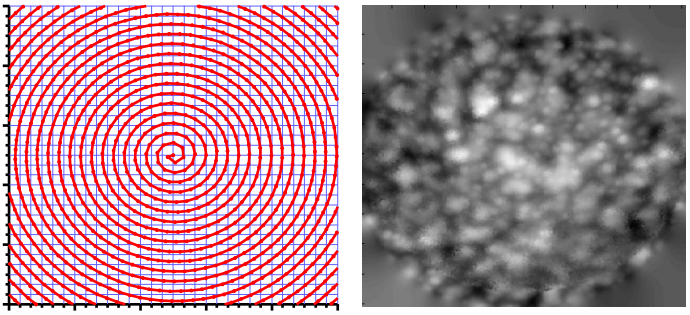

Future Plans

The use of gentle high bandwidth probes and fast scanning algorithms will enable Atomic Force Microscopy to probe samples with high spatial and temporal resolution. We will use these techniques to investigate the structure of water, ions, and small organic molecules near clay surfaces at high salt concentration. This will provide a more complete understanding of the diffusion and flow of water and gas in wells after hydraulic fracturing and could help us better utilize this abundant energy source without aquifer pollution. We also intend to investigate a number of interesting biological systems. Initially, we will image the organization and function of synaptic DNA-protein complexes. The synaptosome is involved in site specific recombination, integration, excision, and inversion in genes. We will also image the process of cell migration and attachment of integrins to the extracellular matrix and subsequent maturation into focal adhesions. The development of focal adhesions is crucial for cell motility and vitality.

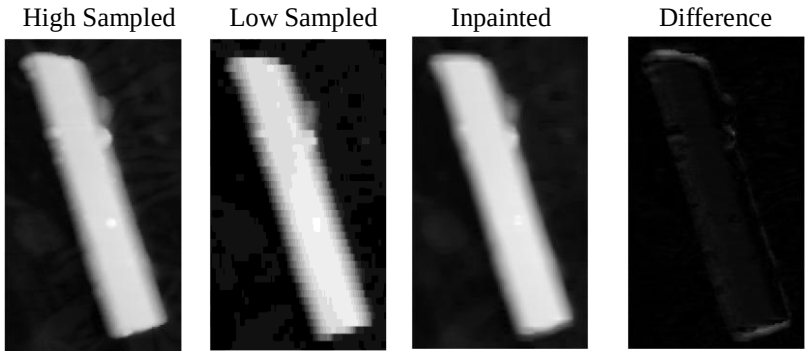

Figure 4 - inpainting diffuses data from known regions of an image to unknown regions by balancing fidelity to the original data and smooth connectedness of the resulting image. For simple images and edges quickly acquired low density data is all that is required enabling higher frame rates.

Nanoscale characterization of protein complexes in physiologic conditions has been limited. Lastly, we will also image the structure of biomimetic materials in solution, specifically peptoid nanosheets. Encased cantilevers offer significantly reduced force noise and higher resonant frequencies and in combination with spiral scanning higher spatial and temporal resolution AFM imaging in solution is possible.

References

[1] Paul D. Ashby, Gentle imaging of soft materials in solution with amplitude modulation atomic force microscopy: Q control and thermal noise, *Appl. Phys. Lett.*, **2007**, *91*, 254102.

[2] Paul D. Ashby, Impact force noise in Frequency Modulation Atomic Force Microscopy, in preparation.

[3] Babak Sanii, Paul D. Ashby, High Sensitivity Deflection Detection of Nanowires, Physical Review Letters, **2010**, *104*, 147203.

[4] Dominik Zieler, Paul D. Ashby, Encased Cantilevers for Ultra Sensitive Force and Mass Detection, in preparation .

[5] Alex Chen, Pascal Getreuer, Yifei Lou, Paul D. Ashby, Andrea Bertozzi, Enhancement and Recovery in Atomic Force Microscopy Images, submitted.

[6] Travis Meyer, Rodrigo Farnham, Nen Huynh, Alex Chen, Jen-Mei Chang, Paul D. Ashby, Andrea Bertozzi, Fast Atomic Force Microscopy Imaging using Self-Intersecting Scans and Inpainting, in preparation.

Program title: Soft Matter Electron Microscopy

Principal Investigators: Nitash Balsara (nbalsara@lbl.gov), Kenneth Downing (khdowning@lbl.gov), Christian Kisielowski (cfkisielowski@lbl.gov), Andrew Minor (aminor@lbl.gov), Ronald Zuckermann (rnzuckermann@lbl.gov)

Research Scope

Our objective is study fundamental aspects of charge transport in nanoscale polymer channels by electron scattering and microscopy. We focus on self-assembled nanostructures formed by bio-inspired peptoids and synthetic block copolymers within which ion transport is restricted to one of the nanostructures. Our objective is to determine the geometry and chain configurations that lead to the most efficient solid-phase ion-transporting channel. Spatially resolved electron microscopy and energy-loss spectroscopy are crucial for obtaining the relationship between morphology and transport. The proposed microscopy techniques focus on maximizing spatial and energy resolution while minimizing radiation exposure and damage. This is achieved by using novel techniques to manipulate and detect the incident, transmitted, and scattered electrons.

Recent Progress

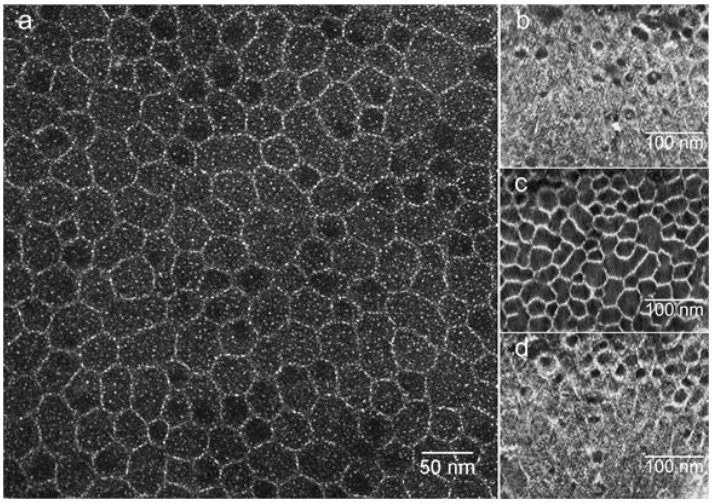

Figure 1. PSS-PMB film prepared by casting and annealing in water vapor showing the honeycomb morphology and ionic clusters (bright spots). a) HAADF image obtained in projection; b, c, d) Slices of HAADF tomographic reconstruction and diagram indicating position of the slice in cross section of the film b) top slice, c) middle slice, and d) bottom slice. The slices reveal that the ionic clusters are distributed uniformly near the top and bottom surfaces and are concentrated in the honeycomb wall structure.

Soft materials will undoubtedly play an important role in the emerging clean energy landscape. Materials that efficiently transport of low atomic weight species, e.g. Li^+ and H^+, are required for propelling vehicles that do not consume gasoline. In order to retain high transport rates and mechanical integrity, it is essential to create ion-transporting channels that must be soft in a high modulus matrix. The multiphase structure is invariably obtained by self-assembly in polymers. We have, in recent months, reported breakthroughs in our ability to image ion-containing phases and systems.

Fuel cells, which hold promise for providing energy without pollution, rely on proton transport through a polymer electrolyte membrane (PEM). The PEM is a single-ion conductor with protons attached to sulfonic acid groups that are attached to the polymer backbone. The clustering of these

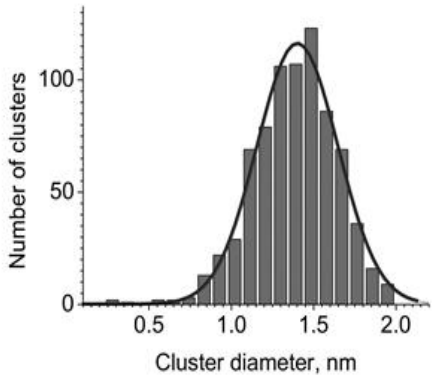

Figure 2. Histogram of ionic cluster size distribution (bars) and Gaussian fit (curve).

groups has important ramifications on proton transport. In spite of several attempts over the past three decades, attempts to image proton-containing clusters by TEM were unsuccessful. Our experiments were conducted on a model PEM comprising poly(styrene sulfonate)-*block*-poly(methyl butylene) (PSS-PMB) copolymers. Our ability to synthesize novel materials is essential for designing efficient membranes and for tailoring the systems for demonstrating novel characterization approaches. Exposing a 35 nm thick free standing electrolyte film to moist air results in the formation of extremely thin cluster-containing layers at the electrolyte/air interfaces and a honeycomb morphology in the interior of the film. This morphology is ideally suited for direct imaging of ionic clusters by electron microscopy. An image thus obtained is shown in Figure 1a. Analysis of the image reveal that the distribution of cluster sizes is Gaussian with an average cluster diameter is 1.4 nm. This work lays the foundation for determining the morphology of ionic clusters in other proton transporting membranes (e.g. Nafion®). Other aspects of our work on fuel cell membranes are reported in refs 2-5.

Solid electrolytes comprising block copolymers with dissolved lithium salts are being considered for developing the next generation of lithium batteries. Batteries with lithium metal anodes will enhance the driving range of electric cars by a factor of two. We have studied poly(styrene-block-ethylene oxide) (PS-PEO) blended with a lithium salt (LiTFSI). We have completed a definitive study of the ability of nanostructured block copolymers to stabilize the lithium metal anode [6]. Of crucial importance is the interface between the electrode and the nanostructured electrolyte. Electron micrographs of this in interface are shown in ref. 6. What we have not yet been able to image is the electrolyte nanostructures at the interface. We have, however, succeeded in obtaining the morphology of PS-PEO/LiTFSI mixtures near the air interface by preparing free-standing films. You our surprise, the films exhibited a honeycomb morphology as shown in Figure 3. It is noteworthy that prior to our work, the honeycomb morphology has never been reported in block copolymers. Other aspects of our work on battery electrolytes are reported in refs. 7.

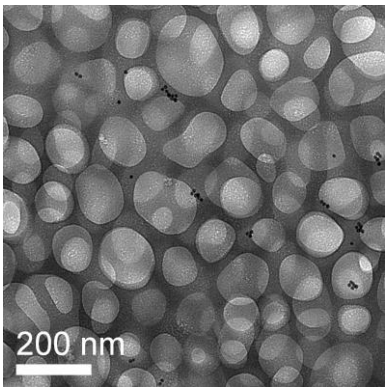

Figure 3. TEM image of a free standing PS-PEO/LiTFSI electrolyte showing a honeycomb morphology. The sample shows a lamellar morphology in the bulk. Unpublished results of Allen and Minor.

In ref. 8 we announce a new approach to mimic the way nature builds precisely defined nanostructures (e.g. proteins and nucleic acids). We accomplish this by arranging

synthetic monomeric building blocks into a specific linear sequence. Such sequence-specific heteropolymers can spontaneously fold into conformationally-defined 3D structures and have the potential to lead to a new generation of highly robust artificial protein-like materials. We have already completed major steps toward developing materials that combine the exquisite architecture and functionality of proteins with the durability of polymers. The polymers of interest are called "peptoids". Our ability to synthesize peptoids for lithium battery applications is described in ref. 8.

Beam damage is a significant problem in soft materials and in ref. 9 we have shown how it can be minimized. The soft matter program has had an influence on other programs at LBNL including that of the Energy Biosciences Institute wherein membranes for biofuel separation were imaged [10]. Our effort to better control the preparation of hydrated samples is described in ref. 11. With the publication of ref. 12, we will conclude the work of C. Kisielowski to develop phase plates for electron microscopy. Other work from this work is reported in refs. 12-15.

Future Plans

Our work described above lays the groundwork for our future studies on battery and fuel cell membranes. Since fuel cells operate in the hydrated state, the morphology of the clusters in the presence of water is crucially important. We are poised to obtain these images due to our experience with frozen samples [11] and earlier work by Moon Park in this program. The imaging of nanostructures near the lithium electrode and identifying dendrites in lithium batteries remains a challenge. We are particularly excited to characterize the precise polypeptoids as the morphology in these systems should be better defined than that in synthetic polymers (all of our imaging work thus far is restricted to synthetic polymers with some polydispersity).

In summary, in the coming years we will:

- Image ion clusters in hydrated fuel cell membranes.
- Study lithium ion transport in an *in situ* cell.
- Image nanostructures including dendrites at the lithium-electrolyte interface.
- Determine the morphology of precise peptoid-based electrolytes.

Publications

1. "Direct Imaging of Nanoscale Acidic Clusters in a Polymer Electrolyte Membrane", S.Yakovlev, X. Wang, P. Erricus, N.P. Balsara, K.H. Downing, *Journal of the American Chemical Society*, vol. 113 (51), p. 20700-20703, 2011.

2. " Limits of Spatial and Compositional Resolution of Electron Energy Loss Spectroscopy of Soft Materials", S. Yakovlev, N.P. Balsara, K.H. Downing, *Ultramicroscopy*, vol. 116, p. 39-46, **2012**.

3. "Counterion Condensation in Nafion", K.M. Beers, D.T. Hallinan, X. Wang, J.A. Pople, N.P. Balsara, *Macromolecules*, vol. 44, p. 8866-8870, **2011**.

4. "Conductivity and Water Uptake in Block Copolymers Containing Protonated Polystyrene Sulfonate and its Imidazolium Salt", X. Wang, K. M. Beers, J.B. Kerr, N.P. Balsara, *Soft Matter*, vol. 47, pg. 647-650, **2011**.

5. "Proton Conduction in Materials with Conducting Domains with Widths less than 6 nm", N.P. Balsara, K.B. Beers, *European Polymer Journal*, vol. 42, pg. 559-562, **2011**.

6. "Resolution of the Modulus versus Adhesion Dilemma in Solid Polymer Electrolytes in Rechargeable Lithium Batteries", G.M. Stone, S.A. Mullin, A.A. Teran, D.T. Hallinan, A.M. Minor, A. Hexemer, N.P. Balsara, *Journal of the Electrochemical Society*, vol. 159 (3), p. A222-A227, **2012**.

7. "Chemical Mapping of a Block Copolymer Electrolyte by Low-Loss EFTEM Spectral Imaging and Principle Component Analysis", F.I. Allen, M. Watanabe, Z.H. Lee, N.P. Balsara, A.M. Minor, *Ultramicroscopy*, vol. 111, pg. 239-244, **2011**.

8. "Structure-Conductivity Relationship for Peptoid-Based PEO-Mimetic Polymer Electrolytes", J. Sung, G.M. Stone, N.P. Balsara, R.N. Zuckermann, *Macromolecules*, vol. 45(12), p. 5151-5156, **2012**.

9. "Minimization of Focused Ion Beam Damage in Nanostructured Polymer Thin Films", S. Kim, M.J. Park, N.P. Balsara, G. Liu, A.M. Minor, *Ultramicroscopy*, vol. 111, pg. 191-199, **2011**.

10. "Master Curve Captures the Effect of Domain Morphology on Ethanol Pervaporation Through Block Copolymer Membranes", A.K. Jha, S.L. Tsang, A.E. Ozcam, R.D. Offeman, N.P. Balsara, *Journal of Membrane Science*, vol. 401-204, p. 125-131, **2012**.

11. "Self pressure freezing for the preparation of frozen hydrated sections", S. Yakovlev and K. H. Downing, *J. Microsc*. **244,** 235-47, **2011**.

12. "The SmartEFTEM-SI method: Development of a new spectrum-imaging acquisition scheme for quantitative mapping by energy-filtering transmission electron microscopy", M. Watanabe and F.I. Allen, *Ultramicroscopy*, vol. 113, pg. 106-119 **2012**

13. "Atomic resolution phase contrast imaging and in-line electron holography using variable voltage and dose rate", B. Barton, B. Jiang, C. Song, P. Specht, H. Calderon and C. Kisielowski, *Microscopy and Microanalysis*, **2012**, in press

14. "Atomic resolution at 50 – 300 kV obtained using low dose rate HRTEM", B. Barton, C. Song,C. Kisielowski, *Microscopy and Microanalysis* 17 (Suppl 2) pg. 1266-1267, **2011**.

15. "The challenge of imaging hard/soft matter interfaces at atomic resolution" B. Barton, R. Buonsanti, A. Dong, D. Milliron, L. Hansen, S. Helveg, B. Jiang, C. Kisielowski, *Microscopy and Microanalysis* 18 (Suppl 2), in press, **2012**.

Nanometer-Scale Surface and Interface Phenomena

Norman Bartelt[1], Peter Feibelman, Gary Kellogg, Kevin McCarty, Nancy Missert, Brian Swartzentruber, Konrad Thürmer, and Kevin Zavadil
Sandia National Laboratories, Livermore, CA and Albuquerque, NM

Program Scope

This program is aimed at atomic/molecular-scale understanding of processes occurring at solid-vacuum, solid-solid and solid-liquid interfaces. Its goal is to provide the scientific underpinnings needed to control surface/interface properties for materials applications, particularly those relevant to energy-related technologies. With the goal of determining how atomic-scale processes relate to the longer-range interactions that control interfacial behavior, our approach combines state-of-the-art experimental capabilities with theory and simulation. The project has four synergistic tasks:

1) *Atomistic dynamics of surfaces* focuses on the mechanisms and energetics of atom transport across surfaces and into the interiors of solids. Experimental tools include scanning tunneling microscopy (STM), *atom-tracking* STM and low-energy electron microscopy (LEEM). Theoretical interpretations emerge from density functional theory (DFT) studies, molecular dynamics/Monte Carlo simulations and thermodynamic modeling. We have identified diffusion processes underlying the growth and stability of surface alloys, thin-film growth and surface nanostructure formation.

2) *Collective phenomena in surface dynamics* quantifies collective processes that govern the surface structures and morphologies of functional materials. We use STM and LEEM to measure the time-evolution of surface structure on nanometer length scales. We develop equations of motion, which account for the observed time dependences precisely and relate their parameters to the atomic processes studied in Task 1. Our new insights into materials behavior include determining the forces that stabilize self-assembling patterns, identifying the kinetic pathways that promote film instability and revealing that unexpected processes of cluster diffusion and bulk/surface mass exchange can guide materials growth.

3) *Materials at interfaces: structural and mechanical properties* measures adhesion, wetting, and mechanical properties at the nanometer to micron scale, using highly sensitive interfacial probes, and interprets them with ideas stemming from atomic-level studies. We have recently been using STM and AFM to probe the structure of the first few layers of atoms or molecules such as water near an interface, and DFT to interpret images and guide experiments.

4) *Nanoscale electrochemistry* uses advanced electrochemical, morphological, chemical and structural analytical tools to clarify corrosion and nanostructure-formation mechanisms. Primary goals are a quantitative understanding of the mechanisms of localized corrosion initiation in passive metals and measurements of the critical parameters governing nanostructure formation in model systems. We apply novel and unique nanofabrication techniques to produce tailored surfaces, and to simulate specific defect types on controlled substrates in well-defined locations.

Recent Progress

Atomistic dynamics of surfaces: Our recent progress includes: 1) understanding defect-mediated diffusion of embedded Ge atoms in Ge/Si(001), 2) analyzing atom transport

[1] bartelt@sandia.gov

during surface alloy formation in the Pd-Cu(001) system, 3) determining the mechanism of Si adatom diffusion on the Au-Si(111) 5x2 surface alloy, 4) understanding labyrinth island growth in Pd/Ru(0001) heteroepitaxy, 5) revealing the competition between bulk and surface diffusion in the chemically reactive system of Al alloying with NiAl, 6) quantifying the mobility of water molecules on ice and 7) determining the atomic structure of graphene on metals.

Collective phenomena in surface dynamics: Our recent progress includes: 1) understanding how B induces self-assembly of one-dimensional nanostructures on Si(001), 2) determining why patterns form after metal deposition on graphene, 3) identifying the mechanism and energetic driving force for 3D pattern formation during thin film dewetting, 4) explaining the ubiquity of nanoscale periodicity of adsorbed phases at high temperature, 5) determining the factors that determine the shape of growing graphene islands (Fig. 1), 6) showing that graphene grows on metals by adding

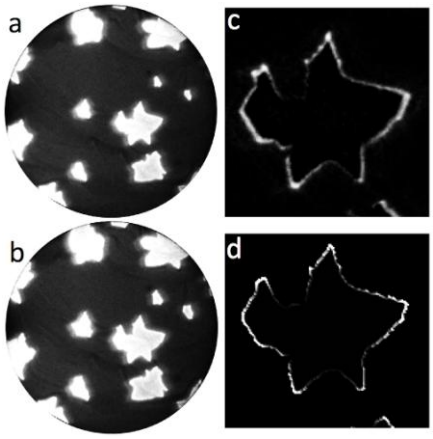

Figure 1. Real-time LEEM imaging of graphene growth on Cu(111). a) Graphene islands are bright. Field of view = 20 μm. b) Same region 60 s later. c) Difference between images a and b enlarged around the island at right of center. The width of the white band is proportional to the local growth rate. d) Simulation of the flux to the island from solving the 2D diffusion equation for the experimental island configuration. The graphene grows faster at the lope tips, which establishes that growth is controlled by surface diffusion of carbon atoms.

clusters of C atoms, 7) revealing the mechanisms of graphene growth by SiC decomposition and 8) characterizing the growth of ice films on Pt(111).

Materials at interfaces: Structural and mechanical properties: Our recent progress includes: 1) explaining epitaxial water nucleation on the surface of salt, 2) first-principles calculations of water-solid interfaces, including water on AgI, Pd(111), Ru(0001) and muscovite, 3) understanding NaCl hydration by ice, 4) measuring friction on a self-lubricating surface, 5) evaluating nanoscale adhesion beyond classical descriptions, 6) developing a molecular basis for interfacial deformation, friction, and wear, 7) determining the structure of the water wetting layer on Pt(111)) and 8) using AFM to image the configuration of molecular-height steps of thick ice films (Fig. 2).

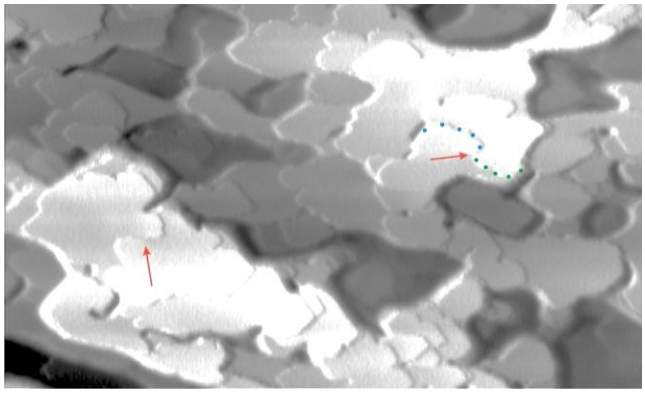

Figure 2. A (600nm x 360nm) AFM image of a 50nm thick insulating ice film on Pt(111) grown at 140K showing the arrangement of molecular-height steps. The red arrows point to threading screw dislocations with a burgers vector equal to the height of two steps (separately marked by the green and blue dots, respectively), establishing that the film is composed of hexagonal ice Ih. In contrast, thinner films are predominately cubic ice Ic.

Nanoscale electrochemistry: Our recent progress includes: 1) characterizing passive oxide breakdown events on Al microelectrodes, 2) defining the role of oxygen vacancy generation in oxide passivity, 3) creating artificial pit nuclei on aluminum at pre-determined locations to measure local pitting susceptibility, 4) using first-principles calculations of Al and O bonding in the presence of a H-impurity atom to conclude that oxide-metal bonding is weaker at interfacial steps, 5) discovering that activation of the oxide surface towards the oxygen reduction reaction occurs in alkaline solutions due to a dramatic increase in electron transfer rates, 6) showing that localized attack in model alloy systems is metastable because of the high pH environment, and 7) showing that self-assembly of surface nanostructures can be controlled electrochemically through manipulation of surface stress from specifically adsorbed anion layers.

DOE Sponsored Publications 2010-2012

[1] P. J. Feibelman, "DFT Versus the "Real World" (or, Waiting for Godft)," *Topics in Catalysis* **53**, 417-422 (2010).

[2] P. J. Feibelman, "The first wetting layer on a solid," *Physics Today* **63**, 34-39 (2010).

[3] P. J. Feibelman, N. C. Bartelt, S. Nie and K. Thurmer, "Interpretation of high-resolution images of the best-bound wetting layers on Pt(111)," *Journal of Chemical Physics* **133**, 154703 (2010).

[4] T. Herranz, K. F. McCarty, B. Santos, M. Monti and J. de la Figuera, "Real Space Observations of Magnesium Hydride Formation and Decomposition," *Chemistry of Materials* **22**, 1291-1293 (2010).

[5] Y. Murata, E. Starodub, B. B. Kappes, C. V. Ciobanu, N. C. Bartelt, K. F. McCarty and S. Kodambaka, "Orientation-dependent work function of graphene on Pd(111)," *Applied Physics Letters* **97**, 143114 (2010).

[6] S. Nie, P. J. Feibelman, N. C. Bartelt and K. Thurmer, "Pentagons and Heptagons in the First Water Layer on Pt(111)," *Physical Review Letters* **105**, 026102 (2010).

[7] T. Ohta, N. C. Bartelt, S. Nie, K. Thurmer and G. L. Kellogg, "Role of carbon surface diffusion on the growth of epitaxial graphene on SiC," *Physical Review B* **81**, 121411 (2010).

[8] B. Santos, J. M. Puerta, J. I. Cerda, T. Herranz, K. F. McCarty and J. de la Figuera, "Structure of ultrathin Pd films determined by low-energy electron microscopy and diffraction," *New Journal of Physics* **12**, 023023 (2010).

[9] Y. Sato, B. Unal, T. A. Lograsso, P. A. Thiel, A. K. Schmid, T. Duden, N. C. Bartelt and K. F. McCarty, "Periodic step arrays on the aperiodic i-Al-Pd-Mn quasicrystal surface at high temperature," *Physical Review B* **81**, 161406 (2010).

[10] J. Soltis, D. P. Krouse, N. J. Laycock and K. R. Zavadil, "Automated processing of electrochemical current noise in the time domain: I. Simulated signal," *Corrosion Science* **52**, 838-847 (2010).

[11] E. Starodub, N. C. Bartelt and K. F. McCarty, "Oxidation of Graphene on Metals," *Journal of Physical Chemistry C* **114**, 5134-5140 (2010).

[12] J. M. Wofford, S. Nie, K. F. McCarty, N. C. Bartelt and O. D. Dubon, "Graphene Islands on Cu Foils: The Interplay between Shape, Orientation, and Defects," *Nano Letters* **10**, 4890-4896 (2010).

[13] E. Bussmann, I. Ermanoski, P. J. Feibelman, N. C. Bartelt and G. L. Kellogg, "Buried Pd slows self-diffusion on Cu(001)," *Physical Review B* **84**, 245440 (2011).

[14] I. Ermanoski, N. C. Bartelt and G. L. Kellogg, "Self-assembly of defect-free nanostripe arrays on B-doped Si(001)," *Physical Review B* **83**, 205432 (2011).

[15] P. J. Feibelman, G. A. Kimmel, R. S. Smith, N. G. Petrik, T. Zubkov and B. D. Kay, "A unique vibrational signature of rotated water monolayers on Pt(111): Predicted and observed," *Journal of Chemical Physics* **134**, 204702 (2011).

[16] T. Herranz, B. Santos, K. F. McCarty and J. de la Figuera, "Real-space study of the growth of magnesium on ruthenium," *Surface Science* **605**, 903-911 (2011).

[17] A. Mascaraque, T. O. Mentes, K. F. McCarty, J. F. Marco, A. K. Schmid, A. Locatelli and J. de la Figuera, "Valence band circular dichroism in non-magnetic Ag/Ru(0001) at normal emission," *Journal of Physics-Condensed Matter* **23**, 305006 (2011).

[18] S. Nie, N. C. Bartelt and K. Thurmer, "Evolution of proton order during ice-film growth: An analysis of island shapes," *Physical Review B* **84**, 035420 (2011).
[19] S. Nie, A. L. Walter, N. C. Bartelt, E. Starodub, A. Bostwick, E. Rotenberg and K. F. McCarty, "Growth from Below: Graphene Bilayers on Ir(111)," *Acs Nano* **5**, 2298-2306 (2011).
[20] S. Nie, J. M. Wofford, N. C. Bartelt, O. D. Dubon and K. F. McCarty, "Origin of the mosaicity in graphene grown on Cu(111)," *Physical Review B* **84**, 155425 (2011).
[21] D. A. Schmidt, T. Ohta and T. E. Beechem, "Strain and charge carrier coupling in epitaxial graphene," *Physical Review B* **84**, 235422 (2011).
[22] A. Seyeux, G. S. Frankel, N. Missert, K. A. Unocic, L. H. Klein, A. Galtayries and P. Marcus, "ToF-SIMS Imaging Study of the Early Stages of Corrosion in Al-Cu Thin Films," *Journal of the Electrochemical Society* **158**, C165-C171 (2011).
[23] E. Starodub, A. Bostwick, L. Moreschini, S. Nie, F. El Gabaly, K. F. McCarty and E. Rotenberg, "In-plane orientation effects on the electronic structure, stability, and Raman scattering of monolayer graphene on Ir(111)," *Physical Review B* **83**, 125428 (2011).
[24] A. L. Walter, S. Nie, A. Bostwick, K. S. Kim, L. Moreschini, Y. J. Chang, D. Innocenti, K. Horn, K. F. McCarty and E. Rotenberg, "Electronic structure of graphene on single-crystal copper substrates," *Physical Review B* **84**, 195443 (2011).
[25] J. I. Cerda, B. Santos, T. Herranz, J. M. Puerta, J. de la Figuera and K. F. McCarty, "CO-Assisted Subsurface Hydrogen Trapping in Pd(111) Films," *Journal of Physical Chemistry Letters* **3**, 87-91 (2012).
[26] J. Knudsen, P. J. Feibelman, T. Gerber, E. Granas, K. Schulte, P. Stratmann, J. N. Andersen and T. Michely, "Clusters binding to the graphene moire on Ir(111): X-ray photoemission compared to density functional calculations," *Physical Review B* **85**, 035407 (2012).
[27] C. F. Lin, A. B. H. Hammouda, H. C. Kan, N. C. Bartelt and R. J. Phaneuf, "Directing self-assembly of nanostructures kinetically: Patterning and the Ehrlich-Schwoebel barrier," *Physical Review B* **85**, 085421 (2012).
[28] S. Maier, I. Stass, T. Mitsui, P. J. Feibelman, K. Thurmer and M. Salmeron, "Adsorbed water-molecule hexagons with unexpected rotations in islands on Ru(0001) and Pd(111)," *Physical Review B* **85**, 155434 (2012).
[29] M. Monti, B. Santos, A. Mascaraque, O. R. de la Fuente, M. A. Nino, T. O. Mentes, A. Locatelli, K. F. McCarty, J. F. Marco and J. de la Figuera, "Magnetism in nanometer-thick magnetite," *Physical Review B* **85**, 020404 (2012).
[30] Y. Murata, S. Nie, A. Ebnonnasir, E. Starodub, B. B. Kappes, K. F. McCarty, C. V. Ciobanu and S. Kodambaka, "Growth structure and work function of bilayer graphene on Pd(111)," *Physical Review B* **85** (2012).
[31] S. Nie, N. C. Bartelt, J. M. Wofford, O. D. Dubon, K. F. McCarty and K. Thürmer, "Scanning tunneling microscopy study of graphene on Au(111): Growth mechanisms and substrate interactions," *Physical Review B* **85**, 205406 (2012).
[32] T. Ohta, T. E. Beechem, J. T. Robinson and G. L. Kellogg, "Long-range atomic ordering and variable interlayer interactions in two overlapping graphene lattices with stacking misorientations," *Physical Review B* **85**, 075415 (2012).
[33] B. Santos, S. Gallego, A. Mascaraque, K. F. McCarty, A. Quesada, A. T. N'Diaye, A. K. Schmid and J. de la Figuera, "Hydrogen-induced reversible spin-reorientation transition and magnetic stripe domain phase in bilayer Co on Ru(0001)," *Physical Review B* **85**, 134409 (2012).
[34] E. Starodub, N. C. Bartelt and K. F. McCarty, "Viable thermionic emission from graphene-covered metals," *Applied Physics Letters* **100**, 181604 (2012).
[35] J. M. Wofford, E. Starodub, A. L. Walter, S. Nie, A. Bostwick, N. C. Bartelt, K. Thürmer, E. Rotenberg, K. F. McCarty and O. D. Dubon, "Extraordinary epitaxial alignment of graphene islands on Au(111)," *New Journal of Physics* **14**, 053008 (2012).

ERKCM67: Probing phase transitions, chemical reactions, and energy transfer at the atomic scale: Multifunctional imaging with combined electron and scanning probe microscopy

PI: Albina Y. Borisevich **Co-PIs***:* Minghu Pan, (albinab, mpan1)@ornl.gov

Postdocs: Young-Min Kim, Jae Hyuck Jang

Oak Ridge National Laboratory, Oak Ridge, TN 37831

Program scope

This program started in August 2009 as one of the Single-Investigator- Small Group projects. The focus is on probing the mechanisms of reversible and irreversible bias-induced transformations in solids at the atomic level of individual defects using a combination of scanning transmission electron microscopy (STEM) and local-field confinement in *ex-situ* and *in-situ* active device configurations. We aim to unravel the complex interplay between order parameter dynamics, ionic flows, electrochemical reactions, and mechanical behavior by studying three classes of phenomena: (A) *irreversible* electrochemical processes including oxygen vacancy injection, vacancy ordering, and the formation of crystallographic shear defects, (B) *hysteretic* processes including electrostatically-driven structural changes and phase transitions in ferroelectrics and at ferroelectric interfaces and ultimately (C) kinetics of *reversible* electronic transfer, ionic polarization and interfacial reactions at oxide interfaces and oxide grain boundaries. We aim to uncover the mechanisms of these transformations at the nanometer-scale, and ultimately, the single-atom and single electron level, and link these to atomistic and mesoscopic models. This will enable optimization of a broad range of energy and information technologies from solid oxide fuel cells to memristive data storage and logic devices, as well as elucidate the role of vacancies in physical functionality of surfaces and interfaces.

Recent Progress

Mapping Oxygen Vacancies on Atomic Scale. Uncovering the physical and chemical behavior of oxides during bias-induced phase transformations requires capability for probing both vacancy concentration and degree of ordering locally. While some reports of local vacancy concentration measurements via matching observed intensities to High Resolution Transmission Electron Microscopy (HRTEM) simulations at a grain boundary[1] and tracking EELS fine structure in reduced $SrTiO_3$[2] have appeared in the literature, neither of these approaches proved to be sufficiently general to develop into a quantitative tool. Here, we extended the direct image analysis approach originally developed for ferroics to vacancy ordered systems, specifically, analyzing STEM images to extract the intensity of columns and atomic positions and utilizing lattice parameter (i.e. locally measured ***chemical expansivity***) as a measure of oxygen vacancy concentration.

The new approach was successfully applied to lanthanum strontium cobaltite ($La_{0.5}Sr_{0.5}CoO_{3-\delta}$) thin films epitaxially grown on substrates of different symmetry, where Polarized Neutron Reflectometry revealed strong difference in magnetic properties. Different vacancy content found in the two films (Fig.1) suggests the change in oxygen chemical potential as a source of distinct magnetic properties. Furthermore, we demonstrated that the tilt effect imposed by substrate symmetry can influence the overall oxygen stoichiometry in the film, opening pathways for structural

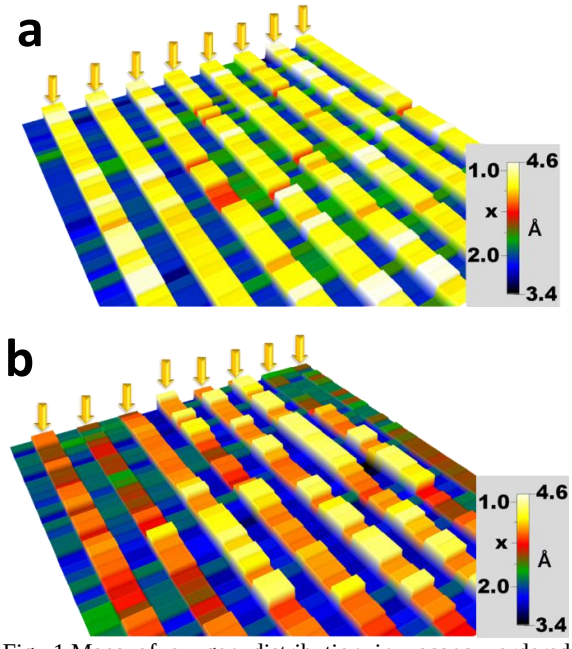

Fig. 1.Maps of oxygen distribution in vacancy ordered $La_{0.5}Sr_{0.5}CoO_{3-\delta}$ films grown on different substrates given as oxygen content x in CoO_x layer: (a) film grown on $NdGaO_3$ is highly ordered brownmillerite $La_{0.5}Sr_{0.5}CoO_{2.5}$ while (b) film on (La, Sr)(Al,Ta)O_3 has overall composition of $La_{0.5}Sr_{0.5}CoO_{2.75}$ with a significant degree of disorder (from [2]).

tuning of the vacancy concentrations and their gradients.

Control of Polar State via Octahedral Tilts and Interface Charge: Many novel oxide device concepts, e.g. magnetoelectric [3], orbitronic [4], and others call for electric field control of structural and spin degrees of freedom. The electric field is directly coupled to polarization, i.e. zone center mode instability. At the same time, most physical behaviors tied to spin and structural distortions are linked to zone boundary modes, the coupling between the two being weak. The emerging strategy to implementation of these couplings is through the multilayers, where a ferroelectric with secondary antiferrodistortive (e.g. octahedral tilts) order parameter is coupled with second component close to tilt-controlled metal insulator transition[5],[15,16]. Realization of such control necessitates understanding the coupling between octahedral tilts (controllable through the substrate) and interface charge (that stabilizes polar state).

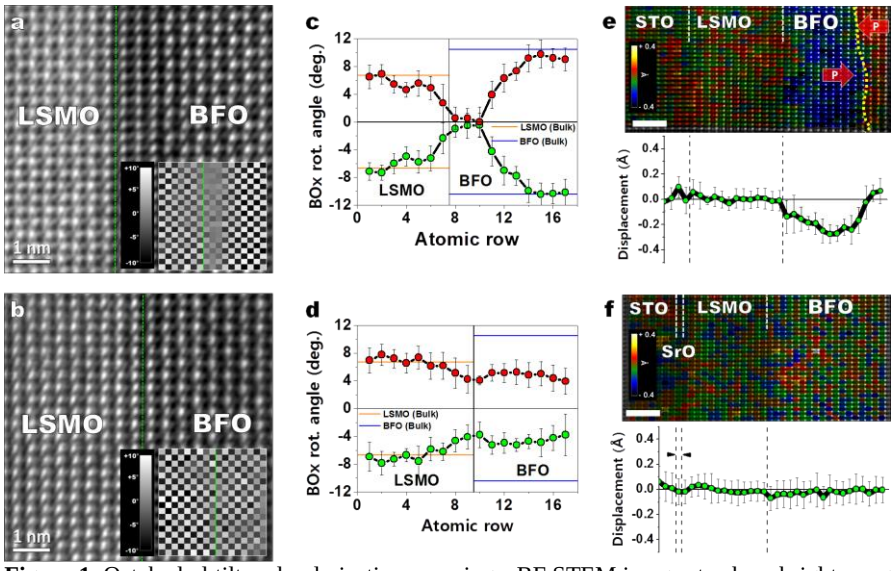

Figure 1. Octahedral tilt and polarization mappings: BF STEM images to show bright oxygen contrast in the respective BFO film structures grown on (a) MnO_2-terminated LSMO and (b) (La,Sr)O-terminated LSMO, taken at the $[110]_{pc}$ orientation. The derived octahedral tilt maps (inset) show checkerboard patterns. (c and d) Line profiles of octahedral tilts averaged over vertical rows of the respective tilt maps in **a** and **b**. The solid line in each graph represents the tilt of the respective bulk BFO and LSMO. (e and f) Out-of-plane (*dz*) displacement maps and the corresponding averaged line profiles of B-site cations in both BFO thin film heterostructures, showing the polarization behavior (data given on the same scale for both films). The maps are overlaid on the respective ADF STEM images. Scale bars are 2 nm.

To illustrate feasibility of this concept, we have studied BFO films grown in $(La,Sr)MnO_3$ with different surface terminations. Figure 2 shows the results of polarization and tilt mapping at these two interfaces. For MnO_2-terminated LSMO, the tilts are fully suppressed at the interface and then quickly recover to bulk values. For (La,Sr)O-terminated LSMO, tilt suppression at the interface is incomplete, and saturation tilts for near-interface region differ from bulk (Fig. 2(a)-(d)). Cation displacement measurements (Fig 2(e),(f)) show that this new interface phase is non-polar, which is confirmed by the detection of small in-plane antiphase displacements and PFM measurements. With the aid of first-principles theory, we interpret this behavior as patterning of the octahedral tilt system and polar order via different layer sequence at the interface. Using similar approach, we further demonstrate that structure of charged domain walls and their pinning at interfaces can be explored, revealing dominant role of screening by oxygen vacancies.

Dynamic Studies of Bias-Induced Processed in a-TiO_2 based memristor heterostructures: As a prototypical system to explore hysteretic and irreversible vacancy dynamics, we have explored bias-induced electrochemical processes in TiO_2, a key material for resistive switching memories (ReRAM), and memristors. These structures can assume one of the two resistance states –high resistance state (HRS) or low resistance state (LRS), which can be switched by application of electrical bias. Several mechanisms have been proposed for switching from HRS to LRS, such as filamentary switching and interfacial effect mechanisms.[6] Most of proposed mechanisms imply local inhomogeneity, yet were formulated based on the electrical response of the device as a whole. In fact, there are very few microscopic studies among the published literature, especially for oxide systems other than TiO_2 (such as Hf/Ta based oxides). We intend to understand the exact electroforming process and resistance switching phenomena in oxide films by (Scanning) Transmission Electron Microscopy ((S)TEM) and electron energy loss spectroscopy (EELS), combined with (a) in situ bias application or (b) ex situ atomic force microscopy (AFM).
Here, an amorphous TiO_2 (a-TiO_2) thin films on Pt were prepared by atomic layer deposition and investigated by TEM before and after applying bias sweep with AFM tip. In addition to ex-situ experiments, in-situ current-voltage measurements were performed. The as-deposited TiO_2 films are amorphous. After applying voltage, a-TiO_2 film was crystallized in the area where bias was applied, as detected by appearance of characteristic rutile reflections in image diffractograms; the degree of crystallinity was enhanced with increasing voltage (Fig. 3(a)).

As the voltage increased, longer-period reflections indicative of TiO_2 reduction were detected. Observations from in-situ and ex situ studies suggest that both crystallization and reduction start at the bottom electrode and then propagate throughthe film (see schematic in Fig.3(b)). At the early stages of reduction, it manifests as stacking faults in stoichiometric TiO_2 (Fig. 3(c)). Similar phenomena are also observed in the Al/amorphous layer/epi-NiO structures, with direct relevance to the switching of the memory state from HRS to LRS.[7] Direct in-situ observations of the crystallization and formation of conductive pathways in ReRAM structures can reveal key information for fundamental understanding and optimization of this technology.

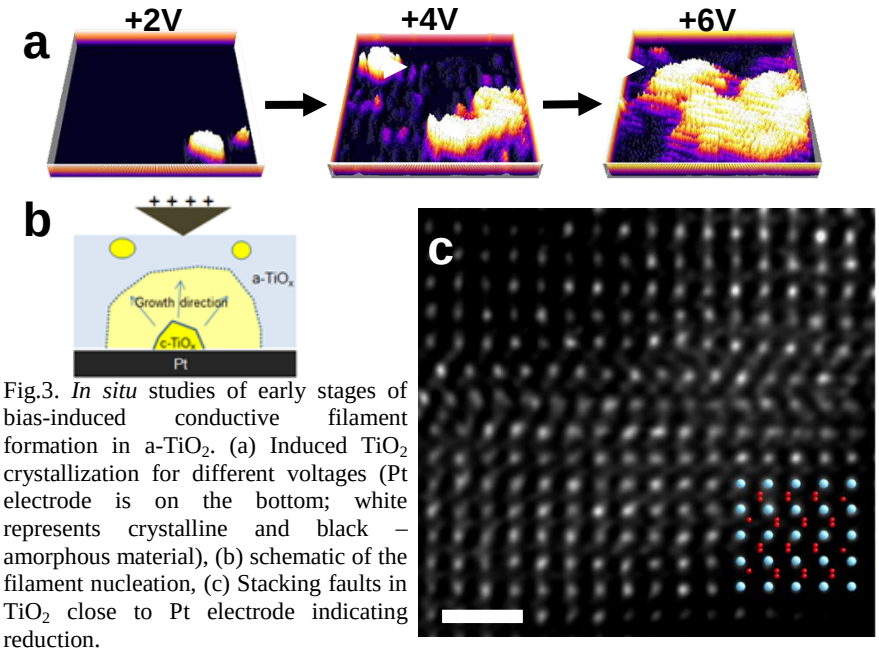

Fig.3. *In situ* studies of early stages of bias-induced conductive filament formation in a-TiO_2. (a) Induced TiO_2 crystallization for different voltages (Pt electrode is on the bottom; white represents crystalline and black – amorphous material), (b) schematic of the filament nucleation, (c) Stacking faults in TiO_2 close to Pt electrode indicating reduction.

Future plans: To date, we have created the robust imaging and data analysis tools for mapping polarization and structural order parameter in oxides, and demonstrated method for sub-unit cell mapping of vacancy concentrations. We further developed the home-built in-situ STM-STEM system, and demonstrated in-situ studies of polarization switching and bias-induced electrochemical crystallization in oxides. In the next period, we aim to integrate these areas to explore (a) electronic and vacancy mediated phenomena at static and moving ferroelectric domain walls and wal-interface junctions, (b) atomic level electrochemical behaviors at the metal-mixed electronic/ionic conductor interfaces, and (c) static electrochemical properties and bias controlled polarization at oxide-oxide interfaces. These studies will reveal the interplay between polarization and structural order parameters, strain, and vacancy-controlled electrochemistry in oxides, and will enable optimization of a broad range of energy and information technologies from fuel cells to memristive data storage and logic devices.

This work is sponsored by the Materials Science and Engineering Division, Office of Basic Energy Sciences of the U S DOE. The work is done in collaboration with S.V. Kalinin and A. Kumar (ORNL), P.Yu, Y.-H. Chu, R. Ramesh (UC Berkeley), M. Biegalski, H. Christen, V. Lauter and H. Ambaye (ORNL), A. Morozovska and E.Eliseev (Ukrainian Academy of Sciences), J. Rondinelli (Drexel U.), A. Hatt (LBNL) Authors also acknowledge instrument access (FEI Titan, Hitachi NB-5000 FIB, Nion UltraSTEM 100) via ORNL's ShaRE user facility, which is sponsored by the Scientific User Facilities Division, Office of Basic Energy Sciences, U.S. DOE.

DOE-sponsored publications 2010-2012 [in total 17 journal papers supported or partially supported by the project were published – 2 Phys Rev. Lett, 2 Adv. Mater, 3 Nanolett., 3 ACS Nano (plus 1 Nature Materials and 1 Phys. Rev. Lett. accepted for publication), 1 patent disclosure]

1. A.Y. Borisevich, A.N. Morozovska, Y.-M. Kim, D. Leonard, M.P. Oxley, M. Biegalsky, E. A. Eliseev, and S.V. Kalinin, Exploring mesoscopic physics of vacancy-ordered systems through atomic scale observations of topological defects, *Phys. Rev. Lett*., accepted (2012).
2. Y.-M. Kim, J. He, Michael D. Biegalski, H. Ambaye, V. Lauter, H. M. Christen, S. T. Pantelides, S. J. Pennycook, S. V. Kalinin, and A. Y. Borisevich, Probing Oxygen Vacancy Concentration and Homogeneity in Solid Oxide Fuel Cell Cathode Materials on the (sub) Unit Cell Level, *Nature Materials*, accepted (2012).
3. P. Maksymovych, M. Huijben, M. H. Pan, S. Jesse, N. Balke, Y. H. Chu, H. J. Chang, A. Y. Borisevich, A. P. Baddorf, G. Rijnders, D. H. A. Blank, R. Ramesh, and S. V. Kalinin, Physical Review **B 85**, 014119 (2012).
4. A.N. Morozovska, E.A. Eliseev, and S.V. Kalinin, *Electrochemical Strain Microscopy with Blocking Electrodes: The Role of Electromigration and Diffusion*, J. Appl. Phys. **111**, 014114 (2012).

5. (**journal cover**) H.J. Chang, S. V. Kalinin, S. Y. Yang, S. Bhattacharya, P. P. Wu, N. Balke, S. Jesse, L. Q. Chen, R. Ramesh, S. J. Pennycook, and Albina Y. Borisevich, *Watching Domains Grow: In-situ studies of polarization switching by combined Scanning Probe and Scanning Transmission Electron Microscopy*, J. Appl. Phys. **110**, 052014 (2011).
6. H.J. Chang, S.V. Kalinin, A.N. Morozovska, M. Huijben, Y.H. Chu, P. Yu, R. Ramesh, E.A. Eliseev, G.S. Svechnikov, S.J. Pennycook and A. Borisevich, *Atomically-resolved mapping of polarization and electric fields across ferroelectric-oxide interfaces by Z-contrast imaging*, Adv. Mater. **23,** 2474 (2011)
7. A. Tselev, J. D. Budai, E. Strelcov, J. Z. Tischler, A. Kolmakov, S. V. Kalinin, "Electromechanical actuation and current-induced metastable states in suspended single-crystalline VO2 nanoplatelets," *Nano Letters* **11**(8), 3065-3073 (2011).
8. A. N. Morozovska, E. A. Eliseev, G. S. Svechnikov, and S. V. Kalinin, "Nanoscale electromechanics of paraelectric materials with mobile charges: Size effects and nonlinearity of electromechanical response of $SrTiO_3$ films", Phys. Rev. B **84**, 045402 (2011).
9. A. N. Morozovska, E. A. Eliseev, A. K. Tagantsev, S. L. Bravina, Long-Qing Chen, and S. V. Kalinin, "Thermodynamics of electromechanically coupled mixed ionic-electronic conductors: Deformation potential, Vegard strains, and flexoelectric effect", Phys. Rev. B **83**, 195313 (2011).
10. A. Tselev, I. A. Luk'yanchuk, I. N. Ivanov, J. D. Budai, J. Z. Tischler, E. Strelcov, A. Kolmakov, S. V. Kalinin, "Symmetry Relationship and Strain-Induced Transitions between Insulating M1 and M2 and Metallic R Phases of Vanadium Dioxide," *Nano Letters* **10**(11), 4409-4416 (2010).
11. A. Tselev, V. Meunier, E. Strelcov, W. A. Shelton, I. A. Luk'yanchuk, K. Jones, R. Proksch, A. Kolmakov, and S. V. Kalinin, "Mesoscopic MetalInsulator Transition at Ferroelastic Domain Walls in VO_2," *ACS Nano* **4**(8), 4412 (2010).
12. A. Tselev, E. Strelcov, I. A. Luk'yanchuk, I. N. Ivanov, J. D. Budai, J. Z. Tischler, K. M. Jones, R. Proksch, S. V. Kalinin, A. Kolmakov, "Interplay between Ferroelastic and Metal-Insulator Phase Transitions in Strained Quasi-Two-Dimensional VO2 Nanoplatelets," Nano Letters 10(6), 2003-2011 (2010)
13. E. J. Crumlin, E. Mutoro, S.-J. Ahn, G. J. la O', D. N. Leonard, A. Borisevich, M. D. Biegalski, H. M. Christen, Y. Shao-Horn, *Oxygen Reduction Kinetics Enhancement on a Hetero-Structured Oxide Surface for Solid Oxide Fuel Cells*, J. Phys. Chem. Lett., **1**, 3149 (2010).
14. Jun He, Albina Borisevich, Sergei V. Kalinin, Stephen J. Pennycook, Sokrates T. Pantelides, *Control of the structural and magnetic properties of perovskite oxide ultrathin films through the substrate symmetry effect*, Phys. Rev. Lett. **105**, 227203 (2010).
15. A.Y. Borisevich, O. Ovchinnikov, H.J. Chang, M. Oxley, P. Yu, J. Seidel, E.A. Eliseev, A.N. Morozovska, R. Ramesh, S.J. Pennycook, S.V. Kalinin, *Mapping octahedral tilts and polarization across a domain wall in $BiFeO_3$ from Z-contrast STEM image atomic column shape analysis*, ACS Nano **4**, 6071 (2010).
16. A.Y. Borisevich, H. J. Chang, M. Huijben, M. P. Oxley, S. Okamoto, M. K. Niranjan, J. D. Burton, E. Y. Tsymbal, Y. H. Chu, P. Yu, R. Ramesh, S. V. Kalinin, and S. J. Pennycook**,** *Suppression of Octahedral Tilts and Associated Changes in Electronic Properties at Epitaxial Oxide Heterostructure Interfaces*, Phys. Rev. Lett. **105**, 087204 (2010)
17. A.N. Morozovska, E. A. Eliseev, S. V. Svechnikov, A. D. Krutov, V. Y. Shur, A. Y. Borisevich, P. Maksymovych, and S. V. Kalinin, *Finite size and intrinsic field effect on the polar-active properties of ferroelectric-semiconductor heterostructures*, Phys. Rev. **B 81,** 205308 (2010)
18. J. Shin, A.Y. Borisevich, J. Zhou, V. Meunier, E.W. Plummer, S.V. Kalinin, and A.P. Baddorf, *An oxygen-induced surface reconstruction of* $SrRuO_3$ *and its effect on the* $BaTiO_3$ *interface*, ACS Nano **4**, 4190 (2010).
19. S. V. Kalinin, B. J. Rodriguez, A. Y. Borisevich, A. P. Baddorf, N. Balke, H. J. Chang, L. Q. Chen, S. Choudhury, S. Jesse, P. Maksymovych, M. P. Nikiforov and S. J. Pennycook, "Defect-Mediated Polarization Switching in Ferroelectrics and Related Materials: From Mesoscopic Mechanisms to Atomistic Control," *Adv. Mater.* **22**, 314 (2010).

References:

1. Jia, C. L.; Lentzen, M.; Urban, K. *Science* 2003, 299, (5608), 870-873.
2. Muller, D. A.; Nakagawa, N.; Ohtomo, A.; Grazul, J. L.; Hwang, H. Y. *Nature* 2004, 430, (7000), 657-661.
3. Spaldin, N. A.; Fiebig, M. *Science* 2005, 309, (5733), 391-392.
4. Tokura, Y.; Nagaosa, N. *Science* 2000, 288, (5465), 462-468.
5. Rondinelli, J. M.; Spaldin, N. A. *Physical Review B* 2010, 82, (11), 113402.
6. Waser, R. and Aono, M. *Nature Mat.* 2007, 6 (11), 833-40.
7. Jang, J.H.; ; Jung, H.-S.; Kim, J.H.; Lee, S.Y.; Hwang, C.S.; Kim, M. *J. Appl. Phys.* 2011, 109, 023718.

Complex Fundamental Mechanisms of Transient States in Materials Quantified by DTEM

Geoffrey H. Campbell, PI
Thomas LaGrange, Bryan W. Reed, Melissa K. Santala, and Joseph T. McKeown, Co-I
Lawrence Livermore National Laboratory, Condensed Matter and Materials Division
PO Box 808, Mailstop L-356, Livermore, CA 94550
E-mail: ghcampbell@llnl.gov

Project Scope

The thrust of this project is to reveal the fundamental parameters of strongly driven phase transformations with the novel capabilities offered by the LLNL DTEM instrument. We strive to map the kinetics of phase transformations (both diffusive and martensitic) by developing time-temperature-transformation (TTT) diagrams with nanosecond time resolution. The imaging capabilities of the instrument allow us to quantitatively measure nucleation and growth rates directly, and these measurements are used in analytical models of the transformation kinetics. Moreover, the observations allow us to identify changes in the mechanism of transformation as the driving force is changed in order to assess the applicability of models to the various driving force regimes of the transformation.

Recent Results

Phase Change Materials

Phase change materials (PCMs) used in optical recording media and non-volatile random access memory applications rely on rapid switching between amorphous and crystalline phases, which have distinct optical and electrical properties. In these applications it must be possible to switch between the phases in nanoseconds during the write and erase processes, but the amorphous materials must be stable against crystallization for years, thus the relevant timescales for crystallization span sixteen orders of magnitude. There exist well-developed models for crystallization kinetics, but use of them to predict materials behaviors over all relevant temperatures and timescales requires more detailed knowledge of many materials parameters, such as atomic mobilities and interfacial energies, than is often available. It is experimentally challenging to determine the parameters affecting crystallization under conditions where it is fastest. As a result, experimentation on crystallization kinetics is often performed at lower temperatures, where microstructural changes and temperature may be more easily monitored. Unfortunately, it is difficult to predict behavior under the highly driven conditions arising during laser- or current-crystallization from experiments performed under different conditions. This has motivated experiments using DTEM to collect microstructural data under highly driven conditions. The results on GeTe reveal the course of microstructural evolution at the temperature and heating rates relevant to laser and electrical switching where crystallization rates are the highest.

Stoichiometric GeTe may be switched rapidly and has a high crystallization temperature, T_x, relative to other technologically practical PCMs. Time resolved studies measuring crystal growth rates during crystallization of amorphous GeTe and other PCMs have been performed at temperatures near T_x (~450 K for GeTe) with optical microscopy and electron microscopy but the growth rates are orders of magnitude lower than what occurs during laser crystallization. Time resolved measurement of optical and electrical properties may be made on the nanosecond scale, but these methods yield data on the overall fraction and do not provide the microstructural information needed to extract nucleation and crystal growth rates independently.

Figure 1 shows four of nine frames of a movie captured during crystal growth in amorphous GeTe induced by a 12-ns pump laser pulse. Growing crystalline grains appear as roughly circular light gray areas in the otherwise featureless amorphous material; many grains also have dark bend contour bands. For images in **Figure** 1, the electron beam and specimen laser were aligned such that the imaging occurs at the center of the

laser spot, where the specimen receives the greatest laser irradiation. Nucleation events are fairly sparse where the temperature is highest (approaching T_m) and the crystalline grains grow inward toward the center. Growth rates were measured for several crystallization events. Having multiple images from each crystallization event allows for changes in crystal growth rate with time to be measured. Growth rates were 3 m/s during the first microsecond of growth and dropped off to 2 m/s after 2 μs.

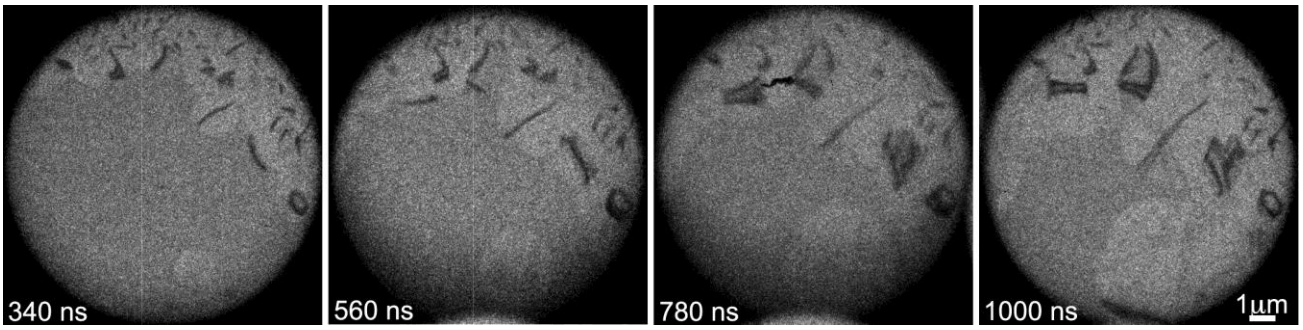

Figure 1 Bright-field 15-ns pulsed TEM images of laser-induced crystallization of amorphous GeTe. The time indicates the delay between the laser pulse that initiated crystallization and the electron imaging pulse.

Crystallization further out in the laser spot progresses differently. **Figure 2**a shows an image taken off the center of the laser spot with a 1400 ns delay. The top half appears to have a fine, dense crystalline microstructure and the bottom half appears featureless and amorphous. The entire area is crystalline minutes after (**Figure 2**b) and the area crystallized after the 1400 ns delay has a very fine (sub-micron) grain size in its wake, indicative of a high nucleation rate relative to the growth rate. The discrete crystallization front sweeping outward hundreds of microseconds after heating laser has ceased, suggests the enthalpy of devitrification released during crystallization enhances the nucleation rate locally by increasing the temperature.

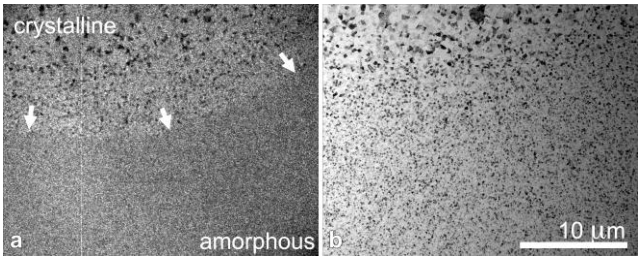

Figure 2 Bright-field 15-ns pulsed TEM image (a) taken 1400 ns after initiation of a 4.2-μJ pump laser pulse and (b) a conventional TEM image of the same area taken minutes later. The arrows in (a) indicate the edge of the crystallization front.

Alloy Solidification

The melting and solidification of metals and alloys is a ubiquitous manufacturing process used to fabricate components for an enormous number of applications. Strong technological interest in alloy solidification currently exists, particularly in additive manufacturing techniques such as direct metal laser sintering used to produce metal and alloy components by rapid prototyping. The properties and performance of these components is dictated by the phases and final microstructure of the material, which is determined in turn by the thermal and compositional conditions as well as thermodynamic and kinetic constraints of the system that exist during solidification. Solidification proceeds by heat extraction from a liquid and motion of a solid-liquid interface. This extraction of heat generally controls the rate of solidification, but the resultant microstructure will be dependent on numerous factors, including solidification rate, temperature gradients, composition, crystallography, phase formation, and kinetics. Initial alloy solidification experiments in the DTEM reveal the evolution of the solid/liquid interface and morphological regions that develop during

solidification in an Al-Cu thin film. Measurements of the velocity of the solid/liquid interface provide insight into the relation between the observed morphologies and the driving forces and kinetics of solidification.

Figure 3a shows an example DTEM experiment that follows the solidification of an initially nanocrystalline Al-7at%Cu thin film alloy. A laser pulse fluence of ~300 mJ/cm^2 was used to melt the alloy film. The solid/liquid interface appears morphologically smooth at the observed scale, and solidification is complete by ~30 μs after melting. The images also reveal an abrupt transition in solidification morphology from columnar grains to a banded morphology at a time between 20 and 25 μs. Figure 3b shows a conventional bright-field TEM montage image of an entire re-solidified region of the film. Four distinct morphological zones can be identified: 1) a small-grained region at the perimeter of the laser-irradiated area that exhibits a hypoeutectic microstructure, 2) an occlusion zone, in which a subset of grains expands at the expense of neighboring grains, 3) a region of columnar growth, and 4) large grains with a banded morphology.

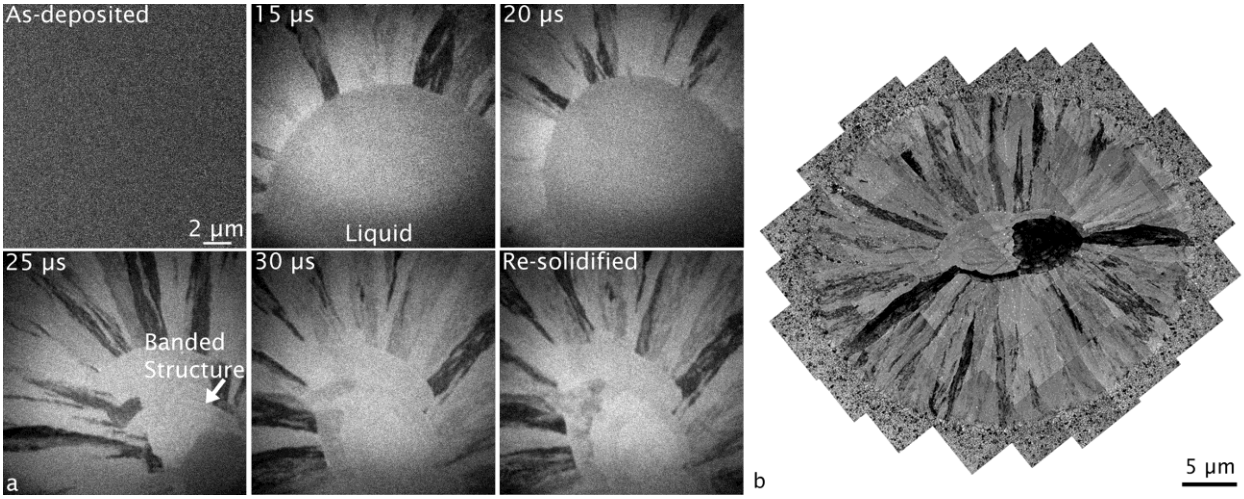

Figure 3 a) Bright-field 15-ns pulsed TEM images taken before and with different time delays after laser melting. b) Conventional bright-field TEM montage image of an entire laser-melted and re-soldified region.

The velocity of the solid/liquid interface was measured as a function of time from the *in-situ* DTEM images of the solidification front. The velocity was taken to be the change in semi-major or semi-minor axis of the elliptical melt pool divided by the delay time, and thus bounds to the velocity as a function of position along the interface were measured. The velocity of the solid/liquid interface increases as the solidification process progresses, accelerating from ~0.5 m/s in the early stages of columnar growth to ~1.5 m/s when banding is observed. Banding occurs when the velocity exceeds a threshold value for interface stability, leading to an oscillatory instability at the solid/liquid interface. The acceleration of the interface can be related to an increasing driving force for solidification (undercooling in the liquid) as a result of solute rejection, local interface curvature, and a kinetic undercooling.

Future Work

In the near future we will be concentrating on using our newly commissioned capability to acquire multiple images of a single event as it unfolds in time to make our quantitative measurements extremely precise. For example, in GeTe phase change materials the lack of a precise time for a nucleation event that leads to a growing grain creates uncertainty in the measurement of nucleation and growth rates. Typically, the single shot images can give bounds to these quantities, which are helpful in bounding the models. With multiple images of a growing phase boundary (whether in phase change materials, alloy solidification, etc.), we can plot its progression as function of time and extract the growth rate from the slope of the curve and the time of the nucleation event from the intercept with the time axis. We anticipate that these types of

observations as a function of driving force for the transformation will provide unique new understanding of the transformation mechanisms operating and the regimes for which they are valid.

This work performed under the auspices of the Division of Materials Sciences and Engineering, Office of Basic Energy Sciences, U.S. Department of Energy by Lawrence Livermore National Laboratory under Contract DE-AC52-07NA27344.

2010 – 2012 Publications

[1] D.J. Masiel, B.W. Reed, T. LaGrange, G.H. Campbell, T. Guo, and N.D. Browning, "Time-Resolved Annular Dark Field Imaging of Catalyst Nanoparticles," *Chem. Phys. Chem.* **11** [10] 2088 – 2090 (2010).

[2] G.H. Campbell, T. LaGrange, J.S. Kim, B.W. Reed, N.D. Browning, "Quantifying Transient States in Materials using the Dynamic Transmission Electron Microscope," *J. Electron Microsc. – Oxford*, **59** [S1] S67-S74 (2010).

[3] N.D. Browning, G.H. Campbell, J.E. Evans, T.B. LaGrange, B.W. Reed, "Electron Microscopy and Spectroscopy on the Ultrafast Timescale," *Chem. Phys. Chem.*, **11** [4] 781 – 782 (2010).

[4] B. W. Reed, T. LaGrange, R. M. Shuttlesworth, D. J. Gibson, G. H. Campbell, and N. D. Browning, "Solving the Accelerator-Condenser Coupling Problem in a Nanosecond Dynamic Transmission Electron Microscope," *Review of Scientific Instruments* **81**, 053706 (2010).

[5] J.S. Kim, T. LaGrange, B.W. Reed, R. Knepper, T.P. Weihs, N.D. Browning, G.H. Campbell, "Direct characterization of moving reaction zones in Al/Ni nanolaminates using DTEM," *Acta Materialia* **59** [9] 3571 – 3580 (2011).

[6] L. Nikolova, T. LaGrange, B.W. Reed, M.J. Stern, N.D. Browning, G.H. Campbell, J.-C. Kieffer, B.J. Siwick, and F. Rosei, "Nanocrystallization of amorphous germanium films observed with nanosecond temporal resolution," *Applied Physics Letters* **97**, 203102 (2010).

[7] N.D. Browning, G.H. Campbell, J.A. Hawreliak, M.A. Kirk, "*In situ* characterization of metals at extremes," *MRS Bulletin* **35** [12] 1009 – 1016 (December 2010).

[8] A. Kulovits, J.M.K. Wiezorek, T. LaGrange, B.W. Reed, and G.H. Campbell, 'Revealing the transient states of rapid solidification in aluminum thin films using ultrafast in situ transmission electron microscopy', *Philosophical Magazine Letters* **71** [4] 287 – 296 (2011).

[9] N.D. Browning, M.A. Bonds, G.H. Campbell, J.E. Evans, T. LaGrange, K.L. Jungjohann, D.J. Masiel, J. McKeown, S. Mehraen, B.W. Reed, M. Santala, "Recent Developments in Dynamic Transmission Electron Microscopy," *Current Opinion in Solid State and Materials Science*, **16** [1] 23 – 30 (2012).

[10] T. LaGrange, B.W. Reed, M.K. Santala, J.T. McKeown, A. Kulovits, J.M.K. Wiezorek, L. Nikolova, F. Rosei, B.J. Siwick, and G.H. Campbell, "Approaches for ultrafast imaging of transient material processes in the transmission electron microscope," *Micron*, in press.

[11] M.K. Santala, B.W. Reed, T. Topuria, S. Raoux, S. Meister, Y. Cui, T. LaGrange, G.H. Campbell, and N.D. Browning, "Nanosecond *in situ* TEM studies of the reversible $Ge_2Sb_2Te_5$ cubic ⇔ amorphous phase transformation," *Journal of Applied Physics*, **111** [2] 024309-1 – 024309-6 (2012).

[12] J.T. McKeown, N.A. Roberts, J.D. Fowlkes, Y. Wu, T.B. LaGrange, B.W. Reed, G.H. Campbell, and P.D. Rack. "Real-time observation of nanosecond liquid-phase assembly of nickel nanoparticles via pulsed-laser heating," *ACS Nano*, in press.

[13] T. LaGrange, B.W. Reed, W.E. King, J.S. Kim, and G.H. Campbell, "Dynamic Transmission Electron Microscopy," Chapter 3 in In-situ Electron Microscopy, eds. G. Dehm, J.M. Howe, and J. Zweck, Wiley-VCH Verlag, Weinheim (2012).

[14] N.D. Browning, G.H. Campbell, J.E. Evans, T. LaGrange, K.L. Jungjohann, J.S. Kim, D.J. Masiel, B.W. Reed, "Dynamic Transmission Electron Microscopy," Chapter 9 in Handbook of Nanoscopy, eds. G. van Tendeloo, D. van Dyck, and S.J. Pennycook, Wiley-VCH Verlag, Weinheim (2012).

Spectroscopic Imaging STM for Complex Electronic Matter

J. C. Séamus Davis
LASSP, Physics Department, Cornell University, Ithaca, NY 14853, USA.
CMP&MS Department, Brookhaven National Laboratory, Upton, NY 11973, USA
Office: 607-254-8965 / Mobile: 607-220-8685 / Email: jcdavis@ccmr.cornell.edu

Research Objectives

Among our long-term objectives are to understand the electronic phase diagrams and the microscopic interactions leading to the strong Cooper pairing and higher critical temperature superconductivity. Additionally, electronic liquid-crystalline states are a new area of study in condensed matter physics; our long-term goals here are to pursue the preliminary evidence that they play a fundamental role in high temperature superconductivity. The broad scientific areas of focus are: (i) DoE Grand Challenge "How do remarkable properties of matter emerge from complex correlations of atomic or electronic constituents and how can we control these properties?" and, (ii) several PRD's from BASIC RESEARCH NEEDS FOR SUPERCONDUCTIVITY (http://www.er.doe.gov/bes/reports/files/SC_rpt).

Research Progress Significant research progress has been achieved in recent years:

Spectroscopic Signature of Phase-Incoherent Superconductivity in the CuO_2 Pseudogap Phase

One possible explanation for the existence of the cuprate pseudogap state is that it is a *d*-wave superconductor without quantum phase rigidity. Transport and thermodynamic studies provide evidence that supports this proposal, but few spectroscopic explorations of it have been made. A spectroscopic signature of d-wave superconductivity is the particle-hole symmetric "octet" of dispersive Bogoliubov quasiparticle interference modulations (QPI). We measured this octet's evolution from low temperatures to well into the pseudogap regime. No pronounced changes occur in the octet phenomenology at T_c, and it survives up to at least temperature $T \sim 1.5\ T_c$. Thus the pseudogap exhibits the phenomenology predicted for QPI in a phase-incoherent d-wave superconductor; ***Science 325***, 1099 (2009)

Real-space and Momentum-space Imaging of a Heavy Fermion Superconductor

Within a Kondo lattice, the strong hybridization between electrons localized in ***r***-space and those delocalized such that they are defined in ***k***-space, generates exotic electronic states called 'heavy fermions'. We used SI-STM to image the evolution of the heavy fermion superconductor URu_2Si_2 electronic structure simultaneously in **r**-space and ***k***-space. At low temperatures in this material we introduced heavy f-electron quasiparticle interference imaging, revealing the rapid splitting of a light ***k***-space band into two new heavy fermion bands. This is the first visualization of heavy fermion formation and paves the way to explore the possible spin fluctuation exchange mechanism of Cooper pairing in HF superconductivity; ***Nature 465***, 570 (2010).

Atomic Scale Impact of Kondo Hole in a Heavy Fermion Superconductor

When, in a heavy fermion compound, a spinless atom replaces a magnetic atom, it generates a quantum state referred to as a 'Kondo-hole'. This is dual to the 'Kondo resonance' at a single magnetic atom in a metal. We recently achieved the first visualization of the electronic structure of a Kondo-hole at a spinless Thorium atom substituted for magnetic Uranium atom in URu_2Si_2. Surrounding each Thorium atom we find the heavy-fermion hybridization modulations predicted to occur at Kondo-holes. By introducing the 'hybridization gapmap' technique to heavy fermion studies, we observed nanoscale hybridization heterogeneity due to a combination of the randomness of Kondo-hole doping and the long-range hybridization oscillations; ***PNAS 108,*** 18233 (2011).

Future Plans

A powerful way to examine the electronic structure of exotic superconductors is using Bogoliubov QPI from which the band structure, Fermi surface, and the anisotropic superconducting energy gap $\Delta(\mathbf{k})$ can be measured. QPI is a uniquely powerful technique because it can determine both ***r***-space and ***k***-space electronic structure, it has demonstrated energy resolution up to 50 times better than standard ARPES while retaining the equivalent ***k***-space resolution, it can measure electronic structure above and below E_f and it works in high magnetic fields where ARPES does not. We plan the following BQPI studies:

A ***F-electron Heavy Fermion Superconductivity***

Our planned studies of heavy fermion superconductivity include:

(1) Magnetic Field SI-STM studies of Heavy Fermion Superconductivity

At the most elementary level we propose to explore if and how the Zeeman energy can overwhelm the hybridization interactions and undo the heavy fermion formation. More specific to superconductivity (and at a lower field scale) we propose to study the vortex core structure in heavy fermion superconductors to explore order parameter symmetry issues.

(2) Kondo Hole Effects on Heavy Fermion Superconductivity

Individual impurity atoms can be used to probe the microscopic electronic structure of an unconventional superconductor. Specifically the detailed spatial/energetic structure of the bound states that occur at each impurity atom can be highly revealing of the microscopic order parameter symmetry. In the case of HFSC, the situation is more complex because the impurity atom may undo the hybridization and destroy the heavy fermions instead of breaking the Cooper pairs directly. We propose an extensive study of impact of specific impurity atoms substituted on the magnetic site in heavy fermion compounds to examine all these issues.

B ***Copper-based Superconductivity***

Within the cuprate pseudogap phase it has been unclear which electronic symmetries (if any) are broken, what the identity of any associated order parameter might be, and which microscopic electronic degrees of freedom are active. With DoE EFRC support, we recently reported breaking of rotational symmetry by the electronic structure within each CuO_2 unit cell. Moreover, we show that these phenomena arise from electronic differences at the two oxygen sites within each unit cell; **Nature 466**, 347 (2010). Thus, both nematic and smectic broken symmetry states have been reported in underdoped cuprates. The challenge was then to understand the interactions between these states and how they determine the cuprate phase diagram. With DoE EFRC support, we also carried out an SI-STM study of the coexisting smectic and nematic broken symmetries in underdoped $Bi_2Sr_2CaCu_2O_{8+d}$. By visualizing their spatial components separately, we identified 2π topological defects throughout the smectic states. Imaging the locations of such topological defects simultaneously with nematicity revealed the coupling between the two broken symmetry states. A Ginzburg-Landau description of quantum nematic/smectic coupling was identified; **Science 333**, 426 (2011). Building upon these we now plan the following studies:

(1) Ultra-high Magnetic Field SI-STM in Cuprates

Underdoped cuprates seem to have no closed Fermi surface, but only disconnected 'Fermi arcs'. Whereas, quantum oscillations in the electrical resistance of $YBa_2Cu_3O_{6.5}$ established the existence of what appears to be a well-defined small Fermi surface pockets in the high-field state of underdoped cuprates. It is unknown whether these pockets are electron-like, hole-like, how many there are, and where they are in ***k***-space. And the standard approach of using ARPES to explore the ***k***-space is

impossible because this technique does not work in magnetic fields. However we can determine ***k***-space electronic structure in ultra high magnetic fields using quasiparticle inference imaging. We propose to pursue such QPI studies to the highest magnetic fields presently possible and have therefore constructed the world's first 20 Tesla SI-STM to explore ***k***-space changes in underdoped cuprates due to very high fields.

(2) Nanoscale C_2 Domain Percolative Transition to Superconductivity

Hole doping the cuprate Mott insulator first destroys the Mott state yielding a weak insulator where electrons localize only at low temperatures. Then the pseudogap state, with intra-unit-cell breaking of 90º-rotational (C_{4v}) symmetry appears. SI-STM studies of $Ca_{2-x}Na_xCuO_2Cl_2$ show that at lowest dopings, nanoscale regions exhibiting pseudogap spectra and 180º-rotational (C_{2v}) symmetry form unidirectional clusters within a weakly insulating and the C_{4v}-symmetric matrix that has its own spectral shape. It seems (very surprisingly) that cuprate doping proceeds by the appearance of meso-scale clusters of localized holes within which the broken-symmetry pseudogap state is stabilized and when the C_{2v}-symmetric clusters touch each other the long-range high-T_c superconductivity appears; ***Nature Physics 8****, 534* (2012). We propose to explore this same set of phenomena in BiSrCaCuO to determine the universality of this percolative transition to superconductivity picture.

(3) Bragg Peak Fourier Transform SI-STM

By studying the Bragg peaks in Fourier transforms of electronic structure images, and particularly by resolving both the real and imaginary components of the Bragg amplitudes, distinct types of intra-unit cell symmetry breaking can be studied. Bragg-peak Fourier analysis of an electronic structure image g(***r***,V) focuses upon g(***q***,V)=Reg(***q***,V)+iImg(***q***,V). Several measures of intra-unit-cell breaking of crystal symmetry by the electronic structure become possible from the study of the real and imaginary components of the Bragg amplitudes. For example, if the crystal unit-cell is tetragonal with 90º-rotational (C_{4v}) symmetry, one can search for intra-unit-cell "nematicity" by considering Reg(***q***,V); similarly, if the unit-cell is centrosymmetric, one can search for intra-unit-cell breaking of inversion symmetry in electronic structure using Img(***q***,V). We propose to continue development of this approach to categorize IUC broken symmetries of underdoped cuprates.

C *Iron-based Superconductivity*

The mechanism of high-temperature superconductivity in the iron-based superconductors is proposed to be magnetic spin fluctuation exchange but how this emerges from the 'parent' antiferromagnetic state is poorly understood. With DoE EFRC support, we used SI-STM to study the electronic structure of $CaFe_{1.94}Co_{0.06}As_2$ in the "parent" state. Static, unidirectional electronic nanostructures of size $\sim 8a_{Fe\text{-}Fe}$, and aligned along the crystal *a*-axis were observed. In contrast, the delocalized electronic states detectable by QPI were found to be dispersive along the *b*-axis only and consistent with a nematic α_2 band; ***Science 327***, 181 (2010). Near optimal doping in iron-pnictide superconductors, distinct anisotropic superconducting energy gaps $\Delta i(\boldsymbol{k})$ were predicted on the different electronic bands *i*. But it was impossible to detect these effects by other techniques. Again using DoE EFRC support, we introduced intra-band Bogoliubov QPI techniques for determination of $\Delta i(\boldsymbol{k})$ in iron-based superconductivity(LiFeAs). We identified the hole-like bands and determine the anisotropy, magnitude and orientation of their $\Delta i(\boldsymbol{k})$; ***Science 336****,* 426 (2012).

(1) Ultra-high Magnetic Field SI-STM in Iron-based Superconductors We propose to study the vortex core structure in iron-based superconductivity to explore order parameter symmetry issues.

(2) Impurity Atoms in Underdoped Ferro-Pnictides

Electronic nematicity (***Science 327***, 181 (2010)) appears to be a driver in the phase diagram of most iron-based superconductors. For example, substituting Co for Fe atoms in $CaFe_2As_2$ to create superconductivity also generates a dense population of unusual unidirectional electronic nanostructures. We propose to study these eight-unit-cell electronic anisotropic impurity states that are distributed randomly but all aligned with the antiferromagnetic $\vec{a}$-axis. We plan studies of scattering from these anisotropic impurity states to reveal an explanation for the $\vec{b}$-axis-oriented QPI effects consistent with the band structure and, perhaps more importantly, for the anisotropic electronic transport in underdoped iron-based superconductors.

Recent Relevant Publications:

1. Spectroscopic Fingerprint of Phase Incoherent d-Wave Superconductivity in the Cuprate Pseudogap State, Jhinhwan Lee, K. Fujita, Chung Koo Kim, A. R. Schmidt, H. Eisaki, S. Uchida, & J.C. Davis, ***Science 325,*** 1099 (2009).
2. Heavy d-Electron Quasiparticle Interference and Real-space Electronic Structure of the Electronic Nematic Material $Sr_3Ru_2O_7$, Jinho Lee, M. Allan, M. Wang, J.E. Farrell, S.A. Grigera, F. Baumberger, J.C. Davis and A.P. Mackenzie. ***Nature Physics 5,*** 800 (2009).
3. Nematic Electronic Structure in the 'Parent' State of Iron-based Superconductor $Ca(Fe_{1-x}Co_x)_2As_2$, T.-M. Chuang, M.P. Allan, Jinho Lee, Yang Xie, Ni Ni, S.L. Bud'ko, G. Boebinger, P.C. Canfield & J.C. Davis, ***Science 327***, 181 (2010).
4. Imaging the Fano Lattice to Hidden Order transition in URu_2Si_2, A.R. Schmidt, M.H. Hamidian, P. Wahl, F. Meier, A.V. Balatsky, T.J. Williams, G.M. Luke and J.C. Davis, ***Nature 465,*** 570 (2010).
5. Intra-unit-cell Electronic Nematicity of the High-Tc Cuprate Pseudogap States, M. J. Lawler, K. Fujita, Jhinhwan Lee, A.R. Schmidt, Y. Kohsaka, Chung Koo Kim, H. Eisaki, S. Uchida, J.C. Davis, J.P. Sethna, and Eun-Ah Kim, ***Nature 466***, 374 (2010).
6. Topological Defects Coupling in Cuprates A. Mesaros, K. Fujita, H. Eisaki, S. Uchida, J.C. Davis, S. Sachdev, J. Zaanen, M.J. Lawler and Eun-Ah Kim, ***Science 333***, 426 (2011)
7. Electronic Structure of the Cuprate Superconducting and Pseudogap Phases from Spectroscopic Imaging STM, A.R. Schmidt, K. Fujita, E.–A. Kim, M. J. Lawler, H. Eisaki, S. Uchida, D-H Lee and J.C. Davis, ***New J. Phys.*** 13, 065014 (2011).
8. Topological Defects Coupling in Cuprates A. Mesaros, K. Fujita, H. Eisaki, S. Uchida, J.C. Davis, S. Sachdev, J. Zaanen, M.J. Lawler and Eun-Ah Kim, ***Science 333***, 426 (2011
9. How Kondo Holes Create Intense Nanoscale Heavy-Fermion Hybridization Disorder, M.H. Hamidian, A.R. Schmidt, I. Firmo, P. Bradley, J.D Garrett, T.J. Williams, G.M. Luke, Y. Dubi, A.V. Balatsky, and J.C. Davis, ***Proc. Nat. Acad. Sci. 108*** 18233 (2011).
10. Spectroscopic Imaging STM Studies of Electronic Structure in the Superconducting and Pseudogap Phases of Cuprate High-T_c Superconductors. K. Fujita, A. R. Schmidt, E.–A. Kim, M. J. Lawler, D.-H. Lee , J. C. Davis, H. Eisaki, S. Uchida. ***J. Phys. Soc. Jpn. 81,*** 011005 (2012).
11. Picometer Registration of Zn Impurity States in $Bi_2Sr_2CaCu_2O_8$ - Phase Determination for Intra-unit-cell Fourier Transform STM. H. Hamidian, I. Firmo, K. Fujita, S. Mukopadhayay, H. Eisaki, S. Uchida, J.W. Orenstein and J.C. Davis ***New J. Phys. 14,*** 53017 (2012).
12. Anisotropic Energy-Gaps of Iron-based Superconductivity from Intra-band Quasiparticle Interference in LiFeAs M. P. Allan, A. W. Rost, A. P. Mackenzie, Yang Xie, J. C. Davis, K. Kihou, H. Eisaki, and T.-M. Chuang ***Science 336,*** 563 (2012).
13. Visualizing the emergence of the pseudogap state and its evolution to superconductivity in a lightly hole-doped Mott insulator; Y. Kohsaka, T. Hanaguri, J.C. Davis, M. Azuma, M. Takano and H. Takagi. ***Nature Physics 8****, 534* (2012).

ATOMISTIC MECHANISMS OF METAL-ASSISTED HYDROGEN STORAGE IN NANOSTRUCTURED CARBONS

Nidia C Gallego, Cristian I Contescu, James R Morris, Stephen J Pennycook, Takeshi Egami

Oak Ridge National Laboratory, Oak Ridge, TN 37831

Research Scope

Nanoporous carbons - also known as activated carbons – are carbon materials containing micropores (<2 nm) and mesopores (2-50 nm). These materials have long played an important role in areas associated with energy and environment (e.g. air cleaning, water purification), but are expected to play an even broader role in the future. For example, nanoporous carbons are already at the core of energy storage in batteries and supercapacitors, used on large scale in portable energy sources, electric vehicles, and for smart grid technologies; nanoporous carbons are a strong alternative for capturing CO_2 from flue gases and for storage of hydrogen and natural gas in adsorbed rather than compressed state; and they are used as catalysts or catalyst supports in chemical and pharmaceutical industries. For too long the research on porous carbons has been carried out only by interested industries and mostly with a strict product-oriented focus.

In this project we focus on developing realistic models of nanoporous carbons that allow understanding the role of local atomic structure, composition, and order on the mechanisms of gas adsorption. The task is challenging because of the lack of a clear atomic picture of nanoporous carbon materials. We have addressed this challenge using existing expertise at ORNL, including strengths in materials synthesis, advanced X-ray and neutron scattering techniques for characterization of disordered materials, electron microscopy with sub-Ångstrom resolution, and atomistic modeling of structure, dynamics, and adsorption in carbon nanostructures. Our specific goals include (1) identification of atomic structures in disordered carbons and metal-doped carbons; (2) exploration of the nature of hydrogen binding on such sites and of the role of metal particles and modifiers; (3) identification of H_2 adsorption mechanisms and characterization of energetics and dynamics of adsorbed hydrogen.

Recent Progress

It has been experimentally observed that H_2 uptake by Pd-modified activated carbon fibers (Pd-ACF) is about 30% higher than what would be expected based on total conversion of Pd into $PdH_{0.66}$ (Fig. 1). We obtained evidence in support of the "spillover mechanism" according to which H_2 the Pd hydride phase is destabilized by contacts with nanoporous carbon and released H atoms migrate on carbon surface and form new C-H bonds with unsaturated carbon atoms. Closer examination of Pd-ACF by high resolution STEM led us to discover the presence of single Pd atoms stabilized by the carbon matrix, and their concentration was determined [1]. Single transition metal atoms can form multiple coordinative bonds with H_2 molecules (known as Kubas complexes), but

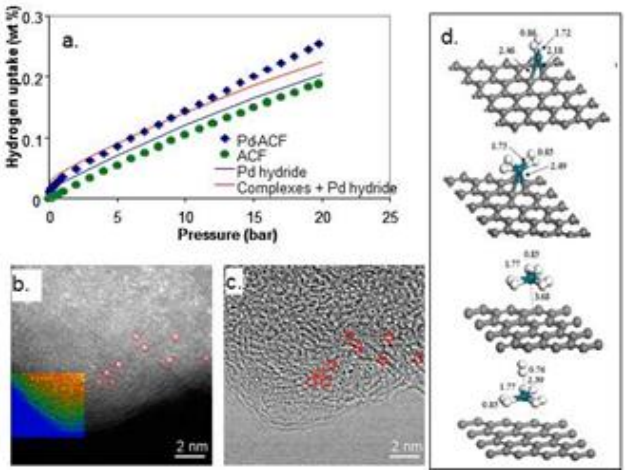

Fig. 1 (a) Experimental H_2 adsorption on ACF and Pd-ACF compared with behavior expected if all Pd is converted to Pd hydride and based on Kubas mechanism hypothesis. Also shown are (b) single Pd atoms and (c) carbon structures identified by HR-STEM; and (d) predicted Kubas structures for multiple bonding of H_2 to single Pd atoms. [1,2]

isolated metal atoms are in general unstable on carbon substrates, and Kubas complexes have not been experimentally studied. Using first-principle calculations we estimated that each Pd atoms can bind up to four H_2 molecules in our experimental conditions. We concluded that Kubas binding is another possible route leading to enhanced H_2 uptake on Pd-ACF, along with physisorption on carbon support, hydride formation, and spillover leading to new C-H bonds [2].

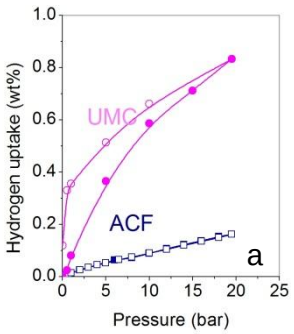

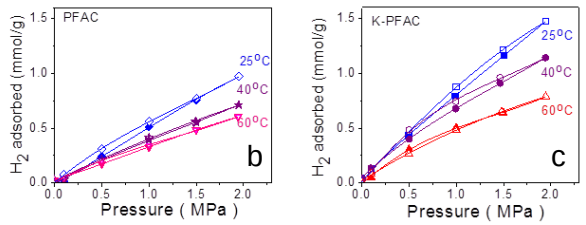

Fig. 2 (a) Adsorption (filled symbols) and desorption (open symbols) data points for H_2 on UMC and ACF materials at 298 K, showing higher uptake on UMC and adsorption - desorption hysteresis on UMC; (b) Adsorption-desorption isotherms on PFAC and (c) on K-doped PFAC showing enhanced H_2 uptake in presence of K.

Doping nanoporous carbon with alkali metals can also promote enhanced H_2 uptake, albeit by a different mechanism. High surface area ultramicroporous carbon (UMC) has atypically high H_2 uptake (0.8 wt% at 300 K and 20 bar) compared with ACF (Fig. 2), which we explained using the concept of polarization-induced physisorption at K^+ and Na^+ ions reminiscent from chemical activation [3,4].In a control experiment we introduced controlled amounts of K or Li in a polymer-derived carbon (PFAC) and observed enhanced H_2 uptake at 298 K (Fig. 2) and higher heats of adsorption [5,6]. These results confirm that polarization-induced physisorption is an alternate mechanism for enhancing H_2 uptake on nanoporous carbons.

All our data suggest that physisorption remains the most important mechanism for H_2 adsorption on nanoporous carbons. Adsorption models predict that strong adsorption forces in narrow carbon nanopores determine high density of the adsorbed phase, but direct confirmation is not available because of numerous experimental difficulties. Using in-situ high-pressure small-angle neutron scattering (SANS) experiments at room temperature, we obtained the first direct evidence of enhanced densification of H_2 trapped in narrow carbon nanopores (Fig. 3) [7]. The data show that *at room temperature* the density of H_2 adsorbed in 9 Å pores is close to that of liquid H_2 when the external gas pressure is about 200 bar. The densification factor depends on external pressure and pore size, causing internal pressures some 40-50 times larger than in the bulk gas phase. An estimate of adsorption energy in the narrowest pores gave ~10 kJ/mol, which is twice large than the value reported from measurements at cryogenic temperatures.

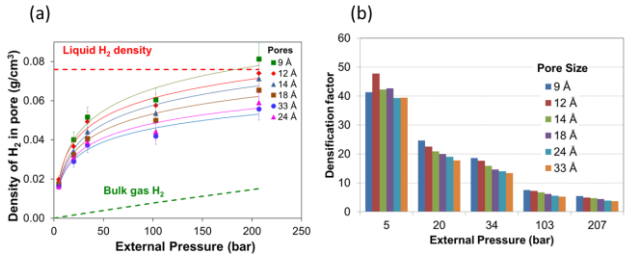

Fig. 3: (a) Estimated densities of H_2 trapped in PFAC nanopores as a function of pore size and external H_2 pressure, and (b) the densification factors showing the large increase in density at low pressures and the gradually weaker effect at higher pressures.

The mobility of small molecules confined in narrow nanopores is severely limited at cryogenic temperatures. Using in-situ quasi-elastic neutron scattering (QENS), we found that H_2 trapped in nanopores becomes mobile some 9-12 K above the triple point temperature (13.9 K). Diffusion is described by a solid-like jumping mechanism with large activation energy. Moreover, at these low temperatures, H_2 diffusion is strongly affected by quantum effects resulting from its thermal de Broglie wavelength being comparable with the size of confining nanopores [8].

Structural investigation of nanoporous carbons using small angle neutron and X-ray scattering revealed that all materials investigated have a dominant 2D character consistent with the sp^2 hybridization on C atoms, but with limited (PFAC) or extremely weak (UMC) coherent stacking of graphene sheets in the direction perpendicular to their main orientation.

Detailed information on the local atomic arrangement was obtained by X-ray and neutron atomic pair distribution function (PDF) methods [9], which allow for studying both local and medium range structures of disordered materials in real space (Fig. 4). It was found that in-plane coherence is limited to about 13-14 Å (or 8-9 hexagonal units) and that most graphene sheets are likely to have local folds and cusps that limit the extent of flat areas. Depending on the particular carbon's origin (ACF, UMC), the micro-texture defined by graphene stacking in the perpendicular direction is different, which results in substantially different gas adsorption characteristics.

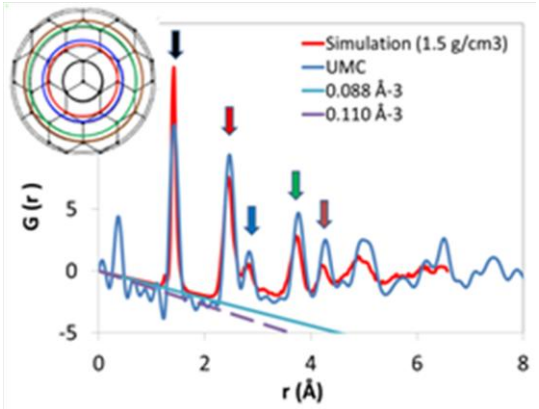

Figure 4: Experimental PDF for UMC versus 1.5 g/cm^3 simulated structure. The straight line slope scales with atomic density of scattering atoms: 0.088 Å^{-3} (UMC; blue) and 0.11 Å^{-3} (graphite, purple). Insert: origin of PDF peaks graphite structure.

Theoretical modeling of gas hydrogen adsorption in nanoporous carbons provided similar results. We used tight binding molecular dynamics (TBMD) to generate carbon structures with various densities and calculated the amounts of H_2 adsorbed as a function of pressure [10,11,12]. With increasing carbon density, the structures develop domains of hexagonal symmetry of C atoms, interrupted by defects. Adsorption calculations identified pockets in the porous structure with favorable adsorption energy (Fig. 5 a). The heat of adsorption increases with carbon density, but the available volume drops, so that carbon density is an important structural parameter that controls practical uptake capacity. Calculations demonstrate that small pores in dense carbon materials adsorb very strongly, with isosteric heat of adsorption at zero coverage of 12-22 kJ/mol. This range is suitable for hydrogen storage and delivery, but the scarcity of narrow pores leads to poor uptake in real materials. In contrast, although carbons simulated at low densities have lower heat of adsorption (due to weaker interactions in larger pores), the available pore volume is larger, and overall effect is an increase of uptake. Figure 5 b shows the competition between optimizing the available pore volume and optimizing the adsorption potential in narrow pores for high gas uptake.

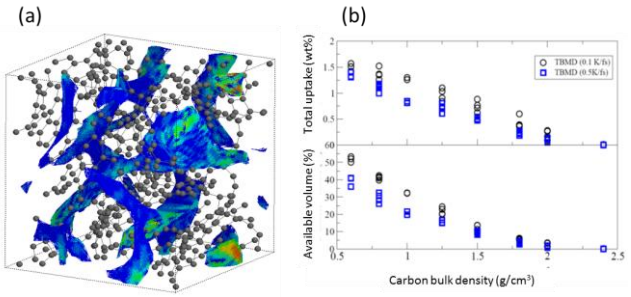

Fig. 5: (a) Simulated carbon structure (1.25 g/cm^3) showing pockets for H_2 adsorption with favorable adsorption energy (< -10 kJ/mol), with blue indicating weaker, and red stronger adsorption sites; (b) Correlation between total H_2 uptake (298 K at 50 bar), available volume, and bulk carbon density. Data show reproducibility between structures obtained in repeated simulations with two quenching rates (black - 0.1 K/fs; blue – 0.5 K/fs).

The presence of non-hexagonal atom rings in the structure of nanoporous carbons has been confirmed by atomic resolution STEM of PFAC and UMC materials [13]. Topological defects are frequently observed in graphene sheets as energetically favorable 5-7 rings pairs, highly correlated with each other, typically near other 5-7 rings (Fig. 6). Atomic level modeling showed that these defects induce localized rippling which interfere with the graphitic stacking and create nanopores with enhanced adsorption energy

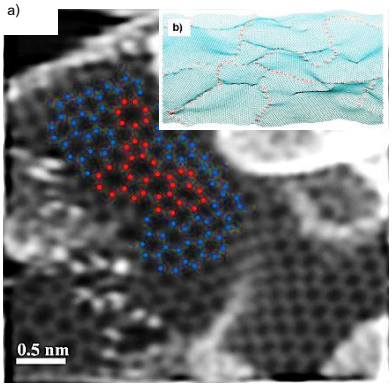

Fig. 6: Atomic resolution STEM image typical for graphenes in nanoporous carbons, showing defective rings of 5-7 atoms (a) and 3D relaxed graphene sheet with ripples and folds introduced by topological defects (b).

for H_2 (and presumably other) molecules. PFAC contains larger regions of stacked layers and consequently develops smaller surface area and porosity than UMC.

The simulation results are consistent with all previous information obtained from in-situ-SANS, STEM, and PDF analysis. Local defects in graphene cause curling and imperfect stacking, and create narrow porosity which is the locus of high energy sites for adsorption and densification of H_2. Other light molecules are expected to follow the same mechanism. The adsorbed fluid may experience restricted severe confinement conditions, which limit its mobility.

Future Plans

Our goal for the next few years is to understand the relationship between local atomic structures and large scale architecture of nanoporous carbons, and the impact of these two elements on the nature of interaction with the surrounding gaseous environment; leading to the understanding of the phase behavior and properties of molecular species confined in carbon's nanopores.

To achieve this goal we will focus on the interactions at the atomic and molecular scale between carbon atoms, electronic spins, topological defects, and defectively stacked graphenes; and the interaction with the gaseous environment surrounding nanoporous carbons. We will employ advanced characterization tools available on the ORNL campus and in other DOE facilities, such as neutron and X-ray scattering, diffraction, spectroscopy; atomic resolution electron microscopy; and powerful computing resources. The results will materialize in fundamental understanding of materials for energy storage and conversion, and development of new techniques and procedures that will be applicable to similar adsorption processes on other porous materials.

References to publications of DOE sponsored research (2010-2012)

1 K. van Benthem, C.S. Bonifacio, C.I. Contescu, N.C. Gallego, S. J. Pennycook, "STEM imaging of single Pd atoms in activated carbon fibers considered for hydrogen storage", *Carbon* **49** (2011): 4059-4073.

2 C.I. Contescu, K. van Benthem, S. Li, C. S. Bonifacio, S. J. Pennycook, P. Jena, N. C. Gallego, "Single Pd atoms in activated carbon fiber and their contribution to hydrogen storage", *Carbon* **49** (2011): 4050-4058.

3 V. V. Bhat, C. I. Contescu, N. C. Gallego, F. S. Baker, "Atypical hydrogen uptake on chemically-activated, ultramicroporous carbon". *Carbon*, **48** (2010) 1331-1340.

4 V. V. Bhat, C. I. Contescu, N. C. Gallego, "Kinetic effect of Pd addition on the hydrogen uptake of chemically-activated ultramicroporous carbon". *Carbon*, **48** (2010) 2361-2364.

5 D. Saha, C. I. Contescu, N. C. Gallego, "Tetrahydrofuran-induced K and Li doping onto poly(furfuryl alcohol)-derived activated carbon (PFAC): Influence on microstructure and H_2 sorption properties", *Langmuir* **28** (2012): 5669-5677.

6 H. Zhang, V. V. Bhat, P. X. Fang, C. I. Contescu, N. C. Gallego, "Effect of potassium-doping on the microstructure development in polyfurfuryl alcohol-derived activated carbon", *Carbon* (accepted, 2012).

7 N. C. Gallego, L. He, D. Saha, C. I. Contescu, Y. B. Melnichenko, "Hydrogen confinement in carbon nanopores: Extreme densification at ambient temperature", *JACS* **133**, 13794-13797 (2011).

8 C. I. Contescu, D. Saha, N. C. Gallego, E. Mamontov, A. I. Kolesnikov, V. V. Bhat, "Restricted dynamics of molecular hydrogen confined in activated carbon nanopores", *Carbon* **50** (2012) 1071-1082.

9 W. Dmowski, C. I. Contescu, A. Llobet, N. C. Gallego, T. Egami, "Local atomic density of microporous carbons", *J Phys Chem C* **116** (2012) 2946-2951.

10 L. Peng, J. R. Morris, "Hydrogen adsorption calculations in expanded graphite and amorphous carbons", *Mater. Res. Symp. Proc*. Vol. 1216 © 2010 Materials Research Society, 1216-W01-08.

11 L. Peng, J. R. Morris, "Prediction of hydrogen adsorption properties in expanded graphite model and in nanoporous carbon". *J. Phys. Chem. C*, **114** (2010) 15522-15529.

12 L. J. Peng, J. R. Morris, "Structure and hydrogen adsorption properties of low density nanoporous carbons from simulations", *Carbon* **50** (2012) 1394-1406.

13 J. Guo, J. R. Morris, Y. Ihm, C. I. Contescu, N. C. Gallego, G. Duscher, S. J. Pennycook, M. F. Chisholm, "Topological defects: Origin of nanopores and enhanced adsorption performance in nanoporous carbons", *Small* (accepted, 2012)

Nematicity in Fe-pnictide and chalcogenide superconductors

From FWP 10028: Correlated Materials - Synthesis and Physical Properties

PIs: I. R. Fisher, T. H. Geballe, A. Kapitulnik, S. A. Kivelson, and K. A. Moler

Abstract by Ian Fisher

Geballe Laboratory for Advanced Materials, Stanford University, and

Stanford Institute for Materials & Energy Science, SLAC National Laboratory.

Email: irfisher@stanford.edu

1. Program Scope

This FWP is part of the newly-formed Stanford Institute for Materials and Energy Sciences (SIMES), which is the Materials Science Division at the SLAC National Accelerator Laboratory. Within our specific FWP, our efforts aim to address the grand challenge of "emergence" as well as a number of "Basic Research Needs" areas for energy applications in the realm of quantum materials. Understanding and ultimately controlling this class of materials has the potential to profoundly impact the next generation of electronic materials relevant to addressing our nation's energy needs. From new quantum states that enable computing with vastly lower power consumption, to new superconductors that better suit power transmission requirements, quantum materials hold the promise of advanced applications as well as providing some of the deepest and most challenging intellectual questions. In the last two years our research has encompassed the fields of superconductivity, novel forms of charge and spin order, non-Fermi liquid behavior and topological insulators. Our focus is on understanding fundamental factors determining the often complex electronic properties of these materials. We combine crystal growth and characterization of novel materials with measurements of their bulk electronic properties (Fisher & Geballe), with measurements of local electronic (Kapitulnik) and magnetic (Moler) properties, and theory (Kivelson). We collaborate extensively, both within SIMES and externally, and materials synthesized as part of this program enable research at diverse other universities and laboratories.

2. Recent Progress

This abstract relates principally to recent work addressing nematicity in Fe-pnictides, but also outlines results of quantum oscillation studies of both Fe-pnictides and of topological insulators and a brief commentary on other materials studied as part of this FWP. Separate abstracts from A. Kapitulnik and K. A. Moler from our FWP address research in our FWP using scanning magnetic probes, STM and Kerr effect measurements.

(a) Electronic nematic order in Fe-pnictides

Correlated electron fluids can exhibit a startling array of complex phases, among which one of the more surprising is the electron nematic, a translationally invariant metallic phase with a spontaneously generated spatial anisotropy (See [20] for a recent review). These ideas are pertinent in the recently discovered Fe-arsenide superconductors. The parent phases harbor an antiferromagnetic transition which is either preceded or accompanied by a structural transition that breaks the four fold symmetry of the lattice. Previously, we (SAK) developed a minimal spin Hamiltonian that explains the structural transition in terms of an emergent electronic nematic phase transition (PRB **77**, 224509 (2008)). Some analogies can be drawn with the high T_c cuprates (Nature Materials **7**, 927 (2008)), possibly providing a unified theoretical approach (NJP **11**, 085007 (2009).).

Motivated by these theoretical ideas, we developed a new experimental methodology using uniaxial strain to probe the nematic response of the Fe-pnictides. Uniaxial strain couples linearly to the nematic order parameter, and as such provides an ideal probe of the nematic response of a material. By measuring the induced electronic anisotropy as a function of the applied strain one can determine the "nematic susceptibility", which describes the tendency of the electronic system to favor orientational order, even in the absence of an actual phase transition. Our measurements of the prototypical system $Ba(Fe_{1-x}Co_x)_2As_2$ reveal a divergent nematic susceptibility, demonstrating that the structural transition is driven by an instability in the electronic part of the free energy [1]. These measurements also revealed an electronic nematic quantum phase transition at optimal doping (Fig. 1), raising the much deeper theoretical question of what role nematic fluctuations might play in the superconducting pairing mechanism. Related measurements of $BaFe_2(As_{1-x}P_x)_2$ revealed the coupling between the superconducting, magnetic and nematic order parameters [2] and can be understood within our (SAK) theoretical framework [3].

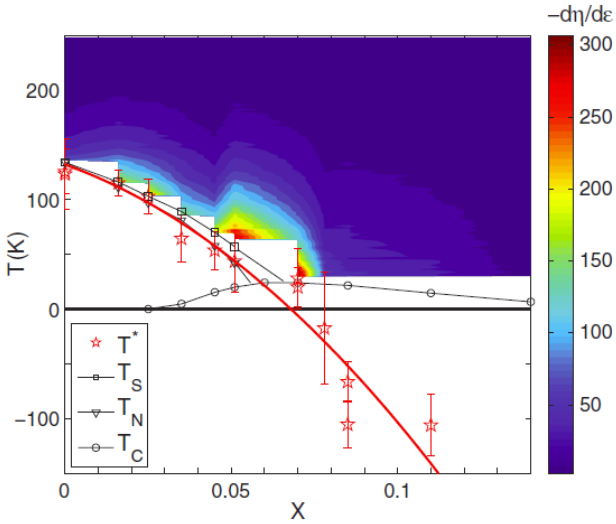

Figure 1. *Colorscale plot showing the temperature an d composition dependence of the nematic susceptibility $d\eta/d\varepsilon$ of the archetypical Fe-arsenide superconductor $Ba(Fe_{1-x}Co_x)_2As_2$. Solid black lines show the structural (T_S), magnetic (T_N) and superconducting (T_c) transitions. Red data points and line show the bare mean-field nematic critical temperature extracted from these measurements, which is renormalized by interaction with the crystal lattice to give the structural transition. An electronic nematic quantum phase transition occurs for compositions close to optimal doping. From [1].*

The intrinsic electronic anisotropy in the nematic state of the Fe-pnictides can be hidden by twin formation. We uncovered a large in-plane resistivity anisotropy by detwinning small single crystal samples in situ, using both in-plane magnetic fields [6,14] and uniaxial stress [8,15]. These measurements also showed an unusual non-monotonic doping dependence of the electronic anisotropy, possibly related to a Lifshitz transition [9]. The new techniques that we developed motivated and enabled additional collaborative measurements based on reflectivity [7,11], and ARPES [12] that clearly revealed how the nematic transition affects the electronic structure.

(b) Quantum oscillation studies

Quantum oscillatory phenomena provide detailed information about the Fermi surface (FS) and quasiparticle properties of metals. Our research in this area during the last two years revealed important insights in the following areas:-

- Fe-pnictides: our measurements of $BaFe_2(As_{1-x}P_x)_2$ revealed the morphology of both electron and hole pockets, revealing enhanced nesting for superconducting compositions [16]. These results support a key role for FS nesting in the superconducting pairing mechanism.
- Topological insulators: By growing samples with very low carrier densities, approaching 10^{16} cm^{-3}, we were able to reach the lowest Landau levels of the surface states [17]. These

measurements not only directly established that the surface states contribute to the conductivity of bulk crystals, but also opened the door for studies of interaction effects among Dirac Fermions. Additional experiments comparing quantum oscillation measurements with ARPES data revealed the effects of band-bending towards the surface of the material, of particular importance for any technological applications [13].

(c) Crystal growth of novel materials

Access to high quality single crystals of a variety of materials is a crucial enabling component of our program, ensuring rapid response to developments in the field as well as pioneering new directions for experimental study (see [5] for a recent review). We collaborate widely, sharing the materials synthesized as part of our DOE-supported work and enabling research both within SIMES and at other institutions (within the US and abroad) that would not be possible without access to such high quality single crystal samples. Beyond the Fe-pnictide and chalcogenide superconductors, and the topological insulators described above, other materials that we have studied in the last two years include:-

- R_2Te_5 (R=rare earth element): material supports multiple CDW phases associated with separate nesting of FS sections associated with single and double Te planes [19].
- $Pb_{1-x-y}Tl_xIn_yTe$: counter-doping of Tl-doped PbTe with In reveals correlation between superconductivity and anomalous normal-state properties, adding weight to the suggestion that the material harbors an unusual charge Kondo effect [18].
- $Ba_3(Mn_{1-x}V_x)_2O_8$: heat capacity measurements reveal an exotic random singlet phase at low temperatures[10].
- $Bi_2Ir_2O_7$ & $Y_2Ir_2O_7$: groundstates on the metallic and insulating sides respectively of a coupled magnetic/electronic phase transition [4,5]

3. Future Plans

Our ongoing experiments will continue to emphasize the use of uniaxial strain as a probe of electronic nematic order in strongly correlated quantum materials, including various cuprates and ruthenates. We will also continue to develop crystal growth techniques for a range of new/novel materials.

4. References to publications of DOE sponsored research that have appeared in 2010-2012

The following is a partial list of selected publications from our FWP relevant to the work described in this abstract.

[1] *Divergent nematic susceptibility in an iron arsenide superconductor*, Jiun-Haw Chu, Hsueh-Hui Kuo, James G. Analytis, Ian R. Fisher, arXiv:1203.3239 (Accepted for publication in Science)

[2] *Magneto-elastically coupled structural, magnetic and superconducting order parameters in* $BaFe_2(As_{1-x}P_x)_2$, H-.H. Kuo, J. G. Analytis, J.-H. Chu, R.M. Fernandes, J. Schmalian and I. R. Fisher, arXiv:1207.3858 (Accepted for publication in Phys. Rev. B)

[3] *Pressure effects on magnetically driven electronic nematic states in iron pnictide superconductors*, J-P. Hu, S. Chandan, and S. A. Kivelson, Phys. Rev. B **85**, 100507 (2012).

[4] *Structure and Magnetic Properties of the Pyrochlore Iridate* $Y_2Ir_2O_7$, M. C. Shapiro, S. C. Riggs, M. B. Stone, C. R. de la Cruz, S. Chi, A. A. Podlesnyak & I. R. Fisher Phys. Rev. B **85**, 214434 (2012) [5 pages]

[5] *Principles of crystal growth of intermetallic and oxide compounds from molten solutions*, I. R. Fisher, M. Shapiro and J. G. Analytis, Phil. Mag. Vol. **92**, Nos. 19–21, 2401–2435 (2012) [34 pages]

[6] *Susceptibility anisotropy in an iron arsenide superconductor revealed by x-ray diffraction in pulsed magnetic fields*, J. P. C. Ruff, J.-H. Chu, H.-H. Kuo, R. K. Das, H. Nojiri, I. R. Fisher, Z. Islam
Phys. Rev. Lett. **109**, 027004 (2012) [5 pages]

[7] *Anisotropic in-plane optical conductivity in detwinned* $Ba(Fe_{1-x}Co_x)_2As_2$,
A. Dusza, A. Lucarelli, A. Sanna, S. Massidda, J.-H. Chu, I. R. Fisher and L. Degiorgi,
New Journal of Physics **14**, 023020 (2012) [20 pages]

[8] *In-plane electronic anisotropy of underdoped '122' Fe-arsenides revealed by measurements of detwinned single crystals*, I. R. Fisher, L. Degiorgi and Z. X. Shen, Rep. Prog. Phys **74**, 124506 (2011) [21 pages]

[9] *Possible origin of the nonmonotonic doping dependence of the in-plane resistivity anisotropy of* $Ba(Fe_{1-x}T_x)_2As_2$ *(T=Co, Ni and Cu)*, H.-H. Kuo, J.-H. Chu, S. C. Riggs, L. Yu, P. L. McMahon, K. De Greve, Y. Yamamoto, J. G. Analytis and I. R. Fisher, Phys. Rev. B **84**, 054540 (2011) [11 pages]

[10] *Heat capacity of the site-diluted spin dimer system* $Ba_3(Mn_{1-x}V_x)_2O_8$
E. C. Samulon, M. C. Shapiro, and I. R. Fisher, Phys. Rev. B **84**, 054417 (2011) [11 pages]

[11] *Anisotropic charge dynamics in detwinned* $Ba(Fe_{1-x}Co_x)_2As_2$
A. Dusza, A. Lucarelli, F. Pfuner, J.-H. Chu, I. R. Fisher and L. Degiorgi,
Euro. Phys. Letters **93**, 37002 (2011). (6 pages)

[12] *Symmetry breaking orbital anisotropy observed for detwinned* $Ba(Fe_{1-x}Co_x)_2As_2$ *above the spin density wave transition*, M. Yi, D. H. Lu, J.-H. Chu, J. G. Analytis, A. P. Sorini, A. F. Kemper, B. Moritz, S.-K. Mo, R. G. Moore, M. Hashimoto, W. S. Lee, Z. Hussain, T. P. Devereaux, I. R. Fisher, Z.-X. Shen
PNAS **108** (17) 6878-6883 (2011) (6 pages)

[13] *Bulk Fermi surface coexistence with Dirac surface state in* Bi_2Se_3*: A comparison of photoemission and Shubnikov–de Haas measurements*, J. G. Analytis, J.-H. Chu, Y. Chen, F. Corredor, R. D. McDonald, Z. X. Shen and I. R. Fisher, Phys. Rev. B **81**, 205407 (2010) (6 pages; Editor's Suggestion)

[14] *In-plane electronic anisotropy in underdoped* $Ba(Fe_{1-x}Co_x)_2As_2$ *revealed by partial detwinning in a magnetic field*, Jiun-Haw Chu, James G. Analytis, David Press, Kristiaan De Greve, Thaddeus D. Ladd, Yoshihisa Yamamoto, Ian R. Fisher, Phys. Rev. B **81**, 214502 (2010). (5 pages)

[15] *In-plane resistivity anisotropy in an underdoped iron pnictide superconductor*
Jiun-Haw Chu, James G. Analytis, Kristiaan De Greve, Peter L. McMahon, Zahirul Islam, Yoshihisa Yamamoto, Ian R. Fisher, Science **329**, 824 (2010). (3 pages)

[16] *Enhanced Fermi surface nesting in superconducting* $BaFe_2(As_{1-x}P_x)_2$ *revealed by the de Haas-van Alphen effect*, J.G. Analytis, J.-H. Chu, R.D. McDonald, S. C. Riggs, I.R. Fisher,
Phys. Rev. Lett. **105**, 207004 (2010). (4 pages).

[17] *Two-dimensional surface state in the quantum limit of a topological insulator*
J.G. Analytis, R.D. McDonald, S. C. Riggs, J.-H. Chu, G. S. Boebinger, I.R. Fisher
Nature Physics **6**, 960 (2010).

[18] *Correlation of anomalous normal state properties with superconductivity in* $Pb_{1-x-y}Tl_xIn_yTe$
A. S. Erickson, N. P. Breznay, E. A. Nowadnick, T. H. Geballe and I. R. Fisher,
Phys. Rev. B **81**, 134521 (2010) (6 pages)

[19] *Observation of two separate charge density wave transitions in* Gd_2Te_5 *via transmission electron microscopy and high-resolution X-ray diffraction*, K.Y. Shin, N. Ru, I.R. Fisher, C.L. Condron, M.F. Toney, Y.Q. Wu and M.J. Kramer, Journal of Alloys and Compounds **489**, 332 (2010). (4 pages)

[20] *Nematic Fermi Fluids in Condensed Matter Physics*, Eduardo Fradkin, Steven A. Kivelson, Michael J. Lawler, James P. Eisenstein, Andrew P. Mackenzie, Annual Reviews of Condensed Matter Physics **1**, 153 (2010).

Spin Physics and Nanoscale Probes of Quantum Materials

David Goldhaber-Gordon and Hari C. Manoharan

Stanford Institute for Materials and Energy Sciences, SLAC National Accelerator Laboratory
Department of Physics, Stanford University, Stanford, CA 94305
goldhaber-gordon@stanford.edu • manoharan@stanford.edu

Program Scope

The goal of this program is to directly measure and manipulate low-dimensional spin, isospin, and electron correlations using scanning probes. The quantum materials and physics targeted in this program span many dimensionalities and are summarized in Figure 1. A diverse array of experimental tools is being applied to these investigations: scanning tunneling microscopy and spectroscopy (STM/STS), atom manipulation STM, Scanning Gate Microscopy (SGM), and a new tool termed a "Virtual STM." A common theme is the precise control of nanoscale geometry through nanofabrication and nanoassembly. The scientific work has been spread over two main thrusts: (A) topological and spin effects in novel quantum materials [1], and (B) mapping low-dimensional electronic structure and manipulating single electronic wavefunctions in nanostructures.

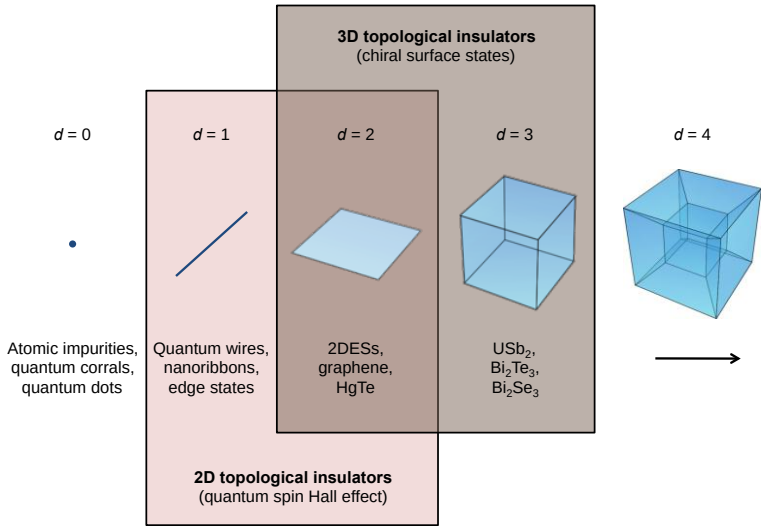

Fig. 1 Summary of materials and physics examined in this program, involving scanning probe interrogation and manipulation across quantum materials of various dimensionality (*d*).

Recent Progress

A. Imaging Dirac Materials and Topological Order

Targeting 2D topological insulator physics, we have studied Quantum Spin Hall (QSH) edge states by SGM. In the QSH state, counter-propagating states exist at the edge of a two-dimensional system, whereas the bulk is insulating. While backscattering between the counter-propagating states in general is prohibited by time-reversal symmetry, several mechanisms have been theoretically proposed where a potential fluctuation can lead to a suppression of the edge state conductance. We applied SGM techniques to study the QSH state in HgTe heterostructures, which is the only material where the QSH effect has been demonstrated experimentally so far. By applying a bias voltage to the scanning gate tip, a potential fluctuation is induced in the device, and the modulation of the conductance is measured as a function of the tip position (Fig. 2, left).

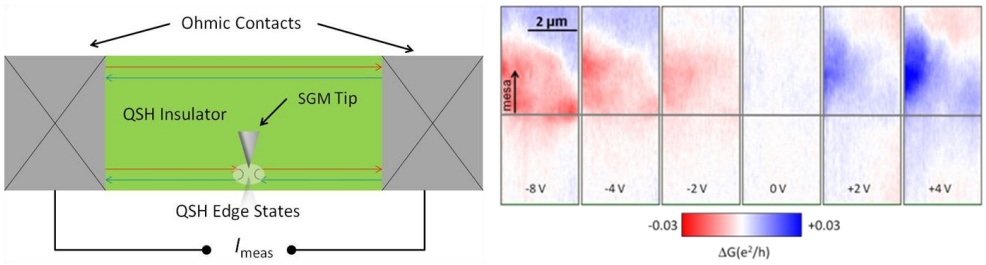

Fig. 2 (Left) Schematic of the SGM setup for study of the 2D topological insulator (not to scale). (Right) In the vicinity of the mesa edge (grey solid line), a clear tip effect on the conductance can be observed.

The length of the studied devices is 5 µm, comparable to the mean free path of the QSH edge states. The large width of 150 µm prevents any interaction between states on the opposite edges, so that the states propagating at opposite edges can be regarded as independent channels. Our first generation of devices all showed a *p*-type bulk carrier density of $n \sim 10^{11}$ cm^{-2}. Nonetheless, we were able to observe signatures of the QSH state. When a negative voltage is applied, the conductance is suppressed when the tip is near the mesa edge (Fig. 2, right). On the other hand, an increase of conductance is observed for positive voltages. This behavior can be understood when the bulk carriers are taken into account. These form a reservoir of states into which the carriers in the QSH edge states can scatter. The amount of backscattering of the edge states due to the bulk carriers increases with the bulk carrier density. When a negative tip voltage is applied, the density of the p-type bulk carriers is increased locally, resulting in the observed decrease of conductance. In contrast, a positive tip voltage will decrease the density or can possibly even tune the system locally into the bulk-insulating regime, which will decrease backscattering and thus increase the edge state conductance. A clear gate effect can be observed approximately 2 µm into the bulk. We have also recently found that particular sites along the edge are susceptible to producing enhanced backscattering as their potential is tuned.

Our STM work involves the full-time operation of several custom STM systems including a variable-temperature UHV STM and an ultra-stable high-magnetic-field low-temperature UHV STM. The measurement techniques employed cluster around STM and STS, and include specializations such as atomic manipulation, inelastic electron tunneling spectroscopy (IETS), and simultaneous measurements in a high magnetic field. Figure 3 shows recent results for STM-based work in this program.

We made significant progress during this period in STM/STS and atomic manipulation studies of quantum materials and spin/pseudospin-based topological ground states. By manipulating molecules, we achieved the first "designer" Dirac fermions by transforming normal surface states on Cu(111) into hosts for massless Dirac fermions. This new 2D material is called "molecular graphene" since it involved up to ~1000 individual CO molecules manipulated into precise lattices to obtain new states arising from pseudospin textures (see Fig. 3A and 3B). For example, we formed atomic scale *p*-*n* junctions to study the propagation of Dirac fermions, created massive Dirac fermions by texturing surface graphene bonds to form a gap, and generated gauge (pseudo) electric and magnetic fields by straining molecular graphene. These fields were manifested in either a change in the effective doping of the crystal or, in the most striking case, a quantum Hall state generated in zero real magnetic field but with a gauge magnetic field of strength 60 Tesla. This state is akin to a 2D topological insulator with time-reversal invariance. These results were reported in Nature [2] (co-selected for the cover), and was also covered by a News & Views [3], as well as Physics Today [4] and Scientific American [June 2012]. These efforts compliment our earlier work in other local fabrication and manipulation of graphene nanostructures [5]. Other STM/STS work involved other complex materials synthesized in other SIMES groups. We made progress imaging CVD graphene devices fabricated by Goldhaber-Gordon group. We succeeded in isolating ultrathin Bi_2Te_3 topological insulator nanoribbons on top of graphite (collaboration with Y. Cui group) [see Fig. 3C and 3D], complementing earlier work on Bi_2Se_3 topological insulator nanoribbons on SiO_2 [6].

Using FT-STS, we have mapped pseudospin-flipping and chirality-reversing scattering processes on bare graphene, and extended measurements to investigation of magnetic adatoms. STM/STS work on individual atomic spins on graphene led to a theoretical understanding of observed Fano resonances and a unique polarity switching effect stemming from the underlying Berry phase of graphene pseudospin [7].

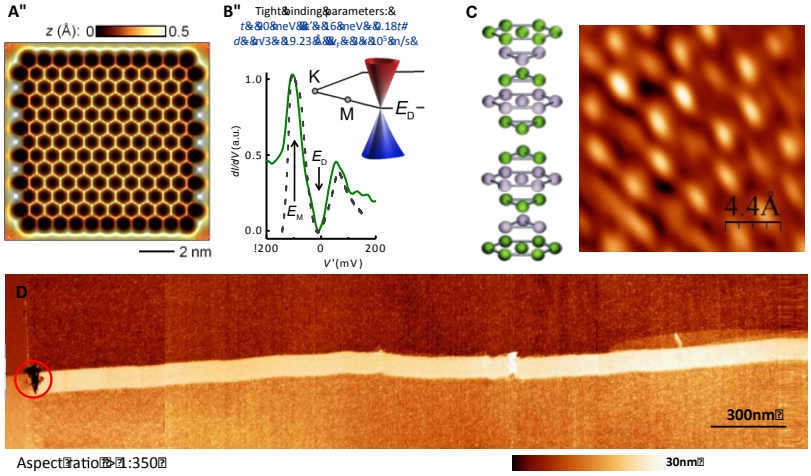

Fig. 3 (A) STM topograph acquired after many sequential manipulation steps to assemble "molecular graphene" from CO molecules patterning the Cu(111) surface state. (B) Scanning tunneling spectroscopy of molecular graphene showing a signature graphene-like density of states. Inset: fit to tight-binding model, extracted hopping parameters, and the resulting Dirac cone in momentum space. (C) Atomic structure of Bi_2Te_3 nanoribbons imaged by STM. (D) Wide field STM image of single Bi_2Te_3 topological insulator nanoribbon.

B. Imaging and Manipulating Quantum Wavefunctions

The combination of natural or engineered electronic structure creating exact degeneracies due to geometry is a fertile area for robust topological effects in condensed matter. Not surprisingly, quantum mechanical phase often plays a role in the underlying ground states. In nanoassembled materials we have been mapping the effects of quantum mechanical phase in various forms, guided by ideas such as real-space and *k*-space exact degeneracies in band structure. Our atom manipulation and high resolution STS capabilities in magnetic fields up to 11 T were additionally used for sensitivity to Aharonov-Bohm phase, flux effects such as Landau level quantization, and coupling to the spin degree of freedom. Using STM and theoretical modeling, a new method of interrogating and cloaking single molecules in a nanostructure was discovered via inelastic tunneling spectroscopy [8].

We are also developing a new kind of scanned probe called the Virtual STM (VSTM) [9]. This probe will also be able to map 2DESs, but instead of relying on backscattering of current flowing in the 2DES, it will use localized tunneling from a nearby parallel electron layer into the 2DES. This offers the benefit of directly mapping the spatial organization and energy states of electrons. Such an instrument is motivated by many predicted, complex electron phases which are expected to occur only in low-disorder heterostructures. In this past, this has limited observation of the phases to indirect bulk transport measurements due the large (near 1 eV) surface potential barrier restricting direct access. Inside a sample, however, barriers can be engineered to be as low as we wish. We take advantage of this with a second "probe" 2DES layer grown above the first, and with a few meV barrier between the two 2DESs. We have shown that Coulomb effects should not strongly suppress such local tunneling [11]. With proper heterostructure design, a scanned metal tip at the surface should be able to induce tunneling locally from the probe into the 2DES phases below, as if STM were being performed on a buried 2DES. Since induced tunneling follows the scanned tip above, we call this scanning probe system Virtual STM.

The bilayer heterostructure used in VSTM is effectively a vertical quantum transistor, which we have developed as the Wavefunction Extension Transistor (WET) [10]. Current through this transistor is

modulated by changing the decay of electrons into the interlayer potential barrier, and we have empirically shown that this mechanism can increase tunnel current by two to three orders of magnitude at low temperature. Because the cryogenic scanning system we plan to use is under construction (tested at room *T* and 3 K), we have relied on WET structures with large area, non-local measurements to show the feasibility of the VSTM. We can predict a high spatial resolution for VSTM based on the sensitivity of induced tunneling to electric field. We can also show that the probe 2DES excels at screening the sensitive interface below from surface fields, such as from a metal tip. Finally, we have successfully applied the spectroscopic capabilities of the bilayer heterostructure to the quantum Hall regime.

Future Plans

For the next generation of SGM devices and STM studies, we plan to implement a back gate, i.e. a gate electrode at the bottom of the device. In this way, we can control the bulk carrier density and possibly tune the devices into the bulk insulating regime which is required to observe and study the pure topological insulator state in 2D and 3D materials. In the coming year, we will incorporate our functioning scanning systems into a recently received cryogen-free dilution refrigerator. When combined with improved VSTM samples, which should exhibit higher tunnel modulation and mobilities, we expect to be able to probe several exotic electron phases. For example, Wigner crystallization is predicted to appear in low disorder samples as electron-electron interactions overtake electron kinetic energy. Wigner crystallization may arise through a series of "microemulsion" states possible to image. We plan to probe quantum Hall stripes, which are so far only manifested as transport anisotropy in low-disorder quantum Hall systems. Finally, we also plan to probe lithographically-defined structures, such as quantum point contacts and quantum dots in SGM, STM, and VSTM. New forms of graphene and topological insulators will be shared between groups to study in all experimental scanning probe systems in this program.

Literature cited

Publications attributed to work done under BES funding of this task

1. H. C. Manoharan, "Topological insulators: A romance with many dimensions," *Nature Nanotechnology* **5**, 477-479 (2010).
2. K. K. Gomes, W. Mar, W. Ko, F. Guinea, H. C. Manoharan, "Designer Dirac fermions and topological phases in molecular graphene," *Nature* **483**, 306–310 (2012).
3. J. Simon, M. Greiner, "Condensed-matter physics: A duo of graphene mimics," *Nature* **483**, 282–284 (2012).
4. "Designer Dirac fermions," *Physics Today* **65**, 76 (2012).
5. S. Lee, M. F. Toney, W. Ko, J. C. Randel, H. J. Jung, K. Munakata, J. Lu, T. H. Geballe, M. R. Beasley, R. Sinclair, H. C. Manoharan, A. Salleo, "Laser-synthesized epitaxial graphene," *ACS Nano* **4**, 7524-7530 (2010).
6. D. Kong, J. C. Randel, H. Peng, J. J. Cha, S. Meister, K. Lai, Y. Chen, Z.-X. Shen, H. C. Manoharan, and Y. Cui, "Topological insulator nanowires and nanoribbons," *Nano Letters* **10**, 329-333 (2009).
7. T. O. Wehling, H. P. Dahal, A. I. Lichtenstein, M. I. Katsnelson, H. C. Manoharan, and A. V. Balatsky, "Theory of Fano resonances in graphene: The influence of orbital and structural symmetries on STM spectra," *Physical Review B* **81**, 085413 (2010).
8. J. Fransson, H. C. Manoharan, and A. V. Balatsky, "Detection and cloaking of molecular objects in coherent nanostructures using inelastic electron tunneling spectroscopy," *Nano Letters* **10**, 1600-1604 (2010).
9. A. Sciambi, M. Pelliccione, S. R. Bank, A. C. Gossard, and D. Goldhaber-Gordon, "Virtual scanning tunneling microscopy: a local spectroscopic probe of 2D electron systems," *Appl. Phys. Lett.* **97**, 132103 (2010).
10. A. Sciambi, M. Pelliccione, M. P. Lilly, S. R. Bank, A. C. Gossard, L. N. Pfeiffer, K. W. West, and D. Goldhaber-Gordon, "Vertical field-effect transistor based on wavefunction extension," *Physical Review B* **84**, 085301 (2011).
11. K. Luna, E.-A. Kim, P. Oreto, S.A. Kivelson, and D. Goldhaber-Gordon, "Local interlayer tunneling between two-dimensional electron systems in the ballistic regime," *Physical Review B* **82**, 235317 (2010).

Presentation Title:

Nano-Scale Optical Spectroscopy in Correlated Electron Systems

Principal Investigator: Adrian Gozar
Address: Condensed Matter and Materials Science Department, Brookhaven National Laboratory, Bldg. 510B, Upton, NY 11973, USA.
Email: agozar@bnl.gov

Period covered: June 10, 2010 – July 18, 2012

Research Scope:

The aim of this program is to understand electronic properties of complex materials and low dimensional structures by means of optical spectroscopy with nanometer-scale spatial resolution. The main objectives are to elucidate the emergence of metallic transport and superconductivity as a function of temperature and carrier concentration in correlated electron systems and to probe quasi-particle dynamics in nano-structures made out of such materials.

Our approach is topographic imaging along with local spectroscopic interrogation of these materials in the infrared and terahertz range by using a variable temperature scattering-type scanning near-field spectroscope (VT s-SNOM) system. This technique relies on the interaction between the sample and the enhanced electromagnetic field induced by antenna effects in the proximity of a sharp metallic atomic force microscope (AFM) tip whose size also determines the spatial resolution. This electromagnetic coupling allows extraction of the nano-scale dielectric properties of metallic and/or insulating phases. In case of systems having more complicated phase diagrams VT s-SNOM enables probing of the evolution of their optical response across metal-insulator and metal-superconducting transitions. We seek to establish in this latter case the nature, percolative or homogeneous, of these transitions and the static or dynamic nature of the phase coexistence.

The motivation for doing local optical spectroscopy is a broad array of experimental evidence obtained by other techniques relating competing interactions to the tendency towards phase segregation. We are also stimulated in this work because nano-scale spectroscopy opens up the possibility to probe excitations away from the Brillouin zone center, with a depth in q-space roughly given by the inverse of the achieved spatial resolution ($q \sim 1/r$ where r is the AFM tip radius). The access to this extra degree of freedom, exploited in inelastic neutron or X-ray scattering, photoemission or electron-loss spectroscopy, is absent in traditional far-field infrared spectroscopy or inelastic light (Raman) scattering.

Recent Progress:

We have tested an atomic force microscope system working in the T = 300 K to T = 6 K in a setup optimized for s-SNOM. Optical studies with spatial resolution of the order of 10 nm using pointed probes require the integration of atomic force microscopy within a variable temperature cryogenic system. Because such VT s-SNOM systems are, to the best of PI's knowledge, not yet commercially available the first step was to develop the necessary instrumentation which was done along with the entire laboratory infrastructure. Besides the VT s-SNOM, described below, the lab is equipped with a far-field Bruker FTIR spectrometer. The following main aspects were considered in the design of the system: **a)** mechanical stability and possibility for fast thermal cycling and stabilization; **b)** a base temperature as low as possible; **c)** optimization of the sample compartment for optical access and light focusing; **d)** control of the tapping motion of the AFM probe and avoiding interference with the direct laser beam focused on the tip; **e)** synchronization of the AFM scanning to an independent data acquisition system fed by the output of an infrared light detector. The constraints resulted in a setup adapting and integrating available instrumentation and functionalities. Fig.1 shows our VT s-SNOM reaching a base temperature of 5.9 K.

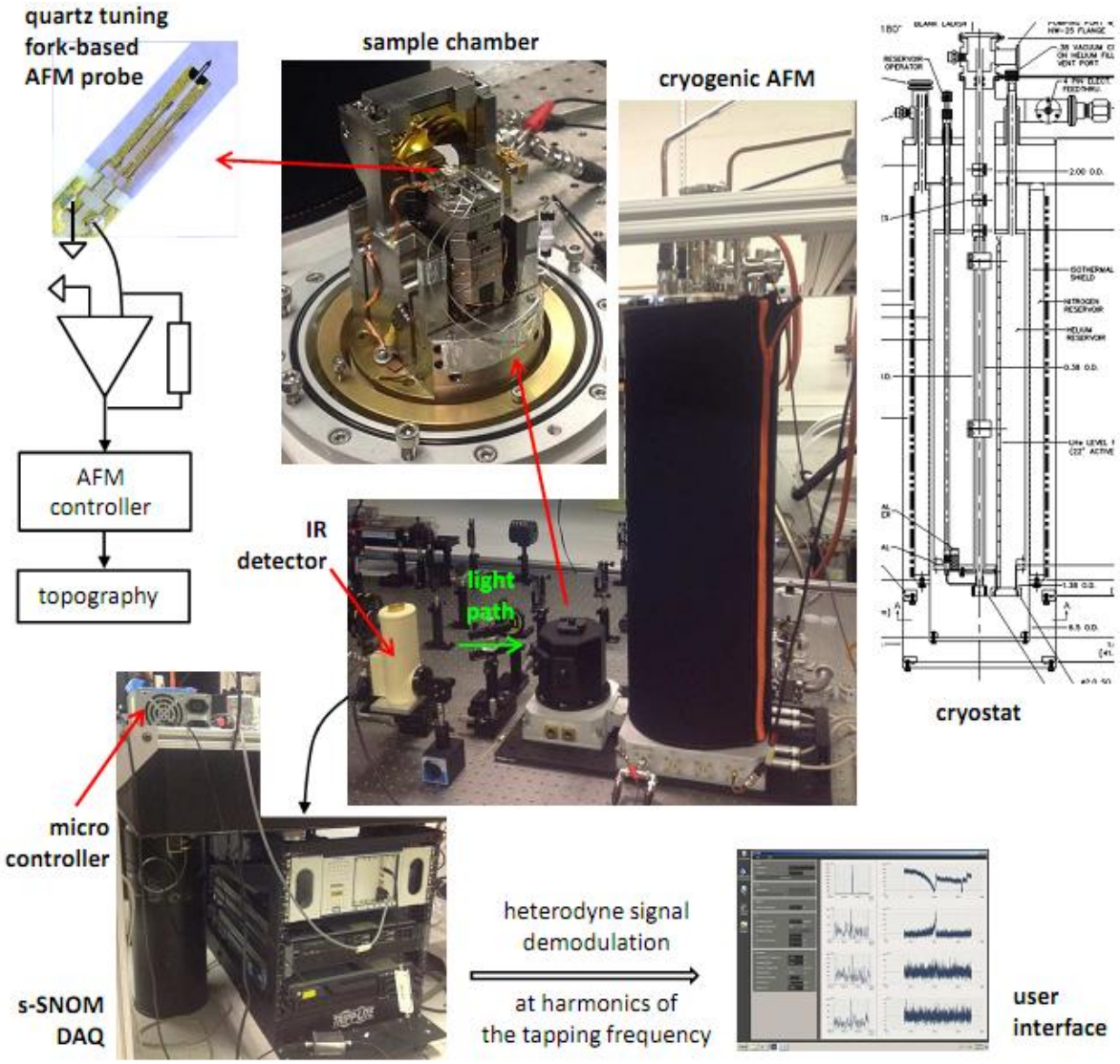

Fig.1: The VT s-SNOM system. **Cryogenics**: This is based on a vacuum cold plate LHe + LN2 shielding system (Janis Research) whose tail piece was extended with the AFM chamber (Attocube Systems). An integrated needle-valve controlled capillary flow connects the LHe volume to a variable temperature (VT) plate. Two flexible thermal links connect the VT plate to the thermally isolated sample holder and the 4K plate of the cryostat to the rest of the AFM chamber. The sample chamber has a 77 K radiation shield. **Optical Access**: Six windows mounted on the AFM housing allow access of the incident beam which is in turn focused by an off-axis parabolic mirror onto the AFM tip. Two XYZ piezo stacks support the AFM probe and the sample allowing independent positioning of the tip in the beam focus. **AFM Signal**: The conventional laser-based control of the cantilever deflection was replaced by electrical detection to avoid constraints for the incident beam. We use mechanically actuated probes consisting of a quartz tuning fork (TF) whose prongs are connected by a softer Si cantilever (Akiyama probes). The piezo current generated by the oscillating TF prongs (in the nA range) is detected in a similar manner to scanning tunneling microscopes. **s-SNOM signal**: The light scattered from the AFM tip is amplified in a heterodyne-type scheme and focused onto a detector (MCT). The output is fed into a separate data acquisition system and is synchronized to the AFM topography. Corresponding pixel, line and scan pulses are sent to a microcontroller in charge of the acquisition timing of a ADC card of a computer which in turn provides the Fourier analysis and demodulation of the s-SNOM signal. A dedicated user interface allows real time visualization of the spectral content of the data enabling the recording of the actual 2D s-SNOM scans.

We performed AFM operation tests at various temperatures and results are shown in Fig.2. We also show in this figure the first s-SNOM data obtained in the PI's lab at room temperature very recently. We note that the data in panel a) were taken in a tip amplitude detection scheme which turned out to be unstable due to low temperature self-oscillating behavior. We have implemented and are currently doing final tests for the robustness of another detection scheme at low temperatures (see Fig.1). Demonstrating s-SNOM operation in this range is our immediate next goal.

Our proposal for collaboration with the Center for Functional Materials at Brookhaven has been accepted. This work is currently focused on metal deposition and characterization of our tuning fork based AFM probes. The commercially available probes have semiconducting tips (Si). Metallic coatings significantly increase the electromagnetic field strength at the tip apex.

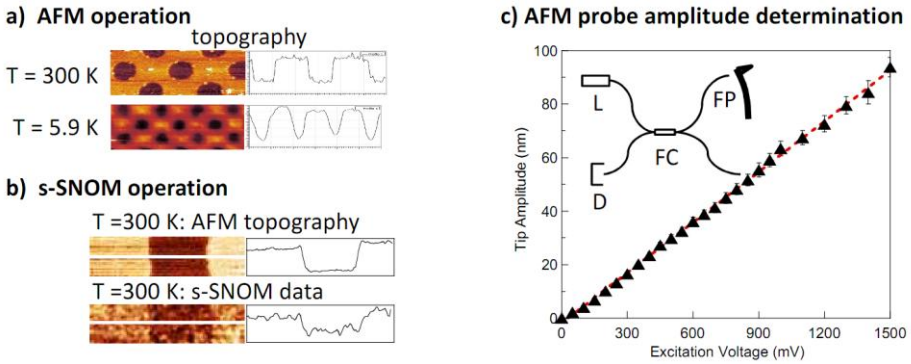

Fig.2: **a)** AFM operation tests at room and base temperatures (T = 5.9 K). **b)** s-SNOM scan along with topography at room temperature. The data were obtain by demodulating the signal at the second harmonic (S_2) of the tapping frequency (44 kHz) obtained from a calibration sample (20 nm thick SiO_2 lines patterned on Si). The true nature of the near-field data was checked by approach curves and by performing resonant contrast measurements taking advantage of the surface phonon excitation at the air-SiO2 interface with an energy $\omega \sim 1160\ cm^{-1}$, i.e. comparison of S_2(SiO2)/ S_2(Si) signals for two CO_2 laser excitation wavelengths: λ = 9.27 μm and 10.53 μm. c) Optical fiber based interferometry results for tip oscillation amplitude determination. L – laser, D – detector, FC – fiber coupler, FP Fabry – Perot cavity.

Future Plans:

- Metal-insulator transitions: **a)** vanadium oxides (V_2O_3); **b)** ferromagnetic semiconductors (Eu chalcogenides).
- Fe-based superconductors: inhomogeneous behavior and superconductivity.
- Studies of HTS cuprates (especially $La_{2-x}Sr_xCuO_4$): **a)** search for inhomogeneous behavior in the pseudogap phase of underdoped samples; **b)** plasmon excitations in hybrid structures; **c)** superconductivity in single-phase crystals/films, multi-layered structures and superlattices.
- Instrumentation: **a)** extend our mid-infrared capabilities to the far-infrared range by using broad band sources and the AFM tip as a part of an interferometer (asymmetric FTIR configuration) and/or a time-domain Terahertz setup; **b)** expand on the collaboration with Brookhaven's nano-center for fabrication of ultra-sharp probes and AFM tip shape tailoring.

Publications of DOE sponsored research (2010 – 2012):

J. Phys. Chem. Solids 71, 1098 (2010).
Physical Review Letters 106, 237003 (2011).
Physical Review Letters 108, 217401 (2012).

Current Trends in Scanning Probe Microscopy at the Center for Nanoscale Materials: Low-dimensional Materials at the Atomic Scale

Nathan P. Guisinger
Center for Nanoscale Materials, Argonne National Laboratory – Lemont, IL 60439
nguisinger@anl.gov

Research Scope and Definition

Low-dimensional materials functioning at the nanoscale are a critical component for a variety of current and future technologies. From the optimization of light harvesting solar technologies to large-scale catalytic processes, the key physical processes are occurring at the nanometer and atomic level and predominately at interfaces. For instance, graphene is a nearly ideal two-dimensional conductor that is comprised of a single sheet of hexagonally packed carbon atoms. In order fully realize the potential of graphene for novel electronic applications, large-scale synthesis of high quality graphene and the ability to control the electronic properties of this material on a nanometer length scale are key challenges. At the same time, the 2-dimensional interface of complex oxide heterostructures play a dominant role in the resulting physical properties of these strongly correlated materials. These interfaces present a difficult challenge for direct characterization. This poster highlights how scanning probe microscopy presents a series of powerful experimental tools that can overcome several challenges and allow for the direct characterization of several advanced materials.

Recent Progress

Here we will cover our novel cross-sectional scanning tunneling microscopy techniques for directly probing these interfaces at the atomic scale for the first time, as illustrated in Fig 1. We have demonstrated the reversible and local modification of the electronic properties of graphene by hydrogen passivation and subsequent electron-stimulated hydrogen desorption with a scanning tunneling microscope tip, as illustrated in Fig. 2. In this poster, I will also present our studies of graphene on single crystal Cu(111) surfaces and Cu foil by variable temperature scanning tunneling microscopy and spectroscopy.[1-4] We studied the bonding configurations between copper and carbon, as well as the atomic-scale electronic structure of the graphene on the copper surface. Our results provide valuable information for understanding the growth mechanism and the electronic quality of graphene on copper. The poster will also cover some of our recent studies of molecular technologies.

Future Plans

Future work includes optimized synthesis for large-scale "low-defect" graphene and advanced functionalization and modification. The study of several complex oxide interfaces and molecular systems that have applications ranging from organic photovoltaics to novel catalysis.

References

1. L. Gao, J. R. Guest, and N. P. Guisinger: Epitaxial Graphene on Cu(111), *Nano Lett.* **10**, 3512 (2010).
2. Q. Yu, *et al.*: Control and characterization of individual grains and grain boundaries in graphene grown by chemical vapour deposition, accepted *Nature Materials*, **10**, 443 (2011).
3. J. Cho, *et al.*: Atomic-scale investigation of graphene grown on Cu foil and the effects of thermal annealing, under review *ACS Nano*, **5**, 3607 (2011).
4. J. Cho, *et al.*: Structural and Electronic Decoupling of C60 from Epitaxial Graphene on SiC. *Nano Lett.* **10**, 3512 (2012).

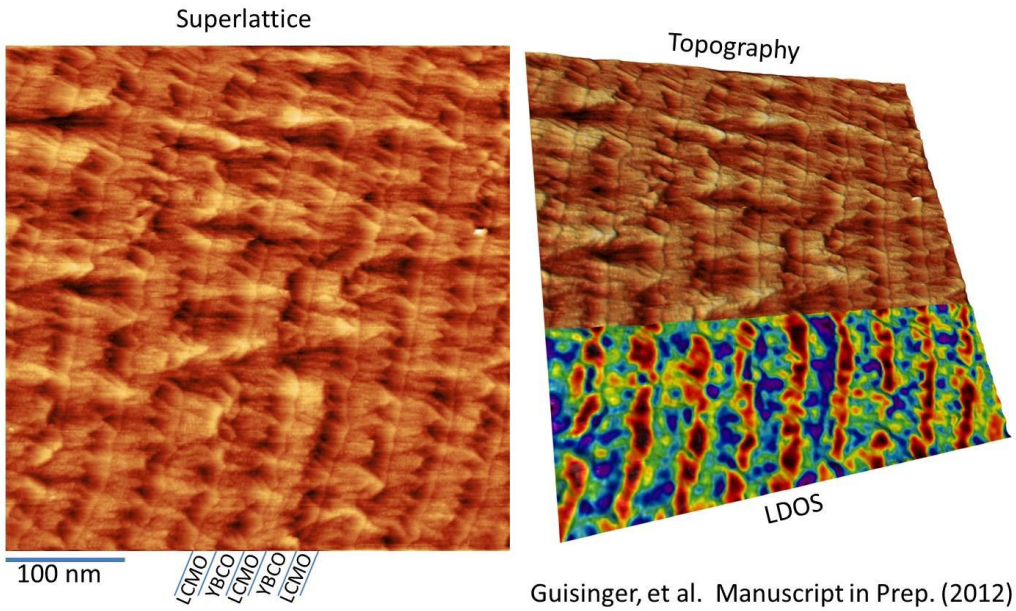

Figure 1: Cross-sectional STM utilized to study the interfaces of an oxide superlattice that includes simultaneous topographic and electronic band mapping.

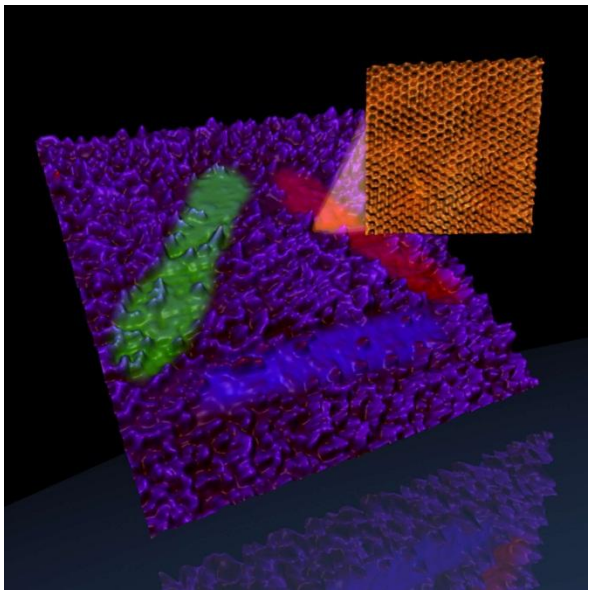

Figure 2: Argonne National Laboratory logo patterned at the atomic-scale (STM image rendered with false coloring added). Hydrogen saturated graphene was controllably patterned via STM induced electron stimulated desorption. The inset shows an atomic-scale image of the patterned graphene, which is structurally preserved and demonstrates the reversible nature of this process.

Probing electrochemical reactivity of solids in-operandi *below the 10 nm level*

S. Jesse, S.V. Kalinin, and A.P. Baddorf (sjesse, sergei2, baddorfap)@ornl.gov)

Postdocs and students: A. Kumar and E. Strelcov

Oak Ridge National Laboratory, Oak Ridge, TN 37831

Program scope

Many emerging information and energy storage and conversion technologies are based on systems in which the motion and reactions of ions define functionality. Batteries, fuel cells, and photo-electrochemical cells form the technological foundations of a greener future. Similarly, electroresistive and memristive materials hold the key to low-power, non-volatile memory storage and new generations of logic devices. However, as long as the nanoscale details of ionic transport and electrochemical processes in solids remain unknown and largely inaccessible, progress has been incremental. Here, we aim to explore electrochemical reactions and ionic flows in solids with resolution at the 10 nm level. This goal is being accomplished through a synergistic effort involving (a) development of advanced Scanning Probe Microscopies (SPM) for probing ionic transport and electrochemical behavior on the nanoscale over broad temperature and electric field ranges, (b) exploring the effects of single defects, interfaces, and catalyst particles on electrochemical activity and (c) control reactions at the tip surface junction by including "in-the-loop" reaction monitoring in order to study irreversible processes in detail. Once successful, these studies provide insight into atomistic mechanisms of bias-induced and field induced phase transformations on a single defect level and can be further integrated with in-situ structural studies to establish associated atomistic mechanisms.

Recent Progress

Local probing of bias-induced transformations: The SPM group at the CNMS is actively working on the development of scanning probe microscopy techniques for probing bias-induced (ferroelectric polarization switching, electrochemical reactions) and thermal (glass transition, melting) transformations on the nanoscale. In these experiments, the SPM tip focuses an electric or thermal field in a small (5 – 30 nm) region of material, inducing local transformations. In parallel, measured dynamic strain, resonance frequency shift, or quality factor of the cantilever (piezoresponse force microscopy, electrochemical strain microscopy) or tip-surface current (conductive AFM) provides information on processes in the material (polarization, domain size, ionic motion, second phase formation, melting) induced by the local stimulus. In the future, the detection strategies can include microwave, Raman, focused X-ray, electron microscopy, and other high-bandwidth local (~10 nm and below) structural and chemical probes. The unique aspect of this approach is that transformation can be probed in material volumes containing zero or single individual extended defects, paving a pathway for studying ***phase transformations and electrochemical reactions on a single defect level*** (as opposed to volume averaging for typical materials science methods; compare to the impact of molecular unfolding spectroscopy in biomolecular chemistry), a target of crucial importance for material science to link defect structure to its functionality.

Need for multidimensional SPM: The hardware platforms for these studies can be realized on 30,000+ SPMs worldwide and necessitate a classical development path of minimizing by noise level, improving drift stability, and introducing proper chemical and thermal environments. However, probing local bias- and temperature induced phase transitions in solids requires drastic improvement in the capability to collect and analyze multidimensional data sets, well beyond classical 2D imaging or 3D spectroscopic imaging. This can be demonstrated as follows:

- Spatial scanning necessitates data acquisition over 2D dense grid of points.

- Probing local transformation requires sweeping local stimulus (tip bias or temperature) while measuring the response.
- First order phase transitions are hysteretic and hence history dependent. This necessitates first order reversal curve type studies, increasing dimensionality of the data by one.
- First order transition often possess slow time dynamics, necessitating probing kinetic hysteresis (and differentiating it from thermodynamics) by measuring response as a function of time.
- Detection of force-based SPMs necessitates probing response in a frequency band around resonance .

These simple physical arguments illustrate that complete probing of local temperature-or bias induced transformations necessitate 6D (space x frequency x (voltage x temperature) x time) detection schemes. To date, we have realized several 5D detection schemes (first order reversal curves, time relaxation within hysteresis loop methods, amplitude sweeps). The time line of these techniques, corresponding technical requirements, and resultant publications is illustrated in **Table 1**. Note that the progress from 3D (Band Excitation (BE), Switching Spectroscopy Piezoresponse Force Microscopy (SSPFM)) to more complex 4D and 5D modes was realized on time scale from 2006 to the present. A broad set of these applications have been fully transferred to the CNMS user program including piezoresponse force microscopy and spectroscopy of ferroelectric materials, giving rise to multiple user-led publications.

Table 1. Development of multidimensional SPM methods

Technique	*Dimensionality*	*Data size**	*Data volume*
Band Excitation	3D, space and ω	(256 x 256) x 64,	32 MB
SS- PFM	3D, space and voltage	(64 x 64) x 128,	4 MB
Time relaxation PFM	3D, space and time	(64 x 64) x 128	4 MB
AC sweeps	4D, space, ω, voltage	(64 x 64) x 64 x 256	512 MB
BE SSPFM	4D, space, ω, voltage	(64 x 64) x 64 x 12	256 MB
BE thermal	4D, space, ω, temp	(64 x 64) x 64 x 256	512 MB
Time relaxation BE	4D, space, ω, time	(64 x 64) x 64 x 64	128 MB
First order reversal curves	5D, space, ω, voltage, voltage	(64 x 64) x 64 x 64 x16	2 GB
Time relaxation on voltage sweep, BE	5D, space, ω, voltage, time	(64 x 64) x 64 x64x64	8 GB
Temperature-Voltage-Time BE*	6D, space, ω, voltage, time, Temp	(64 x 64) x 64 x 64 x 64 x 16	128 GB

* As realized to date. For many parameters we aim to increase the number of data points
** Not yet realized

Electrochemical Strain Microscopy: In the last several years, we have developed the instrumental framework that has enabled a set of scanning probe microscopy techniques for probing bias-induced phase transitions locally, as exemplified by Electrochemical Strain Microscopy. In ESM, a biased SPM tip concentrates an electric field in a nanometer-scale volume of material, inducing interfacial electrochemical processes at the tip-surface junction and diffusive and electromigrative ionic transport through

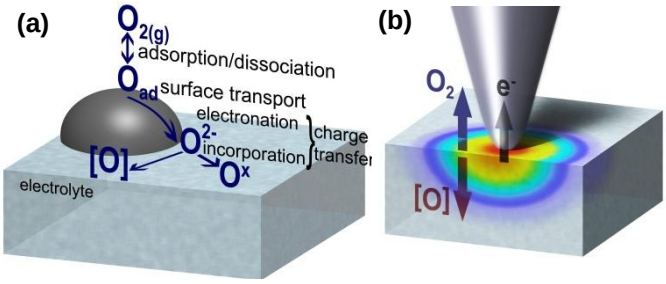

Figure 1. (a) Schematic representation of ORR/OER reaction mechanism in pure conductors and mixed-ionic electronic electrodes (b) ESM approach for probing local ORR/OER activity

the solid. The intrinsic link between the concentration of ionic species and/or oxidation states of the host cation and molar volume of the material results in strain and surface displacement. The sensitivity of standard SPM platforms allows for detection of 2-5 pm surface allows for a 6-8 order of magnitude reduction in probing volume as compared to classical electrochemical strategies based on Faradaic current measurements.

S. Jesse has led the effort towards the application of ESM to solid oxide fuel cell material as illustrated in **Figure 1**. In classical fuel cells, the gas-solid reaction (e.g., oxygen reduction reaction (ORR) and oxygen evolution reaction (OER)) is catalyzed by a metallic nanoparticle on the surface and can proceed through multiple surface and bulk transport and reaction steps. In ESM, a sharp SPM tip plays the triple role of mobile electrode that creates a local electrochemical potential gradient, electrocatalytic nanoparticle (depending on the tip coating), and probe of local surface deformation induced by the bias. The measured strain signal provides information on local electrochemical functionality.

To illustrate the reactivity mapping of oxygen vacancies, ESM was applied to LSCO and to Pt-nanoparticles on a Yttrium Stabilized Zirconia (YSZ) surface as shown. In **Figure 2a**, close agreement is found in a comparison between the local ESM measurements of hysteresis loop width to the standard, macroscale electro-chemical impedance spectroscopy measurement (EIS) of area specific resistance of oxygen for several, differently prepared samples [Kumar, submitted]. In **Figure 2b**, the aim was to probe the triple phase boundary, at which the catalyst electrode is in contact with the reactants and the electrolyte, forming a critical unit in a catalyzed reaction. The ESM response was mapped over a 300 nm region containing the nanoparticles. The reactivity map is overlaid on topography revealing increased reactivity close to the triple phase boundary in comparison to the free YSZ surface. Note the relatively weak ESM response of the particle itself, the sharp increase of reactivity at the triple-phase junction, and low reactivity in the YSZ surface. For a tip positioned on the nanoparticle, the particle is biased as a whole, and the oxygen reduction/evolution reaction (ORR/OER) is activated.

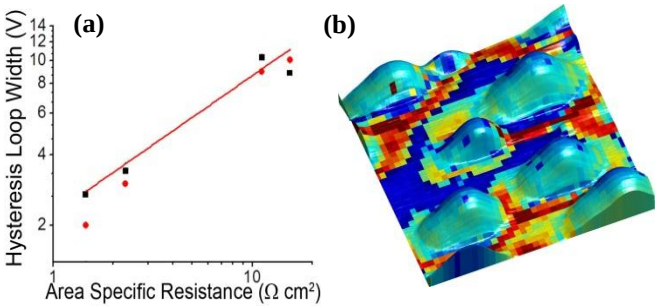

Figure 2. ESM on oxygen conductors. (a) Comparison of nanoscale ESM loop width with EIS macroscale measurements of LSCO surfaces (b) Overlay of electrochemical activity on the topography of Pt nanoparticles on YSZ reveals enhanced activity at the triple phase boundary.

Future plans:

Our goal is to understand the basic mechanisms of temperature and gas-solid reactions in electrochemical processes for energy and information technologies on the nanoscale. An SPM tip will be used as a combined local heat source, electrode, and displacement/strain sensor, thus allowing one to induce and control local electrochemical processes while probing the temperature and voltage dependence of the kinetics and thermodynamics of local reactivity. To reach this goal we will focus on three specific aims: (1) Understanding ionic transport and electrochemical behavior on the nanoscale over broad temperature and electric field ranges at the junction between the tip and the surface. This will involve constructing local temperature-voltage phase diagrams from multi-dimensional ESM measurements of material on the order of $(10\ nm)^3$ in size. (2) Determine the effects of single defects and catalysts particles on electrochemical activity by mapping variations in local phase diagrams to ultimately image activation energy with nanoscale resolution. (3) Control reactions at the tip surface junction by including reaction monitoring "in-the-loop" in order to study in detail irreversible processes by adjusting local temperature and voltage to slow or arrest reactions.

These goals will be achieved through the development of scanning probe microscopy based methods capable of mapping the local (< 30 nm) voltage and temperature dependent ionic, electronic,

and electrochemical processes in oxygen-ion conducting materials. Accomplishing this will involve developing an experimental platform for manipulating experimental conditions locally, decipher mechanisms of electrochemical processes at the tip-surface junction and linking these to experimentally measurable signals, extend this framework to acquire functional maps of systems with well-defined defect types, and develop instrumentation and control schemes to investigate irreversible electrochemical processes.

- **Bi-crystal Grain Boundaries (GB)** in materials such as YSZ and Ceria potentially allow one to distinguish the variability of diffusion coefficients for different ions on well characterized defects. It has been reported that in these materials the oxygen diffusivity is reduced at the GB's, whereas proton diffusion is enhanced
- **Metal nanoparticles on ionic conductor surfaces** are ideal model systems for probing triple-phase boundary effects in electrocatalysis. Individual nanoparticles and combinatorial arrays of varying geometries, sizes, and composition within the nanoparticles are readily available to the PI through existing collaborations.
- **Crystallographic Shear Planes (CSP)** in oxides such as TiO_2 offer an ideal model defect that possesses high electronic conductivity but reduced ionic conductivity. Note that ionic motion in materials such as TiO_2 can be probed directly by ESM, suggesting the feasibility of these studies. The CSP can be induced by the application of significantly high biases using interdigitated electrode geometries or heating under strongly reducing conditions. These systems will allow probing of the role of local electronic conductivity on ESM signal formation mechanisms.
- **Superionic interfaces** between materials such as $SrTiO_3$ and YSZ offer an example of a low-dimensional object with greatly enhanced ionic conductivity. Note that the enhancement of ionic conductivity can be due to space charge effects (Maier model), or from the formation of vacancy-rich or amorphous layers. We expect that ESM will both provide identifiable signals and will contribute to establishing origins of enhanced ionic conductance.

As the project progresses and the technique matures, knowledge acquired from model systems will be applied to more realistic systems including polycrystalline SOFC electrolyte.

Research sponsored by the U.S. Department of Energy, Office of Basic Energy Sciences, Division of Scientific User Facilities (SVK, SJ, BJR, and APB) and by the Laboratory Directed Research and Development program. The work is done in collaboration with L.Q. Chen (Penn State), R. Ramesh (UC Berkeley), M. Alexe (MPI Halle) and A. Morozovska (Ukrainian Academy of Science). The SS-PFM and Band Excitation SPM capabilities are available for user research at the CNMS.

DOE-sponsored publications 2009-2012 enabled by this work [In total, ~32 peer-reviewed papers (1 Nature Mat, 1 Nat Chem, 1 PNAS, 1 Phys. Rev. Lett., 3 Adv. Mat., 3 Nano Lett, 4 ACS Nano)]

References

1. KUMAR, F. CIUCCI, A.N. MOROZOVSKA, S.V. KALININ, and S. JESSE, *Measuring oxygen reduction/evolution reactions on the nanoscale,* Nature Chem. **3**, 707 (2011).
2. S. JESSE, N. BALKE, E. ELISEEV, A. TSELEV, N. DUDNEY, A.N. MOROZOVSKA, and S.V. KALININ, *Direct mapping of ionic transport in* Si-*anode on the nanoscale: time domain electrochemical strain spectroscopy study,* ACS Nano **5**, 9682 (2011).
3. (Invited review) S. JESSE and S.V. KALININ, *Band Excitation in Scanning Probe Microscopy: Sines of Change,* J. Phys. **D 44**, 464006 (2011).

Probing Coupled Metal-Insulator and Ferroic Transitions from the Atomistic to Mesoscopic Scales

S.V. Kalinin and P. Maksymovych (sergei2, maksymovych)@ornl.gov)

Postdocs: A. Tselev (research professor), Y. Kim, W. Lin

Oak Ridge National Laboratory, Oak Ridge, TN 37831

Program scope

The coupling between electronic and ferroic behaviors has emerged as one of the most intriguing aspects of condensed matter physics, with examples including phase separation in complex oxides, metal-insulator transitions in ferroelastic oxides, and complex electronic ordering patterns in superconducting and charge-density wave materials. Both structural and electronic aspects of these behaviors are currently of interest for energy generation and storage applications, and are uniquely accessible through high-resolution probe-based studies. The overarching goal of this project is to reveal the mechanisms of coupled electronic (metal-insulator) and ferroic (ferro- and antiferroelastic, ferro and antiferroelectric) transitions from atomistic to mesoscopic scales by exploring coupled electronic and atomistic structures on the length-scale of a single domain, structural defect, and domain wall. The research will develop and exploit the synergy between advanced scanning probe microscopy, artificial-intelligence and multivariate methods for theory-experiment matching, and established methodologies of surface science and oxide growth. The SPM tip will act as a local probe of the ferroic and electronic state of matter, communicating local properties to the outside world through measured electronic current, dynamic and static electromechanical response, resonant frequency and quality factor of the cantilever, and microwave response, thus ***exploring*** and ***actively manipulating*** local order parameters in nanoscale volumes. Unraveling and subsequently understanding the energy balance between competing interactions will pave the way to deterministic design of novel electronic materials, and reveal the key structural and electronic mechanisms involved in energy storage, generation and dissipation processes. This will provide a fundamental scientific basis for optimization and engineering of energy-related materials, with enormous potential benefits to fuel cells, batteries, solar energy, data storage, energy transport, and other vital energy technologies.

Recent Progress

The present FWP is a new initiative, and much of the effort is directed towards development of the instrumental base. However, in the concurrence period the available experimental facilities at the Center for Nanophase Materials Sciences, ORNL, have allowed for experimental progress. The exploration of ferroelectric domain walls and ferroelectric vortex cores at the mesoscopic level has elucidated the non-trivial role of oxygen vacancies in measured responses. This, in turn, led us to explore the ionically-mediated electromechanical phenomena and metal insulator transitions in simple oxides such as TiO_2 and NiO, an effort required to build comprehensive picture of nanometer-scale physical functionalities allowing for electrochemical degrees of freedom. In pursuance of the primary goal of the proposal, we have explored structure - order parameter coupling in model layered pnictide systems and developed data analysis tools for correlating structural and spectroscopic image data. Finally, initial progress was achieved on the in-situ oxide growth. This progress is summarized below.

Mesoscopic polarization mediated functionality at ferroic walls. Topological defects in ferroic materials are attracting much attention both as a playground of unique transport, magnetic, and ferroic phenomena and due potential applications in reconfigurable electronic devices. In a joint effort with the Center for Nanophase Materials Sciences, we have explored transport phenomena in 2D (domain walls) and 1D (vortexes and antivortexes) in ferroelectric materials by combination of piezoresponse force microscopy, phase-field modeling, and density functional theory. Unexpectedly, conductance in

domain walls and vortex cores was found to exhibit pronounced memory effects and hysteresis, behaviors that cannot be explained by a simple physical picture of wall-induced static conductive channel. For domain walls, these observations are consistent with carrier accumulation due to presence of charged wall segments. Exploring these behaviors, we demonstrate that a continuum of non-volatile metallic states across decades of conductance can be encoded in the size of ferroelectric nanodomains using electric field. These studies were further extended to demonstrate metallic conductivity of ferroelectric walls, a long predicted but not until now observed behavior. Similar studies were extended to conductivity in vortex cores. For vortexes, phase field modeling predicts that the core structure can undergo a reversible transformation into a metastable twist structure, extending charged domain walls segments through the film thickness. The vortex core is therefore a dynamic conductor controlled by the coupled response of polarization and electron/mobile vacancy subsystems with external bias. This controlled creation of conductive 1D channels opens a pathway for design and implementation of integrated oxide electronic devices based on domain patterning.

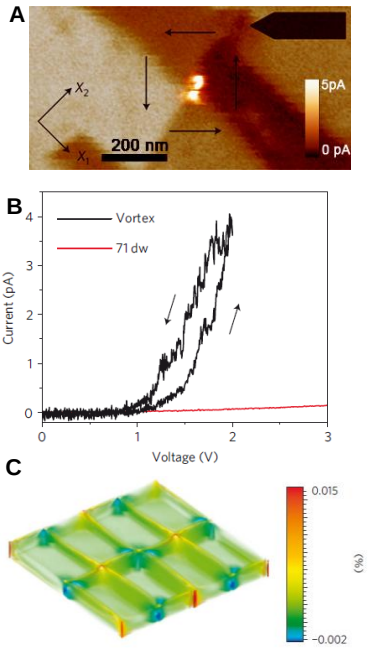

Fig. 1. Enhanced conductivity at vortex cores. (A) The in-plane PFM image of a fabricated vortex structure, with c-AFM overlay showing conductivity at the core. **(B)**The I-V curve at the vortex core, in comparison with 71° domain walls. **(C)** Trace of strain tensor of the vortex/anti-vortex lattice

Ionically-controlled physical properties in oxides: The analysis of the conductivity data combined with recent electron microscopy observations strongly suggests that ionic dynamics can play a significant role in nanoscale behaviors of oxides. This lead us to explore the electromechanical phenomena and coupling between ionic behaviors and physical phenomena in simple (non-ferroelectric) oxides including TiO_2, $SrTiO_3$, and NiO. Using local scanning probe microscopy approach, electromechanical activity, remanent polarization states, and hysteresis loops in paraelectric TiO_2 and $SrTiO_3$ are observed. The coupling between the ionic dynamics and incipient ferroelectricity is analyzed using extended Ginsburg Landau Devonshire (GLD) theory. Possible origins of electromechanical coupling including ionic dynamics, surface-charge induced electrostriction, and ionically-induced ferroelectricity are identified. For the latter, the ionic contribution can change the sign of first order GLD expansion coefficient, rendering material effectively ferroelectric. These studies provide explanation for ferroelectric-like behavior in centrosymmetric transition metal oxides.

These studies were further extended to demonstrate the presence of inverse effect, namely pressure induced changes in vacancy concentration and concurrent MIT in simple oxides. We have predicted and experimentally observed the pressure-induced changes in conductivity of transition metal oxides presumably mediated by changes in oxygen stoichiometry, behavior we refer to as ***piezochemical effect***. This behavior is expected to be universal in transition metal oxides and can be predicted based on deformation potential, flexoelectric effect, and chemical expansivity. The piezochemical effect allows mechanical manipulation of local resistivity down to the nanometer level. This provides insight into the pressure-controlled physics of transition metal oxides, and also allows development of novel information storage devices with mechanical recording and current readout.

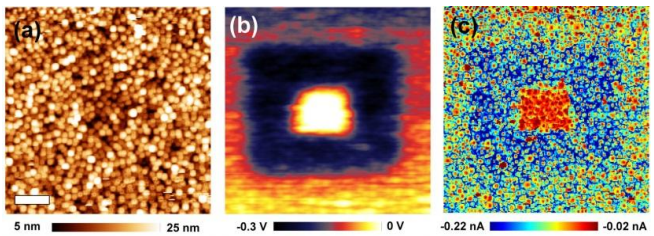

Figure 2. Piezochemical switching of surface conductance in NiO. (a) Topography, (b) KPFM, and (c) CAFM images after box patterning by a diamond coated tip: background box pattern: bias voltage of -6 V, inner box pattern: set point of 1.5 V. CAFM images in (c) were taken under -2 V. Scale bar is 1 μm.

Structure-order parameter coupling on the atomic level in model systems. We aim to explore the coupling between ferroic order parameters and electronic properties on the atomic level. In oxides, these behaviors are additionally mediated by mobile defects such as oxygen vacancies, the role of which increases for small length scales. To develop the necessary know-how and analysis methods for probing the coupling between electronic properties and structural order parameters, we teamed with Minghu Pan (CNMS) to explore model superconductive FeTeSe system. These materials offer the advantage of atomically flat defect-free surfaces that can be prepared by cleaving and readily identifiable from dI-dV curves superconductive order parameter. Here, we explored the surface structure of Fe(TeSe) using high resolution structural mapping. The atomic positions extracted from STM images were used to construct chemical composition map that can further be correlated with superconductive gap derived from dI/dV spectroscopic mapping. Using this approach, we have identified 1D chemical defects formed by Se segregation and quantitatively determine its effect on local supercondictivity. We now aim to extend this approach to structural and topological defects in oxides.

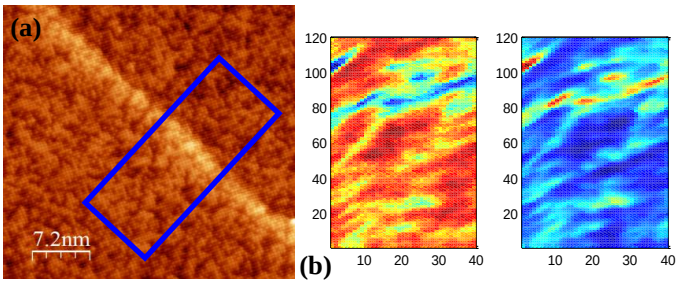

Figure 3. (a) Atomically-resolved STM image and (b) principal component analysis of the I-V spectroscopic image acquired in the box in (a). Electronic inhomogeneity at the defect is clearly seen.

In-situ oxide growth. We aim to extend the mesoscopic studies of order parameter-electronic property couplings and atomic level studies to realistic oxide surfaces. To achieve this goal, the surfaces should be grown in situ. Via a peer reviewed user project, the CNMS NanoTransport system combining PLD growth and surface characterization, was used to grow and characterize by atomically resolved STM surfaces of $SrRuO_3$, a prototypical perovskite. In the near future, we aim to switch from resistive to laser heating of the sample plate to enable growth at higher temperatures necessary for ferroelectrc materials.

Future plans: Understanding of the fundamental physics of coupling between electronic properties and ferroic behaviors on strongly correlated oxide surfaces necessitates a synergistic effort that involves (a) *in-situ* studies of grown or cleaved surfaces free of chemisorbed species, (b) development of strategies for comprehensive structural and property measurements locally, (c) advanced software and hardware for fast data acquisition and processing beyond conventional probe microscopy, and (d) theoretical framework that allows describing the coupling between structural degrees of freedom described by appropriate order parameter fields, electronic properties, and (as a newly realized parameter) concentration of oxygen vacancies. Our research will pursue these directions, aimed at the following fundamental issues:

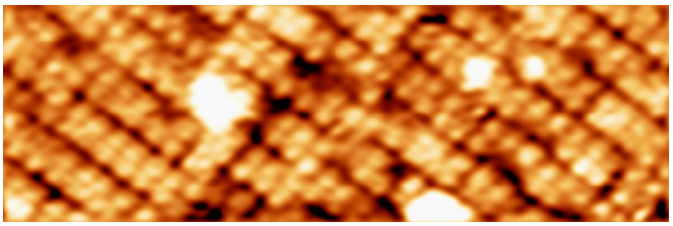

Figure 4. Atomically-resolved STM image of PLD grown $SrRuO_3$ on $SrTiO_3$.

- **Structure and electronic properties at topological defects:** We will pursue a systematic approach to characterization and manipulation of existing topological defects on one hand, and material design on the other to answer the fundamental question of how topological and structural defects give rise to novel electronic behaviors. We will explore the static and dynamic properties of existing topological defects in the order parameter field (e.g. domain walls corresponding to different

order parameters and their junctions), as well as those dynamically created in the sub-surface volume by the confined electric and elastic fields of a scanning probe tip.

- **Designing and probing local order parameters at epitaxial interfaces**. We aim to pursue the effect of mismatch in an order parameter (e.g. octahedral tilts, Jahn-Teller distortion, in-plane orderings) on ferroic and electronic states. We aim to answer (a) whether suppression of a structural order parameter such as octahedral tilts across the interface can lead to novel ferroic states in materials with a soft-phonon instability; (b) whether a similar effect can tune or suppress correlated-electron phase transitions; (c) explore the evolution of in-plane and thickness-dependent structural and polarization instabilities, and (d) whether these properties can be manipulated and controlled locally. We will utilize tunneling spectroscopy and microscopy to obtain direct and local measurements of the electronic structure in these systems with epitaxial interfaces.
- **Atomistic origins of order parameters and defect interactions.** We aim to reveal the atomistic structure of the order parameter and order-parameter defect interactions in several model materials with strong coupling between electronic properties and atomic level structural deformations amenable to high-resolution scanning tunneling microscopy. The questions include (a) can we understand the atomistic aspects of collective interactions leading to the emergence of a polar order parameter, (b) can the changes in bonding and electronic structures induced by discontinuities by an order parameter field and structural defects be probed on the atomic level, and (c) can the order parameter be manipulated and used to tailor local electronic properties of surfaces.

Research supported by the U.S. Department of Energy Office of Basic Energy Sciences Division of Materials Sciences and Engineering and performed at the Center for Nanophase Materials Sciences supported by Division of Scientific User Facilities (SVK, PM, YK WL, and AT). The work is done in collaboration with L.Q. Chen (Penn State), M. Alexe (MPI Halle) and A. Morozovska (Ukrainian Academy of Science).

DOE-sponsored publications 2010-2012 [10 peer-reviewed papers including 1 *Nature Phys*., 1 *Nature Comm*., 1 *Phys. Rev. Lett*., 2 *ACS Nano*, 1 *Nano Lett*., 1 plenary and 4 invited talk**s]**

1. N. BALKE, B. WINCHESTER, W. REN, Y.H. CHU, A.N. MOROZOVSKA, E.A. ELISEEV, M. HUIJBEN, R.K. VASUDEVAN, P. MAKSYMOVYCH, J. BRITSON, S. JESSE, I. KORNEV, R. RAMESH, L. BELLAICHE, L.Q. CHEN, and S. V. KALININ, *Enhanced electric conductivity at ferroelectric vortex cores in* $BiFeO_3$, Nature Physics **8**, 81 (2012).
2. A.Y. BORISEVICH, E.A. ELISEEV, A.N. MOROZOVSKA, C.J. CHENG, J.Y. LIN, Y.H. CHU, D. KAN, I. TAKEUCHI, V. NAGARAJAN, and S.V. KALININ, *Atomic-scale evolution of modulated phases at the ferroelectric-antiferroelectric morphotropic phase boundary controlled by flexoelectric interaction*, Nature Communications **3**, 775 (2012)
3. P. MAKSYMOVYCH, A.N. MOROZOVSKA, P. YU, E.A. ELISEEV, Y.H. CHU, R. RAMESH, A.P. BADDORF, and S.V. KALININ, *Tunable metallic conductance in ferroelectric nanodomains*, Nano Lett. **12**, 209 (2012).
4. Y. KIM, A. KUMAR, O. OVCHINNIKOV, S. JESSE, H. HAN, D. PANTEL, I. VREJOIU, W LEE, D. HESSE, M. ALEXE, and S.V. KALININ, *First-Order Reversal Curve Probing of Spatially Resolved Polarization Dynamics in Ferroelectric Nanocapacitors*, ACS Nano **6**, 491 (2012).
5. P. MAKSYMOVYCH, M. HUIJBEN, M. PAN, S. JESSE, N. BALKE, Y.H. CHU, H.J. CHUNG, A.Y. BORISEVICH, A.P. BADDORF, G. RIJNDERS, D.H.A. BLANK, R. RAMESH, and S.V. KALININ, *Ultrathin Limit and Dead-layer Effects in Local Polarization Switching of* $BiFeO_3$, Phys. Rev. **B 85**, 014119 (2012).
6. E.A. ELISEEV, A.N. MOROZOVSKA, G.S. SVECHNIKOV, P. MAKSYMOVYCH and S.V. KALININ, *Domain wall conduction in multiaxial ferroelectrics*, Phys. Rev. **B 85**, 045312 (2012).
7. A.N. MOROZOVSKA, E.A. ELISEEV, S.L. BRAVINA, F. CIUCCI, G.S. SVECHNIKOV, L.Q. CHEN, and S.V. KALININ, *Frequency Dependent Dynamical Electromechanical Response of Mixed Ionic-Electronic Conductors*, J. Appl. Phys. **111**, 014107 (2012).
8. A.N. MOROZOVSKA, E.A. ELISEEV, and S.V. KALININ, *Electrochemical strain microscopy with blocking electrodes: the role of electromigration and diffusion*, J. Appl. Phys. **111**, 014114 (2012).
9. A.N. MOROZOVSKA, E.A. ELISEEV, S.V. KALININ, L.Q. CHEN and V. GOPALAN, *Surface polar states and pyroelectricity in ferroelastics induced by roto-flexo field*, Appl. Phys. Lett. **100**, 142902 (2012).

CORRELATED MATERIALS: SYNTHESIS AND PHYSICAL PROPERTIES

PIs: I. R. Fisher, T. H. Geballe, A. Kapitulnik, S. A. Kivelson, K. A. Moler,

Abstract by: **Aharon Kapitulnik**

Geballe Laboratory for Advanced Materials, Stanford University, and
Stanford Institute for Materials & Energy Science, SLAC National Laboratory.
Email: aharonk@stanford.edu

Program scope

This FWP is part of the newly-formed Stanford Institute for Materials and Energy Sciences (SIMES), which is the Materials Science Division at the SLAC National Accelerator Laboratory. Within our specific FWP, our efforts aim to address the grand challenge of "emergence" as well as a number of "Basic Research Needs" areas for energy applications in the realm of quantum materials. Understanding and ultimately controlling this class of materials has the potential to profoundly impact the next generation of electronic materials relevant to addressing our nation's energy needs. From new quantum states that enable computing with vastly lower power consumption, to new superconductors that better suit power transmission requirements, quantum materials hold the promise of advanced applications as well as providing some of the deepest and most challenging intellectual questions. Our research encompasses the fields of superconductivity, charge and spin order, non-Fermi liquid behavior, and most recently topological insulators. Our focus is on understanding fundamental factors determining the often complex, electronic properties of these materials. We combine crystal growth and characterization of novel materials (Fisher, Geballe), local electronic and magnetic (Kapitulnik, Moler) measurements, and theory (Kivelson). We collaborate extensively, both within SIMES and externally, and materials synthesized as part of this program enable research at diverse other universities and laboratories.

High Resolution Magneto-optics and STM Studies of complex electronic materials

I. Progress report

In the past two years we emphasized three different directions in exploring novel properties of complex electronic systems. Below we describe these efforts.

a) Optical studies of the pseudogap in high-Tc superconductors

One of the most challenging puzzles that has emerged within the phenomenology of the high-temperature superconductors (HTSC) is to understand the occurrence and role of the normal-state "pseudogap" phase in underdoped cuprates. This phase exhibits anomalous behavior of many properties including magnetic, transport, thermodynamic, and optical properties below a temperature, T*, large compared to the superconducting (SC) transition temperature, Tc. To date, not only do we not know the origin of the pseudogap state, there is also no consistent experimental picture of its relation to superconductivity. While in one class of theories, T* represents a crossover into a state with preformed pairs with a d-wave gap symmetry, in other, T* marks a true transition into a phase with broken symmetry which ends at a quantum critical point. While at low-doping this phase may compete with superconductvity, it might provide fluctuations that are responsible for the enhanced Tc near its quantum critical point.

Our work emphasizes high-resolution linear-birefringence and magneto-optical (MO) data on several HTSC systems. While the birefringence measurements accurately locate structural phase transitions and/or transitions into a charge-ordered phase, while an onset of a MO-Kerr effect indicates that time-reversal-symmetry (TRS) is broken below that temperature. The above effects exhibit a

markedly stronger signal in the case of $La_{2-x}Ba_xCuO_4$ (LBCO) with x=1/8. For this system a first-order structural transition from an orthorhombic to tetragonal phase is accompanied by an onset of a Kerr signal. The signal then exhibits a weak inflection at the charge order transition, rises to a maximum around the spin-order transition, and decreases to a finite value when superconducting correlations are substantial. However, despite the sharp onset of the Kerr signal, hysteretic training effects are observed, indicating that TRS has been broken at much higher temperatures. Such an effect was previously observed in YBCO, especially close to x=1/8 doping on single-layer BSCO, and has recently reported on similar LBCO crystals These results, together with detailed magnetic studies on similar crystals may point to a unique magnetic structure in the material that is strongly altered when charge-ordering takes place so as to allow the Kerr effect to be visible.

b) STM studies of the topological insulators Bi_2Te_3 and Bi_2Se_3.

A topological insulator (TI) has a full energy gap in the bulk, and contains gapless surface states that cannot be destroyed by any non-magnetic impurities. Because of time reversal symmetry, the surface states cannot be back-scattered by non-magnetic impurities. When a thin magnetic layer is applied on the surface, a full insulating gap is opened, and an electric charge close to the surface is predicted to induce an image magnetic monopole. When a thin superconducting layer is applied on top of the surface, elementary excitations are predicted to be Majorana fermions. This brief account of TI systems suggest that they may provide a novel platform for device physics, including low-impedance interconnects, unique switching devices, or provide basic building blocks for topological quantum computing systems. However, to date most applications of these materials are hampered by bulk and surface defects. Thus, it is of utmost importance to understand the electronic properties of the surface of TIs in the presence of impurities and defects. Scanning tunneling spectroscopy (STM) is particularly suitable for such studies.

STM studies on high-quality 3D topological insulators (TI) Bi_2Te_3 and Bi_2Se_3 crystals exhibit perfect correspondence to ARPES data, hence enabling identification of different regimes measured in the local density of states (LDOS). Oscillations of LDOS near a step are analyzed. Within the main part of the surface band oscillations are strongly damped, supporting the hypothesis of topological protection. At higher energies, as the surface band becomes concave, oscillations appear which disperse with a particular wave-vector that is shown to result from an unconventional hexagonal warping term.

Further analysis of the data, beyond the oscillations, reveal a one-dimensional bound state that runs parallel to the step-edge and is bound to it at some characteristic distance. This bound state is clearly observed in the bulk gap region, while it becomes entangled with the oscillations of the warped surface band at high energy, and with the valence band states near the Dirac point. We obtain excellent fits to theoretical predictions that properly incorporate the three-dimensional nature of the problem to the surface state. Fitting the data at different energies, we can recalculate the LDOS, originating from the Dirac band without the contribution of the bulk bands or incoherent tunneling effects.

Finally, we look at the effect a local impurity on the surface of the TI, on the local density of states. We find that the LDOS around the Dirac point of the electronic spectrum at the surface is significantly disrupted near the impurity, exhibiting a low-energy resonance state. However, we find that for most common impurities, this is not sufficient to locally destroy the Dirac point.

c) Theoretical investigations of some unconventional superconductors.

Using an asymptotically exact weak coupling analysis of a multi-orbital Hubbard model of the electronic structure of Sr_2RuO_4, we show that the interplay between spin and charge fluctuations leads unequivocally to triplet pairing which originates in the quasi-one dimensional bands. The resulting superconducting state spontaneously breaks time-reversal symmetry and is of the form "p_x+ip_y" with sharp gap minima and a d-vector that is only weakly pinned. The superconductor is topologically trivial and hence lacks robust chiral Majorana fermion modes along the boundary. The absence of

topologically protected edge modes could explain the surprising absence of experimentally detectable edge currents in this system.

Given that indeed Sr_2RuO_4 is a two-component p-wave superconductor, there exists the possibility of well-defined collective modes corresponding to fluctuations of the relative phase and spin-orientation of the two components of the order parameter. We demonstrate that at temperatures much below Tc, these modes have energies small compared to the pairing gap scale if the superconductivity arises primarily from the quasi 1D (d_{xz} and d_{yz}) bands, while it is known that their energies become comparable to the pairing gap scale if there is a substantial involvement of the quasi 2D (dxy) band. Therefore, the orbital origin of the superconductivity can be determined by measuring the energies of these collective modes.

II. Future Plans

We plan to continue the above studies emphasizing our unique capabilities and broadening our materials selection. In particular we plan to study the magneto-optic properties of several other High-Tc systems including the Hg-based compounds and Bi:2212; Preparing high-quality topological insulator films, we also plan to expand our STM work in that field to include TI films and devices.

III. Publications in the past two years

1. Suk Bum Chung, Srinivas Raghu, Aharon Kapitulnik, Steven A. Kivelson, "Charge and spin collective modes in a quasi-1D model of Sr_2RuO_4," arXiv:1206.5330, accepted for publication in Phys. Rev. B (2012).

2. Hovnatan Karapetyan, M. Hucker, G. D. Gu, J. M. Tranquada, M. M. Fejer, Jing Xia, A. Kapitulnik, "Magneto-optical signatures of a cascade of transitions in $La_{2-x}Ba_xCuO_4$," arXiv:1203.2977 , Accepted for publication in Phys. Rev. Lett. (2012).

3. Zhanybek Alpichshev, Rudro R. Biswas, Alexander V. Balatsky, James G. Analytis, Jiun-Haw Chu, Ian R. Fisher, Aharon Kapitulnik, "STM imaging of impurity resonances on Bi_2Se_3," Phys. Rev. Lett 108, 206402 (2012).

4. Rui-Hua He, M. Hashimoto, H. Karapetyan, J. D. Koralek, J. P. Hinton, J. P. Testaud, V. Nathan, Y. Yoshida, Hong Yao, K. Tanaka, W. Meevasana, R. G. Moore, D. H. Lu, S.-K. Mo, M. Ishikado, H. Eisaki, Z. Hussain, T. P. Devereaux, S. A. Kivelson, J. Orenstein, A. Kapitulnik, Z.-X. Shen, "From a single-band metal to a high-temperature superconductor via two thermal phase transitions," Science 331, 1579-1583 (2011).

5. Nicholas P. Breznay, Karen Michaeli, Alexander M. Finkel'stein, Mihir Tendulkar, Konstantin S.Tikhonov, and Aharon Kapitulnik, "Fluctuation Hall conductivity in superconducting films," Phys. Rev. B 86, 014514 (2012).

6. S. Raghu, A. Kapitulnik, S. A. Kivelson, "Hidden quasi one-dimensional superconductivity in Sr_2RuO_4," Phys. Rev. Lett. 105, 136401 (2010).

7. Zhanybek Alpichshev, J. G. Analytis, J.-H. Chu, I. R. Fisher, and A. Kapitulnik, "STM Imaging of a bound state along a step on the Surface of Bi_2Te_3," Phys. Rev. B 84, 041104 (2011) [Editor's Choice].

8. Zhanybek Alpichshev, J. G. Analytis, J.-H. Chu, I. R. Fisher, Y. L. Chen, Z. X. Shen, A. Fang, and A. Kapitulnik, "STM imaging of Electronic Waves on the surface of the topological insulator Bi2Te3: Topologically Protected Surface States and Hexagonal Warping Effects," Phys. Rev. Lett. 104, (2010), 016401 [cover page].

Probing transport and structure relations on the nanoscale with cryogenic four-probe scanning tunneling microscopy

An-Ping Li, Arthur P. Baddorf

(apli@ornl.gov, baddorfap@ornl.gov)

Postdocs: Kendal Clark, Tae-Hwan Kim, Shengyong Qin

Center for Nanophase Materials Sciences, Oak Ridge National Laboratory, Oak Ridge, TN 37831

Program scope:

Electron transport at the nanoscale is the key to the novel applications of nanomaterials in electronic and energy technologies. Due to the restricted dimensionality, one distinctive character of nano-systems is transport properties that are critically dependent on the structural details. Therefore, an important requirement for transport research of a specific nanomaterial system is to examine its structures and properties in a coherent manner. In this program, we aim to understand the transport on multiple length-scales and its coupling to the electronic and structural properties down to the atomic scale. Our effort has involved (a) development of advanced techniques and processes capable of probing electronic transport on the nanometer scale based on cryogenic multiple-probe STM measurements, (b) combined scanning tunneling and electron microscopies for probing local metal-insulator transitions on the sub-micron level, (c) correlated study on the effects of atomic defects and interwire coupling on the electronic and transport properties of ultra thin quantum wire system, and (d) direct measurement of individual grain boundary resistances in copper nanowires with one-to-one correspondence to the grain boundary structure. (e) demonstration of ferroelectric field effect transistor in individual CdS nanotetrapods. Our recent progress and future plans are summarized in the following sections grouped by research projects.

Research progress:

Correlating electronic transport to atomic structures in self-assembled quantum wires. Quantum wires are extremely narrow one-dimensional (1D) materials where electron motion is allowed only along the wire direction, and is confined in the other two directions. Quantum wires, as a smallest electronic conductor, are expected to be a fundamental component in all quantum electronic architectures. The electronic conductance in quantum wires, however, is often dictated by structural instabilities and electron localization at the atomic scale. In this project, we have performed the first correlated study of electronic properties by utilizing both scanning tunneling microscopy and nanotransport measurements on the same nanowire as the nanowires are assembled *wire-by-wire*. Individual nanowires have a width of 16.7 Å, a height of 4 Å, and lengths of micrometers, and embody one of the closest realizations of 1D conductors. Amazingly, these nanowires can be grown either in the form of isolated nanowires or bundles with a number of constituent wires separated by an atomic interwire spacing. We have examined the correlation between structure, electronic properties, and electronic transport in the quantum wire system by combining nanoscale transport measurements, scanning tunneling microscopy, and density functional theory calculations. The approach takes advantage of our developments in fabricating nanocontacts using a field-induced atom emission process to bridge the atomic wires and the mesoscopic transport electrodes. A metal-insulator transition (MIT) is revealed in

isolated nanowires, while a robust metallic state is obtained in wire bundles at low temperature. Observations are interpreted as atomic defects leading to electron localization in isolated nanowires, and interwire coupling which stabilizes the structure and promotes metallic. The results thus provide a rare glimpse of the intrinsic structure-transport relations and the influence of local environments at an unprecedented atomic scale.

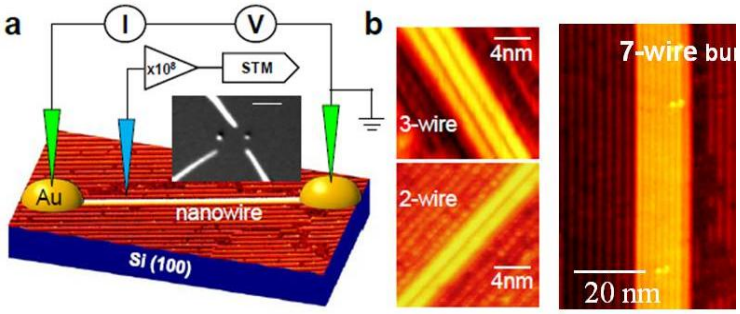

Fig. 1 (a) A cryogenic four-probe STM is used to probe both the electrical transport and the electronic structures of individual $GdSi_2$ nanowires (b) STM images of self-assembled nanowires with different width.

Structural dependent grain boundary resistance in Cu interconnect nanowire. Copper nanowire is currently used as interconnect in integrated circuits. As interconnect dimensions decrease, the resistivity of copper increases dramatically because of electron scattering from surfaces, impurities, and grain boundaries (GBs), and threatens to stymie continued device scaling. Lacking direct measurements of individual scattering sources, understanding of the relative importance of these scattering mechanisms has largely relied on semi-empirical modeling. In this project, we have made a first ever attempt to measure and calculate individual GB resistances in copper nanowires with one-to-one correspondence to the GB structure. By directly measuring both intra- and inter-grain resistance with a unique four-probe scanning tunneling microscope, we observed surprisingly large resistance jumps across high-angle random GBs, while the resistance of coincidence boundaries are negligibly small. Strikingly, the high resistance for random boundaries is found to be an intrinsic result arising from the scaling of the electron mean free path with the size of the relaxation region near the GBs. These results have shown for the first time that the GB scattering effect can differ by orders of magnitude depending on the level of structural symmetry. The results thus provide compelling evidence on the importance of GB scattering process, particularly at random GBs, and also suggest a path to suppressing the GB scattering effect in polycrystalline nanowires through the conversion of random GBs into coincidence GBs.

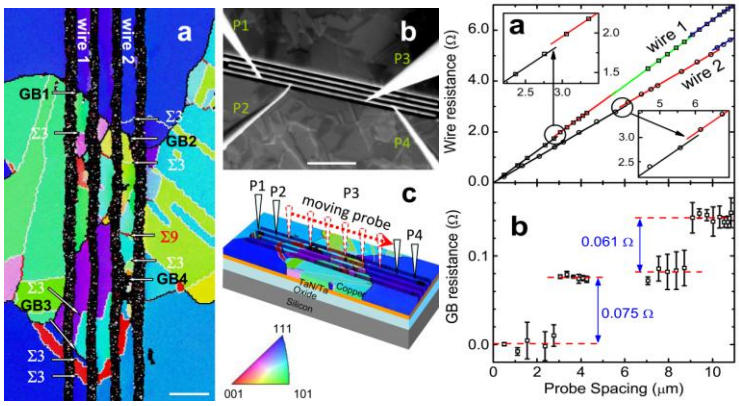

Figure 2. Left Figure: Structures of copper nanowires. (a), The inverse pole figure of EBSD map showing the orientations of grains and GBs. (b), SEM image showing four-probe STM contacted onto the same copper nanowire. (c), A schematic illustrating the resistance measurement procedure with 4-probe STM. Right Figure: resistance jumps near random GBs.

Imaging and manipulating electronic phases near a Mott transition in complex oxide. The complex interplay between electron and lattice degrees of freedom produces many nearly degenerate electronic states in correlated electron materials. These states determine the functionality of the system, but competition between these states produces highly variable properties whose mechanism remains in debate. By imaging phase domains with electron microscopy and interrogating individual domains in situ via point probe electron transport spectroscopy in double-layered $Sr_3(Ru_{1-x}Mn_x)_2O_7$ (x = 0 and 0.2), we have showed (right figure) the first real-space evidence that the microscopic phase competition and the Mott-type metal-insulator transition can be tuned by applying a mechanical stress. Studies were enabled by novel application of a cryogenic four-probe scanning tunneling microscope system, which both images the microscopic phase domains using a scanning electron microscope and simultaneously interrogates the electronic properties of each domain using the scanning tunneling probes in either spectroscopic or transport modes. Dramatic changes were observed in the size and shape of phase domains in response to thermal cycling and mechanical stress. A quantitative correlation between the macroscopic metal-insulator transition and the microscopic phase percolation has been revealed.

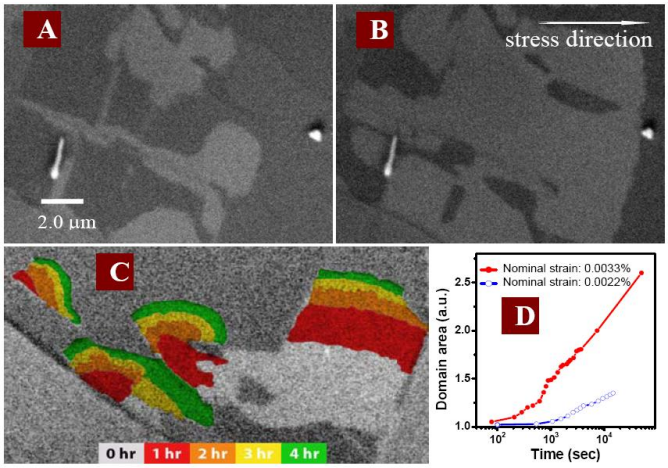

Figure 3. Strain-induced domain evolutions in the cleaved surface of a $Sr_3(Ru_{0.8}Mn_{0.2})_2O_7$. **(A),** Domain image before stress and **(B),** after applying an uniaxial compressive stress in the *ab* plane. **(C),** Domain evolution in time with nominal strain of 0.0022%. **(D),** Domain area change with time.

Ferroelectric Gated Electron Transport in CdS Nanotetrapods. The continuing miniaturization of electronic device has inspired extensive research efforts to develop the bottom-up fabrication of unique nanoelectronic devices by taking advantages of the nanostructured materials and motifs. In this context, the multi-armed semiconductor nanotetrapods are of particular interest due to their unique nanoscale three-dimensional (3D) architectures that can deliver functionalities of delicate multi-terminal nanodevices for potential logic circuits, sensors, and memory applications. However, a technological challenge for experimentally modulating the conductance of the semiconductor nanotetrapods lies in their unique 3D geometric shape that makes the tetrapod structures impossible to lie flat on the planar substrate surfaces and thus seriously hampers the capacitance coupling between the gating electric field and the tetrapod conduction channels. In this project, we have demonstrated the ferroelectric field effect transistor (FeFET) devices by integrating individual CdS nanotetrapods with the high-κ, switchable ferroelectric $Ba_{0.7}Sr_{0.3}TiO_3$ (BST) film as gate dielectrics. A *p*-type field effect is observed up to room temperature, owing to the enhanced gate capacitance coupling. And the reversible remnant polarization of the ferroelectric gate dielectric leads to a well-defined nonvolatile memory effect. The field effect is shown to originate from the channel tuning in the arm/core/arm junctions of nanotetrapods. At low temperature (8.5 K), the nanotetrapod devices exhibit a ferroelectric-modulated single-electron transistor (SET) behavior. The results illustrate how the characteristics of a ferroelectric such as switchable polarization and

high dielectric constant can be exploited to control the functionality of individual 3-dimensional nano-architectures.

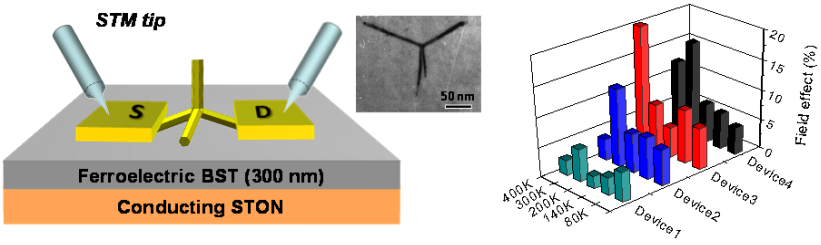

Figure 4. A cryogenic four-probe scanning tunneling microscopy (STM) is used to probe the electrical transport through individual CdS nanotetrapods with a ferroelectric $Ba_{0.7}Sr_{0.3}TiO_3$ (BST) film as gate dielectric. A ferroelectric field effect transistor (FeFET) operation is demonstrated.

Future work:

The next direction for our nanotransport research will be to extend the capabilities to the atomic spacial resolution and control the electron transport by tuning the local structures at the atomic scale. Atomic resolution transport measurements will expose effects from individual point defect and impurities. The correlation between the transport and the local structures will be deterministically addressed.

This work is sponsored by the Scientific User Facilities Division, Office of Basic Energy Sciences, U.S. DOE.

Publications:

1 Shengyong Qin, Tae-Hwan Kim, Wenjie Ouyang, Yanning Zhang, Hanno H. Weitering, Chih-Kang Shih, Arthur P. Baddorf, Ruqian Wu, and An-Ping Li, "Correlating Electronic Transport to Atomic Structures in Self-Assembled Quantum Wires", *Nano Letters*, 12 (2), 938-942 (2012).

2 Shengyong Qin, Sondra Hellstrom, Zhenan Bao, Boyan Boyanov, and An-Ping Li, "Contacting nanowires and nanotunes with atomic precision for electronic transport", *Applied Physics Letters* 100 (10), 103103 (2012).

3 Xiangdong Li, Guowen Meng, Shengyong Qin, Qiaoling Xu, Zhaoqin Chu, Xiaoguang Zhu, Mingguang Kong, and An-Ping Li, "Nanochannel-Directed Growth of Multi-Segment Nanowire Heterojunctions of Metallic $Au_{1-x}Ge_x$ and Semiconducting Ge", *ACS Nano*, 6 (1), 831-836 (2012).

4 Shengyong Qin, Tae-Hwan Kim, Zhouhang Wang, and An-Ping Li, "Nanomanipulation and manofabrication with multi-probe scanning tunneling microscope: From individual atoms to nanowires", *Review of Scientific Instruments*, 83, 063704 (2012).

5 Tae-Hwan Kim, D. M. Nicholson, X.-G. Zhang, B. M. Evans, N. S. Kulkarni, E. A. Kenik, H. M. Meyer, B. Radhakrishnan, and An-Ping Li, "Structural Dependence of Grain Boundary Resistivity in Copper Nanowires", *Japanese Journal of Applied Physics*, 50 (8), 08LB09 (2011).

6 Wangyang Fu, Shengyong Qin, Lei Liu, Tae-Hwan Kim, Sondra Hellstrom, Wenlong Wang, Wenjie Liang, Xuedong Bai, An-Ping Li, and Enge Wang, "Ferroelectric Gated Electrical Transport in CdS Nanotetrapods", *Nano Letters*, 11 (5), 1913–1918 (2011).

7 Xiangdong Li, Guowen Meng, Qiaoling Xu, Mingguang Kong, Xiaoguang Zhu, Zhaoqin Chu, and An-Ping Li, "Controlled Synthesis of Germanium Nanowires and Nanotubes with Variable Morphologies and Sizes", *Nano Letters*, 11 (4), 1704–1709 (2011).

8 Tae-Hwan Kim, X. G. Zhang, Don M. Nicholson, Boyd M. Evans, Nagraj S. Kulkarni, B. Radhakrishnan, Edward A. Kenik & An-Ping Li "Large discrete resistance jump at grain boundary in copper nanowire", *Nano Letters*, 10 (8), 3096–3100 (2010).

9 Tae-Hwan Kim, M. Angst, B. Hu, R. Jin, X. G. Zhang, J. F. Wendelken, E. Ward Plummer, and An-Ping Li, "Imaging and Manipulation of the Competing Electronic Phases near the Mott Metal-Insulator Transition", *Proc. Nat. Acad. Sci.*, 101, 5272 (2010).

Nanoscale materials research by transmission electron microscopy

Y. Liu*, X-M Lin, Y. Sun, T. Rajh, A. K. Petford-Long

Center for Nanoscale Materials, Argonne National Laboratory, 9700 S. Cass Ave., Argonne 60439

*Contact e-mail for TEM at Center for Nanoscale Materials: yuziliu@anl.gov

The Center for Nanoscale Materials (CNM) at Argonne National Laboratory provides expertise, instruments, and infrastructure for interdisciplinary nanoscience and nanotechnology research through a peer-reviewed user proposal system. Transmission electron microscopy (TEM) provides a platform to investigate nanomaterials from devices to individual nanostructures by using in-situ [1] and ex-situ techniques.[2, 3] Advanced analytical TEM is being employed to study the microstructure and chemical structure of nanomaterials including catalysts, energy materials, electronic materials and multilayer heterostructures. These microstructural characterizations can be correlated with growth parameters, post-growth treatments and physical properties of the nanomaterials. At the CNM we are using a variety of in-situ TEM techniques, including development of a program to use an environmental electrochemical cell platform. We use two examples to demonstrate our recent progress.

Theoretical work has shown that Ag nanowires (NWs) can show different behavior depending on whether they are twinned or single crystal. [4] We used a dual-beam scanning electron microscope/focused-ion beam (DB-SEM/FIB) system to prepare cross-section TEM samples which allow the microstructure of very specific regions of five-fold twinned Ag NWs to be studied. [5] Electron nanobeam diffraction and high resolution electron microscopy (HREM) images revealed the presence of body centered tetragonal (bct) Ag in the five-fold (111) twinned NWs. This is induced by strain that compensates for the 7.53°-missing angle. A cross sectional TEM specimen of a Ag NW prepared by DB-SEM/FIB milling is shown in Figure 1. The bright field image and high resolution images of a 90° cross-sectional TEM specimen shown in Figure 1 (a) and (b) reveal that the core area of the Ag NW is more strained than the surrounding material. Release of this strain has resulted in the extra stacking faults seen in Fig 1 (b). In order to image the bct structure directly (from the difference between the (100) and the (001) reflections in electron diffraction), a cross-sectional TEM specimen was prepared at an angle of 45° with respect to the [011] growth direction, as shown in the inset of Fig 1 (c). This allows the electron beam to lie parallel with [010]. From the nanobeam electron diffraction, we found the lattice parameter difference between $\boldsymbol{a}$ and $\boldsymbol{c}$ is 3.6% at position 1 (core) and 0.6% at position 2 (sheath), indicates that the core area of the Ag NW is more strained than the sheath area.

Revealing the physics and chemistry that drive the self-assembly processes for nanoparticles (NPs) will enable us to design hybrid material systems exhibiting new functionalities such as semiconductor/magnetic, metal catalyst/semiconductor, plasmonic/magnetic. The self-assembly of Au nanoparticles (NP) covered with positive-charged cetyltrimethylammonium (CTA^+) and negative-charged citric surfactants, in deionized (DI) water, were monitored by in-situ liquid cell TEM experiments. The electron beam leads to a potential on the sample which frees the CTA^+-covered Au NPs from the Si_3N_4 membrane as shown in Fig 2 (b). The solvated negative charges will then reduce the over-all positive charges of the CTA^+-covered Au particles in solution (Fig 2 (b), (c) and (d)), leading to their self-assembly. The anisotropic dipole-dipole interaction drives the CTA^+-

covered Au NPs to form one-dimensional chains as shown in Fig 2 (d). On the contrary, the citric-covered Au NPs are stable on the Si_3N_4 membranes.

This work was performed at the Center for Nanoscale Materials, a U.S. Department of Energy, Office of Science, Office of Basic Energy Sciences User Facility under Contract No. DE-AC02-06CH11357.

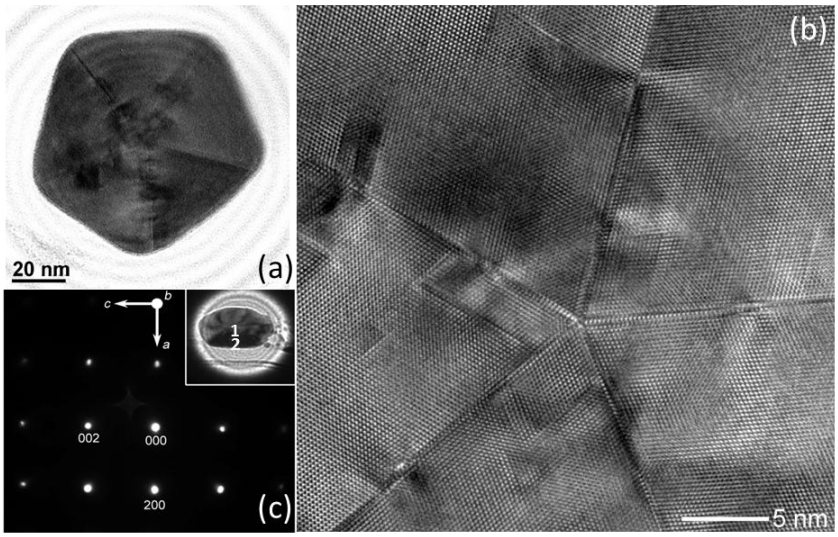

Figure 1 (a) bright field TEM image of 90°-cross sectional Ag NW. (b) HREM image of core area of (a) (by ACAT). (c) electron diffraction pattern of 45°-cross section of Ag NW with electron beam parallel with [010]. The inset is a shadow image. [5]

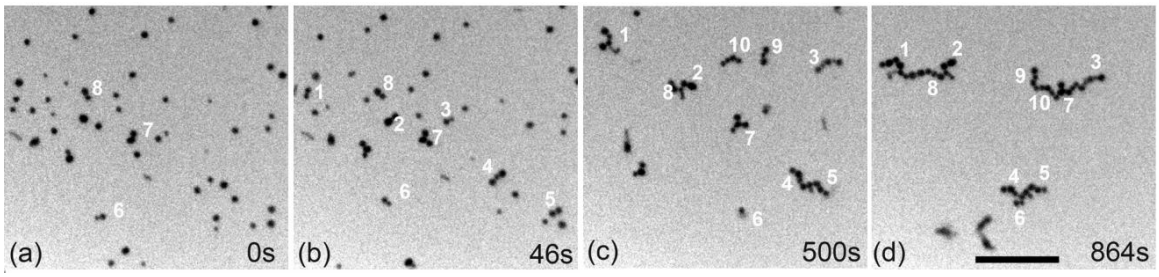

Figure 2 Time sequential images of Au NPs self-assembly in solution. (a) NPs separated on Si_3N_4 membrane. (b) after exposure by electron beam with intensity of 1.0pA/cm^2 the dimers, trimers formed. (c) and (d) show the short chains formed by existing dimers, trimers and individual NPs attachment. The scale bar is 500nm.

[1] Y. Liu, A.N. Chiaramonti, D.K. Schreiber, H. Yang, S.S.P. Parkin, O.G. Heinonen, A.K. Petford-Long, Effect of annealing and applied bias on barrier shape in CoFe/MgO/CoFe tunnel junctions, Phys. Rev. B, 83 (2011) 165413.
[2] E.R. Hemesath, D.K. Schreiber, E.B. Gulsoy, C.F. Kisielowski, A.K. Petford-Long, P.W. Voorhees, L.J. Lauhon, Catalyst Incorporation at Defects during Nanowire Growth, Nano Lett., 12 (2011) 167-171.
[3] Y. Liu, D.K. Schreiber, A.K. Petford-Long, K.-Z. Gao, Three-dimensional characterization of near-field transducers by electron tomography, Mater. Charact.
[4] A.M. Leach, M. McDowell, K. Gall, Deformation of Top-Down and Bottom-Up Silver Nanowires, Adv. Funct. Mater., 17 (2007) 43-53.
[5] Y. Sun, Y. Ren, Y. Liu, J. Wen, J.S. Okasinski, D.J. Miller, Ambient-stable tetragonal phase in silver nanostructures, Nat Commun, 3 (2012) 971.

A Reactive Regime of Electron Transport

Petro Maksymovych
Center for Nanophase Materials Sciences, Oak Ridge National Laboratory, Oak Ridge, TN

The overwhelming majority of electron transport studies aim to identify intrinsic electronic properties of materials in the regime of least perturbation, thus avoiding large electric fields, hysteresis, chemical reactions and hot electrons. On the other hand, the studies that employ electronic excitation to drive chemical reactions (e.g. photochemistry) are primarily focused on the chemical reactions themselves rather than the excitation that drives them. In this presentation we will discuss the intersection of these two paradigms, where the magnitude of electronic or electrochemical excitation is intentionally large enough to drive chemical changes or phase-transitions. It is demonstrated that in this reactive regime one can probe hot-electron transport at the nanoscale, create intrinsic and highly localized conducting channels in otherwise insulating reactions and reveal new types of chemical reactions, many of which are inaccessible by thermal excitation. Though a number of methods can potentially be applied to explore the joint phenomena of electron transport, phase-transitions and chemical reactions, scanning probe microscopy offers several unique advantages, particularly in the form of scanning tunneling and conductive atomic force microscopies. Atomic resolution provides a direct measure of the effect of electron transport on the surface or adsorbates, while a sharp localization of applied fields and hot-electron currents enables point-source and differentiation between intrinsic and defect-mediated processes.

1. Metal-insulator Transition Driven by Ferroelectric Switching

Ferroelectric oxides are almost universally dielectrics, or at most wide-gap semiconductors. Yet, we have found that switching of sponatneous polarization at the nanoscale in a canonical lead-zirconate-titanate perovskite oxide is always associated with a dramatic, up to 10000-fold enhancement of electronic conductance [1]. Upon detailed analysis of coupled resistive and ferroelectric switching as a function of temperature, we have established metallic conductivity in nanoscale ferroelectric domains and a metal-insulator transition controlled solely by ferroelectric switching in an insulating perovskite oxide [2]. This was the first time metallic conductivity has been found in a ferroelectric, despite a variety of theoretical scenarios dating back to the early 70's that hypothesized such a behavior. Conductive atomic force microscopy was pivotal to separate this effect from extrinsic phenomena, such as displacement or leakage currents. Moreover, in our studies metallic conductivity is exclusive to nanoscale polarization structures, created in the regime of high-electric field local polarization reversal, while the rest of the crystal lattice remains an insulator. Therefore, it remained largely inaccessible to macroscopic transport measurements.

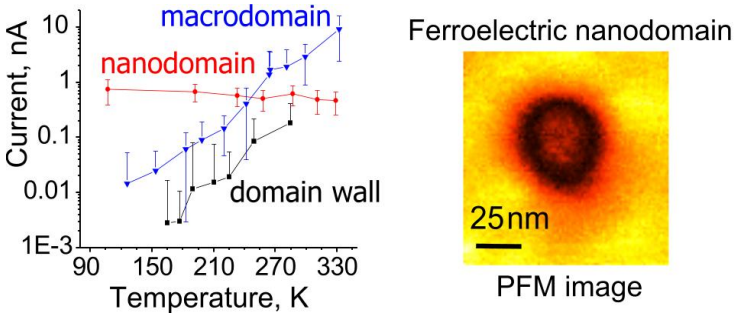

Left: temperature dependence of various conducting entities on the surface of lead zirconate. Nanodomains are metallic in stark contrast to both macrodomains and their domain walls. Right: SPM image of a typical ferroelectric nanodomain.

Equally intriguing is the experimental, and corollary theoretical evidence, that the polarization-controlled metallic conductivity is tunable by orders of magnitude simply by changing of size of a ferroelectric nanoscale domain. This phenomenon is a new manifestation of the notorious ferroelectric field effect, involving a homo- rather than a heterointerface of a ferroelectric material. Our findings

highlighted new electronic properties and entities occurring during local switching of the ferroelectric order parameter or redistribution of oxygen vacancies, and provided new insight into the structural dynamics of the materials themselves, including a possible role of flexoelectric coupling in mediating the phenomeon. Though a number of conducting phenomena have recently been observed in ferroelectric and multiferroic oxides, none have been nearly as dramatic as the polarization-induced metallicity: we have observed large current densities (up to 30000 A/cm^2), giant resistive switching ratios (up to 10000:1) and temperature-independent conductance from 100K to 400K in a relatively thick film of an insulating oxide. These properties pave the way to new prospects of ferroic interfaces in oxide nanoelectronics, such as information storage and neuromorphic computing. Furthermore, the methodologies developed in our study can prospectively reveal new electronic properties in a broad family of structurally-correlated transition metal oxides.

[1] Maksymovych, Science 324 (2009) 1421.
[2] Maksymovych, Nano Lett. 12 (2012) 209.

2. Surface Reactions as a Probe of Hot-electron Transport

Scanning tunneling microscopy provides unique insight into surface chemistry of adsorbed molecules due to its high resolution and ability to excite chemical events using tunneling current. Indeed, the STM tip is a highly efficient source of hot charge carriers by virtue of a large resistance of the tunneling gap, and there are therefore a number of dynamic processes on the surface that can be triggered by inelastic scattering in an STM experiment. If the surface possesses distinct surface states, a large fraction of electrons that have crossed the tunnel junction will continue propagating in the surface plane. Standing wave microscopy and spectroscopy is a direct manifestation of this phenomenon. Several years ago, we discovered that propagating hot electrons can also drive chemical reactions under certain conditions, and that astonishingly large, mesoscale surface areas are "irradiated" by hot-electrons from a precisely localized tunneling source [1]. From a chemical perspective, this method provides a direct access to the kinetics of hot-electron reactions, and crucially it largely eliminates STM-tip artifacts from the analysis of the chemical reaction. Furthermore, one can quantitatively probe the kinetics of fast electron-induced reactions, the time-scales of which far exceed the limited time-resolution of the STM. From the perspective of hot-electron transport, the reaction rate is a direct measure of the hot-electron current in plane of the surface. From a statistical analysis of the spatial distribution of the reaction events, we have been able to directly estimate the inelastic mean-free path of hot-electrons on this surface, with a finite coverage of adsorbates [1]. But by far the biggest advantage of this approach is the ability to directly access electron transport across point and extended defects. Initially, we have observed that single-atoms steps are almost transparent for hot-electrons. The rationale for this behavior is a significant propagation of the surface resonance state into the bulk, which renders the step as a comparatively transparent barrier. However, by varying the injection conditions, we have found a regime where the step becomes very efficient at suppressing the

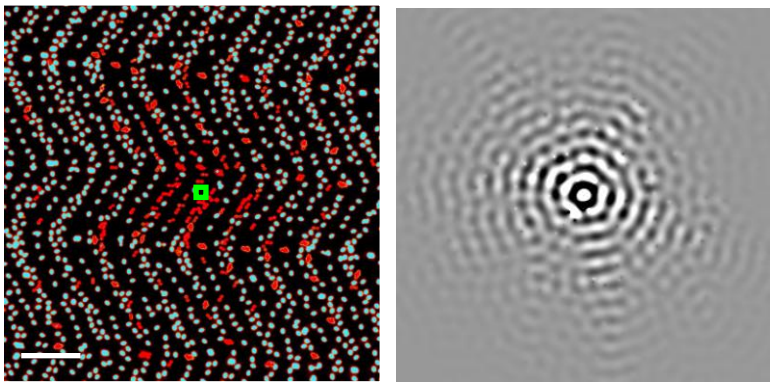

Left: reacted CH_3SSCH_3 molecules (red) surrounding a pulse of hot-electrons injected into the surface from an atomically-sized STM tip (green square). Right: probability density of hot-electrons around a point of origin (center) on the gold surface with finite density of elastic scatterers and an inelastic mean-free path of ~ 5nm. This observable is effectively probed in delocalized reaction experiments.

hot-electron flow [2]. From the analysis of the hot-electron transport within a extended-Huckel model, coupled to the non-equillibrium Green's function formalism, we have surmised that the reflectivity of the step signals the transition from a far-field to a near-field regime of the STM tip as an electron source, with respect to the position of the single-atom step. Experiments have directly verified the associated reverse focusing, and thus and effect k-filtering of hot-electron current across the surface. Future applications of this approach will target 2D materials, where current propagation across the surface is the foundation for the very diverse and practical properties of these materials.

[1] Maksymovych, Phys. Rev. Lett. 99 (2007) 016101.

[2] Maksymovych, submitted (2012)

3. Collective Reactivity and Self-assembly of Adsorbed Molecules Beyond the Ground-state

3.1. Collective reactivity mediated by delocalized electronic states

Electron delocalization in organic molecules underpins the use of conjugated polymer chains and crystals or films with significant degree of pi-stacking in organic electronics, energy harvesting and solid state lighting applications. Electron transport and injection into such materials is rarely associated with possible chemical changes, though the reality is likely otherwise. While investigating the mechanism of alkanethiol self-assembly on the gold surface, we found an example of highly peculiar chain reaction that is mediated by a hot-electron injected into a delocalized electronic state of CH_3SSCH_3 molecules, naturally self-assembled on the gold surface into linear chains several molecules long [1].

The chain reaction involves dissociation and subsequent reassociation of the CH_3SSCH_3 molecules, and therefore, and effective redistribution of the bonding among the self-assembled and self-aligned molecules. The products can also be related to the reagents as mirror images – a reaction trajectory that is inaccessible either thermally (preceded by dissociation) or electronically (likewise preceded by dissociation) on a single molecule scale. However, perhaps most puzzling is the non-trivial reaction patterns observed on Au(100) surface, which are counterintuitive and countermechanistic – they seem to violate the momentum conservation along the reacting chain. One of the hypotheses is that the delocalized electronic state is responsible for initiating the reaction, *and* defining the reaction trajectory at the same time, when this state is populated by a hot-electron. Indeed, first-principles calculations reveal that the pattern of the reaction and the charge distribution of the delocalized state can be related. The reaction therefore reveals a form of coherent control of chemical reactions, where the coherency of the delocalized state defines the reaction pattern.

[1] Maksymovych, Science 322 (2008) 1664.

3.2. Hot-electron control over molecular self-assembly

Today’s paradigm of molecular adsorption and self-organization on the surface, along with the emergent properties of supported supramolecular, monolayer and multilayered structures, is almost entirely dominated by thermally activated chemical reactions. While this is not necessarily perceived as a problem, reliance on ground electronic-state chemistry and comparatively small activation barriers, accessible around room temperature, severely limits the range of accessible reaction mechanisms. These limitations may explain why the entire field of molecular self-assembly on metal and many semiconductor surfaces, including those of nanoparticles, is dominated by the chemical reactions of thiol and dithiol groups. Indeed, although almost every single molecule adsorbed on a surface can form an ordered two-dimensional monolayer, that is often self-assembled, very few headgroup chemistries have been able to rival the ability of organosulfur compounds to form a three-dimensional monolayer, which is most desired for applications and is often made synonymous with the self-assembly itself.

Recently we have discovered that electron-induced excitation of physisorbed phenylacetylene on the gold surface creates a surprisingly ordered and robust layer of upright oriented molecules, the size and shape of which can be precisely controlled by the excitation conditions. The driving force for this transformation was traced to hot electron and hot hole-induced reactions of the alkyne group that produces very strong (excess of 3 eV/molecule) bonding to the surface. Curiously, thermal excitation can only desorb the molecule, and so attachment and self-assembly of alkyne derivatives on gold has been inaccessible experimentally, despite a growing interest in this system from the theoretical community. These experiments have also demonstrated a distinct novel approach to molecular self-assembly, which is somewhat reminiscent of the e-beam lithography. Specifically, we have utilized a layer of physisorbed weakly bonded molecules on the surface as a precursor "wetting" layer, where the molecules are disordered and diffuse appreciably under the reaction conditions. Electron-induced excitation then produces the attachment reaction and immobilizes the molecules in the region of the excitation, but the mobility of the precursor layer is vital to assure the formation of a continuous and ordered layer. Prospectively the precursors can be supplied directly from the gas-phase. The exact mechanisms of the electron-induced processes involving phenylacetylene molecules are not yet understood, and will be subject to future work. One of the most intriguing possibilities is the tautomerization of the alkyne group, where a hydrogen atom switches to a C2 carbon while the lone-pair of the sigma-orbital of the C1 carbon attaches to gold. This product is an upright and fully conjugated aromatic molecule directly at the metal-organic interface. Preliminary theoretical calculations indicate that it exhibits a vanishing transport gap at the anchor-group – an unprecedented phenomenon on its own, with strong implications for electronic and potentially plasmonic applications. We believe that electronic control will pave way to next-generation self-assembly methodologies, with deterministic design of the structure and topology of self-assemblies from nanoscale to mesoscale as well as the direct control over the reactivity and properties of the metal-organic interface. Furthermore, harnessing electron-induced reactions can lead to a variety of new self-assembled structures composed of molecules that are not amenable to thermally-induced surface reactions.

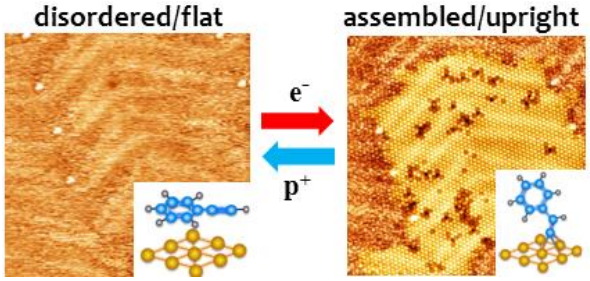

Transformation of a disordered mobile layer of physisorbed phenylacetylene molecules on the gold surface into a self-assembled arrangement of strongly bonded upright conjugated molecules by injection of hot electrons. Hot holes reverses the process.

[1] Li, Pan, Maksymovych, Nat. Sci. Rep. In review (2012)

Experiments were carried out at the Center for Nanophase Materials Sciences, sponsored by the Division of User Facilities, Office of Basic Energy Sciences, U.S. Department of Energy. The research on ferroelectric oxides was partially supported by the U.S. Department of Energy, Office of Basic Energy Sciences, Materials Sciences and Engineering Division (contracts ERKCZ07, DE-AC02-05CH1123), and by the SRC-NRI-WINS program. The research on dimethyldisulfide was partially supported by the W. M. Keck Foundation and the Army Research Office, and by NSF through grant CHE0518253.

Scanning SQUID Microscopy of Novel Materials

From FWP 10028: Correlated Materials - Synthesis and Physical Properties

PIs: I. R. Fisher, T. H. Geballe, A. Kapitulnik, S. A. Kivelson, and K. A. Moler

Abstract by K.A. Moler

Geballe Laboratory for Advanced Materials, Stanford University, and

Stanford Institute for Materials & Energy Science, SLAC National Laboratory.

Email: kmoler@stanford.edu

1. Program Scope

FWP *10028* is part of the newly-formed Stanford Institute for Materials and Energy Sciences (SIMES), which is the Materials Science Division at the SLAC National Accelerator Laboratory. Efforts in our specific FWP aim to address the grand challenge of "emergence" as well as a number of "Basic Research Needs" areas for energy applications in the realm of quantum materials. Understanding and ultimately controlling this class of materials has the potential to profoundly impact the next generation of electronic materials relevant to addressing our nation's energy needs. From new quantum states that enable computing with vastly lower power consumption, to new superconductors that better suit power transmission requirements, quantum materials hold the promise of advanced applications as well as providing some of the deepest and most challenging intellectual questions. In the last two years our research has encompassed the fields of superconductivity, novel forms of charge and spin order, non-Fermi liquid behavior and topological insulators. Our focus is on understanding fundamental factors determining the often complex electronic properties of these materials. We combine crystal growth and characterization of novel materials with measurements of their bulk electronic properties (Fisher & Geballe), with measurements of local electronic (Kapitulnik) and magnetic (Moler) properties, and theory (Kivelson). We collaborate extensively, both within SIMES and externally. Separate abstracts from A. Kapitulnik and I.R. Fisher from our FWP address research in our FWP on nematicity in Fe-pnictides, and STM and Kerr effect measurements.

This abstract describes scanning SQUID microscopy in three families of materials:

- Fe-pnictide superconductors (a collaboration within this FWP),
- complex oxide heterostructures (in collaboration with FWP #10069, "Atomic Engineering Oxide Heterostructures: Materials by Design"), and
- HgTe/HgCdTe quantum wells (in collaboration with members of FWP#10029, "Spin Physics"; made possible by a seed grant on Topological Insulators).

2. Recent Progress

(a) Superfluid density in Fe-pnictide superconductors.

The London penetration depth is the length scale on which a superconductor can shield magnetic fields. The inverse of the London penetration depth squared is the superfluid density. It is one of the most fundamental and important quantities by which to understand a superconductor. Its temperature dependence is generally considered a key signature of the superconductor order paremeter that reveals information about the mechanism of superconductivity. We developed methods to measure variations in superfluid density in bulk superconductors using scanning SQUID microscopy and magnetic force microscopy.

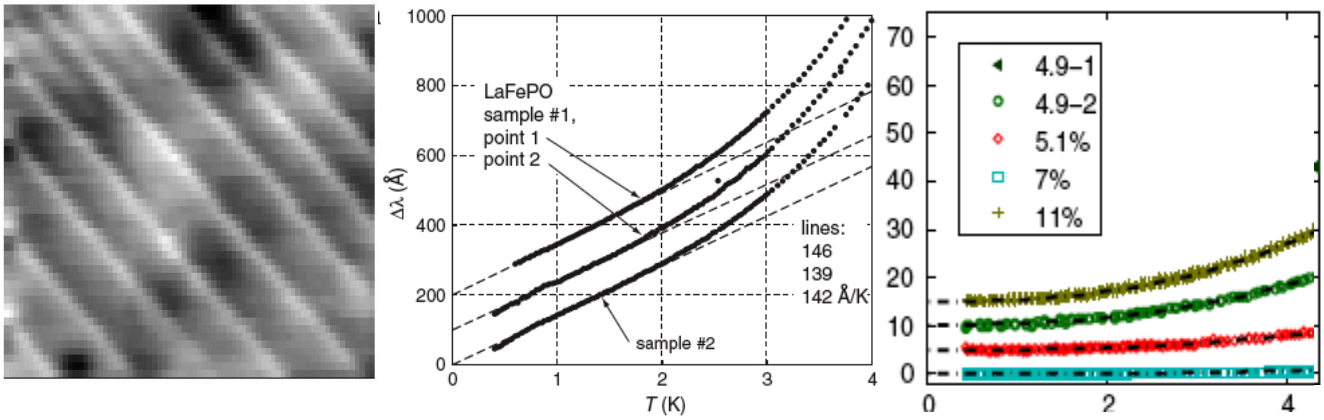

Figure 1. **Superfluid Density in Pnictides**. *Using local scanning probes to map the superfluid density can reveal variations associated with doping, scattering, or structure, and help identify uniform samples for fundamental studies. Left: a map of the superfluid density in underdoped Co-doped BaFe2As2 shows strongly enhanced superfluid density on twin boundaries. Middle and right: The temperature dependence of the penetration depth in LaFePO (middle) and Co-Doped BaFe2As2 (right).*

We used these measurements and analysis to establish the following:

- We matched variations in topography and doping with variations in the apparent local penetration depth. This result indicates a need to compare global and local measures of penetration depth, especially in new and complex materials, which may be prone to disorder.
- In LaFePO, a pnictide superconductor with a critical temperature of 6 Kelvin, we found that the penetration depth has a linear temperature dependence at low temperatures. This result established that some pnictide superconductors have order parameters with line nodes.
- In $Ba(Fe_{1-x}Co_x)_2As_2$, we found the temperature dependence of the penetration depth is consistent with either a two-gap model or with a power law, and the details across the superconducting dome are consistent with spin-fluctuation-based superconductivity.
- In underdoped $Ba(Fe_{1-x}Co_x)_2As_2$, we found that the superfluid density is strongly enhanced on twin boundaries. By imaging vortices together with superfluid density, we found that the twin boundaries repel vortices.

(b) Superfluid density and magnetism in LAO/STO heterostructures

$LaAlO_3$ and $SrTiO_3$ are both nonmagnetic insulators. When 3 or more unit cell layers of $LaAlO_3$ are grown on a $SrTiO_3$ substrate, the interface between them is conducting and even superconducting. The superconductivity can be tuned with a gate voltage, making it seem like an ideal system to study the superconductor-insulator transition. With this in mind, we carried out magnetic imaging with the intent to study the gate-tuned superconductor-insulator transition. Surprisingly, we found patches of nanoscale ferromagnetism, indicating that multiple states are important in this engineered interface. In follow-up work, we showed that the nanomagnetism appears only when the $LaAlO_3$ is at least 3 unit cells thick, which shows that the migration of electrons to the surface, called "electronic reconstruction," is a necessary but not sufficient condition for the magnetism to arise. We also showed that the magnetism can be dramatically changed by in situ contact with a local scanning probe. These results and the known importance of Rashba spin-orbit coupling at the interface have led theorists to speculate that the

superconductivity may have various forms, but so far we have found no evidence of exotic superconducting behavior.

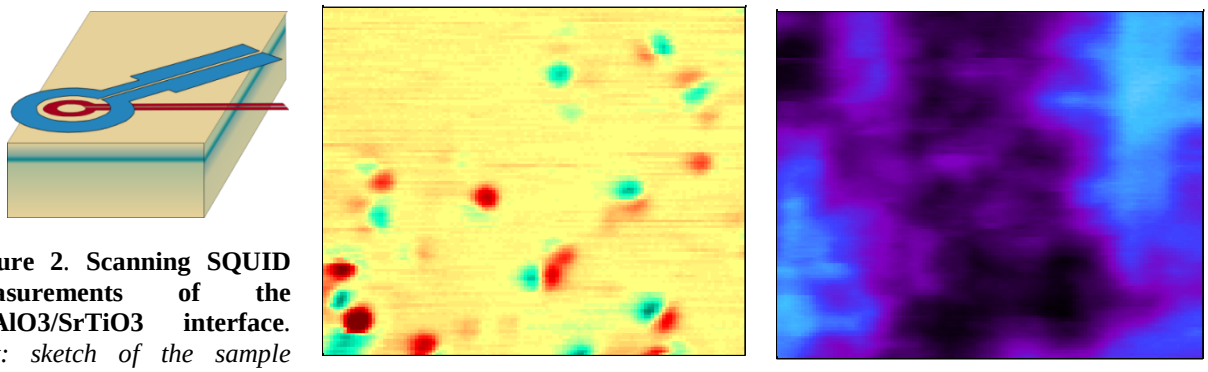

Figure 2. Scanning SQUID measurements of the LaAlO3/SrTiO3 interface. *Left: sketch of the sample (beige), interface (green), SQUID pickup loop (red), and SQUID field coil (blue). We measure the magnetic field through the pickup loop, and can use the field coil to apply a local magnetic field. Center: a map of the flux through the pickup loop corresponds to a map of the sample's static magnetic field, and reveals nanoscale patches of ferromagnetism. Green and red correspond to north and south poles. Right: a map of the sample's diamagnetic susceptibility reveals the local superfluid density. These images show that magnetism and superconductivity exist in the same samples. Future measurements will further investigate the correlation between the two.*

(c) Imaging edge currents in a Quantum Spin Hall Insulator

In 2004 and 2005, theorists calculated that the interaction between the spin and orbital degrees of freedom of the electrons in a two-dimensional (2D) system could lead to a nontrivial energy gap. They predicted that under some conditions, such systems would have an insulating interior, but with conducting edge states. In these edge states, electrons with spin up would propagate in one direction and those with spin down would propagate in the opposite direction. This state is similar to the quantum hall state, but is invariant under time reversal, and is dubbed the "quantum spin Hall insulator" (QSHI). In 2007, Laurens Molenkamp and others from the University of Würzburg, in collaboration with Stanford theorists, confirmed that prediction by observing quantized conduction in sufficiently small (micron-scale) Hall bars of HgTe/(Hg, Cd)Te quantum wells, which they attributed to the edge states. They subsequently added additional evidence for the nonlocal nature of the edge state through transport measurements.

Working with the University of Würzburg, we imaged the magnetic field produced by transport current in a larger Hall bar of HgTe/(Hg, Cd)Te, and found that the current does flow on the edge in the Quantum Spin Hall Insulator regime [preliminary unpublished data]. This finding provides a way to characterize the micron-scale disorder potential in this samples and to seek edge states in novel candidates for the QSHI regime.

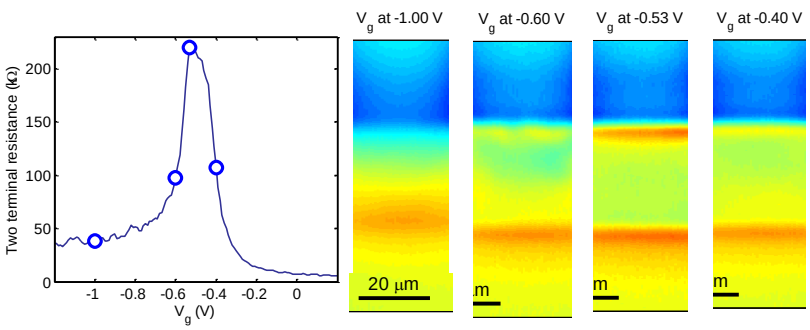

Figure 3. Images of the edge state in a HgTe/HgCdTe Hall bar. *Left: resistance of a 30 μm by 60 μm Hall bar. The peak is believed to indicate the Quantum Spin Hall Insulator (QSHI), where the current should flow in edge states. Right: images of the magnetic field from the transport current indicate that current flows uniformly through the interior away from the peak, but flows on the edges in the QSHI state.*

3. Future Plans

These experiments are unifed by the us of magnetic microscopy for interfaces, including both naturally occuring interfaces such as twin boundaries and engineered interfaces. Work on LAO/STO and HgTe/(Hg, Cd)Te is further unified by the possibility of exotic superconductivity that will support Majorana fermions in two-dimensional superconducting systems, whether that superconductivity occurs naturally or as the result of a proximity effect, and whether the needed spin properties are provided by spin-orbit coupling or by topological insulator behavior. We plan to continue to characterize interfaces to work towards the possibility that engineered interfaces can lead to sufficient Rashba coupling to realize predicted exotic superconductivity.

4. References to publications of DOE sponsored research that have appeared in 2010-2012

(a) Selected publications on Fe-pnictides.

Evidence for a Nodal Energy Gap in the Iron-Pnictide Superconductor LaFePO from Penetration Depth Measurements by Scanning SQUID Susceptometry, Clifford W. Hicks, Thomas M. Lippman, Martin E. Huber, James G. Analytis, Jiun-Haw Chu, Ann S. Erickson, **Ian R. Fisher**, **Kathryn A. Moler,** Phys. Rev. Lett. **103**, 127003 (2009).

Stripes of increased diamagnetic susceptibility in underdoped superconducting $Ba(Fe_{1-x}Co_x)_2As_2$ single crystals: Evidence for an enhanced superfluid density at twin boundaries, Beena Kalisky, John R. Kirtley, James G. Analytis, Jiun-Haw Chu, Arturas Vailionis, **Ian R. Fisher**, **Kathryn A. Moler**, Phys. Rev. B **81**, 184513 (2010) (Accompanied by a Viewpoint by John Tranquada, *Physics* **3**, 41 (2010).)

Local measurement of the penetration depth in the pnictide superconductor $Ba(Fe_{0.95}Co_{0.05})_2As_2$, Lan Luan, Ophir M. Auslaender, Thomas M. Lippman, Clifford W. Hicks, Beena Kalisky, Jiun-Haw Chu, James G. Analytis, **I. R. Fisher**, John R. Kirtley, **Kathryn A. Moler**, Phys. Rev. B 81, 100501(R) (2010). (Editor's Suggestion, Accompanied by an Editor's Synopsis in *Physics*.)

Local Measurement of the Superfluid Density in the Pnictide Superconductor $Ba(Fe_{1-x}Co_x)_2As_2$ across the Superconducting Dome,Lan Luan, Thomas M. Lippman, Clifford W. Hicks, Julie A. Bert, Ophir M. Auslaender, Jiun-Haw Chu, James G. Analytis, **Ian R. Fisher**, and **Kathryn A. Moler**, Phys. Rev. Lett. **106**, 067001 (2011).

(b) Selected publications on LAO/STO heterostructures

Direct imaging of the coexistence of ferromagnetism and superconductivity at the $LaAlO_3/SrTiO_3$ interface, Julie A. Bert, Beena Kalisky, Christopher Bell, Minu Kim, Yasuyuki Hikita, Harold Y. Hwang, and **Kathryn A. Moler,** *Nature Physics* **7**, 767-771 (2011).

Critical thickness for ferromagnetism in $LaAlO_3/SrTiO_3$ heterostructures,Beena Kalisky, Julie A. Bert, Brannon B. Klopfer, Christopher Bell, Hiroki K. Sato, Masayuki Hosoda, Yasuyuki Hikita, Harold Y. Hwang, **Kathryn A. Moler**, *Nature Communications* **3**, 922 (2012).

Scanning probe manipulation of nanomagnetism at the $LaAlO_3/SrTiO_3$ heterointerface Beena Kalisky, Julie A. Bert, Christopher Bell, Yanwu Xie, Hiroki K. Sato, Masayuki Hosoda, Yasuyuki Hikita, Harold Y. Hwang & **Kathryn A. Moler,** Nano Lett., Article ASAP, DOI: 10.1021/nl301451e (2012).

Measurements of the gate tuned superfluid density in superconducting $LaAlO_3/SrTiO_3$, Julie A. Bert, Katja C. Nowack, Beena Kalisky, Hilary Noad, John R. Kirtley, Chris Bell, Hiroki K. Sato, Masayuki Hosoda, Yasayuki Hikita, Harold Y. Hwang, **Kathryn A. Moler** arXiv:1205.4064v1 (Accepted for publication in Phys. Rev. B).

From Graphene to Molecular Assembly: Probing at Atomic/Single Molecular Scale

Minghu Pan, Petro Maksymovych, Arthur P. Baddorf
panm@ornl.gov

Postdocs: Qing Li

Oak Ridge National Laboratory, Oak Ridge, TN 37831

Program scope

The overarching scientific driver for our research is the question, "*How do atoms, molecules and defects interact with external stimuli to define physical properties?"* The key to answering this question is the development of new analytical tools for understanding the mechanisms of electronic and ionic functionalities on the atomic and molecular level. To quote Freeman Dyson, one of the visionary physicists of 20th century, "*Major events in the history of science are called scientific revolutions. There are two kinds of scientific revolutions, those driven by new concepts and those driven by new tools."* At the CNMS, this effort is underpinned by a vigorous program of scanning probe microscopy development, including in-house design and construction of low-temperature high-magnetic field scanning tunneling microscope (STM) and variable temperature STM for probing electronic properties of solid surfaces and molecular systems. These systems are presently used to explore in-depth intertwined electronic and structural phenomena on materials such as grapheme, layered transition metal oxides and pnictides, and further extend this knowledge to probe and control molecular systems.

Recent Progress

We have built two cryogenic STM systems, one operates at low temperature (2.2-4.2K) and high magnetic field (9 Tesla) and another is designed for variable temperature. The instrumental development had been finished in 2010. Since that point, by collaborating with chemical vapor deposition (CVD) graphene synthesis groups, we have carried out a series of experiments to study the novel structural and related electronic properties down to atomic scales in doped graphene and graphene nanostructures. High stabilities and resolutions of our home-made STM and skilled graphene synthesis capabilities of the collaborators, led us to explore the effects of quantum confinements at graphene edges and controllable substitutional doping in 2D graphene lattices. Furthermore, starting from single molecules, we have explored the surface molecular self-assembly via weakest hydrogen bonding, cooperative CH/π interaction. More interesting, a high strained, corrugated linear polymerization supported by Cu-coordinating metal-organic complex could be formed and well-organized on copper surfaces. This progress is summarized below.

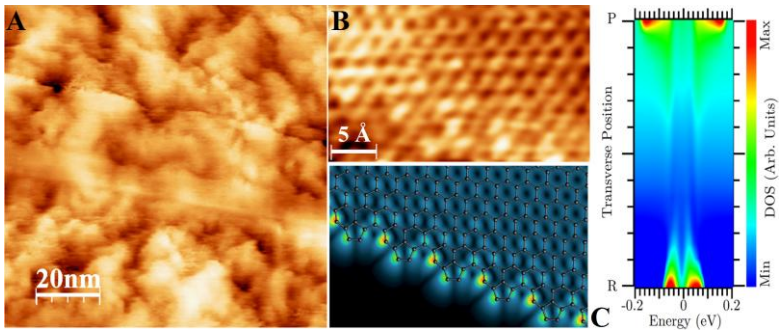

Fig. 1. (a) A typical GNR placed on a Si/SiO_2 substrate observed in STM measurements (b) Atomic resolution image of an edge region with simulated STM images based on a reconstructed edge structure.(c) Color mapping for the calculated local density of states shows two spin-split peaks around the Fermi energy taken perpendicularly to the axis of a graphene ribbon.

Atomic Characterization of Edges in CVD Grown Graphene Nanoribbons: It has been predicted that graphene nanoribbons (GNRs) with armchair shaped edges can be either metallic or semiconducting

depending on their widths, and that GNRs with zigzag shaped edges are metallic with peculiar edge states on both sides of the ribbon regardless of its widths. To analyze the relationships between the edge shape and the electronic edge state of graphene nanoribbons (GNRs) in a more practical model, we used scanning tunneling microscopy and spectroscopy (STM/S) techniques to analyze as-grown CVD GNRs. A rich variety of single-layered graphene nanoribbons exhibiting a width of several to 100 nm and up to 1 μm long were studied. High-resolution images highlight highly crystalline nanoribbon structures with well-defined and clean edges. Theoretical calculations indicate clear spin-split edge states induced by electron-electron Coulomb repulsion. The edge defects can significantly modify these edge states, and different edge structures for both sides of a single ribbon produce asymmetric electronic edge states, which reflect the more realistic features of CVD grown GNRs, and thereby suggesting the possibility of a defective morphology at the edge of CVD grown nanoribbons. This determination is made only possible from our high resolution STM/S data and the simulation using state-of-the-art computational methods.

Nitrogen-doped graphene from atmospheric-pressure CVD: beyond single substitution: In particular, N-doping graphene, expected to introduce additional n-type carriers in carbon systems, is crucial for applications in high-frequency semiconductor devices and enhanced catalysis for energy conversion and storage. Although some attention has been paid to the synthesis and potential applications of N-doped graphene (NG), the nature of the dopants, e.g. the bonding type, the dopant location and the induced perturbation in the graphene lattice, are important to both basic research and practical applications, have not been fully understood. Here, we explored the synthesis of large-area, highly-crystalline monolayer N-doped graphene (NG) sheets via an atmospheric-pressure chemical vapor deposition (AP-CVD) method, yielding a unique N-doping site composed of two quasi-adjacent substitutional nitrogen atoms within the same graphene sub-lattice ($N2^{AA}$). STM/STS of NG reveal the presence of localized states in the conduction band induced by $N2^{AA}$–doping. We also noted the coexistence of pyridine-like nitrogen atoms and other unconventional substitutional N-doped sites in our NG samples. Such N-doping bonding diversity is now opening different possibilities in the fabrication of unprecedented NG-based nanodevices and sensitive/selective molecular sensors.

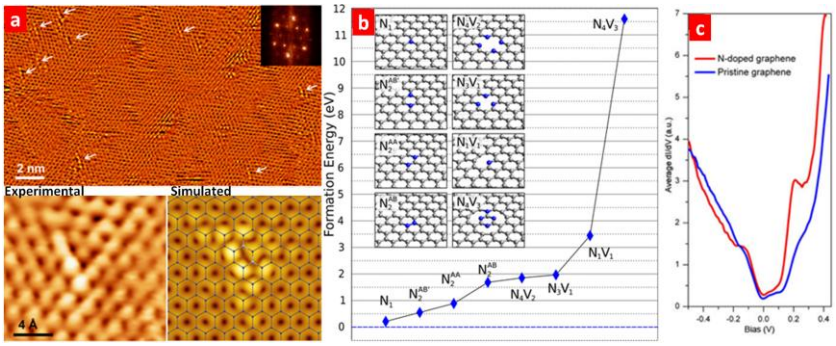

Figure 2. (a), Highly resolved experimental and simulated STM images of $N2^{AA}$ dopants from as-synthesized NG sheets. (b) Calculated formation energy of different N-doping configurations. (c) Local electronic characteristics of NG sheets based on dI/dV curves measured on $N2^{AA}$ dopants (red curve) and on pristine graphene (blue curve).

Supramolecular Self-Assembly of π-conjugated Hydrocarbons via 2D Cooperative CH/π Interaction. The CH/π interaction is the weakest and yet a very unique type of hydrogen bonding found in a large number of gas-phase and bio-molecular clusters. We report, that the supermulecular self-assembly can be formed via purely 2D CH/π interaction by introducing the ethyne fragments. In our case, the CH/π bonding introduces an attractive interaction among hydrocarbon molecules that would otherwise be only repulsive. CH/π bonding not only plays an important role in intermolecular interactions on a metal surface, but that by its characteristic property of multicentricity it effectively induces supramolecular self-assembly of robust molecular clusters with an almost perfectly uniform size distribution across the surface. The multicentricity is manifested in the ability of the ethyne group of a phenylacetylene molecule to act as both an electron density donor and a proton acceptor, enabling

each molecule to participate in multiple CH/π bonding interactions with several of its neighbors. The unique self-assembly process reported here enables deterministic tunability of supramolecular self-assembly via chemical functionalization (e.g., by introducing one or several ethyne groups into a parent molecule) and thus control over both shape and size of supramolecular assemblies, as well as the transition between supramolecular and extended self-assembled structures.

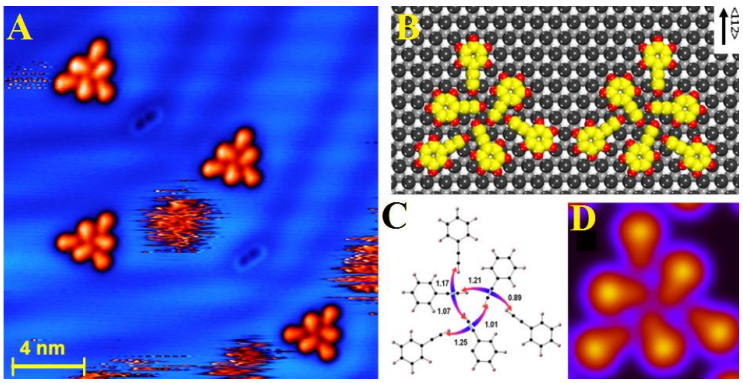

Fig. 3. (a). Topographic STM images of "magic" clusters of phenylacetylene on Au(111). (b) The fully relaxed hexamer.(c) Natural Bond Orbital analysis of the CH/π bonding motif.(d) Simulated STM image for fully relaxed hexamer.

Mesoscopic Aligned and Cu-Coordinated Surface Linear Polymerization: In contrast to supramolecular structures, a key challenge for molecular electronics is the controlled assembly of molecules into desired architectures by strong, that is, covalent, intermolecular connections, enabling efficient electron transport between the molecules and providing high stability. However, most reactions require high temperatures and pressures and do tend to lack control. Here we demonstrate a surface-coordinated linear polymerization, which occurred at liquid nitrogen temperature (100 K), forms long chain poly(phenylacetylenyl)s, well-organized into a "circuit-board" pattern on Cu(100) surface. Such polymerization reaction was confined epitaxially to copper lattice, which suggests the formation of high strained and Cu-coordinating polymer. This highly strained 1D conjugated polymer alters greatly the electronic structure compared to unperturbed polymer. The processes of polymerization and depolymerization can be controlled locally within nanoscale by a charged metal tip. This work thus demonstrates the feasibility of accessing and controlling chain-growth polymerization at low temperature that may lead to the bottom-up construction of sophisticated architectures for molecular nano-devices.

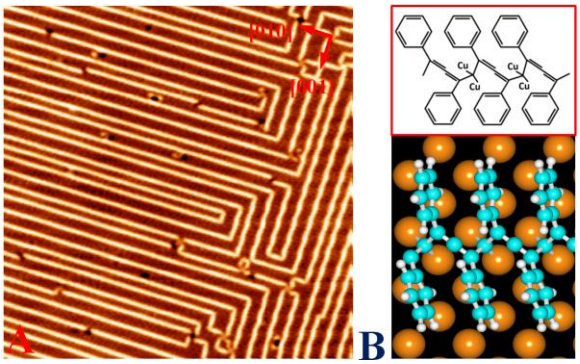

Fig. 4. (a) Highly ordered self-assembled linear polymer on Cu(100). (b) Chemical structure and ball-and-stick model of linear polymer from relaxed DFT calculations (lime is carbon, orange is copper substrate and cyan is hydrogen atoms).

Future plans:

Our research will pursue to understand the fundamental scientific aspects of graphene or graphene-like nanomaterials, manipulate the electronic properties, aimed at the following fundamental issues:

- **Structure and electronic properties of novel graphene-based nanostructures:** We will pursue a systematic study to investigate of existing graphene nanostructures, such as GNRs, ripples, and other geometrically and morphologically controlled structures. We will explore the graphene-molecule hybridized system, which has potentially applications for molecular device and electronics.

- **Probing single doping center in various doped graphene materials**. Substitutional doping of graphene with different atoms (e.g. B, N, S and Si) results in the disruption of the ideal sp2

hybridization of the carbon atoms, thus locally inducing significant changes in their electronic properties and chemical reactivity. We aim to study the doping effects on single layer CVD graphene sample, with addressing the atomic structure and electronic properties of single dopant. We aim to answer (a) How much electronic perturbation induced by a local dopant (b) whether lattice distortion induced by a substitutional dopant affects electronic properties.

- **Surface synthesis of novel graphene nanostructures by 2D conjugated polymerization.** We aim to chemically synthesize graphene nanostructures on a template surface. A precursor, e.g. a polycyclic aromatic hydrocarbon (PAH), is deposited onto the template surface, where the terraces support epitaxial growth of graphene and ordered adsorption of precursors. The step-array template breaks the symmetry of the low-index terrace surface, resulting in a preferred orientation of the precursor and therefore a predetermined orientation of the GNRs, which can be macroscopically long. We plan to perform STM/STS to image the GNRs and to determine their band structures. Our capabilities of molecular assembly imaging, atomic structure determination, and GNR edge state spectroscopy, collaborated with first-principles calculations will be employed to understand the surface and molecular dynamics that enable synthesis of tailored GNRs through self-assembly. The atomic resolution images and spectra will then be compared with first-principles calculations to provide insight into the structure and related properties of fabricated GNRs. Moreover, the microscopic origins of the emerging electronic and magnetic properties of the GNRs can be theoretically investigated.

Research was conducted at the Center for Nanophase Materials Sciences, which is sponsored at Oak Ridge National Laboratory by the Scientific User Facilities Division, Office of Basic Energy Sciences, U.S. Department of Energy. (MP, PM, AB, QL). The work is done in collaboration with Mildred S. Dresselhaus (MIT), M. Terrones (Penn State), V. Meunier (Rensselaer Polytechnic Institute) and J. Bernholc (North Carolina State University).

DOE-sponsored publications 2010-2012 [5 peer-reviewed papers including 1 *PNAS*, 1 *ACS Nano*, 1 *Nano Lett*., 7 talk at conferences**)]**

1. QING LI, CHENGBO HAN, MIGUEL FUENTES-CABRERA, HUMBERTO TERRONES, BOBBY G. SUMPTER, WENCHANG LU, JERRY BERNHOLC, JIEYU YI, ZHENG GAI, ARTHUR P BADDORF, PETRO MAKSYMOVYCH & MINGHU PAN, Electronic Control over Attachment and Self-assembly of Alkyne Groups on Gold, Submitted to *NATURE SCIENTIFIC REPORTS*, In Review

2. RUITAO LV, QING LI, ANDRÉS R. BOTELLO-MÉNDEZ, TAKUYA HAYASHI, BEI WANG, AYSE BERKDEMIR, QINGZHEN HAO, ANA LAURA ELÍAS, RODOLFO CRUZ-SILVA, HUMBERTO R. GUTIÉRREZ, YOONG AHM KIM, HIROYUKI MURAMATSU, JUN ZHU, MORINOBU ENDO, HUMBERTO TERRONES, JEAN CHRISTOPHE CHARLIER, MINGHU PAN AND MAURICIO TERRONES, Nitrogen-doped graphene from atmospheric-pressure CVD: beyond single substitution and enhanced molecular sensing, *NATURE SCIENTIFIC REPORTS*, DOI: 10.1038/srep00586

3. MINGHU PAN, EDUARDO COSTA GIRÃO, XIAOTING JIA, SREEKAR BHAVIRIPUDI, QING LI, JING KONG, VINCENT MEUNIER, AND MILDRED S. DRESSELHAUS, "Topographic and Spectroscopic Characterization of electronic edge states in CVD Grown Graphene Nanoribbons", *NANO LETT*, (2012) DOI: 10.1021/NL204392S

4. LI Q., HAN C.B., HORTON S.R., FUENTES-CABRERA M., SUMPTER B. G., LU W.C., BERNHOLC J., MAKSYMOVYCH P., AND PAN M.H., "Supramolecular Self-Assembly of π-Conjugated Hydrocarbons via 2D Cooperative CH/π Interaction", *ACS NANO* 6(1), 566(2012)

5. R. JIN, M. H. PAN, X. B. HE , GUORONG LI , DE LI , RU-WEN PENG , J. R. THOMPSON, B. C. SALES, A. S. SEFAT, M. A. MCGUIRE, D MANDRUS, J. F. WENDELKEN , V. KEPPENS AND E. W. PLUMMER, "Electronic, magnetic and optical properties of two Fe-based superconductors and related parent compounds", *SUPERCOND. SCI. TECHNOL*. 23 054005(2010

Single Atom Imaging and Spectroscopy of Defects in Graphene

Stephen J. Pennycook, Andrew R. Lupini, Matthew F. Chisholm, Sokrates T. Pantelides
Postdoctoral scientists: Junjie Guo, Jaekwang Lee
Collaborators: Wu Zhou and Juan-Carlos Idrobo
pennycooksj@ornl.gov, arl1000@ornl.gov, chisholmmf@ornl.gov, pantelides@vanderbilt.edu
Materials Science and Technology Division, Oak Ridge National Laboratory, Oak Ridge, TN 37831

Program Scope

This program develops and utilizes imaging and spectroscopy techniques in the scanning transmission electron microscope aiming for the highest resolution and sensitivity. Here we present a number of examples concerning defects in monolayer graphene, in which atomic configurations, their dynamics, and their optical and electronic properties are extracted through a combination of annular dark field (ADF) imaging, electron energy loss spectroscopy (EELS) and first-principles theory.

Recent Progress

The Nion UltraSTEM is a latest-generation scanning transmission electron microscope (STEM) with a cold field emission gun, 5th order aberration corrector and flexible column optics to maximize the efficiency of imaging and spectroscopic signals. In addition, it is equipped with a bakeout system to avoid carbon contamination which allows five samples to be loaded into the microscope at one time. The UltraSTEM provides atomic resolution of the graphene lattice at only 60 kV accelerating voltage, well below the threshold for knock-on damage in the perfect graphene lattice. At defects, however, some beam-induced motion can occur, which allows metastable configurations and cluster dynamics to be studied experimentally. Individual impurity atoms can be identified based on their intensity in the ADF image, and if sufficiently stable their chemical bonding can be identified by EELS. An example is shown in Fig. 1, in which a Si-N defect pair is identified based on comparing ADF image intensity to simulations, also spectroscopically by EELS. Moreover, in the elemental maps it is clear that the carbon map is dark at the sites of the impurity atoms, hence they are *substitutional* in the graphene lattice.

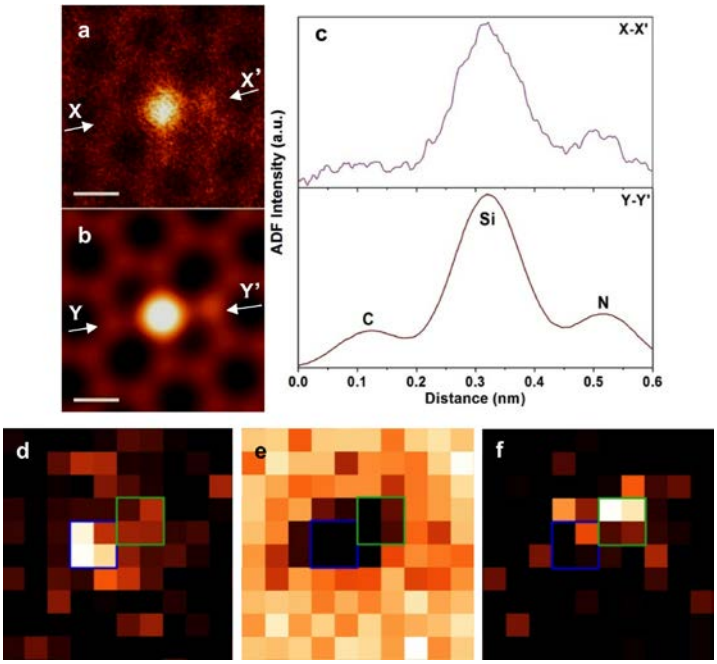

Figure 1: *Atomic structure of a point defect complex in monolayer graphene. (a) ADF image showing the presence of two dopant atoms, (b) simulated ADF image. (c) Corresponding intensity profiles along X-X' and Y-Y' in the experimental and simulated images respectively. Experimental images have been low-pass filtered. (d-f) Si-L-, C-K-, and N-K- edge maps with blue and green squares indicating the positions of the substitutional Si and N atoms respectively. Scale bars are 0.2nm, reproduced from Zhou et al., 2012.*

Low loss EELS can also give information on optical properties, and Fig. 2 shows a surprisingly localized enhancement at the plasmon energy at the Si-N point defect shown in Fig. 1. The exponential decrease moving away from the two-layer region in the lower right of the image is consistent with the expected delocalization, however, the enhancement at the point defect is surprisingly localized, with a full-width-half-maximum of around 4 Å. The point defect complex is acting as an atomic-scale antenna in the petaHertz (10^{15} Hz) frequency range (11 eV is equivalent to a frequency in the order of 10^{15} Hz), and is the smallest resonant structure seen to date.

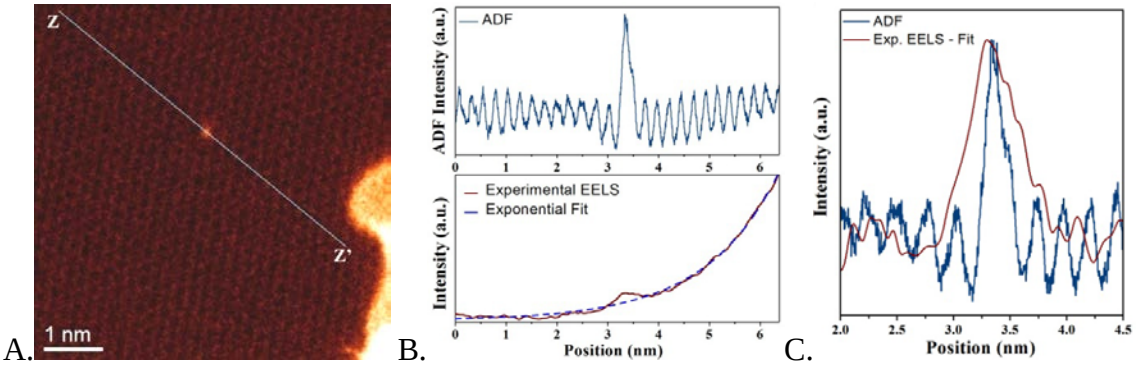

Figure 2: STEM-EELS line scan across a point defect in monolayer graphene. (A) Low-pass filtered ADF survey image. (B) Simultaneously collected ADF and integrated EELS signals from 11 to 18 eV (raw data) as a function of probe position along the line (Z-Z') indicated in Figure A. (C) Comparison of the full-width-half-maximum between the ADF signal and the enhanced plasmon intensity from the substitutional Si atom. Reproduced from Zhou et al., 2012.

At the low beam energies we use here, these point defects are stable under the beam for a sufficient time that spectral fine structure can be collected with good signal to noise ratio. In this case it is possible to directly interpret the chemical bonding. Comparing fine structure from 3- and 4-fold coordinated Si atoms in graphene, Si-C_3 and Si-C_3N point defects, respectively, we find very different near edge fine structures. The Si-L edge fine structure at the Si-C_3 pont defect shows a prominent peak around 104 eV, similar to what is observed from Si, SiC and Si_3N_4, all of which have sp^3 hybridized Si. We therefore infer that the Si-C_3 defect also adopts sp^3 hybridization, which implies that the configuration of the defect is non-planar and that the Si lies above the plane of the graphene. In the case of the Si-C_3N defect, however, this peak is essentially absent. As the Si L edge results from transitions to empty *d*-orbitals, this suggests that the *d* orbitals are now partially full, i.e., taking part in the bonding, with a sp^2d configuration. Thus, unlike the Si-C_3 configuration Si-C_3N is likely to be planar. These conclusions were all confirmed by density functional calculations (see abstract by Pantelides et al., work submitted for publication.)

Defects that are not so stable can also provide useful information if provoked by the electron beam to explore some metastable configurations. Images of a Si_6 magic cluster trapped in a graphene nanopore have revealed configurational changes induced by the beam. One of the atoms executes an oscillatory motion from left to right. Density functional calculations were used to extract the three-dimensional structure of the cluster in these two different configurations and the energy barrier between the two is 0.8 eV from left to right but 1.44 eV from right to left. If these transitions were excited thermally at room temperature they would take approximately 10 and 10^{11} seconds, respectively. However, if we estimate the rate of transformation via direct energy transfer

from the electron beam we find only a factor of two difference in transition rate. This shows how useful beam induced processes can be for revealing energy landscapes of small clusters (work submitted for publication.)

Future Plans

The 200 kV UltraSTEM is equipped with a stage allowing electrical contacts to be made to the specimen and an accelerator design that can be optimized for even lower voltage operation. We will use a heating holder to explore the effects of thermal excitation on defect configurations, also we plan to pass electrical current through the graphene to look for any effects on defect stability or impurity atom diffusion.

Acknowledgements: The PI's and postdocs were sponsored by the DOE Office of Basic Energy Sciences, Materials Sciences and Engineering Division, J-CI by ORNL's ShaRE User Facility supported by the Scientific User Facilities Division, Office of Basic Energy Sciences, WZ by the National Science Foundation through Vanderbilt University and computations were supported by the National Energy Research Supercomputer Center, supported by the DOE Office of Basic Energy Sciences, Scientific User Facilities Division.

DOE-sponsored journal publications 2010-2012

(Publications with Maria Varela are listed solely in her abstract).

C. Cantoni, et al., "Strain-Driven Oxygen Deficiency in Self-Assembled, Nanostructured, Composite Oxide Films," *ACS Nano* **5,** 4783-4789 (2011).

H. B. Cao, et al., "Evolution of the nuclear and magnetic structures of $TlFe_{1.6}Se_2$ with temperature," *Phys. Rev. B* **85**, 054515 (2012).

J. C. Idrobo and S. J. Pennycook, "Vortex beams for atomic resolution dichroism," *J. Electron Microsc*. **60**, 295 (2011).

H. Cun, et al., "Tuning Structural and Mechanical Properties of Two-Dimensional Molecular Crystals: The Roles of Carbon Side Chains," *Nano Lett*. **12**, 1229-1234 (2012).

H. J. Chang, et al., "Atomically Resolved Mapping of Polarization and Electric Fields Across Ferroelectric/Oxide Interfaces by Z-contrast Imaging," *Adv. Matls*. **23,** 2474-2479 (2011).

H. J. Chang, et al., "Watching domains grow: In-situ studies of polarization switching by combined scanning probe and scanning transmission electron microscopy," *J. Appl. Phys.*, **110**, 052014 (2011).

Woo Seok Choi, et al., "Wide bandgap tunability in complex transition metal oxides by site-specific substitution," *Nature Communications* **3**, 689 (2012).

R. M. Stroud, et al., "Supernova Shock-Wave-Induced Co-Formation of Glassy Carbon and Nanodiamond," *Astrophysical Journal Letters* **738**, L27, (2011).

Ondrej L. Krivanek, et al., "Atomic-resolution STEM at low primary energies," in *Scanning Transmission Electron Microscopy; Imaging and Analysis*, Ed by S.J. Pennycook and P.D. Nellist, Springer, New York, 615-658 (2011).

J. W. Lee, et al., "Vacancy-Driven Anisotropic Defect Distribution in the Battery-Cathode Material $LiFePO_4$," *Phys. Rev. Lett.* **107**, 085507 (2011).

Y. Li, et al, "An oxygen reduction electrocatalyst based on carbon nanotube-graphene complexes," *Nature Nanotechnology,* **7**, 394-400 (2012).

Andrew R. Lupini, “The Electron Ronchigram,” for *Scanning Transmission Electron Microscopy: imaging and analysis*, Ed. by P. Nellist and S. Pennycook. Springer, New York, 117-160 (2011).
A. R. Lupini and N. De Jonge, “The Three-Dimensional Point Spread Function of Aberration-Corrected Scanning Transmission Electron Microscopy,” *Microscopy & Microanalysis* **17,** 817-826 (2011).
S J Pennycook, “A Scan Through the History of STEM,” for *Scanning Transmission Electron Microscopy: imaging and analysis*, Ed. by P. Nellist and S. Pennycook. pp. 1-90, Springer, New York, (2011).
S. J. Pennycook and C. Colliex, "Spectroscopic imaging in electron microscopy," *MRS Bull.* **37**, 13-18 (2012).
Stephen J. Pennycook, et al., “Z-Contrast Imaging,” pp 109-152 in *Handbook of Nanoscopy* **1**, eds. G. Van Tendeloo, D. Van Dyck and S. J. Pennycook, Wiley-VCH, Weinheim, Germany (2012).
T. J. Pennycook, et al., "Dynamic Fluctuations in Ultrasmall Nanocrystals Induce White Light Emission," *Nano Lett* **12**, 3038–3042 (2012).
Ö. Polat, et al. “Pinning Enhancements in YBCO Films via Nanoengineered Composite Cap Layer,” *IEEE Transactions on Applied Superconductivity* **21**, No. 3, 3171-3174 (2011).
Murari Regmi, Matthew F. Chisholm and Gyula Eres, “The effect of growth parameters on the intrinsic properties of large-area single layer graphene grown by chemical vapor deposition on Cu,” *Carbon* **50** (1), 134-141 (2012).
D. L. Sales, et al., “Distribution of bismuth atoms in epitaxial GaAsBi,” *Appl. Phys. Lett.* **98,** 101902 (2011)
J. Seidel, et al., "Prominent electrochromism through vacancy-order melting in a complex oxide," *Nature Communications* **3**, 799–6 (2012).
K. van Benthem, et al., "STEM imaging of single Pd atoms in activated carbon fibers considered for hydrogen storage," *Carbon* **49**, 4059 (2011).
G. Van Tendeloo, D. Van Dyck and S. J. Pennycook (eds.), *Handbook of Nanoscopy*, Wiley-VCH (2012).
Z. Q. Yang, et al., "Role of crystal defects on brittleness of C15 Cr2Nb Laves phase," *Acta Mater* **60**, 2637–2646 (2012).
H. Yurdakul, J. C. Idrobo, S. J. Pennycook and S. Turan, "Towards atomic scale engineering of rare-earth-doped SiAlON ceramics through aberration-corrected scanning transmission electron microscopy," *Scripta Mater.* **65**, 656 (2011).
H. Zhou, M. F. Chisholm, T. H. Yang, S. J. Pennycook and J. Narayan, "Role of interfacial transition layers in VO2/Al2O3 heterostructures," *J Appl Phys* **110**, 073515 (2011).
W. Zhou et al., "Atomically Localized Plasmon Enhancement in Monolayer Graphene," *Nature Nanotechnology* **7**, 161-165 (2012).

3D Visualization of Emergent Behavior in Nanoscale Functional Heterostructures

C. Phatak, S. Hong, A. K. Petford-Long
Materials Science Division, Argonne National Laboratory, 9700 S Cass Avenue, Argonne, IL 60439
cd@anl.gov, hong@anl.gov, petford.long@anl.gov

Program Scope

This research is focused around a single theme: **three-dimensional in-situ visualization of the emergent behavior that is seen in patterned functional nanostructures and heterostructures as their dimensions are reduced to the nanoscale.** We are focusing our research on understanding the complex energy landscape in heterostructure nanosystems whose building blocks show resistance switching, ferroelectric, ferromagnetic, and superconducting properties. Our aim is to obtain a fundamental understanding of domain behavior and charge transport properties in these nanostructures through control of the parameters that contribute to their energy landscape, such as interlayer coupling, geometric effects that lead to anisotropy, and the interaction between adjacent nanostructures. A variety of methods can be used to probe emergent behavior on a global scale, but in nanoscale materials it is essential to be able to probe the local behavior, which can best be done through direct imaging as a function of external stimuli such as applied fields, temperature and/or time. Our multi-modal approach involves an interwoven combination of aberration-corrected Lorentz transmission electron microscopy (ALTEM) and advanced scanning force microscopy to solving scientific questions related to the behavior of ferroic nanostructures. A particular focus of our effort will be on the use of three-dimensional analysis and imaging techniques that we have developed to visualize domain and transport behavior in nanostructures.

Recent Progress

Visualization and Magnetic reversal studies of artificial spin ices:

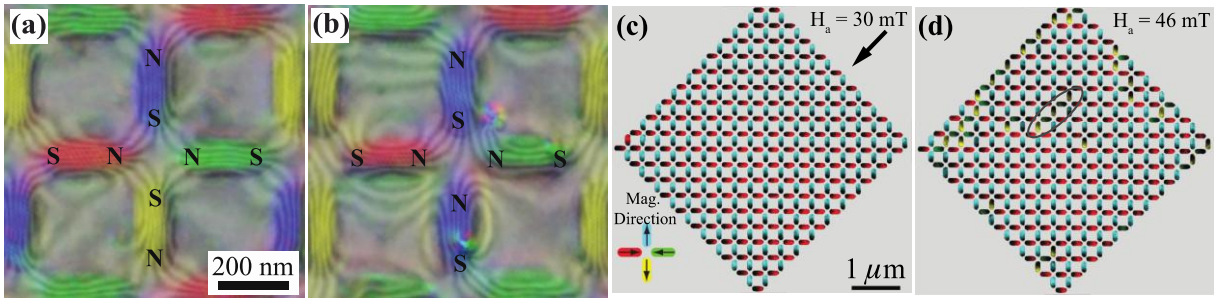

Fig. 1. Experimental images of the magnetic induction in an artificial spin ice lattice. (a), (b) ALTEM images showing detail at (a) node obeying spin ice rule and (b) node exhibiting a magnetic monopole defect. (c), (d) MFM images at different values of applied field showing part of the reversal process. Schematics show how color relates to magnetization direction for all four images. The oval in (d) shows the formation of a chain of reversed islands equivalent to a Dirac string.

Magnetic frustration in artificial spin ices arises when the system tries to minimize the magnetostatic interaction energy of an individual island as well as that of the entire geometric lattice of islands. We have used ALTEM to study the magnetic frustration behavior in individual islands and magnetic force microscopy (MFM) to study the magnetization reversal process of entire lattices and thus gain an understanding of the way in which the magnetostatic interaction can be controlled in square spin ice lattices. The spin ice lattice shown in Fig. 1 consisted of 290 nm ×130 nm islands patterned from a 20 nm thick Permalloy film into a square lattice of side 390 nm. Using ALTEM, with a world-leading spatial resolution of 0.4 nm, we were able to visualize the fine structure of the magnetic induction around nodes obeying spin ice rules (Fig. 1a) and those displaying a magnetic monopole defect structure (Fig. 1b). The colors indicate the direction magnetization in the islands. We were also able to study the formation of so-

called “Dirac strings defects”, which are formed during the magnetization reversal of the lattice. The formation of these string defects is directly related to formation of monopole defects and achieving a demagnetized ground state in the lattice. More recently, in collaboration with Prof. M. De Graef (Carnegie Mellon University), we have also studied the magnetization reversal behavior of the lattices using a combined approach involving ALTEM and MFM correlated with Monte Carlo models. Our MFM studies enabled statistical analysis of large areas of the spin ice arrays that could not easily be achieved using ALTEM, allowing us to develop a model for the reversal process that, for the first time, takes into account the true shape of the islands and thus correctly accounts for their interactions. The fundamental understanding of physics of magnetic frustration gained through this research provides a playground to exploit such novel emergent behavior under the influence of external stimuli such as temperature or magnetic field, which could lead to potential applications in low-power magnetic logic devices.

In-situ studies of resistance-switching oxide heterostructures:

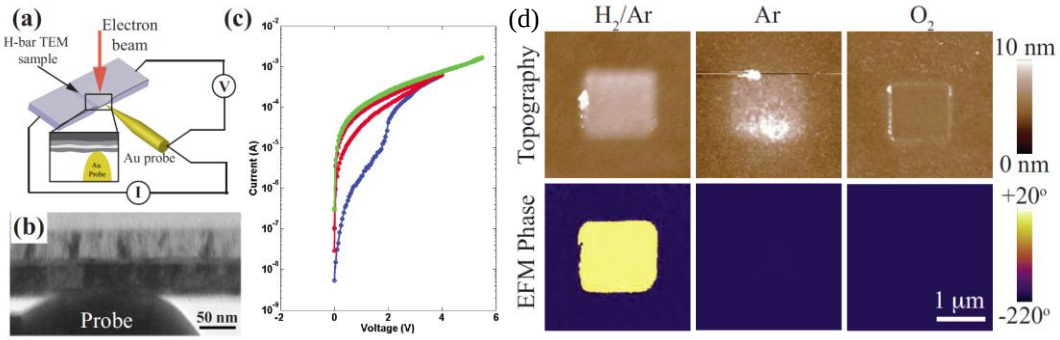

Fig 2. (a) Schematic showing in-situ TEM transport measurement set-up, (b) cross-section image of a Pt/HfO_x/Pt heterostructure, and (c) electroforming curves recorded from the same region. (d) Topography (upper row) and EFM phase images (lower row) after tip-induced stress analysis of a 1.5 µm×1.5 µm square region of TiO_2 in H_2/Ar, Ar, and O_2 environments.

Our preliminary studies of these materials have focused on exploring the spatial distribution of the conducting pathways that form during the electroforming process, and on the role of applied voltage in controlling the local energy landscape and thus the transport behavior. We are carrying out in-situ TEM studies that allow simultaneously observation of changes to the microstructure and composition whilst measuring in-situ I-V curves. Fig. 2(a)-(c) show a schematic of the configuration used to make local in-situ TEM transport measurements, together with a cross-section image of a Pt/HfO_x/Pt resistive-switching oxide heterostructure and electroforming curves recorded from the same region. Recent results have shown a clear change to the shape of the oxygen K-edge spectrum measured via electron energy loss spectroscopy (EELS) upon electroforming (changing from high resistance to low resistance) a 25 nm thick NiO layer, with further changes to the O K-edge observed upon resetting the NiO layer to the high resistance state. Preliminary density functional theory simulations carried out in collaboration with H Iddir (Materials Science Division, Argonne) have shown that these changes can only result from ordering of vacancies within the NiO crystal structure, as a result of electric field-induced changes to the local enthalpy. Furthermore, we are exploring the effect of surface potential on the free energy of the surface of single crystal TiO_2 using electrostatic force microscopy (EFM). Fig. 2(d) shows the results: the square area at the center of each image was scanned by the scanning probe microscopy (SPM) tip with a DC bias (V_{dc}) of +10 V in contact mode to induce ‘tip-induced stress’. Fig. 2(d) shows topographical images for three different ambient gases. The height of the stressed region increases, and the relative height difference is dependent on the ambient gas. Our experiments were carried out in a cell filled with highly pure (> 99.999%) gas and under a positive tip bias, which excludes the possibility of a surface

anodization process. The EFM phase images in Fig. 2(d) show that a phase of 0° occurs only under H_2/Ar, indicating a considerable modification of V_{surf} (ΔV_{surf} = 0.30 eV) and thus its free energy. Quantitative measurement of the influence of ambient gas on V_{surf} led us to develop a model in which the adsorbed oxygen molecules interact with oxygen vacancies at the TiO_2 surface, leading to a change in surface potential. These results provide insights into ambient-dependent physical phenomena in resistive switching oxide materials and provide important clues about the role of oxygen vacancies and adsorbed oxygen anions in the change of charge transport.

Selected Future Directions

***Domain behavior in ferroic nanostructures*:** The energetics of domain structure, nucleation and reversal in ferroic nanostructures is the key to understanding the way in which their behavior evolves at the nanoscale. We seek to understand the contribution and relative scale of the various energy terms to domain behavior, such as the energy imparted by an applied field, the pinning energy of defects, the effect of shape on demagnetizing/depolarizing energy, intrinsic exchange or dipolar energy. Our investigations of confined nanostructure arrays will additionally focus on the interactions laterally between elements arranged in an array or vertically between the layers in heterostructures, and on the effect of artificial defects using a focused ion-beam, which can change the energetics of the systems. Our efforts will focus on developing a 3-D view of the domain structure and associated electric/magnetic fields, using a combination of vector field tomography and three-dimensional PFM.

We will expand our investigations of the artificial spin ices to different lattice geometry and island shapes, and to lattices in which the magnetization can rotate in 3D. Using our in-situ thermal stages we will also study and visualize the frustration behavior as a function of temperature. Building on our research on artificial spin ice structures, we will focus on developing artificial systems to investigate the energy landscape of ferrotoroidic behavior at a microscopic scale. Ferrotoroidic materials are of importance as they form a novel class of materials with strong magnetoelectric coupling properties but the fundamental understanding and experimental control of their domains has not yet been accomplished.

Patterning of FE thin films to different shapes changes the electrostatic boundary conditions, which results in different domain variants and influences the polarization and switching behavior. We will investigate these effects and their responses to external stimuli such as applied electric field. Furthermore, we will correlate the behavior with parameters such as lattice strain, initial domain state, and geometry. We will also carry out temperature-dependent studies in FE and FM systems to understand the effect of size confinement on transition temperatures.

Microstructural origins of charge transport behavior: Charge transport in functional oxide heterostructures occurs by either electronic or ionic conduction of electrons, holes and charged defects. The charged defects can either diffuse or order themselves to contribute to both ionic and electronic conductivities by creating additional energy levels inside the forbidden bandgap. Our goal is to explore the microstructural origins of emergent charge transport phenomena such as resistive switching behavior displayed by functional oxide heterostructures. We aim to do this by developing a quantitative understanding of the effect of local energy landscape on diffusion of charge defects and inhomogeneous phase transitions.

Several models have been proposed to explain the transport behavior but no clear experimental evidence supporting the role of local changes in the microstructure or microchemistry has been presented. We will use the expertise in our group to probe the local transport behavior, whilst simultaneously probing the composition and crystal structure of the same region using complementary in-situ TEM experiments combined with conductance AFM (c-AFM) experiments and hard X-ray Nanoprobe experiments (through user proposals to CNM). Our goal is to image the local conduction paths, to identify the majority charge carriers inside the local conduction channels and then to measure their mobility. This will give insights into the mechanism, which can then be correlated with models to allow us to predict and

control this behavior. Understanding the charge transport in the presence of polarization, magnetization, and domain and grain boundaries in addition to charged defects in multiferroic materials is a challenging task. The role of each factor will be carefully explored to understand the effect of local transport behavior.

The submitted manuscript has been created by UChicago Argonne, LLC, Operator of Argonne National Laboratory ("Argonne"). Argonne, a U.S. Department of Energy Office of Science Laboratory, is operated under Contract No. DE-AC02-06CH11357.

References to selected publications of DOE-sponsored research (2010–2012)

"Magnetic interactions and reversal of artificial square spin ices", C. Phatak, M. Pan, A. K. Petford-Long, S. Hong and M. De Graef, *New J. Phys. accepted* (June 2012).

"Direct Observation of Unconventional Topological Spin Structure in Coupled Magnetic Discs", C. Phatak, A. K. Petford-Long, and O. Heinonen, *Phys. Rev. Lett.* **108**, 067205 (2012).

"Ambient effects on electric-field-induced local charge modification of TiO_2," H. Kim, S. Hong, and D.-W. Kim, *Appl. Phys. Lett.* **100**, 022901 (2012)

"Quantitative measurement of in-plane cantilever torsion for calibrating lateral piezoresponse force microscopy, H. Choi, S. Hong, and K. No, *Rev. Sci. Instr.* **82**, 113706 (2011)

"Nanoscale ferroelectric switching behavior at charged domain boundaries studied by angle-resolved piezoresponse force microscopy," M. Park, S. Hong, J. Kim, J. Hong, K. No, *Appl. Phys. Lett.* **99**, 142909 (2011)

"Structure-property relationships in self-assembled MOCVD-grown $CoFe_2O_4$-$PbTiO_3$ multiferroic nanocomposites using three-dimensional characterization," M. Pan, Y. Liu, G.-R. Bai, S. Hong, V. P. Dravid, A. K. Petford-Long, *J. Appl. Phys.* **110**, 034103 (2011)

"Direct observation of fatigue in epitaxially grown $Pb(Zr,Ti)O_3$ thin films using second harmonic piezoresponse force microscopy," N. M. Murari, S. Hong, H. N. Lee, R. S. Katiyar, *Appl. Phys. Lett.* **99**, 052904 (2011)

"Elastic Relaxation and Correlation of Local Strain Gradients with Ferroelectric Domains in (001) $BiFeO_3$ Nanostructures," J. A. Klug, M. Holt, R. N. Premnath, A. Joshi-Imre, S. Hong, R. S. Katiyar, M. J. Bedzyk, O. Auciello, *Appl. Phys. Lett.* **99**, 052902 (2011)

"In situ Lorentz TEM magnetization study of a Ni–Mn–Ga ferromagnetic shape memory alloy", A. Budruk, C. Phatak, A. K. Petford-Long, and M. De Graef, *Act. Mater.* **59**, 4895-4906 (2011).

"In situ Lorentz TEM magnetization studies on a Fe–Pd–Co martensitic alloy", A. Budruk, C. Phatak, A. K. Petford-Long, and M. De Graef, *Act. Mater.* **59**, 6646-6657 (2011).

"Nanoscale structure of the magnetic induction at monopole defects in artificial spin-ice lattices", C. Phatak, A. K. Petford-Long, O. Heinonen, M. Tanase, and M. De Graef, *Phys. Rev. B.* **83**, 174431 (2011).

"On the magnetostatics of chains of magnetic nanoparticles", C. Phatak, R. Pokharel, M. Beleggia, and M. De Graef, *J. of Magn. and Magn. Mater*, **323**, 2912-2922 (2011).

"Effect of annealing and applied bias on barrier shape in CoFe/MgO/CoFe tunnel junctions", Y. Liu, A. N. Chiaramonti, D. K. Schreiber, H. Yang, S. S. P. Parkin, O. G. Heinonen, and A. K. Petford-Long, *Phys. Rev. B*, **83**, 165413 (2011)..

"Effects of Cantilever Buckling on Vector Piezoresponse Force Microscopy Imaging of Ferroelectric Domains in $BiFeO_3$ Nanostructures," R. Nath, S. Hong, J. A. Klug, A. Imre, M. J. Bedzyk, R. S. Katiyar, and O. Auciello, *Appl. Phys. Lett.* **96** (2010) 163101 [Journal Cover]

"Three-dimensional ferroelectric domain imaging of epitaxial $BiFeO_3$ thin films," M. Park, S. Hong, J. A. Klug, M. J. Bedzyk, O. Auciello, K. No, A. K. Petford-Long, accepted for publication in *Appl. Phys. Lett.* (2010).

"Three-dimensional study of the vector potential of magnetic structures", C. Phatak, A. K. Petford-Long and M. De Graef, *Phys. Rev. Lett.* **104**, 253901 (2010).

"Effect of deposition temperature on surface morphology and magnetic properties in epitaxial $CoFe_2O_4$ thin films deposited by MOCVD," M. Pan, G. Bai, S. Hong, V. P. Dravid and A. K. Petford-Long, *J. Appl. Phys.* **107**, 043908 (2010).

"Correlating structural and resistive changes in Ti:NiO resistive memory elements," O. Heinonen, M. Siegert, A. Roelofs, A. K. Petford-Long, M. Holt, K. D'Aquila and W. Li, *Appl. Phys. Lett.* **96**, 103103 (2010).

"The role of interfaces in the behavior of magnetic tunnel junction structures," A. K. Petford-Long, *Internat. J. Mat. Res.* **101**, 16–20 (2010).

Imaging Magnetism by Spin-Polarized Low-Energy Electron Microscopy

Andreas Schmid, *National Center for Electron Microscopy, Lawrence Berkeley National Lab, Berkeley, CA, 94720. Email: akschmid@lbl.gov*

Research Scope

By using a spin-polarized low-energy electron beam to illuminate sample surfaces (SPLEEM), one can simultaneously image a samples magnetic structure while observing MBE-growth of nanoscale materials, or the formation and properties of adsorbate layers, in controlled *in-situ* environments and under dynamic conditions.
Magnetic properties including transition temperatures, the easy-axis of magnetization, etc., depend on sample size and are a sensitive function of contact with other materials, such as substrates or adsorbates, even when the contacting materials are not magnetic. To understand these proximity and confinement phenomena, it is useful to monitor magnetic properties in-situ, during well-controlled sample processing steps.

Recent Progress

Determination of spin-polarized quantum well states and spin-split energy dispersions of Co ultrathin films grown on Mo(110). [1] While imaging by spin-polarized low-energy electron microscopy, epitaxial Co thin films were grown on Mo(110). We find that the spin asymmetry of the electron reflectivity from the Co film alternates its sign as a function of both the electron energy and the Co film thickness as a result of spin-polarized quantum well states in the Co film. By measuring spin-dependent quantum well states, we are able to resolve the spin-split energy dispersions of the Co film. The determined spin-resolved energy bands are further tested by fitting the quantum well states using the phase accumulation model, and the result shows an excellent agreement between the fitting and the experimental data.

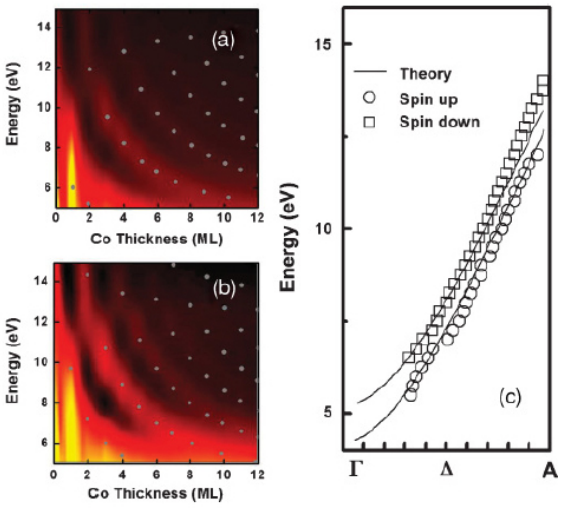

Figure 1: Electron reflectivity for (a) spin-down electrons and (b) spin-up electrons shows layer resolved quantum well states. (c) Spin-split energy bands retrieved from this data. Resonances predicted from the phase accumulation model phase accumulation model [dots in (a) and (b)] which gives the quantization condition of [2]
$2kd_{Co} + \varphi = 2n\pi n = integer$
are in excellent agreement with the experimentally observed reflectivity maxima. (Here d_{Co} is the Co film thickness, k is the electron wave vector, and φ is the phase accumulation of the electron upon reflection at the two boundary surfaces of the Co film.)

This work was done in collaboration with J. S. Park, Y. Meng, J. Li, E. Jin, H. Son, A. Tan, J. Wu, Z. Q. Qiu (UC Berkeley), C. Hwang (KRISS, Korea), H. W. Zhao (CAS, Beijing, China), and A. Quesada (LBNL, Berkeley).

Hydrogen-induced reversible spin-reorientation transition and magnetic stripe domain phase in bilayer Co on Ru(0001). [3] Imaging the change in the magnetization vector in real time by spin-polarized low-energy electron microscopy, we observed a hydrogen-induced, reversible spin-reorientation transition in a cobalt bilayer on Ru(0001). Initially, hydrogen sorption reduces the size of out-of-plane magnetic domains and leads to the formation of a magnetic stripe domain pattern,which can be understood as a consequence of reducing the out-of-plane magnetic anisotropy. Further hydrogen sorption induces a transition to an in-plane easy axis. Desorbing the hydrogen by heating the film to 400 K recovers the original out-of-plane magnetization. By means of ab initio calculations we determine that the origin of the transition is the local effect of the hybridization of the hydrogen orbital and the orbitals of the Co atoms bonded to the absorbed hydrogen. It is conceivable that the high sensitivity of the Co magnetization easy axis to small doses of hydrogen could be employed in devices designed to detect and signal the presence of hydrogen. [4]

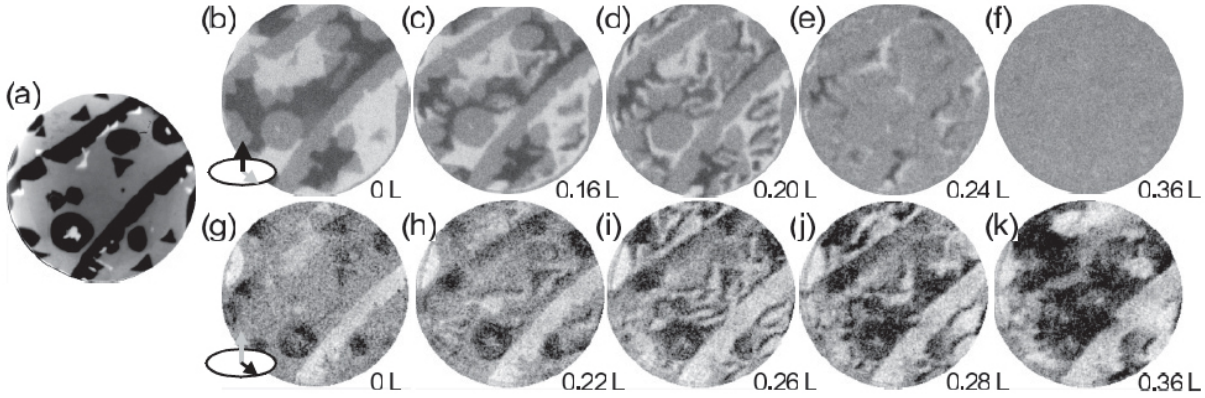

Figure 2: (a) LEEM image of a Co film with 3-ML Co islands (dark areas) on a nearly continuous 2-ML film (medium gray areas). (b)–(f) SPLEEM images with out-of-plane magnetic domain contrast as a function of hydrogen exposure. (g)–(k) SPLEEM images showing the in-plane magnetic domains of the same region during hydrogen exposure after desorbing the initial hydrogen by annealing to 400 K. The dose is indicated in the lower right corner of each SPLEEM image. The field of view (FOV) is 4 μm, and the beam energy is 5.2 eV.

This work was done in collaboration with Juan de la Figuera, Benito Santos, Silvia Gallego (CSIC, Madrid, Spain), Arantzazu Mascaraque (UC Madrid, Spain), Kevin F. McCarty (Sandia, CA), Adrian Quesada, and Alpha T. N'Diaye (LBNL, Berkeley).

Future Plans

Much of our previous work using spin-polarized low-energy electron microscopy addressed structures composed of metals, semiconductors, and adsorbed gases; less has been done on oxides. Exploring low dimensional effects in oxides and oxide heterostructures is an area in which we plan to expand our efforts. To this end, we've started to look at magnetite.

Micromagnetism in (001) Magnetite by Spin-Polarized LEEM. Magnetite has played an important role throughout the history of science and technology [5], e.g., the discipline of paleomagnetism relies to a large extent on its properties. Interest in magnetite as a candidate material for spintronic applications [6] is driven by the predicted half-metal character [7], high conductivity, chemical stability and high-Curie temperature. Promising recent results include the use of magnetite as a spin-injector source [8] as well as observations suggesting that the magnetic properties of magnetite are robust even in the nanometer thickness limit [9]. Using spin-polarized low-energy electron

microscopy, we find that domains are magnetized along the surface [110] directions, and domain wall structures include 90° and 180° walls. A type of unusually curved domain walls are interpreted as Néel-capped surface terminations of 180° Bloch walls.

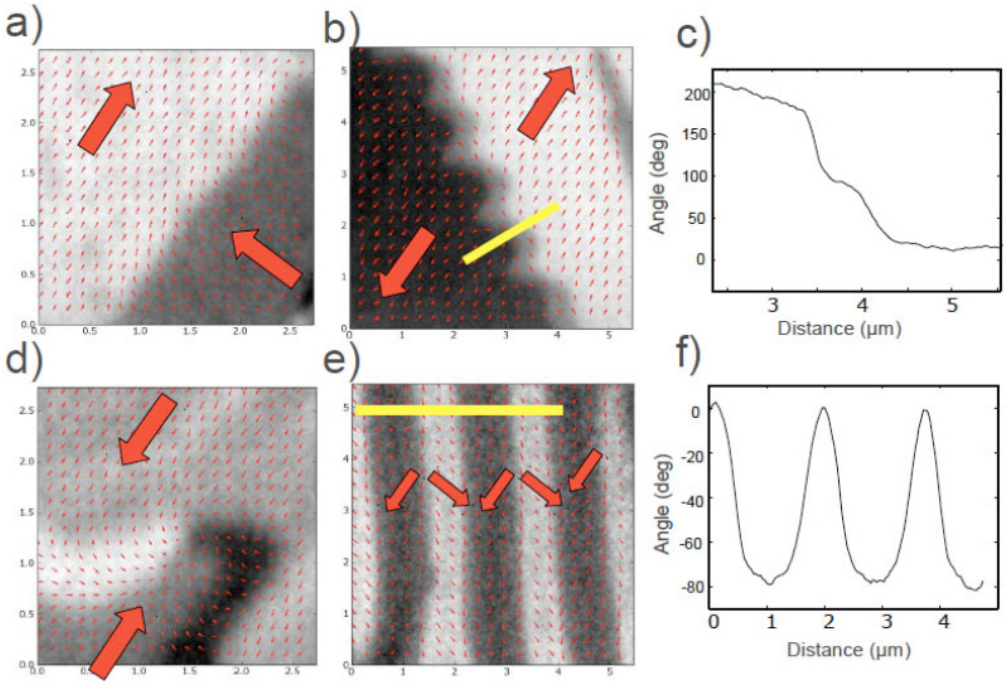

Figure 1. Details of particular magnetization configurations observed on (100) magnetite. Panels (a) and (b): SPLEEM images acquired with spin polarization along the [011] direction, (d) and (e) are acquired with [01-1] spin alignment. Small red arrows show the in-plane magnetization directions as measured from pairs of SPLEEM images acquired with orthogonal beam polarizations, large red arrows indicate average magnetization in each domain. (a) 90° wall, image size 2.7 μm. (b) Wavy 180° wall, image size 5.3 μm. (c) Intensity profile along the line indicated in previous panel suggests that the structure is a 180° Néel-capped Bloch wall. (d) Bloch line separating two sections of opposite chirality within Néel-capped 180° Bloch wall; image size 2.7 μm. (e) Periodic array of 90° walls, image size is 5.3 μm. (f) Image intensity profile across array of 90° walls (along the line indicated in previous panel).

We are pursuing these plans in collaboration with J. de la Figuera, L. Vergara, M. Monti, A. Quesada (CSIC Madrid, Spain), A. T. N'Diaye, G. Chen (LBNL Berkeley)

References

[1] Park J. S., et al., Phys. Rev. B 83, 113405 (2011)
[2] Z. Q. Qiu and N. V. Smith, J. Phys.: Condens. Matter 14, R169 (2002)
[3] Santos B., et al., Phys. Rev. B 85, 134409 (2012)
[4] A. K. Schmid, et al., US Patent No. 032990 (2010)
[5] Allan A. Mills. The lodestone: History, physics, and formation. Ann. Sci. 61, 273, (2004).
[6] M. Bibes and A. Barthelemy. Oxide spintronics. IEEE Trans. Elec. Dev. 54, 1003, (2007).
[7] M. I. Katsnelsonet al., Rev. Mod. Phys. 80, 315, (2008).
[8] E. Wada, et al., Appl. Phys. Lett. 96,102510, (2010).
[9] M. Monti, et al., Physical Review B, 85, 020404, (2012).

DOE sponsored recent publications

1. "Hydrogen-induced reversible spin-reorientation transition and magnetic stripe domain phase in bilayer Co on Ru(0001)", Santos Benito et al., Phys. Rev. B 85, 134409, (2012)
2. "New synthesis method for the growth of epitaxial graphene". Yu X. Z.; Hwang C. G.; Jozwiak C. M.; et al., J. Electron Spectroscopy and Related Phenomena 184, 100 (2011)
3. "Determination of spin-polarized quantum well states and spin-split energy dispersions of Co ultrathin films grown on Mo(110)". Park J. S.; Quesada A.; Meng Y.; et al., Phys. Rev. B 83, 113405, (2011)
4. "Floating two-dimensional solid monolayer of C(60) on graphite". Shin Heekeun; O'Donnell S. E.; Reinke P.; et al., Phys. Rev. B 82, 235427, (2010)
5. "Magnetic imaging with spin-polarized low-energy electron microscopy". N. Rougemaille, A. K. Schmid Eur. Phys. J. Appl. Phys. 50, 20101, (2010)
6. "Periodic step arrays on the aperiodic i-Al-Pd-Mn quasicrystal surface at high temperature".Sato Y, Unal B, Lograsso TA, Thiel PA, Schmid AK, Duden T, Bartelt NC, McCarty KF, Phys. Rev. B 81, 161406 (2010).
7. "A high-efficiency spin-resolved photoemission spectrometer combining time-of-flight spectroscopy with exchange-scattering polarimetry". Jozwiak C, Graf J, Lebedev G, Andresen N, Schmid AK, Fedorov AV, El Gabaly F, Wan W, Lanzara A, Hussain Z, Review Of Scientific Instruments 81, 053904 (2010)
8. "Valence band circular dichroism in non-magnetic Ag/Ru(0001) at normal emission". Arantzazu Mascaraque, T Onur Menteş, Kevin F McCarty, Jose F Marco, Andreas K Schmid, Andrea Locatelli and Juan de la Figuera, J. Phys.: Condens. Matter 23, 305006 (2011)
9. "Design of a hybrid double-sideband/single-sideband (schlieren) objective aperture suitable for electron microscopy". Bart Buijsse, et al., Ultramicroscopy 111(12):1688-1695 (2011)
10. "Depth-dependent magnetism in epitaxial MnSb thin films: effects of surface passivation and cleaning". Aldous, JD et al., Journal Of Physics-Condensed Matter 24 , 146002, (2012)
11. "Widespread spin polarization effects in photoemission from topological insulators". Jozwiak C., Phys. Rev. B 84, 165113, (2011)
12. "Air-Protected Epitaxial Graphene/Ferromagnet Hybrids Prepared by Chemical Vapor Deposition and Intercalation". Coraux, Johann et al., Journal of Physical Chemistry Letters, in press.
13. "Perpendicular magnetic anisotropy of cobalt films intercalated under graphene", N. Rougemaille et al., Appl. Phys. Lett., in press.
14. "Progress Towards An Aberration-Corrected Low Energy Electron Microscope for DNA Sequencing and Surface Analysis", M. Mankos et al., Journal of Vacuum Science and Technology B, in press.

Mapping nanoscale chemical and optoelectronic properties by multidimensional nanospectroscopic imaging

***P. James Schuck*[1]**

with Wei Bao,[1,2] Mauro Melli,[1] Alex Weber-Bargioni,[1] Paul Ashby,[1] D. Frank Ogletree,[1] F. Intonti,[3] D. S. Wiersma,[3] J. Bokor,[1,2] Miquel B. Salmeron,[1,2] Stefano Cabrini[1]

[1] *Molecular Foundry, Lawrence Berkeley National Laboratory, One Cyclotron Road, Berkeley, Ca 94720, USA*

[2] *UC Berkeley, 210 Hearst Mining Building, Berkeley, CA 94720, USA*

[3] *European Laboratory for Non-linear Spectroscopy, 50019 Sesto Fiorentino (FI), Italy*

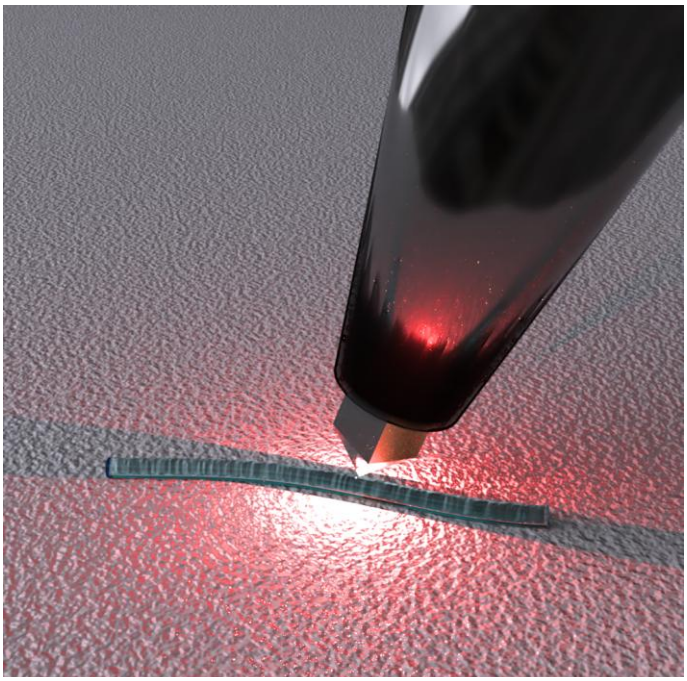

With the promise of combining the rich chemical information and ultrafast temporal resolution inherent to optical spectroscopy with the high-spatial-resolution capabilities of modern scan-probe techniques, tip-enhanced nanospectroscopic imaging is emerging as an important characterization technique in nanoscience.[1] In general, however, the technique has been limited either by relatively low near-field enhancements and signal levels or by experimental geometries that significantly constrain the types of samples that can be studied. In conventional tip-enhanced spectroscopy, a sharp metallic tip is used to locally enhance both the excitation light field and the Raman scattered signal. Enhancement is maximized when optical signals excite surface plasmons on the tip, and spatial resolution is determined by the tip's radius of curvature – typically 10-20 nm.

It is well known that a single sharp metal tip acts as a rather crude far-field to near-field transducer (i.e. – a crude optical antenna), and that much greater enhancements can be achieved with optical antenna geometries based on plasmonically-coupled elements. Such a geometry is realized in the so-called gap-mode configuration, where a metal tip is held ~ 1nm above a metallic substrate (with the sample located in the gap), effectively forming a vertically-oriented coupled dipole- or bowtie-like plasmonic antenna.[2] Ultra-large enhancements have been observed in this geometry, but the requirements of gap mode operation render it quite limiting in practice. It requires both a metallic substrate and very small tip-substrate gap, meaning only

very thin samples (e.g. molecular monolayers) can be investigated, precluding many classes of nanoscale structures and devices.

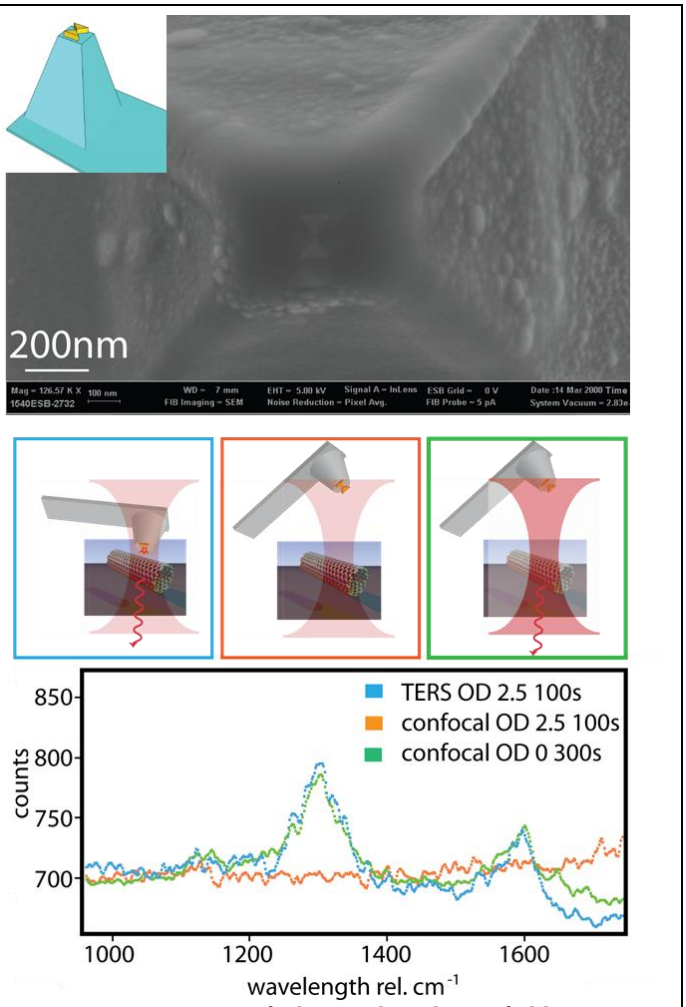

Fig. 1. An SEM image of a bowtie-based near-field tip is shown in the top panel. To date, these tips have provided the largest known TERS enhancements on a dielctric substrate (bottom panels)

This has motivated our efforts to engineer coupled optical antenna structures directly on the scan-probe tip. Initial efforts along these lines had been hindered by fabrication constraints, but recent advances at the Molecular Foundry have made it possible to reliably create such next-generation tip-enhanced nanospectroscopy probes.[3] Here we discuss how such engineered tips offer the solution to the longstanding "nanospectroscopy imaging" problem, using them to hyperspectrally map chemical and optoelectronic properties of at the relevant length scales of critical processes in nanomaterials.

One probe design consisted of a Au bowtie optical antenna fabricated at the end of a tip (Fig. 1). Our nanoantenna-based tips are fabricated using the induced-deposition mask lithography (IDML) technique.[3] This method is useful for reproducibly creating high-resolution plasmonic and photonic nanostructures on nearly any substrate, including the apexes of scan-probe tips. An example of our tip-enhanced Raman spectrosocpy data from carbon nanotubes (CNTs) is shown in Fig. 1. With the bowtie tip in contact with the sample, a TERS spectrum was collected using an incident power of 1 μW and a 100 s integration time (Fig. 1, blue curve). The tip was then retracted approximately 5 μm from the sample and another spectrum was acquired with the same excitation power and integration time. Under these conditions, no significant CNT signal was detected (Fig. 1, orange curve). In order to achieve a spectrum comparable to the tip-down case, we had to increase the excitation power by a factor of 300 and integration time by a factor of 3 (Fig. 1, green curve), demonstrating a tip-down vs. tip-up enhancement (one of the most conservative methods for estimating enhancement) of ~900, the largest non-gap-mode TDTU value to date.

Using another probe geometry, which is based on coaxial plasmonic antennas (Fig. 2), we have demonstrated hyperspectral tip-enhanced Raman imaging on dielectric substrates.[4] Our coaxial probes avoid the limitations associated with the "tip-substrate gap-mode" imaging geometry by again placing the gap at the end of the tip. A full Raman spectrum was acquired at each pixel of a 256 by 256 pixel contact-mode atomic force microscope image of carbon nanotubes grown on a fused silica microscope cover slip, allowing D and G mode intensity and D-mode peak shifts to be measured with ~ 20 nm spatial resolution. Tip enhancement was sufficient to acquire useful Raman spectra in 50-100 ms. Coaxial scan probes combine the efficiency and enhanced, ultralocalized optical fields of plasmonically-coupled antennae with the superior topographical imaging properties of sharp metal tips. The yield of the coaxial tip fabrication process is close to 100%, and the tips are sufficiently durable to support hours of contact-mode force microscope imaging.

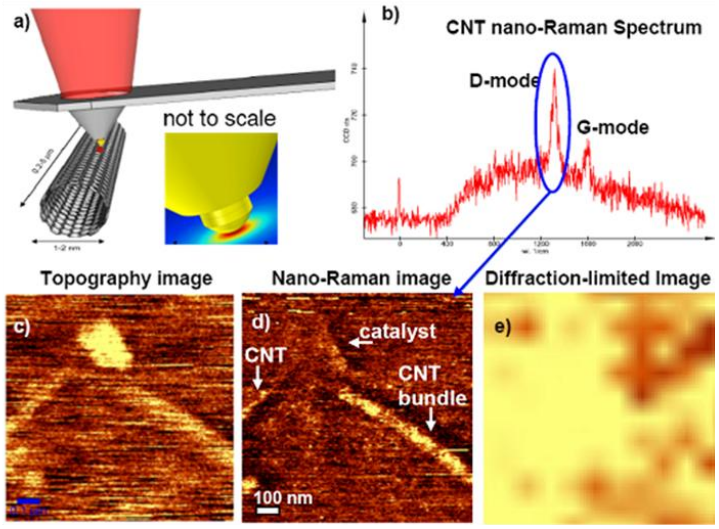

Fig. 2. Plasmonic coaxial antenna tips (a) were used for hyperspectral nano-Raman imaging of carbon nanotubes with 20 nm resolution. A representative nano-Raman spectrum is shown in (b). (c)-(e) show topographic and and spectral images of CNTs using the D-mode vibration peak .intensity.

Finally, we have recently demonstrated a near-ideal nano-optical probe, which we call the "campanile" tip, since it resembles a bell tower of the same name (Fig. 3). Specifically, we have mapped the influence of local trap states within individual nanowires on carrier recombination rates and energies with resolution well below the diffraction limit, i.e. at the length scales relevant to critical processes in nanomaterials. This is achieved using multidimensional nanospectroscopic imaging based on the campanile nano-optical device concept, which overcomes the major limitations currently restricting spectroscopy measurements at the nanoscale. The device, placed at the end of a scan probe, delivers optimal near-field properties including highly-efficient far-field to near-field coupling, ultra-large field enhancement and sensitivity, nanoscale resolution, almost-background-free imaging, and independence from sample and substrate requirements – all with a broadband spectral response. This structure enables the expansion of nano- and nonlinear-optics beyond their current niche roles in nanoscience. Here, ~40 nm resolution hyperspectral imaging of InP nanowires is performed via excitation and collection through the probes, revealing optoelectronic structure along individual indium phosphide nanowires that is not accessible with other existing methods.[5]

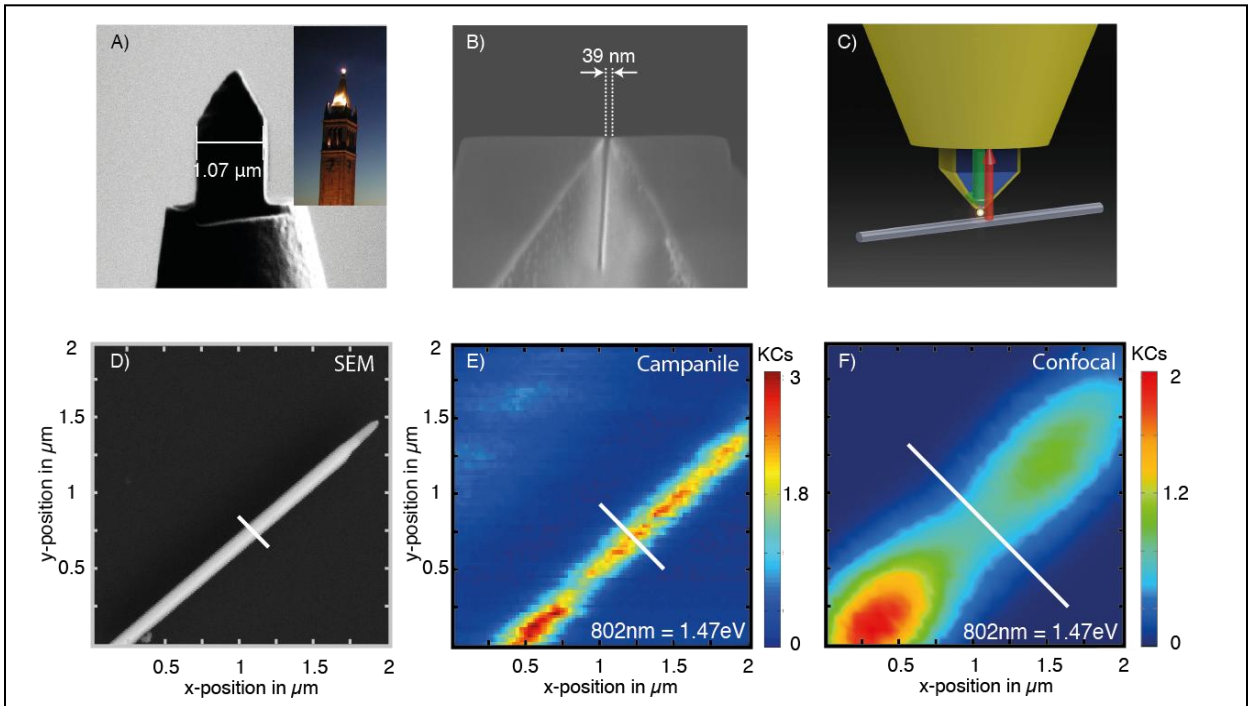

Fig. 3. Fabricated next-generation near-field "Campanile" tips used for nano-optical hyperspectral mapping of InP nanowires. The campanile structure was fabricated at the end of a tapered glass fiber (A) via focused ion beam milling, resembling a bell tower of the same name (inset: photo of the Berkeley Campanile), with a 39 nm (±2 nm) gap between the 3D-tapered Au plates (B). These near-field probes were used to both locally excite InP NWs and collect the scattering/emission through the campanile structures (C). Shown in D) is an SEM image of the InP NW, which had emission from its surface states hyperspectrally mapped with the Campanile tip (E) (100uW excitation power, 10msec/spectrum, map at 802nm), and confocally (F) (900uW, 10msec/spectrum, map at 802nm). The near-field map shows considerably higher spatial resolution then the confocal map

1 L. Novotny and B. Hecht, *Principles of Nano-Optics*. (Cambridge University Press, 2006).
2 J. Stadler, T. Schmid, and R. Zenobi, Nanoscale **4**, 1856 (2012).
3 A. Weber-Bargioni, A. Schwartzberg, M. Schmidt et al., Nanotechnology **21**, 065306 (2010).
4 A. Weber-Bargioni, A. Schwartzberg, M. Cornaglia et al., Nano Lett. **11**, 1201 (2011).
5 Wei Bao, M. Melli, N. Casseli et al., In Prep. (2012).

Direct observation of Ferromagnetic Nanoclusters and Their Role in Colossal Magnetoresistance

J. Tao, L. Wu, V.V. Volkov, and Y. Zhu
Dept. of Condensed Matter Physics and Materials Science
Brookhaven National Laboratory, Upton, NY 11973
Email: jtao@bnl.gov

Research Scope

The focus of this research task under the FWP Number MA-015-MACA is to explore nanoscale phenomena that control the functionality of technologically important materials having significant relevance to the DOE's energy mission. It covers three major research areas: 1) understanding the interplay between charge, orbital, spin and lattice in strongly correlated systems; 2) electronic structures, structural defects and interfaces in oxides; and 3) energy materials. Emphasis is on the understanding of structure-property relationships and the underlying mechanisms for the complex physical behavior of various functional materials including high-temperature superconductors, multiferroics, thermoelectric materials, catalysts, and batteries. Advanced quantitative electron microscopy techniques, such as coherent electron diffraction, electron nanodiffraction, atomic imaging, electron spectroscopy, Lorentz imaging and phase retrieval methods are extended to study these materials. Experiments are closely coupled with structural modeling and theory. Although electron scattering and microscopy are the primary tools, complementary methods such as synchrotron x-ray, neutron scattering and scanning tunnel microscopy are also used.

Recent Progress

Electronic inhomogeneities that give rise to unique material properties have been considered as one of the most important discoveries in condensed matter physics in the past decade. In the area of strongly correlated electron systems, we have studied manganites with intriguing colossal magnetoresistance (CMR) and focused on a nanoscale phase with structural modulation that resulted from the complex spin-charge-orbital-lattice interplay. Our earlier work showed that this nanoscale phase is in form of nanoclusters and is a key to understand the CMR [1]. However, the measurement of the magnetic and physical properties of these nanoclusters that are embedded in bulk materials becomes a challenging task. Without direct experimental evidence, the role of the nanoclusters in CMR remains illusive.

In order to understand magnetic and physical properties of the nanoclusters, we used advanced transmission electron microscopy (TEM) techniques including Lorentz imaging (Fig. 1) and scanning electron nanodiffraction (Fig. 2), and the TEM observations were intimately correlated with property measurements. In particular, we discovered unexpected magnetic behavior in doped $La_{1-x}Ca_xMnO_3$ systems, which cannot be interpreted by any existing theoretical models. Surprisingly, TEM observations enable us to reach a unique solution to successfully explain the bulk measurements by the following findings. Unlike the longstanding hypothesis that the nanoclusters are antiferromagnetic and insulating, we found, for the first time, that the nanoclusters are ferromagnetic and conducting at the CMR temperature, while they become antiferromagnetic and insulating at temperatures well below the CMR transition. We unveiled a new level of complexity of nanoscale phase separation scenario in doped manganites that upon cooling, parts of the material undergo a phase transition from paramagnetic phase to ferromagnetic nanoclusters (first-order transition) while the others go through a conventional second-order transition from paramagnetic to ferromagnetic in a different form as submicron lamellar domains. Through the phase transitions, the ferromagnetic nanoclusters compete with the surrounding paramagnetic phase and ferromagnetic submicron domains. The spin moments of the nanoclusters and the submicron domains are antiparallel to each other, and such alignment can be changed by applied magnetic field. Therefore, the magnetization and the resistivity were measured to be a function of temperature, magnetic field and doping levels. More importantly, a new CMR mechanism was thus proposed based on those results in doped manganites that the percolation of the conducting nanoclusters with structural modulation forms an electron path to cause a drastic change in the resistivity measurements [2, 3].

Furthermore, the findings here led to a deeper understanding of the nature of the nanoclusters. Since the discovery of the nanoclusters with the structural modulation, they have been called "charge-ordered" nanoclusters, named by a long-range-ordered phase that is the ground state at different doping level in $La_{1-x}Ca_xMnO_3$ with superstructural modulation as well. However, we found the ferromagnetic to antiferromagnetic transition inside the nanoclusters is accompanied by a structural transition. Considering the nanoclusters could possess different magnetic order and resistivity (ferromagnetic and conducting) than the "charge-ordered" phase (antiferromagnetic and insulating), this fact of the structural transition evidently indicates that the ferromagnetic nanoclusters are intrinsically different with the long-range "charge-ordered" phase, but the antiferromagnetic nanoclusters at low temperatures have similar superstructure as that in the "charge-ordered" state. We believe such results are necessary to answer the questions raised in previous reports such as why the estimation of the volume fraction of nanoclusters is inaccurate by using the diffraction intensities [1-3].

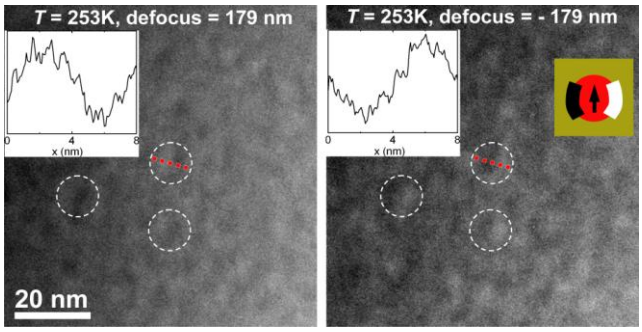

Fig.1 Direct observation of ferromagnetic nanoclusters in doped manganites. Using Lorentz imaging technique, nanoclusters at the temperature corresponding to CMR in $La_{0.55}Ca_{0.45}MnO_3$ show black and white line-contrast at cluster edges, which can be switched with positive and negative defocus values. Such contrast disappears in the Lorentz images at temperatures without nanoclusters. Therefore, the figures on right provide direct evidence of in-plane ferromagnetism in the nanoclusters. Size of the nanoclusters was measured to be consistent with the result from other microscopic methods.

Future Plans

We will continue our study of the CMR phenomenon, focusing on the competing degrees of freedom of spin, charge, orbital and lattice and quantification of the interactions among these orders (temperature affects the entropy of different orders, magnetic field strongly influences spin-lattice, chemical potential and Coulomb energy play a critical role in the charge-orbital coupling). TEM observations will be correlated with property measurements for manganites with various dopant concentrations (e.g., the nanoscale phase separation of $La_{0.33}Ca_{0.67}MnO_3$, as shown in Fig. 2). The nanoscale phase separations will be characterized by in-situ electron diffraction, electron nanodiffraction, electron energy-loss spectra and high-resolution TEM. We will also investigate the electron-electron and electron-phonon interaction and separate their contribution to the CMR effects using a time-resolved pump-probe approach. Evolution of various charge/orbital ordered phases will also be studied with the time-resolved ultrafast electron diffraction instrument (2MeV and 100fs) we recently built. The study will provide not only insights into manganites, but also guidance for understanding correlated materials which may reveal completely new laws of physics.

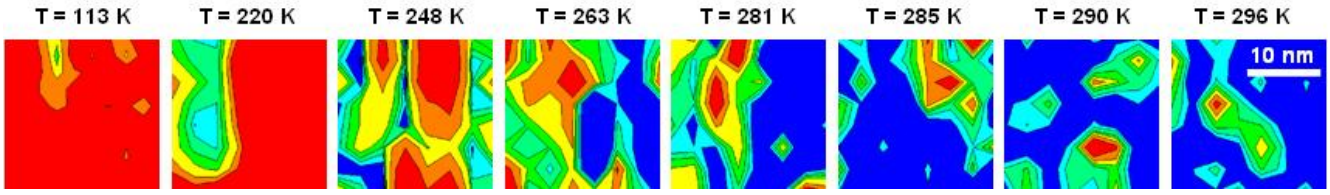

Fig. 2. Evolution of phase separation scenario during phase transition in $La_{0.33}Ca_{0.67}MnO_3$ mapped by scanning electron nanodiffraction. Areas in warm color are corresponding to structural modulation while areas in blue means no structural modulation.

The work was supported by the U.S. Department of Energy, Division of Materials Science and Engineering, Office of Basic Energy Science, under Contracts No. DE-AC02-98CH10886.

References

[1] Tao, J., et al., "Direct imaging of nanoscale phase separation in $La_{0.55}Ca_{0.45}MnO_3$: relationship to colossal magnetoresistance", *Phys. Rev. Lett.* 103, 097202 (2009)

[2] Tao, J., et al, "Role of structurally and magnetically modified nanoclusters in colossal magnetoresistance", *Proc. Natl. Acad. Sci.* 108, 20941 (2011).

[3] Tao, J., "Nanoclusters in Magnetoresistance", *Nanotechnology Reviews* (invited review article), in press (2012)

DOE Sponsored Publications in 2012-2010

The publication list under FWP MA-015-MACA for 2012 and 2010 is attached to an addition abstract in this program book: "Direct Observations of Magnetic Monopoles and Vortex-Core Precession Orbit with Electrons", by Y. Zhu, S. Pollard, M.G. Han, L. Wu, V.V. Volkov and J. Tao.

2011

Cai, Y., Ma, C., Zhu, Y., Wang, J.X., and Adzic, R.R., "Low-Coordination Sites in Oxygen-Reduction Electrocatalysis: Their Roles and Methods for Removal". Langmuir 27 8540-8547 (2011).

Chen, H., Wu, L., Zhang, L., Zhu, Y., Grey, C.P., "LiCoO2 Concaved Cuboctahedrons from symmetry - controlled topological reactions", J. Am. Chem. Soc., 133, 262-270 (2011).

Ciston,J., Si, R., Rodriguez, J.A., Hanson, J.C., Martínez-Arias,A., Fernandez-García,M., and Zhu, Y., "Morphological and Structural Changes during the Reduction and Reoxidation of CuO/CeO2 and Ce1 xCuxO2 Nanocatalysts: In Situ Studies with Environmental TEM, XRD, and XAS", J. Phys. Chem. C 115, 13851–13859 (2011).

Gong, K., Vukmirovic, M.B., Ma, C., Zhu, C., and Adzic, R.R., "Synthesis and catalytic activity of Pt monolayer on Pd tetrahedral nanocrystals with CO-adsorption-induced removal of surfactants", Journal of Electroanalytical Chemistry 662 213 (2011).

Inada, H., Su, D., Egerton, R.F., Konno, M., Wu, L., Ciston, J., Wall, J., and Zhu, Y., "Atomic Imaging Using Secondary Electrons in a Scanning Transmission Electron Microscope : Experimental Observations and Possible Mechanisms", invited articles for the special issue in honor of John Spence, Ultramicroscopy 111 865-876 (2011).

Jang, H. W.; Felker, D. A.; Wang, Y.; Niranjan, M. K.; Zhang, Y.; Nelson, C. T.; Su, D.; Folkman, C. M.; Bark, C. W.; Baek, S. H.; Lee, S.; Janicka, K.; Zhu, Y.; Pan, X. Q.; Fong, D.; M. S. Rzchowski, C. B. E., "Strongly-correlated two-dimensional electron gas at oxide interfaces", Science, 331, 886-889 (2011).

Lu, Z., Chen, H., Robert, R., Zhu, B.X.Y., Deng, J., Wu, L., Chung, C.Y., and Grey, C.P., "Citric Acid- and Ammonium-Mediated Morphological Transformations of Olivine LiFePO4 Particles", Chem. Mater., 23, 2848-2859 (2011).

Meng, Q., Welch, D.O., and Zhu, Y., "Oxygen reordering near room temperature in YBa2Cu3O6+x: A thermodynamic model", Phys. Rev. B 83, 144106 1-6 (2011).

Meng, Y.-S., McGilvray, T., Yang, M.-C., Gostovic, D., Wang, F., Zeng, D., Zhu, Y., and Graetz, J., "In Situ Analytical Electron Microscopy for Probing Nanoscale Electrochemistry", Interface, The Electrochemical Society, 20, 49-53 (2011).

Ofan, A., Gaathon, O., Zhang, L., Evans-Lutterodt, K., Bakhru, S., Bakhru, H., Zhu, Y., Welch, D., Osgood, Jr. R.M., "Twinning and dislocation pileups in heavily implanted LiNbO3", Phys. Rev. B, 83, 064104 1-8 (2011).

Smadici, S., Lee, J.C.T., Morales, J., Logvenov, G., Pelleg, O., Bozovic, I., Zhu, Y., and Abbamonte, P., "Graded orbital occupation near interfaces in a La2NiO4-La2CuO4 superlattice", Phys. Rev. B 84, 155411 1-10 (2011).

Su, D., Meng, Q., Vaz, C. A. F., Han, M.-G., Segal, Y., Walker, F. J., Sawicki, M., Broadbridge, C., and Ahn, C. H., "Origin of 90o domain wall pinning in Pb(Zr0.2Ti0.8)O3 heteroepitaxial thin films", Applied Physics Letters, 99, 102902 (2011).

Sutter, E., Albrecht, P., Wang, B., Bocquet, M.-L., Wu, L., Zhu, Y., and Sutter, P., "Monodisperse Ru nanocluster arrays templated by monolayer graphene on Ru", Surface Science, 605 1676-1684 (2011).

Tao, T., Niebieskikwiat, D., Jie, Q., Schofield, M.A., Wu, L.,, Li, Q., and Zhu, Y., "Role of structurally and magnetically modified nanoclusters in colossal magnetoresistance", *Proc. Natl. Acad. Sci.* 108, 20941–20946 (2011).

Tan, Z., Patel, V., Likharev, K. K., Su, D., and Zhu, Y., "Experimental study of resistive bistability in metal oxide junctions", Appl. Phys. A (2011) 103, 293-300.

Valset, K., Taftø, J., Wu, L., and Zhu, Y., "Anharmonic thermal motion of atoms in thermoelectric Mg2Si studied via convergent-beam electron diffraction", Phys. Rev. B 84, 220301(R) (2011).

Wang, J.X., Ma, C., Choi, Y.-M., Su, D., Zhu, Y., Liu, P., Si, R., Vukmirovic, M.B., Zhang, Y., and Adzic, R.R., " Kirkendall Effect and Lattice Contraction in Nanocatalysts: A New Strategy to Enhance Sustainable Activity", J. Am. Chem. Soc., 133, 13551–13557 (2011).

Wang, X.J., Chen, H.-Y., Yu, X., Wu, L., Nam, K.-W., Bai, J., Li, H., Huang, X., and Yang, X.-Q., "A new in situ synchrotron X-ray diffraction technique to study the chemical delithiation of LiFePO4", Chem. Commun., 47 7170-7172 (2011).

Wang, F., Graetz, J., Moreno, M.S., Ma, C., Wu, L., Volkov, V.V., and Zhu, Y., "?Chemical Distribution and Bonding State of Lithium in Intercalated Graphite: Identification with Optimized Electron Energy-loss Spectroscopy", ACS Nano, 5 1190-1197 (2011).

Wang, F., Robert, R., Chernova, N. A., Pereira, N., Omenya, F., Badway, F., Hua, Ruotolo, X., M., Zhang, R., Wu, L., Volkov, V., Su, D., Key, B., Whittingham, M. S., Grey, C. P., Amatucci, G. G., Zhu, Y., and Graetz, J., "Conversion Reaction Mechanisms in Lithium Ion Batteries: Study of the Binary Metal Fluoride Electrodes", J. Am. Chem. Soc., 133, 18828–18836 (2011).

Wu, L., Nam, K.-W., Wang, X., Zhou, Y., Zheng, J.-C., Yang, X.Q., and Zhu, Y., "Structural Origin of Overcharge-Induced Thermal Instability of Ni-Containing Layered-Cathodes for High-Energy-Density Lithium Batteries", Chem. Mater., 23, 3953-3960 (2011).

Zeng, J.; Tao, J.; Li, W.; Grant, J.; Zhu, Y. and Xia, Y., "A mechanistic study on the formation of silver nanoplates in the presence of silver seeds and citric acid or citrate ions", Chem. Asian J., 6, 376 – 379 (2011).

Zeng J., Tao J., Su D., Zhu Y., Qing. D., and Xia Y., "Selective Sulfuration at the Corner Sites of a Silver Nanocrystal and Its Use in Stabilization of the Shape", Nano Lett. 11, 3010-3015 (2011).

Zheng , Y., Tao, J., Liu, H., Zeng, J., Yu, T., Ma, Y., Moran, C., Wu, L., Zhu, Y., Liu, J., and Xia, Y., "Facile Synthesis of Gold Nanorice Enclosed by High-Index Facets and Its Application for CO Oxidation", Small, 7 2307-2312 (2011).

Zhou, H., Wang, H.-Q., Wu, L., Zhang, L., Kisslinger, K., Zhu, Y., Chen, X., Zhan, H., and Kang, J., "Wurtzite ZnO (001) films grown on cubic MgO (001) with bulk-like opto-electronic properties", Appl. Phys. Let., 99, 141917 (2011).

Zhou, X., Wang, F., Zhu, Y., and Liu, Z., J. of Mater. Chem. "Graphene modified LiFePO4 cathode materials for high power lithium ion batteries", J. Mater. Chem., 21, 3353-3358 (2011).

Zhou, J., Jie, Q., Wu, L., Dimitrov, I., Li, Q., and Shi, X., "Nanostructures and defects in nonequilibrium-synthesized filled skutterudite CeFe4Sb12", J. Mater. Res., 26, No. 15, (2011).

Zhu, Y., and Inada, H., "Scanning Electron Microscopy", Encyclopedia of Nanotechnology, Springer, 2011

An atomic resolution view at magnetic oxides

Maria Varela, Stephen J. Pennycook, Andrew R. Lupini, Sokrates T. Pantelides
Collaborators: Jaume Gazquez, Juan Salafranca, Neven Biskup, Manuel Roldan, Mark Oxley.
mvarela@ornl.gov, pennycooksj@ornl.gov, arl1000@ornl.gov, pantelides@vanderbilt.edu
Materials Science and Technology Division, Oak Ridge National Laboratory, Oak Ridge, TN 37831

Program Scope

This sub-program is aimed at understanding the physical properties of complex oxides through atomic resolution imaging and spectroscopy techniques in the scanning transmission electron microscope (STEM). In this abstract we present a number of examples regarding magnetic oxide thin films, interfaces and nanoparticles through a combination of annular dark field (ADF) imaging, electron energy loss spectroscopy (EELS) and first-principles theory.

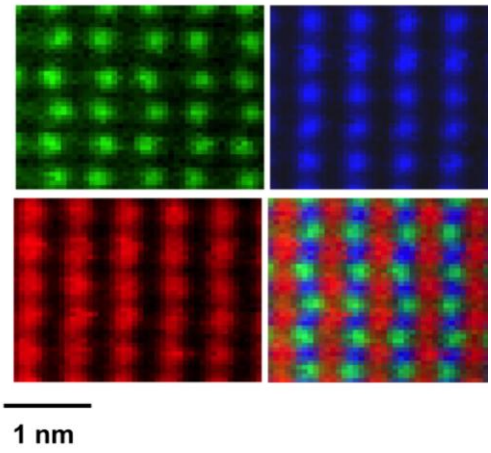

Fig. 1. Spectroscopic imaging of $LaMnO_3$ down the pseudocubic ⟨110⟩ axis, at 60 kV. In green, the O *K* edge image; in blue the simultaneously acquired Mn $L_{2,3}$ image and in red the La $M_{4,5}$ image. The RGB is the overlay of the three elemental maps.

Recent Progress

Magnetic materials exhibit fascinating novel behaviors and have applications ranging from data storage to sensors, spintronic devices, generators, motors and energy materials. Controlling interfacial or surface magnetism at the monolayer level is the key to achieving such devices. This project relies on understanding how magnetism works at the atomic scale, especially in low dimensions and in the presence of defects, surfaces, interfaces, etc. Novel phenomena such as unconventional band filling, charge leakage, symmetry breaking, finite size effects, dead layers or determining defects may arise which can only be studied in real space. Currently, a number of microscopy techniques sensitive to magnetism are available. Unfortunately, none provides a comprehensive tool at high enough spatial resolution. Electron microscopy is the pioneering technique in achieving sub–Å resolution for imaging of materials. Unprecedented advances in instrumentation are pushing the limits into the atomic regime, both in imaging and spectroscopy (even at low acceleration voltages, **Fig. 1**).

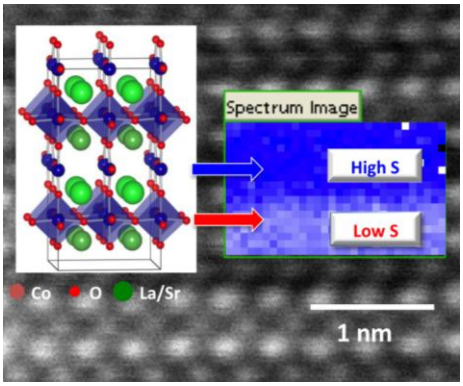

Fig. 2. Real-space, atomic-resolution mapping of a spin state superlattice in $La_{0.5}Sr_{0.5}CoO_{3-\delta}$. Insets: crystal structure along with the map of the O *K* edge normalized pre-peak intensity, which for this compound correlates with the spin state of Co atoms [Gazquez 2011].

Here, we explore new avenues relying on imaging modes sensitive to magnetic properties such as orbital moment or spin. For this purpose, spectroscopic techniques have been exploited in order to develop the full potential of electron beams. Our recent advances have demonstrated the sensitivity of EELS to magnetic quantities through the study of the near edge fine structure, giving proof of principle that atomic resolution mapping of magnetism in real space is indeed possible. In some systems, such as cobaltite oxide thin films, specific features of the near edge fine structure such as the pre-peak of the O *K* edge are sensitive to the Co atoms spin state, as shown in **Fig. 2**. Atomic resolution mapping of the pre-peak feature has recently allowed, for the

first time, the imaging in real space of a superlattice of the spin state of Co in this system [Gazquez 2011].

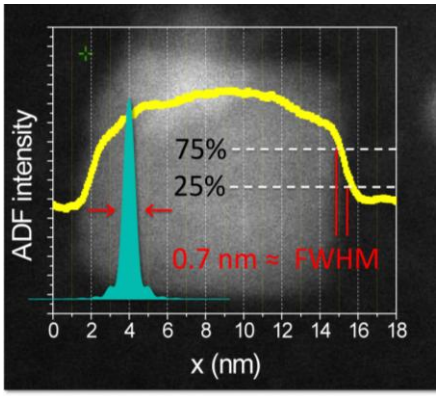

Fig. 3. ADF image of a cubic magnetite nanoparticle acquired at the Nion ultraSTEM100 in ORNL using the nanodiffraction mode. The edge of the particle can be used to estimate the full width at half maximum of the electron beam, 0.7 nm approx.

Among other approaches that we have recently explored is the use of electron magnetic circular dichroism (EMCD) in the electron microscope. EMCD is the counterpart of x-ray magnetic circular dichroism (XMCD). The experimental setup in the electron microscope can be made analogous to the circularly polarized incident beam of photons. A superposition of two plane waves with a relative phase shift of $\pm\pi/2$ can be produced at the target atom and an energy loss with mutually perpendicular momentum transfers can be detected. This approach can be fulfilled by placing the objective aperture on two conjugate positions of the diffraction pattern, thus selecting perpendicular momentum transfers q and q'. This way the chirality of the allowed transitions relative to the magnetic moments can be changed and two electron energy loss spectra can be obtained, one for each configuration. The chiral signal is the difference of two spectra, and as with XMCD, is proportional to the magnetic moment. The optics, cold field emission gun and the high collection efficiency of ORNL's 5th order aberration corrected STEMs provide a unique environment in which to push this line of research. The Nion UltraSTEM100 can produce nanodiffraction (ND) conditions with an electron beam below 1 nm in size (see **Fig. 3**) and with 100% collection efficiency, while the newly installed Nion UltraSTEM 200 is capable of forming an electron probe 0.5 nm in width in convergent beam mode. They enable optimal tuning of beam convergence and spatial resolution, and the trade off between sensitivity to magnetism (best with a parallel beam) and spatial resolution (requiring a convergent beam) can be explored at the click of a mouse.

The optics of the STEM have been optimized to perform high spatial resolution *EMCD spectrum imaging* (EMCDSI) measurements in order to be able to provide quantitative magnetization maps in real space. This approach is ideal to study reduced dimensionality oxide systems - nanowires or nanoparticles – which are of great interest for sensors, biomedical applications, electronic devices, magnetic storage, nano-motors, energy materials and many others. Their magnetic properties are highly dependant on the surface/bulk ratio. This is very often due to the presence of magnetically disordered or even dead layers at the surface that depress the macroscopic magnetic properties. In some cases, outstanding properties can be produced by high temperature methods involving organic acid capped metal oxide nanoparticles, finally making these particles ideal for magnetic storage, energy or medical applications. Understanding the nature of enhanced surface magnetism in these systems is a must towards harnessing their properties.

Our EMCDSI experiments show that it is indeed possible to spatially map the dichroic signal. **Figure 4** shows two

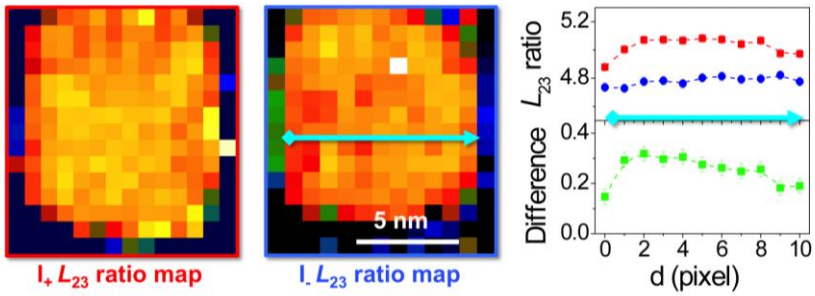

Fig. 4. Color coded $L_{2,3}$ ratio maps obtained from a spectrum image of the nanoparticle shown in **Fig. 3** acquired at I_+ and at I_-, respectively, along with the $L_{2,3}$ profile along the direction of the blue arrow. The right panel shows the difference between the I_+ and I_- L_{23} ratios, which should be proportional to the local magnetic moment.

L_{23} intensity ratio maps obtained from the analysis of the experiment depicted in **Fig. 3**. The lower panels show the values of the L_{23} ratios along the blue arrows for both maps. A clear difference between such values is observed, associated with the local value of the magnetic moment per pixel, the pixels being below 1 nm^2 in size. In this particular case, these experiments show how the surface magnetization of these nanoparticles is relatively high, barely 30% lower than in the center (bulk), confirming that the surface is passivated by the oleic acid surfactant and no dead layer is present. Atomic resolution EELS and Density-Functional Theory (DFT) has been used to understand the nature of the bond between the fatty acid and the surface, and the electronic properties of the surface atoms.

Future directions

A unexplored frontier of magnetic imaging lies at high spatial resolution, beyond the sub-nanometer regime. Novel opportunities such as developing a magneto-optical imaging mode by studying the dichroic signal associated with plasmon and optical excitations will be pursued. Such capabilities could be furthermore enhanced if in the future ORNL were to acquire a monochromated electron source for the aberration corrected STEM. If successful, this approach will open a new realm of possibilities. On the one hand, characterization of magnetic materials will be easier thanks to the high signals of the low loss regime. But also it will allow direct imaging of the interactions of magnetic fields with optical properties in the nanometer scale and in real space. Such techniques will create a unique opportunity to study emerging magnetic phenomena in low dimensional and artificially structured materials such as thin films, interfaces, nanowires, nanoparticles and beyond.

DOE-sponsored journal publications 2010-2012

(Note: this list only includes publications involving M. Varela. For the rest, see S. J. Pennycook's abstract)

C. J. C. Bennett, H. S. Kim, M. Varela, et al., "Compositional tuning of the strain-induced structural phase transition and of ferromagnetism in $Bi_{1-x}Ba_xFeO_{3-d}$," *Journal of Materials Res.* **26,** 1326-1331 (2011).

F. Y. Bruno, J. Garcia-Barriocanal, M. Varela, N. M. Nemes, P. Thakur, J. C. Cezar, N. B. Brookes, A. Rivera-Calzada, M. Garcia-Hernandez, C. Leon, S. Okamoto, S. J. Pennycook, J. Santamaria, "Electronic and magnetic reconstructions in $La_{0.7}Sr_{0.3}MnO_3/SrTiO_3$ heterostructures: A case of enhanced interlayer coupling controlled by the interface," *Phys. Rev. Letts.* **106,** 147205 (2011).

A. Carretero-Genevier, J. Gazquez, C. Magen, M. Varela et al., "Chemical synthesis of oriented ferromagnetic LaSr-2x4 Mn oxide molecular sieve wires," *Chem. Commun.* **50**, 6223-6225 (2012).

A. Carretero-Genevrier, J. Gazquez, J. C. Idrobo, J. Oro, J. Arbiol, M. Varela et al., "Single crystalline LSMO nanowires with high temperature ferromagnetism." *J. Am. Chem. Soc.* **133**, 4053–4061 (2011).

J. Chakalian, J. M. Rondinelli, J. Liu, B. Grey, M. Kareev, E.J. Moon, N. Prasai, J. Cohn, M. Varela et al., "Asymmetric orbital-lattice interactions in ultra-thin oxide films" *Phys.Rev.Lett*. **107,** 116805 (2011).

F. A. Cuellar, G. Sanchez-Santolino, M. Varela et al., "Thermally assisted tunneling transport in $La_{0.7}Ca_{0.3}MnO_3/SrTiO_3$:Nb Schottky-like heterojunctions," *Phys. Rev. B* **85**, 245122 (2012).

N. Galiana, P. P. Martin, L. Garzon, E. Rodriguez, C. Munuera, F. Esteban, M. Varela et al., " Formation of pyramid-like nanostructures in MBE grown Si films on Si(001)." *Applied Physics A* **102**, 731 (2011).

J. Gazquez, W. D. Luo, M. P. Oxley, M. Prange, M. A. Torija, M. Sharma, C. Leighton, S. T. Pantelides, S. J. Pennycook, M. Varela, "Atomic-Resolution Imaging of Spin-State Superlattices in Nanopockets within Cobaltite Thin Films," *Nano Lett.* **11**, 973-976 (2011).

J. Gazquez, M. Varela et al., "Aberration corrected STEM-EELS studies of epitaxial Fe/MgO/(001)Ge heterostructures", *J. Mater. Sci.* **46**, 4157-4161 (2011).

B. S. Guiton, V. Iberi, S. Z. Li, D. N. Leonard, C. M. Parish, P. G. Kotula, M. Varela, G. C. Schatz, S. J. Pennycook and J. P. Camden, "Correlated optical measurements and Plasmon mapping of silver nanorods," *Nanoletters* **11,** 3482-3488 (2011).

D. Hernandez-Maldonado, M. Herrera, P. Alonso-Gonzalez, Y. Gonzalez, L. Gonzalez, J. Gazquez, M. Varela, S. J. Pennycook et al., "Compositional Analysis with Atomic Column Spatial Resolution by 5th-Order Aberration-Corrected STEM," *Microscopy & Microanalysis* **17**, 578-581 (2011).

A. Llordes, A. Palau, J. Gazquez, M. Coll, R. Vlad, A. Pomar, J. Arbiol, R. Guzman, S. Ye, V. Rouco, F. Sandiumenge, S. Ricart, T. Puig, M. Varela et al., "Nanostrain-induced pair suppression as a vortex pinning mechanisms in high-temperature superconductors," *Nature Materials* **11,** 329-336 (2012).

V. K. Malik, I. Marozau, S. Das, B. Doggett, D. K. Satapathy, M. A. Uribe-Laverde, N. Biskup, M. Varela et al., "Pulsed laser deposition growth of heteroepitaxial $YBa_2Cu_3O_7/La_{0.67}Ca_{0.33}MnO_3$ superlattices on $NdGaO_3$ and $Sr_{0.7}La_{0.3}Al_{0.65}Ta_{0.35}O_3$ substrates," *Phys. Rev. B* **85**, 054514 (2012).

S. I. Molina, M. P. Guerrero, P. L. Galindo, D. L. Sales, M. Varela and S. J. Pennycook, "Calculation of integrated intensities in aberration-corrected Z-contrast images," *J. Electron Microsc*. **60**, 29-33 (2011).

C. Moreno, N. J. Divins, J. Gázquez, M. Varela, I. Angurell, J.Llorca, "Improved thermal stability of oxide-supported naked gold nanoparticles by ligand-assisted pinning," *Nanoscale* **4**, 2278-2280 (2012).

S. J. Pennycook, M. Varela, "New Views of Materials through Aberration-corrected STEM," *J. Elect. Micros.* **60,** S213-S223 (2011).

T. J. Pennycook, M. P. Oxley, J. Garcia-Barriocanal, F. Y. Bruno, C. Leon, J. Santamaria, S. T. Pantelides, M. Varela and S. J. Pennycook, "Seeing Oxygen disorder in YSZ/$SrTiO_3$ colossal ionic conductor heterostructures using EELS," *European Physics Journal Applied Physics* **54,** 33507 (2011).

D. Petti, M. Cantoni, C. Rinaldi, S. Brivio, R. Bertacco, J. Gazquez and M. Varela, "Sharp Fe/MgO/Ge(001) epitaxial heterostructures for tunneling junctions," *J. Appl. Phys.* **109,** 084909 (2011).

S. R. C. Pinto, M. Buljan, A. Chahboun, M. A. Roldan, S. Bernstorff, M. Varela, S. J. Pennycook et al., "Tuning the properties of Ge-quantum dots superlattices in amorphous silica matrix through deposition conditions," *J Appl Phys.*, **111**, 074316 (2012).

A. Rivera-Calzada, M. R. Diaz-Guillen, O. J. Dura, G. Sanchez-Santolino, T. J. Pennycook, R. Schmidt, F. Y. Bruno, J. Garcia-Barriocanal, Z. Sefrioui, N. M. Nemes, M. Garcia-Hernandez, M. Varela, C. Leon, S. T. Pantelides, S. J. Pennycook and J. Santamaria, "Tailoring Interface Structure in Highly Strained YSZ/STO Heterostructures," *Adv. Mater*. **23**, 5268-5274 (2011).

J. Salafranca, J. Gazquez, N. Pérez, A. Labarta, S. T. Pantelides, S. J. Pennycook, X. Batlle and M. Varela, "Surfactant Organic Molecules Restore Magnetism in Metal-Oxide Nanoparticle Surfaces," *Nano Lett* **12**, 2499–2503 (2012).

M. Sharma, J. Gazquez, M. Varela, J. Schmitt, C. Leighton, "Coercivity enhancement driven by interfacial magnetic phase separation in $SrTiO_3$(001)/$Nd_{0.5}Sr_{0.5}CoO_3$," *Phys. Rev. B.* **84,** 024417 (2011).

M. Sharma, J. Gazquez, M. Varela et al., "Growth temperature control of the epitaxy, magnetism, and transport in $SrTiO_3$(001) / $La_{0.5}Sr_{0.5}CoO_3$ thin films," *J. of Vacuum Sci & Tech. A.* **29,** 051511 (2011).

S. Singh, M. R. Fitzsimmons, T. Lookman, H. Jeen, A, Biswas, M. A. Roldan and M. Varela, "Role of elastic bending stress on magnetism of a manganite thin film studied by polarized neutron reflectometry," *Phys. Rev. B* **85**, 214440 (2012).

Surendra Singh, M. R. Fitzsimmons, T. Lookman, J. D. Thompson, H. Jeen, A. Biswas, M. A. Roldan and M. Varela, "Magnetic Nonuniformity and Thermal Hysteresis of Magnetism in a Manganite Thin Film," *Phys. Rev. Lett*. **108**, 077207 (2012).

M.K. Stewart, C.-H. Yee, Jian Liu, M. Kareev, R.K. Smith, B.C. Chapler, M. Varela et al., "Optical study of strained ultrathin films of strongly correlated $LaNiO_3$." *Phys. Rev. B* **83**, 075125 (2011).

M. A. Torija, M. Sharma, J. Gazquez, M. Varela et al., "Chemically-driven nanoscopic magnetic phase separation at the $SrTiO_3$(001)/$La_{1-x}Sr_xCoO_3$ interface," *Adv. Mater.* **23,** 2711-2715 (2011).

M. Varela, J. Gazquez and S. J. Pennycook, "STEM-EELS imaging of complex oxides and interfaces," *MRS Bull.* **37**, 29-35 (2012).

M. Varela et al., "Applications of Aberration Corrected STEM-EELS to Complex Oxide Materials", for *STEM: imaging and analysis*, Springer, New York, 429-466 (2011).

M. Varela, T. J. Pennycook, J. Gazquez, A. Y. Borisevich, S. T. Pantelides, S. J. Pennycook, "Complex Oxide Materials," pp 1179-1212, *Handbook of Nanoscopy* **2**, Wiley-VCH, Weinheim, Germany (2012).

C. Visani, J. Tornos, N. M. Nemes, M. Rocci, C. Leon, J. Santamaria, S. G. E. te Velthuis, Y. H. Liu, A. Hoffmann, J. W. Freeland, M. Garcia-Hernandez, M. R. Fitzsimmons, B. J. Kirby, M. Varela and S. J. Pennycook, "Symmetrical interfacial reconstruction and magnetism in $La_{0.7}Ca_{0.3}MnO_3$/ $YBa_2Cu_3O_7$ /$La_{0.7}Ca_{0.3}MnO_3$ heterostructures," *Phys. Rev. B* **84**, 060405 (2011).

Real Time TEM Imaging of Materials Transformations in Liquid or Gas Environments

PI: Haimei Zheng
Email: hmzheng@lbl.gov; Early Career FY2011
Materials Sciences Division, Lawrence Berkeley National Laboratory, Berkeley, CA 94720

Program Scope

The objective of this project is to study the physical and chemical processes of materials with high spatial resolution using in situ liquid or gas environmental cell transmission electron microscopy (TEM). Understanding how materials grow and function at the nanometer or atomic scale in their working environments is essential to developing efficient and inexpensive energy conversion and storage materials and devices. With real time imaging in liquids or gases, this project will develop environmental cell TEM and result in better understandings of growth and chemical reactions induced structural changes of nanocrystals important for energy applications.

Recent Progress

In situ liquid cell TEM study of nanocrystal growth in solution: The study of nanomaterials growth mechanisms is a significant common theme among all materials sciences and materials chemistry. Although colloidal nanocrystal growth has advanced remarkably, nanocrystal growth is still hard to predict and mechanisms of growth remain controversial. Our recent development of in situ liquid cell TEM, which has the ability of revealing single nanoparticle growth trajectories in solution, offers many opportunities in the study of colloidal nanocrystal growth mechanisms. Our initial focus of liquid cell TEM study is on nucleation and growth pathways of metal or alloy nanocrystals for catalytic applications.

We have studied the growth of Bi nanoparticles in an engineered precursor-scarce environment in a liquid cell at an elevated temperature (180 ºC). We observed oscillatory growth dynamics of Bi nanoparticles in situ. Both individual and pair-wise growth oscillations and collective fluctuations at global length scales were identified (Figure 1). Tracking single particle growth trajectories allows us to analyze quantitatively the novel kinetic growth. We believe the oscillatory dynamics is associated with the growth/dissolution driven by precursor dependent chemical potential and it is resemble to the growth at critical point. This study suggests the possibility to counteract the energetically favorable Ostwald ripening process to prevent the coarsening of nanoparticles, which is highly beneficial to many industrial reactions, such

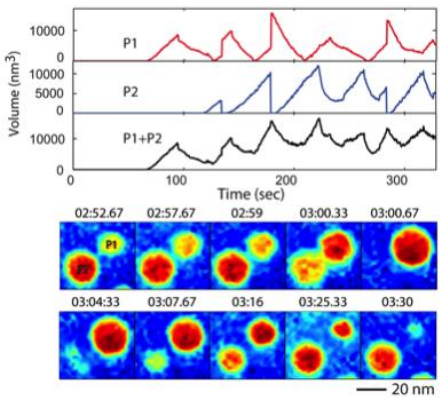

Figure 1 Oscillatory growth of Bi nanoparticles. Trajectories of two particles showing pairwise oscillation.

as the heterogeneous nanoparticle catalysis.

The growth of colloidal nanocrystal architectures by nanoparticle attachment is frequently reported as an alternative to the conventional growth by monomer attachment. However, the underlying mechanism for how nanoparticle attachment proceeds microscopically remains unclear. Our development of imaging through liquids using liquid cell TEM provides the opportunity to resolve the issue. We have achieved the growth of Pt_3Fe nanorods (with the aspect ratio up to 40:1) in the liquid cell. Our real time imaging of the dynamic growth reveals many details of shape directed nanoparticle attachment that has not been approachable previously.

As shown in Figure 2, we show the growth of winding polycrystalline nanoparticle chains by shape-directed nanoparticle attachment followed by straightening (including orientation and shape corrections) to yield single-crystal nanorods. Tracking nanoparticle growth trajectories allows us to distinguish the force fields exerted by single nanoparticles and nanoparticle chains. Such quantification of nanoparticle interaction and understanding the growth pathways are important for the design of hierarchical nanomaterials and controlling nanocrystal self-assembly for functional devices.

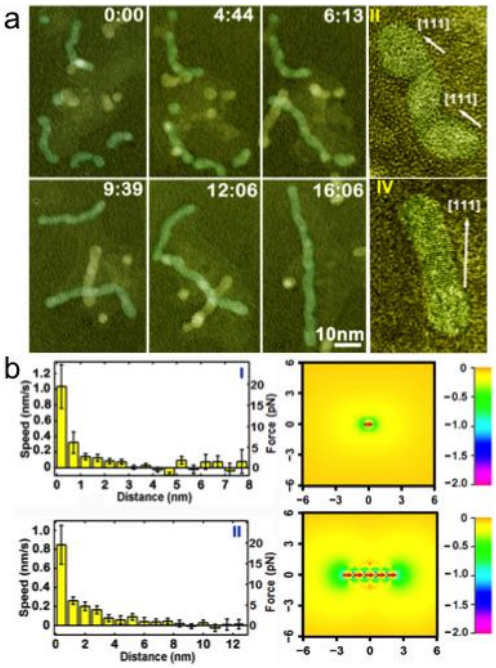

Figure 2 Growth of Pt_3Fe nanorods by shape directed nanoparticle attachment. (a) Sequential TEM images show the attachment of Pt_3Fe nanoparticles to form windy nanowires and the subsequent straightening process into nanorods. (b) Nanoparticle interaction as a nanoparticle approaches another nanoparticle or a nanoparticle chain as a function of interpartcle distance. It illustrates that our observation of nanoparticles preferring to attach to the ends of a chain is consistent with dipolar forces mediating nanoparticle attachment.

In situ environmental TEM probing Co-based nanocatalysts: Simultaneous probing the electronic structure and morphology of materials at the nanometer or atomic scale while a chemical reaction is proceeding is significant for understanding the underlying reaction mechanisms and optimizing a materials design. This is especially important in the study of nanoparticle catalysts, yet such experiments have rarely been achieved. With the development of gas environmental (cell) TEM and electron energy loss spectroscopy (EELS), the valence state of nanoparticles can be measured concurrently with atomic-resolution imaging during the reaction. We study structural dynamics of nanoparticle catalysts in situ during oxidation or reduction reactions (in O_2 or H_2 gas) using an environmental transmission electron microscope (ETEM) at the user facility of Center for Functional Materials (CFN) at Brookhaven National Laboratory (BNL) as well as our custom-made gas flow cell TEM holder at Lawrence Berkeley National Laboratory (LBNL).

We have studied the valence state of nanoporous cobalt-containing particles and its correlation with the structural coarsening during the hydrogen reduction reaction for Fischer-Tropsch (F-T) synthesis - an industrial reaction that converts syngas (a mixture of hydrogen and carbon monoxide) to liquid fuels. During the in situ experiments, a 15 mTorr hydrogen environment was maintained while various temperatures (300-600 ºC) were used. Nanoporous cobalt nanoparticle catalysts coated with silica were studied under the above reaction conditions. Studies reveal quantitative correlation of the cobalt valence states with the particles' nanoporous structures.

As shown in Figure 3, when the nanoporous particles were reduced, the valence state changed from cobalt oxide to metallic cobalt and concurrent structural coarsening was observed. In situ mapping of the valence state and the corresponding nanoporous structures allows quantitative analysis necessary for the understanding and improving of the mass activity and lifetime of cobalt-based catalysts, i.e., for Fischer-Tropsch synthesis. This approach provides the unique opportunity to uncovering the catalyst optimization mechanisms.

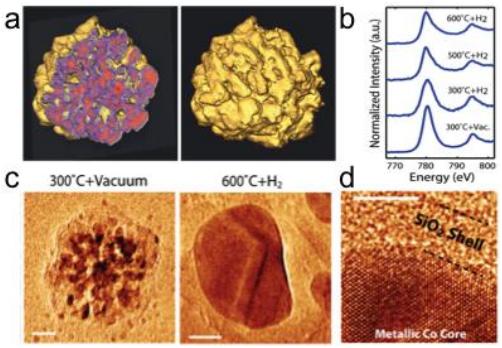

Figure 3 Revealing the correlation of valence state with nanoporous structure in cobalt catalysts by in situ environmental TEM. (a) 3-D tomographic reconstruction of an as-prepared CoO_x/SiO2 nanoparticle. (b) Co $L_{2,3}$ edges of the catalysts from in situ EELS measurements. (c) In situ TEM of structural changes of the catalysts at different reduction conditions. (d) An only 3.5 nm silica shell can prevent the particle from oxidation at room temperature.

Future Plans

We will advance liquid cell TEM in the stud y of nanocrystal growth in solution and develop gas flow environmental cell TEM in probing nanoparticle catalysts in situ. By real time imaging, we plan to focus on (1) shape control of colloidal nanocrystals; (2) mass transport in nanocrystals; (3) structural dynamics of bimetallic nanoparticle catalysts. To assist the study, we will continue to advance liquid cell TEM techniques including the development of flow cells, integrated in situ high resolution TEM imaging and EELS, electrochemical biasing liquid cells, etc.

Publications during 2011-2012 [In total, ~16 peer-reviewed papers including 2 in *Science*, 1 in *PNAS*, 1 in *Nano Lett*, 1 in *JCAS*; 1 patent disclosure; 10 invited talks**]**

1. K. Niu, H.G. Liao, H. Zheng*, "Revealing dynamic processes of materials in liquids using liquid cell transmission electron microscopy" ***JoVE*** in press.
2. H. Liao, L. Cui, S. Whitelam, H. Zheng*, " Real time imaging Pt_3Fe nanorod growth in solution " ***Science*** 336, 1011 (2012).
3. H. L. Xin, E.A. Pach, R.E. Diaz, E. A. Stach, M. Salmeron, H.Zheng*, "Revealing correlation of valence state with nanoporous structure in cobalt catalyst nanoparticles by in situ environmental TEM " ***ACS Nano*** 6, 4241 (2012).

4. H. L. Xin, H. Zheng*, “In situ observation of oscillatory growth of bismuth nanoparticles” ***Nano Lett.*** 12, 1470 (2012).
5. U. M Mirsaidov, H. Zheng, D. Bhattacharya, Y. Casana, P. Matsudaira, “Direct observation of stick-slip movements of water nanodroplets induced by an electron beam" ***PNAS*** 109, 7187 (2012).
6. U. M. Mirsaidov+, H. Zheng+, Y. Casana, P. Matsudaira, “Imaging protein structure in water at 2.7 nm resolution by transmission electron microscopy”, ***Biophys. J.*** 102, L15 (2012).
7. H. Zheng, “Transmission electron microscopy imaging of structural transformation dynamics in a single nanocrystal” ***Microscopy Today*** 20, 18 (2012). (Invited)
8. L. Ji+, H. L. Xin+, T. R. Kuykendall, S. Wu, H. Zheng, M. Rao, E. J. Cairns, V. Battagliac, Y. Zhang “SnS2 nanoparticle loaded graphene nanocomposites for superior energy storage” ***Phys. Chem. Chem. Phys.*** 14, 6981 (2012).
9. L. Ji, M. Rao, H. Zheng, L. Zhang, Y. Li, W. Duan, J. Guo, E. J. Cairns, and Y.Zhang, “Graphene oxide as a sulfur immobilizer in high performance lithium/sulfur cells” ***J. Am. Chem. Soc.*** 133, 18522 (2011).
10. K. Niu, H. Zheng, Z. Li, J.Yang, J. Sun, X. Du, “Laser dispersion of detonation nanodiamonds”. ***Angew. Chem. Int. Ed.*** 50, 4099 (2011).
11. H. Zheng*, J. B. Rivest, T. Miller, B. Sadtler, A. Lindenberg, M. F Toney, L-W. Wang, C. Kisielowski, A. P. Alivisatos, “Observation of transient structural-transformation dynamics in a Cu_2S nanorod” ***Science*** 333, 206 (2011).

Direct Observations of Magnetic Monopoles and Vortex-Core Precession Orbit with Electrons

Y. Zhu, S. Pollard, M.G. Han, L. Wu, V.V. Volkov and J. Tao
zhu@bnl.gov, spollard@bnl.gov, mghan@bnl.gov, ljwu@bnl.gov, volkov@bnl.gov, and jtao@bnl.gov
Dept. of Condensed Matter Physics and Materials Science
Brookhaven National Laboratory, Upton, NY 11973

Research Scope

The focus of this research task under the FWP Number MA-015-MACA is to investigate spin-related phenomena, including nanoscale magnetic structure and spin-spin, spin-electron and spin-lattice correlation that control the functionality of technologically important materials relevant to the DOE missions. It encompasses three major areas of research: 1) switching behavior of patterned magnetic architecture to understand nanoscale magnetism, 2) ferroelectric, ferromagnetic and ferroelastic coupling in multiferroic materials; and 3) the role of the magnetic degree of freedom in strongly correlated electron systems. Emphasis is on revealing structure-property relationships and the underlying mechanisms for the complex physical behavior of various functional materials such as high-temperature superconductors, rare-earth-alternative energy-storage materials, multiferroics, and spintronic devices. Advanced quantitative electron microscopy techniques, especially Lorentz phase imaging, off-axis electron holography and in-situ biasing with electromagnetic field and spin-polarized-current are developed and implemented to study these materials. Experiments are closely coupled with structural modeling and theory. Although electron scattering and microscopy are the primary tools, complementary methods such as synchrotron x-ray, neutron scattering and scanning probes are also used.

Recent Progress

Our recent progress includes the understanding of dynamic behavior of emergent magnetic charges, or monopoles, in artificially structured spin-ice lattices, which represent a new paradigm in the study of frustrated and correlated systems where in-situ microscopy can be used to uncover the ordering processes that occur with competing interactions and correlation. With our unique differential phase imaging methods we show the presence of flux channels similar to Dirac string in the systems, which has represented a holy grail in physics for more than 70 years [1]. The Dirac string, connecting pairs of magnetic charges (monopoles or anti-monopoles) plays an indispensable role in nucleation, propagation, and annihilation of the monopoles during the magnetic reversal. Statistical analysis of monopole populations and system correlations illustrated the detailed evolution of the magnetic charge ordering processes that result in achieving a highly frustrated, low energy quasi-ground spin state, as well as their crucial role in the reversal behavior, providing key insights into the physics of spin ordering and of frustrated materials systems [2].

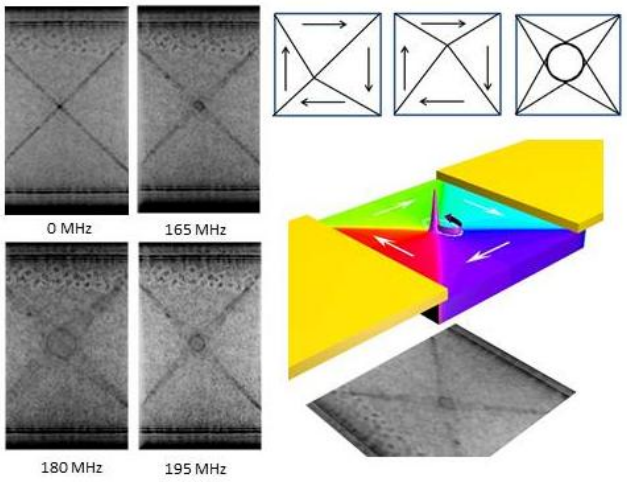

Fig.1 Direct observations of vortex-core precession orbit with electrons. A novel in-situ dynamic Lorentz microscopy method was developed to apply ac current with high frequencies on the sample while observing directly vortices in motion in TEM. The method allows us to determine the torque contributions exerted by spin polarized currents on magnetic structures, thus valuable to the study of emerging spintronic technologies. (Left): Lorentz micrographs of the core precession orbit of permalloy square with Landau domain structure at various driving frequencies (remnant; 0MHz, resonant: 180MHz). During off-resonant excitations, the orbit becomes elliptical, and its shape and size depend strongly on the chirality and polarity of the vortex. (Right): Schematic illustration of how the vortex motion leads to the pattern observed as images of the dynamic orbits.

Another recent accomplishment that will be presented at the DOE contract meeting is the understanding of the origin of non-adiabatic spin torques in ferromagnetic materials, since spin-dependent transport and current-driven magnetization dynamics underlies a number of emerging spintronic technologies. For instance, in magnetic memory and logic applications that rely on the control of domain wall locations within a magnetic film, the speed at which domain walls may be moved by spin polarized currents is governed by the magnitude of non-adiabatic spin torques. We have developed a new sample stage capable of applying high-frequency dynamic excitations and spin-polarized-currents to a sample in an electron microscope. It allows us to directly observe, with unprecedented spatial resolution and phase sensitivity, the subtle change of vortex-core-orbits under various excitations and the influence due to the chirality and polarity of the vortex (Fig.1). It further permits us to accurately measure the non-adiabatic spin-torque, excluding extraneous influences, which is the key to the development of spintronic devices including domain wall racetrack memories [3].

Future Plans

We will study a variety of patterned tri-layer systems (e.g. Py/Cu/Co) with magnetic vortex configurations in which we can extract quantitative information about the interlayer spin-spin coupling, the damping constant and the degree of non-adiabaticity. The research will be complemented with x-ray magnetic circular dichroism experiment. With our unique capabilities we will be able to answer some of the fundamental questions related to the origin of spin torques. Among many other exciting projects, we also plan to explore the use of electric field to control magnetic structure by quantifying the magnetic response to piezo-electric induced strain in Pb-Mg-Nb/Pb-Ti/Ni heterostructures. In multiferroics, emergent properties of ferroelectric domain walls, effects of oxygen vacancy migrations, and photovoltaic applications are of great interest as well. Local broken symmetries at ferroelectric domain walls engender unexpected unusual domain properties, yielding recent findings of conduction modulation and net magnetic moments at domain walls in hexagonal manganites. All these activities will advance our knowledge on spin-electron-lattice interactions and can lead to discoveries of novel functionalities in advanced materials including ferroelectrics and multiferroics [4].

The work was supported by the U.S. Department of Energy, Division of Materials Science and Engineering, Office of Basic Energy Science, under Contracts No. DE-AC02-98CH10886.

References

[1] Dirac, P.A.M., "Quantised singularities in the electromagnetic field", Proc. of Royal Society of London. Series A **133**, 60 (1931).

[2] Pollard, S.D., Volkov, V.V., and Zhu, Y., "Propagation of magnetic charge monopoles and Dirac flux strings in an artificial spin-ice lattice ", Phys. Rev. B (Rapid Comm. as Editors' suggestions), **85**, 180402(R) (2012).

[3] Pollard, S. D., Huang, L., Buchanan, K.S., Arena, D.A., Zhu, Y., "Direct Dynamic Imaging of Non-Adiabatic Spin Torque Effects", Nature Communications, in press (2012).

[4] Polking, M. J., Han, M.-G., Yourdkhani, A., Petkov, V., Kisielowski, C. F., Volkov, V.V., Zhu, Y., Caruntu, G., Alivisatos, A. P., and Ramesh, R., "Ferroelectric order in individual nanometer-scale crystals", Nature Materials, **11** 700 (2012).

DOE Sponsored Publications in 2012-2010

The publication list under FWP MA-015-MACA for 2011 is attached to an additional abstract in this program book: "Role of Structurally and Magnetically Modified Nanoclusters in Colossal Magnetoresistance", by Tao, Wu, Volkov and Zhu.

2012

Akey, A.J., Lu, C., Wu, L., Zhu, Y., and Herman, I.P., "Anomalous photoluminescence Stokes shift in CdSe nanoparticle and carbon nanotube hybrids", Phys. Rev. B 85, 045404 (2012).

Bo, S-H., Wang, F., Janssen, Y., Zeng, D.L., Nam, K-W., Xu, W.Q., Du, L-S., Stephens, P., Graetz, J., Yang, X-Q., Zhu, Y., Parise, J., Grey, C., and Khalifah, P., "Degradation and (De)lithiation Processes in the High Capacity Battery Material LiFeBO3", J. Chem. Mater, 22 8799 (2012).

Chen, H., Hautier, G., Jain, A., Moore, C., Kang, B., Doe, R., Wu, L., Zhu, Y., Tang, Y., and Ceder, G., "Carbonophosphates: A New Family of Cathode Materials for Li-Ion Batteries Identified Computationally", Chem. Mater., 24, 2009-2016 (2012).

Chen, W.F., Sasaki, K., Ma, C., Frenkel, A.I., Marinkovic, N., Muckerman, J.T., Zhu, Y., and Adzic, R.R., "Hydrogen-Evolution Catalysts Based on Non-Nobel Metal Nickel-Molybdenum Nitride Nanosheets", Angew. Chem. Int. Ed. 51 6131 (2012).

Ji H.; Allred J. M.; Ni N.; Tao J.; Neupane M.; Wray A.; Xu S.; Hasan M. Z.; and Cava R. J., "Bulk intergrowth of a topological insulator with a room-temperature ferromagnet", Phys. Rev. B 85, 165315 (2012)

Jiang, M.; Lim, B.; Tao, J.; Camargo, P. H. C.; Ma, C.; Zhu, Y. and Xia, Y., "Epitaxial overgrowth of platinum on palladium nanocrystals", Nanoscale 2, 2406-2411 (2010).

Nam, K.-W., Bak, S.-M., Hu, E., Yu, X., Zhou, Y., Wang, X., Wu, L., Zhu, Y., Chung, K.-Y., Yang, X.-Q., "Combining In Situ Synchrotron X-Ray Diffraction and Absorption Techniques with Transmission Electron Microscopy to Study the Origin of Thermal Instability in Overcharged Cathode Materials for Lithium-Ion Batteries", Adv. Funct. Mater. (2012).

Polking, M. J., Han, M.-G., Yourdkhani, A., Petkov, V., Kisielowski, C. F., Volkov, V.V., Zhu, Y., Caruntu, G., Alivisatos, A. P., and Ramesh, R.,"Ferroelectric order in individual nanometer-scale crystals", Nature Materials, 11 700-709 (2012).

Pollard, S. D., Huang, L., Buchanan, K.S., Arena, D.A., Zhu, Y., "Direct Dynamic Imaging of Non-Adiabatic Spin Torque Effects", Nature Communications, in press (2012).

Pollard, S.D., Volkov, V.V., and Zhu, Y., "Propagation of magnetic charge monopoles and Dirac flux strings in an artificial spin-ice lattice ", Phys. Rev. B (Rapid Comm. as Editors' suggestions), 85, 180402(R) (2012).

Raabe, S., Mierwaldt, D., Ciston, J., Uijttewaal, M., Stein,H., Hoffmann, J., Zhu, Y., Blöchl, P., and Jooss, Ch., "In-situ electrochemical electron microscopy study of oxygen evolution activity of doped manganite perovskites", Advanced Functional Materials, DOI: 10.1002/adfm.201103173 (2012).

Saucke, G., Norpoth, J., Jooss, Ch., Su, D., and Zhu, Y., "Polaron absorption for photovoltaic energy conversion in a manganite-titanate pn heterojunction", Phys., Rev., B 85, 165315 (2012).

Tao J. "Nanoclusters in Magnetoresistance", Nanotechnology Reviews, invited review article, in press.

Wu, L., Egerton, R.F., and Zhu, Y., "Image simulation for atomic resolution secondary electron image", Ultramicroscopy, in press.

Xin, X., Zhou, X.F., Wang, F., Yao, X.Y., Xu, X.X., Zhu, Y., and Liu, Z.P., "A 3D Porous Architecture of Si/Graphene Nanocomposite as High-Performance Anode Materials for Li-Ion Batteries", J. Mater. Chem., 22, 7724-7730 (2012).

Xu, Z., Hine, C.R., Maye, M.M., Meng, Q.P., and Cotlet, M., "Shell Thickness Dependent Photoinduced Hole Transfer in Hybrid Conjugated Polymer/Quantum Dot Nanocomposites: From Ensemble to Single Hybrid Level", ACS Nano, 6 4984–4992 (2012).

Zeng, J., Zhu, C., Tao, J., Jin, M., Zhang, H., Li, Z.-Y., Zhu, Y., and Xia, Y., "Controlling nucleation and growth of silver on palladium nanocubes by manipulating the reaction kinetics" Angew. Chemie Int. Ed., 51, 2354-2358 (2012)

Zhang, Yu., Ma, C., Zhu, Y., Si, R., Cai, Y., Wang, J.X., Adzic, R.R., "Hollow core supported Pt monolayer catalysts for oxygen reduction", Catalysis Today (in press).

Zhu, Y., Milas, M., Rameau, J., and Sfeir, M., "The Multimodal Optical Nanoprobe for Advanced Electron Microscopy", invited article, Microscopy Today, in press, 2012

Zhu, Y., and Wu, L., "Shadow Imaging for Charge Distribution Analysis", Book Chapter in "Electron Crystallography Meets Powder Diffraction", U. Kolb, K. Shankland, L. Meshi, A. Avilov, and W. David Eds., Springer, in press.

2010

Ferrari, L., Matteucci, G., Schofield, M.A., Beleggia, M., and Zhu, Y., "Near-Curie magnetic anomaly at the Ni/C interface observed by electron holography", J. of Mag. Mag. Mater., 322 858–865 (2010).

Han, M.-G., Zhu, Y., Sasaki, K., Kato, T., Fisher, C.A.J., Hirayama, T., "Direct measurement of electron beam induced currents in p-type silicon", Solid-State Electronics 54 777–780 (2010).

Han, W., Su, D., Murphy, M., Ward, M., Sham, T.K., Wu, L., Zhu, Y., Hu, Y., and Aoki, T., "Microstructure and electronic behavior of PtPd@Pt core/shell nanowires", J. of Materials Research 25, 711 (2010).

He J. Q.; Volkov V. V.; Beleggia M.; Asaka T.; Tao J.; Schofield M. A.; Zhu Y., "Ferromagnetic domain structures and spin configurations measured in doped manganites", Phys. Rev. B 81, 094427 (2010).

He, J.Q., Sootsman, J.R., Joseph, R., Girard, S.N., Zheng, J.C., Wen, .JG., Zhu, Y., Kanatzidis, M.G., Mercouri, G., Dravid, V.P., "On the Origin of Increased Phonon Scattering in Nanostructured PbTe Based Thermoelectric Materials", J. Am. Chem. Soc., 132 8669-8675 (2010).

He, J.Q., Volkov, V. V., Asaka, T., Chaudhuri, S., Budhani, R. C., and Zhu, Y., "Competing two-phase coexistence in doped manganite: direct observations by Lorentz electron microscopy", Phys. Rev. B 82 224404 (2010).

Huang, L., Schofield, M.A., and Zhu, Y., "Control of Double-Vortex Domain Configurations in a Shape-Engineered Trilayer Nanomagnet System", Adv. Mater., 22, 492–495 (2010).

Jiang, M., Lim, B., Tao, J., Camargo, P. H. C., Ma, C.. Zhu, Y., and Xia, Y., "Epitaxial overgrowth of platinum on palladium nanocrystals", Nanoscale, 2, 2406–2411 (2010).

Kolpak, A.M., Walker, F. J.; Reiner, J. W., Segal, Y., Su, D., Sawicki, M. S., Broadbridge, C. C., Zhang, Z., Zhu, Y., Ahn, C. H., and Ismail-Beigi, S., "Interface-induced polarization and inhibition of ferroelectricity in epitaxial SrTiO3/Si", Phys. Rev. Lett, 105, 217601 (2010).

Kumah, D. P. , Reiner, J. W., Segal, Y., Kolpak, A. M., Zhang, Z., Su, D., Zhu, Y., Sawicki, M. S., Broadbridge, C. C., Ahn, C. H., and Walker, F. J., "The atomic structure and polarization of strained SrTiO3/Si", Appl. Phys. Lett., 97, 251902 (2010).

Lau, J.W, Morrow, Read, J.C., Hoink, V., Egelhoff, W.F., Huang, L., Zhu, Y., "In situ tunneling measurements in a transmission electron microscope on nanomagnetic tunnel junctions", Appl. Phys. Lett., 96 262508 (2010).

Morosan E., Wagner K. E., Zhao L., Hor, Y., Williams A.J., Tao J., Zhu Y., and Cava, R.J., "Multiple electronic transitions and superconductivity in PdxTiSe2", Phys. Rev. B 81, 094524 (2010), highlighted as Editor's suggestion.

Ngai, J. H., Segal, Y., Su, D., Zhu, Y., Walker, F.J., Ismail-Beigi, S., Le Hur, K., and Ahn1, C.H., "Electric field tuned crossover from classical to weakly localized quantum transport in electron doped SrTiO3", Phys. Rev. B 81, 241307 (R) (2010).

Ofan, A., Zhang, L., Gaathon, O., Bakhru, S., Bakhru, H., Zhu, Y., Welch, D.O., and Osgood, Jr. R.M., "Spherical solid He nanometer bubbles in an anisotropic complex oxide", Phys. Rev. B 82, 104113 (2010).

Pan, Z., Tao, J., Zhu, Y., Huang, J.-H., and Paranthaman, M.P., "Spontaneous Growth of ZnCO3 Nanowires on ZnO Nanostructures in Normal Ambient Environment: Unstable ZnO Nanostructures", Chem. Mater., 22, 149–154 (2010).

Si,W., Jie, Q., Wu, L., Zhou, J., Gu, G., Johnson, P.D., and Li, Q., "Superconductivity in epitaxial thin films of Fe1.08Te:Ox", Physics Review B 81, 092506 (2010).

Solovyov, V.F., Develos-Bagarinao, K., Si, W.D., Wu, L., Zhou, J., Qing, J., and Li, Q., "High irreversibility field of YBa2Cu3O7 films intercalated with a long-period metastable cuprate phase", J. Appl. Phys., 108, 113912 (2010).

Su, D., Yang, B., Jiang, N., Sawicki, M., Broadbridge, C., Couillard, M., Reiner, J.W., Walker, F.J., Ahn, C.H., and Zhu, Y., "Valence electron energy-loss spectroscopy of ultrathin SrTiO3 films grown on silicon (100) single crystal", Appl. Phys., Lett., 96, 121914 (2010).

Su, D., and Zhu, Y., "Scanning moire´ fringe imaging by scanning transmission electron microscopy", Ultramicroscopy 110 229–233 (2010).

Tao J., Niebieskikwiat D., Varela M., Luo W., Schofield M. A., Zhu Y., Salamon M. B., Zuo J. M., Pantelides S. T., and Pennycook S. J., "Direct imaging of nanoscale phase separation in La0.55Ca0.45MnO3: relationship to colossal magnetoresistance", Phys. Rev. Lett., 103 097202 (2009) (selected by Virtual Journal of Nanoscale Science & Technology; highlighted in Physics Today, Nov. issue, p20-23.

Wang, H., Altman, E., Broadbridge, C., Zhu, Y., and Henrich, V., "Determination of electronic structure of oxide-oxide interfaces by photoemission spectroscopy", Materials views article, Adv. Mater., 22, 2950–2956 (2010).

Wang, J.X., Inada, H., Wu, L., Zhu, Y., Choi, Y.-M., Liu, P., Zhou, W.-P., and Adzic, R.R., "Oxygen Reduction on Well-Defined Core-Shell Nanocatalysts: Particle Size, Facet, and Pt Shell Thickness Effects", J. Am. Chem. Soc., 131, 17298–17302 (2009).

Zeng, J., Zheng, Y., Rycenga, M., Tao, J., Li, Z.-Y., Zhang, Q., Zhu, Y., and Xia, Y., "Controlling the Shapes of Silver Nanocrystals with Different Capping Agents", J. Am. Chem. Soc., 132, 8552–8553 (2010).

Zhang, Y., Chen, H., Choi, G., Raghothamachar, B., Dudley, M., Edgar, J.,Grasza, K., Tymicki, E., Zhang, L., Su, D., and Zhu, Y., "Nucleation Mechanism of 6H-SiC Polytype Inclusions Inside 15R-SiC Crystals", J. Electronic Materials, 39 799-804 (2010).

Zheng, J.C., Frenkel, A.I., Wu, L., Hanson, J., Ku, W., Božin, E.S., Billinge, S. J. L., and Zhu, Y., "Nanoscale disorder and local electronic properties of CaCu3Ti4O12: An integrated study of electron, neutron, and x-ray diffraction, x-ray absorption fine structure, and first-principles calculations", Phys. Rev., B 81, 144203 (2010).

Zhou, W.P., Sasaki, K., Su, D., Zhu, Y., Wang, J.X., and Adzic, R.R., "Gram-Scale-Synthesized Pd2Co-Supported Pt Monolayer Electrocatalysts for Oxygen Reduction Reaction", J. Phys. Chem. C 114, 8950–8957 (2010).

UNIVERSITY GRANT PROJECTS

Discovery of Dielectric Response and Forces in Nanoscale Objects

P.E. Batson and M.J. Lagos

Institute for Advanced Materials, Devices, and Nanotechnology,
Department of Physics and Astronomy
Department of Materials Science and Engineering
Rutgers, The State University
136 Frelinghuysen Road
Piscataway, New Jersey 08854
batson@physics.rutgers.edu

Surface plasmons in nanometer-sized metal structures have been studied for many years to better understand the interaction of light with sub-wavelength sized materials structures [1]. Theoretical studies show that coupling of optical energy into a confined structure results in enhanced local electric fields, producing *forces* of 10's of pico-Newtons, which have the potential to alter local structure [2] or to encourage nanoscale self-assembly [3]. Plasmon modes are also accessible using electron scattering, allowing selective excitation of modes having well defined orientation or symmetry through precise placement of a small electron beam [4,5,6]. Recently, these studies have been extended to practical nano-antenna structures [7].

This project seeks to explore the dielectric response of very small objects using aloof inelastic scattering of a sub-Angstrom fast electron beam. This information will be useful for better understanding of the coupling of light to these objects. Important systems include reporter-molecule/particle structures designed for Surface Enhanced Raman Scattering, nano-antenna arrays for improved absorption of light for energy generation, and semiconductor-organic hybrid structures useful for photon up/down energy conversion. We also wish to understand inter-object forces, the strength of near and far-field photonic coupling, and possible unanticipated optical behavior in molecular and nano-scale objects. Since the objects to be studied here involve only a few tens to hundreds of atoms, we expect structural changes in response to local forces, and we hope to gain some understanding of these changes for different materials in the presence of well defined substrates.

This effort requires unique electron beam equipment, a strong post-doctoral involvement in the experiments, and collaboration with a dedicated theoretical group to understand results. We are beginning with a VG Microscopes 3rd order aberration corrected instrument equipped with a high resolution Wien filter electron spectrometer capable of sub-Angstrom performance [8]. This equipment, though dated, is perhaps the sole instrument in the world today that is capable of a calibrated measurement of the energy position of an EELS feature in the soft x-ray energy region [9]. In the spring of 2013, we will have delivered a new 5th order corrected Nion instrument, designed to operate as low as 40 kV,

and having a new monochromator-spectrometer system that will deliver <30 meV energy resolution.(Supported under NSF grant #0959905.) This instrument will be installed in ultra-quiet space currently under construction at Rutgers. We were fortunate recently to attract M.J. Lagos to Rutgers as a Post-Doctoral Research Associate to participate in this project. He brings experience with mechanical and electrical properties of nanometer-sized wires, obtained using high resolution electron microscopy [10] and low temperature transport measurements [11]. Finally, we have the committed participation of J. Aizpurua, P.M. Echenique, and A. Rivacoba of the Donostia International Center for Physics in San Sebastian for theoretical understanding of the plasmonic behavior of nanoscale systems in the presence of a swift electron beam.

During the past two years, we have published a theoretical treatment of electron beam driven forces in small metal particles [12], receiving a Phys. Rev. B Editor's Choice designation. We looked closely at very close approaches of the electron beam with ~ 1nm sized particles, finding that a simple, classical dielectric response could generate a *repulsive* force, as well as an attractive force expected based on image charge arguments. In addition, coalescence of pairs of particles was found to be favored by coupled plasmon modes having bonding symmetry [13], driven by beam passage outside a pair, while placement of the electron beam within a group of particles drives them apart by excitation of coupled plasmon modes having anti-bonding symmetry, also called "dark modes" in the experimental literature [14].

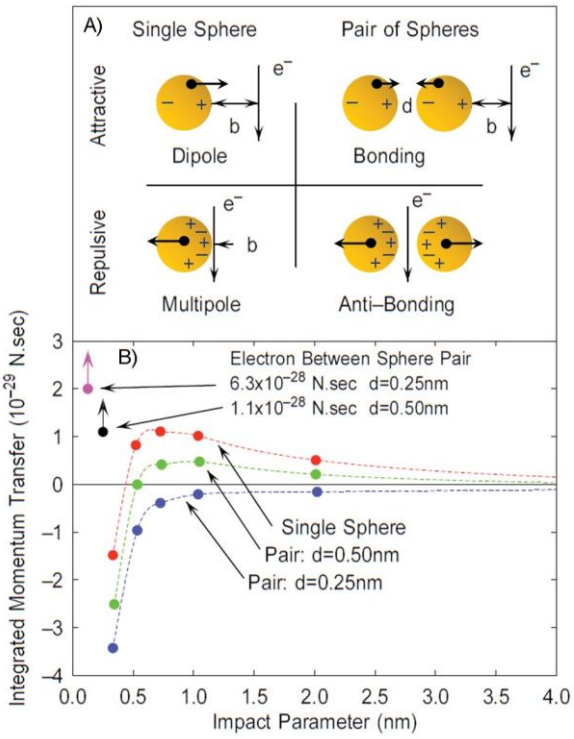

In Fig. 1, on the right, we summarize four beam-sphere geometries tested in this work, including repulsive and attractive forces in single spheres, and bonding and anti-bonding modes in sphere pairs. Transferred momentum are calculated for an isolated 1 nm radius Au sphere (red), pairs of 1 nm radius spheres separated by d= 0.25 nm (blue) and 0.5 nm (green), as a function of electron impact parameter, b. For the isolated sphere the momentum transfer is positive (towards the electron) for moderate impact parameter and negative (away from the electron) for small impact parameter. For a pair of spheres sufficiently close together, the momentum transfer always forces the two spheres together. Positioning the electron beam between a pair (black and pink points)forces them apart. (Reproduced from [15].

We have followed up on this theoretical work with experimental results published in NanoLetters [15] and in press in Ultramicroscopy [16] confirming the unexpected repulsive force for the case of the very near approach of the electron beam. Experimental results are summarized in the Fig. 2, to the right. Briefly, we show A) *pulling* of a particle towards a region of high beam current density at the left edge of the imaged area, B) *pushing* of the same particle when the left edge of the scanned area (denoted by the dashed square) is brought closer to the 1nm particle, C) the onset of *coalescence* of two particles and D) *separation* of particles when the left edge of the scanned area lies between the two particles. These results are enjoying attention in the plasmonics community with an invited presentation this coming fall in at NFO-12, an international meeting on near-field optics and nano-photonics, and participation in a plasmonics review in the MRS Bulletin [17]. Three conference abstracts supported by this project [18,19,20].

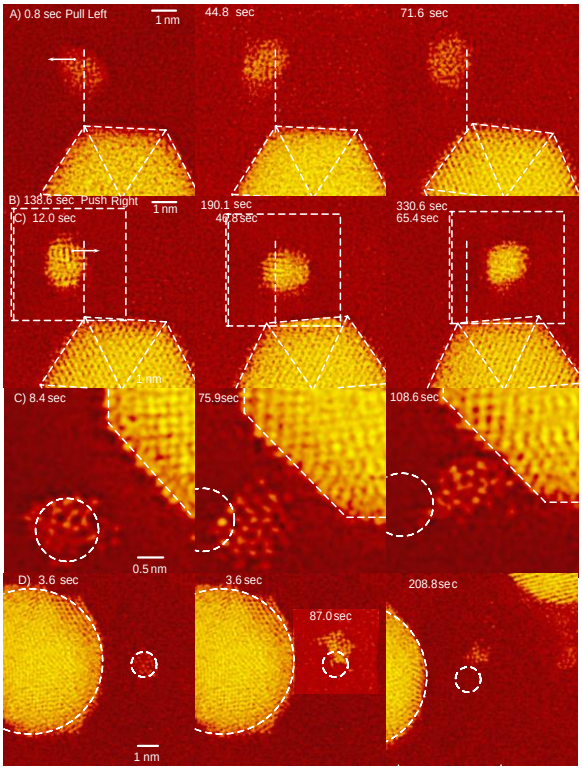

This project is intended to explore a range of scattering geometries, substrates and materials. To that end, we have acquired a four pocket miniature evaporation source by Mantis and have been gaining experience with evaporation of Au, Pt and Cu onto various substrates, including graphene, obtained from other groups at Rutgers. We have modified the VG Microscopes specimen air-lock to accept the source, and will therefore be able to produce samples in a clean environment for STEM inspection. With the experience brought to the project by Dr. Lagos, we will spend some time with nanowire geometries, as well as small particles, to better understand structural transformations in these very small objects.

Finally, we are continuing theoretical work towards understanding the physics involved in the force reversal at very small impact parameter. While this appears to be fundamentally related to the plasmonic response of the material, details of the field behavior are not at all clear. This unexpected finding is interesting because it may provide a basis for electron beam manipulation of molecular-sized objects. One could envision, for instance, controlling the rotation and position of a pentacene molecule on graphene, by trapping the molecule within a rectangular scan of a sub-Ångstrom beam. This would not be possible without the very short ranged *push* discovered in this work.

References:

[1] W. L. Barnes, A. Dereux, and T. W. Ebbesen, *Nature*, 424 (2003) 824-830.

[2] A. J. Hallock, P. L. Redmond, and L. E. Brus, *Proc. Nat. Acad. Sci.*, 102 (2005) 1280 – 1284.

[3] P. A. Smith, C. D. Nordquist, T. N. Jackson, T. S. Mayer, B. R. Martin, J. Mbindyo, and T. E. Mallouk, *Applied Physics Letters*, 77 (2000) 1399-1401.

[4] P. E. Batson, *Phys. Rev. Lett.*, 49 (1982) 936 – 940.

[5] P. E. Batson, *Surface Science*, 156 (1985) 720 – 734.

[6] J. Nelayah, M. Kociak, O. Stephan, F. J. García de Abajo, M. Tence, L. Henrard, D. Taverna, I. Pastoriza-Santos, L. M. Liz-Marzan, and C. Colliex, *Nat. Phys.*, 3 (2007) 348-353.

[7] T. Coenen, E. J. R. Vesseur, and A. Polman, *ACS Nano*, 6 (2012) 1742-1750.

[8] P. E. Batson, N. Dellby, and O. L. Krivanek, *Nature*, 418 (2002) 617 – 620.

[9] P. E. Batson, *Rev. Sci. Inst.*, 57 (1986) 43–48.

[10] M. J. Lagos, F. Sato, D. S. Galvão, and D. Ugarte, *Phys. Rev. Lett.*, 106 (2011) 055501.

[11] M. Lagos, V. Rodrigues, and D. Ugarte, *J. of Elect. Spect. and Rel. Phenom.*, 156-158 (2007) 20 - 24.

[12] A. Reyes-Coronado, R. Barrera, P. Batson, P. Echenique, A. Rivacoba, and J. Aizpurua, *Phys. Rev. B*, 82 (2010) 235429.

[13] E. Prodan, C. Radloff, N. J. Halas, and P. Nordlander, *Science*, 302 (2003) 419-422.

[14] M. Chu, V. Myroshnychenko, C. Chen, J. Deng, C. Mou, and F. García de Abajo, *Nano Letters*, 9 (2009) 399-404.

[15] P. E. Batson, A. Reyes-Coronado, R. Barrera, A. Rivacoba, P. Echenique, and J. Aizpurua, *Nano Letters*, 11 (2011) 3388 – 3393.

[16] P. E. Batson, A. Reyes-Coronado, R. Barrera, A. Rivacoba, P. Echenique, and J. Aizpurua, *Ultramicroscopy*, (in press) .

[17] E. J. R. Vesseur, J. Aizpurua, T. Coenen, A. Reyes-Coronado, P. E. Batson, and A. Polman, *MRS Bulletin*, (in press) .

[18] P. E. Batson, A. Reyes-Coronado, R. Barrera, A. Rivacoba, P. Echenique, and J. Aizpurua, *Microscopy and Microanalysis*, 17-S2 (2011) 1288 – 1289.

[19] P. E. Batson, A. Reyes-Coronado, R. Barrera, A. Rivacoba, P. Echenique, and J. Aizpurua, *Microscopy and Microanalysis*, (in press) .

[20] M. J. Lagos, F. Sato, D. S. Galvão, and D. Ugarte, *Microscopy and Microanalysis*, (in press) .

Mapping interactions in hybrid systems with active scanning probes

PI: Jesse Berezovsky, jab298@case.edu
Physics Department, Case Western Reserve University
10900 Euclid Avenue
Rockefeller Building
Cleveland, OH 44106

An understanding of interactions between confined electrons in nanostructures and integrated optical or magnetic systems is essential for many future applications in energy conversion, opto-electronics, and spintronics. Many such applications will involve hybrid nanosystems that incorporate two or more materials or structures in a single device. By opening the door to combinations of disparate materials and structures, the possibilities for devices are greatly expanded, but so are the difficulties involved in realizing them. In this new project, beginning summer 2012, we plan to design, construct, and employ a scanning probe system to investigate interactions in hybrid systems in which one component is fabricated on a scanned microcantilever, and the other on a fixed substrate. For interactions based on proximity of the hybrid components (via e.g. evanescent optical interactions, or magnetic or electric fields), we will separate the system into two separate components, one of which can be positioned relative to the other with nanometer precision, allowing us to controllably study and optimize interactions in the hybrid system.

The power of this idea is that once the two components are individually fabricated, one component can be scanned spatially about the other, fixed component, and furthermore can be sequentially scanned over different fixed components. This will allow for investigation of interactions as a function of the relative position of the components, and for rapid serial testing of coupling between many different components.

First, a scanning probe microscope will be constructed that is optimized for this scheme. Second, we will develop a process for cantilever fabrication around an arbitrary component. This scanned component will be situated near the end of the cantilever, with electrical and/or optical inputs and outputs extending to the supporting chip.

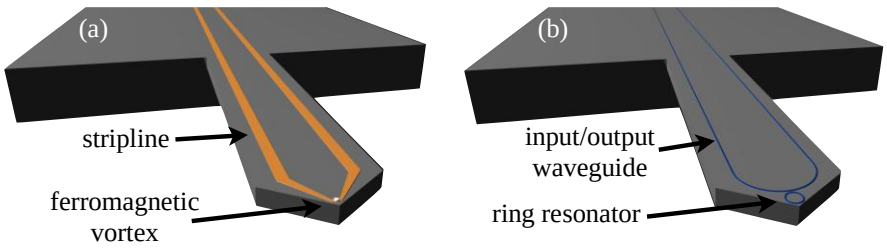

Figure 1. (a) Active magnetic probe. (b) Active optical probe.

We plan to develop two types of active probes, building off of our ongoing research: a magnetic vortex probe, and a photonic ring resonator probe (see Fig. 1). These probes will serve as a basis for other magnetic and optical probes, and may spark collaborations with other researchers studying hybrid devices. The magnetic vortex probe consists of a ferromagnetic film, patterned into a micron-scale disk near the end of the cantilever, and a microstripline patterned nearby to supply a time-varying magnetic field. By using this magnetic field to control the

magnetic domain dynamics of the ferromagnet, we will use this probe to investigate interactions between highly localized magnetic field gradients or large AC magnetic fields (see Fig. 2a), and confined electrons in nanostructures.

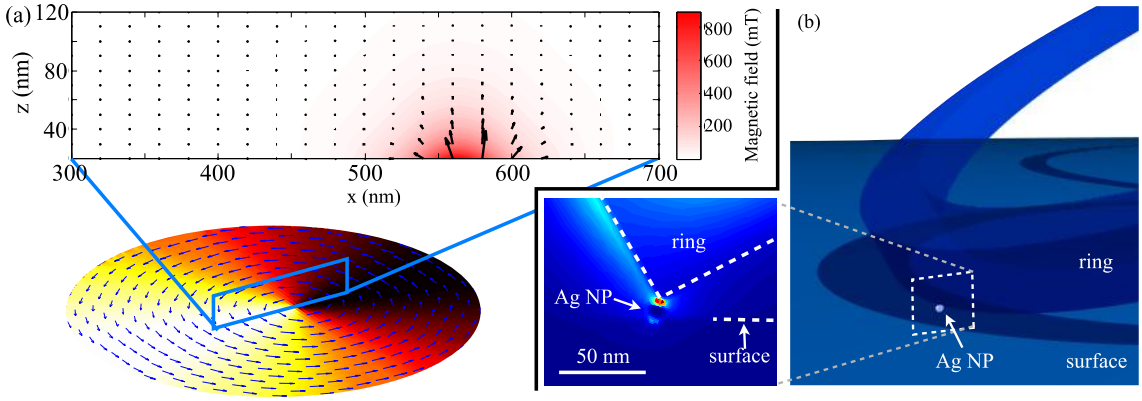

Figure 2. (a) Bottom: Micromagnetic simulation of magnetization of a 2 μm diameter Permalloy disk. Top: Magnetic field in a region above the disk. (b) Right: Schematic of a ring resonator above a nanoparticle. Cantilever is not shown. Left: Finite-difference time domain simulation of electric field amplitude in and around the ring, in proximity to a nanoparticle.

The second active probe we plan to fabricate is comprised of a photonic ring resonator near the end of the cantilever, with a waveguide coupling light in and out of the ring. This system will allow us to investigate interactions between the resonator and nanostructures on a surface (Fig. 2b). In these experiments, we will study how coupling between an optical resonator and different nanostructures affects interaction strengths and optical loss, and how electron spins couple to light in an optical resonator.

This planned scheme offers a significant increase of flexibility and efficiency for investigating hybrid systems over traditional nanoassembly. Recently, a number of tantalizing proof-of-concept hybrid nanosystems have been demonstrated, but the difficulties involved in fabrication hold back progress in understanding and optimizing these systems. Scanned active probes will comprise a powerful new tool for investigating interactions in hybrid nanosystems, which we will employ to map new routes towards future technology.

Local Properties at Nanosized Interfaces:

Metal-Semiconductor and Ionic Conductor-Electrode Systems

PI: Dawn Bonnell
The University of Pennsylvania
3231 Walnut St, Philadelphia, PA 19104
bonnell@lrsm.upenn.edu

Research Scope

The goal of this project is to determine the fundamental processes that underlie the behavior of nanosized interfaces and nanoscale property variations at interfaces in energy related systems. Electronic and ionic transport are the basis for the operation of devices critical to many energy generation, harvesting, storage, and efficiency strategies. Iconic examples involving electrons are solar cells, catalysts, and low power electronics: involving ions are fuel cells, and batteries. In this research we take one ideal example for each class of interfaces, develop tools and analysis to characterize local properties and relate these to relevant mechanisms. The two classes of interfaces/behavior are metal-semiconductor interfaces with size dependent Schottky barriers and resistive switching; and ionic conductor-electrode interfaces in operating fuel cells.

Recent Progress: Size Dependence of Gold-$SrTiO_3$ (100) Interface Properties

At small scales interfaces become critically important to device behavior and interface properties are often size dependent. The Bonnell group developed instrumentation based on scanning probe microscopy that can find and image metal nanoparticles, make local electrical contact to each individual particle and characterize complex electrical properties of each interface. Using the model system of a metal-semiconductor interfaces, Au-SrTiO3 (100), we have shown that in the size range of 10nm to 200 nm Schottky barriers and ideality factors are size and orientation dependent. We have recently shown that these system also exhibit the characteristics of resistive switching, which also manifests size dependent behavior.

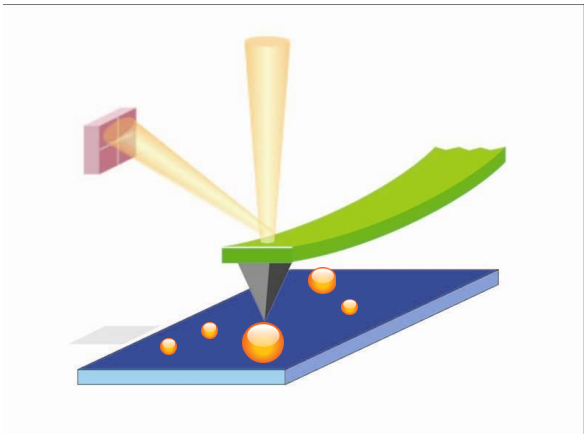

Figure 1. Schematic representation of electrical analysis of nano sized interface with SPM.

This poster will describe the size dependence of these various properties and relate them to the interfaces structure.

Recent Progress: Local Property Variations in Operating Solid Oxide Fuel Cells

The area of fuel cell technologies is an intensely studied field in the context of potential solutions to rapidly growing energy concerns. To ensure adequate conversion efficiencies, an operational fuel cell must fulfill two requirements: 1) elevated temperatures - solid oxide fuel cells (SOFCs) of the highest conversion efficiencies operate at temperatures ranging from 400°C - 1000°C; 2) variable gaseous environments – full SOFCs operate under H_2-based environments on the anode side and O_2-based environments on the cathode side. Advancing fuel cell technologies requires understanding of complex electrochemical processes through studies within their operating regime by in situ performance measurements. Scanning probe microscopy (SPM) offers a platform of a variety of complex properties on the exact size scale at which they occur. Here, the design and developmental of a miniature reaction chamber for use with a standard commercial atomic force microscope while operating under fuel cell operating conditions (temperature, gas environment)t is presented.

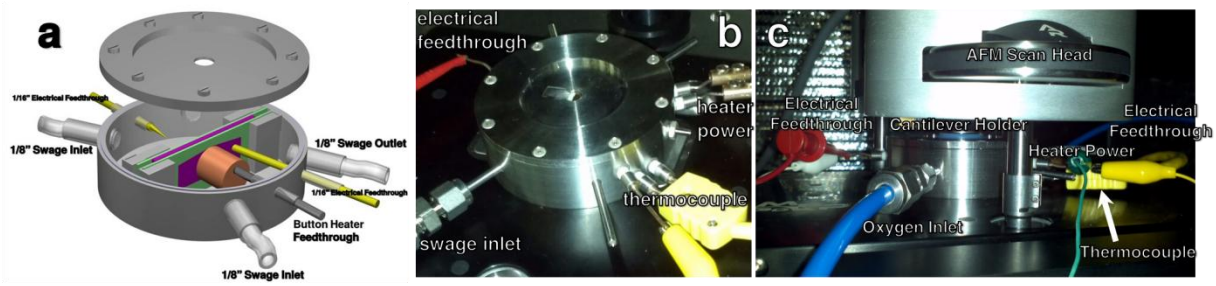

Figure 2: (a) schematic of the miniature environmental chamber design; (b) digital photograph of the actual miniature chamber as fabricated; (c) digital photograph of miniature chamber integrated with a commercial AFM scan head, while operating.

The design and fabrication of the miniature chamber shown in Figure 2 accounts for the various required stimuli of the fundamental fuel cell redox reaction while providing direct physical access for scanning probe measurements. Briefly, the chamber hosts separate electrical feedthroughs, gas inlet/outlets, and resistive heating elements (Figs. 2a,b) complete with a chamber lid with a sealed access port for SPM analysis (Fig. 2c). To ensure system performance, elevated temperature scanning surface potential microscopy (SSPM) of $La_{0.8}Sr_{0.2}MnO_3$ (LSM)-YSZ symmetrical fuel cells served as the test study

Scanning surface potential microscopy (SSPM) is a two-pass, non-contact technique; the first pass collects the topographic image of the sample surface, the second pass detects the surface potential of the sample. Figure 3 represents topographic (Fig. 3a) and SSPM (Figs. 3b-d) images collected of LSF-YSZ symmetrical cells at a temperature of 400°C. As expected, unbiased 0V conditions displayed random-like surface potential contrast (Fig. 23), while an applied bias of ±5V (Figs. 3c,d) yielded distinct potential gradients across the surface. Individual line trace analysis of each scan further clarifies the

gradients for each respective scan under differing bias conditions (Figs. 3e-h). Here the red lines represent the line slices taken of each respective scan, with the dotted red circle representing a single grain topographic feature, or the dotted black vertical lines through all the line traces found on the right. The black dotted lines represent the grain found in the red dotted circle (topographic trace) and local linear resistance characteristics of said grain features, trending with their respective bias conditions.

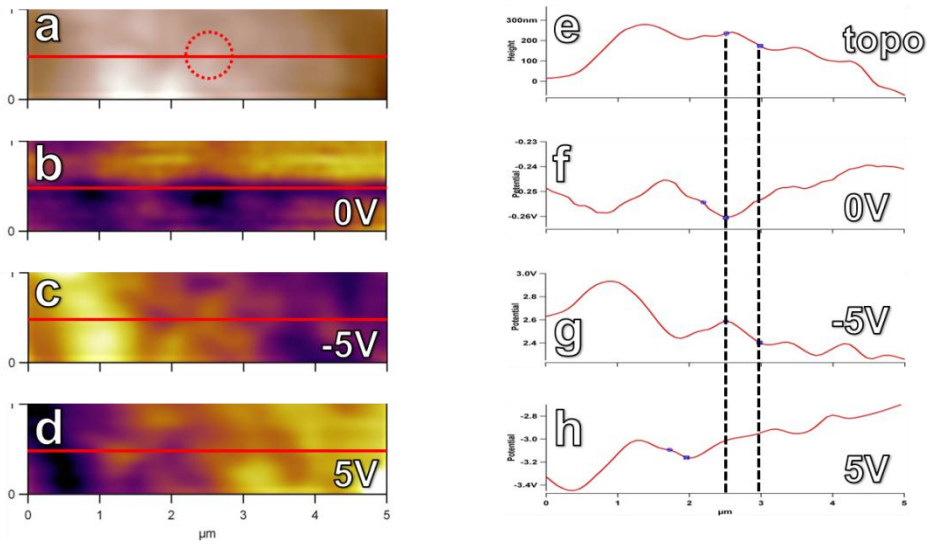

Figure 3: Line profiles of topographic and SSPM images (red lines) collected under various bias conditions at 400°C applied thermal load. The vertical black dotted lines represent the individual grain topographic feature (red dotted circle). The surface potential line traces indicate local linear resistances are observed across individual grains, trending with their bias conditions.

In summary, we have developed methodologies to conduct scan probe studies of fuel cell energy materials *in-situ*, with an operating regime comprising extreme temperatures and variable gaseous environments, using simple integration with existing, commercially available AFM systems. The SSPM studies of YSZ fuel cell electrolyte demonstrate the first direct, local observation of redox processes under operating temperatures to date.

Publications

Scanning Probes for New Energy Materials: Probing Local Structure and Function ed: N. Balke, D.A. Bonnell, D. Ginger, M. Kemerink *MRS Bulletin Focus Issue* July 2012

Nano Impedance and Complex Properties in Energy Related Systems

Wonyoung Lee, Fritz B. Prinz, Xi Chen, S. Nonneman, Dawn A. Bonnell, Ryan P. O'Hayre *MRS Bulletin* July 2012

Probing Local Phenomena: from electrons to photons spanning continuum to quantum interactions.
D.A. Bonnell, *et al. Review for Modern Physics* July 2012

Scanning Probe Microscopy in Energy Research: Materials, Devices and Applications Ed. S. Kalinin, D. A. Bonnell World Scientific Publishers in review

Probing High Sensitivity Dielectric Properties in Energy Related Systems
S. Nonneman, X. Chen, D. A. Bonnell Scanning Probe Microscopy in Energy Research: Materials, Devices and Applications Ed. S. Kalinin, D. A. Bonnell World Scientific Publishers submitted

In Situ Characterization of Interface Potential in Operating Fuel Cells
S. Nonneman, , D. A. Bonnell Scanning Probe Microscopy in Energy Research: Materials, Devices and Applications Ed. S. Kalinin, D. A. Bonnell World Scientific Publishers submitted

Orientation Controlled Schottky Barrier Formation at Au Nanoparticle-SrTiO3 Interfaces
R. Kraya, L. Y. Kraya , D. A. Bonnell *Nano Letters* **10** (2010) 1224-1228.

Materials Properties at Interfaces in Nanostructured Materials: Fundamental Atomic Scale Issues

N. D. Browning, nigel.browning@pnnl.gov

Chemical and Materials Sciences Division, Pacific Northwest National Laboratory, 902 Battelle Boulevard, P.O. Box 999, MSIN K8-87, Richland, WA 99352 USA

and

Department of Chemical Engineering and Materials Science and Department of Molecular and Cellular Biology, University of California-Davis, One Shields Avenue, Davis, CA 95616

Program Scope

The aim of this research program is to develop a robust method to quantify the atomic scale changes in structure, composition and bonding that occur at grain boundaries and interfaces under a variety of environmental conditions. Although scanning transmission electron microscopy (STEM) has long had the ability to deliver atomic resolution Z-contrast images, linking the atomic structure to the overall properties of the material being studied has primarily been on an image by image basis – in some cases extrapolating a single image that covers only a few nanometers of a defect to represent the properties of the larger scale system as a whole . However, to truly quantify the properties of interfaces, any atomic scale study must give statistical relevance to the analysis. In addition to an increase in spatial resolution, the advent of aberration correctors has provided a stability and robustness of experimental approach that means the experiment can be precisely defined and the statistical variations across many images can be correlated and quantified. This research is building on statistical crystallography methods developed for structural biology and applied previously in materials science to study doping changes in bulk materials. Research is focusing specifically on grain boundaries in oxide systems, supported metal nanostructures and the analysis in gas and liquid environments. Through such a detailed systematic analysis the most important compositional and structural effects controlling properties can be ascertained, and the mechanism by which the properties can be manipulated on the atomic scale can be determined.

Recent Progress

Grain boundaries (GBs) in complex oxides such as perovskites have been shown to readily accommodate nonstoichiometry, changing the electrostatic potential at the boundary plane and effectively controlling material properties such as capacitance, magnetoresistance and superconductivity. Understanding and quantifying exactly how these atomic scale variations in stoichiometry extend to the practical operational mesoscale is therefore a critical step towards improving the overall properties. Recent results have shown that statistical analysis of aberration corrected scanning transmission electron microscope (STEM) images acquired from a large area of grain boundary is an effective route to understanding precisely these variations in boundary structure and stoichiometry. In the case of the $SrTiO_3$ 22.6° $\sum$13 (510)/ [100] GB shown here (Figure 1), the atomic structures observed from a micron-long GB can be categorized as being composed of two different structural arrangements.

This statistical analysis from these large grain boundary areas suggests that the rigid body shift structure has the lowest energy, which is contrary to previous first principles calculations that indicated the symmetric structure to be the only stable structure at this misorientation angle.

However, careful analysis of the structure indicates the origin of this discrepancy - a difference in cation stoichiometry was discovered between the two structures. By reducing the Sr/Ti ratio from 1.0 to 0.86±0.02 in the simulations (a value close to the 0.83±0.05 ratio obtained from STEM-EDS measurements), the resultant grain boundary energy of the rigid-body shift structure was reduced to 0.97±0.01 J/m^2 (40% lower than the energy calculated for the stoichiometric structure and the same value as obtained for the symmetric structure shown in Figure 1a). This significant reduction in grain boundary energy highlights the important role stoichiometry plays in understanding grain boundary formation and structure over large length scales. Furthermore, while a comparison between the simulated structure and simultaneously acquired HAADF and ABF images (Figure 2) shows good agreement in the cation positions, there are two more oxygen columns in the ABF image that are not in the simulated structure. While this further difference between the experimental image and the simulation would seem to account for the energy difference (the rigid body shift structure is seen twice as often as the symmetric structure) this is hard to simulate, as incorporating these columns in the simulation makes the grain boundary plane charged. However, the statistical analysis described here can provide an understanding of the relative importance of stoichiometric effects on the grain boundary energies and provide the framework for in-situ observation of properties such as ionic conductivity.

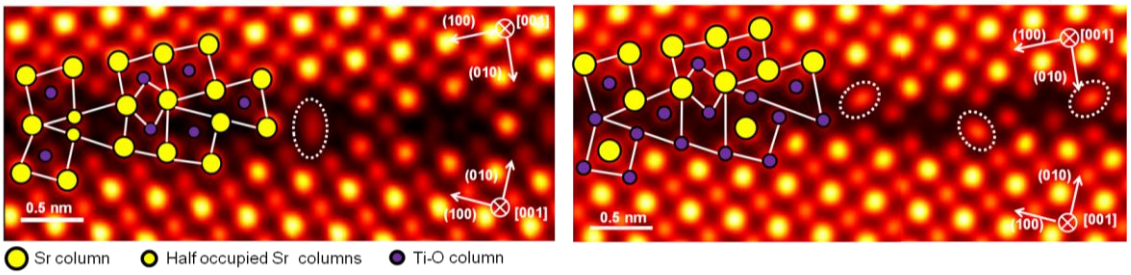

Figure 1: Average images of the two different atomic structures from a dataset of over 400 cropped experimental images. Of these cropped images, 35% images show the symmetric structure in a); and 65% images show the rigid-body shift structure in b). The identified structural units are overlaid on the left part of each image. In the average image, atomic columns showing elongated shapes suggest the presence of varying positions along the boundary.

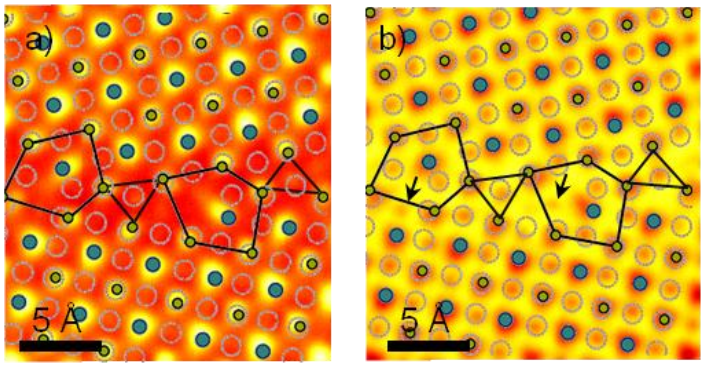

Figure 2: Average (a) HAADF and (b) ABF images of the rigid-body shift structure overlaid with the model from first principles calculations. The Sr/Ti columns show good agreement between theory and experiment. However, two oxygen columns are present in the ABF image as compared to the calculated structure (arrowed).

A second area of research is in the use of STEM techniques to image dispersed metal clusters on oxide supports, with a focus on beam sensitive materials such as zeolites. A summary, of the results obtained for Au/NaY zeolite is shown in figure 3. In particular, the results indicate that the use of a crystalline zeolite support and a reactive organogold precursor leads to an atomically dispersed gold catalyst with a high degree of uniformity that can be characterized precisely with

atomic resolution STEM. The STEM images identify the catalytic sites as site-isolated gold complexes and indicate that the observed change in activity during operation of the catalyst is associated with a change in the gold–support interface. Thus, aberration-corrected STEM can be used to probe the metal–support interface in the most highly dispersed supported metal catalysts, even when they consist of beam-sensitive materials. Such results open up the range of catalytic systems that can be analyzed by these methods and indicate that it is possible to control the beam damage to a level where quantitative information can be obtained.

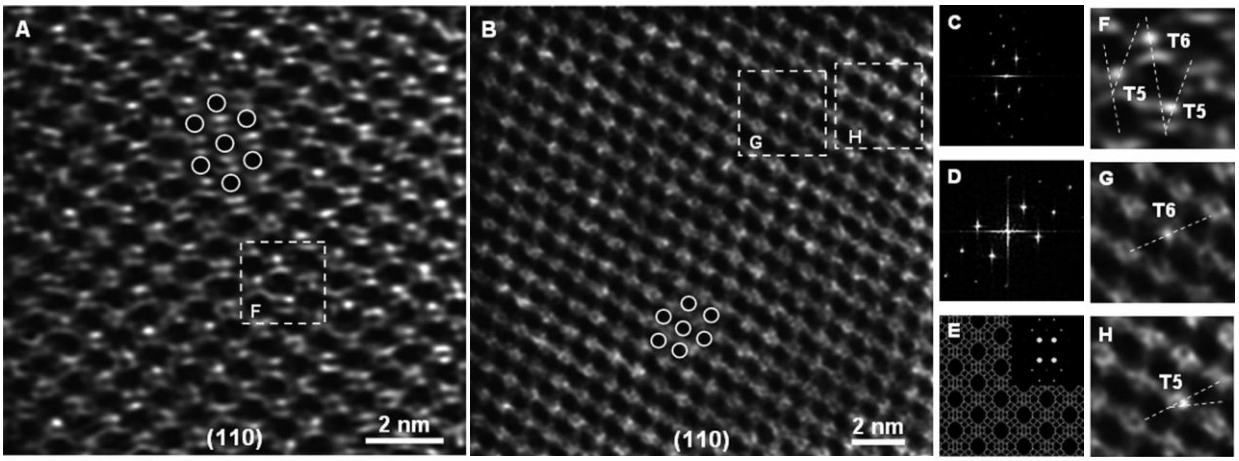

Figure 3: Aberration-corrected HAADF-STEM images of a Au/Zeolite sample prepared by adsorption of $Au(CH_3)_2(acac)$ in zeolite NaY. (a) Initially prepared sample. (b) Sample after treatment in flowing $CO+O_2$ (during CO oxidation catalysis) for 30 min. (c) FFT of the experimental image shown in (a). (d) FFT of the experimental image shown in (b). (e) Simulated framework and theoretical diffraction pattern of zeolite Y in the [110] projection. (f–h) Higher magnification images of the regions shown in rectangles in (a) and (b).

Future Plans

The results from recent work have shown several key points for understanding the effect of interface structure on properties: a) grain boundary variability can be observed and quantified, and the statistics can be related to the energetics of the interface, b) low-dose high-resolution imaging of sub-nm clusters can be obtained from the STEM, and c) the effect of the electron beam on the in-situ observations can be characterized in terms of a reducing agent (results not shown in this abstract). The aim for the future is to tie together these analyses in the following complete set of in-situ experiments:

1. The grain boundaries from a variety of systems (perovskite, fluorite, etc.) and dopants (Pr, Eu, etc.) will be reduced in-situ to observe the effect of variable oxygen stoichiometry on the stability of the grain boundary network.
2. The nanoscale catalysts will be observed under dynamic reduction/oxidation conditions to understand diffusion/reaction effects under realistic reaction parameters.
3. Methods of multivariate statistical analysis will be introduced to identify and correlate the most relevant structure/composition variations in the structures as a function of processing and environmental conditions.

DOE Sponsored Publications (2010-2012)

22. "A "Smart" Catalyst: Sinter Resistant Supported Ir Clusters Visualized with Electron Microscopy", C. Aydin et al, *Angewandte Chemie***51**, 5929 - 5934 (2012)
21. "Imaging isolated gold atom catalytic sites in zeolite Na Y", C. Aydin et al, *Angewandte Chemie***51**, 5842-5846 (2012)
20. "Single-Crystal Tungsten Oxide nanosheets: Photochemical Water Oxidation in the Quantum Confinement Regime", M. R. Waller et al, *Chemistry of Materials* **24**, 698-704 (2012)
19. "Photocatalytic Water Splitting with Suspended Calcium Niobium Oxides: Why Nanoscale is Better than Bulk – A Kinetic Analysis", E. Sabio et al, *J. Physical Chemistry C***116**, 3161-3170 (2012)
18. ""The Effect of Interfacial Charge Transfer on Ferromagnetism in Perovskite Oxide Superlattices", F. Yang et al, *Journal of Applied Physics***111**, 013911 (2012)
17. "Femtosecond Ligand/Core Dynamics of Microwave Assisted Synthesized Silicon Quantum Dots in Aqueous Solution", T. M. Atkins et al, *JACS***133**, 20664-20667 (2011)
16. "Tracking Iridium Atoms with Electron Microscopy: First Steps of Metal Nanocluster Formation in One Dimensional Zeolite Channels", C. Aydin et al, *Nanoletters***11**, 5537-5541 (2011)
15. "Ir(6) Clusters Compartmentalized in the Supercages of Zeolite NaY: Direct Imaging of a Catalyst with Aberration Corrected STEM", C. Aydin, J. Lu, M. Shirai, N. D. Browning and B. C. Gates, *ACS Catalysis* **1**, 1613-1620 (2011)
14. "Photocatalytic water oxidation with suspended alpha-Fe(2)O(3) particles-effects of nanoscaling", T. K. Townsend et al, *Energy and Environmental Science* **4**, 4270-4275 (2011)
13. "Atomic and Electronic Structures of the $SrVO_3$-$LaAlO_3$ Interface", M. Chi et al, *Journal of Applied Physics***110**, 046104 (2011)
12. L. Sudheendra et al, "Gold coated up-converting rare-earth nanophosphor", *Journal of Materials Chemistry* **23**, 2987-2993 (2011)
11. "Point defect characterization in HAADF-STEM images using multivariate statistical analysis", M. C. Sarahan et al, *Ultramicroscopy* 111, 251-257 (2011)
10. "Photocatalytic Water Oxidation with Non-Sensitized IrO2 Nanocrystals under Visible and UV Light", F. Frame et al, *JACS* **133**, 7264-7267 (2011)
9. "Improved Niobate Nanoscroll Photocatalysts for Partial Water Splitting", T. M. Townsend et al, *ChemSusChem* **4**, 185-190 (2011)
8. "Investigation of strain in self-assembled multilayer InAs/GaAs quantum dot heterostructures", S. Adhikary et al, *J. Crystal Growth* **312**, 724-729 (2010)
7. "Synthesis and Characterization of $K_{8-x}(H_2)ySi_{46}$", D. Neiner et al, *Inorganic Chemistry* **49**, 815-822 (2010)
6. "Evolution of Physical and Photocatalytic Properties in layered Titanates A(2)Ti(4)O(9) (A=K,H) and in nanosheets Derived by Chemical Exfoliation", M. R. Allen et al, *Chemistry of Materials***22**, 1220-1228 (2010)
5. "Charge Separation in Niobate Nanosheet Photocatalyst Studied with Photochemical Labeling", E. M. Sabio et al, *Langmuir* **26**, 7254-7261 (2010)
4. "Synthesis and Spectroscopic Characterization of P-doped Na_4Si_4", J. L. Wang et al, *J. Solid State Chemistry* **183**, 2522-2527 (2010)
3. "Decomposition pathway of Ammonia Borane on the Surface of Nano-BN", D. Neiner et al, *J. Phys Chem C* **114**, 13935-13941 (2010)
2. "Effect of InAlGaAs and GaAs Combination Barrier Thickness on the Duration of Dot Formation in Different Layers of Stacked InAs/GaAs Quantum Dot Heterostructure Grown by MBE", N. Halder et al, *Journal of Nanoscience and Nanotechnology* **10**, 5202-5206 (2010).
1. "Direct evidence for cation non-stoichiometry and Cottrell atmospheres around dislocation cores in functional oxide interfaces", M. A. Arredondo et al, *Advanced Materials***22**, 2430-2432 (2010).

Applications of STEM/EELS to Plasmon-related Effects in Optical Spectroscopy

PI: Jon P. Camden
Department of Chemistry, University of Tennessee, Knoxville, TN 37996-1600, USA
E-mail: jcamden@utk.edu

Research Scope

A large number of optical phenomena rely on the unique ability of metallic nanostructures to concentrate light on length scales that are smaller than the diffraction limit of visible light. Noble metal nanoparticles such as silver and gold have optical properties that make them suitable for various applications including imaging beyond the diffraction limit, solar energy harvesting, and surface-enhanced spectroscopy. These special properties result from an excitation of the localized surface plasmon resonance (LSPR), which is a collective oscillation of the conduction band electrons. LSPRs are known to depend strongly on the size and shape of the nanostructure and can be excited by both electrons and photons. Recently, electron energy loss spectroscopy (EELS) in a scanning transmission electron microscope (STEM) has emerged as a technique capable of mapping plasmonic properties on a scale 100 times smaller than optical wavelengths. While this technique has great potential, the connection between electron-driven plasmons, encountered in EELS, and optically driven plasmons, encountered in plasmonic devices, is not well understood.

Our research focuses on correlating optical spectroscopy and electron microscopy from the exact same nanostructures. Our approach is twofold. (1) We are imaging plasmon modes in single nanoparticle structures as well as nanoparticle aggregates and correlating these measurements with optical scattering measurements and fully 3D electrodynamics simulations of the exact same structures. (2) We seek to image directly the molecules that give rise to surface enhanced spectroscopies and establish their location relative to the plasmons which underlie these optical scattering spectroscopies.

Recent Progress

1. Correlated Optical and Electron Scattering from Individual Nanoparticles

While it is clear that LSPRs can be excited by far-field optical excitation and fast moving electrons, the detailed connection between resonance-Rayleigh scattering, EELS mapping, and electrodynamics remains unexplored at the single particle level. Theoretical studies have shown that the photonic density of states is related to the EELS intensity,[1] although it has been cautioned that a quantitative description of this coupling may not be possible.[2] Our research group recently demonstrated the first correlated optical scattering and STEM/EELS from the *exact* same nanostructure,[3] a critical first step to the application of STEM/EELS to plasmon-driven processes (Figure 1). In this study, we also apply a method of multivariate statistical analysis (MSVA) to extract the complex and

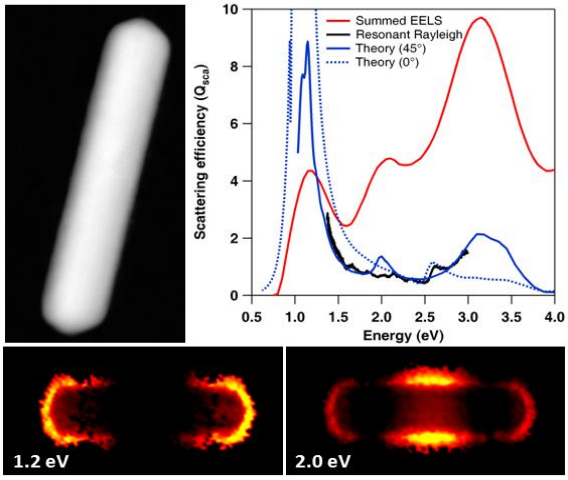

Figure 1: (Top) Annular dark field (ADF) image of a Ag nanorod with STEM/EELS spatial maps. (Bottom) Experimental and classical electrodynamics resonance-Rayleigh scattering spectra

overlapping plasmon modes encountered in nanoparticles with high aspect ratios. The calculated field-enhancement plots obtained from plane wave excitation are in good agreement with the EELS extracted plasmon maps; however significant differences are also observed.

Our initial study on high-aspect ratio silver nanorods was followed with a detailed investigation of silver nanocubes, which offer the possibility of exploring a truly 3D structure. Unlike nanorods and quasi-planar structures, which have occupied most of the previous STEM/EELS imaging studies, nanocubes have distinct LSPRs that emerge upon interaction with the substrate. This investigation (Figure 2) has given insight into the challenges associated with extracting plasmon modes from 3D structures, as well as explored the effects of the electron beam on the optical scattering spectra.

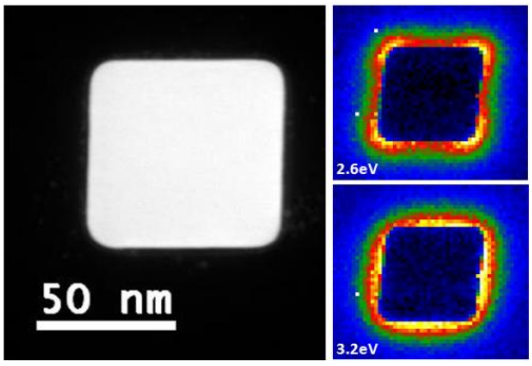

Figure 2: ADF image and STEM/EELS derived plasmon maps for a Ag nanocube. The 2.6 eV mode appears in the optical spectrum; however the mode at 3.2 eV is optically dark.

2. Comparison between photon-and electron-excitation of plasmon modes in metallic nanostructures

Our work on correlated optical and electron scattering from individual nanoparticles demonstrates the need for theories capable of describing the electron-driven excitation of plasmonic nanoparticles of arbitrary geometry and composition. Collaborator Masiello (University of Washington) integrated the motion of a swift electron into the framework of the discrete dipole approximation (DDA). This code, in conjunction with large scale parallel computing, allows us to quickly explore the following questions: (1) Is there a difference between the plasmons generated at the same excitation energy but by an electron rather than a photon? (2) What is the difference between their associated evanescent near-fields?

We use this theory to directly compare with our experimental results on nanorods, nanocubes, and complex aggregates. Figure 3 shows that theory reproduces well our experiments and that there are significant differences between the EELS loss probability map and the near-electric-field enhancements for a given energy.

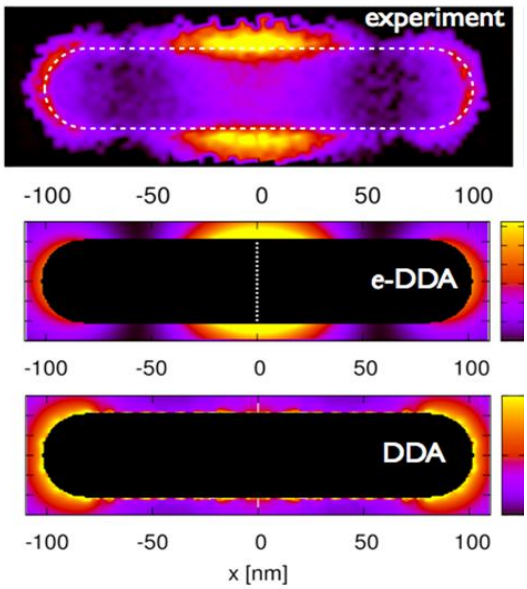

Figure 3: Comparison of the experimentally measured EEL probability map (top) for a loss energy of 2.0 eV. The dimensions of the Ag nanorod are 202x40nm and corresponds to the n=2 mode of the rod. The theoretically calculated EEL probability map for 2.0 eV (middle) is also compared to the electric field enhancement obtained under plane wave excitation at the same energy (bottom).

3. Using STEM/EELS to Elucidate Electromagnetic Hot Spots

It is widely accepted that electromagnetic hot spots play a critical role in a variety of plasmon-driven processes, especially single molecule surface enhanced Raman scattering (SMSERS). These regions of

intense electromagnetic near-fields are often found in the gaps between coupled plasmonic nanostructures.[4] Despite their importance, hot spots are challenging to measure as they require spatial resolutions better than 2 nm; therefore we have used STEM/EELS to investigate the plasmonic properties of nanoaggregates confirmed to be SMSERS active. Surprisingly, our STEM/EELS measurements do not show a strong localization of the EEL probability in either space or energy in the gap regions between coupled nanoparticles (Figure 4). In order to examine this observation in detail we use our modified version of DDA to compare the optically driven and electron driven plasmons in the aggregate structures. The calculated loss-probability map compares well with the experiment although small differences are observed. Under plane-wave excitation this structure is predicted to have an intense electromagnetic hot spot in the junction region and is known to be SMSERS active; however, a strong EEL probability in the junction region at 532 nm is *not* observed in *either* the STEM/EELS experiment or the e-DDA. We do find, however, signatures of the hot spot are observed *external* to the junctions. Interestingly, this means that the electromagnetic hot spot can indeed be excited by the electron beam, and that it is in principle possible to induce Raman scattering from the single molecule with the electron beam.

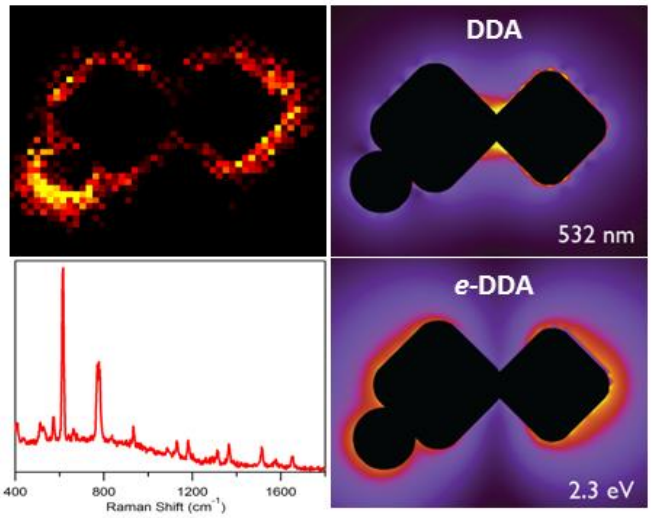

Figure 4: Experimental plasmon map of Ag aggregate responsible for Raman enhancement (top left) and single-molecule SERS of Rhodamine 6G (bottom left). Near-electric-field enhancement obtained from plane wave excitation at 532nm (2.3 eV) (top right) and EEL probability at 2.3 eV (bottom right).

Future Work

While STEM/EELS imaging of plasmonic nanostructures has demonstrated great promise, the field remains mostly unexplored and many unanswered questions exist. Moving forward, our work will build on the foundation established by our previous experiments. We are expanding our work on single nanoparticles to dimer structures and nanoparticle aggregates. Combining these detailed experiments with our newly modified version of the DDA will further enhance our understanding of hot spots and correlation between electron and photon driven plasmons. STEM/EELS is also ideally suited to the study of particles with more complex dielectric properties, such as core-shell and alloyed particles, which are important in a range of heterogeneous catalysis.

Another important aspect of single-molecule SERS that still remains unaddressed is whether an optically dark plasmon mode could possibly lead to single-molecule detection. It is widely believed that optically bright plasmon modes are responsible for SERS detection but no experimental proof of this has been reported yet. We will tackle this issue by directly probing the spatial location of the molecule on the nanoparticle responsible for the SERS signal. We will achieve the aforementioned goals by using a cold field emission, 5th order aberration-corrected Nion UltraSTEM 100. This microscope can operate at low voltages (60 kV) while still maintaining an atomic size probe. Our experiments will investigate molecules with high atomic number (Z)-values such as ruthenium which will enable us to use Z-contrast imaging to determine the precise location of the molecule in nanostructure and correlate the structure with the simultaneously acquired atomic resolved electron energy-loss spectra. Our success in this project will

ultimately provide the answers to the questions that are very important not only to the SERS community but to the entire plasmonics community as well.

References

1. de Abajo, F. J. G.; Kociak, M., Probing the Photonic Local Density of States with Electron Energy Loss Spectroscopy. *Phys. Rev. Lett.* **2008,** *100* (10).
2. Hohenester, U.; Ditlbacher, H.; Krenn, J. R., Electron-Energy-Loss Spectra of Plasmonic Nanoparticles. *Phys. Rev. Lett.* **2009,** *103* (10).

References to Publications from DOE Sponsored Work (2010-2012)

3. Guiton, B. S.; Iberi, V.; Li, S.; Leonard, D. N.; Parish, C. M.; Kotula, P. G.; Varela, M.; Schatz, G. C.; Pennycook, S. J.; Camden, J. P., Correlated Optical Measurements and Plasmon Mapping of Silver Nanorods. *Nano Lett.* **2011,** *11* (8), 3482-3488.
4. Litz, J. P.; Camden, J. P.; Masiello, D. J., Spatial, Spectral, and Coherence Mapping of Single-Molecule Sers Active Hot Spots Via the Discrete-Dipole Approximation. *J. Phys. Chem. Lett.* **2011,** *2* (14), 1695-1700.

Collaborators

Prof. Beth Guiton (University of Kentucky)
Prof. David Masiello (University of Washington)
Dr. Stephen Pennycook (Oak Ridge National Laboratory)

Properties of $LaAlO_3/SrTiO_3$ interface structures

***Venkat Chandrasekhar**, Department of Physics and Astronomy, Northwestern University, 2145 Sheridan Road, Evanston, IL*
***Chang-Beom Eom**, Department of Materials Science and Engineering, 1150 Engineering Drive, University of Wisconsin, Madison, WI*

Recent Progress

Coexistence of superconductivity and ferromagnetism at the LAO/STO interface

The two dimensional conducting gas formed at the interface between $LaAlO_3$ (LAO) and $SrTiO_3$ (STO) has attracted a lot of attention since its discovery in 2004. The system exhibits a rich variety of behaviour including superconductivity, magnetism, a superconductor-to-insulator transition (SIT), and a metal-to-insulator transition. The system shows superconductivity below $\sim$ 200 mK and has been shown to undergo a SIT by the tuning of a back gate voltage. Figure 1a shows this behaviour in the temperature dependence of resistance for a 10 unit cell thick LAO grown on TiO_2 terminated single crystal (001) STO substrates. As the back gate is changed from 80 to -100 V, the system transitions from a superconducting to an insulating state.

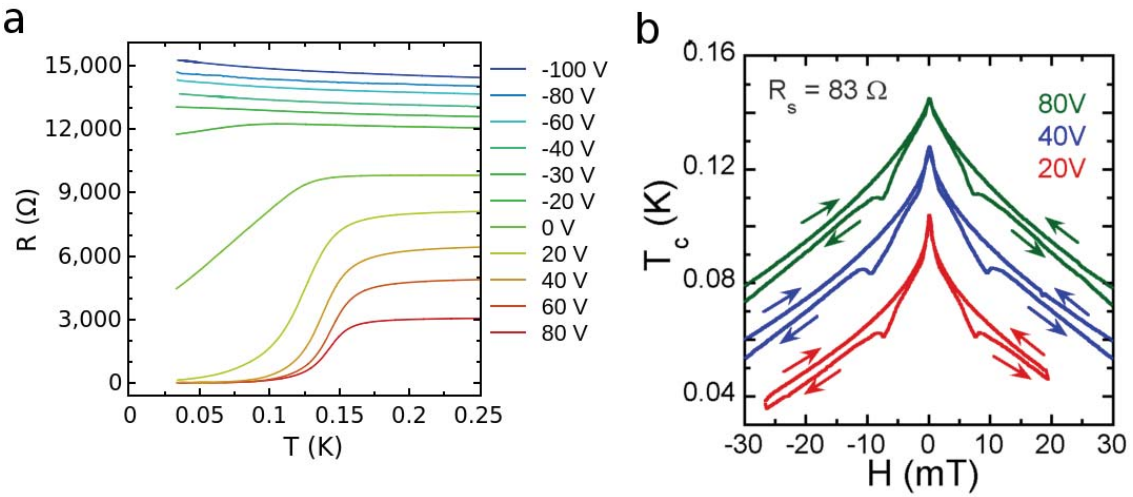

Figure 1: (a), Superconductor to insulator transition (SIT) tuned by a back gate voltage, V_g. (b) Phase diagrams, T_c vs. H, at a bias point of $R_S = 83\ \Omega$, at the foot of the resistive transition, at three different gate voltages. Data for $V_g = 40$ V are shifted by 10 mK and data for $V_g = 80$ V by 20 mK for clarity (from Publication 1).

Although both superconductivity and ferromagnetism had been observed in this system in different samples (typically under different growth conditions) by other groups, they had not been observed simultaneously in the same sample. In 2011, we reported for the first time the observation of the coexistence of superconductivity and ferromagnetism at the LAO/STO interface in the same sample [Publication 1]. These two physical phenomena are usually considered to be antagonistic to each other because of the pair breaking effect of the ferromagnetic field on the superconductor. Our magnetotransport measurements revealed the classic signature of ferromagnetism, hysteresis, while the sample was in the superconducting state. This is shown in Fig. 1b, where the critical temperature, T_c, of the superconductor is mapped continuously as the perpendicular external magnetic field is ramped, for three different gate voltages. In a separate study, discussed below, we showed that the hysteretic suppression of T_c, at $H_\perp \sim \pm$ 7 mT, can be attributed to

the motion of vortices in the superconductor induced by the magnetization dynamics in the ferromagnet at the time of magnetization reversal.

Charge-vortex duality in the superconductor-to-insulator transition

It is not yet known to what extent the magnetic and the superconducting order parameters of the LAO/STO system interact with each other. The experimental evidence obtained so far indicates that the effect of the ferromagnetism on the charge carriers is "passive," i.e., all the transport experimental features can be explained by considering the effect of the field due to the ferromagnet on the charge carriers. However, this interplay between the two phenomena of superconductivity and ferromagnetism gives rise to a novel manifestation of the phenomenon of charge-vortex duality in the SIT transition. This is shown in Fig. 2a, which shows the gate voltage dependence of the magnetoresistance of the system in a parallel external magnetic field. First, it is immediately seen that the magnetoresistance is hysteretic for all the gate voltages, due to the effect of the magnetization dynamics of the ferromagnet on the charge carriers. As the system is tuned through the SIT, the *peaks* in resistance change into *dips*. This transition from peaks to dips occurs at exactly the same gate voltage as the transition from the superconducting to the insulating regime in the R versus T dependence (Fig. 1). In a 2D SIT, the superconducting and the insulating states are related by a duality transformation. Under this transformation, the role of charge and flux interchanges between the

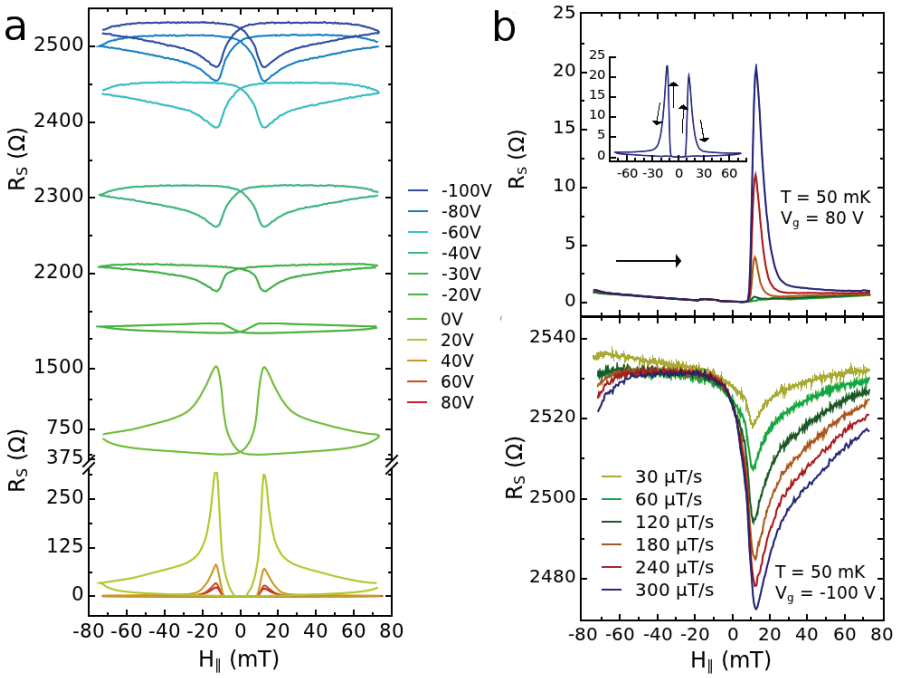

Figure 2: (a) Parallel field MR with the external magnetic field being swept at 300 μT/s as a function of gate voltage, tuning the system from the superconducting to the insulating regime. The top and bottom halves of the panel are for insulating and superconducting regimes respectively. Charge-vortex duality manifests itself as the conversion of the *peak* in the superconducting regime to a *dip* in the insulating regime. The peak and dip occur at the external field value of $H_\parallel \sim \pm$ 12 mT. (There is an axis break on the y-axis in the bottom panel.) (b) Sweep rate dependence of the peaks in the superconducting regime (top panel) and the dips in the insulating regime (bottom panel). The magnitude of the peaks and dips increases with the external magnetic field sweep rate. $T = 50$ mK (from Publication 3).

two states, giving rise to an observable interchange of current and voltage, or resistance and conductance of the two states. This is exactly what is seen in Fig. 2a.

In order to understand this behavior, it is useful to model the sample as a two-dimensional random network of superconducting grains, each grain coupled to its neighbor by the Josephson effect, parametrized by an energy scale E_j. In addition, each grain is small enough that there is a Coulomb energy E_c required for a Cooper pair to tunnel between grains. If $E_j >> E_c$, the sample is in the superconducting regime; if $E_j << E_c$, the sample is in the insulating regime. The ratio E_j/E_c can be controlled by the back gate voltage.

The ability to control the magnetization of the ferromagnet by means of an external magnetic field gives rise to another unique signature of charge-vortex duality in this system: the magnitude of the peaks in the superconducting regime and of the dips in the insulating regime is related to the sweep rate of the external magnetic field: the faster the sweep rate, the larger the magnitude of the peaks/dips (Fig. 2b). This is due to the magnetization dynamics during the reversal of the moment of the ferromagnet, which results in a time-dependent magnetic field perpendicular to the plane of the film. In the superconducting regime, the resulting dynamic perpendicular magnetic field generates moving superconducting vortices that increase the resistance of the sample. The faster the sweep rate, the larger the resistance increase. In the insulating regime, where the charging energy dominates, the dynamic perpendicular magnetic field generates an emf on the superconducting islands that acts to overcome the charging energy, reducing the resistance: the larger the sweep rate, the larger the induced emf, and hence the larger the decrease in resistance. A consequence of the model is that the magnitude of the peaks in the superconducting regime should decrease exponentially with the measured critical current, while in the insulating regime, the magnitude of the dips should scale exponentially with sweep rate. This is exactly what is observed [Publication 3].

Publications (2010-2012)

1. Dikin, D. A., Mehta, M., Bark, C. W., Folkman, C. M., Eom, C. B. and Chandrasekhar, V., Coexistence of superconductivity and ferromagnetism in two dimensions. *Phys. Rev. Lett.* **107**, 056802 (2011).

2. Mehta, M., Dikin, D. A., Bark, C. W., Folkman, C. M., Eom, C. B. and Chandrasekhar, V., Hysteretic Hall resistance at the $LaAlO_3$-$SrTiO_3$ interface - interplay between superconducting and ferromagnetic properties. *To appear in IOP conference series for LT26*

3. Mehta, M., Dikin, D. A., Bark, C. W., Ryu, S., Folkman, C. M., Eom, C. B. and Chandrasekhar, V., Evidence for charge-vortex duality at the $LaAlO_3/SrTiO_3$ interface. *Nat. Comm.* **3**, 955 (2012) doi:10.1038/ncomms1959.

Future plans

Superconducting tunnel junctions formed between LAO/STO interfaces

The coexistence of ferromagnetism and superconductivity at the LAO/STO interface opens up the possibility that the pairing mechanism in the superconductor may be unconventional. One way to probe the symmetry of the superconducting order parameter is to perform spectroscopic measurements by tunneling into the interface electron gas. We have attempted to make tunneling contacts to the interface electron gas at the edge of the mesa defined by etching the LAO/STO structure, using an Al counter-electrode. However, the process of etching apparently depletes the electron gas at the edge to a distance of about 100 nm, so contacting the interface electron gas has not been successful.

Consequently, we have moved to fabricating superconductor-insulator-superconductor (SIS) junctions directly in the LAO/STO interface, using a top gate. Figure 3(a) shows an image of one such sample we

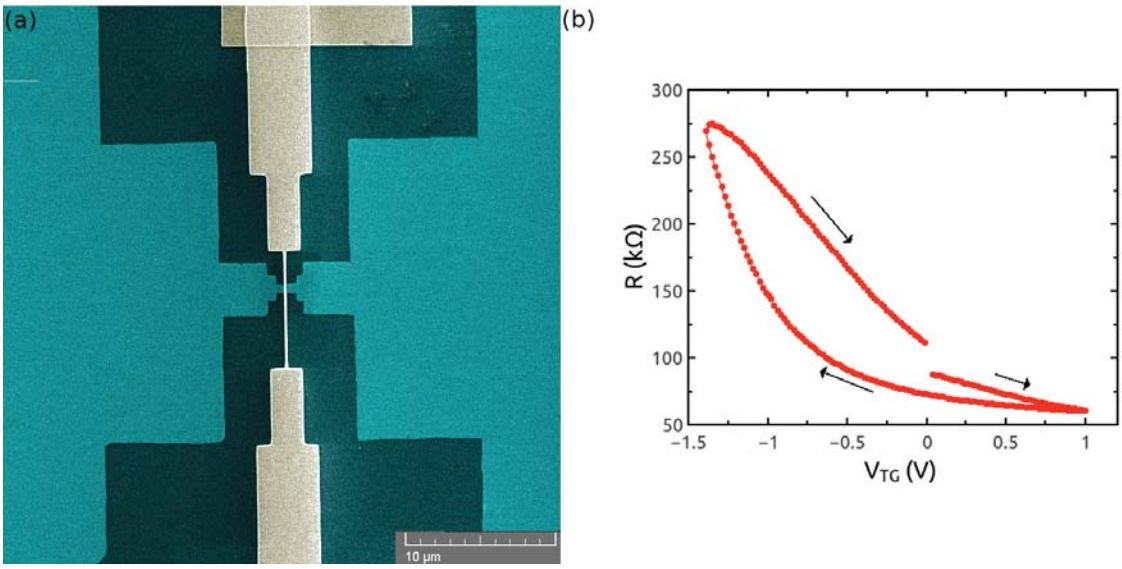

Figure 3: (a) False color scanning electron micrograph of a LAO/STO interface device fabricated by photolithography, electron-beam lithography and dry etching. Light blue-green areas are LAO/STO, dark blue areas are STO, and the gold areas are a metallic top gate. (b) Differential resistance as a function of the top gate voltage of the device of (a), at 77 K.

have fabricated. We define a constriction 1 micron long and 800 nm wide in the LAO using electron-beam lithography followed by argon ion milling, and subsequently fabricate an 80 nm wide top gate across it using e-beam lithography. The top gate is formed by first depositing 10 nm of aluminum oxide followed by gold to ensure electrical insulation between the top gate electrode and the 2DEG. Since the top gate is placed only a few tens of nanometers from the electron gas, it is very effective in controlling the density of the electron gas. Figure 3(b) shows that potentials of order of only a volt are required to deplete the electron gas, in contrast with the hundreds of volts required with a conventional back gate. We plan to measure the current-voltage characteristics of this and similar devices in the superconducting state, and then fabricate devices with additional large-area top gates, so that we can tune the state of one or the other electrode.

Scanned probe studies of LAO/STO interfaces

While two other groups have confirmed the coexistence of ferromagnetism and superconductivity in the LAO/STO system using scanned SQUID techniques (Kam Moler's group at Stanford) and torque magnetometry (Ray Ashoori's group at MIT), the nature of both the superconductivity and the ferromagnetism at the LAO/STO interface is not clear. We are in the final stages of constructing a millikelvin range multimode scanning probe microscope in order to perform magnetic force microscopy (MFM) measurements at low temperatures. Given the apparently inhomogeneous nature of the electron gas at the LAO/STO interface, we hope to correlate the MFM measurements with electrostatic force microscopy (EFM) measurements in order to gain a better understanding of the origins of both the ferromagnetism and superconductivity at the LAO/STO interface.

Structure and Dynamics of Domains in Ferroelectric Nanostructures – Phase-field Modeling

Long-Qing Chen, Department of Materials Science and Engineering, The Pennsylvania State University, University Park, PA 16802; lqc3@psu.edu

Program scope

This program is focused on investigating the basic science of domain structures and dynamics in ferroelectric thin films and nanostructures using the phase-field method, in close collaboration with experimental groups using High Resolution Transmission Electron Microscopy (HRTEM), In Situ TEM with Scanning Probe Microscopy (SPM), or Piezoresponse Force Microscopy (PFM). The main objective is to fundamentally understand the electromechanical effects on ferroelectric domain stability and on mesoscale domain switching mechanisms by close integration of computer simulations and experiments. The primary material systems to be studied are $BiFeO_3$ and related oxides. $BiFeO_3$ is one of the most promising single-phase candidates for magnetoelectric device applications due to the coexistence of ferroelectricity and antiferromagnetism at room temperature. Specifically, the program is aimed to (1) develop the modeling capability of three-dimensional (3D) ferroelectric domain evolution with spatial distributions and transport of charged defects; (2) study the fundamental roles of electric boundary conditions, film thickness, and strain in the formation of ferroelectric and ferroelastic domain structures; and (3) investigate the interactions between domain walls and charged defects as well as their influence on switching mechanisms, remnant polarization, and coercive field.

Recent Progress

In collaboration with Pan's group at University of Michigan, we studied the effect of electrical boundary conditions on domain structures in $BiFeO_3$ thin films deposited on $TbScO_3$ using the phase-field method [6,19]. It was shown that the domain structure under short-circuit boundary conditions formed (101)-oriented domain structures while the open-circuit domain structures formed (010)-oriented domains to reduce the bound charge at the film/substrate interface. It was discovered that small triangular nanodomains (Fig.1), formed at the domain/domain/substrate and domain/domain/surface interfaces in the open-circuit case, result primarily from the minimization of electrostatic energy. These nanodomains may be important for controlling in-plane switching in rhombohedral ferroelectric thin films as they represent spontaneous backswitched regions.

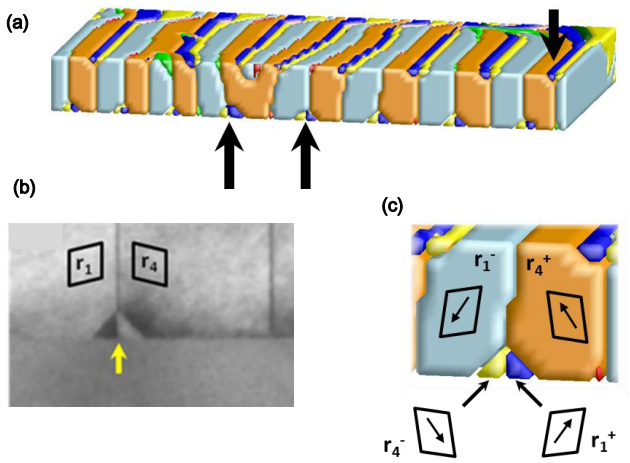

Figure 1. (a) Cross-section of a $BiFeO_3$ film with vertical 109° domains along the $[100]_p$ direction. (b) Cross section dark field TEM image of a 20nm $BiFeO_3$ film on insulating $TbScO_3$ substrate. (c) Enlarged cross-section of (a) showing an example of triangular domains at the film/substrate interface from simulation.

We also studied the effect of electrostatic boundary conditions on the temperature-strain phase diagram of (001) $BiFeO_3$ thin film under tensile in-plane strains [7, 20]. We demonstrated the open-circuit boundary condition lead to dramatically different strain – temperature phase diagram of a $BiFeO_3$ thin film. It was shown the depolarization field arising from the open circuit boundary conditions at the surface and film/substrate interface suppressed the out of plane polarization and promoted the formation of orthorhombic domains. Our simulation predicted the $BiFeO_3$ film grown on $NdScO_3$ substrate with

approximately ~1.1% tensile strain will exhibit orthorhombic phase at room temperature, which was later confirmed by experimental measurements by Ramesh's group at UC Berkeley and others.

In collaboration with Kalinin's group at Oak Ridge National Laboratory, we studied the properties of topological defects in $BiFeO_3$ thin films [15, 19]. These defects represent a junction of four polarization variants with the same out-of-plane polarization, forming a 1-D wall through the thickness of the film (Fig. 2). Experimental results showed much higher-than-usual electrical conduction at these defects, and simulation results demonstrated peculiarly high electroelastic fields which contribute to charged defect segregation. Through theoretical analysis and phase-field simulations, the properties of the defects were shown to be primarily governed by the electrostrictive properties of the material. These defects offer a path towards writable/rewritable nanoelectronics, in which we can control the conductive paths of a film through domain structure control.

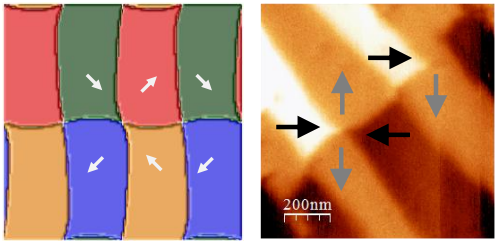

Simulation Experiment

Fig.2. Comparison between predicted four-junction anti-votex/votex domain configuration by phase-field simulation (left) and experimental observations by Kalinin's group (right).

We studied the ferroelectric domain structures of epitaxial $BiFeO_3$ thin films on miscut substrates using a phase-field model [14, 19]. In particular, we examined the effects of substrate vicinality towards (100) by assuming charge-compensated surface and film/substrate interface. The predicted domain structures show remarkable agreement with existing experimental observations with TEM and PFM observations, including domain wall orientations and local topological domain configurations (Fig. 3). A combination of computer simulations and experimentally observed domain structures allows us to understand the roles of elastic, electric, and gradient energies on the domain structures. We showed that the substrate strain anisotropy due to the miscut largely determines the domain variant selection and domain configurations.

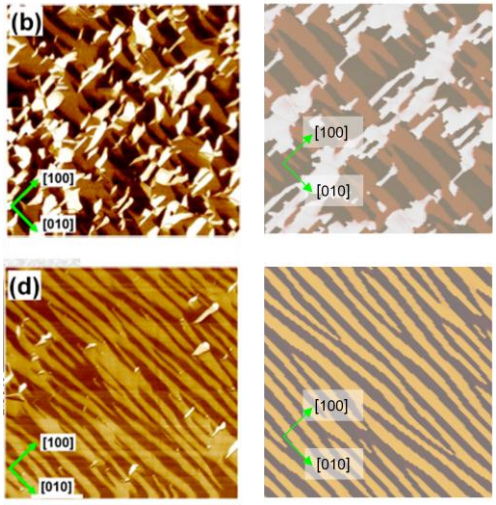

Experiment Simulation

Fig.3. Comparison between experimentally observed 4-variant and 2-variant domain structures of $BiFeO_3$ films using PFM (left) (Ramesh) and those obtained from phase-field simulations (right).

A three-dimensional phase-field model is developed for predicting the thickness effect on domain stability and Curie temperature in ferroelectric films [17]. The model simultaneously takes into account the ferroelectric domain structures, the electrostrictive effects, as well as the strain relaxation due to the thickness effect. As an example, the thickness – strain domain stability diagram was constructed for $PbTiO_3$ thin films, using both Matthews-Blakeslee (MB) and People-Bean (PB) for the estimation of critical thickness and strain relaxation. The relative domain populations as a function of thickness are plotted for $PbTiO_3$ thin films grown on $SrTiO_3$ and $KTaO_3$ substrates and compared with available experiments.

We extended our three-dimensional phase field code to incorporate strain fields resulting from edge dislocation loops in a thin film. Incorporating dislocations allowed us to simulate and understand experimentally observed interfacial dislocations in $PbTi_{0.8}Zr_{0.2}O_3$ thin films grown on $SrTiO_3$ substrates

by Pan's group. Our results agreed remarkable well with the microscopy results for films under similar mechanical and electric boundary conditions. The computational results successfully explained the fundamental driving forces underlying the domain development around the dislocations. Using the phase-field approach we were able to model the strain distribution of the system and the total elastic energy released by the domain growth around the dislocation.

Future Plans

Based on our recent progresses, we will focus on the following tasks in the near future:

In collaboration with Pan's group at University of Michigan, we will model the kinetics of domain switching in $PbTi_{0.8}Zr_{0.2}O_3$ thin films containing inhomogeneous domain structures. We will consider a 45° *a*-domain embedded in a film that is otherwise a single poled c-domain and model the mechanisms that a switched c-domain grows through the film under an applied potential. Strain states and electric fields around the domain nucleation sites will be analyzed to help to under the nucleation and growth mechanism of a *c*-domain around the *a*-domain. Using this model we will also study the reverse switching process and compare results with experimental observations using TEM.

In collaboration with Kalinin's group at Oak Ridge National Lab, We will extend our current phase-field codes of 3D ferroelectric domain structures to study the influence of mobile charged defects on domain stability and switching. In particular, we will design a series of phase-field simulations to understand the relative roles of electrostatic, strain, and domain-wall energies in determining the domain structures in BFO films at different thickness. Our strategy is to first examine some artificial, simple domain structures, e.g. domain structures containing a single domain wall. We will study more realistic 3D inhomogeneous domain structures in BFO by solving the polarization evolution equations starting from the paraelectric phase. We will perform phase-field simulations of transport of oxygen vacancies, electrons and holes in a single BFO domain film on a substrate under a uniform electric field by including interactions between defects with polarization and stress. We will also perform uniform and local switching simulations in the presence of charged defects.

We will continue developing a new phase-field model of $BiFeO_3$ which takes into account both the spontaneous polarization and antiferromagnetic order, as well as the coupling of them. The model will have a more complete description of the Landau free energy functional than the current model which ignored the antiferromagnetic order. The model could be used to predict antiferromagnetic transitions and domain structure as well as the ferroelectric polarization in $BiFeO_3$ thin films.

Publications of DOE sponsored research in 2010-2012

1. G. Sheng, Y.L. Li, J.X. Zhang, S. Choudhury, Q.X. Jia, V. Gopalan, D.G. Schlom, Z.K. Liu, and L.Q. Chen, *Phase transitions and domain stabilities in biaxially strained (001) $SrTiO_3$ epitaxial thin films.* Journal of Applied Physics, 2010. **108**(8).
2. Y. Wang, J.E. Saal, Z.G. Mei, P.P. Wu, J.J. Wang, S.L. Shang, Z.K. Liu, and L.Q. Chen, *A first-principles scheme to phonons of high temperature phase: No imaginary modes for cubic $SrTiO_3$.* Applied Physics Letters, 2010. **97**(16).
3. Y. Wang, J.J. Wang, J.E. Saal, S.L. Shang, L.Q. Chen, and Z.K. Liu, *Phonon dispersion in Sr_2RuO_4 studied by a first-principles cumulative force-constant approach.* Physical Review B, 2010. **82**(17).
4. M.D. Biegalski, D.H. Kim, S. Choudhury, L.Q. Chen, H.M. Christen, and K. Dorr, *Strong strain dependence of ferroelectric coercivity in a $BiFeO_3$ film.* Applied Physics Letters, 2011. **98**(14).
5. C.T. Nelson, P. Gao, J.R. Jokisaari, C. Heikes, C. Adamo, A. Melville, S.H. Baek, C.M. Folkman, B. Winchester, Y.J. Gu, Y.M. Liu, K. Zhang, E.G. Wang, J.Y. Li, L.Q. Chen, C.B. Eom, D.G. Schlom, and X.Q. Pan, *Domain Dynamics During Ferroelectric Switching.* Science, 2011. **334**(6058): p. 968-971.

6. C.T. Nelson, B. Winchester, Y. Zhang, S.J. Kim, A. Melville, C. Adamo, C.M. Folkman, S.H. Baek, C.B. Eom, D.G. Schlom, L.Q. Chen, and X.Q. Pan, *Spontaneous Vortex Nanodomain Arrays at Ferroelectric Heterointerfaces.* Nano Letters, 2011. **11**(2): p. 828-834.
7. G. Sheng, *Strain Effect on Ferroelectric Phase Transitions, Ph.D. Thesis,* , in *Materials Science and Engineering* 2011, The Pennsylvania State University.
8. R.K. Vasudevan, Y.C. Chen, H.H. Tai, N. Balke, P.P. Wu, S. Bhattacharya, L.Q. Chen, Y.H. Chu, I.N. Lin, S.V. Kalinin, and V. Nagarajan, *Exploring Topological Defects in Epitaxial $BiFeO_3$ Thin Films.* Acs Nano, 2011. **5**(2): p. 879-887.
9. J. Wang, Y.F. Xia, L.Q. Chen, and S.Q. Shi, *Effect of strain and deadlayer on the polarization switching of ferroelectric thin film.* Journal of Applied Physics, 2011. **110**(11).
10. Y. Wang, J.E. Saal, S.L. Shang, X.D. Hui, L.Q. Chen, and Z.K. Liu, *Effects of spin structures on Fermi surface topologies in $BaFe_2As_2$.* Solid State Communications, 2011. **151**(4): p. 272-275.
11. Y. Wang, J.E. Saal, P.P. Wu, J.J. Wang, S.L. Shang, Z.K. Liu, and L.Q. Chen, *First-principles lattice dynamics and heat capacity of $BiFeO_3$.* Acta Materialia, 2011. **59**(10): p. 4229-4234.
12. Y. Wang, S.L. Shang, L.Q. Chen, and Z.K. Liu, *Magnetic Excitation and Thermodynamics of $BaFe_2As_2$.* International Journal of Quantum Chemistry, 2011. **111**(14): p. 3565-3570.
13. Y. Wang, C.L. Zacherl, S.L. Shang, L.Q. Chen, and Z.K. Liu, *Phonon dispersions in random alloys: a method based on special quasi-random structure force constants.* Journal of Physics-Condensed Matter, 2011. **23**(48).
14. B. Winchester, P. Wu, and L.Q. Chen, *Phase-field simulation of domain structures in epitaxial $BiFeO_3$ films on vicinal substrates.* Applied Physics Letters, 2011. **99**(5).
15. N. Balke, B. Winchester, W. Ren, Y.H. Chu, A.N. Morozovska, E.A. Eliseev, M. Huijben, R.K. Vasudevan, P. Maksymovych, J. Britson, S. Jesse, I. Kornev, R. Ramesh, L. Bellaiche, L.Q. Chen, and S.V. Kalinin, *Enhanced electric conductivity at ferroelectric vortex cores in $BiFeO_3$.* Nature Physics, 2012. **8**(1): p. 81-88.
16. K. Kathan-Galipeau, P.P. Wu, Y.L. Li, L.Q. Chen, A. Soukiassian, Y. Zhu, D.A. Muller, X.X. Xi, D.G. Schlom, and D.A. Bonnell, *Direct Determination of the Effect of Strain on Domain Morphology in Ferroelectric Superlattices with Scanning Probe Microscopy.* Journal of Applied Physics, 2012. **submitted**.
17. G. Sheng, J.M. Hu, J.X. Zhang, Y.L. Li, Z.K. Liu, and L.Q. Chen, *Phase-field simulations of thickness-dependent domain stability in $PbTiO_3$ thin films.* Acta Materialia, 2012. **60**(8): p. 3296-3301.
18. Y. Wang, S.L. Shang, Z.K. Liu, and L.Q. Chen, *Mixed-space approach for calculation of vibration-induced dipole-dipole interactions.* Physical Review B, 2012. **85**(22).
19. B. Winchester, *A Phase-field Investigation of Domain Structure in $BiFeO_3$ Thin Films, Ph.D. Thesis,* , in *Materials Science and Engineering* 2012, The Pennsylvania State University.
20. J.C. Yang, Q. He, H.J. Liu, C.Y. Kuo, L.C. W., C.Y. Peng, R. Haislmaier, G. Sheng, L.H. J., C. Adamo, Z. Hu, L. Chang, C.T. Chen, L.H. Tjeng, D.G. Schlom, V. Gopalan, L.Q. Chen, Y.H. Chu, and R. Ramesh, *Orthorhombic $BiFeO_3$ Multiferroic Thin Films.* 2012. **submitted**.

Combined microscopy studies of complex electronic materials

David H. Cobden (cobden@uw.edu)
Department of Physics, University of Washington, Box 351560, Seattle, WA 98195

Scope

Many interesting electronic materials have complex microstructure and exhibit high sensitivity to experimental conditions, impeding their study and utilization. For example, strongly correlated oxides exhibiting first-order phase transitions, such as VO_2 with its famous and intriguing metal-insulator transition (MIT) at T_c = 68 °C, have inevitable domain structure and twinning in the bulk resulting from the transition itself. Other topical materials, such as two dimensional semiconductors like MoS_2, only exist as delicate micron-scale sheets. Therefore, studies of small single crystals under carefully controlled conditions are called for in order to determine the intrinsic properties and to understand the fundamental physics of these systems, such as the mechanisms underlying the MIT. The goal of this program is to perform such studies, employing a combination of microscopy techniques. As an essential component we are developing an apparatus in which we can achieve simultaneous control of temperature, magnetic field, vapor environment, and uniaxial strain all while performing ultrafast scanning optics, electrical transport and photocurrent measurements. In addition, collaborations allow us to perform other microscopies on the same microcrystal samples, including scanning-probe, transmission electron microscopy, and ultrafast X-ray spectroscopy. The work also relies on developing crystal synthesis, sample preparation, and device technology.

Recent progress

1. Scattering-scanning optical microscopy (s-SNOM) and scanning Raman spectroscopy on VO_2. In s-SNOM one detects scattering of a laser from an atomic force microscope tip above the sample, allowing determination of optical properties at a scale of tens of nm. s-SNOM and Raman studies of VO_2 nanobeams and platelets were done in collaboration with Markus Raschke (Department of Physics, University of Colorado at Boulder), with whom this project began as an SISGR project. The role of the intermediate insulating M2 phase in the MIT is likely critical but remains poorly understood. We found that small M2 domains form inevitably at the interfaces between the low-temperature M1 and metallic rutile R domains during the MIT, and quantified the behavior [1].

2. Photocurrent microscopy on VO_2 nanobeams. An intimate combination of high-resolution and ultrafast optics with dc electrical measurements is enabled by working with small samples having electrical contacts. Not only can photocurrent measurements reveal many aspects of the behavior of a material but also the quantities thereby determined are key to optoelectronic applications. In band semiconductors, depletion fields associated with interfaces separate long-lived photo-induced carriers. However, in systems with strong electron-electron and electron-phonon correlations such as VO_2 it is unclear what physics will dominate the photoresponse. In our scanning photocurrent

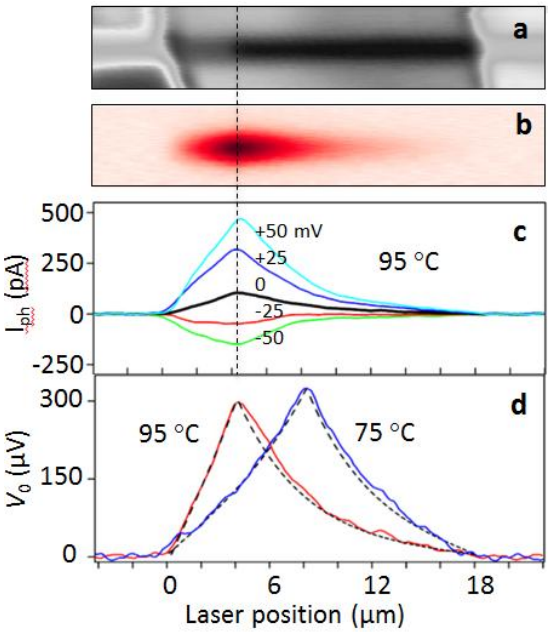

Figure 1. SPCM applied to a suspended VO_2 nanobeam. (a) Reflection image of a device at 95 °C: the darker region is metallic (M), the paler insulating (I). (b) Photocurrent image at bias V=0, showing a peak at the M-I interface. (c) Line traces of photocurrent Iph along nanobeam center for series of V. (d) Line traces of determined photo-emf V0 = RIph at two temperatures. Dashed lines are the predicted photothermal voltage.

microscopy (SPCM) setup, constructed in collaboration with Xiaodong Xu (University of Washington), a diffraction-limited 800 nm laser spot, chopped at 1 kHz, is scanned over the sample on a temperature stage. The resulting photocurrent is measured with a lock-in amplifier referenced to the chopper. Using SPCM on suspended VO_2 nanobeams undergoing the MIT, we observed photoresponse peaked at the metal-insulator boundary but extended throughout both insulating and metallic phases (Fig. 1). We determined that the response is photo-thermal, with no evidence for nonequilibrium carrier effects, implying efficient carrier relaxation to a local equilibrium in a manner consistent with strong electron-electron and electron-phonon correlations [2]. We also demonstrated switching of the photocurrent by optical control of the metal-insulator boundary arrangement.

3. Ultrafast photocurrent microscopy on graphene p-n junctions. We have also constructed a setup for time-resolved SPCM. In a typical degenerate pump-probe arrangement, 800 nm laser pulses of 250 fs width repeated at 76 MHz are split into pump and probe beams and then recombined with a relative delay before focusing on the sample by a microscope objective. The probe beam can be down-converted to infrared (up to ~4 μm), and can be scanned independently over the sample. It is chopped at 1 kHz and the corresponding current at that frequency is detected. Our first measurements were on gated graphene [3], a well characterized and topical material system with open questions concerning its nonequilibrium electron behavior and ultrafast dynamics. Selected results are shown in Fig. 2. We demonstrated that hot carriers, rather than phonons, dominate energy transport. The photocurrent response time was found to vary from 1.5 ps at room temperature to 4 ps at 20 K (Fig. 2d). Gate-dependent measurements proved that both thermoelectric and built-in electric field effects contribute to the photocurrent in graphene, with the contribution from each depending on the junction configuration. The photocurrent produced by a single pulsed laser also displayed multiple polarity reversals as a function of carrier density, which is a possible signature of impact ionization.

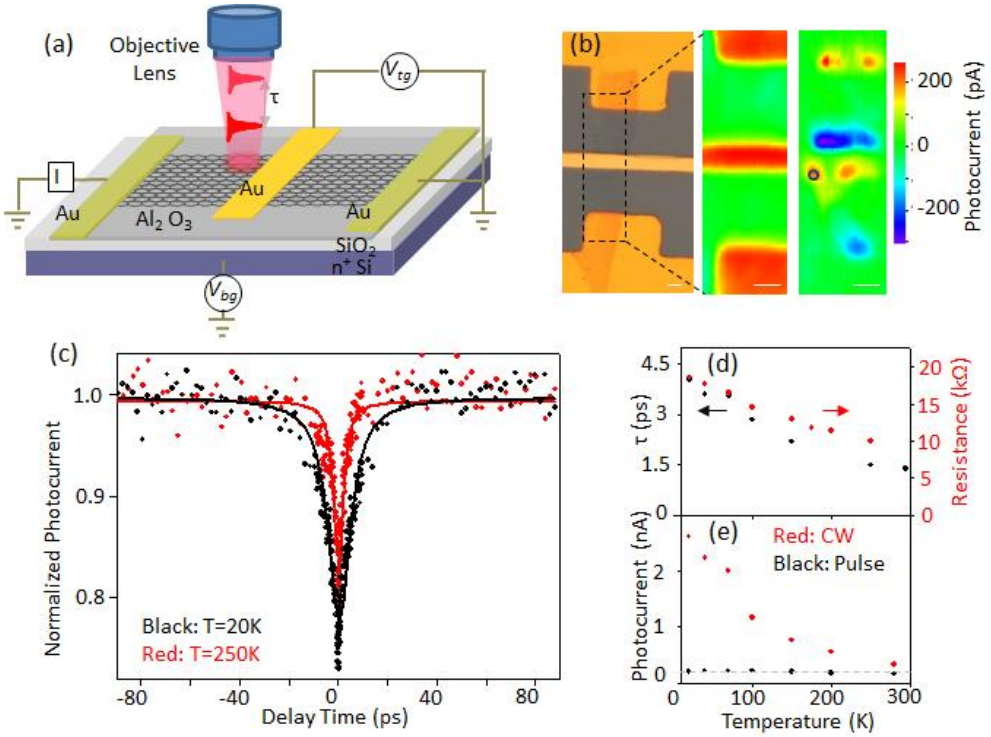

Figure 2. Ultrafast scanning photocurrent microscopy on graphene p-n junctions. (a) Pump and probe laser pulses are focused on the junction near the edge of an Au/Al_2O_3 top gate on an exfoliated graphene sheet. (b) White-light (left), reflection (middle), and photocurrent (right) images of a device with Au source and drain at top and bottom. (c) Variation of probe-induced photocurrent with pump delay at two temperatures, showing relaxation in a few ps. (d) Relaxation time τ vs *T*. (e) Dramatic difference in *T*-dependence of the photocurrent between CW and pulsed excitation.

4. Ultrafast polarized response of single-domain VO_2 crystals. VO_2 has been a popular system for application of ultrafast techniques, because the MIT appears to take place in as little as 50 fs and its dynamics remain an open question. However all previous studies have been on bulk crystals or thin films where orientational averaging or inhomogeneity has to be allowed for and prevents measurements of, eg, polarization dependence. In collaboration with Xiaodong Xu we have performed the first polarization-dependent ultrafast studies on VO_2 [manuscript in preparation], using individual single-domain microcrystals with known crystal axes, such as the one shown in Fig. 3a. The crystals were grown on SiO_2 using a modified physical vapor transport process and transferred to sapphire substrates, so that optical transmission could be measured at varying temperatures up to T_c. Fig 3b illustrates a nondegenerate pump-probe measurement at room temperature. The MIT is induced for fluences above about 1 mJ/cm^2, and the response settles in a timescale of hundreds of ps, broadly consistent with previous results on thin films. It has been suggested that this settling timescale corresponds to nucleation of the rutile phase, although shock wave propagation of the M-I interface has also been mooted. One key new feature of our results is coherent acoustic oscillations, which we see only when the probe polarization is perpendicular to the c-axis. The oscillation period is proportional to crystal thickness (Fig. 3c), consistent with compression waves generated by the pump propagating normal to the substrate and modulating the absorption anisotropically. These oscillations occur irrespective of the MIT, and decay on the same time scale as the settling, indicating that the settling process is in fact associated with elastic relaxation.

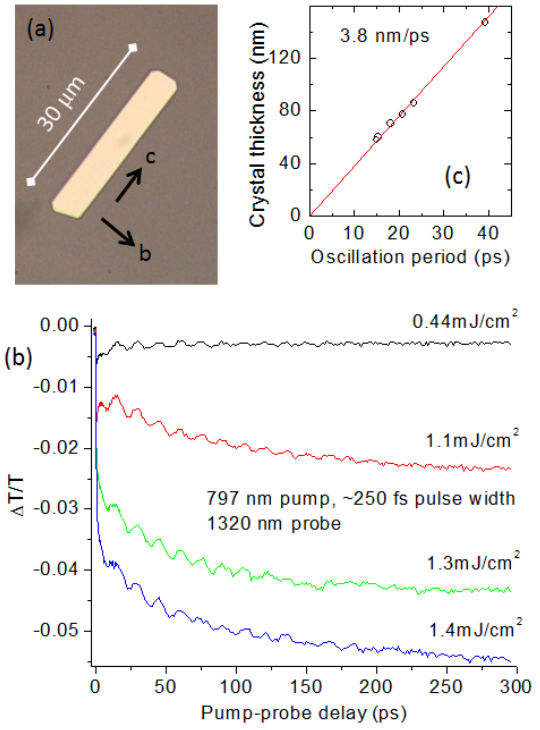

Figure 3. (a) Optical image of a VO_2 microcrystal on a sapphire substrate. c indicates the rutile c-axis. (b) Representative pump-probe measurements on this crystal: $\Delta T/T$ is the fractional change in normal incidence transmission of the probe produced by the pump. Results are shown for several pump fluences with probe polarization in the b-direction. (c) Period of oscillations as seen in (b), for six different crystals, plotted against crystal thickness measured by AFM.

Future plans

1. The fundamental nature of the MIT in vanadium oxides. We will continue to focus on VO_2 as a paradigm for demonstrating the effectiveness of the approach of applying multiple microscopy-related techniques combined with thorough control of sample conditions to micro- and nano-scale single crystals. Rutile c-axis strain greatly modifies the MIT in VO_2 with many ramifications, but in most experiments it is uncontrolled and unknown. Motivated by this we are completing a unique system for applying axial strain to nanobeams or 2D sheets with nm precision under a microscope in a cryostat. This will allow us amongst other things to home in on the evasive M1-M2-R triple point in VO_2, whose precise location and relationship to T_c is important to establish. We will extend the single-microcrystal ultrafast studies to shorter times and higher resolution (using s-SNOM, with Markus Raschke), to photocurrent measurements, and to Cr- and H-doped crystals in which either the M2 or R is stabilized at low temperatures. We are developing low-stress single-crystal VO_2 Hall bars on boron nitride and graphene for transport and optical measurements in high magnetic fields and with actively tunable hydrogen doping. Pump-probe and other microscopy studies of M2-stabilized samples will allow us to determine the importance of dimerization of the vanadium chains for the ultrafast MIT. Time-resolved polarization-

dependent near-edge X-ray spectroscopy (with Jerry Seidler, University of Washington) using VO_2 microcrystals on high thermal conductivity low-friction substrates (graphene on diamond) to minimize strain and thermal inertia, at the Advanced Photon Source may allow separation of lattice and electronic processes in the MIT at ps timescales. New high-resolution transmission electron microscopy techniques developed by our collaborators (Richard Beanland, University Warwick) are capable of producing strong contrast between very similar structures such as M1 and M2 and will be used to further investigate the role of M2 and the putative related trigonal phase. The polarization-resolved far-infrared conductivity, which is expected to reflect correlations and to be extremely sensitive to the MIT, will be measured in all phases (with Mumtaz Qazilbash, College of William and Mary). Ultrasonic force microscopy (with Neil Wilson, Warwick) will yield elastic moduli with AFM spatial resolution, important for disentangling stress complications at the MIT. Also, we hope to perform similar experiments on microcrystals of the related material V_2O_3, with its MIT at ~150 K which intriguingly resembles that in VO_2 in some ways but not others. We will try to obtain V_2O_3 microcrystals by reducing our VO_2 crystals in vacuum or in controlled O_2 partial pressure, as well as by cleaving larger existing crystals.

2. Two-dimensional semiconductors and other materials. We will continue to diversify the range of systems under study. We will apply the techniques and approach to single sheets of exfoliated semiconductors such as MoS_2, $MoSe_2$ and WS_2. These two-dimensional materials resemble graphene in having a hexagonal Brillouin zone with Dirac-like properties, but in contrast with graphene they have single-particle bandgaps in the infrared or visible and have therefore greater potential for diverse interactions with light as well as interesting dependences on strain, magnetic field, vapor environment, and so on. They also exhibit finite Berry curvature and strong spin-orbit coupling relevant for spin- and valleytronics. Extensions of our ultrafast photocurrent microscopy techniques will be appropriate for exploring these phenomena.

DoE sponsored publications, 2010-2012

1. A.C. Jones, S. Berweger, J. Wei, D.H. Cobden, M.B. Raschke, “Nano-optical Investigations of the metal-insulator phase behavior of individual VO_2 microcrystals”, Nano Letters 10, 1574 (2010).
2. T.S. Kasirga, D. Sun, J.H. Park, J.M. Coy, X. Xu, D.H. Cobden, “Photoresponse of a strongly correlated material determined by scanning photocurrent microscopy”, under review, Nature Nanotechnology (2012).
3. D. Sun, G. Aivazian, A.M. Jones, J.S. Ross, W. Yao, D.H. Cobden, X. Xu, “Ultrafast hot-carrier-dominated photocurrent in graphene”, Nature Nanotechnology 7, 114 (2012).
4. J.H. Son, J. Wei, D.H. Cobden, G.Z. Cao, Y.N. Xia, “Hydrothermal synthesis of monoclinic VO_2 micro- and nanocrystals in one step and their use in fabricating inverse opals”, Chemistry of Materials 22, 3043 (2010).

In Situ Light Illumination of Photocatalytic Materials in an Environmental Transmission Electron Microscope

Peter A Crozier (PI), Ben Miller and Liuxian Zhang
School for Engineering of Matter, Transport and Energy, Arizona State University,
Tempe, AZ 85287-6106
Email: crozier@asu.edu

Program Scope

Photocatalysis has the potential to play an important role in the development of sustainable energy technologies. In principle, hydrogen can be generated from water and carbonaceous fuels can be generated from CO_2 using photocatalytic or electrophotocatalytic processes. An advantage of this approach to solar energy is that the energy of the sun is simultaneously captured and stored in the fuel molecule. This energy can then be released either for electricity generation or in transportation based combustions processes. The current efficiency and long term performance of photocatalysts for solar fuel generation is very low and there are many fundamental problems that must be solved related to photon absorption, charge separation and catalytic activity. The scope of this project is to develop novel *in situ* microscopy techniques for probing structure-reactivity relations in photocatalytic materials. Specifically we are developing a variable wavelength light illumination system which will allow photocatalysts to be studied in the TEM under near reactor conditions. The first phase of this project involved construction and installation of a variable wavelength light source onto an environmental transmission electron microscope so that materials can be studied under light irradiation, variable temperature and reactive gases. This phase has now been completed and we are currently investigating the surface changes taking place on titania nanoparticles during photon illumination in atmospheres of water, hydrogen and vacuum. Interfacial interactions between titania and cadmium sulfide and metal co-catalysts are also under investigation. The fundamental information that emerges from this project should lead to a deeper understanding of the effect of light, heat and gas on the properties of nanomaterials relevant to solar fuels.

Recent Progress

The initial stage of this project was to design and construct a system for performing *in situ* photon irradiation of TEM samples under conditions relevant to solar energy applications. This requires photon irradiation from the IR to the UV at intensities, integrated over all wavelengths, on the order of 100 mW/cm^2. Moreover, the system should provide variable wavelength capability, should not limit the use of TEM holders and should not impose significant constraints on sample tilting capability. Initially we want to irradiate samples in an FEI Tecnai environmental transmission electron microscope in the presence of reactive gases at variable temperature. Thus the system should be resistant to chemical attack and should be fully bakable. We also intend to install the system (in slightly modified form) into a future NION superSTEM equipped with a monochromator for photon induced charge transfer studies.

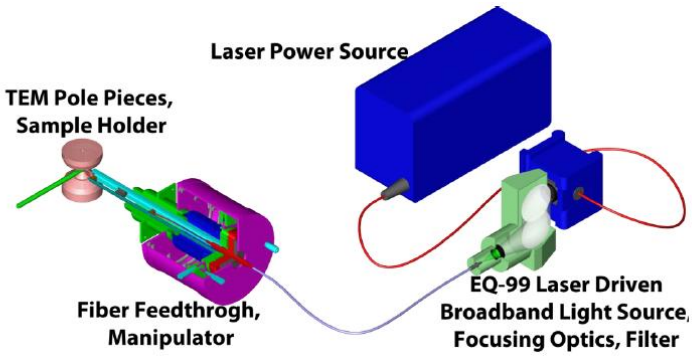

Figure 1: Overview of *in situ* illumination showing IR laser, broadband light source and fiber feed through and manipulator.

Taking all these requirements into consideration lead to the design illustrated schematically in Figure 1 consisting of an Energetic laser driven light source providing a high brightness white light source that was coupled into an optical fiber which was directed toward the TEM sample. The light source focusses an infrared laser into a xenon gas that generates a plasma approximately 100 μm in

diameter at a temperature of 7200°K. After passing through suitable optical filters, the light is coupled onto the entrance surface of a 600 μm fiber using a set of parabolic mirrors. Mirrors rather than lenses are employed because they do not suffer from chromatic aberration and so the entire spectrum of light can be focused onto the fiber if desired. The solarization fiber employed is resistant to damage from UV radiation and transmits across a wide range of wavelengths with reasonable efficiency. A standard high vacuum feed through was used to couple the light from the external optical fiber to a similar fiber inside the TEM. The fiber in the TEM is coated with aluminum to prevent charging. One important feature of our design is illustrated in figure 2. There is very limited space inside the TEM and the fiber cannot be bent through a radius of curvature of less than 25 cm. To ensure that light strikes the TEM sample, the end of the fiber is cut at an angle of 30° which refracts light towards the sample. This ensures that the sample is illuminated in any of our existing TEM holders in an untilted position.

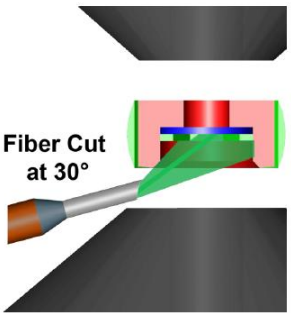

Figure 2: Schematic diagram of end of fiber in the ETEM adjacent to TEM sample located in hot stage furnace between upper and lower pole pieces of objective lens. The 30° cut refracts light towards the TEM sample.

Before installing the system on the TEM it was necessary to characterize the light distribution on the sample *ex-situ* using a CDD camera. Figure 3 shows the light distribution integrated over all wavelengths when the fiber is positioned 2 mm from the sample. The peak intensity is approximately 1460 mW/cm^2 which is 10 times the solar flux on the earth's surface. The intensity distribution has an elliptical profile and figure 3 shows various contours corresponding to intensity levels of 90%, 50% and 10% of the peak intensity. The zone containing 90% of the peak intensity lies within an elliptical area with major and minor axes of approximately 1 and 0.2 mm respectively. This is certainly large enough to intensely irradiate large areas of the TEM sample. The 10% contour (corresponding to a little over one sun) has major and minor axes of almost 4 and 1.6 mm. To align the fiber inside the TEM, we built a photodiode into an old TEM holder and translate the fiber to maximize the intensity falling on the detector. Figure 4 shows the peak intensity as a function of wavelength over the wavelength range 200 – 800 nm. The effect of variations in transmission of the various optical components (fibers, mirrors, filters etc..) is also shown on the diagram. This shows that the intensity varies by no more than a factor of 2 over the range 400 – 800 nm although some additional attenuation takes place with the insertion of filters. For comparison the solar spectrum striking the earth is also shown.

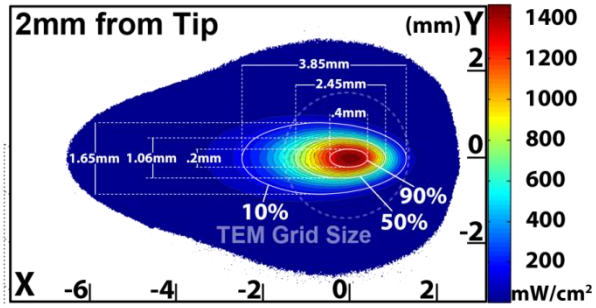

Figure 3: The light distribution as a function of position on the TEM sample when the end of the optical fiber is located 2 mm from the TEM sample at zero tilt angle. The maximum intensity is about 1460 mW/cm^2 and the contours show the wavelength integrated intensity levels of 90%, 50% and 10% of this maximum.

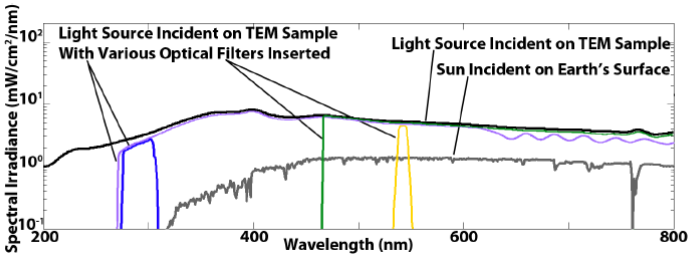

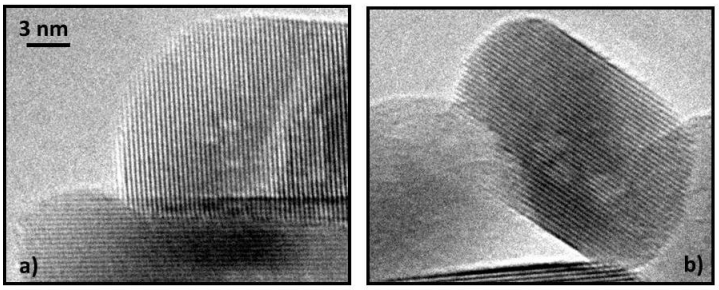

Figure 5: a) HREM image of initial anatase particles at 150°C showing (101) lattice fringes. b) HREM of anatase particle at 150°C in 0.5 Torr of H_2 after 44 hours of irradiation at 1460 mW/cm^2 (through fused silica) with other

For our initial application of the

ısity as a function of wavelength striking the center
. The effect of various filters is also shown along
ty at the earth's surface.

in situ illumination system, we are studying titania based photocatalysts. In spite of pure titania's limited absorption in the visible, these materials remain a major focus of photocatalytic research because of their very high stability in aqueous and organic environments. The response in the visible region can be enhanced through functionalization with other semiconductors or doping. Titania nanoparticles, nanotubes and nanowires were prepared using hydothermal and electrochemical techniques with and without functionalization. These materials were sometimes supported on SiO_2 spheres and dispersed onto Pt grids for image and spectroscopic observation in the TEM. The materials were typically heated to 150°C to remove hydrocarbons from the surface and then exposed to various reactive gases and light for periods up to 60 hours. HREM images and electron energy-loss spectra were recorded before, after and during irradiation to look for evidence of phase changes. Electron beam effects in titania are significant and techniques such as low dose imaging must be employed. Figure 5a shows a typical anatase crystallite at 150°C in the absence of light or gas showing a reasonably ordered surface termination. Figure 5b shows a similar anatase crystallite after a 44 hour exposure to the complete spectrum of light and 0.5 Torr of H_2. Very little change is observed on the surface or bulk of the anatase crystallite after this treatment. However, changing the gaseous atmosphere to H_2O gives a very different result. Figure 6 shows the change that takes place in anatase at 150°C in an atmosphere of 1 Torr of H_2O after exposure to light. Significant surface roughening and disorder appeared and quantitative analysis showed that of the number of (101) lattice spacings across the width of the crystal decreased by about 2. This proves that the top 0.4 nm (approximate a (101) lattice spacings) transformed from a crystalline to amorphous structure during irradiation. Prolonged continued irradiation under the same conditions for a further 40 hours resulted in this disorder layer approximately doubling in thickness. Images from other crystallites, including those not previously exposed to the electron beam, confirmed this surface amorphization phenomena.

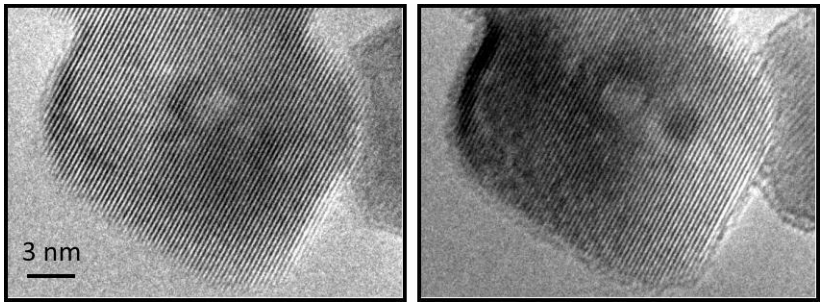

Figure 6: a) a) HREM image from anatase nanoparticle at 150°C before exposure to light and H_2O. b) Same anatase particle after exposure to 1 Torr of H_2O and 30 minutes of light at 150°C showing presence of disordered layer up to a few monolayers (~ 0.4 nm) thick.

This set of observations can be explained by considering the processes taking place on the surface of the titania during irradiation with light. It is known that oxygen desorption takes place from the top one or two layers of the crystal during light (and electron beam) exposure resulting in the creation of oxygen vacancies at the surface. This was confirmed with high spatial resolution EELS analysis which showed that the surface titanium atoms are close to the +3 oxidation state. In the H_2 atmosphere (or vacuum), very little additional change is observed suggesting H_2 is not activated on the bare anatase surface under these experimental conditions. In the water atmosphere, water adsorbs dissociatively at the oxygen vacancy site giving rise to two hydroxyl groups on the surface. This causes the surface to transform from a crystalline reduced titanium oxide to an amorphous titanium hydroxide. This is a major disruption to the catalyst surface with will certainly have a major effect on charge transfer process, catalysis and metal

support interactions. We hypothesize that this may be the structure of the titania in an aqueous environment during photon irradiation. We also observed that the underlying crystal structure remains unchanged by this process and it is just the top two monolayers that are affected. Effectively the hydroxyl layers passivate further hydroxylation leading to long term stability of titania.

Future Plans

We expect our NION SuperSTEM to be delivered sometime this fall and after completion and testing of the instrument we plan to install a similar light delivery system. We believe that our design will be mostly transferable to the NION with minor adjustments reflecting changes in the geometry around the pole piece and sample. We plan to investigate light induced charge transfer phenomena across heterostructures using ultra high energy resolution EELS. With the current set up in the environmental microscope, we will continue to study changes taking place in titania based catalysts. Having complete baseline studies on anatase, we plan to perform similar studies in rutile and also to explore the wavelength dependence of the changes in the water environment. Does the surface roughening only occur when irradiation is carried out with photon energy above the bandgap? We are particularly interested in investigating the changes taking place on functionalized titania. At the moment we are functionalizing titania nanowires and nanotubes with semiconductors that absorb in the visible and with metal catalytic particles. Several questions are critical for developing an understanding of the fundamental phenomena that take place on these materials. Do metal particles undergo sintering at low temperature in the presence of UV irradiation? Does this depend on the photon energy relative to the bandgap? What happens to the structure of the interface during light induced charge transfer processes. How are these phenomena influenced by the gas environment around the catalyst? Can we make similar measurement in a liquid environment? How do these structural observations correlate with catalytic properties?

References to publications of DOE sponsored research that have appeared in 2010-2012

V. Sharma, P.A. Crozier, R. Sharma and J.B. Adams, (2012) "Direct Observation of Hydrogen Spillover in Ni-Loaded Pr-Doped Ceria ", Catalysis Today **180**(2) 2-8.

P. P. Dholabhai, S. Anwar, J. B.Adams, P. A.Crozier, R. Sharma (2012) "Predicting the optimal dopant concentration in gadolinium doped ceria: a kinetic lattice Monte Carlo approach." Modelling and Simulation in Materials Science and Engineering **20**(1): 13.

P. P. Dholabhai, J. B.Adams, P. A. Crozier, R. Sharma, (2011) "In search of enhanced electrolyte materials: a case study of doubly doped ceria", Journal of Materials Chemistry, 21(47): 18991-18997.

P. P. Dholabhai, S. Anwar, J. B.Adams, P. A. Crozier, R. Sharma, (2011) "Kinetic lattice Monte Carlo model for oxygen vacancy diffusion in praseodymium doped ceria: Applications to materials design ", Journal of Solid State Chemistry 184(4): 811-817.

Pratik Dholabhai, James Adams, Peter Crozier and Renu Sharma, (2011) "First-principles Study of Defect Migration in RE-doped Ceria (RE = Pr, Gd)", MRS Online Proceedings Library, 1311, mrsf10-1311-gg05-08 doi:10.1557/opl.2011.158

P.P. Dholabhai, J.B. Adams, P. Crozier, R. Sharma, (2010) "A Density Functional Study of Defect Migration in Gadolinium Doped Ceria", Phys. Chem. Chem. Phys., 12 7904-7910.

P.P. Dholabhai, J.B. Adams, P. Crozier, R. Sharma, (2010) "Oxygen Vacancy Migration in Ceria and Pr-Doped Ceria: A DFT plus U Study", Journal of Chemical Physics, 132 8.

V. Sharma, K.M. Eberhardt, R. Sharma, J.B. Adams, P.A. Crozier, (2010) "A Spray Drying System for Synthesis of Rare-Earth Doped Cerium Oxide Nanoparticles", Chemical Physics Letters, 495 280-286.

Benjamin K. Miller and Peter A. Crozier (2012). "A System for *In Situ* UV-Visible Illumination of ETEM Samples" (under review, Microscopy and Microanalysis).

Interfacial Thermal Resistance of Carbon Nanotubes
Principal Investigator: John Cumings
Department of Materials Science and Engineering
Bldg. 90, Stadium Dr.
College Park, MD 20742-2115
Email: cumings@umd.edu

Project Scope

Many studies have shown that carbon nanotubes have superlatively high thermal conductivity [1,2], but unfortunately, the scientific understanding about how heat can be transferred into and out of nanotubes is lacking. Some studies have even shown that bulk collections of nanotubes can behave as thermal insulators due to the interface resistance between nanotubes, despite their high intrinsic thermal conductivity [3]. This project seeks to create a comprehensive understanding of the interfacial thermal conductivity and the mechanisms that drive it by careful measurements of the interfacial resistance in a variety of relevant environments. This includes measuring the thermal contact resistance of nanotubes to variety of materials, but also measuring the dependence upon temperature and electronic state of the nanotubes.

The project makes use of a novel thermal imaging technique developed to make use of and to be compatible with transmission electron microscopy (TEM), that we call electron thermal microscopy (EThM) [4]. The technique makes use of a thermal indicator material to generate a temperature-dependent contrast in TEM images. The embodiment currently employed uses nanoscale islands of indium metal (T_{MP} = 156.6° C). When the indium melts, this generates a contrast in dark-field TEM imaging, and this contrast can be used to build thermal maps of test platforms carrying carbon nanotubes or other nanostructures. This technique has been used to measure the thermal contact resistance of a nanotube sitting on a silicon nitride substrate (very high, > 200 K·m/W) or beneath a palladium metal contact (much lower, $4.2^{+5.6}_{-2.1}$ K·m/W) [5]. The lower contact resistance from the palladium metal contact can be easily understood from the increased contact area between the nanotube and a conformal palladium layer on top of it. However, the contact resistance between the nanotube and the substrate is very high, and it is at odds with other published values in the literature[6,7]. It is the goal of this project to understand this discrepancy and to develop a foundational understanding of the science of interfacial thermal resistance in carbon nanotubes.

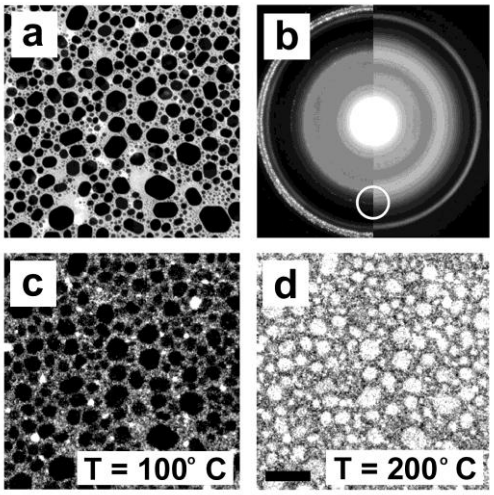

Figure 1. Demonstration of the principle of electron thermal microscopy. a) bright-field image of indium islands. b) a composite diffraction part of solid (left) and molten (right) islands. With the objective aperture at the circle, images c) and d) are produced in the solid and molten phases, respectively.

Recent Progress

Remote Joule Heating. From the knowledge gained about the contact resistance for a nanotube on a substrate vs. that with a metal contact, it is readily expected that the effects of heating should first make themselves detectable near the electrical contacts, even in the case of uniform power dissipation throughout the length of the nanotube. However, thermal imaging experiments on current-carrying nanotubes show that the heat is readily transferred to the substrate underneath the nanotube and diffuses out from that region, as shown in Figure 2.

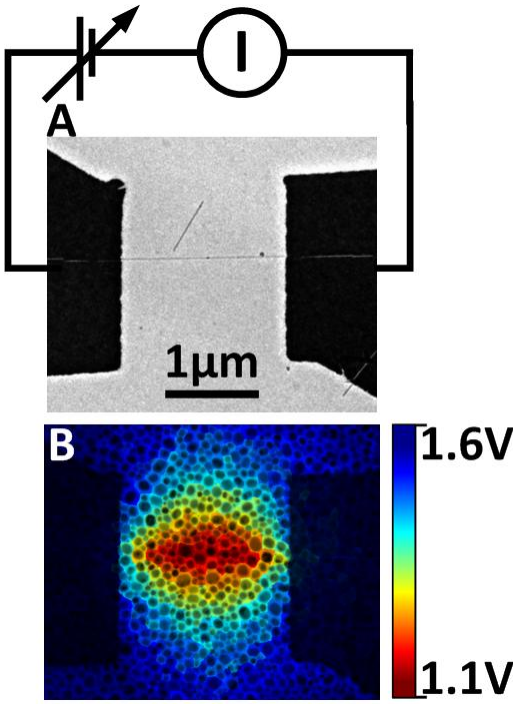

Figure 2. Thermal dissipation about a current-carrying nanotube. (A) measurement schematic and TEM image of the nanotube and contacts, prior to indium deposition. (B) (original in color) Thermal map of the platform where color indicates the melting voltage of each indium island, overlaid with a black and white image of the indium islands.

This effect can be attributed either to near-field radiation from the nanotube to the substrate (via a very high temperature of the nanotube while carrying a current) [8] or to a remote Joule heating effect where the charge carriers of the nanotube (electrons) scatter directly off the phonons of the substrate, thus transferring their power directly [9]. Separate results (not shown) indicate clearly that the nanotube remains cold while carrying the current, which is a surprising effect, given that the nanotubes are able to effectively heat the substrate significantly at the same time. This confirms the remote Joule heating effect and suggests the possibility that this effect could be used for thermal engineering of other dissipative nanostructures, such as transistors in computer processors. These results have been published in *Nature Nanotechnology* [S1] and have generated significant interest from thermal management and semiconductor electronics communities.

Nanotube Crossings. More recently, we have successfully repeated the above experiments on current-carrying channels composed of exactly two carbon nanotubes, electrically contacting one another. The results of these more recent experiments show that both nanotubes can dissipate power, with the contact itself showing no specifically notable role as, for example, a source of extra resistance. Furthermore, we see no appreciable sign of dissipation into the substrate from nanotube segments that carry no current, further indicating that indeed remote Joule heating is the dominant mechanism for transfer of heat to the substrate, with traditional conduction playing only at most a negligible role in the thermal transport. A collaboration has been initiated with S.V. Rotkin from Lehigh University, who has initially proposed and perfected the theories of remote joule heating, to optimize the model for our specific results and to

extract specifically meaningful parameters for our nanotubes and experimental measurement platforms.

Future Plans

Thermal Biasing. One of the key limitations of our measurement approach is that the thermal indicators (melting indium islands) show no response until 156.6° C. Due to this limitation, we typically cannot obtain any information from our measurements until the dissipated power reaches the level of 50-100 μW, from the nanotube itself. Currently, We are seeking to remove this limitation by thermally biasing the platform to within just a few degrees of the melting point. This would allow to image the heat dissipation at much lower applied voltage bias and power dissipation from the nanotube itself. In this regime, the remote Joule heating effect is expected to be suppressed according to the theories, and we should see a crossover to ordinary thermal conduction, where the heating would be expected to appear first at the metal contacts. We are currently in the design and testing phase for new measurement platforms that incorporate both the nanotube contacts and biasing heaters to enable this experimental approach

Boron Nitride Nanotubes. Boron nitride is a layered material, analogous to graphitic carbon, that can also form into a nanotube structure. Using high quality boron nitride nanotube samples have obtained from Dmitry Golberg at NIMS, in Japan, we will develop experiments to repeat many of the past experiments on these new materials. Predictions and some prior experiments (from other groups) show that BN nanotubes have a similar thermal conductivity to carbon nanotubes. However, any near-field effects (such as remote Joule heating) will be significantly modified due to the greatly different optical and electronic properties of BN compared to carbon. We will perform experiments to measure the contact resistance of BN nanotubes with the SiN substrates and also with contacting Pd metal contacts, both described previously for carbon nanotubes [5].

Affirmative Measurements of Substrate Contact Resistance. Past measurements using our platform of the thermal conductivity of the interface between nanotubes and our silicon nitride substrates has determined that this interface carries very low thermal conductivity. In fact, in all previous attempts, this thermal conductivity has been too low to measure, even using out platforms with low intrinsic thermal conductivity. It would be preferable to obtain a verifiable measurement of these thermal conductances, even if they are quite small, so as to probe how they might be affected by different materials and varying temperatures. We will design experiments to test this by removing the parasitic thermal conductivity through the SiN substrate that occurs in our past experimental geometries. This will be achieved by fabricating holes or slits in the SiN membrane that will eliminate this extraneous heat path. From there, experimental platforms will be fabricated that are much more sensitive to this contact resistance. Hopefully, in future experiments, we will be able to observe the ordinary thermal conduction between the nanotube and the SiN substrate, under conditions when the remote Joule heating effect is not playing a role. In this case, near-field thermal conduction, perhaps including plasmon resonances, may start to play a role [8,10].

References

[1] P. Kim, L. Shi, A. Majumdar, and P. L. McEuen, Thermal Transport Measurements of Individual Multiwalled Nanotubes, *Physical Review Letters*, 87, 215502 (2001).
[2] Motoo Fujii, Xing Zhang, Huaqing Xie, Hiroki Ago, Koji Takahashi, Tatsuya Ikuta, Hidekazu Abe, and Tetsuo Shimizu, Measuring the Thermal Conductivity of a Single Carbon Nanotube, *Physical Review Letters*, 95, 065502 (2005).
[3] Ravi S. Prasher, X. J. Hu, Y. Chalopin, Natalio Mingo, K. Lofgreen, S. Volz, F. Cleri, and Pawel Keblinski, Turning Carbon Nanotubes from Exceptional Heat Conductors into Insulators, *Physical Review Letters*, 102, 105901 (2009).
[4] Todd Brintlinger, Yi Qi, Kamal H. Baloch, D. Goldhaber-Gordon, and John Cumings, Electron Thermal Microscopy, *Nano Letters*, 8(2), 582 (2008).
[5] Kamal H. Baloch, Norvik Voskanian, and John Cumings, Controlling the thermal contact resistance of a carbon nanotube heat spreader, *Applied Physics Letters*, 97(6), 063105 (2010).
[6] Hareem Maune, Hsin-Ying Chiu, and Marc Bockrath, Thermal resistance of the nanoscale constrictions between carbon nanotubes and solid substrates, *Applied Physics Letters*, 89, 013109 (2006).
[7] Adam W. Tsen, Luke A. K. Donev, Huseyin Kurt, Lihong H. Herman, and Jiwoong Park, Imaging the electrical conductance of individual carbon nanotubes with photothermal current microscopy, *Nature Nanotechnology*, 4, 108 (2009).
[8] A. I. Volokitin and B. N. J. Persson, Near-Field Radiative Heat Transfer and Noncontact Friction, *Reviews of Modern Physics* 2007, 79, 1291-1311
[9] 17. S. V. Rotkin, V. Perebeinos, A. G. Petrov , and P. Avouris, An Essential Mechanism of Heat Dissipation in Carbon Nanotube Electronics, *Nano Letters* 9 (5) , 1850-1855 (2009)
[10] Andrei M. Nemilentsau and Slava V. Rotkin, Vertical Single-Wall Carbon Nanotube Forests as Plasmonic Heat Pipes, *ACS Nano*, 6, 4298-4304 (2012).

Publications of DOE sponsored research (2010-2012)

[S1] Kamal H. Baloch, Norvik Voskanian, Merijntje Bronsgeest, and John Cumings, Remote Joule heating by a carbon nanotube, *Nature Nanotechnology*, 7(5), p. 316 (2012).

Materials Applications of Aberration-Corrected Lorentz Microscopy

Marc DeGraef (PI) and Emma Humphrey (PhD student)
degraef@cmu.edu, ehumphre@andrew.cmu.edu
Department of Materials Science and Engineering,
Carnegie Mellon University, Pittsburgh, PA 15213

Program Scope

The increasing complexity of today's materials systems must be accompanied by improvements in the methods used to study those materials. In this project (DOE# DE-FG02-01ER45893), we develop and apply tomographic reconstruction methods to the three-dimensional study of magnetic field distributions around nano-scale magnetic samples. The program consists primarily of an experimental component, supported by a strong modeling component. The modeling component is used to validate experimental observations, by using numerical simulations and analytical evaluation of error propagation. The experimental component makes use of a series of carefully selected samples, used in a series of increasingly more advanced electron microscopes, and on a series of length scales. The program also further develops methods for the computation of magnetostatic interactions between nano-particles, based on the shape amplitude formalism (developed with prior DOE support). This theoretical work has produced more than twenty publications in peer-reviewed journals over the past decade.

The research is carried out by the P.I., Prof. Marc De Graef, and a graduate student, Emma Humphrey; Emma joined the group in 2008, and is currently working towards her Ph.D. degree. She has successfully presented her thesis overview in 2012 and is in the final year of her degree program. The work benefits from a strong collaboration with the group of Dr. Amanda Petford-Long at ANL.

Recent Progress

We have continued our theoretical work in the area of magnetostatic properties of and interactions between nano-scale objects. This approach relies on the use of the *shape amplitude*, i.e., the Fourier transform of the object's indicator or shape function (a discontinuous function equal to 1 inside and 0 outside the object). The following list itemizes some of the most important findings of our work (citations are listed at the end of this abstract):

- Exchange-coupled composite (ECC) particles are the basic constituents of ECC magnetic recording media. In collaboration with Marco Beleggia (Danish Technical University) and David Vokoun (Czech Academy of Science), we have employed the shape amplitude formalism to examine core-shell structures, consisting of a hard magnetic core and a coaxial soft magnetic shell, and conventional ECC particles with a hard magnetic core topped by a soft cylindrical element. Our results show that the switching field and the zero-field energy barrier are strongly dependent on the details of the particle geometry.
- With our colleagues at Argonne National Laboratory (ANL), we have successfully modeled the interactions between rectangular and stadium shaped thin elements that make up square spin-ice lattices. The magnetostatic interactions between the rectangular islands were computed and expressed in analytical form; for the stadia, we obtained an energy expression that only required a single numerical integration. We implemented these interaction energies in a Monte Carlo frame-work to study the demagnetization and switching behavior of these frustrated lattices.
- In collaboration with Marco Beleggia (Danish Technical University) we completed work on a theoretical and numerical technique to compute the mechanical stability and bending energy of a chain of uniformly magnetized particles of arbitrary shape. The approach can deal with chains of arbitrary length and may have applications in a variety of fields, e.g., magnetic colloids, magnetotactic bacteria, etc. Our approach makes use of the shape amplitude formalism when the chain components are close together, and the standard dipolar approach for spacings larger than a threshold distance.

- We are currently completing work on the use of the "image method" to compute magnetostatic forces between magnetic elements and semi-infinite objects. This approach is novel and makes use of the shape amplitude formalism to compute the interactions between a uniformly magnetized object of arbitrary shape and a nearby soft magnetic material with a arbitrary permeability. This work is currently being written up for submission to a peer-reviewed journal.
- We have started work in the area of electrostatic phase shift computations for the study of domain walls in ferroelectric materials. Our analysis has provided novel insights in the area of domain wall visibility that explain some uncertainties and conflicting statement in the literature. It turns out that the equivalent of a uniformly magnetized object (a uniformly polarized object) would have a huge electrostatic phase shift that has never been observed due to depolarization effects. Our new model accounts for all the relevant contributions and is currently being prepared for submission to a peer-reviewed journal.

In addition to the theoretical work summarized above, a significant portion of our work has focused on the application of tomographic reconstruction methods to the 3-D analysis of magnetic fields. We apply exit wave reconstruction methods and 3D scalar and vector field electron tomography algorithms developed during the previous portion of the program to determine the magnetic field distribution in and around magnetic materials at the nano-scale. Vector field electron tomography (VFET) extends the concept of conventional tomography to the reconstruction of vector objects (e.g., velocity field, magnetic induction or vector potential). The example to the right shows a schematic of a square Permalloy island with a closure domain state (blue magnetization arrows) and four magnetic domain walls (black lines) along with the corresponding magnetic vector potential (red arrows). Note that the vector potential is non-zero outside the particle, despite the fact that the magnetic induction (fringing field) mostly vanishes outside. A typical VFET experimental setup is shown in (b), illustrating the fact that two tilt series around perpendicular axes are needed. The input to the tomographic reconstruction consists of the magnetic phase shift for each sample tilt; this phase shift is obtained from a through-focus series of images, such as the series shown (c)-(e), acquired for the sample in the conventional orientation, and also a series with the sample flipped upside down (to eliminate the electrostatic phase shift).

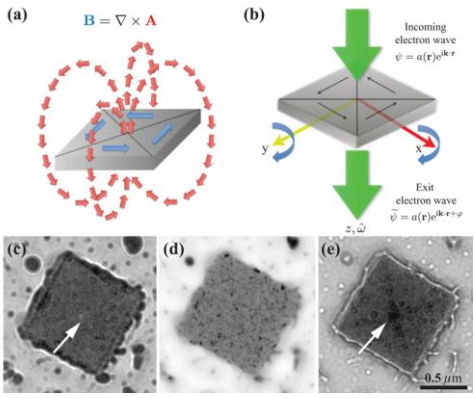

During Spring '12, Emma Humphrey spent time at the Argonne National Laboratory, working with Charudatta Phatak and Amanda Petford-Long, acquiring a number of experimental data sets for vector field electron tomography on ANL's aberration corrected Lorentz microscope. The data sets are currently being analyzed (image registration and phase reconstruction) and should produce 3-D reconstructions by the end of the Summer of 2012. Simultaneously, we have interacted with Prof. C. Bouman (Purdue University) to learn the fundamentals of model-based iterative reconstruction (MBIR). This technique, which is used primarily in the medical tomography community, has significant potential in the area of VFET as well, and we are evaluating its applicability and comparing the approach to the more standard Simultaneous Iterative Reconstruction Technique (SIRT). All algorithms currently under development will be applied to data sets of the following materials: patterned permalloy islands; patterned spin-ice lattices; and nano-twinned Ni_2MnGa alloy microstructures (the latter is a ferromagnetic shape memory alloy, used for magnetic actuation).

We have started to work on the magnetostatics of magnetically frustrated spin-ice lattices with a Kagome structure. We have derived analytical expressions for the magnetostatic interactions between thin circular disks; the interactions are expressed as integrals over Bessel functions of the first kind and exponentials, and lead to a compact expression of the total energy of an interacting Kagome spin-

ice lattice. The interaction energy for two disks at distance r, with magnetic moment m along the (unit) direction vector (indicated by a hat above the symbol) can be written as:

$$E(\boldsymbol{\rho}_{ji}) = \frac{\mu_0 \mu^2}{4\pi\rho^3}\left[\hat{\boldsymbol{\mu}}_i \cdot \hat{\boldsymbol{\mu}}_j \, \mathcal{F}_1(\frac{2R}{\rho},\tau) - (\hat{\boldsymbol{\mu}}_i \cdot \hat{\boldsymbol{\rho}}_{ji})(\hat{\boldsymbol{\mu}}_j \cdot \hat{\boldsymbol{\rho}}_{ji})\mathcal{F}_2(\frac{2R}{\rho},\tau)\right],$$

where the functions *F* are defined by the following integrals:

$$\mathcal{F}_1(\sigma,\tau) = \frac{8}{\tau^2\sigma^2}\int_0^\infty \frac{\mathrm{d}K}{K^3} J_1^2(K) J_1(\frac{2K}{\sigma})[2K\tau - 1 + e^{-2K\tau}];$$

$$\mathcal{F}_2(\sigma,\tau) = \frac{16}{\tau^2\sigma^3}\int_0^\infty \frac{\mathrm{d}K}{K^2} J_1^2(K) J_2(\frac{2K}{\sigma})[2K\tau - 1 + e^{-2K\tau}].$$

The dimensionless variables are defined as s=2R/ r, and t=t/2R, with R the disk radius and t the thickness. These integrals represent no numerical problems. In addition, we have derived the elements of the magnetic torque vector as a function of the disk shape parameters and the relative position and magnetization direction of pairs of disks. The *z* component of the torque vector (the only non-zero component) is given by:

$$T_z(\rho,\phi;\sigma,\tau) = \frac{\mu_0\mu^2}{4\pi\rho^3}\left[\mathcal{F}_1(\sigma,\tau)\sin(\theta_j-\theta_i) + \right.$$
$$\left. \mathcal{F}_2(\sigma,\tau)[\cos^2\phi\sin\theta_i\cos\theta_j - \sin^2\phi\cos\theta_i\sin\theta_j - \cos\phi\sin\phi\cos(\theta_i+\theta_j)]\right],$$

where r and f are polar coordinates of the relative position of two disks and the angles q_i represent the magnetization directions.

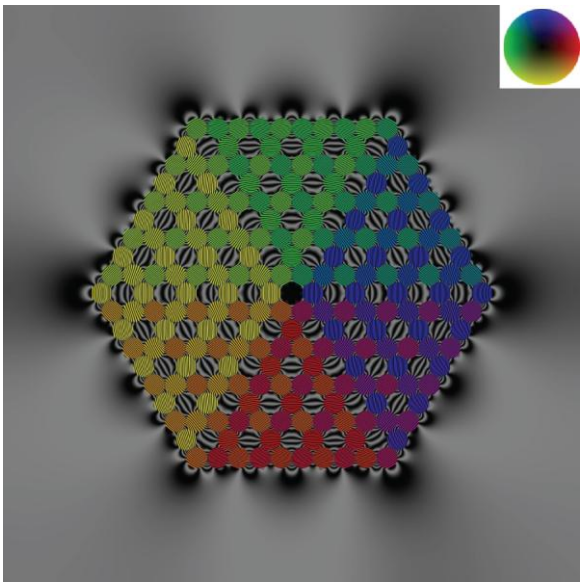

Both sets of expressions have been implemented in a Monte Carlo framework, and we have considered the special cases of three, six, and twelve disks as well as large arrays of disks; one result is shown to the right, representing a low energy state of the lattice. The color indicates the local direction of the magnetization, whereas the contours represent the cosine of the magnetic phase shift (Lorentz phase shift). We are currently in the process, in collaboration with researchers at ANL, of recording Lorentz phase maps for these structures so that we can compare them with the simulated results. In addition, micromagnetic simulations are underway to verify the extent to which the uniform magnetization state represents a good approximation of reality.

Finally, we are also in the process of analyzing how one can quantify "magnetic resolution." While spatial resolution can be defined in terms of electron optical lens parameters, it is not so easy to derive an equivalent resolution for Lorentz observations, in particular when aberration correction is used. The relatively small deflection angles imply that one does not even begin to approach the zero-crossings of the phase contrast function, so a different approach must be used. We are currently analyzing whether or not magnetic resolution needs to incorporate the properties of the sample itself; our work so far indicates that it does not appear to be possible to define magnetic resolution in terms of microscope parameters alone. A magnetic phase gradient (which depends on the sample) will need to be taken into account.

Future Plans

During the calendar year 2013, the PI will spend part of his time at the Ohio State University (sabbatical). During that time, several visits to ANL will be carried out, to acquire tomographic data sets as well as work with Dr. Petford-Long's group on the modeling side. To compare the tomographic reconstruction process for different microscopes, we will also carry out VFET observations on the same samples using our own Titan 80-300 corrected microscope; this data will be acquired during the second half of 2012.

We will continue our work on the implementation of a standardized file format for the archival storage of tomographic data. This file format, which has been partially designed with AFOSR support, consists of a series of high-level routines (in C++ and IDL) written on top of the public domain Hierarchical Data Format 5 (HDF5), created at and supported by the University of Illinois. We will work towards making this file format a new standard in the electron microscopy community, in particular for the long-term archival storage of tomographic data. A Fortran-90 version is currently being prepared for release to the microscopy community.

While GPU implementation of the tomographic reconstruction algorithms was put on hold in favor of searching for better algorithms (which we now believe we have found in the form of model-based iterative reconstructions), we plan to resume the process of implementing our algorithms in a GPU frame-work. We currently have a 2-GPU system available to us, and the graduate student working on the project will take a training course to learn how to write efficient programs for this hardware. All algorithms created under this program will be made available to the microscopy community and to the DOE user facilities.

Finally, we will expand our exploration of iterative reconstruction methods, combined with a new phase reconstruction approach that directly produces the magnetic phase shift, without the need to explicitly subtract the electrostatic component. We anticipate that the iterative approach, which starts from the filtered back-projection reconstruction, will allow for a much more accurate reconstruction of the magnetic vector potential and/or the magnetic induction in the presence of a missing wedge.

The personnel currently working on the project consists of the PI, Prof. Marc De Graef, and a graduate student, Emma Humphrey. Emma has the necessary background to be successful at executing the research plan, and is closely monitored by the PI. Dr. Amanda Petford-Long from the Argonne National Laboratory will be a member of the thesis overview committee, thereby guaranteeing a close collaboration and knowledge transfer between the PI's group and ANL.

DOE Sponsored Publications in 2010-2012

- A. Budruk, C. Phatak, A.K. Petford-Long, and M. De Graef, “Domain observations in Fe-Pd-Co by dynamic in-situ Lorentz TEM,” Microscopy and MicroAnalysis, vol. 16, pp. 1236CD, 2010.
- C. Phatak, A.K. Petford-Long, and M. De Graef, “Three-dimensional study of the vector potential of magnetic structures,” Phys. Rev. Lett., vol. 104, 253901, 2010.
- N.T. Nuhfer, A. Budruk, and M. De Graef, “Aberration-corrected Lorentz microscopy,” Microscopy and MicroAnalysis, vol. 16, pp. 142CD, 2010.
- D. Vokoun, M. Beleggia, M. De Graef, H.C. Hou, and C.H. Lai, “The influence of magnetostatic interactions in exchange-coupled composite particles,” J. Phys. D, vol. 43, pp. 275001, 2010.
- C. Phatak, A.K. Petford-Long, M. Tanase, O. Heinonen, M. Pan, and M. De Graef, “Nanoscale structure of the magnetic induction at monopole defects in artificial spin-ice lattices,” Phys. Rev. B, vol. 83, pp. 174431, 2011.
- C. Phatak, R. Pokharel, M. Beleggia, and M. De Graef, “On the magnetostatics of chains of magnetic nanopar- ticles,” J. Magn. Magn. Mat., vol. 323, pp. 2912–2922, 2011.
- C. Phatak, M. Pan, A.K. Petford-Long, S. Hong and M. De Graef, “Magnetic interactions and reversal of artificial square spin ices,” New Journal of Physics, in press (2012).
- C. Phatak, A.K. Petford-Long, M. Beleggia, and M. De Graef, “Theoretical study of ferroelectric domain wall images using phase reconstructed electron microscopy,” Ultramicroscopy, 2012 (in preparation).

In-Situ TEM Observations of Degradation Mechanisms in Next-Generation High-Energy Density Lithium-Ion Battery Systems

Shen J. Dillon, sdillon@illinois.edu

Department of Materials Science and Engineering, University of Illinois Urbana-Champaign, 1304 West Green Street, Urbana, IL

Program Scope

This project seeks to characterize nanoscale processes associated with the degradation of next-generation high energy density lithium-ion battery electrodes via in-situ transmission electron microscopy. Dynamic processes active in the electrodes, electrolyte, and intervening interfaces, which are chemical, electrical, and mechanical in nature, have been correlated with capacity fade in lithium ion batteries. However, without direct in-situ observation of these degradation mechanisms, with high spatial and temporal resolution, it remains difficult to understand and predict how these processes initiate, propagate, and interact. This work seeks to develop a fundamental understanding of degradation mechanisms in representative environmental conditions using commercial electrolytes and electrode designs that mimic commercial electrodes. The research will also develop the experimental techniques necessary for investigating electrochemical systems by in-situ transmission electron microscopy and will provide a framework for distinguishing and limiting electron beam effects that could potentially influence experimental results.

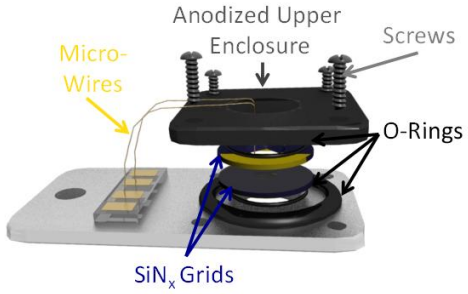

Fig. 1 Schematic of the in-situ electro-chemical cell

Recent Progress

In-situ Cycling of High-Strain Electrodes in Liquid Electrolyte

Fig. 1 provides a schematic of the environmental cell utilized for the experiments. Preliminary results demonstrate in-situ cycling of a Sn electrode against a Li counter electrode in ethylene carbonate dimethyl carbonate-1M $LiPF_6$ electrolyte in an enclosed environmental cell. Sn anodes display large volumetric strain during lithiation and delithiation. How the microstructure

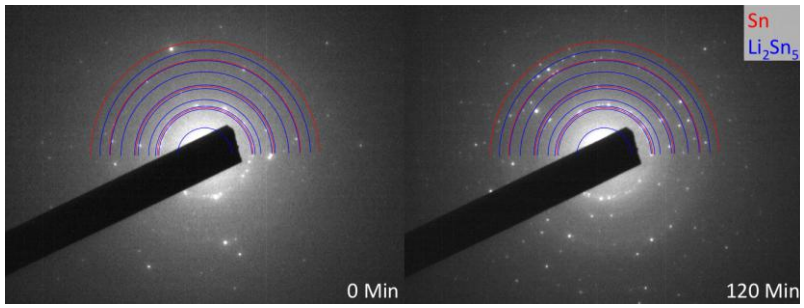

Fig. 2: Time-lapse diffraction patterns of Sn lithiation showing the formation of Li_2Sn_5.

accommodates cyclic volumetric strains in excess of 200% remains unclear. However, these processes likely affect cycle life and the practical function of the electrode. Fig. 2 present time-lapse electron diffraction data for a Sn thin film electrode during lithiation, where the formation of Li_2Sn_5 is clearly observed. The time-lapse image sequence in Fig. 3 captures the delithiation process. A non-uniform morphological evolution within individual grains during de-alloying indicates that the process must be accommodated by significant Sn diffusion. Similar features are observed after ex-situ cycling of micron scale Sn particles. The process has a morphological analogue in chemical dealloying processes in alloys with high surface diffusivity, such as Au-Ag. However, the dealloying of compounds and solid solutions should develop by different mechanisms. This may account for what appears to be crystallographic preference in the direction of void growth. We are currently investigating this phenomena and developing a model that discribes the process.

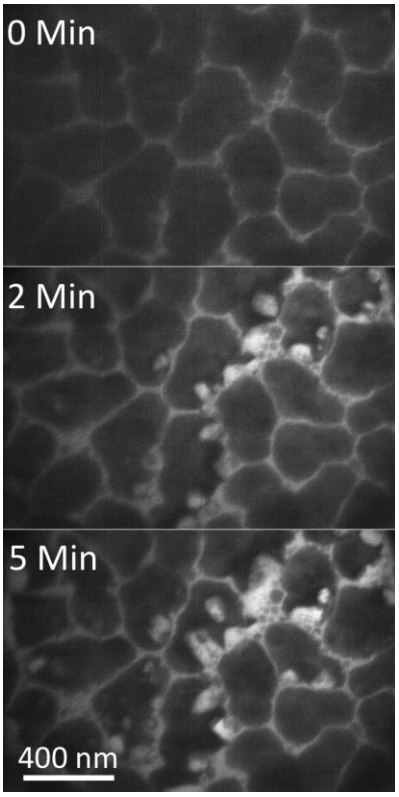

Fig. 3: Time-lapse images of a Li containing Sn electrode during delithiation.

Electron Beam Induced Effects in Liquid Systems

While a number of investigators have reported results of in-situ TEM studies in liquid environments, limited understanding of electron beam interactions with such systems exist in the literature. Beam induced effects in chemical environments differ dramatically from those in vacuum. We performed three sets of experiments which demonstrate that (i) secondary electron-hole pairs generated at the environmental cell window contribute significantly to beam induced chemical reactions due to their large absorption cross-sections, (ii) the reaction rate is sensitive to beam current density and solution composition, and (iii) the chemical potential of the solution also radically impacts beam induced effects. These experiments indicate that the beam may impact the evolution of environmental systems dramatically, and that the interactions must be understood in detail to enable appropriate interpretation of our in-situ experiments.

We demonstrated that secondary electron-hole pairs originating at the cell window dominate beam induced chemical effects in liquid environments by characterizing the beam-induced reduction of $SiCl_4$ liquid. Due to the high rate of secondary electron absorption by the solution and the irreversibility of the reaction, this system serves as a reasonable proxy for the rate of absorption by inorganic electrolyte, and enables the reaction rate to be quantified simply. Amorphous silicon is deposited from the $SiCl_4$ liquid and the volume of the deposited features may be measured by ex-situ AFM. This allows the number of electrons absorbed by the solution to be quantified. The results are detailed in Ref. 1. Calculations based on these data suggest that ~10^3-10^4 molecules/μm^2s should be ionized by secondary electrons under standard imaging

conditions. The results suggest that best practice for imaging in-situ battery cycling utilizes intermittent imaging coupled with beam blanking (e.g. Fig.'s 2 & 3).

We developed the first quantitative model describing electron beam induced reaction rates between solids and liquid solvents (Ref 2). Aqueous Ag-Ag_2SO_4 served as a model experimental system for developing trends in beam effects with respect to beam current density and solution composition. Silver in the system could grow, dissolve, or be relatively stable under different conditions of beam current density and solution composition. Two distinct regimes of kinetic response exist; a reaction rate limited regime and a diffusion-limited regime. A model for each regime was described based on a simple oxidation-reduction reaction mechanism and a chemical kinetics model. Ref 2 describes the results in detail.

We have also characterized beam induced reactions in the more complex $Zn(NO_3)_2$-HMTA aqueous system. This system produces a ZnO product phase during electron irradiation in a specific range of chemical potential (Fig. 4). By maintaining a constant $Zn(NO_3)_2$ composition and varying the HMTA composition, the nucleation and growth of ZnO may be tuned. The results indicate that chemical activity not concentration is the dominant factor in affecting beam-induced reactions in aqueous solution. This system also exhibited an incubation time for nucleation that was consistent with an activation barrier. The results produce trends that are qualitatively consistent with traditional chemical reactions, but results primarily from the presence of the electron beam. The results indicate that the interpretation of chemical reactions and interactions within the microscope must be carefully analyzed if claims are to be made about the intrinsic behavior of a chemical system.

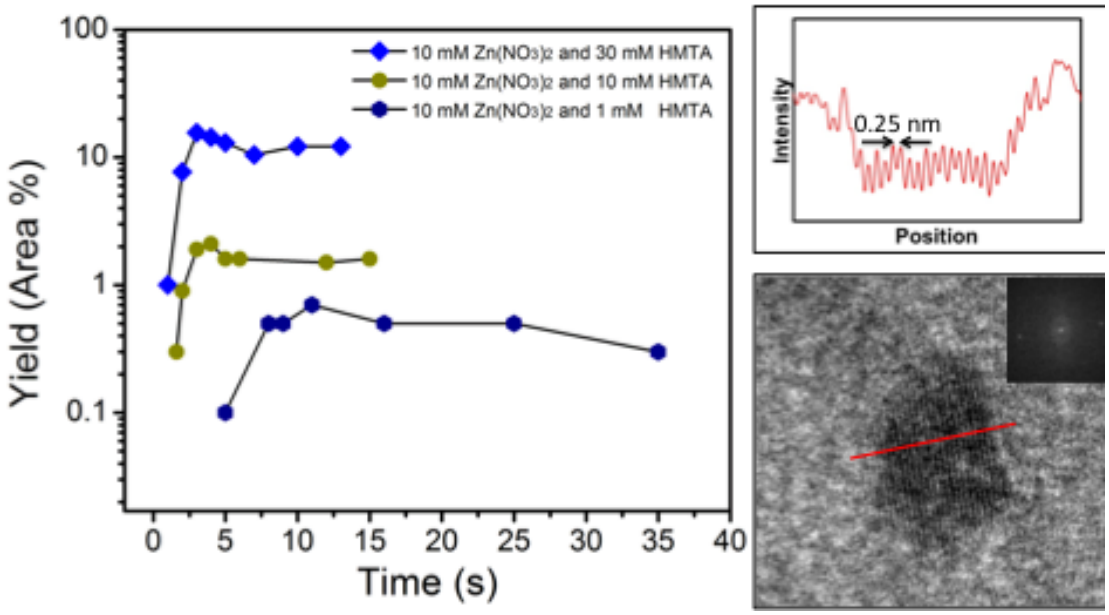

Fig. 4: Growth kinetics of beam induced ZnO precipitation from solutions of different composition and an associated HRTEM image take during in-situ nucleation and growth. Note that no growth was observed for 10 mM $Zn(NO_3)_2$ solutions containing no HMTA.

Future Plans

During the first year of the project, we demonstrated in-situ cycling of Sn anodes

(Fig. 2 & 3) known to exhibit high strain and rapid capacity fade. With subsequent cycling, these same electrodes partially amorphize and recrystallize during lithiation and delithiation. These processes will be characterized in more detail and interpreted in the context of appropriate thermodynamic and kinetic models. We also intend to extend these studies to high-capacity cathode materials under consideration for next-generation lithium ion batteries.

Preliminary work has also focused on the development and testing of all solid-state thin film batteries. These will also be tested in-situ to achieve high-resolution imaging and spectroscopy during cycling.

References to Publications from our DOE-sponsored Research

1. Liu, Y., X. Chen2, K.W. Noh, and S.J. Dillon, *"Electron beam induced deposition of silicon nanostructures from a liquid phase precursor," Nanotechnology*, **In press**.
2. Noh, K.W., Y. Liu, L. Sun, and S.J. Dillon, "Challenges associated with in-situ TEM in environmental systems: The case of silver in aqueous solutions," *Ultramicroscopy*, 2012. **116**: p. 34-8.
3. Dillon, S.J. and K. Sun, "Microstructural design considerations for Li-ion battery systems," *Current Opinion in Solid State and Materials Science*, 2012. **16**: p. 153-62.

Abstract for DOE Electron & Scanning Probe Microscopy PI Meeting

Title : Quantum Control of Spins in Diamond for Nanoscale Magnetic Sensing and Imaging

PI: Gurudev Dutt

Address: Department of Physics & Astronomy
University of Pittsburgh
3941 O'Hara Street
Pittsburgh, PA 15260

E-mail: gdutt@pitt.edu

Research Scope:

The goal of this research is to develop a magnetic field imaging technique with nanoscale resolution that would allow for non-invasive, non-destructive probing of a variety of important physical phenomena such as quantum tunneling in single molecule magnets and quantum bits encoded into spins in quantum dots. Diamond single spin magnetic sensors are a highly promising material platform featuring high magnetic field sensitivity, nanometer spatial resolution and the important ability to operate under ambient or harsh environmental conditions required to study many material systems. The proposed work will take a multi-faceted approach toward improving the accuracy, sensitivity and robustness of this platform through a unique combination of fundamental investigations into quantum control and precision quantum metrology coupled tightly to innovative design, sophisticated nano-fabrication and advanced measurement techniques.

Recent Progress:

The error in magnetic field precision measurements is commonly improved by noise averaging the signal through increased measurement time. However, the best precision typically requires restricting the dynamic range (maximum possible field strength B_{max}) to be much less than the sensor's spectral linewidth; or else a trade-off with the precision occurs, necessitated by increasing the measurement bandwidth and thus reducing the signal to noise ratio. Quantum effects such as entanglement and squeezing usually improve the precision only in the first scenario, and they are difficult to achieve in practice, especially in solid-state environments. We have recently implemented novel phase estimation algorithms (PEAs) on a single electronic spin associated with the nitrogen-vacancy (NV) defect center in diamond to achieve ~ 10x improvement compared to standard measurements, over a field sensing range ~ +/- 0.3 mT that is large (~ 100x) compared to the spectral linewidth. The field uncertainty in our approach now scales as $1/T^{0.88}$, in contrast to the standard measurement scaling of $1/T^{0.5}$. Besides their direct impact on magnetic sensing and imaging at the nanoscale, these results open the way for quantum control and feedback techniques to be applied to sensitive magnetometry applications. This work was published in Nature Nanotechnology [2].

Fig 1 illustrates the principle behind standard imaging and sensing approaches for DC magnetic fields such as e.g. frequency modulation spectroscopy (CW) or Ramsey techniques (pulsed). Due to the resonant response of the sensor, *only a single contour of constant magnetic field* is mapped out per each 2D scan over an unknown sample. This means that to fully reconstruct the spin density in real samples, one must take many scans at different heights from the sample, thereby greatly reducing the data acquisition rate. We emphasize that this is a fundamental problem, because the measurement bandwidth $\Delta\upsilon$ must be kept small to obtain the best resolution $\Delta x = \Delta\upsilon\,(d\upsilon/dx)^{-1}$; but this automatically reduces the acquisition rate and leads to loss of information from the scan.

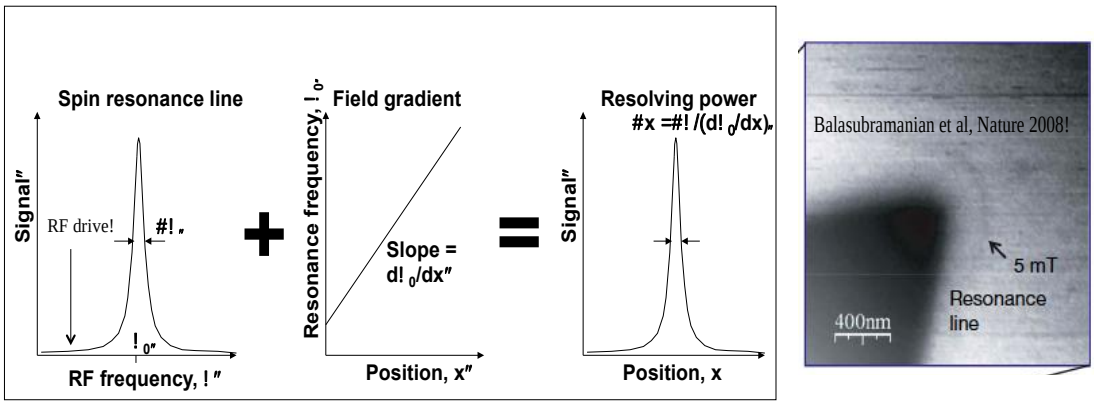

Figure 1: a) Principle of DC magnetic field imaging. The RF drive is kept detuned from the resonance, and whenever the field in the sample matches the difference between the two, we get a signal. (b) Image of resonance slice, obtained using a diamond nanocrystal tip, from a magnetic nanostructure. Taken from Ref. [1].

This limitation is common to many forms of precision spectroscopy, e.g. frequency-modulated AFM; however in magnetic imaging with defect spins in diamond, this limitation may be particularly problematic. Because the sensing element in such a system is an atomic-scale defect, the location of this defect must be controlled very carefully if one is to achieve nanometer resolution. For instance, suppose we know that we have two electron spins in the sample located 5 nm below the diamond tip, and spaced 5 nm apart. Since only a single contour of pre-set field strength can be imaged in one scan, then the location of the NV center in the tip must be known with a precision better than 0.5 nm, as seen by a straightforward calculation, otherwise the two spins will not even be detected. The precision needed on the NV center position will become greater as we increase the sensitivity, not lower. Thus we have now introduced a new problem of controlling the NV center position with angstrom-scale precision.

By contrast, our method provides a full-field readout, with a linear response to the magnetic field, over a wide dynamic range, while maintaining the high sensitivity of the traditional techniques. We proposed and implemented a method borrowed from quantum information science,

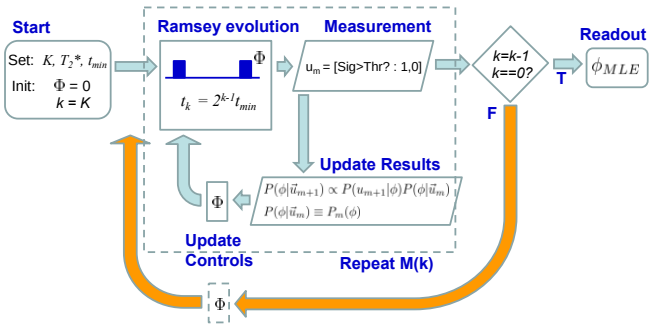

Figure 2: Flowchart for phase estimation algorithm (PEA).

i.e. phase estimation algorithms. The algorithm we used is illustrated in Figure 2. With our method, it should be possible now to obtain directly a "density plot" of the magnetic field values over the scan region, while maintaining the resolution afforded by the standard approach. The results from our experiments are summarized in Figure 3.

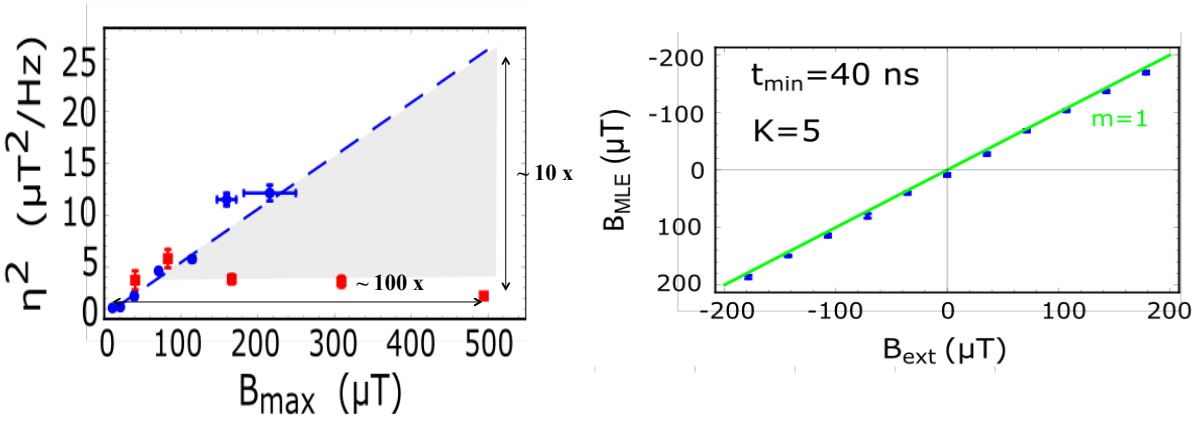

Figure 3: (a) Comparison of sensitivity and dynamic range between our technique (red squares) and standard measurement techniques (blue dots). For more details, see Ref. [2]. (b) Demonstration of the excellent linearity of our technique (blue dots) over a wide dynamic range. The green line is not a fit, but the expected theoretical readout of a perfect sensor.

Future Plans:

We will also explore the other quantum control techniques outlined in our proposal, such as controlling nuclear spin for magnetometry, and pursue various questions raised by our new results on quantum phase estimation algorithms. In particular, the most sensitive magnetometry techniques involve driving the spins in the samples to be imaged using various protocols (AC magnetometry), and the same issues of sensitivity and dynamic range can be expected to play an important role. Thus, we are exploring improvement to AC magnetometry using our current phase estimation algorithms as well as others.

References:

[1] G. Balasubramanian, I. Y. Chan, R. Kolesov, et al., Nanoscale imaging magnetometry with diamond spins under ambient conditions. *Nature*, **455**, 648 (2008).
[2] N. M. Nusran, M. Ummal Momeen, M. V. Gurudev Dutt, High-dynamic-range magnetometry with a single electronic spin in diamond, *Nature Nanotechnology* **7**, 109–113 (2012). *The work reported in this publication was carried out with support from the DOE.*

Electronic States and Transport in Semiconductor Nanostructures

Rachel S. Goldman[1] and Harley T. Johnson[2]
[1]Department of MSE, University of Michigan, Ann Arbor, MI 48109; rsgold@umich.edu
[2]Department of MechSE, University of Illinois, Urbana, IL 61801; htj@uiuc.edu

Program Scope

The understanding of electronic states and transport through dimensionally-confined semiconductor structures is a classic problem in materials physics. Advances in experimental probes and computational methods have led to several important breakthroughs including lattices of quantum dots (QDs) and accurate electronic structure models for nanostructures. Yet, a number of critical fundamental questions regarding the effects of QD size, spacing, and arrangements on the electronic states and transport through semiconductor nanocomposites remain unanswered. For example, how many atoms are needed in a QD for it to cross over from behaving as an impurity state to a band of states? How do point defects and dopants (magnetic and non-magnetic) influence the band structure, the positions of confined states, and transport through ensembles of QDs? How do interface disorder and strain affect the QD electronic states and transport through QD nanocomposites? The program combines leading edge experimental and computational methods to answer these questions and develop a set of design rules for predicting the electronic states and transport in semiconductor nanocomposites.

This program seeks to understand electronic states and transport in dimensionally-confined semiconductor structures. Specifically, the effects of nanostructure size, spacing, and arrangement; strain and interface disorder; and the presence of point defects and dopants on the electronic band structure, confined states, and transport will be investigated using a novel combination of state-of-the-art experiments and theory. Using the probe tip of a scanning tunneling microscope, electronic spectroscopy measurements with nanoscale spatial resolution are performed on precisely fabricated QD nanocomposites. The imaging and spectroscopy measurements are performed over a wide temperature range, thereby facilitating measurements of the influence of magnetic dopants on nanostructure confined states and the probing of transport properties over a wide range of electron-phonon scattering conditions. Simultaneously, electronic structure based calculations of confined states and electron transport will be performed using experimentally-determined QD morphologies. Comparisons between experimental and computational studies will reveal both the origins of the electronic states and transport properties in semiconductor nanostructures, as well as the validity of the physical assumptions underlying the experimental and computational techniques.

Recent Progress and Future Plans

In addition to the development of instrumentation and analysis methods, we are developing new understanding of electronic states in several QD systems, including InAs:Mn, GaSb/GaAs, InAs/GaAs, and GaN/GaAs. Each of these are described below.

Influence of Dopants on QDs

We have investigated the influence of Mn dopants on the electronic states in the vicinity of InAs/GaAs quantum dots QDs and the surrounding GaAs matrix. A

comparison of cross-sectional scanning tunneling microscopy, scanning tunneling spectroscopy, and tight binding calculations of the local density of states reveals that the Mn dopants primarily influence the electronic states at the QD edges and the surrounding GaAs matrix. These results suggest that the Mn dopants reside at the QD edge, consistent with the predictions of a thermodynamic model for the nanoscale-size dependence of dopant incorporation in nanostructures [Dasika, 2011].

We have further examined the surfactant nature of p-type dopants in InAs/GaAs QDs, via a comparison of the height and width distributions of undoped, Be-doped, and Mn-doped InAs QDs. As shown in Fig. 1, comparison of undoped InAs QDs, InAs:Be QDs, and InAs:Mn QDs have shown the most probable QD height and width being smallest for InAs:Be QDs. Specifically, the most probable height and widths were 3.9 nm x 5.3 nm for InAs:Be QDs, 4.7 nm x 12.4 nm for InAs:Mn QDs, and 9.0 nm x 18.0 nm for undoped InAs QDs. The smaller (larger) sizes of the InAs:Be (Mn) QDs are likely due to a delayed (promoted) island transition, suggesting the surfactant (anti-surfactant) action of Be (Mn) during InAs/GaAs QD growth. The surfactant nature of the p-type dopants likely leads to smaller, lower density QDs. Further plan-view STM experiments on the effects of Mn and Be doping on the formation of InAs QDs are planned.

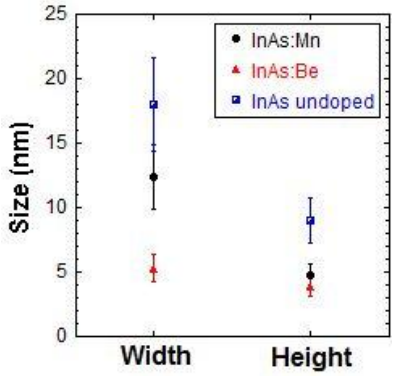

Fig. 1: Comparison of widths and heights of Mn-doped, Be-doped, and undoped InAs QDs. These values are based upon an analysis of several high resolution images of the QDs.

Effective Mass and Tight-Binding Computations

In our modeling work, we studied complexity reduction in our tight-binding calculations and effects of heterogeneous composition on the confined electronic states. The moments of the electronic local density of states (LDOS) were collected within some radius of neighborhood of the target atom. According to theory, the variance of the LDOS estimate for a fixed number of moments M decreases with the number of neighborhood atoms J as $(JM)^{-1/2}$ and with the radius of neighborhood R, as $R^{-3/2}M^{-1/2}$. Figure 2 shows LDOS on a Ga atom calculated by collecting moments from

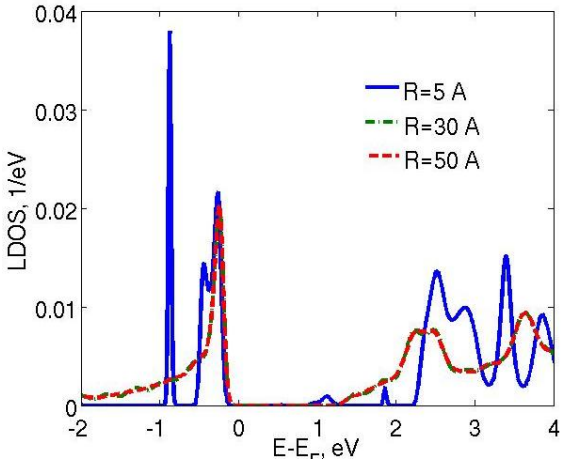

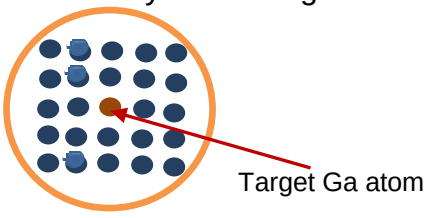

Fig. 2: LDOS on a Ga atom in GaAs as functions of $E-E_F$ computed using moment-based tight-binding method for different neighborhood radii used to collect the LDOS moments. The inset shows schematically the lattice and two different radii of neighborhood in which LDOS moments are collected.

neighborhoods of different radii. For homogeneous GaAs, it is sufficient to 'carve out' a neighborhood of 3-5 nm radius from a larger domain without the loss of precision in LDOS. Using this smaller neighborhood instead of a larger set of atoms allows significant reduction in the computation time, while the variance of LDOS estimate increases only by a few percent. Tight-binding calculations of LDOS were also carried out for InAs/GaAs to quantify the influence of the Ga cations in the matrix on the InAs QD electronic states. This should allow us better understand the influence of the matrix atoms on the localized states in QDs.

GaSb/GaAs QDs

Due to the predicted composition dependence of band offset type, As-Sb QDs have been identified as promising systems for light emitters (type I) and photovoltaics and photodetectors (type II). In the case of InGaSb QDs, a composition-dependent transition from type I to type II offsets has been reported. Although type II band offsets have been reported for GaSb/GaAs QDs, a variety of atomic structures ranging from clusters to rings to dots have been observed. Furthermore, type I band offsets have been reported for Sb clusters on GaAs. The precise growth conditions for tuning the GaSb/GaAs QD atomic structure and its influence on type I vs type II band offsets have not been reported. Therefore, we have investigated the influence of growth conditions on the nanoscale structure and band offsets of GaSb/GaAs QDs using a combination of variable temperature XSTM and STS. For GaSb/GaAs QD grown on both As- and Sb-terminated surfaces, mostly clusters and a few dots are observed. In addition, for GaSb/GaAs QD grown on Sb-terminated GaAs surfaces, rings are also apparent. STS in the vicinity of the clusters reveals type I offsets with ΔE_C and ΔE_V similar to that of Sb clusters on GaAs and of InAsSb/GaAs QDs, as shown in Figs. 3 and 4. Additional studies on the influence of doping concentration, QD growth mode, and the role of misfit dislocations on the QD size, shape, distribution, and band structure are in progress.

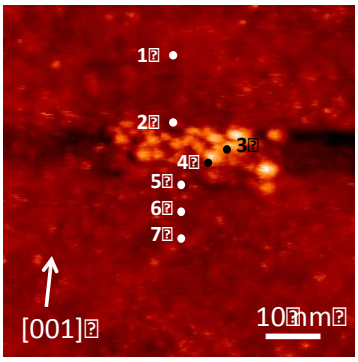

Fig. 3: XSTM image of GaSb/GaAs cluster. The numbered spots show positions of STS data in Fig. 4.

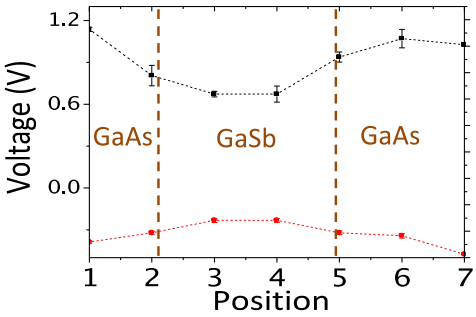

Fig. 4: Plot of effective conduction and valence band edges across the cluster in Fig. 3

InAs/GaAs and GaN/GaAs QDs by droplet epitaxy

Droplet epitaxy has emerged as a promising alternative method for fabrication of QDs. For this method, metallic surface droplets are formed in the absence of group V flux. Subsequent exposure to group V flux results in the conversion of the metal droplets to islands. It is expected that droplet epitaxy will result in a higher density of smaller QDs without wetting layers; very little is known about the confined states in such nanostructures. We are currently investigating the detailed interface structure and

electronic states in both the InAs/GaAs and GaN/GaAs QD systems, using a combination of plan-view STM, XSTM, and STS.

To date, we have investigated the influence of In exposure and substrate temperature on growth of InAs/GaAs QDs by droplet epitaxy. A set of conditions to produce > $3x10^{10}$ cm^{-2} QDs has been identified (Fig. 5). Furthermore, the apparent WL thickness varies with increasing In exposure, suggesting a critical exposure of ~3.5ML for minimal WL thickness. In addition, droplet epitaxy of GaN QDs has been achieved on p-type Si using MBE. Fig. 6 shows an AFM image of the GaN QDs grown on silicon. To enable examination the confined states in such QDs using XSTM/STS, droplet epitaxy of GaN QDs on heavily-doped Si and GaAs is planned. The influence of Bi and Sb surfactants for InAs/GaAs QD growth will also be investigated.

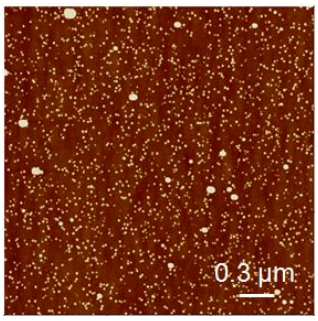

Fig. 5: AFM image of high density ($3x10^{10}$ cm^{-2}) InAs QDs grown by droplet epitaxy on GaAs.

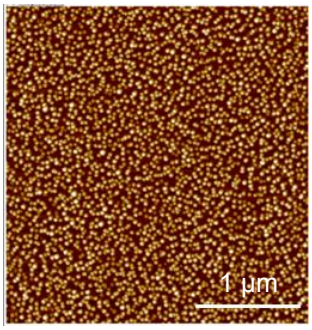

Fig. 6: AFM image of GaN QDs grown by droplet epitaxy on a (001) Si substrate.

Publications supported by the Grant: 2010-2012

[Dasika, 2011] V. D. Dasika, A. Semichaevsky, J.P. Petropoulos, A. M. Dangelewicz, J.C. Dibbern, M. Holub, P.K. Bhattacharya, J.M.O. Zide, H.T. Johnson, and R. S. Goldman, "Influence of Mn Dopants on InAs/GaAs Quantum Dot Electronic States," *Appl. Phys. Lett.* 98, 141907 (2011).

[Dasika, 2011b] V.D. Dasika and R.S. Goldman, "STM of Self Assembled III-V Nanostructures," Handbook of Instrumentation and Techniques for Semiconductor Nanostructure Characterization, Volume 2, Chapter 9. World Scientific Publishing Company (2011).

[Hossain, 2010] M. Z. Hossain, N. V. Medhekar, V. B. Shenoy, and H. T. Johnson, "Enhanced quantum confinement due to nonuniform composition in alloy quantum dots," *Nanotechnology* **21**, 095401 (2010).

[Huang, 2011] S. Huang, A.V. Semichaevsky, L. Webster, H.T. Johnson, R.S. Goldman, "Influence of wetting layers and quantum dot size distribution on intermediate band formation in InAs/GaAs superlattices," J. Appl. Phys. 11, 073105 (2011).

[Kumah, 2011] D.P. Kumah, J.H. Wu, N.S. Husseini, V.D. Dasika, R.S. Goldman, Y. Yacoby, and R. Clarke, "Resolving the interfacial and internal structure of self-assembled quantum dot systems", *Appl. Phys. Lett.,* 98, 021903 (2011).

[Semichaevsky, 2011] A. V. Semichaevsky, R. S. Goldman, and H. T. Johnson, "Linking computational and experimental studies of III-V quantum dots for optoelectronics and photovoltaics," JOM: Journal of the Minerals, Metals, and Materials Society, 63, 20-26 (2011).

[Zech, 2012] E.S. Zech, A.S. Chang, A.J. Martin, Y.H. Lin, J.M. Millunchick, and R.S. Goldman, "Influence of Quantum Dot Atomic Structure on GaSb/GaAs Band Offsets", in preparation (2012).

Resistive Switching Behavior in Ferrelectric Tunnel Junctions Studied at Nanoscale

Alexei Gruverman

Department of Physics and Astronomy, UNL, Lincoln, NE 68588-0111

Email: alexei_gruverman@unl.edu

Research Scope:

Most of the nanoscale studies of the tunneling electroresistance (TER) effect are based on electrical control of polarization using scanning probe microscopy (SPM). For experiments involving electrical poling by an SPM tip in ambient environment there is always a concern that electrically-induced changes in surface conditions, e.g. due to redox chemical reactions or charge deposition, may significantly affect resistive switching measurements. This has raised questions regarding whether this surface modification is in fact the primary mechanism for the reported resistive switching effect as opposed to the mechanism based on the polarization-related change in energy barrier between top and bottom electrodes. For example, redox reactions and associated band bending at the interfaces have been recently proposed as possible mechanisms for the TER in ultrathin ferroelectric films. In our research, we demonstrated that the nonvolatile TER effect in ultrathin (several nanometer-thick) ferroelectric films could be induced by purely mechanical means and showed that this effect could be realized without any involvement of surface electrochemical processes commonly expected in SPM poling of oxide films. Comparison between electrically and mechanically induced TER effects allows assessment of the surface charge influence on resistive switching.

A mechanically-induced TER effect is facilitated by the recently discovered flexoelectric switching of ferroelectric polarization [1] resulting from application of a local mechanical load to an ultrathin ferroelectric film via an SPM tip. It has been found, that the tip-generated strain gradient in the film can produce a flexoelectric field that is strong enough to switch polarization in a way similar to an external electric field. To explore the mechanically-induced TER effect, we have used epitaxial single-crystalline ultrathin (12-unitcell-thick, or ~4.8 nm) $BaTiO_3$ films grown by pulsed laser deposition on atomically smooth TiO_2-terminated (001)-$SrTiO_3$ substrate with $SrRuO_3$ as a bottom electrode.

Figures 1a and 1b show the PFM amplitude and phase images, respectively, of two downward-oriented domains written in as-grown film: the left domain has been written with an electrically biased tip (+3V) and a loading force of 20 nN (which is a typical value for the PFM operation mode), whereas the right domain has been produced by scanning the film surface with a grounded tip while applying a loading force of 1400 nN. After writing, PFM imaging of the resulting domain pattern has been carried out with the same tip at a contact loading force of 20 nN. Both domains exhibit a saturated PFM amplitude signal and 180º phase inversion, indicating a fully switched single domain state. Switchable polarization behavior is confirmed by the local PFM spectroscopic measurements (Fig 1c), which show rather symmetric piezoelectric hysteresis loops with a coercive voltage of ~2.0 V (or coercive field of ~4 MV/cm). Noteworthy features of the mechanically written domains are that they are stable and electrically erasable.

Additional analysis of the written domain pattern has been performed using electrostatic force microscopy (EFM) (Fig 1d). Note that EFM is sensitive to the presence of the surface charge and thus can be used to assess the difference between surface charge

density of electrically and mechanically produced domains. In the EFM imaging conditions used in our study, dark contrast of the written domains corresponds to a positive surface charge. This is opposite to the negative bound polarization charge of the domains suggesting that the signal detected by EFM is due to a surface charge that screens polarization of the downward-oriented domains. There is a clear disparity of the EFM signal between electrically written and mechanically written domains. Much darker contrast for the electrically produced domain indicates a higher screening charge density. This effect could be due to the field-induced redox reaction resulting in deposition of extra charge in addition to the adsorption of ionic species from ambient.

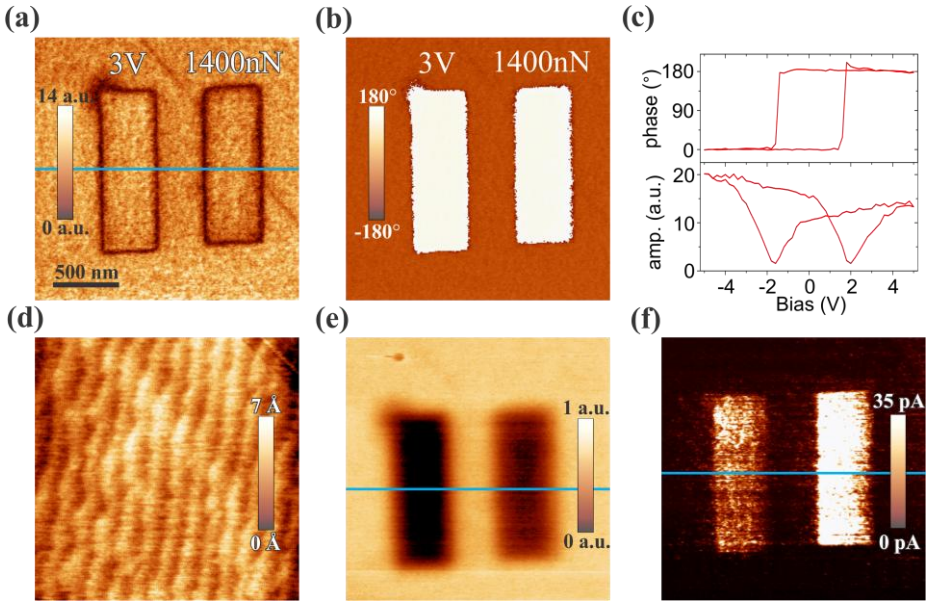

Figure 1. SPM data illustrating the mechanically and electrically induced TER effects. (a, b) PFM amplitude (a) and phase (b) images of the the 4.8-nm-thick $BaTiO_3$ film after generation of the downward-oriented domains by electrical poling (left) and mechanical loading force (right). (c) Local PFM hysteresis loops measured in the same $BaTiO_3$ film (top - phase signal, bottom - amplitude signal). (d) Topographic image of the same area acquired after mechanical writing showing that the film surface was not affected by the writing process. (e) EFM image taken at the same location as the PFM images. Regions of dark contrast represent downward oriented domains and correspond to a positive surface screening charge. (f) Tunneling current map acquired in the C-AFM mode with a dc read bias 0.3V at the same location as the PFM and EFM images. Bright contrast corresponds to higher conductivity. The scan size is the same for all SPM images.

The resistive switching behavior has been studied by simultaneous imaging of the electrically and mechanically written domains in the C-AFM mode. Figure 1e shows a tunneling current map where contrast variations correspond to changes in conductivity. It can be seen that both electrically and mechanically poled domains with downward polarization have higher conductivity in comparison to the as-grown $BaTiO_3$ film with upward polarization, which is indicative of the TER effect. It can be concluded that it is the change in the energy barrier height due to polarization reversal that lead to the electroresistance effect. Also, the fact that the TER effect can be induced by mechanical pressure without any electrical bias application indicates that the electrochemical surface modification as the main mechanism of resistive switching in ferroelectrics can be ruled out.

It is interesting that, while there is no discernible difference between the PFM images of electrically and mechanically written domains, the mechanically-induced TER is larger than the electrically-induced TER as is shown by local spectroscopic measurements (Fig 2): the resistance changes by 2300% for electrically poled domain versus 7300% resistance change for the mechanically written domain.

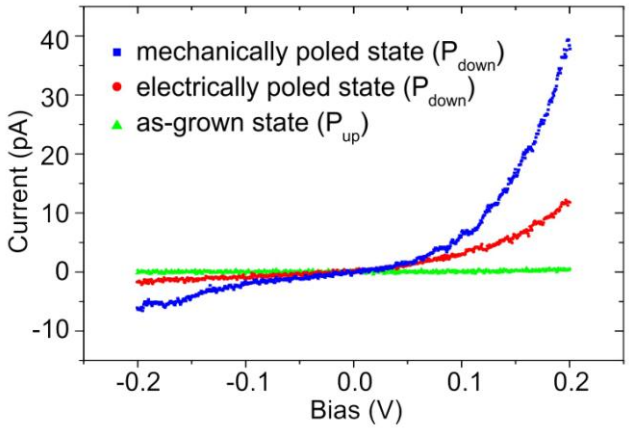

Figure 2. Comparative analysis of the mechanically and electrically induced TER effects. Local I-V curves measured for the as-grown film area with upward polarization (green), electrically downward-switched domain (red) and mechanically downward-switched domain (blue).

Future plans:

1. Investigate mechanically induced resistive switching in ferroelectric tunnel junctions in conjunction with theoretical simulations.

2. Explore a bi-stable behavior of oxygen vacancies in $LaAlO_3/SrRuO_3$ where our preliminary experimental studies show a bistable switching behavior. Correlate these results with the experimental studies.

3. Compute the associate change in the tunneling conductance across this system. Correlate theory with the experiment.

Papers:

1. H.Lu, C.W.Bark, D. Esque de los Ojos, J.Alcala, C.B.Eom, G.Catalan, and A.Gruverman, "Mechanical Writing of Polarization", Science **6,** 59-61 (2012).
2. H.Lu, X.Liu, J.D.Burton, Y.Wang, Y.Zhang, D.J.Kim, A.Stamm, P.Lukashev, C.W.Bark, D.A.Felker, C.M.Folkman, P.Gao, X.Q.Pan, M.S.Rzchowski, C.-B.Eom, E.Y.Tsymbal, and A.Gruverman, "Enhancement of Ferroelectric Polarization Stability by Interface Engineering", Adv. Mat. **24**, 1209-1216 (2012).
3. E.Y.Tsymbal, A.Gruverman, V.Garcia, M.Bibes and A.Barthélémy, "Ferroelectric and Multiferroic Tunnel Junctions", invited review in *MRS Bulletin* **37**, No 2, 138-143 (2012).
4. D. Pantel, H. Lu, S. Goetze, P. Werner, D. J. Kim, A. Gruverman, D. Hesse, and M. Alexe1, "Tunnel electroresistance in junctions with ultrathin ferroelectric Pb(Zr0.2Ti0.8)O3 barriers", Appl. Phys. Lett. (accepted, 2012).

5. H. Lu, T. A. George, Y. Wang, I.Ketsman, J. D. Burton, C.-W. Bark, S. Ruy, D. J. Kim, J. Wang, C. Binek, P. A. Dowben, A. Sokolov, C.-B. Eom, E. Y. Tsymbal, and A. Gruverman, "Electric Modulation of Magnetization at Ferroelectric - Ferromagnetic Interfaces", submitted to Appl. Phys. Lett. (2012).
6. A. Stamm, D. J. Kim, H. Lu, C.-W. Bark, C.-B. Eom, and A. Gruverman, "Polarization Relaxation Kinetics in Ultrathin Ferroelectric Capacitors", submitted to Appl. Phys. Lett. (2012).
7. H. Lu, D. J. Kim, C.-W. Bark, S. Ryu, C. B. Eom, E. Y. Tsymbal, and A. Gruverman "Mechanically-Induced Tunneling Electroresistance Effect in Ultrathin Ferroelectrics", to be submitted (2012).

Contributed conference papers:

1. X. Liu, H. Lu, J. D. Burton, Y. Wang, C. W. Bark, Y. Zhang, D. J. Kim, A. Stamm, P. Lukashev, D. A. Felker, C. M. Folkman, P. Gao, M. S. Rzchowski, X. Q. Pan, C. B. Eom, and A. Gruverman, and E. Y. Tsymbal, "Enhancement of ferroelectric polarization by interface engineering," *Nature Materials Conference on Frontiers in Electronic Materials: Correlation Effects and Memristive Phenomena*, Aachen, Germany, June 2012.
2. D. J. Kim, H. Lu, A. Stamm, J. D. Burton, C.-W. Bark, S. Ryu, C.-B. Eom, E. Y. Tsymbal, A. Gruverman, "Memristive Behavior of Ferroelectric Tunnel Junctions," *MRS Fall Meeting*, San Francisco, CA, April 2012.
3. X. Liu, Y. Wang, P. Lukashev, J. D. Burton, and E. Y. Tsymbal, "Exploring and alleviating detrimental interface dipole effects in ultra-thin all-oxide metal-ferroelectric-metal heterostructures," *APS March Meeting*, Boston, MA, March 2012.
4. T. R. Paudel, Y. Wang, J. D. Burton, and E. Y. Tsymbal, "Oxygen vacancy shuttle across the $LaAlO_3/SrTiO_3$ interface," *APS March Meeting*, Boston, MA, March 2012.

Nanoscale understanding of exchange bias and spin wave manipulation using advanced MRFM imaging techniques

P. Chris Hammel
Departments of Physics and Electrical and Computer Engineering, The Ohio State University
191 West Woodruff Ave.
Columbus, OH 43210
hammel@mps.ohio-state.edu

Project scope

We are applying the microscopic imaging capabilities of Ferromagnetic Resonance Imaging (FMRI) to two important systems: exchange biased ferromagnetic films and spin wave logic structures. In the first case, we are mapping the interfacial exchange coupling between an antiferromagnet and an adjacent ferromagnetic film. We are studying both intentionally introduced spatial variations of the exchange bias field and naturally occurring and unavoidable microscopic variation of the exchange bias field. These properties are relevant for spin wave device functionality which will rely on efficient mechanisms for controlling magnetization and manipulating spin waves. We microscopically study two techniques for manipulating spin waves—localized, intense magnetic fields and exchange bias—to develop a detailed knowledge of the interaction mechanisms and their effect on the spin waves.

Exploiting the spin degree of freedom of the electron offers new and powerful opportunities for enhancing the capabilities and performance of information processing systems. Technical limitations to the continuing improvement of charge-based electronics makes it is essential to develop novel information processing technologies with improved functionality and energy efficiency. Spin waves have been used for information transmission and for logic operations. These demonstrations indicate an attractive approach to information processing and logic that avoids charge transport with its attendant power dissipation.

Exchange bias already plays a central role in information storage through its role in giant magnetoresistance magnetic field sensors employed in high density disk drive read heads. However, understanding of the detailed mechanisms by which exchange bias couples to and pins the magnetization of an adjacent ferromagnetic layer remain incomplete. This is due in part to the complicating fact that observed behavior represents the spatial average over a nonuniform interfacial layer of the antiferromagnet leading to complex and poorly understood behavior.

Spatially resolved probes of exchange bias fields and magnetic properties are needed in order to unravel the complex phenomena occurring at the buried antiferromagnet/ferromagnet interface at the heart of exchange bias systems. As spin devices become smaller to enable large scale applications, microscopic imaging of spin wave phenomena including interactions with the local fields used to manipulate the spin waves will also be essential.

Our DOE supported research has enabled the development of a novel and powerful technique, scanned probe Ferromagnetic Resonance Imaging (FMRI), that can provide microscopic information regarding static and dynamic properties of buried ferromagnetic structures and interfaces. We have shown (see DOE sponsored publication [1]) that the intense, spatially confined magnetic field of the micromagnetic probe tip mounted on a cantilever can localize the FMR mode immediately under the probe. With this microscope we have demonstrated imaging in ferromagnets with 200 nm spatial resolution and 1 Gauss/$\sqrt{\text{Hz}}$ field resolution in nanoscale volumes. Straightforward improvements of this approach will allow this dimension to be decreased to tens of nanometers. This important milestone provides a mechanism for obtaining detailed, quantitative understanding of the magnetic properties of buried ferromagnetic structures and interfaces.

Recent progress

We have applied our microscopic imaging studies of exchange bias to a series of specially prepared, exchange-biased permalloy (Py) films. In these samples the exchange bias is patterned by means of ion-irradiation to produce microscale patterns in the exchange bias fields separated by sharp interfaces (width ~ 20-30 nm). These samples, schematically diagrammed in Fig. 1, were prepared by our collaborators led by Dr. Jeffrey McCord at the Helmholtz-Zentrum Dresden-Rossendorf (HZDR) Institute of Ion Beam Physics and Materials Research (Dresden, Germany). The exchange bias system consists of two coupled layers; one ferromagnetic (FM), and one antiferromagnetic (AF). Exchange interactions across the FM/AF interface produce an effective magnetic field experienced by the FM layer. The direction of this field is defined by the polarization of the top atomic layer of the antiferromagnet.

Fig. 1 schematically depicts the structure of our samples. The sample was fabricated by coating a 20 nm thick continuous Py film with a 7 nm IrMn (AF) layer capped by a 3 nm Ru layer (not shown for clarity in Fig. 1) to avoid oxidation. A striped pattern of exchange bias field is fabricated by depositing an IrMn layer in the presence of external in-plane magnetic field followed by selective irradiation of IrMn layer with He ions through a striped mask pattern. The sample is irradiated in the presence of an in-plane magnetic field applied with an orientation opposite to that used during the initial deposition. Ion irradiation the AF areas not protected by the mask causes the direction of the exchange bias field to reverse in the irradiated stripes thus forming a striped pattern of exchange bias fields in the Py film. The results presented here were obtained on samples with as-deposited regions of width D and irradiated regions of width D_I where $D{:}D_I$ = 20 μm:20 μm. In what follows, this will be referred to as the 20 μm stripe sample.

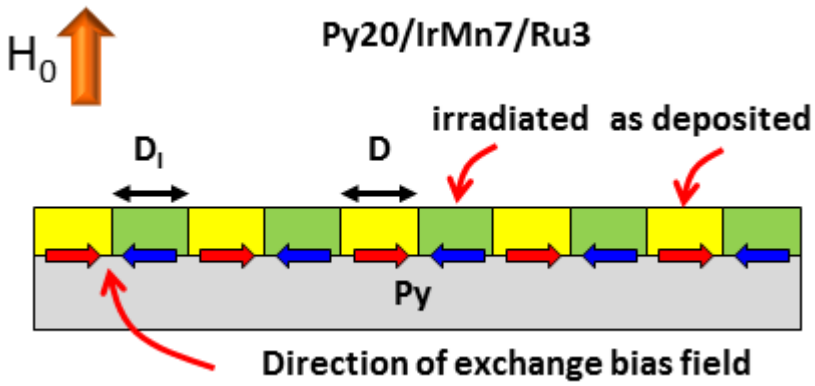

Figure 1: Schematic of a permalloy (Py) exchange biased sample fabricated by coating a 20 nm thick continuous Py film with a 7 nm IrMn layer capped by a 3 nm Ru layer (not shown) to avoid oxidation. A striped pattern of exchange bias field is generated by depositing the IrMn layer while exposed to an external, in-plane magnetic field followed by selective irradiation of IrMn layer with He ions in a reversed, in-plane magnetic field.

We have used our scanned probe FMRI technique for spatially resolved mapping of the internal magnetic field in exchange-biased Py films with typical results shown in Fig. 2. Panel a) shows a Magnetic Force Microscopy (MFM) image of the interfacial region between the as-deposited and ion-irradiated regions of the 20 μm stripe sample. The MFM image is acquired simultaneously with the FMRI measurements presented in b), which demonstrate a ~ 350 Gauss change in the internal magnetic field due to the reversal of the exchange bias field orientation in the as-deposited regions relative to the irradiated regions of the sample. While the change in internal field due to exchange bias reversal was intentionally engineered, panel c) shows micron-scale, spontaneously occurring internal magnetic field variations in the ion-irradiated region of the sample. The nature of these variations is still under investigation but they can be attributed to variations in the local strength of the exchange bias coupling. The magnetic parameters of the sample measured using spatially resolved FMRI are in a good agreement with globally averaged measurements obtained by means of conventional FMR. The details of our studies of the exchange-biased samples will be discussed in DOE sponsored publication [5]. The FMRI measurements of the internal field shown here were obtained using our recently developed experimental protocol described in DOE sponsored publication [6].

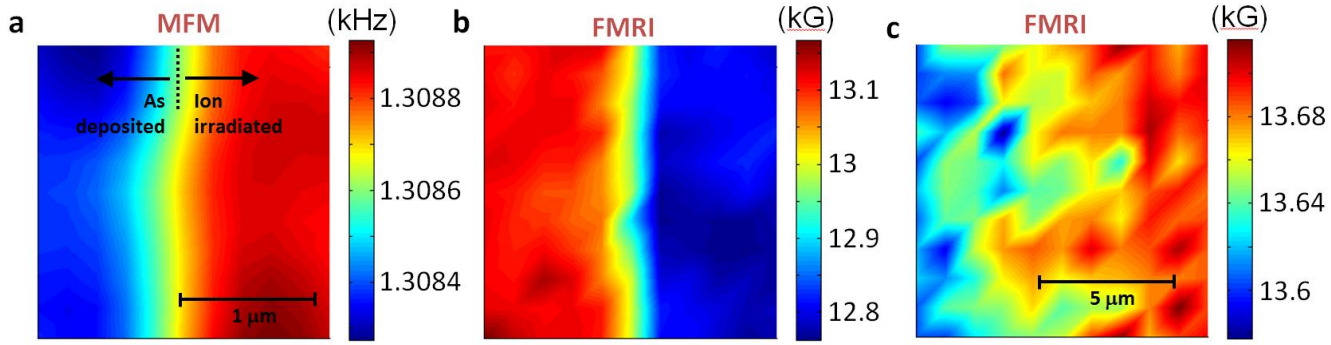

Figure 2: MFM and FMRI images of a Py film subjected to an exchange bias field patterned by ion-irradiation into 20 μm wide stripes. a) MFM image of the interfacial region between the as-deposited and ion-irradiated regions of the sample which was acquired simultaneously with the FMRI measurements. b) FMRI image of the internal magnetic field in the buried Py film. The reversal of the orientation of the local exchange bias field is clearly visible. c) FMRI image of the internal magnetic field in the ion-irradiated region of the sample demonstrating ~ 100 Gauss local magnetic field variations on micron scale.

Future plans

A primary thrust will be to use our imaging technique to better understand the spin dynamics of Spin Torque Nano Oscillators (STNO) and adjacent ferromagnetic films. This work will be performed in collaboration with Prof. Ilya Krivorotov (UC Irvine), an expert in fabrication and operation of STNOs. We will study multi-layered vertical pillar STNOs with characteristic dimensions of ~ 150 nm. The heart of the device is a set of three ferromagnetic (FM) layers separated by nonmagnetic layers. Both the ferromagnetic and nonmagnetic layers are typically ~ 2-4 nm thick. Two of the FM layers are antiferromagnetically coupled thus forming a synthetic antiferromagnet that "pins" the FM layer. The magnetization of the third, "free" layer undergoes large amplitude oscillations in response to current driven through the nanopillar. The ability of our scanned probe FMRI instrument to obtain spatially resolved maps of magnetic properties of thin magnetic films at the nanoscale offers a unique opportunity to study the magnetic properties of *individual* STNOs. We expect that further improvements in the sensitivity of our instrument will allow mapping of the spatial variations of the magnetic properties within individual FM layers in the STNO, and to map the spatial variation of the exchange bias coupling in the "pinned" layer of the STNO. We will map the dynamics of STNO magnetization oscillations in response to externally applied microwave radiation and/or electric current flowing through the STNO nanopillar.

Selected DOE sponsored publications

[1] "Nanoscale scanning probe ferromagnetic resonance imaging using localized modes", I.H. Lee, Yu Obukhov, G. Xiang, A. Hauser, F. Yang, P. Banerjee, D.V. Pelekhov, Hammel, P.C., *Nature* **466**, 845-848 (2010).

[2] "Magnetic force microscopy in the presence of a strong probe field" I.H. Lee, J. Kim, Yu. Obukhov, P. Banerjee, G. Xiang, D.V. Pelekhov, A. Hauser, F. Yang, and P.C. Hammel, *Appl. Phys. Lett.* **99**, 162514 (2011).

[3] "Nanoscale confined mode ferromagnetic resonance imaging of an individual $Ni_{81}Fe_{19}$ disk using magnetic resonance force microscopy (invited)", I.H. Lee, Yu. Obukhov, A.J. Hauser, F.Y. Yang, D.V. Pelekhov, and P.C. Hammel, P.C. *J. Appl. Phys.* **109**, 07D313 (2011).

[4] "Local magnetic characterization of (Ga, Mn) As continuous thin film using scanning probe force microscopy", I.H. Lee, Yu. Obukhov, J. Kim, X. Li, N. Samarth, D.V. Pelekhov, and P.C. Hammel, , *Phys. Rev. B*, **85**, 184402 (2012).

[5] “Dipolar Coupling in Patterned Exchange Bias Films by Ferromagnetic Resonance", by I.H. Lee, R. Adur, Yu. Obukhov, C. Hamann, J. McCord, D.V. Pelekhov, and P.C. Hammel, in preparation.

[6] “Experimental protocol for mapping internal magnetic fields in ferromagnetic samples using FMRFM", I.H. Lee, R. Adur, Yu. Obukhov, A. Reed, F. Wolny, T. Muhl, D.V. Pelekhov, and P.C. Hammel, in preparation.

NANOSCALE SWITCHING DYNAMICS IN DATA STORAGE MATERIALS

Bryan D. Huey

University of Connecticut

Institute of Materials Science

97 N. Eagleville Rd., unit 3136

Storrs, CT 06269

bhuey@ims.uconn.edu

http://www.ims.uconn.edu/~bhuey/

Scope

Optimizing the performance of data storage devices requires a thorough understanding of the nanoscale switching dynamics. Leveraging High Speed SPM (HSSPM) imaging, the local device state is simultaneously detected and manipulated in situ by biasing through a conducting AFM tip, achieving temporal resolution down to 10 nsec [1]. This enables switching nucleation times, growth velocities, growth directions, switching patterns (spatial and temporal), and activation energies to be mapped and analyzed as a function of position, processing, switching parameters, defects, etc., the emphasis of this DOE award.

For example, Figure 1 displays a switching movie acquired by polarizing a 3 µm x 3 µm region of epitaxial (001) PZT, first positively, then negatively. The switching mechanism completely changes from growth dominated to nucleation controlled depending on bias polarity, corresponding to a built-in polarization preference according to hysteresis measurements. Leveraging complementary measurements such as topography (AFM), local mechanical compliance (AFAM or nanoindentation), or chemical content (*ex situ* x-ray microanalysis), switching dynamics can further be correlated to step edges, ferroelastic domain walls or intersections, or concentration.

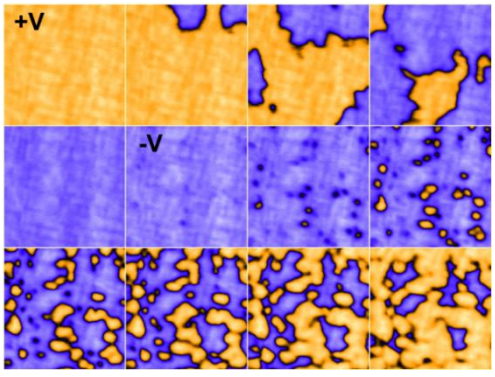

Figure 1: 3 µm x 3 µm HSSPM images extracted from a sequence of 256 consecutive images, with steps of ±55 mV_{dc} for each to cycle through an entire hysteresis loop for a (001) epitaxial PZT thin film. 3 seconds/image frame.

Recent Progress

Applying HSSPM to epitaxial (001) $BiFeO_3$, with eight possible <111> domain variants, requires simultaneous resolution of both out-of-plane and in-plane piezoactuation signals during the switching process. Recombining these signals at every image pixel then allows 3-d domain orientation maps to be generated. More interestingly, it also enables local and statistical analyses of the number, type, charging, and/or angle of domain boundaries [3]. Performing such measurements with simultaneous DC biasing, as in Figure 1, therefore yields movies of the switching event resolved in 3 dimensions, providing novel insight into the switching process.

For example, Figure 2 displays the evolution of domain orientations for a 2 µm by 2 µm area. The ferroelectric begins oriented 100% in the $[001]$ out of plane ('OP') direction (frame 1) due to uniform pre-poling by scanning with a strongly DC biased tip. The initial distribution of in-plane ('IP') domains ($[1v1]$ and $[\bar{1}v1]$) is almost equal (53% vs. 47% respectively), as they are energetically equivalent. While then scanning with an opposite DC bias superimposed on the PFM signal, nearly complete switching towards the $[uv\bar{1}]$ direction develops (93% by the final frame, 53). This is coupled with a remarkably complex sequence of changes in the IP domain configuration.

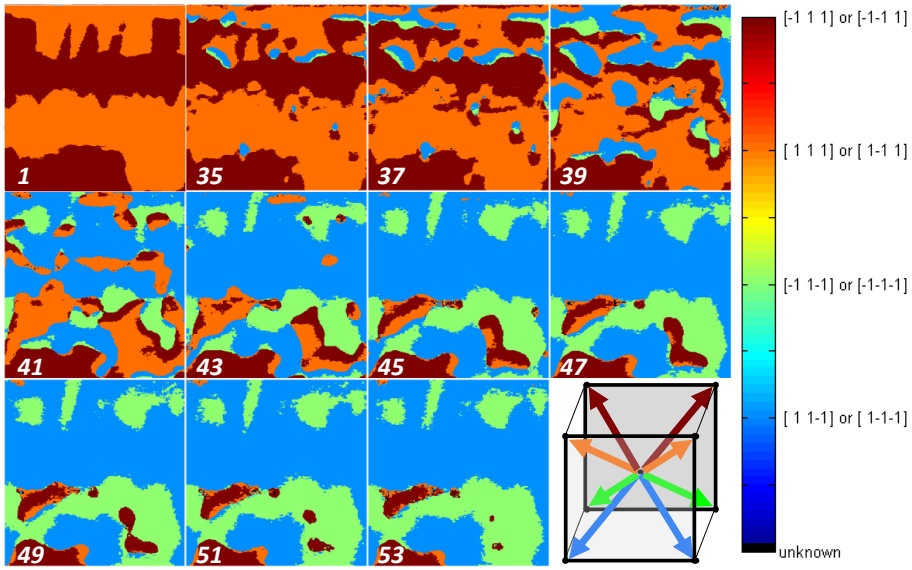

Figure 2: Montage of domain orientation maps during switching, 4 µm^2.

Having developed a procedure to analyzing the movie of Figure 2 frame by frame, Figure 3 presents the proportion of domain orientations as a function of poling time. Proportionally, OP switching prefers $[1v\bar{1}]$ orientations as compared to $[\bar{1}v\bar{1}]$ regions by approximately 2:1. $[1v1]$ domains were also observed to be sacrificed 15% more than $[\bar{1}v1]$ domains, many of which remained unswitched.

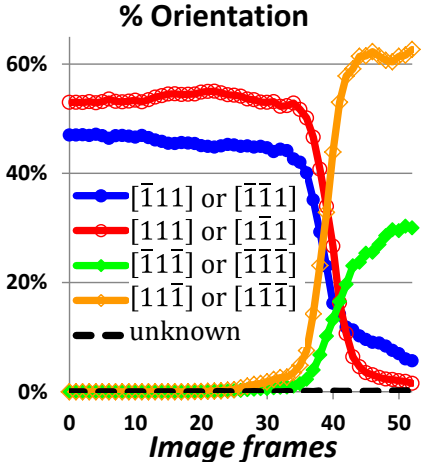

Figure 3: Domain orientations as a function of poling time.

But such average statistics overlook critical local details in the

switching process. For example, the OP reversal is dominated by domain growth from a few nucleation sites which are almost entirely located at pre-existing domain boundaries (frame 35). The growth of these nucleation sites often straddles domain interfaces (frames 37-39), growing in multiple directions by consuming the adjacent areas. Frequently, one in-plane configuration is preferred over the other as well. In fact, before switching out of plane to the $[1v\bar{1}]$ direction, $[1v1]$ domains often grow at the expense of $[\bar{1}v1]$) IP domains (and vice versa, frames 37-43). This switch does not diminish the electrostatic energy of the domain as it is still tilted 71° from the normally applied field. Therefore, it must result from other influences such as substrate effects or mechanical stress imposed by the surrounding domain microstructure. Only with additional poling is the free energy further reduced by OP switching. Such observations were not previously possible.

A newly developed procedure for pixel by pixel analysis enables such 3-d switching steps to be quantified at the nanoscale (Figure 3, with 193536 total pixels, ~21 nm^2 each). Based on the initial and final orientation maps only, Figure 4(a) shows whether any given location switched laterally ('IP', 3% of the imaged area), normally and laterally ('IP+OP', 63%), normally and possibly also laterally (30%), or either in-plane or did not switch at all ('IP or none', 4%). The uncertainty is caused by the possibility of unresolved in-plane switches from $[u1w]$ to $[u\bar{1}w]$ directions. Less than 1% of domains could not be resolved due to image noise. Altogether, this implies that the almost-total normal repolarization is accompanied by an in-plane switch of at least 63%, and as much as 97%, of the 4 µm^2 area imaged. This is somewhat surprising, since electrostatically an IP switch provides no appreciable benefit for OP poling.

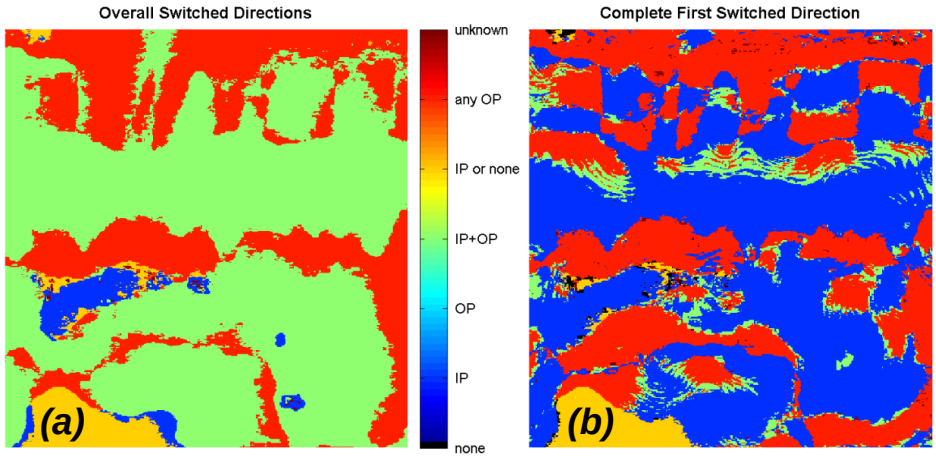

Figure 4: Maps of (a) overall change in orientation during polarization reversal, and (b) first switching direction during the switching process, from Figure 2.

Uniquely, a method was also developed to track the switching process step by step. This reveals the number and order of polarization switching steps at any given position. Accordingly, Figure 4(b) presents the *first* switching direction for the entire area, with 51% of domains laterally reorienting (IP) before eventually normally switching (OP). 37% of the investigated area first switched out of plane, while 4% either initially switched in-plane or did not switch at all. This high proportion of non-

electrostatically favored reorientations during poling is both surprising and significant for poling speeds and reliability, and is therefore the primary focus of current work.

The total number of orientation changes per pixel is also an interesting measure of the switching evolution, Figure 5. Roughly 1/3rd of the specimen switched at least once, one half exhibited two switching steps, a small fraction changed orientation three times, and 4 or more switches were observed at the borders of relatively static domains during the switching movie (dark rings). Since each switching step relates to an energetic relaxation, this novel approach for visualizing the number and location of switching events, not just the end stages, is crucial to ultimately controlling the switching procedure for optimal device performance.

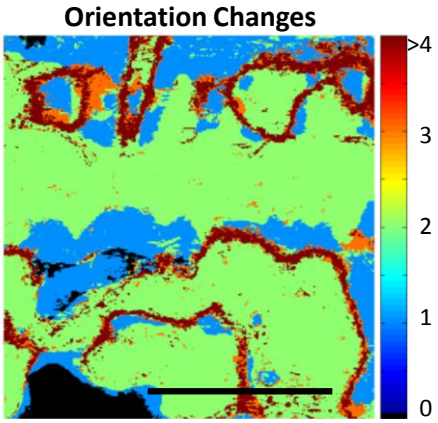

Figure 5: Map of orientation changes per pixel (1 µm scale bar).

Future Plans

- The ability to detect, and track, domain and domain boundary orientations with HSSPM is being applied to a wider range of related ferroelectrics and multiferroics, in order to ascertain the generality of the multi-step switching process observed in the $BiFeO_3$ system.
- Domain evolution is being measured and compared for $BiFeO_3$ specimens with controlled domain variants, supporting efforts to engineer devices with higher speed and reliability.
- Switching dynamics are being investigated in resistive media ($SrTiO_3$), an increasingly promising industrial system with many remaining questions for the switching mechanism.
- Nanostructured III/V photovoltaics are being studied by coupling optics and HSSPM. Photoconductivity, V_{oc}, and I_{sc} are each being measured and mapped to better leverage interfacial effects and functional grading in solar cell devices.

Acknowledgements

Specimens are provided by Y. H. Chu and R. Ramesh, UC Berkeley; J. Ihlefeld and D. Schlom, Cornell University; and E. D. Spoerke and Jose Luis Cruz-Campa, Sandia National Labs.

Publications (in print thus far, 4 additional manuscripts in progress)

[1] B. D. Huey, R. Nath, S. Lee, N. A. Polomoff, J. American Ceramic Society, **95** (4), (2012).

[2] J. Desmarais, J. F. Ihlefeld, T. Heeg, J. Schubert, D. G. Schlom, B. D. Huey, Applied Physics Letters, **93**, 162902, (2011).

Vortex Matter in Confined Superconductors and Mesoscopic Hybrid Herostructures

Principal Investigator: Maria Iavarone
Physics Department, Temple University
Barton Hall, 1900 N. 13th Street
Philadelphia, PA 19122
e-mail: iavarone@temple.edu

Project Scope

The primary emphasis of this project is on the physics of vortices in confined superconductors and hybrid heterostructures such as superconductor-normal metal and superconductor-ferromagnet systems. The goal is to understand how the physics of vortex matter changes in order to be able to predict and control the electronic properties of new hybrid systems. Scanning Probe Microscopy and Spectroscopy is an integral part of this study. The vortex configuration in confined superconductors can be probed with high spatial resolution using Magnetic Force Microscopy or by mapping the spatial variations in the electronic density of states with Scanning Tunneling Microscopy (STM). The understanding of the local changes in the electronic density of states is crucial as it also affects all the thermodynamic properties of the material.

Recent Progress

When the superconductor and the ferromagnet are brought in contact the superconductivity in both subsystems is modified due to the exchange field h and the electromagnetic interaction. The exchange field tends to align the spins of the Cooper pair, leading to pair breaking in s-wave superconductors (paramagnetic effect). On the other hand, the electromagnetic interaction results from the interplay between the magnetization of the ferromagnet and the screening currents in the superconductor. If a thin insulating layer is placed between the ferromagnet and the superconductor the electromagnetic interaction will dominate and the proximity effect at the interface between superconductor and ferromagnet will be suppressed. The S/F systems with purely electromagnetic interaction can be described phenomenologically using Ginzburg-Landau and London formalisms. In this case, in contrast to the situation of a uniform applied field where the critical temperature is constant throughout the volume of the superconductor, the critical temperature in such S/F systems depends on the position.

We have made significant advancement in the study of F/S structures magnetically coupled in the areas of:

1. Spontaneous Vortex-Antivortex pairs in S/F structures magnetically coupled.
2. Pinning and the avalanche region in the H-T phase diagram in S/F structures magnetically coupled.
3. Domain wall superconductivity and reverse domain wall superconductivity in S/F structures magnetically coupled.

Spontaneous formation of vortex-antivortex pairs

In S/F structures magnetically coupled we observed a rich variety of phenomena deriving from a combination of pinning and confinement of vortices in channels defined by the underlying ferromagnetic magnetic stripe domain structure.

Magnetic Force Microscopy (MFM) showed the spontaneous formation of vortex-antivortex in S/F hybrid structures, induced by the stray field of the ferromagnet (Figure 1). *We confirmed experimentally for the first time the theoretical criterion for spontaneous formation of V-AV pairs in F/S hybrids. The key role for formation of V-AV is played by the out-of-plane magnetization of the ferromagnet and by the ratio of the magnetic domain width to the superconducting film thickness.* The samples studied are Py/Nb bilayer magnetically coupled.

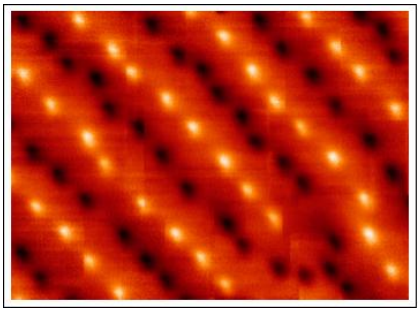

Figure 1 MFM image of Vortex-Antivortex pairs acquired on a Py/Nb bilayer magnetically coupled at T=5.7 K. The image is in zero applied magnetic field. V-AV pairs are spontaneously generated by the stray field of the Py. The scan area is 11.4x8.7 μm^2.

Pinning in S/F structures magnetically coupled

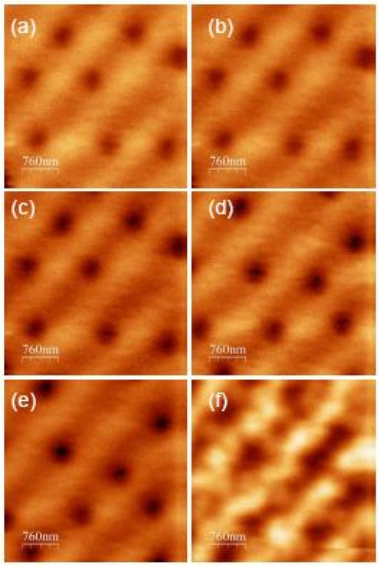

Figure 2 MFM images of a Py/Nb bilayer at T=5.5 K. The applied magnetic field perpendicular to the surface is swept from (a)H= -16 Oe, to (b)=+14 Oe, (c) H=+34 Oe, (d) H=+37 Oe, (e) H=+47 Oe, (f) H=+95 Oe. The scan area is 3800 nm x 3800 nm.

As far as the *non-equilibrium state of F/S structures we observed different regimes in the H-T phase diagram. Close to the superconducting critical temperature T_c, where magnetic pinning is predicted to be effective, we observe an enhancement of vortex pinning. We also found an enlarged region of the H-T phase diagram, compared to the reference Nb films, where flux avalanches occur.* Avalanches have been observed as sharp jumps in DC magnetization, that are fingerprints of sudden penetration of flux into the sample, and have been visualized by low temperature MFM (Figure 2). The observed behavior is related with channeling of vortices by the underlying magnetic stripe domains in the Py. These findings are important since avalanches can limit the applicability of the S/F structures in devices at low temperatures.

Domain wall and reverse domain wall superconductivity

In F/S structures, since the critical temperature is suppressed by the magnetic field, the highest critical temperature is reached at position with lowest magnetic field. As a result, the superconductivity will nucleate in the low magnetic field regions. If an external magnetic field is applied, due to compensation effects, the minimum magnetic field regions will change position and consequently the superconductivity will move towards these regions. This effect manifests itself in a non-trivial evolution of the effective critical temperature as a function of the applied magnetic field $T_c(H)$. The T_c can indeed increase as increasing applied magnetic field (reentrant superconductivity). In zero applied magnetic field the superconducting order parameter will be localized above the magnetic domain wall. When increasing the magnetic field, the total field above the compensated domains will decrease, and the order parameter will be relocated below the domains with opposite polarity to the applied field.

Therefore, a nonuniform magnetic field is an alternative way to confine the superconducting order parameter and study the effects related to superconductivity and confinement. Using applied magnetic field and temperature as external parameters one can tune the confinement conditions within the same sample.

We have explored different magnetic materials that were prepared in a dedicated system while the superconductor layer was prepared in the UHV chamber linked to the STM chamber. We first optimized the growth of superconducting film on a Si substrate and we characterized the superconducting and vortex properties of these films by low temperature STM. We succeeded in fabricating Pb films with a thickness of ~30 nm characterized by *flat surfaces with atomic step terraces, suitable for STM investigation.* The films have a superconducting critical temperature T_c=7.2 K as revealed by the temperature dependence of the tunneling spectra with a gap $\Delta(0)$=1.5 meV and Hc2(0)=1100 Oe at T=350 mK determined from the vortex core size and from the evolution of the zero bias conductance as a function of the applied magnetic field.

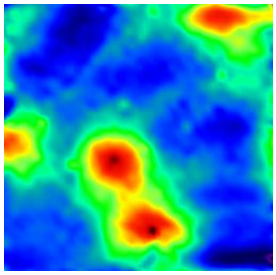

Figure 3
STM conductance map at zero bias showing spontaneous V-AV in Co-Pd/Pb at T=2.0 K. Scan area 600 nm x 600 nm.

We fabricated F/S structures consisting of Co-Pd multilayers having stripe domains of 200-300 nm, covered by 10 nm of oxide and 30 nm of Pb deposited in the UHV STM system at low temperature. STM measurements showed the presence of spontaneous vortex-antivortex pairs at T=2.0 K (Figure 3). The stray field of the ferromagnetic layer estimated by the distance between vortices is of the order of 700 Oe (i.e. much higher than the Py films). *STM temperature dependence revealed the region when the superconductivity nucleates at first being of the order of 100 nm on the top of the domain walls. Measurements in applied magnetic field directly visualized for the first time the shifting of the superconductivity toward the centre of the domains.*

Future Plans

We will continue to advance on the fundamental understanding of vortex matter and its impact on applications. Indeed, the studies of vortex-antivortex dynamics could have far-

reaching impact going beyond the basic understanding and control of vortex dynamics. Many applications of superconductors in sensors are limited by noise believed to be due to dissipation from vortex-antivortex dynamics.

We will correlate STM measurements with MFM, transport and magnetization measurements on the same samples in order to address in a systematic approach fundamental questions related to the formation and annihilation of vortex-antivortex pairs in S/F bilayers. Specific planned activities include:

- Imaging of vortex-antivortex pairs subjected to Lorenz force by superconducting transport current would elucidate the strength of the vortex-antivortex binding potential as well as non-equilibrium vortex-antivortex states. The basic dynamics of such system remains unknown.
- S/F structure in the regime of proximity effect to image directly the oscillatory behavior of the superconducting order parameter inside the magnetic metal near the interface.
- Based on our preliminary results on Pb islands on Si substrates we will explore mesoscopic superconductors on different substrates.

Publications

" Observation of spontaneous vortex-antivortex pairs in superconductor/ferromagnet hybrid structures", M. Iavarone, A. Scarfato, F. Bobba, M. Longobardi, G. Karapetrov, V. Novosad, V. Yefremenko, F. Giubileo, and A. M. Cucolo, *Phys. Rev. B* **84**, 024506 (2011)

"Visualizing vortex dynamics in Py/Nb thin film hybrids by low temperature magnetic force microscopy", A.M. Cucolo, A. Scarfato, M. Iqavarone, M. Longobardi, F. Bobba, G. Karapetrov, V. Novoisad, V. Yefremenko, *J. Supercond. Nov. Magn*. (2012)

"Vortex Confinement in Planar Superconductor/Ferromagnet Hybrid Structures", M. Iavarone, A. Scarfato, F. Bobba, M. Longobardi, S. A. Moore, G. Karapetrov, V. Yefremenko, V. Novosad, and A. M. Cucolo, *IEEE-transaction on Magnetics* 48 (11), 1 (2012)

"Evolution of the Charge Density Wave state in Cu_xTiSe_2", M. Iavarone, R. Di Capua, X. Zhang, M. Golalikhani, S. A. Moore, and G. Karapetrov, *Phys. Rev. B* ***85***, 155103 (2012)

"Evidence of Vortex Jamming in Abrikosov Vortex Flux Flow Regime", G. Karapetrov, V. Yefremenko, G. Mihajlovic, J. E. Pearson, M. Iavarone, V. Novosad, and S.D. Bader, in preparation

"Local Stray Field of thick Py films effects on superconductors", A. Scarfato, M. Iavarone, F. Bobba, M. Longobardi, G. Karapetrov, V. Novosad, V. Yefremenko, A. Di Bartolomeo, and A.M. Cucolo, in preparation

"Direct visualization of domain wall superconductivity and inverse domain wall superconductivity" in preparation

High-resolution photoemission electron microscopy

Rolf Könenkamp
Physics Department, Portland State University, 1719 SW 10th Avenue, Portland OR 97201
(503) 725 4224 rkoe@pdx.edu

Research scope and definition

We study new instrument designs in photoemission electron microscopy and explore new applications for this type of microscopy. Our photoemission microscope (PEEM) is a home-built instrument featuring a hyperbolic electrostatic mirror for the correction of chromatic and spherical aberration. It is equipped with a 244nm cw laser and a femtosecond pulsed laser system with wavelengths between 200 and 800nm.

In the past years we have brought the spatial resolution of this instrument to 5.4 nm for 1μm-diameter images and to 4.4 nm for smaller size images. These are currently the best published resolutions for PEEM. We have calculated and recently built a new, more complex aberration corrector based on a 3-electrode mirror which is to be operated in conjunction with a mirror entry lens. This corrector system is currently being installed. It is expected that the new corrector will again allow for a resolution improvement, bringing us closer to our 2nm goal.

We are utilizing the increased sensitivity and contrast of the aberration-corrected instrument in non-linear photoemission microscopy in plasmonics and two-dimensional photonics. Surface plasmon propagation and the possibility of coherent optical control of surface plasmons are explored in specifically designed metal nanostructures. Similarly, we explore photon propagation in two-dimensional waveguides made of transparent metal oxide films using the same methodology as in plasmonics. Both plasmon and photon propagation can directly be visualized in the microscope with a resolution better than ~1/20 of the optical wavelength. We hope to use this type of microscopy to obtain a detailed and quantitative description of optical near-field dynamics and non-linear interaction effects.

In other applications we utilize the strong surface sensitivity of PEEM to study thin two-dimensional layers, such as graphene, with the goal to explore structural properties and growth mechanisms.

Recent progress

A. Mirror development: Low electron energy microscopes, such as PEEM and LEEM have comparably large chromatic aberrations and for this reason mirror-based aberration correctors are being developed for these instruments. The first generation of these mirrors encompassed mirrors with one controllable and one grounded electrode (1). In these mirrors the chromatic and spherical aberration coefficients are intimately coupled, and by adjusting the mirror potential both coefficients are altered in a deterministic way. This, of course, limits the optimal adjustment of the microscope to a small number of configurations. This case coupling between chromatic and spherical aberration is illustrated in figure 1a where the two aberration coefficients are plotted as a function of mirror image distance which in turn is a function of electrode potential. The undesirable coupling is relaxed when more electrodes are available. 4-electrode mirrors have been proposed and implemented (2), but the resolution improvement in PEEM has so far not been very strong. This may in part be due to the complexity of these devises and the lack of analytical description of their optical properties. Our 3-electrode mirror uses only 2 controllable and one grounded electrode and is run in conjunction with a standard electrostatic einzellens. Mathematically this is a simpler object than a four-electrode mirror. We were able to develop an approximate analytical description that agrees to within 5% accuracy with

numerical simulations. For this mirror-lens combination the correlation between chromatic and spherical aberration is shown in Fig. 1b. Essentially, the line-like correlation is now widened to a 2-dimensional surface which allows – within fairly wide margins – an independent choice of the aberration coefficients

With the available analytical description an optimized combination of electrode potentials for mirror and lens are easily derived, and it is expected that the appropriate electrode potentials can be applied in a simple real-time process during operation.

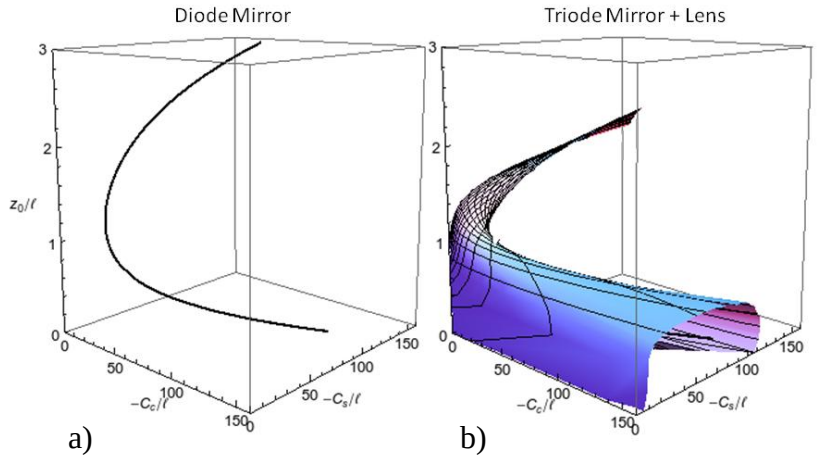

Figure 1a: Correlation of chromatic and spherical aberration coefficients (C_c and C_s) in an electrostatic hyperbolic mirror. Z_o is the image distance of the mirror which can be adjusted with the controllable mirror voltage. B: Same correlation for a triode mirror with 2 controllable electrodes operated in combination with the mirror entry lens. The correlation is now a 2-dim. surface in which the position can be chosen by adjusting the two mirror electrode potentials. Curves of equal electrode potentials are plotted in black on this surface.

B. Photonics and plasmonics: Basic research on plasmonics and two-dimenensional photonics is currently directed towards applications in imaging, sensing and energy conversion. The essential promise in this field is that dynamic electronic processes can be controlled at the microscopic level and at optical frequencies. Photoemission microscopy is capable of combining nanoscale resolution with femtosecond temporal resolution and may therefore become a key tool in this arena. Aberration-corrected instruments with their improved sensitivity, contrast and resolution have received considerable attention in this field.

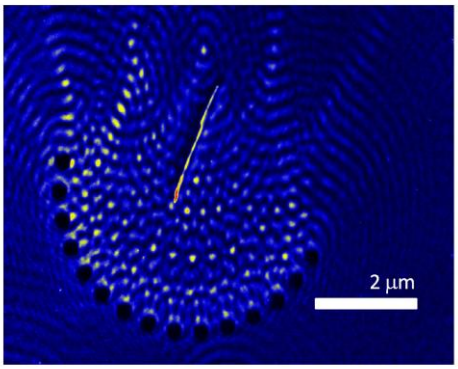

Figure 2: PEEM micrograph of light waves propagating in a 2-dim. indium-tin-oxide waveguide. The light waves are seen to couple to surface plasmons in a gold nanowire. The 410nm excitation light is used as excitation, Photoelectron emission occurs in a non-linear 2-photon photoemission process.

Figure 2 shows an example from our recent work on photon propagation in two-dimensional waveguides. Light at 410 nm is coupled into a 60nm thick transparent indium-tin-oxide layer at cylindrical ion-milled holes. From the holes the light propagates with circular wavefronts giving rise to an intricate interference pattern with multiple focal points. This pattern can be captured in PEEM with high contrast using a non-linear two-photon electron emission process. The spatial resolution is ~ 10nm, i.e. far below the wavelength of the propagating light. In the center of the figure a gold nanowire acts as an antenna in the guided photonic wave field. The micrograph shows that surface plamon modes are coherently excited along the nanowire axis in the evanescent field of the optical wave. By varying polarizations, phases and wavelengths these photon/plasmon interactions can directly be visualized and studied in PEEM. The direct access to the spatial plasmon and photon distributions in PEEM strongly facilitates the design of devices as shown below.

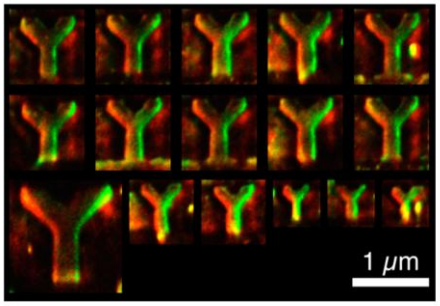

a)

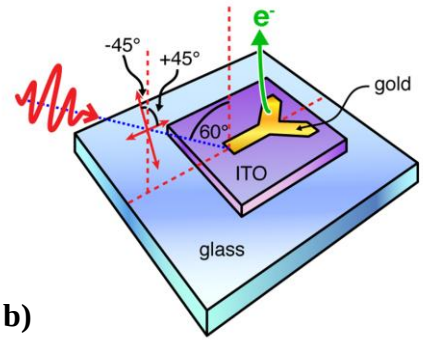

b)

Figure 3a: Composite PEEM micrograph showing plasmon distributions in gold nanostructures when excited with visible light of different polarizations: green color relates to +45^{o} polarization, red color to -45^{o} polarization as defined in the excitation scheme in part b) of the figure.

Figure 3 shows a simple plasmonic router that switches the propagation path of surface plasmons in response to light polarization changes. Single-crystalline Y-shaped gold structures prepared by ion-milling from chemically grown gold platelets are used. Depending on the polarization of the excitation light the plasmon propagation through the Y-structure can be directed towards the right or left tip of the Y. The propagation path is again visualized in a non-linear photoemission process. In part a) the initial plasmon distribution in the gold film is shown for two different polarization directions of the excitation light. Part b) of the figure shows the experimental set up. In more detailed work we can also observe the out-coupling of the plasmon energy at the tip periphery of the Y- structure.
Beyond these practical applications PEEM allows insight into the details of the non-linear electron emission process that underlies the imaging process. Some of the questions which are currently being addressed relate to the extent of coherence in multi-photon and multi-plasmon excitations and the role of intermediate states.

Finally in figure 4 we present work building on the high surface sensitivity of PEEM. Single- and multi-layer graphene growth is easily resolved in photoemission microscopy, as electron scattering strongly affects the photoemission probability for near-threshold electrons in PEEM. Dynamic in-situ observation is, in principle, possible with PEEM and electrical and optical properties for low energy electrons can be studied.

Future Plans

In the remaining grant period we will install and optimize the new aberration corrector to improve the resolution in PEEM towards 2 nm. Using specifically designed single-crystalline gold structure we will continue to study a number of fundamental questions in plasmonics and and plasmon-induced electron emission. These will relate to interaction effects of localized and propoagting plasmonic

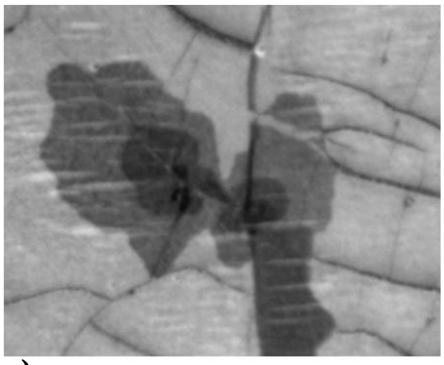

a)

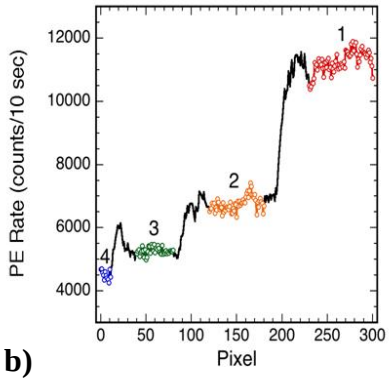

b)

Figure 4: a: PEEM micrograph of multi-layer graphene growth on copper. Areas with 1 to 4 layer coverage are clearly discernible; b: line scan for the photoemission rate (1 pixel corresponds to 10nm.

modes in metals, the excitation of plasmonic modes in the near-field confined photonic modes, and questions on the enhancement of electron emission in the near-field vicinity of surface plasmons. We hope that these questions can be addressed in high-resolution photoemission micrographs under proper operating conditions where the various excitations become visually apparent in the same image.

References

(1) G. F. Rempfer, J. Appl. Phys. 67, 6027 (1990)

(2) Z. Shao and X.D. Wu, Rev. Sc. Inst. 61 (1990), 1230 (1990)

Publications with DOE acknowledgments (2010-12)

5.4 nm resolution in a photoelectron-microscopy

R. Word, T. Dixon, T. Jones, L. Almaraz, G. Rempfer and R. Könenkamp, Ultramicroscopy 110, 899 (2010).

Photoemission from localized surface plasmons in fractal metal nanostructures

Word R. C.; Dornan T.; Könenkamp R., APL 96, 251110 (2010), (also in Virtual Journal of Ultrafast Science (7/10))

Photoelectron emission control with polarized light in plasmonic metal random structures

Word R. C.; Fitzgerald J.; Könenkamp R., APL 99 (2011) (also in Virtual Journal of Ultrafast Science (8/11))

S and P-Polarization Dependence of Localized Surface Plasmon Enhanced Photoelectron Emission from Fractal Gold/ITO Nanostructures

R. Word, J. Fitzgerald and R. Könenkamp, Proceedings of the IEEE-NANO-2011 conference, Portland, OR. (2011)

Aberrations in asymmetrical electron lenses

J.P.S. Fitzgerald, R.C. Word and R. Könenkamp, Ultramicroscopy (Nov. 25, 2011 available on line, in press)

Simultaneous and independent adaptive correction of spherical and chromatic aberration using an electron mirror and lens combination

J. P. S. Fitzgerald, R. C. Word and R. Könenkamp, Ultramicroscopy 115, 35 (2012)

Adaptive aberration correction using a triode hyperbolic electron mirror

J. P. S. Fitzgerald, R. C. Word and R. Könenkamp, Ultramicroscopy 111, 1495 (2012)

Electron emission in the near-field of surface plasmons

Robert C. Word, J. Fitzgerald and R. Könenkamp, Surface Science (submitted)

Controlled spatial switching and routing of surface plasmons in designed single-crystalline gold nanostructures

R. Könenkamp, R. C. Word, J. Fitzgerald, Athavan Nadarajah and S. Saliba, APL (submitted)

Atom chip microscopy: A novel probe for strongly correlated materials

Benjamin Lev
Departments of Applied Physics and Physics
Ginzton Laboratory, Box 305
Stanford University
Stanford, CA 94305-4088
benlev@stanford.edu

Research Scope:

This program is focused on introducing a novel magnetic field microscopy technique into the toolbox of strongly correlated (and topologically nontrivial) material imaging. We have completed the construction of a magnetic microscope that uses atom chips---substrates supporting micron-sized current-carrying wires that create magnetic microtraps near surfaces for thermal gases and Bose-Einstein condensates (BECs)---to enable single-shot and raster-scanned large-field-of-view detection of magnetic fields emanating from electronic transport. Figures 1 and 2 depict the principles of atom chip trapping and the target sensitivity and resolution of the microscope, respectively.

We are working to demonstrate the use of cryogenic atom chip[1] microscopy for single-shot, large-area detection of magnetic flux at the 10^{-7} flux quantum Φ_0 level and below; namely, sub-micron resolution of sub-nanotesla fields over millimeter detection lengths. By harnessing the extreme sensitivity of atomic clocks and Rb and Dy quantum gases to external perturbations, the cryogenic atom chip technology developed here will provide a magnetic flux detection capability that surpasses other techniques---such as scanning SQUIDs---by a factor of 10^1--10^3.

Cryogenic atom chip microscopy introduces three very important features to the toolbox of high-resolution, strongly correlated material microscopy: simultaneous detection of magnetic and electric fields (down to the sub-single electron charge level); no invasive large magnetic fields or gradients; simultaneous micro- and macroscopic spatial resolution; DC to MHz detection bandwidth; freedom from $1/f$ flicker noise at low frequencies; and, perhaps most importantly, the complete decoupling of probe and sample temperatures. The first of these features will play an important role in studying the interplay between magnetic and electric domain structure. The last two are crucial for low frequency magnetic noise detection in, e.g., the cuprate pseudogap region, and for precision measurements of transport throughout the technologically relevant temperature regimes of topological insulators and unconventional superconductors. These temperature regimes are currently inaccessible to other techniques based on superconducting scanning probes.

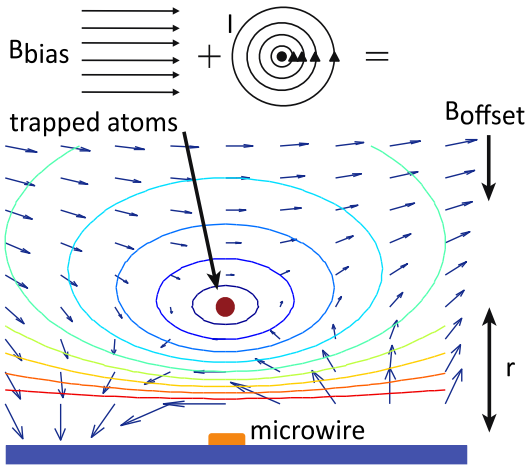

Figure 1: (a) Atom chip trapping principle. A cylindrically symmetric quadrupole magnetic field is created by superimposing a weak, homogeneous bias field B_{Bias} with that from a microwire with current I. Weak-field seeking atoms---i.e., atoms in a Zeeman state whose energy increases for increasing magnetic field magnitude---are trapped in a small region around the zero of the magnetic quadrupole field.

[1] J. Fortagh and J. C. Zimmermann, Rev. Mod. Phys. **79**, 235 (2007).

The atom chip microscope can operate at maximum sensitivity and resolution without regard to the substrate temperature. While the BEC is among the coldest objects realizable (100 nK temperatures are typical), the atom chip substrate can be positioned 1 micron away from the BEC and be as hot as 400 K or as cold as a cryostat can cool. This is because unlike superconducting probes, whose temperature is closely coupled to nearby materials, quantum gases are immune to radiative heating[2]. The energy gap between a Rb or Dy atom's ground state and first excited state far exceeds the typical energy of room temperature blackbody radiation[3]; such atoms are therefore transparent to radiation heating by materials at room temperature or below. With Dy, this technique would now allow transport imaging with micron resolution and sub-10^{-8} Φ_0 magnetic flux sensitivity at any temperature below 400 K, a feat that cannot be performed with current techniques.

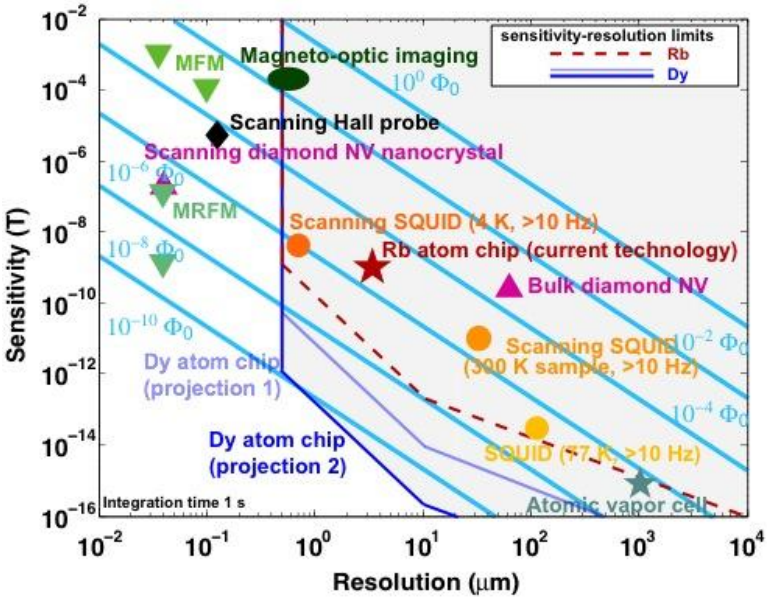

Figure 2: Comparison of techniques for high sensitivity, high-resolution magnetic field measurement. The red dashed (Rb) and blue solid (Dy) lines denote the sensitivity--resolution limits for atom chip microscopy with either Rb atoms or the more exotic, highly magnetic element Dy. The leftmost boundary is due to a 500-nm imaging resolution limit and the lower bounds arise from limits arising from collisional BEC mean field energy and depth in the presence of gravitational pull. Projection 1 is the 20-fold sensitivity improvement provided by our Dy BEC and Fermi gas capability. Projection 2, a 1000-fold Φ_0 improvement over Rb atom chip microscopy and scanning SQUIDs, may be reached by reducing Dy BEC mean field energy.

Recent Progress:

From an empty lab at the start of this DOE funding, we succeeded in building---and rebuilding at Stanford after a move from the University of Illinois at Urbana-Champaign---a Rb BEC cryogenic atom chip microscope, and we are now in the process of taking data characterizing its sensitivity and resolution for publication. The current liquid He flow cryostat allows the sample mount to reach 30 K, and implementation of copper heat shields and an LN_2-cooled atom chip will bring the temperature down from 30 to <10 K once installed. We are able to create a nearby Rb BEC of 10^5 atoms at 100 nK using an atom chip of our own design and fabrication. An ultracold gas of Rb can be created in 10 s and transported to the atom chip and Bose-condensed within 10 s. The mm-long BEC can be recreated and imaged within a few microns of a condensed matter sample with a duty cycle of < 20 s.

The existing imaging system is capable of 3-um resolution, but the UHV chamber infrastructure is designed for a 1-um resolution system. We are currently implementing stroboscopic imaging for DC to kHz bandwidth detection of magnetic field noise arising from current flow fluctuations. Figure 3 shows an image of the current Rb microscope apparatus. Moreover, we have created the world's first BEC and Fermi gas of Dy[4], which in future years will allow us enhance the microscopes sensitivity 20-1000 fold.

[2] All experiments operate within an ultrahigh vacuum (UHV); convective heating is absent.
[3] At room temperature, blackbody radiation wavelength peaks at λ = 10 um; electronic transitions have λ < 1 um.
[4] M. Lu, N. Q. Burdick, S.-H. Youn, and B. L. Lev, PRL **107**, 190401 (2011); *ibid.*, PRL **108**, 215301 (2012).

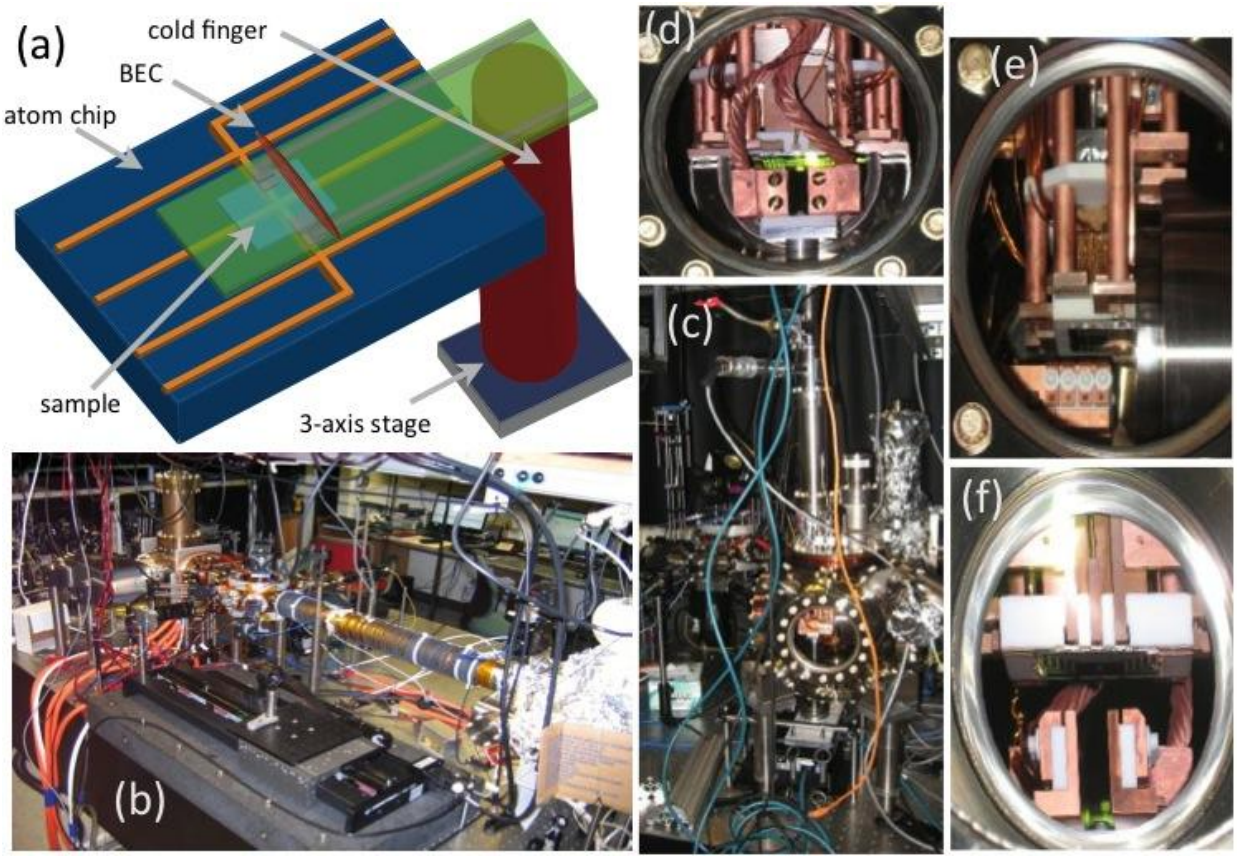

Figure 3: (a) Schematic of the atom chip microscope core. The atom chip suspends the BEC near the condensed matter sample mounted on a cantilevered substrate. This substrate is heat-sunk to a LHe-flow cryostat, and may also be postitioned with sub-micron accuracy via a 3-axis translation stage. (b) Image of our BEC production apparatus: atomic beam oven, Zeeman slower, and MOT coils and laser optics. (c) Image of cryogenic system chamber and BEC produciton chamber in background. Ultracold atoms are transferred via optical tweezer. (d--f) Images of cold finger, atom chip, condensed matter sample mount, high-NA lens access port.

Future plans:

The topological insulator is a unique state of topologically nontrivial quantum matter that has sparked a tremendous amount of interest in the condensed matter community. Interest is not only focused on the novel manner in which this matter organizes, which is distinct from the standard Landau symmetry-breaking paradigm of phase transitions, but also on the potential use of topological insulators in spintronic devices and in topologically protected quantum information processing.

Unfortunately, all known topological insulator materials suffer from large bulk conduction: they are not truly insulating due to chemical imperfections and so are not readily amenable to traditional transport measurements. This makes surface transport properties very difficult to measure, let alone manipulate[4]. A challenge lies in acquiring the ability to distinguish the interesting surface state dynamics from the less interesting dynamics in the bulk. Only then will the promise of novel electronic devices, exotic quantum phenomena, and quantum information processors be realized with topological insulators.

Extant methods are not wholly satisfying from the standpoint of robustly detecting topologically protected surface states in presumptive topological insulators in a model-independent fashion. By contrast, the cryogenic atom chip microscope presents an independent technique that enables the

[4] J. G. Analytis, R. D. McDonald, S. C. Riggs, J.-H. Chu, G. S. Boebinger, and I. R. Fisher, Nature Physics **6**, 960 (2010).

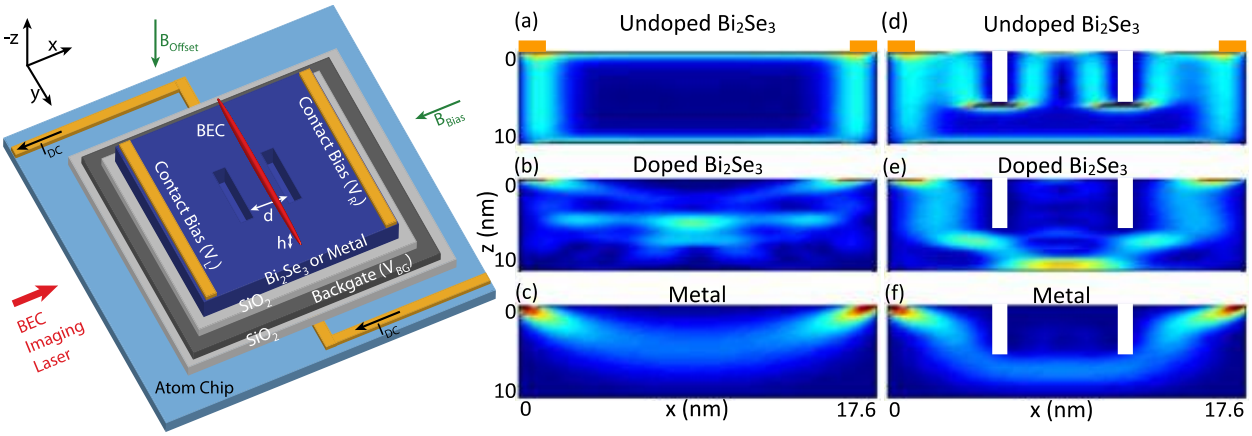

Figure 4: Leftmost panel; schematic of device for imaging transport in a topological insulator. Contacts induce a longitudinal current across the channel, which is back-gated to be within the bulk gap. (a--f) Current profile in topological insulator, where red/bright (blue/dark) denote high (low) current density in: (a) and (d) undoped Bi_2Se_3; (b) and (e) doped Bi_2Se_3; and (c) and (f) metal thin films. Positions of contact leads shown as gold rectangles in (a) and (d); leads in the other panels not shown. (a) Current is closely tied to within 3 nm of the top and bottom surfaces of the undoped TI Bi_2Se_3. (b) Doping by raising the chemical potential to 0.2 eV opens a parallel bulk conducting path as carriers reach the conduction band. The structure in the current density is due to finite simulation size effects. (c) Carriers in the metal immediately diffuse and flow through the bulk of the channel. (d--f) Current flow around two trenches in the top surface of the material. Trenches in these plots are 1 nm wide, 5 nm deep, and separated by 7 nm. (d) Current hugs the upper surface contour in the undoped Bi_2Se_3 sample, but (e) fails to do so in the doped Bi_2Se_3. (f) As in the doped TI, the trenches in a metal serve to spatially low-pass filter the **z** current modulation seen in the undoped TI. Atom chip microscopy can image depth of the current flow between the trenches, thus providing a measure of surface--to--bulk conductivity. See details of calculation and description of proposed surface--to--bulk conductivity measurement in Ref. [1].

direct detection of the surface current in a manner that provides a relatively model-free measure of the surface conductivity versus the bulk conductivity.

Our atom chip microscope may also advance topological insulator physics in other manners. The surface state of existing topological insulators seems to be fragile in that the Fermi level shifts away from the Dirac point over time and exposure. Such aging effects will hamper device functionality unless fabrication techniques mitigate this effect. A surface transport probe such as the atom chip microscope should be a powerful tool to diagnose these aging effects under various preparation conditions.

In the future, we will utilize the magnetic field signatures from electronic transport in TIs as a means of characterizing the topologically protected surface state. Specifically, we will use our microscope to enable single-shot and raster-scanned large-field-of-view detection of magnetic fields emanating from electronic transport in a corrugated TI. This will provide a relatively model-independent measure of the TI's surface—to—bulk conductivity ratio as described in Ref. 1 (see also Fig. 4).

Additionally, STM, transport, and x-ray scattering experiments have, among others, revealed the existence of a quantum liquid crystal state in iron (pnictide) and cuprate superconductors. This strongly correlated state of matter could also be detected by imaging the fluctuating flow (spatially and/or in time) of electrons as the phase/regime boundary is crossed between the pnictide non-Fermi liquid (cuprate strange metal) and the pnictide magnetic phase (cuprate pseudogap regime). We aim to image the developing domain structure as the sample temperature is tuned through the respective temperatures T*, both at DC and in stroboscopic AC detection mode.

References:

1) B. Dellabetta, T. L. Hughes, M. J. Gilbert, and B. L. Lev, Phys. Rev. B 85, 205442 (2012).

Tailoring electronic properties of graphene via defect engineering and doping

Principle Investigator: Lian Li

Mailing Address: 1900 E Kenwood Blvd, Milwaukee, WI 53211

Email: lianli@uwm.edu

Research Scope

The focus of our program is to attain new functionalities in graphene by defect engineering and chemical modification using an integrated approach of STM/AFM imaging and spectroscopy and density functional theory (DFT) calculations.

Recent Progress

1. Atomic structure and growth mechanism of epitaxial graphene/SiC(0001): role of the warped interfacial layer

During the 2010-2012 funding period, we have made significant advances in the understanding of the atomic structure and growth of epitaxial graphene on SiC(0001). We have discovered a new warped interface structure involving the incorporation of pentagon-hexagon-heptagon ($H_{5,6,7}$) defects; and a novel Si diffusion path through this layer for pit free graphene growth on SiC(0001). We show that epitaxial graphene growth on Si-face SiC(0001) starts with the formation of warped interfacial layer with periodic inclusions of $H_{5,6,7}$ complexes within the honeycomb lattice, which relieves the strain between graphene and the SiC substrate, while still retaining the three-fold coordination for each carbon atom. During the subsequent growth, the warped interfacial layer remains, while the succeeding layers assume the usual graphene honeycomb lattice. The model explains the consistencies and variation in the structural and electronic properties of the epitaxial graphene/SiC(0001), which has eluded the community for decades This work has been published in *Phys. Rev. Lett.* [PRL **105**, 085502 (2010)] and a book chapter in *"Physics and Applications of Graphene: Experiments"*.

We have further investigated the impact of this warped interfacial layer on the growth kinetics of epitaxial graphene on SiC(0001). We discovered a novel vertical diffusion path for the Si through the interfacial layer, where the pentagon and heptagon of the $H_{5,6,7}$ complex facilitates the diffusion of the Si atom through a series of configurations involving the dissociation and formation of C-C and Si-C bonds, as shown in Fig. 1. The

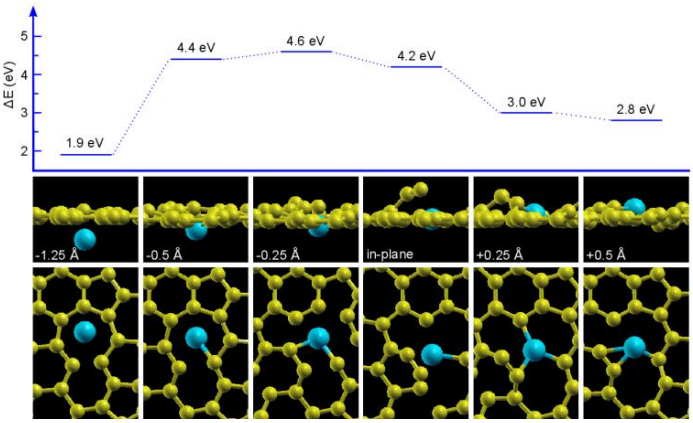

Fig. 1 **Calculated energies and Si diffusion process.** Snapshots of vertical migration process of Si through the warped interfacial layer in cross section (middle panel) and plane (bottom panel) view.

barrier height is calculated to be ~4.7 eV, just slightly larger than interstitial bulk diffusion of ~3.5 eV, but much smaller than the Si self-diffusion of ~ 9.0 eV, making it energetically competitive with the alternative paths for Si diffusion during growth. Based on the understanding of these atomic processes, we have tailored the growth kinetics, and successfully grew pit free graphene on nominal flat SiC in Ar background, as well as on vicinal SiC substrates [Phys. Rev. B **84**, 195455 (2011)].

What made the discovery of this unique warped interfacial structure between graphene and SiC(0001) possible was the use of W tips functionalized with Fe and Cr coating in STM investigations. This functionalization enables the selective imaging of states within a few meV of the Fermi level that are not accessible with conventional W tips, where imaging is typically limited to ~1-2 eV above or below the Fermi level. By modeling these tips using X/W(110) (X=Cr, Fe, W) slabs by DFT calculations, we found that this selectivity is due to the enhanced tunneling from states located at ~0.4-0.6 eV above and below E_F for the Fe/W tips, and 0.3 eV above E_F for the Cr/W tips. Furthermore, we found that the formation of an apex atom is not stable for W/W(110) or Fe/W(110) tips, but is stable for Cr/W(110) tips. This apex atom results in point-like iso-density of states contours for Cr/W tips, enhancing the resolution in the selective imaging of the complex electronic structure of epitaxial graphene on SiC(0001) [PRB **84**, 125425 (2011)].

2. Impact of defects in graphene: resonant scatter as the main cause limiting graphene mobility

We have developed methods to create various types of defect structures by plasma-assisted doping, and carried out comprehensive investigations of the as-modified graphene at the atomic scale. Shown in Fig. 2(a) is an STM image of epitaxial graphene/SiC(0001) after exposure to Ar plasma, where two variants of defect complexes are observed: type *I* structures, where the surrounding graphene lattice is only slightly modified (close-up view in Fig. 2(b)); and type *II*, where strongly enhanced local density of states are seen (close-up view in Fig. 2(c)), with a pronounced $\sqrt{3}\times\sqrt{3}$ periodicity extending over several nanometer around the defect.

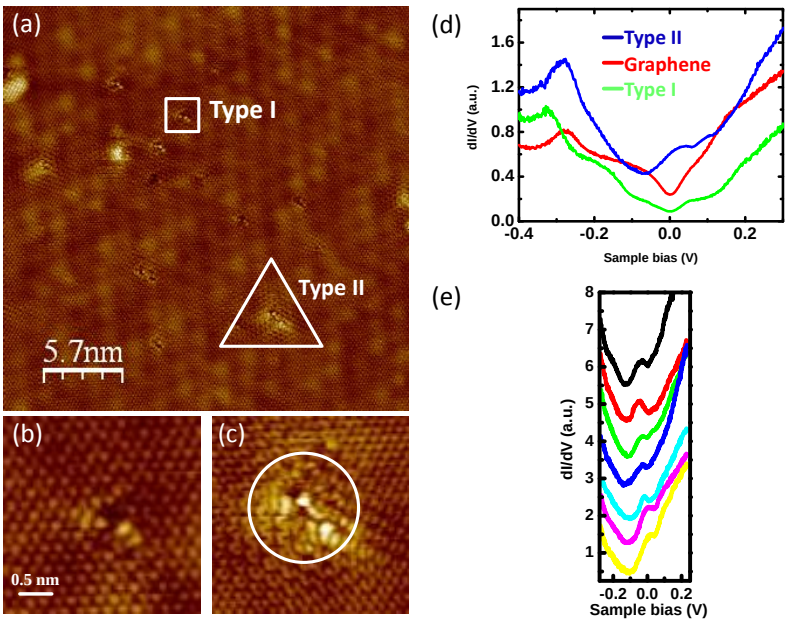

Fig. 2 **STM and tunneling spectroscopy of graphene after modification by Ar plasma.** (a-c) STM images of type *I* and *II* defects (V_s=5 mV, I_t=0.9 nA). (d) Representative dI/dV spectra taken on graphene, type *I* and *II* structures. (e) Spatially resolved dI/dV spectra taken across the type *II* defect.

The modification of graphene electronic structure is further investigated by scanning tunneling spectroscopy. At locations away from the defects, dI/dV spectra exhibit features characteristic of epitaxial graphene/SiC(0001) (Fig. 2(d)), i.e., a Dirac point located ~200 meV below the Fermi energy (V_s = 0), as well as a gap-like feature with a full width at half maximum of ~120 meV centered at E_F, which can be attributed to phonon-assisted inelastic tunneling. Spectra recorded at the type *I* defect show a slightly modified structure, with a state at ~50 meV above E_F. For type *II* complexes, the conductance minimum shifts to ~100 meV below E_F, and a peak appear near the Fermi level, which are better observed in spatially resolved spectra taken within the circled area of the defect (Fig. 2(e)). The observation of state at E_F indicates that the type *II* defect is a resonant scatter.

Energy-dependent dI/dV imaging further reveals that scattering by type *II* complex leads to the reduction in Fermi velocity. Shown in Fig. 3 are STM (a) and simultaneously acquired dI/dV images ((b) & (c)). Clearly evident is the energy-dependent long wavelength (~ several nm) modulations, particularly around the type *II* defects. A two-dimensional Fourier transform (FT) of the dI/dV image in Fig. 3(b) reveals six high-intensity $\sqrt{3}\times\sqrt{3}$ spots (Fig. 3(d)), originated from inter-valley scattering, i.e., wave vector q_1 connecting constant-energy circles at adjacent K_+ and K_- points (Fig. 3(e)); and long wavelength intra-valley scattering, i.e., wave vector q_2 connecting points on a single constant-energy circle.

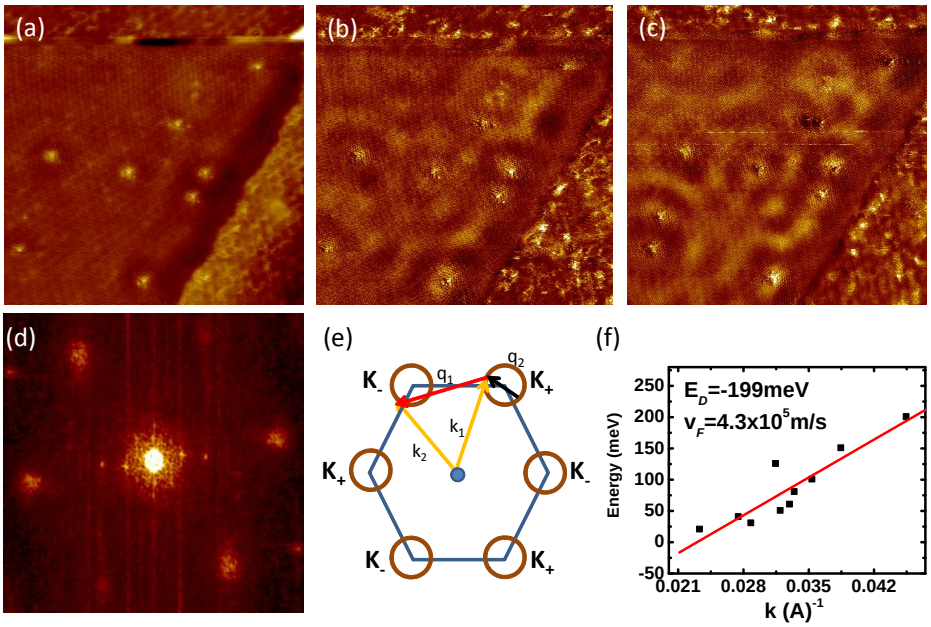

Fig. 3 **dI/dV imaging of defect scattering in graphene.** (a) STM (V_s=-50 mV, I_t=1.0 nA, 45x45 nm^2) and (b) & (c) simultaneously acquired dI/dV images at E_F-50 and E_F-20 meV, respectively, using lock-in technique. (d) FT pattern of image (b). (e) Diagram showing inter- and intra-valley scattering. (f) Dispersion obtained by measuring q_2 as a function of energy.

By measuring the diameter of the circle as a function of bias voltage, the energy dispersion can be determined, as shown in Fig. 3(f). Based on a linear fit, the Fermi velocity is found to be 4.3x10^5 m/s, ~ half of that of typical defect-free graphene. The line intercept at k=0 yields a Dirac point at 199 meV below E_F, consistent with n-type doping of the graphene. Additional measurements on samples with different defect densities establish a direct correlation between an *increase* in the density of type *II* complexes and a *decrease* in the measured Fermi velocity, confirming that these resonant scatters are indeed the leading factor that limits graphene mobility.

Future Plans

We will first continue the experimental work already in progress on the nitrogen doped graphene [Appl. Phys. Lett. **100**, 233119 (2012)] to determine the magnetic properties of N-vacancy complexes using scanning tunneling spectroscopy; as well as experimental and theoretical investigation of the electronic and magnetic properties of hydrogenated graphene.

Second, following our earlier work on the formation of ridges on epitaxial graphene /SiC [Nanotech **20**, 355701 (2009)], we will further investigate the electronic properties of one-dimensional nanowires and zero-dimensional quantum dots confined by the bending and buckling of the graphene using STM imaging and spectroscopy.

References to publications of DOE sponsored research that have appeared in 2010-2012 or that have been accepted for publication

1. "Epitaxial graphene on SiC(0001): More than just honeycomb", Y. Qi, R. H. Rhim, G. F. Sun, M. Weinert, and L. Li, Phys. Rev. Lett. **105**, 085502 (2010).
2. (*Cover article*) "Electron standing waves on GaN(0001) pseudo (1x1): A FT-STM study at room temperature", G. F. Sun, Y. Liu, Y. Qi, J. F. Jia, Q. K. Xue, M. Weinert, and L. Li, Nanotechnology **21**, 435401 (2010).
3. "Epitaxial graphene on SiC(0001): More than just honeycombs", L. Li, book chapter in "Graphene, Theory, Research and Applications" (http://www.intechopen.com/books/show/title/physics-and-applications-of-graphene-experiments).\
4. "Role of functionalized transition-metal coated W tips in STM imaging: Application to epitaxial graphene on SiC(0001)", S. H. Rhim, Y. Qi, G. F. Sun, Y. Liu, M. Weinert, and L. Li, Phys. Rev. B **84**, 125425 (2011).
5. "A novel Si diffusion path for pit-free graphene growth on SiC(0001)", G. F. Sun, S. H. Rhim, Y. Liu, Y. Qi, J. F. Jia, Q. K. Xue, M. Weinert, and L. Li, Phys. Rev. B **84**, 195455 (2011).
6. "Formation of nitrogen-vacancy complexes during plasma-assisted nitrogen doping of epitaxial graphene on SiC(0001)", S. H. Rhim, Y. Qi, Y. Liu, M. Weinert, and L. Li, Appl. Phys. Lett. **100**, 233119 (2012).

Oxide Surfaces: New Tools and Approaches

L. D. Marks

Department of Materials Science and Engineering, Northwestern University, Evanston, IL 60201

Oxide surfaces are an important frontier, with numerous energy-related applications in areas ranging from catalysis to the emerging field of oxide electronics. Despite this, our understanding of oxide surfaces is relatively primitive and more often than not it is assumed that they are essentially the same as the bulk. This is not true. There is a large body of evidence indicating that many oxide surfaces reconstruct with large unit cells, some of which make the reconstructions found for elemental metals or semiconductors look simple. Indeed, the simplest perovskite SrTiO3 has many more reconstructions than silicon, and some of them (those on the (111) surface) are almost certainly more complicated than the Si (111) 7x7 reconstruction. The atomic structure of most of these reconstructions is not known, in large part due to a combination of experimental complications in fabricating them reproducibly and the fact that the workhorses of structure determination for conductors (low energy electron diffraction (LEED) and scanning tunneling microscopy (STM)) are much less effective with insulators.

It would be invaluable to have local information about oxide surfaces where one could read of the atomic structure, independent of whether they are insulators or conductors. For instance, with an oxide supported catalyst or an oxide which is itself used as an active catalyst, knowledge of the detailed atomic structure of the surface as well as its chemical composition is needed to fill the gap between structure and performance paving the way for better catalysts to be engineered. As a second example, there is substantial evidence that the exact structure of the initial surface often plays a critical role in determining the subsequent growth. Without detailed atomic-scale information it is hard to explain or predict properties with much confidence, and one often has to fallback to a trial-and-error approach.

In some cases this surface information is already available from transmission electron microscopy experiments. For instance, at least for small surfaces the profile imaging method [1, 2] can be quite powerful, and the equivalent method for interfaces has been used for many years. However, In a profile or edge-on imaging mode for either a surface or an interface all that is obtained is projected data, and if the structure does not project well along the direction used the results could be incorrectly interpreted. Large unit cell reconstructions which are tilted with respect to the primary zone axes typically used for imaging are common at surfaces, for instance the $\sqrt{5}x\sqrt{5}$ R33.7 reconstruction on the LaAlO3 (001) surface [3] as shown in Figure 1 on the left, and the $\sqrt{13}x\sqrt{13}$ R26.6 reconstruction on the SrTiO3 (001) surface [4] in Figure 1 on the right.

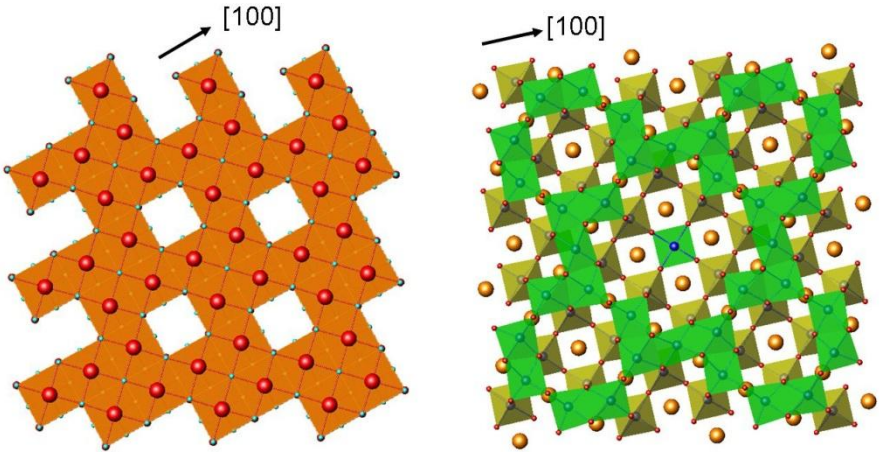

Figure 1: The $\sqrt{5}x\sqrt{5}$ R33.7 reconstruction on the $LaAlO_3$ (001) surface [3] on the left, showing the outer layer with La red and oxygen blue, and the $\sqrt{13}x\sqrt{13}$ R26.6 reconstruction on the $SrTiO_3$ (001) surface [4] in Figure 1 on the right with the five-fold co-ordinated Ti polyhedra in green.

Alternatively one can have reconstructions which are long in one direction such as the series of nx1 reconstructions found on the SrTiO3 (110) surface [5] shown in Figure 2; imaged along [001] the structure would be completely missed, and even orthogonal to this most of the subtleties of the structure would be lost.

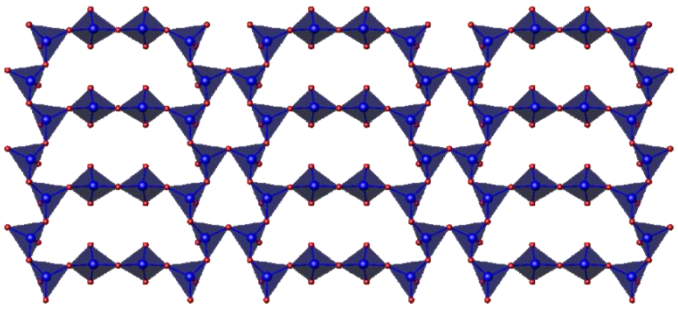

Figure 2: (110) $SrTiO_3$ 4x1 structure [5] showing the tetrahedral TiO_4 units. While something different would be observed in an image, the full richness of the structure would be invisible in a profile image.

Using techniques based upon careful collection of diffraction data coupled with detailed DFT analyses we have made substantial progress in understanding these surfaces over the last few years. For instance, based upon a multi-technique solution for a series of reconstructions on the $SrTiO_3$ (110) surface [6] (see Figure 2) as well as a large reconstruction on $SrTiO_3$ (001) [7] it has became clear that many of the oxide surface structures would be susceptible to water chemisorption, something which is easily missed in refinements from diffraction data (any of TED, LEED or x-ray). Which ones can be predicted from bond-valence analyses [6, 8] which can be done on the back of an envelope and in most cases agrees very well with DFT calculations in the semi-quantitative trends. Based upon the bond-valence analysis we have re-examined the $SrTiO_3$ (001) surface structures, including this as a possibility and using it to guide how water would chemisorb. It would be incorrect to state that all the surfaces have chemisorbed water, but some do. For instance UHV-STM data for the 2x1 reconstruction is in fact more consistent with water chemisorption, plus a structure one can obtain by mild heating is completely consistent with a partially dehydrated surface [9, 10]. More importantly, *all* the different reconstructions have (within error-bars) the same energy with a chemisorbed half monolayer of water [9]. This means that which structure one obtains for $SrTiO_3$ (001) will depend as much or more upon the detailed kinetics of dehydration than just the thermodynamics of which has the lowest free-energy.

However, diffraction is not always an ideal tool and it would be advantageous to have more direct imaging data which can be easily and directly interpreted. There is an "old" technique which can obtain exactly this information – plan view TEM (e.g. [6-13] and references therein). it has been known for about 25 years that one can obtain atomic-scale information which in many cases can be simply interpreted, but it is (or more accurately, was) experimentally very difficult. Very recent experimental data (see later) has demonstrated that this technique has much more potential than at least the PI realized, particularly with modern aberration-corrected instruments. This opens new doors.

There are also new imaging possibilities; since the original work by Zhu *et al* [14] in 2009 it has been clear that the most recent generation of scanning transmission electron microscopy (STEM) instruments can do exceedingly good scanning electron microscopy (SEM), in fact producing images with atomic resolution. What is not (yet) known in detail is exactly what these SEM images are. Are they truly surface images in the same sense that STM images are, or do they see the atomic structure of (for instance) the top 1-2nm? To try and determine this, a definitive test would be to image a sample with a surface reconstruction; quantification of the signal from the reconstruction versus that of the bulk underlying lattice would provide the needed information.

To test this we have produced samples of $SrTiO_3$ (001) and (111) with surface reconstructions, and sent them to J. Ciston and Y. Zhu at BNL so that they could be imaged in plan view, i.e. with the incident electron beam parallel to the plane of the surface, both by "standard" HREM techniques as well as by ADF and SEM imaging.

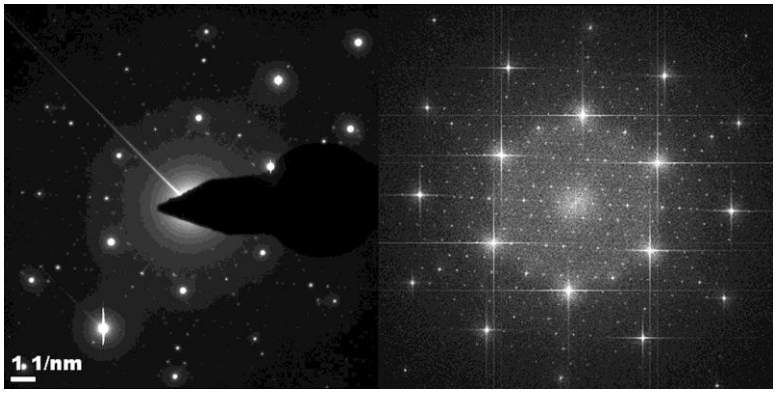

Figure 3: Conventional Diffraction Pattern (left) and the power-spectrum (right), for a $SrTiO_3$ (111) 3x3 surface using HREM. The power spectrum indicates that there is information out to a resolution of about 1.5 Angstroms in the image.

By exploiting techniques which were previously developed for separation of the contributions for the top and bottom surfaces of the Si (111) 7x7 reconstruction [12], we have been able to invert the HREM information as shown in Figure 4 which, after phase extension using diffraction intensities has led to a provisional model for the surface shown in Figure 4 on the right.

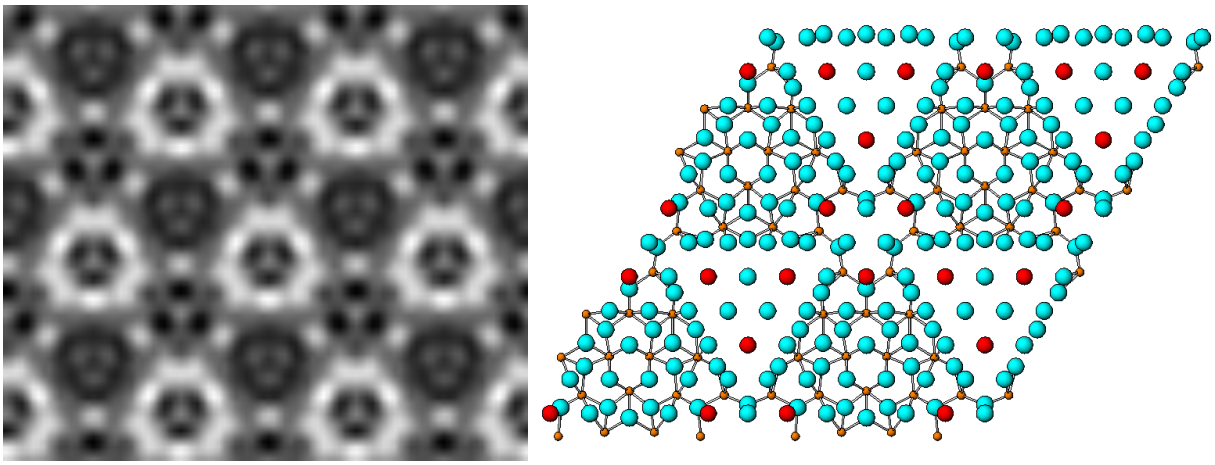

Figure 4: Left, inversion of the raw data from HREM images of the $SrTiO_3$ (111) 3x3 surface, and right, provisional structure with Ti atoms brown, Sr atoms red and O atoms blue.

Future directions will involve taking advantage of recent advancements in electron microscopy to evolve and improve our methods for imaging oxide surfaces by applying them to scientifically relevant materials such as $SrTiO_3$ and $LaAlO_3$. This will not be fully linear research, and an iterative approach may be most fruitful:

1) Obtain experimental image

2) Extract information from the images

3) Combine with diffraction and other information to generate structural models

4) Perform DFT calculations to generate energies and test the feasibility of the structures

5) Do forward simulations to analyze exactly what is in the images

6) Analyze the images and data for artifacts

7) Combine what we find from 2)-6) to generate improved methods of extracting information from the images.

8) Analyze the structural and enegetics results, both the perfect surface and defects, in terms of bond-valence models for oxide surfaces, as well as in terms of packing of octahedral/tetrahedral units similar to what has been found in other cases, as well as for kinetic versus thermodynamic contributions.

References

1. Marks, L.D., *Direct Imaging of Carbon-Covered and Clean Gold (110) Surfaces.* Physical Review Letters, 1983. **51**(11): p. 1000-1002.
2. Marks, L.D. and D.J. Smith, *Direct Surface Imaging in Small Metal Particles.* Nature, 1983. **303**(5915): p. 316-317.
3. Lanier, C.H., J.M. Rondinelli, B. Deng, R. Kilaas, K.R. Poeppelmeier, and L.D. Marks, *Surface reconstruction with a fractional hole: (root 5x root 5)R26.6 degrees $LaAlO_3$(001).* Physical Review Letters, 2007. **98**(8): p. 086102.
4. Kienzle, D.M., A.E. Becerra-Toledo, and L.D. Marks, *Vacant-Site Octahedral Tilings on SrTiO3 (001), the (root 13 x root 13)R33.7 degrees Surface, and Related Structures.* Physical Review Letters, 2011. **106**(17): p. 176102.
5. Enterkin, J.A., A.K. Subramanian, B.C. Russell, M.R. Castell, K.R. Poeppelmeier, and L.D. Marks, *A homologous series of structures on the surface of $SrTiO_3$(110).* Nature Materials, 2010. **9**(3): p. 245-248.
6. Abdelmoula, K., J.J. Metois, and G. Nihoul, *Reconstructed Surface-Structure of (111) Gold Platelets, Observed by High-Resolution Techniques.* Physica Status Solidi a-Applied Research, 1983. **77**(1): p. K5-&.
7. Abdelmoula, K. and G. Nihoul, *Experimental And Theoretical High-Resolution Electron-Microscopy Study Of The (21 X 1) Reconstruction Of Gold (111) Surfaces.* Philosophical Magazine B-Physics of Condensed Matter Statistical Mechanics Electronic Optical and Magnetic Properties, 1988. **58**(4): p. 455-462.
8. Nihoul, G., K. Abdelmoula, and J.J. Metois, *High-Resolution Images Of A Reconstructed Surface-Structure On (111) Gold Platelets - Interpretation And Comparison With Theoretical-Models.* Ultramicroscopy, 1984. **12**(4): p. 353-366.
9. Takayanagi, K., *High-Resolution Surface Study By Insitu UHV Transmission Electron-Microscopy.* Ultramicroscopy, 1982. **8**(1-2): p. 145-161.
10. Haga, Y. and K. Takayanagi, *Single-Atom Imaging in High-Resolution UHV Electron-Microscopy - Bi on Si (111) Surface.* Ultramicroscopy, 1992. **45**(1): p. 95-101.
11. Erdman, N., K.R. Poeppelmeier, M. Asta, O. Warschkow, D.E. Ellis, and L.D. Marks, *The structure and chemistry of the TiO_2-rich surface of $SrTiO_3$ (001).* Nature, 2002. **419**(6902): p. 55-58.
12. Bengu, E., R. Plass, L.D. Marks, T. Ichihashi, P.M. Ajayan, and S. Iijima, *Imaging the dimers in Si(111)-(7x7).* Physical Review Letters, 1996. **77**(20): p. 4226-4228.
13. Xu, P., D. Dunn, J.P. Zhang, and L.D. Marks, *Atomic Imaging of Surfaces in Plan View.* Surface Science, 1993. **285**(1-2): p. L479-L485.
14. Zhu, Y., H. Inada, K. Nakamura, and J. Wall, *Imaging single atoms using secondary electrons with an aberration-corrected electron microscope.* Nature Materials, 2009. **8**(10): p. 808-812.

Nanoscale Imaging of Electrostatic and Magnetic Fields

Martha R. McCartney and David J. Smith
molly.mccartney@asu.edu, david.smith@asu.edu
Department of Physics, Arizona State University, Tempe, AZ 85287

Program Scope

The overall research objectives of this grant are to observe *and* to quantify nanoscale electrostatic and magnetic fields using the technique of off-axis electron holography. There are two major areas of activity:

i) measurement of the 2D electrostatic potential distributions across complex semiconductor heterojunctions and devices; and

ii) investigation of the remanent states and magnetization reversal mechanisms in magnetic thin films and nanostructures.

Recent Progress

i) Electrostatic fields

Our most recent electron holography investigations of electrostatic potential profiles have mainly involved Group IV-IV semiconductor heterojunctions. Our successful study of hole accumulation in epitaxial germanium quantum dots embedded in B-doped silicon has since been followed up by observations of Ge/Si core/shell nanowires in both plan-view and cross-section geometries. Due to the large valence band offset (~500meV) between Ge core and Si shell, hole accumulation occurs in these nanowires, and this charge separation is considered as likely to have applications in high mobility electronic devices. After overcoming practical difficulties involving diffraction contrast effects and determining accurate thickness profiles, it was eventually possible to measure excess phase shifts and to quantify hole densities within the core region as illustrated in Fig 1. Calculations based on a simplified coaxial cylindrical model gave hole densities of $(0.4 \pm 0.2)/cm^2$ in the core region.

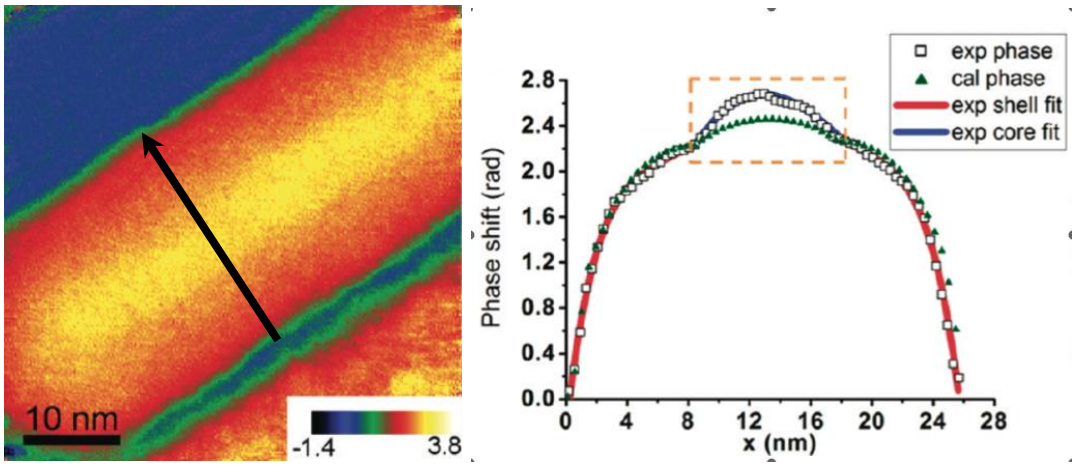

Fig. 1. Reconstructed phase image of SiGe NW with the area used for profile labeled with black arrow with arrow for phase-shift line profile. The result is shown by white squares on the right. The core region is fitted with a polynomial shown in blue and shell region is also fitted with a polynomial shown in red. The green triangles are calculated phase shifts using the projected thicknesses obtained from HAADF intensities. (Li et al., 2011)

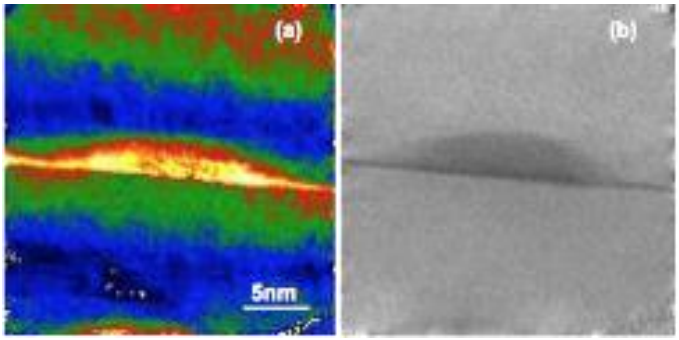

Fig. 2. (a) Phase and (b) amplitude images calculated from the reconstructed hologram of wurzite GaN QD, with base diameter of 23 nm and a height of 3.75nm.

Attention has been directed towards measuring the electric field across individual wurtzite GaN quantum dots (QDs) embedded in an AlN matrix, as shown in Fig. 2 (Zhou et al., 2011). The profiles for individual GaN QDs showed large phase shifts which could be understood in terms of spontaneous polarization and piezoelectric fields and the accumulation of positive and negative charge at the GaN/AlN interfaces. Local fields with magnitude of 7.8 ± 2 MV/cm were measured across the center of a GaN QD, in reasonable agreement with reported simulations. In related work, we have also used electron holography to investigate polarization-induced charge distributions at homogeneous zincblende/wurtzite heterostructural junction in ZnSe nanobelts (Li et al., 2012).

Ongoing studies have involved doped Si and Si/Ge nanowires (NWs), which have electrical transport properties that are considerably different from those of bulk materials due to their one-dimensional structure. Electron holography provides an effective approach to measuring electrostatic profiles along individual NWs. However, we have encountered difficulties attributable to charging of the Au catalyst particles located at the end of the NW, which need to be overcome before reliable *p-n* junction profiles can be determined. Finally, together with former student Suk Chung, we have established an active collaboration with the group of Professor Marek Skowronski at Carnegie-Mellon University (CMU) wherein electron holography is being used to investigate charge accumulation and depletion widths along threading defects in doped SiC samples. The first paper arising from this collaboration was published early in 2011 (Chung et al., 2011).

ii) Magnetic fields

The second major emphases of our electron holography investigations are magnetic thin films and nanostructures, which are of much fundamental and topical interest. Off-axis electron holography represents a powerful tool for evaluating magnetization states and controlling reversal mechanisms as lateral dimensions are reduced since the technique can be used both to determine remanent states of individual elements *and* to follow hysteresis cycles *in situ* with nanoscale spatial resolution. We have continued our investigation of the effects of vortex chirality and shape anisotropy on the reversal mechanisms occurring in notched Py nanowires (He et al., 2010). In situ studies of domain-wall (DW) nucleation and propagation for such nanowires has been the subject of intense activity due to the proposed development of related memory and logic devices based on this configuration. Using notched Permalloy nanowires as test objects, we used electron holography to study various aspects of the field-driven DW motion, including nucleation, injection, pinning and depinning. The relative chirality (i.e., sense of field rotation) of the notch, the domain wall configuration and the nucleation pad were found to have major influences in determining the characteristics of the DW behavior. It was found that the notch either served as a potential well where the transverse DW was trapped, or else it had no obvious effect on the reversal process, as indicated by the pass-through of the transverse DW. The nature of the DW chirality causing this asymmetrical DW motion could be useful for device

design, and extensive experiments are being planned for the future. Micromagnetic simulations using the OOMMF software were also used to confirm the overall trends of these experimental results.

Our holography studies of magnetic materials were temporarily stalled due to recurring instabilities in the Lorentz lens which is essential for samples requiring field-free imaging and/or large-field-of-view observations. Finally, a replacement Lorentz coil was obtained by the microscope manufacturer from a trade-in instrument, thus enabling these types of studies to be resumed. Initial attention was given to CoPd thin films and nanopillars, which are expected to display pronounced perpendicular magnetic anisotropy that is of much topical interest for enhanced storage applications, as well as Ga(Mn)As thin films and nanowires, which have potential spintronics applications. Samples of GaAs/Fe core-shell nanowires have also been examined: initial results suggest non-intuitive remanent states that are not yet well-understood. Finally as shown by the example in Fig. 3, the magnetic behavior of chains of Co/CoO nanoparticles are being investigated.

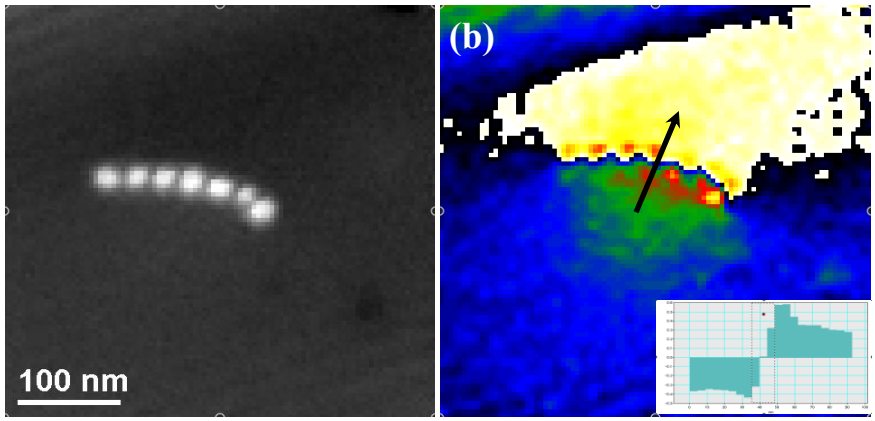

Fig. 3 (a) Holographic phase image of small Fe particles arranged in a chain. (b) Magnetic component of the phase signal obtained by acquiring reversed magnetic orientation holograms and subtracting the phases. Inset shows magnetic flux confined in the particles as steep ramp extending ~13 nm.

Future Plans

Our research over the next year will concentrate on the electrostatic potential profiles developed across undoped and doped heterojunctions, especially highly doped materials with steep concentration profiles which are difficult to characterize using alternative techniques. We will examine further Si/Ge core/shell nanowires with and without B doping in order to gain a better understanding of band-bending effects and charge accumulation. We will also carry out electron holography observations of ZnTe-based thin films, which are of potential interest for ultrahigh-efficiency multijunction solar cells, in particular to provide better insight into the effects of growth and annealing conditions on the potential profiles associated with vertical and lateral *p-n* junctions. Input from electron holography could be decisive in facilitating invention of novel optoelectronic devices, especially for solar-cell applications based on multiple III-V/II-VI heterojunctions.

The second focus of the research over the next year relates to quantifying the nanoscale fields of magnetic thin films and nanostructures:

a) Pronounced perpendicular magnetic anisotropy, as achieved in multilayered Co/Pd and Co/Ni thin films and nanopillars, potentially represents the basis for enhanced memory storage in hard-disk drives. However, changes in magnetic behavior such as reversal mechanisms, and intrinsic properties such as coercivity, that are attributable to reduced particle dimensions and materials defects, need to be identified and then controlled in order for reliable device

applications to be achieved.

b) Domain wall (DW) motion in ferromagnetic nanowires, controlled either by magnetic fields or applied current, is attracting much worldwide attention because of possible enhanced logic and memory storage applications. Information from electron holography about the nucleation, pinning and propagation of individual DWs should greatly assist progress towards a viable device design.

These electron holography observations will be made using an advanced transmission electron microscope equipped with a field-emission electron source that provides highly coherent incident illumination. This instrument is also equipped for Lorentz microscopy and digital recording, as well as permitting imaging in field-free conditions at the sample, which is essential for studying the remanent states of magnetic materials. Conventional transmission electron microscopy and microanalysis with state-of-the-art aberration-corrected electron microscopes will be used as needed to provide complementary information about microstructure and elemental composition that is required for correlation with the nanoscale holography measurements.

References to journal publications of DOE-sponsored research for period 2010-2012:

(invited review) M. R. McCartney, N. Agarwal, S. Chung, D. A. Cullen, M-G. Han, K. He, Luying Li, H. Wang, L. Zhou, D. J. Smith (2010) "Quantitative phase imaging of nanoscale electrostatic and magnetic fields using off-axis electron holography", Ultramicroscopy, **110**, 375-382.

K. He, D. J. Smith, M. R. McCartney (2010) "Effects of vortex chirality and shape anisotropy on magnetization reversal of Co nanorings" (invited) Journal of Applied Physics, **107**, Art. # 09D307.

S. Chung, S. R. Johnson, D. Ding, Y. H. Zhang, D. H. Smith, M. R. McCartney (2010) "Quantitative dopant profiling of p-n junction in InGaAs/AlGaAs light-emitting diode using off-axis electron holography", Journal of Vacuum Science & Technology B, **28**, 1 C1D11–C1D14.

Luying Li, D. J. Smith, E. Dailey, P. Madras, J. Drucker and M.R. McCartney (2011) "Observation of hole accumulation in Ge./Si core/shell nanowires using off-axis electron holography", Nano Letters, **11**, 293-297.

L. Zhou, D. J. Smith, M. R. McCartney, et al., (2011) "Measurement of electric field across individual wurtzite GaN quantum dots using electron holography", Applied Physics Letters, **99** , Art. #101905.

Suk Chung , Ronen A. Berechman , Martha R. McCartney , and Marek Skowronski (2012) "Electronic structure analysis of threading screw dislocations in 4H–SiC using electron holography", J. Appl. Phys. **109**, 034906.

Luying Li, L. Jin, J. Wang, David J. Smith, W-J. Yin, Yanfa Yan, Hongqian Sang, Wallace C. H. Choy, and M. R. McCartney (2012) "Polarization-Induced Charge Distribution at Homogeneous Zincblende/Wurtzite Heterostructural Junctions in ZnSe Nanobelts", Adv. Mater. 2012, **24**, 1328–1332.

In Situ Analytical Electron Microscopy for Probing Electrochemistry at NanoScale

Principle Investigator: Dr. Shirley Meng
Mailing Address: 2703 Atkinson, MC0448, Department of NanoEngineering, University of California San Diego
Email: shirleymeng@ucsd.edu
Student and Postdoc: T. McGilvray and Dr. D. Santhanagopalan
Collaborators: Dr. Feng Wang and Dr. Jason Graetz (BNL); Dr. Nancy Dudney (ORNL)

Program Scope and Objectives

Lithium ion batteries have been the key component of consumer electronics and will play a crucial role in environmentally friendly transportation, such as electric vehicles in the near future. To continuously improve the energy density and power density of lithium ion battery (LIB) electrodes, it is becoming increasingly important to understand the complex dynamic processes that occur during electrochemical cycling. Traditional characterization methods fall short in describing the actual processes occurring during electrochemical cycling, such as, how does the lithiation front move within an electrode as a function of state of charge and charging rate? This work aims to observe these processes in a high resolution analytical transmission electron microscope equipped with energy dispersive X-ray spectroscopy (EDXS) and Electron Energy Loss Spectroscopy (EELS). To enable the observation of lithiation front in an all solid state thin film battery by STEM and EELS, we developed a comprehensive strategy with Focused Ion Beam (FIB) to fabricate electrochemically active "nano-battery"[1-3], with STEM/EELS to quantitatively probe the electrochemistry at the electrode/electrolyte interfaces.

Summary of Recent Progress

Fabrication of all solid-state thin film battery by PLD

Formation of the spinel structure at 600°C using the pulsed laser deposition (PLD) method showed a dense yet relatively faceted crystal morphology with well-defined grains ranging between 100-200 nm. The grains exhibited an octahedral-type morphology reflecting the cubic spinel structure as shown in Figure 1(a). Figure 1(b) shows the XRD patterns for the NiMn spinel thin film deposited on a SS substrate at 600°C. All diffraction peaks from the thin film electrode could be indexed to the spinel structure with an Fd-3m space group and the SS substrate. A (111) textured structure is seen for the thin film, as evidenced by the XRD pattern. The electrochemical properties of the NiMn spinel thin film were investigated in lithium half-cells. The charge/discharge profiles between 3.6 and 5.0V are shown in Figure 2(a). The NiMn spinel thin film electrodes have a reversible capacity of 125 mAh/g. For the thin film NiMn spinel, when the rate increases from C/4 to 4C, there is only a relatively small capacity loss of around 20% (Figure 2(b)). Such rate capability is superior to that of the powder NiMn spinel samples, particularly for the reason that there is absolutely no conduction additive in the NiMn thin film sample.

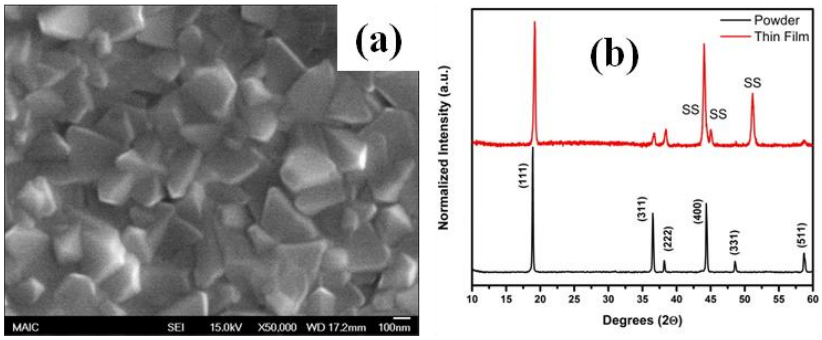

Figure 1: (a) SEM image of the $LiNi_{0.5}Mn_{1.5}O_4$/SS and (b) XRD patterns of $LiNi_{0.5}Mn_{1.5}O_4$ thin film and powder for comparison. [1,2]

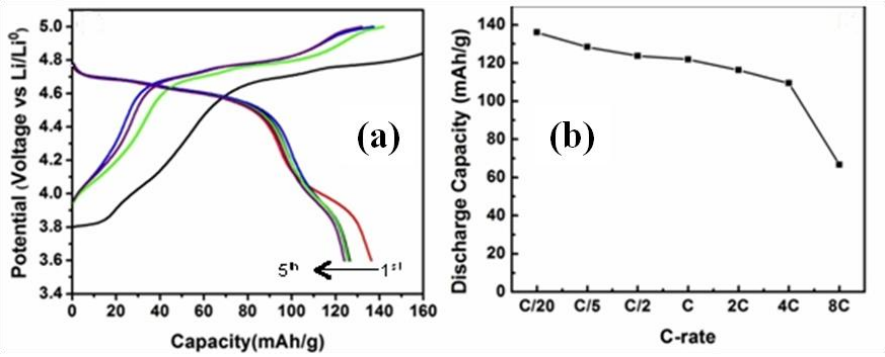

Figure 2: Electrochemical properties of $LiNi_{0.5}Mn_{1.5}O_4$ thin film (a) charge-discharge curves for 5 different cycles and (b) discharge capacity as a function of c-rate. [2]

Anode TiO_2 thin films were deposited on stainless steel at different temperatures. The films are composed of well-defined grains in a range between 50 and 100 nm as shown in Figure 3(a). Figure 3(b) shows the XRD patterns of the TiO_2 thin film deposited on stainless steel substrate at different temperatures. The film is amorphous. The first discharge/charge profiles between 3.5 and 1.0V are shown in Figure 3(c). The plateau around 1.75V for TiO_2 thin film corresponds to the occurrence of the two phase equilibrium of Lithium-poor ($Li_{0.01}TiO_2$) and Lithium-rich ($Li_{0.6}TiO_2$) domains.

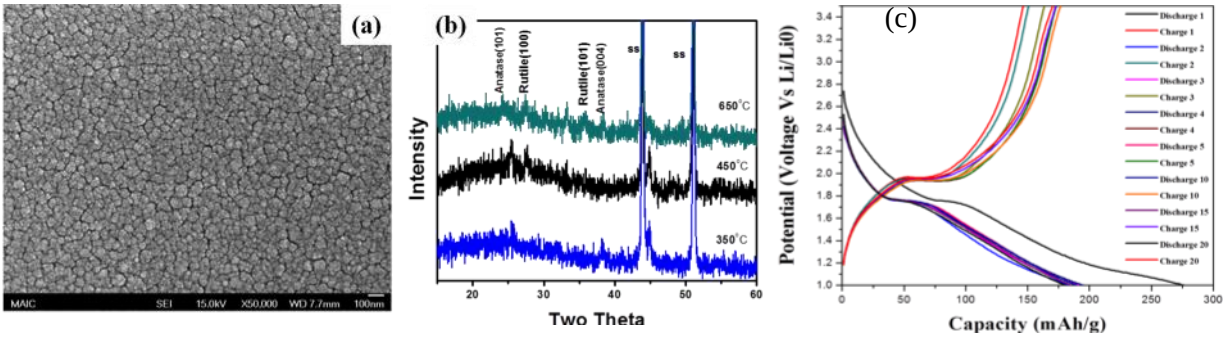

Figure 3: (a) SEM image of the TiO_2 thin-film and (b) XRD Pattern of TiO_2 thin films deposited at different temperatures and (c) Typical charge/discharge curve of the TiO_2 thin film [4]

The all-solid-state thin film battery (TiO_2/LiVSiO/$LiNi_{0.5}Mn_{1.5}O_4$/Stainless Steel) was prepared by PLD. First, the $LiNi_{0.5}Mn_{1.5}O_4$ thin films were deposited on stainless steels substrate (SS). The cross section of TiO_2/$LiNi_{0.5}Mn_{1.5}O_4$ / $L_{3.4}V_{0.6}S_{0.4}O_4$/SiO_2/Si stack was fabricated by focus ion beam. The cross section of all-solid-state thin film battery was examined by SEM as shown in Figure 4. The thickness of the TiO_2 anode, LVSO solid electrolyte and $LiNi_{0.5}Mn_{1.5}O_4$ cathode are 150 nm, 900 nm and 300 nm respectively. The total thickness of the stack is about 1.5 μm, which is suitable for TEM/EELS investigation. Moreover, there were no crack or pin holes even after the anode TiO_2 deposition. In spite of the FIB processing and the STEM observations, the solid electrolyte remains amorphous as examined by diffraction in TEM. The interfaces between the layers are found to be sharp and well defined.

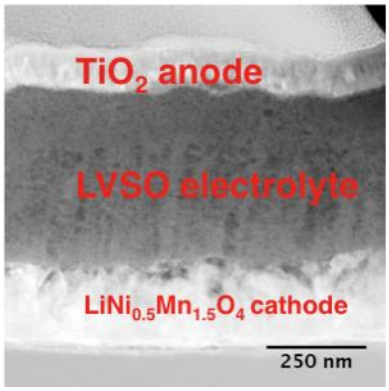

Figure 4: Cross-sectional SEM image of the all-solid-state battery prepared by PLD and subsequent FIB

Minimization of electron and ion beam damage

Preserving the electrochemical activity upon FIB fabrication process is crucial for in situ TEM study. The requirement of such preservation depends on several FIB parameters during fabrication, which needs to be optimized. To do this we used the well known electrochemistry with the solid state batteries ($LiCoO_2$/LiPON/a-Si) made by Dudney at ORNL [3]. During the FIB milling process the

ion beam damages the electrolyte which is very sensitive and the huge re-deposition across the stack are the important factors affecting the electrochemical activity. We have developed a set of procedure to optimize the FIB process which shows electrochemical activity in fabricated cross sectional nano-batteries. Figure 5 below shows three different voltage profiles, (i) very low in voltage of about 0.5 mV which is due to shorted stack of the micro-battery (ii) low voltage of about 1.5 V compared to the expected value indicating un-optimized FIB conditions and (iii) the 3.6 V plateau which was expected indicating a proper electrochemical activity under optimized FIB fabrication conditions. The inset of the Figure 5(a) shows the full charging cycle where the voltage plateau remains at 3.6 V. The effect of two-step FIB processes is shown in Figure 5 (b), after the first step the layers are not observed due to the re-deposition and after the second step all the layers clearly seen.

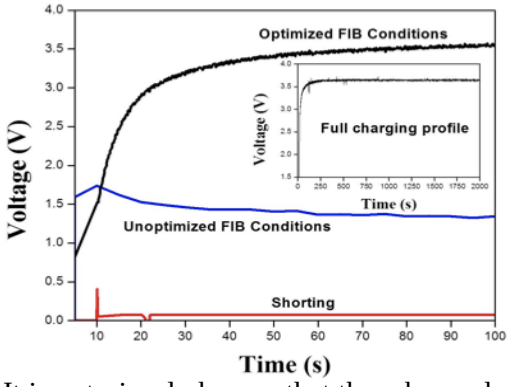

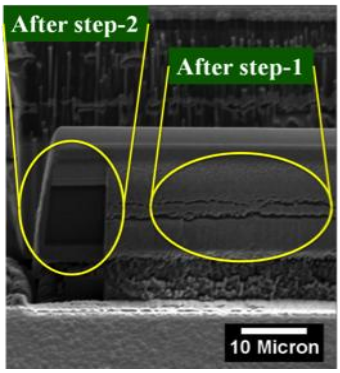

Figure 5: (a) Optimized FIB fabrication condition with preserved electrochemical activity of all-solid-state micro-battery (b) two step fabrication process. [5]

It is notoriously known that the e-beam damages the LiPON solid electrolyte during STEM and EELS investigation. Figure 6 (a) below clearly shows that for longer collection times, the Lithium K-edge in the EELS spectrum is affected while the Phosphorous L-edge is unaffected (shown in the inset). STEM imaging also shows that the electrolyte eventually gets damaged with longer spectrum collections times as shown in Figure 6 (b left). A decrease in damage can be achieved with limited exposure time. More importantly, all-PLD thin-film battery samples with LVSO electrolyte show better stability over e-beam exposure (results not shown here) before and after EELS mapping with almost no visible damage at all.

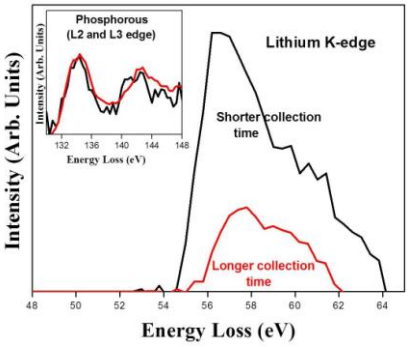

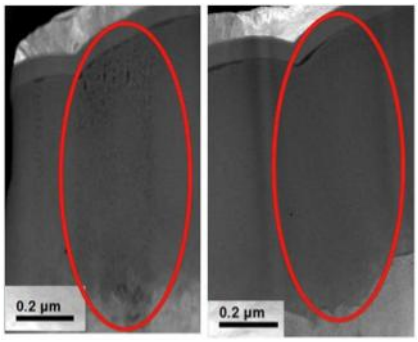

Figure 6: (a) EELS spectrum showing the effect of longer collection time and (b) showing the e-beam damage due to longer collection time (left) and shorter collection time (right). [5]

In-situ biasing in the FIB and *ex-situ* TEM study

The cross section prepared for TEM investigation is characterized by imaging, diffraction and electron energy loss spectroscopic (EELS) methods. Figure 7 below gives a comparison of TEM images and EELS elemental mapping of the pristine, charged and over-charged cross sections. Li signal intensity maps are a way to qualitatively show the distribution of Li over all parts of the samples. For pristine sample, the most intense signal comes from the bulk of the cathode slightly away from the electrode/electrolyte interface. In the charged sample, there is a localized high Li intensity at the $LiCoO_2$/LiPON interface (Figure 7(b)), indicating that this interface has relatively slow Li mobility, likely due to the interfacial impedance. When a large amount of Li is driven to the a-Si anode, the deleption of the LiPON electrolyte can be clearly observed, see Figure 7(c). We estimate that the Li chemical diffusion rate in the LiPON bulk is two to three magntitude higher than that at the

$LiCoO_2$/LiPON interface. Our study clearly shows the lithiation front inside the nanoscale solid state batteries and shed lights on ion transport at the solid-solid electrode/electrolyte interfaces.

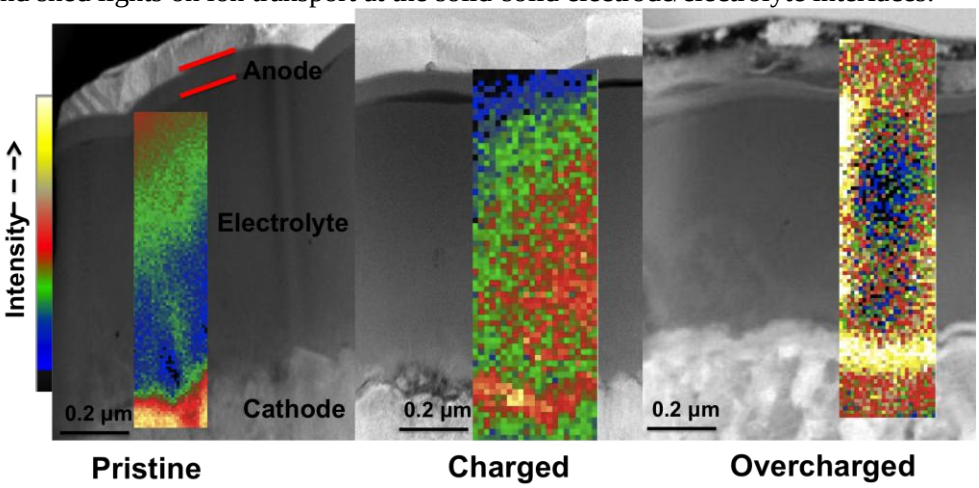

Figure 7: Li intensity mappings for pristine, charged, and overcharged samples. [6]

Future Plans

Several major steps toward the *in-situ* TEM observation of electrochemical dynamics have been successfully completed in the last two years. Bottleneck issues have been overcome and the modifications have been implemented as described in previous sections. With the combination of the expertise, instrumentation and protocol shown in the above section, *in-situ* TEM observation of electrochemical phenomena in an all solid state nano-battery will be used to gain a fundamental understanding of the dynamic chemical and electronic processes at the solid/solid interfaces of the electrochemical cells. The planned future activities for the next three years are focused on the following aspects:

- Choice of new electrolytes and optimization of thin film battery fabrication.
- Diagnostics and quantification of e-beam damage and the development of strategies to minimize e-beam and ion beam damage
- Observation of dynamic electrochemistry at nano-scale using *in-situ* TEM

Paper published and submitted

1. M. Yang, B. Xu, J. Cheng, C. Pan, B. Hwang, and Y. S. Meng, "Electronic, Structural, and Electrochemical Properties of $LiNi_xCu_yMn_{2-x-y}O_4$ ($0 < x < 0.5$, $0 < y < 0.5$) High-Voltage Spinel Materials", **Chemistry of Materials**, 2011, 23(11), 2832-2841.

2. K. Carroll, M. Yang, G. M. Veith, N. J. Dudney, Y. S. Meng, "Intrinsic surface stability in $LiMn_{2-x}Ni_xO_{4-\delta}$ (x=0.45, x=0.5) high voltage spinel materials for lithium ion batteries", **Electrochemical and Solid State Letters**, 2011, 15(5), A72-A75.

3. Y. S. Meng, T. Mcgilvray, M. Yang, D. Gostovic, F. Wang, D. Zeng, Y. Zhu, J. Graetz, "In Situ analytical electron microscopy for probing nanoscale electrochemistry", The Electrochemical Society **Interface**, 2011, 20 (3), 49-53 (**invited featured article**).

4. M. Yang, K. Carroll and Y.S. Meng, "Thin film $Li_4Ti_5O_{12}$ spinel material as high rate anode for all solid state lithium ion batteries", in preparation. 2012.

5. D. Santhanagopalan, T. McGilvray, M. Yang, N. Dudney, F. Wang, J. Graetz and Y. S. Meng, "Preserving functionality of thin-film micro-batteries fabricated by focused ion beams", **Microscopy and Microanalysis**, 2012, submitted.

6. T. McGilvray, F. Wang, D. Santhanagopalan, M. Yang, J. Graetz, N. Dudney, Y.S. Meng, "Probing electrolyte-electrode interfaces upon charging in an all solid-state battery", **Nano Letters**, 2012, submitted.

Program Title: **Structure and Dynamics of Domains in Ferroelectric Nanostructures – In-situ TEM Studies**

Principal Investigator: Xiaoqing Pan
Address: Department of Materials Science and Engineering
University of Michigan
2010 H.H. Dow Building
2300 Hayward Street
Ann Arbor, MI 48109
Tel: 734-647-6822;
E-mail: panx@umich.edu

Program Scope:

The main goal of the proposed research is to explore the structure and dynamic behaviors of ferroelectric domains in ferroelectric thin films and nanostructures by advanced transmission electron microscopy (TEM) techniques in close collaboration with phase field modeling. The experimental techniques used include aberration-corrected sub-Å resolution TEM and *in-situ* TEM using a novel scanning tunneling microscopy (STM) - TEM holder which allows the direct observation of nucleation and dynamic evolution of ferroelectric domains under applied electric field. Specifically, we propose (1) to study the roles of static electrical boundary conditions and electrical charge in controlling the equilibrium domain structures of $BiFeO_3$ thin films with controlled substrate constraints, (2) to explore the fundamental mechanisms of ferroelectric domain nucleation, growth, and switching under an applied electric field in both uniform thin films and nanofabricated nanostructures, and to understand the roles of crystal defects such as dislocations and interfaces in these processes, (3) to understand the physics of ferroelectric domain walls and the influence of defects on the electrical switching of ferroelectric domains. The nucleation and dynamic evolution of ferroelectric domains observed by *in-situ* TEM under applied external electric field are quantitatively analyzed and directly compared with phase field simulations in Professor Long-Qing Chen's group at Penn State University.

Recent Progress

We have extensively explored dynamic nanoscale ferroelectric switching phenomenon using the techniques, equipment, and software analysis tools previously developed under this project. Our work on ferroelectric switching has been published in several journals, including *Science*, Nature Communications, and Advanced Materials, and is highlighted in the following. Details of these results beyond this overview, including real-time video, are available from these publications which are cited below.

<u>Interface assisted switching in inhomogeneous fields</u>

We characterized the nanoscale ferroelectric switching *in situ* and in real-time for two ferroelectric model systems: (rhombohedral phase) $BiFeO_3$ and (tetragonal) $PbZr_{0.2}Ti_{0.8}O_3$. The respective nanoscale switching was found to be the same as for large-scale measurements: a 71° rotation of the out-of-plane axis for $BiFeO_3$ and 180° polarization reversal for $PbZr_{0.2}Ti_{0.8}O_3$. Thin films of these materials were switched via a local electric field from a surface probe (Fig. 1a) while being imaged by TEM. Despite the localization of the applied field by the probe, domain nucleation and switching were influenced primarily by built-in fields from the Schottky junctions formed at the ferroelectric/electrode contacts. Inclusion of these fields (compare Fig.

1b to Fig. 1a) significantly modifies the electrostatic energy landscape, determining the nucleation site for both $BiFeO_3$ and $PbZr_{0.2}Ti_{0.}8O_3$. In the n-type $BiFeO_3$ and p-type $PbZr_{0.2}Ti_{0.8}O_3$ studied here, these built-in electric fields are opposite in sign, negative (toward the electrode) and positive (toward the free surface), respectively. Thus nucleation of 'up' domains occurs at the bottom interface of $BiFeO_3$ (Fig. 1c), but the top interface for $PbZr_{0.2}Ti_{0.}8O_3$ (Fig. 2), and vice-versa for 'down' domains. The nucleation behavior of $BiFeO_3$ was especially anomalous, as demonstrated in Fig. 1c through a chronological TEM image series. We observed two-step switching behavior which would manifest in typical electrical measurements with a too-low transient switching current, possibly misinterpreted as incomplete switching or a reduced polarization, and growth kinetics from latent nuclei, although we have shown this is not the case.

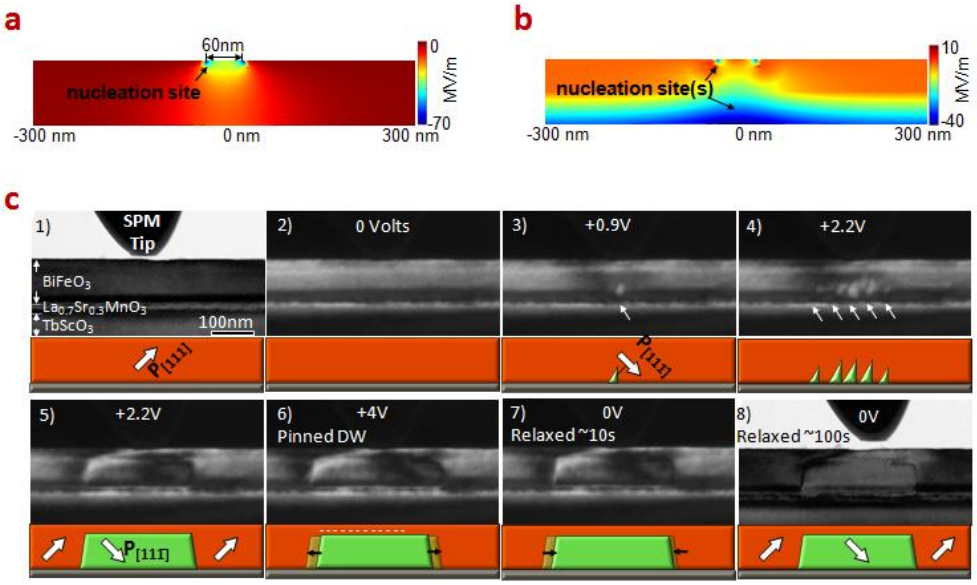

Fig. 1. Interface assisted switching – **a,** Out of plane electric field applied against the polarization direction of a monodomain $P_{[111]P}$ $BiFeO_3$ film results in a large electrostatic energy at the film surface beneath the tip. **b,** The out-of-plane field including a Schottky junction at the bottom electrode **c,** A chronological TEM image series depicts the formation of a $P_{[11\bar{1}]P}$ domain. Nucleation occurs at the $La_{0.7}Sr_{0.3}MnO_3$ electrode interface at 0.9 V (1-3) producing a metastable stationary domain. Additional bias increases the size and number of these domains up to 2.2 V (4). At 2.2 V the domains merge and propagate forward just short of the surface (5) where they remain pinned along a $(001)_P$ plane even after the voltage is nearly doubled (6).

The in-situ switching dynamics of $PbZr_{0.2}Ti_{0.8}O_3$ films, shown for a full cycle in Fig. 2, follows the contemporary switching model for ferroelectric materials: surface nucleation, rapid forward growth forming sharp needle-like domains, and after reaching the opposite interface the domain walls relax to neutral equilibrium vertical planes and propagate slowly laterally. The hysteresis loop in Fig. 2a shows how the built-in fields create several asymmetries in this switching behavior including opposite nucleation sites, as mentioned above, and dissimilar coercive fields and switching rates. The later point is highlighted in Fig. 2b which shows the domain extent versus time. Like the anomalous behavior in $BiFeO_3$ the disparity in switching rates can be explained by the inhomogeneity in the electric field along the film depth. Specifically the 'down' domain is opposed by the positive field from the bottom electrode Schottky contact which slows its progress (Fig. 2b top). In contrast, a similar effect does not

occur for the 'up' domain since the negative field at tip-contact is countered by the tip-induced field enhancement in this region and switching occurs rapidly (Fig. 2b bottom).

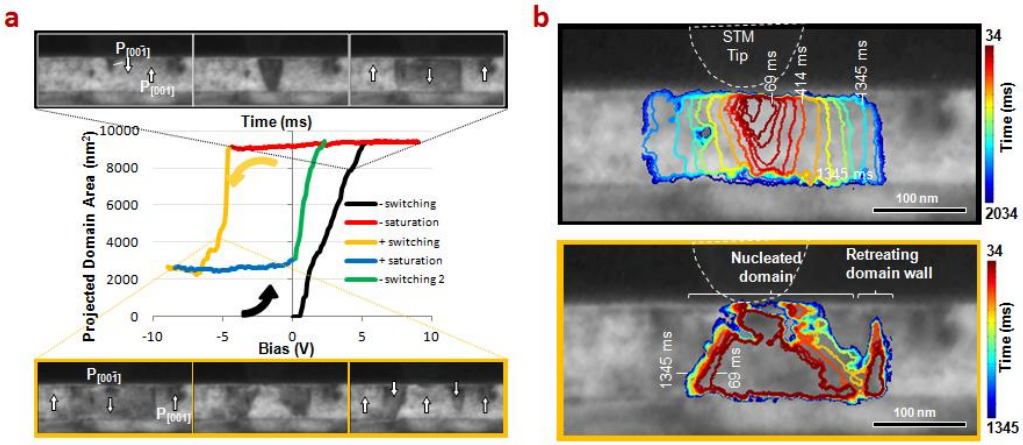

Fig. 2. Interface assisted switching – **a,** Chronological TEM image series of local polarization reversal in $PbZr_{0.2}Ti_{0.8}O_3$ as it traverses the hysteresis loop shown at center. The loop was derived from the total switching domain area. **b,** The same two switching events showing the domain extent versus time.

Domain wall pinning from defects

Our in-situ switching work provides direct experimental support to the contemporary theory for domain wall pinning from defects as a source of ferroelectric fatigue. We have observed defect-domain wall interactions in both $PbZr_{0.2}Ti_{0.8}O_3$ and $BiFeO_3$ films, with the most significant interactions occurring in $BiFeO_3$ where such pinning frequently leads to incomplete switching. The predominant mechanism is for switching domains to become pinned along $(001)_P$ planes. Such pinning sites exhibit perfect repeatability during cyclic switching pointing to fixed defects. These sites have no apparent crystalline defects, cation disorder, nor any difference in the film thickness or sample surface topography to account for the incomplete switching. This points to charged oxygen vacancy planes as the probable cause for pinning the negatively charged domain walls.

We have also observed pinning from extended defects. In a $PbZr_{0.2}Ti_{0.8}O_3$ film we found that dislocations exert a weak pinning force on domain wall motion. This is evidenced by an increase in the domain wall velocity towards the dislocation and a decrease afterwards which is not mirrored on the opposite side. We also observed that the interface domains of $BiFeO_3$ often include point or columnar defects along their lateral edges such as the impurity. However, the causality in this case is not clear, such impurities are a possible contribution to the formation of the interface domains. Both of these affected domain walls are neutrally charged so their interaction with the defects is through strain. However, local strained regions from dislocations in both $PbZr_{0.2}Ti_{0.8}O_3$ and $BiFeO_3$ are not observed to be a significant pinning site for these switching paths, domains readily pass through them. Instead, the aforementioned planar pining of charged domains is the dominant mechanism.

List of publications (2010-2012):

1. P. Gao, C.T. Nelson, J.R. Jokisaari, S.H. Baek, C.W. Bark, Y. Zhang, E.G. Wang, D.G. Schlom, C.B. Eom, and X.Q. Pan, "Direct observations of retention failure in ferroelectric memories", *Adv. Mater.* **24**, 1106-1110 (2012).

2. H. Lu, X. Liu, J. D. Burton, C. W. Bark, Y. Wang, Y. Zhang, D. J. Kim, A. Stamm, P. Lukashev, D. A. Felker, C. M. Folkman, P. Gao, M. S. Rzchowski, X. Q. Pan, C. B. Eom, E. Y. Tsymbal, and A. Gruverman, "Enhancement of Ferroelectric Polarization Stability by Interface Engineering," *Adv. Mater*. **2012**, *24*, 1209–1216 (2012).
3. C.T. Nelson, P. Gao, J.R. Jokisaari, C. Heikes, C. Adamo, A. Melville, S.H. Baek, C.M. Folkman, B. Winchester, Y.J. Gu, Y.M. Liu, K. Zhang, E.G. Wang, J.Y. Li, L.Q. Chen, C.B. Eom, D.G. Schlom, and X. Q. Pan, "Domain dynamics during ferroelectric switching", *Science* **334**, 968-971 (2011).
4. P. Gao, C. T. Nelson, J. R. Jokisaari, S.H. Baek, C.W. Bark, Y. Zhang, E.G. Wang, D.G. Schlom, C.B. Eom, and X.Q. Pan, "Revealing the role of defects on ferroelectric switching with atomic resolution", *Nat. Commun.* 2:591 doi: 10.1038/ncomms1600 (2011).
5. S. H. Baek, J. Park, D. M. Kim, V. Aksyuk, R. R. Das, S. D. Bu, D. A. Felker, J. Lettieri, V. Vaithyanathan, S. S. N. Bharadwaja, N. Bassiri-Gharb, Y. B. Chen, H. P. Sun, C. M. Folkman, H. W. Jang, D. J. Kreft, S. K. Streiffer, R. Ramesh, X. Q. Pan, S. Trolier-McKinstry, D. G. Schlom, M. S. Rzchowski, R. H. Blick, C. B. Eom, "Giant Piezoelectricity on Si for Hyperactive MEMS," *Science* **334**, 958 (2011).
6. H.W. Jang, D.A. Felker, C.W. Bark, Y. Wang, M.K. Niranjan, C.T. Nelson, Y. Zhang, D. Su, C.M. Folkman, S.H. Baek, S. Lee, K. Janicka, Y. Zhu, X.Q. Pan, D.D. Fong, E.Y. Tsymbal, M.S. Rzchowski, C.B. Eom, "Metallic and insulating oxide interfaces controlled by electronic correlations," *Science*, **331**, 886 (2011)
7. C.T. Nelson, B.M. Winchester, Y. Zhang, S.J. Kim, A. Melville, C. Adamo, C.M. Folkman, S.H. Baek, C.B. Eom, D.G. Schlom, L.Q. Chen, X.Q. Pan, "Spontaneous vortex nanodomain arrays at ferroelectric heterointerfaces," *Nano Letters*, **11**, 828 (2011)
8. C. W. Bark, D. A. Felker, Y. Wang, Y. Zhang, H. W. Jang, C. M. Folkman, J. W. Park, S. H. Baek, H. Zhou, D. D. Fong, X. Q. Pan, E. Y. Tsymbal, M. S. Rzchowski, and C. B. Eom, "Tailoring a two-dimensional electron gas at the $LaAlO_3$/$SrTiO_3$ (001) interface by epitaxial strain", *Proceedings of the National Academy of Science (PNAS)* **108**, 4720-4724 (2011).
9. J.W. Park, D.F. Bogorin, C. Cen, D.A. Felker, Y. Zhang, C.T. Nelson, C.W. Bark, C.M. Folkman, X.Q. Pan, M.S. Rzchowski, J. Levy, and C.B. Eom, "Creation of a two-dimensional electron gas at an oxide interface on silicon," *Nature Communications*, **1** (2010)
10. S.H. Baek, H.W. Jang, C.M. Folkman, Y.L. Li, B. Winchester, J.X. Zhang, Q. He, Y.H. Chu, C.T. Nelson, M.S. Rzchowski, X.Q. Pan, R. Ramesh, L.Q. Chen, C.B. Eom, "Ferroelastic switching for nanoscale non-volatile magnetoelectric devices", *Nature Materials*, **9**, 309 (2010)

Future Plans

We will continue exploring the static and dynamic properties of ferroelectric heterostructures to elucidate ferroelectric switching behaviors. We will expand upon our analytical and *in situ* TEM characterization of the prototypical $BiFeO_3$ and $PbZr_{0.2}Ti_{O.8}O_3$ ferroelectrics. Specifically we plan to explore the interplay between electric fields, strain, and ferroelastic domains in switching behaviors. We will also continue surface-probe induced ferroelectric switching experiments, in particular using switching pulses to explore frequency dependence and improve temporal resolution. We plan to expand our measurements to explore switching in fields of greater uniformity using planar electrodes. Constant field studies would be greatly beneficial for analysis such as identifying and exploring the causes for local irregularities in nucleation and pinning and variations in domain velocities. Surface electrodes additionally allow us to switch along in-plane axis, isolate the switching region of the film from tip drift and strain, and if sufficiently large allow for simultaneous electrical characterization of ferroelectric switching to directly correlate TEM observations with conventional measurements.

Physics of complex materials systems through theory and microscopy/EELS

Sokrates T. Pantelides, PI; Mark Oxley, Kalman Varga, co-PIs
Post-docs: (Micah Prange), Myron Kapetanakis; Gradutae students: (Timothy J. Pennycook), Junhua Lin
Department of Physics and Astronomy, Nashville, TN 37235
pantelides@vanderbilt.edu

1. OBJECTIVES

The main objectives of this research program are: a) to create an integrated simulation capability of electron-energy loss spectra (EELS), including both diffraction theory that describes the propagation of the electron beam of a scanning transmission electron microscope (STEM) through the thin film to the detector and density functional theory (DFT) for the calculation of core and valence excitation process, including interference effects (so far, the two objectives have been addressed almost exclusively by different communities, one community leaving out solid-state effects, the other leaving out diffraction and interference); b) pursue calculations to interpret available Z-contrast and EELS data for particular materials systems using available and newly-developed theoretical tools; and c) explore the use of time-dependent density functional theory to simulate advanced imaging techniques. Accomplishments in all three areas are described below.

2. DIFFRACTION + EELS

2.1 Background:

Electron diffraction theory was developed more than 50 years and computer codes for simulating the process in the context of the transmission electron microscope have been written by several groups. Co-PI Mark Oxley is a practitioner of this discipline, having received his training at the group of Les Allen at the University of Melbourne in Australia. The existing diffraction code simulates the propagation of a microscope's electron beam as it travels through the focusing lenses and then traverses the thin film and is diffracted by the periodic crystal potential. EELS simulations for STEM experiments in this context have been limited to atomic approximations for the potential resulting in simulations that lack solid-state effects such as energy-loss near-edge structure (ELNES). When the beam is analyzed in terms of component plane waves, there are plane waves travelling in all directions (different momenta **q**). The transferred momentum determines the scattering angle. Realistic EELS simulations, therefore, require calculations of what is called the mixed dynamical form factor (MDFF), that captures all waves arriving at an atom to be excited, corresponding to the beam position, and tracks the arrival of all scattered waves into the detector, i.e., a sum over **q** and **q**′.

The simulation of ELNES using realistic solid potentials has traditionally been pursued by a different community of researchers that includes the lead PI. This community typically ignores all diffraction effects and essentially assumes that the electron beam travels in vacuum and appears at each atom where it causes an excitation. The contributions of various excitation processes to the experimental signal are calculated from the band structure, which has been the traditional focus of this community. Only the dynamical form factor (DFF), typically calculated at zero momentum transfer (dipole approximation), is needed. The approximation is equivalent to calculating the imaginary part of the dielectric constant as in x-ray or optical absorption.

The main goal of this project is to combine theoretical state-of-the-art spectral and diffraction methods to produce realistic simulations of electron microscope experiments involving dynamical electron diffraction *and* core or valence excitation (e.g. STEM-EELS). Such simulations are increasingly becoming essential in the interpretation of data obtained by aberration-corrected STEMS in complex materials systems.

2.2 Work completed so far

Core excitations

The main elements of the mathematical development and computer code for core excitations have been completed and tested. The new code does not employ the dipole approximation, allowing us to explore the dependence of the near-edge signal on both the magnitude and direction of the momentum transfer for both photon and electron scattering experiments. Most importantly of course is the ability to simulate the dependence of the spectra on probe position. The latest simulation results obtained in conjunction with new experimental data obtained by Maria Varela at ORNL are shown and discussed in Figs. 1 and 2. In Fig. 1 we illustrate the distinct contributions of nonequivalent oxygen columns to the O K EEL spectrum and demonstrate the variation of the EELS spectra as a function of probe position. In Fig. 2 we show the variation of the separation of the first two peaks as a function of probe position and compare with experimental data. Thes variation of this peak separation in different materials has been interpreted as a measure of the variation of the cation oxidation state. The present results show that observed variations of the peak separation within a given material are actually

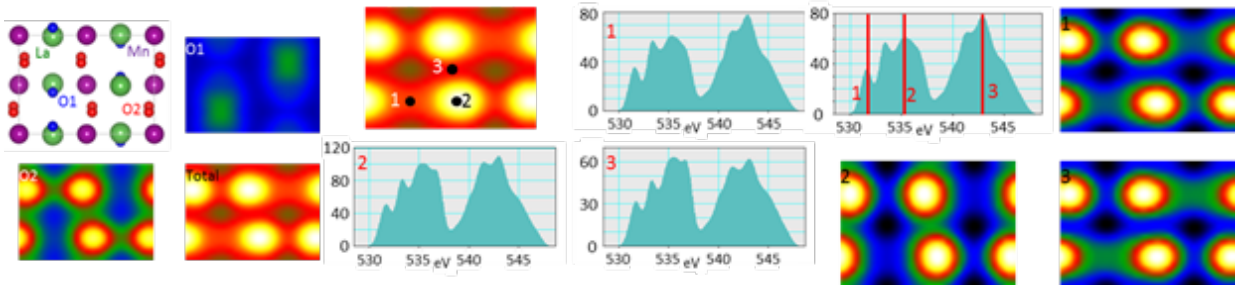

Fig. 1 *Left four panels:* $LaMnO_3$ structural model for the [010] zone axis orientation. The columns containing the O atoms with distinct spectra are indicated by O1 and O2 respectively. Integrated spectrum image simulations for each O type and the total O intensity are also shown. The image intensity is dominated by the O2 atomic columns which contain twice as many atoms as the O1 columns, which also have reduced intensity due to the close proximity of the La atoms. *Middle four panels*: Illustration of the the variation of the total spectrum as a function of probe position within the unit cell. Position 1 is between two adjacent O1 columns and provides the strongest signal. The most significant point here is that different parts of the spectrum vary at different rates as the probe is moved. This effect is due to the dynamical diffractions of the incident electron and its interaction with the mixed dynamical form factor (MDFF). It is illustrated in another way in the four *right panels* where images for 1 eV energy windows are shown for the three energies shown on the spectrum. The variation in shape is due to variation in the MDFF and hence the inelastic scattering potential. These figures demonstrate different delocalizations over a range of energy losses differing by only a few eV, which is contrary to classical estimates of the delocalization of inelastic scattering.

caused by dynamical scattering. The fact that the variation persists for the contributions of each of the two nonequivalent O columns corroborates this conclusion, We have, therefore, demonstrate that simulations using the full MDFF can be a powerful tool in determining when variations of position-dependent spectra can be interpreted in terms of different chemical environments. Such a tool is very promising for the study of interfaces and other inhomogeneous materials systems.

Valence excitations (low loss)

A new computer code is necessary to carry out simulations of valence excitations because the matrix elements are between delocalized Bloch states instead of a localized core level and delocalized final states that are Bloch states modified by electron-hole interactions. As a first pass, we ignore the electron-hole interaction which has a smaller effect compared with core excitations. Programming is still in progress, but we already have an exciting application in graphene. Data have been collected and initial simulations without electron beam focusing or diffraction have already given exciting information. We are waiting for the inclusion of beam focusing and diffraction to finalize the story. The data and initial analysis are described in Section 3.2 below.

3. SELECTED OTHER STUDIES OF REAL MATERIALS SYSTEMS

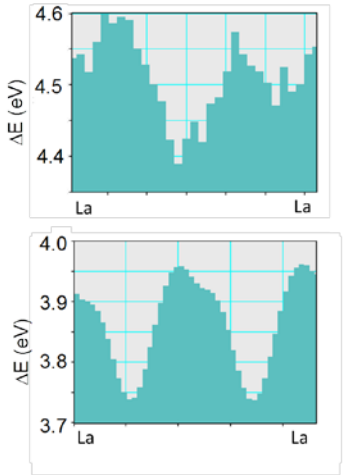

Fig. 2 Variation of the peak separation ΔE as a function of probe position between two La columns. Top: Experiment [M. Varela et al. Phys. Rev. B 79, 085117 (2009)]; bottom: present theory

3.1 The origin of white light emission by ultrasmall CdSe nanoparticles

(This work[1] was part of the Ph.D. thesis of Timothy Pennycook who graduated in January of 2012 and is now a postdoc at the University of Oxford in England).

As the size of semiconductor nanocrystals has been pushed to their lower limits to fully exploit quantum confinement new properties have emerged. Nanocrystals which display size tunable monochromatic emission when small emit across a broader range of energies when their size is reduced into the ultrasmall sub-2nm-range [2]. White light emission from ultrasmall CdSe is a particularly interesting case of such broad emission because of its potential for solid-state lighting [3,4]. The white light consists of a continuum of emission energies spanning the visual range (Fig. 3a). Experiments have ruled out a broad distribution of sizes as the cause, and have shown that individual ultrasmall CdSe nanoparticles emit white light [5]. We have investigated small to ultrasmall CdSe nanocrystals using a combination of state-of-the-art scanning transmission electron microscopy and finite-temperature quantum molecular dynamics simulations. Our findings indicate that following excitation, partial thermalization sets the ultrasmall nanocrystals into a disordered fluxional state. These dynamic fluctuations cause the band gaps of the ultrasmall nanoclusters to vary continuously across the visual range on a femtosec ond time scale (Fig. 3c). When averaged over time, transitions across all these dif-

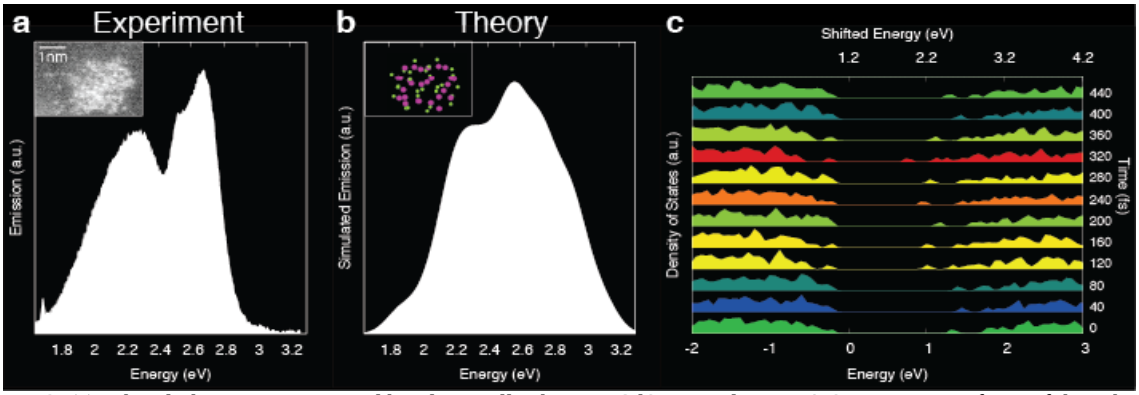

Fig. 3. (a) White light spectrum emitted by ultrasmall sub-2 nm CdSe nanoclusters. A STEM image of one of the sub-2 nm nanoclusters is shown in the inset. (b) The emission spectrum resulting from the dynamic fluctuations of a CdSe nanocluster (shown in the inset) simulated with quantum molecular dynamics simulations. The structural fluctuations cause the density of states (c). The zero of the bottom energy axis has been set to the DFT Fermi level. The top axis has been shifted 1.2 eV to account for the well-known underestimation of the band gap by DFT.

ferent band gaps fill the visual spectrum and produce the white light (Fig. 3b). Furthermore, although the larger monochromatic emitting nanocrystals we have observed possess stable crystal cores, their surfaces are fluxional. Dynamic fluxionality should be taken into consideration when optimizing nanocrystals for applications.

[1] T. J. Pennycook et al. Nano Lett. **12**, 3038-3042 (2012).
[2] C. F. Landes et al. J. Phys. Chem. B **105**, 10554-10558 (2001).
[3] M. J. Bowers II et al., J. Am. Chem. Soc. **127**, 15378 (2005).
[4] J. R. McBride et al. Chem. Phys. Lett. **498**, 1-9 (2010).
[5] A. D. Dukes III et al. J. Phys. Chem. A **115**, 4076 (2011).

3.2 Highly localized excited states in graphene

The low-loss EEL spectrum of graphene is well known. Figure 4 shows a Z-contrast image of graphene and the low loss spectrum taken by Wu Zhou working with Juan Idrobo and Steve Pennycook at ORNL. The two main peaks are known as plasmon because in multilayer graphene they gradually shift with increasing thickness and ultimately match the plasmon peaks of graphite. Figure 1 also shows a faint feature labeled δ, which exhibits an unusual property: a spectrum image obtained from its vicinity shows that the excitations are highly localized at atomic sites, in sharp contrast with spectrum images taken at any other energy range.

Density functional calculations were performed to explore the origin of all peaks in the low loss spectrum. The dielectric function $\varepsilon(\omega)$ was calculated on the basis of interband excitations and the loss function, $\mathrm{Im}[-1/\varepsilon(\omega)]$, was obtained (Fig. 5). We found that $\varepsilon_1(\omega)$ does not go through zero in the vicinity of the low-loss peaks, whereby these peaks are not plasmons (collective excitations), but rather reflect interband transitions. Investigation of the origin of the δ peak led to the surprising conclusion that the final states are *highly localized 3d states* (Fig. 5).

In order to confirm this conclusion, a full MDFF calculation is needed. Similarly, in a recently paper (publication 13 below), the so-called plasmonic peaks were found to be enhanced at a Si impurity in graphene. Full-MDFF low-loss calculations are needed to probe this localization.

4. SIMULATIONS OF ATTO-SECOND IMAGING

We initiated simulations of attosecond imaging of electron dynamics in nanostructures by high-energy electron pulses using time-dependent density-functional theory. These real-time, real-space, time-dependent calculations allow an accurate space-time mapping of electron rearrangement in matter during bond breaking, bond making and ionic dynamics. In the simulations, an attosecond Gaussian wave packet is propagated toward the sample; the scattered and reflected wave packet, as well as the electronic states of the sample, are calculated as a function of time. Figure 6 shows snapshots of the electron density of a wave packet scattering on a single benzene ring from an initial implementation of the method. The objective is to image graphene.

5. FUTURE PLANS

The new codes for STEM/EELS simulations are still evolving, with programming for the low-loss part still in progress. We will complete and validate the codes against experimental data and other simulations, where available, and use the new tools to study real complex materials for which data STEM/EELS become available. Parallel studies of com-

plex materials for which data are already available, e.g., graphene data described above, will also continue. A new post-doc, Myron Kapetanakis is on board, replacing Micah Prange. A new graduate student, Junhua Lin, is also already on board. He has already been trained to do both microscopy and simulations and is currently exploring nitrogen complexes in graphene as a possible catalyst for breaking O_2 molecule for fuel cell applications. We are also continuing explorations using time-dependent density functional theory.

6. PUBLICATIONS (2010-2012):

1. T. J. Pennycook, M. J. Beck, K. Varga, M. Varela, S. J. Pennycook, and S. T. Pantelides, "Origin of Colossal Ionic Conductivity in Oxide Multilayers: Interface-Induced Sublattice Disorder" Phys. Rev. Lett. **104**, 115901 (2010)
2. O.J. Krivanek, M. F.Chisholm, V. Nicolosi, T. J. Pennycook, G. J. Corbin, N. Dellby, M. F.Murfitt, C. S. Own, Z. S. Szilagyi, M. P. Oxley, S. T.Pantelides, and S.J.Pennycook, "Atom-by-atom structural and chemical analysis by annular dark-field microscopy", Nature **464**, 571 (2010).
3. W. Walkosz, R. F. Klie, S. Ogut, B. Mikijelj, S. J. Pennycook, S. T. Pantelides, and J. C. Idrobo, "Crystal-induced effects at crystal/amorphous interfaces: the case of Si_3N_4/SiO_2", Phys. Rev. B **82**, 081412(R) (2010).
4. M. F. Chisholm, W. Luo, M. P. Oxley, S. T. Pantelides and H. N. Lee, "Atomic-scale compensation phenomena at polar interfaces", *Phys. Rev. Lett.* **105**, 197602 (2010).
5. X. Shen, M. Oxley, Y. Puzyrev, B. Tuttle, G. Duscher and S. Pantelides, "Excess carbon in silicon carbide", *J. Appl. Phys.* **108**, 123705 (2010).
6. T. J. Pennycook, M. P. Oxley, J. Garcia-Barriocanal, F. Bruno, C. Leon, J. Santamaria, S. T. Pantelides, M. Varela and S. J. Pennycook, "Seeing oxygen disorder in YSZ/$SrTiO_3$ colossal ionic conductor heterostructures using EELS", *Europ. Phys. J. Appl. Phys.* **54**, 33507 (2011).
7. J. Gazquez, W. Luo, M.P. Oxley, M. Prange, M. A. Torija, M. Sharma, C. Leighton, S.T. Pantelides, S.J. Pennycook, and M. Varela, "Atomic-resolution imaging of spin-state superlattices in perovskite cobaltite films" *Nano. Lett*. **11**, 973 (2011).
8. J. H. Lee, W. Zhou, J. C. Idrobo, S. J. Pennycook and S. T. Pantelides, "Vacancy-driven anisotropic dfefect distribution in the battery cathode material $LiFePO_4$", *Phys. Rev. Lett.* **107**, 085507 (2011).
9. S. Sergiy, B. Wang, S. T. Pantelides, and K. Varga, "Simulation of high-energy ion collisions with graphene fragments", *Phys. Rev. B* **85**, 235435 (2012).
10. T. J. Pennycook, J. R. McBride, S. J. Rosenthal, S. J. Pennycook, and S. T. Pantelides, "Dynamic fluctuations in ultrasmall nanocrystals induce white light emissions", *Nano Lett*. **12**, 3038-3042 (2012).
11. P. Yu P., W. Luo, D. Yi, J. X. Zhang, M. D. Rossell, C.-H. Yang, L. You, G. Singh-Bhalla, S. Y. Yang, Q. He, Q. M. Ramasse, R. Erni, R., L. W. Martin, Y. H. Chu, S. T. Pantelides, S. J. Pennycook, and R. Ramesh, "Interface control of bulk ferroelectric polarization", *Proc. Natl. Acad. Sci.* **109**, 9710-9715, (2012).
12. J. Seidel, W. Luo, S. J. Suresha, P.-K. Nguyen, A. S. Lee, S.-Y. Kim, C.-H. Yang, S. J. Pennycook, S. T. Pantelides, J. F. Scott, and R. Ramesh, "Prominent electrochromism through vacancy-order melting in a complex oxide", *Nature Commun*. **3**, 799 (2012).
13. W. Zhou, N. J. Lee, J. Nanda, S. T. Pantelides, S. J. Pennycook, and J. C. Idrobo, "Atomically localized plasmon enhancement in monolayer graphene." *Nature Nanotechn.* **7**, 161 (2012).

Program Title : ***SISGR- Emerging Functionality in Transition-Metal Oxides Driven by Spatial confinement.*** DOE grant #DE-SC0002136.

Principal Investigator: E. Ward Plummer, Department of Physics and Astronomy, 202 Nicholson Hall, Louisiana State University, Baton Rouge, LA 70803: e mail: wplummer@phys.lsu.edu
Co-PI: Jiandi Zhang, Department of Physics and Astronomy, 202 Nicholson Hall, Louisiana State University, Baton Rouge, LA 70803: e-mail jiandiz@lsu.edu.
Co-PI: Zac Ward, Materials Science and Technology Division, Oak Ridge National Laboratory, Oak Ridge, TN: E-mail **wardtz@ornl.gov**
Co-PI: Jian Shen, Fudan University and Department of Physics and Astronomy, 312 Nielsen, The University of Tennessee, Knoxville, TN, 37996: E-mail— shenj5494@fudan.edu.cn.

Program Scope and Definition:

The exotic properties displayed by correlated electronic materials (CEMs) such as the high temperature superconductors, doped layered perovskites, multiferrocis, and heavy-fermion compounds are intimately related to the coexistence of competing nearly degenerate states which couple simultaneously active degrees of freedom—charge, lattice, orbital, and spin states. This project focuses on the exploration of novel behavior induced by spatial confinement, strain, and chemical or physical modification of the surface or interface. Thin films are grown and characterized *in situ* in an ultra high vacuum environment, using a combination of techniques, such as scanning tunneling microscopy and spectroscopy, low energy electron diffraction, high-resolution X-ray photoemission, angle-resolved photoemission spectroscopy, and low energy electron loss spectroscopy. High resolution scanning transmission electron microscopy, electron loss spectroscopy, x-ray diffraction, and electrical and magnetic transport measurements are conducted *ex situ*. In essence we are combining two of the grand challenges of the 21st century —Complexity and Nano-structured materials to explore and exploit emergent behavior.

Recent Progress (selected examples)**:**

1: Growth diagram and superparamagnetism of multiferroic LuF_2O_4 films. Multiferroics have attracted great attention recently because of their promising new functionality and intriguing fundamental science. A multiferroic material with a large ferroic polarization, high ordering temperature, and strong coupling between the ferroic orders is ideal for applications. So far, those desired properties have not been realized in a single phase material. Multiferroics like $BiFeO_3$ where the magnetic and electric orders originate from different part of the structure have high ordering temperatures but weak coupling between different orders. Other materials like $TbMnO_3$ exhibiting ferroelectricity due to the broken symmetry caused by the spiral magnetic moment have strong magneto-electric coupling. However, here the ordering temperature is very low and the electric polarization is small. $LuFe_2O_4$ contains layers of Fe_2O_2 with a triangular lattice that are sandwiched by LuO_2 layers. Combined with the mixed valance of Fe, the Fe_2O_2 layers in the triangular lattice form a charge ordered state at T_{CO}=320 K, followed by a ferrimagnetic order at T_N = 240 K. Significant changes in dielectric properties have been observed upon application of a small magnetic field at room temperature. The relatively high transition temperature, large polarization, high magnetic coercivity and the strong magneto-electric coupling make $LuFe_2O_4$ a unique multiferroic material.

Recently, the possibility of fast switching and high tunability of $LuFe_2O_4$ due to the electronic origin of its charge order was demonstrated. We have performed a comprehensive study on the growth of Lu-Fe-O compound thin films on MgO(111) substrate using pulsed laser deposition (PLD) [1]. The HRTEM data is shown in **Fig. 1.** The experimentally constructed growth diagram shows that the parameter space for growing epitaxial $LuFe_2O_4$ thin film turns out to be a narrow window of temperature and oxygen pressure, which creates significant experimental difficulty. Based on theses results we have gained fundamental understanding of the growth of Lu-Fe-O

compound films: the growth temperature needs to be high enough to stabilize the metastable phase $LuFe_2O_4$. On the other hand, the loss of Fe at high temperature also changes the resulting phase from $LuFe_2O_4$. These two effects cause the narrow window of the growth condition. Typical LuFeO films exhibit superparamagnetism, which is consistent with the fact that the $LuFe_2O_4$ in the film are epitaxially sandwiched by the impurity phase $LuFeO_3$. The demonstration of epitaxial growth of $LuFe_2O_4$ thin films and the distinct magnetic properties open up new possibilities for studying multiferroicity of low dimensional $LuFe_2O_4$, tuning of its properties, and eventual functionalizations.

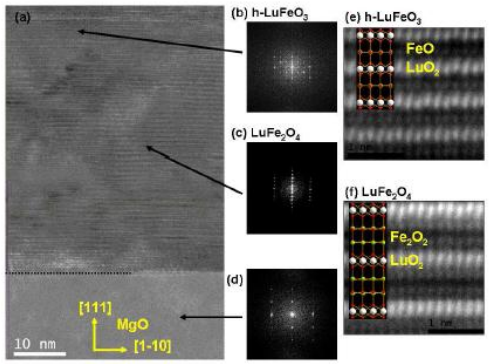

Fig. 1: (a) Typical HRTEM image around the interface, where the interface is marked as a dashed line. (b-d) The Fourier transforms of various positions of (a), where (d) is from MgO substrate and (c) is from the majority of the film, and (b) is from the small top left part of the image. (e) and (f) are the atomic-resolution Z-contrast images corresponding to (b) and (c) respectively.

2: Strain-controlled vertical nanostructured heteroepitaxy and metal to insulator transition [2]. Interfaces of transitional metal oxide heterostructures grown by in-plane epitaxy [layer by layer growth as shown in **Fig. 2(a)**] exhibit many fascinating properties, e.g., high mobility free electron gas and superconductivity. Alternatively, interfaces produced by out-of-plane growth [i.e., a self-assembled or vertical nanostructured heteroepitaxy as shown in **Fig. 2(b)**] of heterostructures surely will generate new and different functionality. In general, layer-by-layer epitaxial growth necessitates a small lattice mismatch (<3%), while achieving vertical growth by forming self-assembled nanostructures is enhanced by a large mismatch. We demonstrated a chemical ratio controlled metal-insulator transition in the nanocomposite films of V_2O_3-$La_{0.7}Sr_{0.3}MnO_3$ (LSMO) grown on $LaAlO_3$ (111) substrate through alternative deposition of LSMO and V_2O_3, two compounds with larger lattice mismatch.

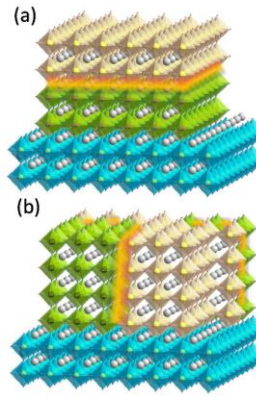

Fig. 2: Schematic view of in-plane epitaxial (a) vs. out-of-plane self-assembled nanostructured (b) interfaces of perovskites-type oxide heterostructures.

We have grown, using PLD, vertically aligned $La_{0.7}Sr_{0.3}MnO_3$ (LSMO) and V_2O_3 [**Fig. 2(b)**] nanostructure on $LaAlO_3$ (LAO)(111) single crystal substrate, where there is a large lattice mismatch of 11% between. The LSMO-V_2O_3 film (~ 10 nm thick) with vertically columnar-like nanostructures can be clearly seen in the high-resolution transmission electron microscopy (TEM) images, shown in **Fig. 3.** By using electron energy loss spectroscopy (EELS) we have found that a V-Mn ion exchange between V_2O_3 and LSMO occurs during the growth and results in the formation of nanoscale and vertically columnar-like insulating Mn_2O_3 and metallic $La_{1-x}Sr_xVO_3$ composite [2].

A metal-insulator transition (MIT) is found in the composite films. This demonstrated a new way to create phase separation, which allows one to control percolation by controlling the ratio of metallic phase. Our artificial phase separation network can be tuned by controlling the relative metallic phase LSVO via tuning the ratio of LSMO and V_2O_3, as a result we can tune the MIT in such system. Multiple functionalities can be obtained since we can tune its properties to one of its component by tuning the relative chemical ratio; hence we have revealed a new pathway to grow advanced materials with multifunctional properties.

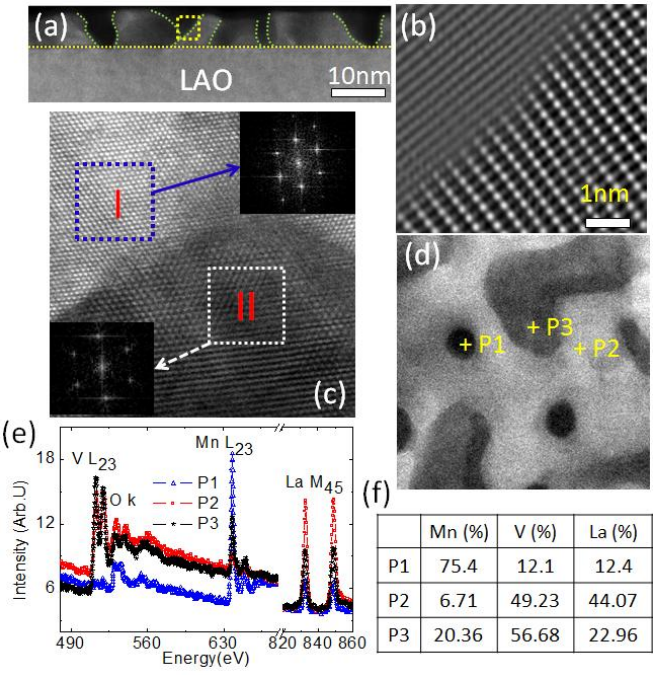

	Mn (%)	V (%)	La (%)
P1	75.4	12.1	12.4
P2	6.71	49.23	44.07
P3	20.36	56.68	22.96

Fig.3: (a) Cross-section view of nanocomposite-thin-film/LAO and (b) zoom-in view of the selected region (marked square) in panel (a) with TEM; (c) TEM image of the interface between dark island and bright matrix, showing well crystallized nanostructures and interface lattice match as confirmed by the difference in diffraction patterns in the insets; (d) Dark field image of planar view of columnar nanocomposite, showing two kinds of brightness with dark islands embedded in bright matrix; (e) EELS spectra of selected spots in (d); (f) the calculated relative quantification of element Mn, V and La from EELS spectra [2].

3: Switching behavior in complex electronic systems. By reducing an electronically phase separated manganite $(La_{1-y}Pr_y)_xCa_{1-x}MnO_3$ single crystal thin film to dimensions on the order of the inherent phase domains, it is possible to isolate and monitor the behavior of single domains at a first order transition. With this technique, we have observed that domain formation is emergent and random, the transition process from the metallic phase to the insulating phase takes longer than the reverse process, electric field effects are more influential in driving a phase transition than current induced electron heating, and single domain transition dynamics can be tuned through careful application of temperature and electric field [3].

Our recent work on spacially confined electronic phase separated manganites is allowing us to create structures dominated by mesoscale phenomena. We are discovering that it is possible to control these systems using local perturbations to the energetic landscape. This means that macroscopic behaviors can be regulated by controlling mesoscale phenomena which opens the door to using localized electric fields to give quantitative information on the question of how Coulombic repulsion shapes electronic phase seeding and distribution.

4: Tunable metal-insulator transition in manganites using surface coated magnetic nanodots. Complex materials exhibit a wide range of fascinating and, potentially, technologically revolutionary behaviors such as, colossal magnetoresistance, multiferroicity, and high temperature superconductivity; however in ultrathin or highly strained films many of these materials have active temperature ranges that are too low for practical applications or lose their exotic properties altogether. This is due to frustration in the delicate electronic balance present in these systems.

To overcome this hurdle, we used the magnetic properties of iron nanodots to control the electron spin in a frustrated complex manganite compound $La_{0.7}Ca_{0.3}MnO_3$, as shown in **Fig. 4.** [4]. The result was a complete recovery of magnetoresistance and active temperature range. It was also discovered that

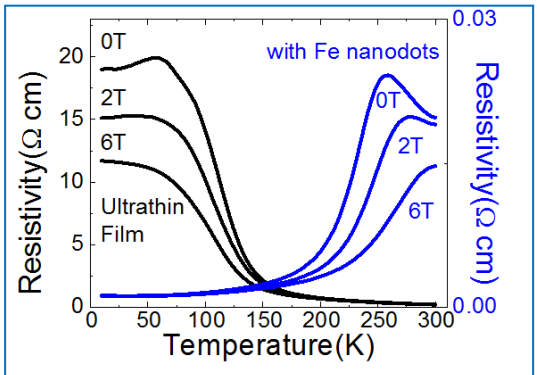

Fig. 4: Transport properties of 20nm ultrathin film of $La_{0.7}Ca_{0.3}MnO_3$ shows insulating behavior. After application of Fe nanodots resistivity data of the same film shows a recovery to bulk-like behavior with a MIT temperature of 255 K at 0 T.

changing the density of the nanodots on the film surface allowed these properties to be highly tunable.

These findings offer a new means to quantitatively investigate the balanced energetics that drive complex materials and promise a simple way to increase and tune critical temperatures in frustrated films for future applications.

Future Plans:

In the future, we will focus on complex doped magnatites, ruthenates, and nichelates exploring the coupled structural, magnetic and electronic transitions. By combining local modifications to order parameters across the range of correlation length scales, we will investigate where the interplay of combinations of spin-charge-orbital-lattice contributions dominate or break down. New nanofabrication capabilities at the Center for Nanophase Materials Sciences at ORNL will be utilized to push the size of spatial confinement into the nanometer range. The electronic and magnetic properties can be tuned in these spatially confined films by depositing electronic donors or acceptors or by patterning of magnetic nano-clusters.

References to papers published 2010 to 2012: First four are references in this document.

1. *Growth Diagram and Superparamagnetism of LuFe2O4 Thin Films,* Wenbin Wang, Zheng Gai, Miaofang Chi, Jason D. Fowlkes, Jieyu Yi, Leyi Zhu, Xuemei Cheng, David Keavney, Paul C. Snijders, Thomas Z. Ward, Jian Shen*, and Xiaoshan Xu, *Phys. Rev.* B **85**, 155411 (2012).
2. *Tuning Functionality in artificial columnar nanocomposite oxides,* Z. L. Liao, P. Gao, S. Stadler, R. Y. Jin, X. Q. Pan, E. W. Plummer, Jiandi Zhang, submitted.
3. *Dynamics of a First-Order Electronic Phase Transition in Manganites*, T.Z. Ward, Z. Gai, H.W. Guo, L.F. Yin, and J. Shen, Phys. Rev. B **83**, 125125 (2011).
4. *Tuning the Metal-Insulator Transition in Manganite Films through Surface Exchange Coupling with Magnetic Nanodots*, T. Z. Ward, Z. Gai, X.Y. Xu, H.W. Guo, L.F. Yin, and J. Shen, Phys. Rev. Lett. **106**, 157207 (2011).

Other publications:

- *Evidence of Coulomb blockade behavior in a quasi-zero-dimensional quantum well on TiO_2 surface*, V. Meunier, F. Moreau. M.H. Pan. K.T. Park, and E.W. Plummer, *Proc. Nat. Acad. Science,* **107** 14968 (2010).
- *An oxygen-induced surface reconstruction of SrRuO3 and its effect on the $BaTiO_3$ interface,"* Junsoo Shin, Albina Y. Borisevich, Vincent Meunier, Jing Zhou, E. W. Plummer, Sergei V. Kalinin, and Arthur P. Baddorf, *ACS Nano* **4**, 4190 (2010).
- *Electroforming and endurance behavior of $Al/Pr_{0.7}Ca_{0.3}MnO_3/Pt$ devices*, Zhaoliang Liao, P. Gao, Y. Meng, H. W. Zhao, X. D. Bai, Jiandi Zhang, and D. M. Chen, *Appl. Phys. Lett.* **98**, 203108 (2011).
- *Engineering of electrodes to improve resistive switching performance in single crystalline CeO_2 thin film*, Zhaoliang Liao, P. Gao, Y. Meng, W. Y. Fu, X. D. Bai, H. W. Zhao, D. M. Chen, *Solid State Electron* **72**, 4(2012).
- *Evidence for electric-field-driven migration and diffusion of oxygen vacancies in $Pr_{0.7}Ca_{0.3}MnO_3$*, Z. L. Liao, Peng Gao, Xuedong Bai, Dongmin Chen, Jiandi Zhang, *J. Appl. Phys.* In press.
- *Room temperature coexistence of ferroelectricity and weak ferromagnetism in hexagonal LuFeO3*, Wenbin Wang, Zheng Gai, Miaofang Chi, Nina Balke, Ho Nyung Lee, Leyi Zhu, Xuemei Cheng, David J. Keavney, Jiyu Yi, Thomas Z. Ward, Jun Zhao, Paul C. Snijders, Hans M. Christen, Jian Shen*, and Xiaoshan Xu, *Nature Comm*.
- *Growth diagram of $La_{0.7}Sr_{0.3}MnO_3$ thin films using pulsed laser deposition*, Hangwen Guo, Dali Sun, Wenbin Wang, Zheng Gai, Ivan Kravchenko, Jian Shao, Lu Jiang, Thomas Z. Ward, Paul C. Snijders, Lifeng Yin, Zhenyu Zhang, Jian Shen, and Xiaoshan Xu, *Phys. Rev. B* (submitted).

1. DOE award # and name of the recipient (Institution)
DE-FG02-07ER46480
The Virginia Polytechnic Institute and State University

2. Project Title and name of the PI / Co-PI
Correlation of Bulk Dielectric and Piezoelectric Properties to the Local Scale Phase Transformations, Domain Morphology and Crystal Structure
Shashank Priya (PI) and Dwight Viehland (co-PI)
310 Durham Hall, Virginia Tech, Blacksburg, VA 24061. (spriya@vt.edu) (viehland@mse.vt.edu)

Research Scope or Definition

Our research addresses the mechanisms controlling the piezoelectric response in lead-free systems by systematically studying the local domain and crystal structures, and their effect on physical properties. $(Na_{1/2}Bi_{1/2})TiO_3$-x%$BaTiO_3$ (NBT-BT) single crystals and textured ceramics of compositions close to morphotrophic phase boundary (MPB) and $K_{0.5}Na_{0.5}NbO_3$-x%$LiNbO_3$ (KNN) single crystals and [001]-grain-textured ceramics near polymorphic phase boundary (PPB) are used as representative lead free system. The nanoscale domain structure and its ferroelectric response were studied as a function of electric field and temperature. In doing so, we have identified the phase transformational sequences in the MPB region, the presence of intermediate bridging phases and identified the similarities and difference in the mechanism of enhanced piezoelectricity for both MPB and PPB Pb-free systems. The nano-structure as a function of composition and temperature was studied by scanning probe microscopy, TEM and HRTEM. We have determined the domain distribution, how elastic compatibility amongst hierarchial domains enhances piezoelectric properties, and how oxygen tilts influence the phase transformational sequence and piezoelectric properties.

Recent Progress

The ferroelectric domain and local structures of $Na_{1/2}Bi_{1/2}TiO_3$-x%$BaxTiO_3$ (NBT-x%BT) crystals for x=0, 4.5 and 5.5% have been investigated by polarized light, piezoresponse force and transmission electron microscopies.[1-4] The results show that the size of polar nano-regions was refined with increasing x (Fig. 1).[2, 4] The tetragonal (T) phase volume fraction, as identified by in-phase octahedral tilting, was found to be increased with BT.[4] We have found a spatial and temporally inhomogeneous polarization under excitation by SS-PFM, which gives evidence of polarization switching by units that are much smaller than conventional macrodomains and that are not confined to regions near domain boundaries in NBT-x%BT crystals. In addition, a giant electric field (E) induced strain of ε=0.60% was found in NBT-5.6%BT, under unipolar fields applied along $[001]_{cub}$ near a E-field induced pseudocubic→T transition at 130°C.[5] The large induced strains for NBT-5.6%BT offer the potential for even higher longitudinal d_{33} coefficients: 2500 and 720pm/V for intermediate and fully transformed T

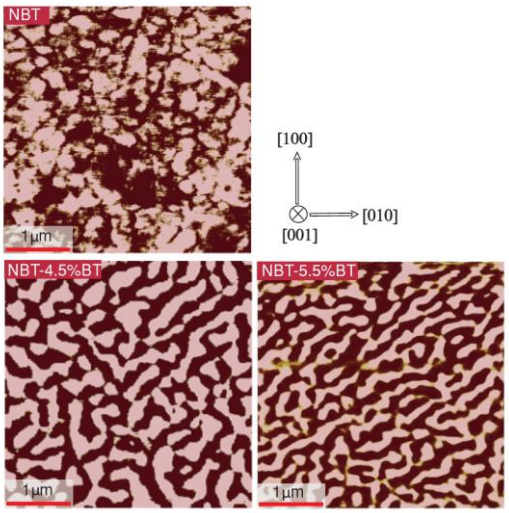

Figure-1 Ferroelectric domains of (001)-oriented NBT, NBT-4.5%BT, and NBT-5.5%BT crystals revealed by PFM.

phase regions.[5]

We have conducted extensive investigations on identifying the origin of large piezoelectric response in single crystal and textured NBT-BT systems for compositions close to MPB. In lead-based ABO_3 compounds, with B-site disorder, the origin of this enhancement has been associated with the presence of an intermediate monoclinic/orthorhombic state that bridges the adjacent ferroelectric rhombohedral and tetragonal phases. However, the origin of high piezoelectric response in lead-free ABO_3 compounds with A-site disorder has not been conclusively established. We have developed a microscopic model derived from comparative analyses of high resolution transmission electron microscopy (HRTEM) and neutron diffraction that explains the origin of high piezoelectric response in lead – free MPB compositions of $(Na_{0.5}Bi_{0.5})TiO_3$ – $BaTiO_3$ (NBT-BT).[6] Direct observation of nanotwins with monoclinic symmetry confirmed the presence of an intermediate bridging phase that facilitates the pathway for polarization reorientation. Monoclinic distortions of an average rhombohedral phase were found to arise from localized displacements of atoms along the non-polar directions (Fig. 2). Such local distortions could be general guiding principle for high piezoelectric response in B-site disordered systems.[7]

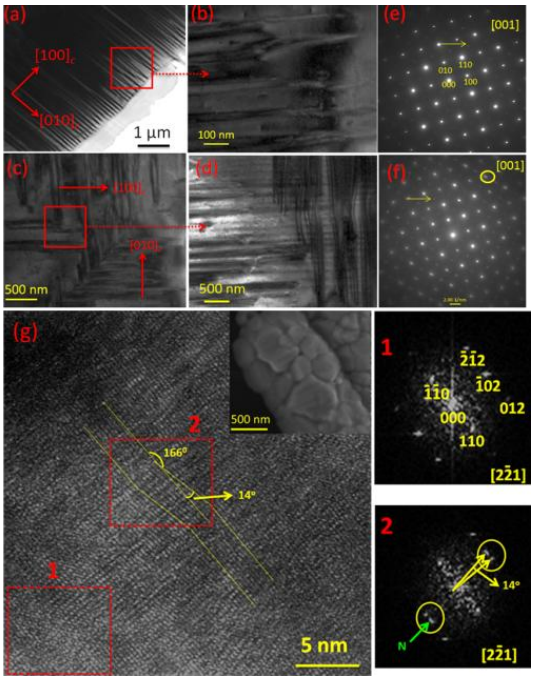

Figure-2 (a) TEM image of thin domains with domain walls planar on (100), the magnified view of these domains is depicted in Fig. 1 (b). (c) The herringbone type domains structure composed of thin domains with domain walls planar on (100) and (010) and intersecting on (110) plane. The magnified view of these domains is depicted in Fig. 1(d). (e) SAED with large probe size, (f) electron diffraction with nano beam. The arrows marked in (e) and (f) indicates superlattice reflections. It was noticed that the $\boldsymbol{g}_{100}/\boldsymbol{g}_{010}$ =1 and the angle between these vectors was ~ 90°, however the SAED with nano beams shows deviation in the ratio and the angles indicating lowering of symmetry. **(g)** A HRTEM image showing the presence of a nanometer twinned region in NBTBT whiskers. The two patterns on the right labeled 1 and 2 are Fast Fourier Transform (FFT) patterns from the corresponding regions of the HRTEM image marked 1 and 2; the split spots in the yellow circles of the FFT of region 2 indicates twinning of the atomic planes. The inset on the HRTEM image is an SEM micrograph of NBTBT whisker.

We also performed comparative analysis of textured and randomly oriented poly-crystalline lead-free piezoelectric $0.93(Na_{0.5}Bi_{0.5}TiO_3)$-$0.07BaTiO_3$ (NBT-BT) ceramics in terms of piezoelectric properties and nature of electric-field induced phase transitions.[8] The $(001)_{PC}$ textured NBT-BT was found to exhibit high longitudinal piezoelectric constant of (d_{33}) ~ 322 pC/N which is almost ~2X of that its randomly oriented counterpart ~160 pC/N. *In-situ* neutron scattering experiments revealed electric-field induced structural phase transformation in randomly oriented polycrystalline NBT-BT. Interestingly, no electric field induced phase transformation was observed in textured NBT-BT (Fig. 3). The nature of phase transformation in NBTBT system is proposed to be related to varying coherence lengths of polar nano regions (PNRs) and internal stress induced by domain switching. We are further working on the Rietveld refinement of the crystal structure after *E*-field induced structural phase transition in NBTBT systems and understanding role of PNRs towards the macroscale properties.[9]

In KNN textured ceramics, our investigations revealed pronounced aging effect in the

orthorhombic single phase field.[10] More uniform and finer domain structures were observed, which are believed to originate from defect-migration. Large sized domains with smooth boundaries were found in the aged condition after poling. Both TEM and HRTEM studies did not reveal the existence of super-reflections, indicative neither of A-site cation ordering or octahedral tilting. In addition, we have found monoclinic C structure in $K_{0.5}Na_{0.5}NbO_3$-x%$LiNbO_3$ Pb-free systems near the PPB.[11] To clearly delineate the symmetry changes, $K_xNa_{(1-x)}NbO_3$ (KNN, x = 0.4, 0.5 & 0.6) single crystals were studied for their optical birefringence behavior in three crystallographic phases. Figure 4 shows the variation of linear optical birefringence of KNN (x = 0.4, 0.5 & 0.6) single crystals [12] in the temperature range 30°C to 600°C. For orthorhombic and tetragonal phases, composition having equimolar amount of Na and K ions, birefringence was found to be higher than the other two compositions. More interestingly, all the three crystals show presence of nonzero birefringence in cubic phase, which persists till 600°C, the upper limit of temperature which could be attained in our instrument. This is a rare finding as according to Neumann principle, a crystal with cubic symmetry should have zero birefringence. $BaTiO_3$ is another rare perovskite composition having presence of nonzero birefringence in cubic phase, but unlike KNN it disappears within few tens of degrees after tetragonal – cubic transition. Presence of linear birefringence in cubic phase of KNN single crystals can be attributed to the existence of localized polar regions in the cubic phase giving rise to quadratic electro – optic effect. This finding indicates the order – disorder behavior of KNN single crystals rather than of displacive type. In this type of ferroelectric compositions local symmetry breaking distortions persist in paraelectric phase of the crystal giving rise to non-ideal cubic unit cell, but random distribution of these distortions prevent any macroscopic net polarization. This distorted cubic structure in KNN single crystals could be either due to: (a) presence of local oxygen octahedral tilting being remnant to the long range octahedral tilting in ferroelectric phase, similar to the findings in PZT or (b) correlated displacement of B site ions (niobium) from their equilibrium positions at the center of oxygen octahedral. These crystals also consist of high concentration of oxygen ion vacancies which incorporate during crystal growth by flux method. From the point of view of both of these distortion mechanisms role of oxygen ion vacancies is critical as well, as they are reported previously giving rise to distortion in the crystal structure of perovskites.

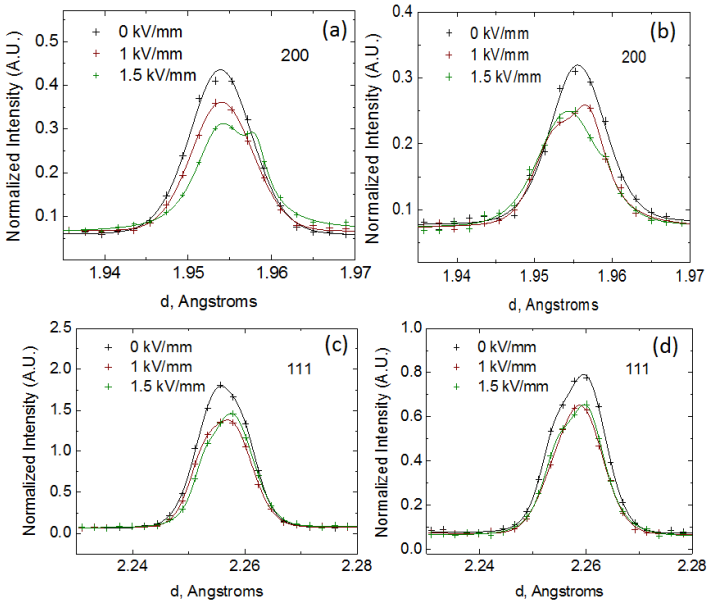

Figure 3: Change in 200 diffraction peak profile for randomly oriented polycrystalline sample, (a) parallel, and (b) transverse, to the direction of applied electric field. Figures (c) and (d) show change in 111 diffraction peak profile for the same sample, parallel, and transverse to the applied electric field direction, respectively.

Future Plans

We are performing investigations of the hierarchial domain structure of Pb-free piezoelectric crystals and textured ceramics for various compositions and dopants. We have purchased a temperature stage for our AFM system, which will allow us to perform investigations in the range of 25<T<250°C: we will use this new tool to determine how the ferroelectric domain structure and organization changes on heating, through the various phases of the transformational sequence. Additional investigations are being planned under in-situ electric fields and by transmission

electron microscopy. We are also investigating field induced transformations, with a focus on developing domain engineered states, via control of the domain hierarchy: which we believe critical to developing lead-free materials with enhanced piezoelectricity. We are studying structurally bridging phases in these crystals and textured ceramics, to determine whether the polarization is free to rotate between various directions: which again could be important to enhanced properties. Detailed crystallographic analysis needs to be done in cubic phase of KNN syste, (T > 450 °C) to preciously determine which of the two above mentioned mechanisms is giving rise to the distortion to the cubic symmetry, and hence the nonzero birefringence. From the point of view of determining local distortions to the cubic cell, pair distribution function (PDF) analysis is an effective tool which taking into account the diffuse scattering of X-rays along with Bragg scattering can reveal the short range ordering in crystals. In conjunction to that high energy neutron diffraction analysis will be used to reveal the average structure distortion in cubic sodium – potassium niobate single crystals.

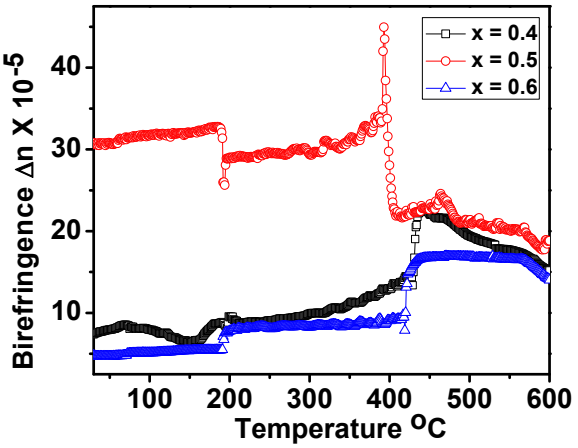

Figure 4: Variation of linear birefringence with temperature for $K_xNa_{(1-x)}NbO_3$ (x = 0.4, 0.5 & 0.6) single crystals.

References:

[1] J.J. Yao, W.W. Ge, L. Luo, et al., Hierarchical domains in $Na_{1/2}Bi_{1/2}TiO_3$ single crystals: Ferroelectric phase transformations within the geometrical restrictions of a ferroelastic inheritance, Appl Phys Lett, 96 (2010) 222905.

[2] J. Yao, L. Yan, W. Ge, et al., Evolution of domain structures in $Na_{1/2}Bi_{1/2}TiO_3$ single crystals with $BaTiO_3$, Physical Review B, 83 (2011) 054107.

[3] J. Yao, Y. Yang, N. Monsegue, et al., Effect of Mn substituents on the domain and local structures of $Na_{1/2}Bi_{1/2}TiO_3$–$BaTiO_3$ single crystals near a morphotropic phase boundary, Appl Phys Lett, 98 (2011) 132903.

[4] J. Yao, N. Monsegue, M. Murayama, et al., Role of coexisting tetragonal regions in the rhombohedral phase of $Na_{0.5}Bi_{0.5}TiO_3$-xat.%$BaTiO_3$ crystals on enhanced piezoelectric properties on approaching the morphotropic phase boundary, Appl Phys Lett, 100 (2012) 012901-012904.

[5] W. Ge, C. Luo, Q. Zhang, et al., Ultrahigh electromechanical response in $(1-x)(Na_{0.5}Bi_{0.5})TiO_3$-x$BaTiO_3$ single-crystals via polarization extension, Journal of Applied Physics, 111 (2012) 093508.

[6] D. Maurya, V. Petkov, M. Murayama, et al., Origin of high piezoelectric response in A-site disordered morphotropic phase boundary systems, Phy. Rev. Lett., Under review (2012).

[7] D. Maurya, V. Petkov, A. Kumar, et al., Mechanism of enhanced piezoelectric instability in lead–free (1-x) $BaTiO_3$ – x $A(Cu_{1/3}Nb_{2/3})O_3$ (A = Sr, Ca, Ba) solid solutions, Phy. Rev. B, Under review (2012).

[8] D. Maurya, A. Pramanick, K. An, et al., Enhanced piezoelectricity and nature of electric-field induced structural phase transformation in textured lead-free piezoelectric $Na_{0.5}Bi_{0.5}TiO_3$-$BaTiO_3$ ceramics, Appl Phys Lett, 100 (2012) 172906.

[9] D. Maurya, V. Petkov, A. Kumar, et al., Nanostructured lead-free ferroelectric $Na_{0.5}Bi_{0.5}TiO_3$–$BaTiO_3$ whiskers: synthesis mechanism and structure, Dalton T, 41 (2012) 5643.

[10] J. Yao, J. Li, D. Viehland, et al., Aging associated domain evolution in the orthorhombic phase of <001> textured $(K_{0.5}Na_{0.5})Nb_{0.97}Sb_{0.03}O_3$ ceramics, Appl Phys Lett, 100 (2012) 132902.

[11] W. Ge, Y. Ren, J. Zhang, et al., A monoclinic-tetragonal ferroelectric phase transition in lead-free $(K_{0.5}Na_{0.5})NbO_3$-x%$LiNbO_3$ solid solution, Journal of Applied Physics, 111 (2012) 103503.

[12] S. Gupta, S. Priya, Ferroelectric properties and dynamic scaling of <100> oriented $(K_{0.5}Na_{0.5})NbO_3$ single crystals, Appl Phys Lett, 98 (2011) 242906.

Nano-imaging and -spectroscopy of correlated electron materials

P.I.: Markus Raschke, markus.raschke@colorado.edu

University of Colorado, Department of Physics, 2000 Colorado Avenue,
Boulder, CO 80309

Introduction: We perform nano-optical imaging and spectroscopy of the nano-domain phase behavior and order phenomena in correlated electron materials. This work is based on our development of variable temperature scattering scanning near-field microscopy (*s*-SNOM) in combination with linear, nonlinear, and ultrafast spectroscopy. The resulting spectroscopic specificity in terms of electronic and vibrational resonances, structural symmetry, and ultrafast dynamics with simultaneous nanometer spatial resolution provides microscopic insight into the underlying mechanisms of the rich phase behavior of metal-insulator transition materials, colossal magneto-resistive manganites, and magnetoelectric multiferroics.

Main research goals: Of the different correlated electron materials, transition metal oxides are often characterized by competing nearly degenerate states, of coupled charge, orbital, spin, and lattice degrees of freedom. In our project we focus specifically on the study of materials that exhibit one or a combination of the following properties: colossal magneto-resistance (CMR), metal-insulator transitions (MIT), and multi-ferroicity. Despite the obvious attractiveness of potentially using these phenomena for technological applications, the largely incomplete understanding of the underlying complex fundamental physics, and even lack of systematic knowledge of relevant driving forces and parameter behind these exotic phases, make materials design and device applications difficult.

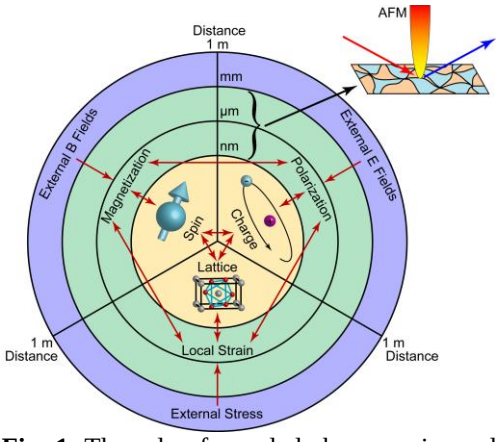

Fig. 1. The role of coupled charge, spin, and lattice degrees of freedom in the formation of *inhomogeneous mesoscopic* domains ranging from the atomic scale, to macroscopic dimensions given by external fields. The interplay of these interactions (red arrows) can result in intrinsic phase coexistence on mesoscopic length scales (1 nm< *l* <1 mm) which we can access spectroscopically on the nanoscale with scattering scanning near-field optical microscopy (*s*-SNOM) with <10 nm spatial resolution.

Phase coexistence and spatial phase separation: The strong correlation of charge, spin, orbital, and lattice degrees of freedom in transition metal oxides and related materials leads to unusually rich phase diagrams with distinct crystallographic, electronic, and magnetic phases with frustration and degenerate ground states. One overarching phenomenon that has became increasingly evident especially during the past 10 years of continuous research effort is that associated with the strong electron correlation, in many cases phase competition and coexistence of multiple phases exists near phase boundaries. This gives rise to structural and electronic inhomogeneities and nanoscale spatial phase separation with complex spatial architecture. This phase co-existence over a wide range of length scales from nano- to microscale, is determined by both intrinsic and extrinsic factors. It can be static or dynamic, and is very sensitive to external stimuli via, e.g., electric field, magnetic field, strain, current, and temperature (see **Fig. 1**).

The origins of these spatial electronic, magnetic, and lattice structural inhomogeneities developing in even nominally homogeneous pure single crystals has been an intensely debated issue. Even their roles in defining the macroscopic materials properties is often unclear. But the problem is not only very difficult to track theoretically. In addition, despite some notable exceptions most experimental evidence is indirect for a lack of versatile imaging techniques, with necessary spatial resolution, that are applicable *in situ*, ideally under variable magnetic and electric fields, and that are simultaneously sensitive to different order parameters.

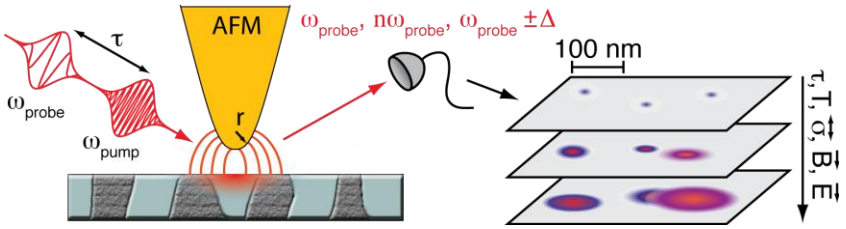

Fig. 2. The concept of scattering scanning near-field optical microscopy (*s*-SNOM) for imaging the nano-domain phase separation in complex oxides. The locally-enhanced optical tip-sample coupling allows for the nanometer resolved probing with different linear, nonlinear, and ultrafast optical techniques. Compatible with variable and low-temperature T, magnetic field B, electric field E, sample strain σ, etc. it allows for mapping domain evolution of the material under those different stimuli.

Our group as developed the new technique of scattering scanning near-field optical microscopy (*s*-SNOM) into a versatile tool for nano- to microscale (10 nm - 10's μm) imaging and spectroscopy of metallic, insulating, and ferroic (ferromagnetic FM, antiferromagnetic a-FM, and ferroelectric FE) domain order (see **Fig. 2**). We have established the basic capabilities in our lab, with *s*-SNOM operating at variable and low-temperature (20 – 500 K)[1], compatible with a high-field magnet, and equipped with broad-band (UV to THz) and ultrafast laser sources with pulse shaping and femtosecond optical control. In collaboration with PNNL and the ALS we have provides the techniques also as an EMSL user facility and have set up IR *s*-SNOM at the newly established ALS IR beamline 5.

In a first series of experiments we have demonstrated the applicability of *s*-SNOM for the determination of the nano-domain order in complex oxides by developing optical phonon nano-Raman crystallography to image ferroelectric domains in $BaTiO_3$ nanocrystals[2], use of the symmetry selectivity of the nonlinear response to image nanoscale ferroic order in multiferroic $YMnO_3$ [3], and use of the mid-IR Drude optical conductivity contrast for the study of the nanoscale phase separation and the discovery of multiphase competition at the metal-insulator transitions in VO_2 micro-crystals[4]. This work has been augmented by the micro-Raman determination of the strain-temperature phase diagram of the insulating phases in VO_2 [5], and characterization of synthetic ferroelectric $LiNbO_3$ micro-crystals [6]. *s*-SNOM and tip-enhanced spectroscopy is fully compatible with essentially all *coherent and incoherent ultrafast wave-mixing and pump-probe* techniques. This opens the door to a new regime of spatio-temporal imaging of electron, spin, and lattice dynamics on nanometer length and femtosecond time scales. We have recently shown the first implementation of nano-scale study of few-femtosecond electron dynamics and free-induction decay vibrational dynamics with time and length scales and sensitivity and spectral resolution virtually inaccessible by any other technique. We have recently reviewed the emerging potential of these new near-field imaging techniques in *Advances of Physics* [7] and *Annual Reviews of Materials Research* [8].

Our ongoing and future work focuses on the investigation of the following representative systems of three main classes of materials: 1) The extension of our investigations of the metal-insulator transitions in oxides (VO_2, V_2O_3) and the thiospinel $CuIr_2S_4$; 2) The systematic study of

the proposed multiple phase coexistence of magnetic, electronic, and lattice degrees of freedom in colossal magnetoresistive manganites (LSMO, LCMO, and $La_{5/8-y}Pr_yCa_{3/8}MnO_3$); and 3) The coupling of the coexisting ferroic order parameter (FE, FM, a-FM) in magnetoelectric multiferroics ($YMnO_3$, $HoMnO_3$, $ErMnO_3$, $BiFeO_3$).

Spatial phase co-existence: Evidence of local phase separation in these materials on mesoscopic length scales and domain formation emerged mostly indirectly from bulk characterization. Here, macroscopic measured quantities expected to exhibit a discontinuous change at the phase transition temperature, are rather found to be broadened. This has been interpreted with the formation of an *inhomogeneous phase distribution*. From the combination with microscopy techniques it emerged that spatial phase separation and coexistence in strongly correlated electron systems spans > 5 orders of magnitudes in length scales ranging from the atomic to the 10's μm scale.

This lead to the phenomenological picture of electronic and structural phase separation (PS), where, e.g., in CMR compounds, FM metallic, CO/OO/a-FM insulating, and PM insulating states may compete. This leads to the formation of an intermediate regime of local mixed phase behavior, and/or local order. This complicates the investigation and microscopic understanding of the origin of the phase behavior.

The goal of our work is the systematic characterization of the electronic, structural, and magnetic *domain texture, spatial and temporal organization, and topology* by nanoscale optical spectroscopy and imaging in these materials. The systematic study of the influence of temperature, strain, electric field, magnetic field, and doping on the domain order will allow us to identify the role and interaction of *intrinsic and extrinsic parameters*. This will help answer the long standing questions where and to which extent domain order is a *side effect or key* to the mechanism of many of the materials properties (e.g., to CMR). And lastly we will explore the possibilities for optical control (static and ultrafast) of correlated electron physics on the nanoscale. Understanding these phenomena might prove essential for practical applications attractive for the very sensitive nonlinear response enabled by the complex phase behavior. However, this being a consequence of percolation following external stimuli, the underlying domain behavior must be understood.

We are able to extend the emergent topic of the selective electronic, lattice, and spin ultrafast dynamics spectroscopy of correlated matter into the nanoscale. We can probe the natural time and length scales and coupling of electron and phonon scattering lengths of 10's of nanometer and associated fs to ps dynamics simultaneously, and on the sub-domain level. From the spatio-temporally resolved relaxation following the ultrafast non-equilibrium photo-excitation we gain direct insight into the formation, stability, and competing processes determining both ground and excited states of the correlated material.

Overarching scientific questions on nano-domain order we will address:

i) What are the underlying competing electronic, lattice, strain, etc, parameters responsible for the formation of the domains?

ii) What are their characteristic length scales?

iii) What are the energetics and how does it influence the domain topology?

iv) What are the reversibility and hysteresis in repeated transitions?

v) What determines multiple phase coexistence on possibly hierarchies of length scales?

vi) What are the relationships of domain size and architecture with crystal quality and impurities?

vi)What are the intrinsic electronic and structural characteristics of the domains near the phase transition as compared to far from the phase transition (T* vs. T_C)?

Answering these question will help us understand the microscopic mechanisms that drive the phase transitions and provide critical input for the development of theoretical models. Unique to our approach is the combination of linear, nonlinear, and ultrafast spectroscopy with *s*-SNOM for i) nano-scale real space imaging and phase identification of the domain order under the influence of temperature, strain, magnetic, or electric field, and ii) local ultrafast spectroscopy providing dynamics information from selective electronic or lattice photo-excitation.

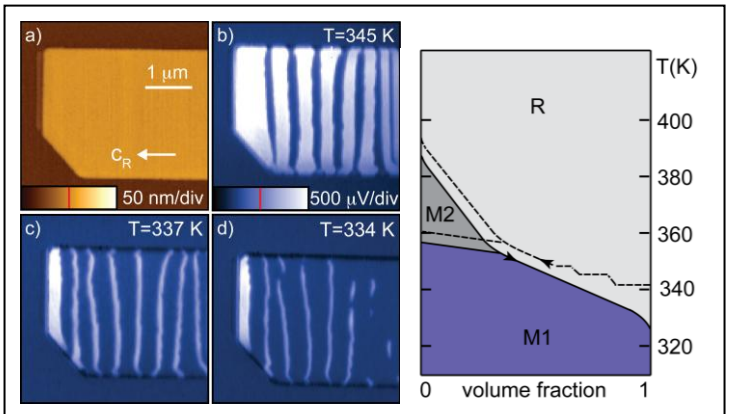

Fig. 13. Topography (a) and *s*-SNOM (b-d) of VO_2 MIT with gradual growth of insulating (dark) domains, with remaining metallic phase islands persisting well below the nominal T_{MIT}. Right: Corresponding volume fraction of M1, M2, and R phases for micro-crystals derived from the combination of *s*-SNOM and micro Raman spectroscopic imaging.

Case study - the insulator-to-metal transition in VO_2: To demonstrate the potential of our approach have studied VO_2 microcrystals under substrate-strain by mid-IR *s*-SNOM. Based on the combined phonon Raman and IR Drude response we were able to identify the i) *spatial domain organization*, ii) *hysteresis*, and iii) *volume fraction* of the coexistence of insulating (M1, M2) and metallic (R) phases as a function of temperature [4]. In extension of this work we have determined the *stress-temperature phase diagram* of the insulating phases using Raman spectroscopy revealing the competition of three insulating M1, M2, and T phases in close proximity to zero strain MIT [5]. And lastly, using *ultrafast pump-probe spectroscopy* we have resolved the ultrafast photo-induced metal-insulator phase transition with response function reconstruction of the few-femtosecond electron dynamics, with insight into the coupled lattice dynamics from the coherent phonon response.

1 H. Yang, E. Hebestreit, and M. B. Raschke, "A cryogenic scattering-type scanning near-field optical microscope for surface investigation of solid matter", Rev. Sci. Inst., *submitted* (2012).

2 S. Berweger, C. C. Neacsu, Y. Mao, H. Zhou, S. S. Wong, and M. B. Raschke, "Optical nanocrystallography with tip-enhanced phonon Raman spectroscopy", Nat. Nanotech. **4**, 496 (2009).

3 C. C. Neacsu, B. B. van Aken, M. Fiebig, and M. B. Raschke, "Second-harmonic near-field imaging of ferroelectric domain structure of $YMnO_3$", Phys. Rev. B **79**, 100107 (2009).

4 A. C. Jones, S. Berweger, J. Wei, D. Cobden, and M. B. Raschke, "Nano-optical investigations of the metal-insulator phase behavior of individual VO_2 microcrystals", Nano Lett. **10**, 1574 (2010).

5 J. M. Atkin, S. Berweger, E. K. Chavez, M. B. Raschke, J. Cao, W. Fan, and J. Wu, "Strain and temperature dependence of the insulating phases of VO_2 near the metal-insualtor transition", Phys. Rev. B, **85**, 020101(R) (2011).

6 A. C. Santulli, H. Zhou, S. Berweger, M. B. Raschke, E. Sutter, and S. S. Wong, "Synthesis of single-crystalline one-dimensional $LiNbO_3$ nanowires", CrystEngComm **12**, 2675 (2010).

7 J. M. Atkin, S. Berweger, A. C. Jones, and M. B. Raschke, "Nano-optical imaging and spectroscopy of order, phases, and domains in complex solids", Advances of Physics, (*in press*, 2012).

8 J. M. Atkin and M. B. Raschke, "Nonlinear and ultrafast nano-imaging and -spectroscopy for systems materials research", Annual Reviews of Materials Research, *invited review* (2012).

Study of Energy Transport at The Nanoscale

Pramod Sangi Reddy
University of Michigan, Ann Arbor, Michigan 48109
Phone: 734-615-5952
E-mail: *pramodr@umich.edu*

Research Scope: The goal of this program is to experimentally study energy and charge transport in nanoscale molecular junctions. It is well known that the transport properties of molecular junctions are specific to the junction and are unlike that of either the metal electrodes or the organic molecules. In support of this view, recent computational studies of thermoelectric effects in molecular junctions have shown that it should be feasible to create extremely efficient thermoelectric devices by engineering the molecular structure of junctions. Large thermoelectric efficiencies are indeed expected on theoretical grounds[1, 2], as molecular junctions can be tuned to have a sharp electronic density of states, which is the key to creating a very efficient thermoelectric material. While some initial progress has been made in understanding electrical conductance of molecular junctions, the thermal conductance and thermoelectric properties of molecular junctions remain largely unexplored. This program seeks to bridge this gap by elucidating the effect of molecular structure, and the chemical composition of the electrodes on 1) the Seebeck coefficient (voltage output per unit temperature differential, also called thermopower), 2) the thermal conductance, and 3) the electrical conductance of MMMJs.

Heat transport in molecular junctions has been investigated computationally for over five decades[3, 4] and several unique effects like the length independence of thermal conductance, phonon-filtering, i.e. the suppression of phonon transport in certain frequency ranges and rectification of heat flow have been predicted. However, in spite of this long history, these interesting *energy* transport phenomena, remain experimentally unverified. This absence of experimental data is due to the lack of tools to 1) trap molecules between electrodes to form a MMMJ, 2) apply known temperature differentials of a few Kelvin across electrodes that are separated by about a nanometer, and 3) measure the small heat currents due to the temperature differential across the electrodes of these junctions. The first steps towards such measurements have been taken recently; first, techniques to form MMMJs have been developed by researchers in the field of molecular electronics. Second, the application of temperature differentials across electrodes to study thermoelectric effects has recently been demonstrated by the PI and coworkers[5, 6]. Finally, ***a novel instrument that combines a picowatt resolution heat-flow calorimeter[7] and a scanning probe microscope***, that can overcome the third challenge—measuring extremely small heat flows in MMMJs—was recently built by the PI and his group as part of this program. Using this technique, investigations will be performed to discover novel phenomena that arise in the transport of MMMJs.

Recent Progress

Thermoelectric Studies at the Molecular Scale: In order to understand the thermoelectric properties at the molecular scale we have recently developed a novel scanning probe technique: thermoelectric atomic force microscopy (ThAFM). Using this technique, we have recently probed the dependence of thermoelectric properties on the structure of molecular junctions and reported the results in a recent publication in the *Journal of American Chemical Society*[8]. These studies identified several interesting effects. These include the length dependence of

thermoelectric properties as well as the effect of end groups on them. For example we find that by just changing the end group of a molecular junction from a thiol (-SH) to isocyanide (-NC) the sign of the Seebeck coefficient is reversed! Our recent theoretical studies of these effects have also provided mechanistic insights into these end group effects[9]. Our current work is exploring the possibility of utilizing quantum interference effects to enhance thermoelectric effects at the nanoscale.

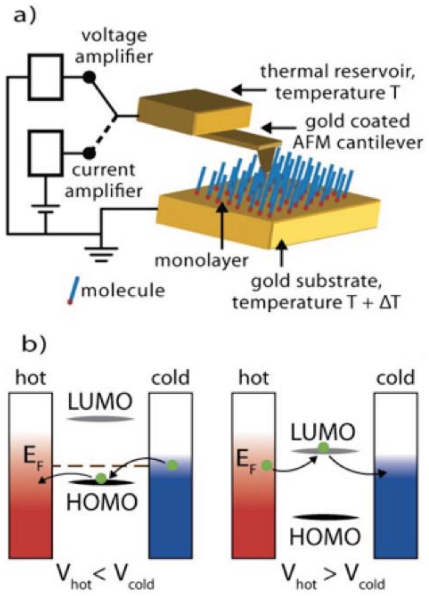

Figure 1: Thermoelectric measurements of molecular junctions. (a) Measurement setup for performing thermoelectric measurements. (b) Schematic picture describing the two scenarios that thermoelectric measurements can distinguish

Scanning Thermal Microscopy: In order to probe temperature fields with nanoscale resolution we have recently developed[10] a novel scanning probe technique that is capable of quantitatively measuring temperature fields with a spatial resolution of ~10 nm and a temperature resolution of ~15 mK. In order to perform such thermal imaging, we custom fabricated AFM probes with a thermocouple integrated into their tips are employed (Fig. 2). Because the thermocouple is integrated into the very end of the tip, the resultant thermoelectric voltage depends only on the temperature of the tip end. When such a custom designed probe is in contact with a metal, dielectric, or a molecular layer the temperature of the tip is directly dependent on the temperature of the surface thus enabling measurement of local temperature with nanoscale resolution.

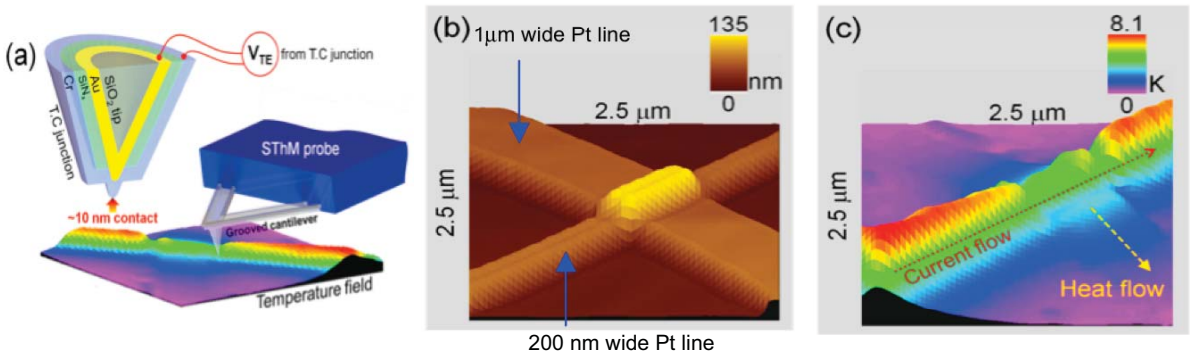

Figure 2: *(a) Depicts a scanning probe with an integrated thermocouple. (b) The topography of a 200 nm wide metal line that is electrically isolated from a 1μm wide line which acts like a fin. (c) Temperature field of the sample when an electric current passes through the 200 nm line. Adapted from [10].*

Picowatt Resolution Heat Flow Calorimetry: In order to characterize thermal transport through molecules and one-dimensional polymer chains it is necessary to measure heat flows with picowatt resolution[11]. To accomplish this goal we have recently developed a novel microdevice—**a picowatt resolution heat flow calorimeter**—that integrates an ultra-sensitive bimaterial cantilever temperature sensor into a thermally isolated suspended region (see Fig. 3). Since the bimaterial cantilever can resolve temperature changes (ΔT) as small as ~6×10^{-6} K, and

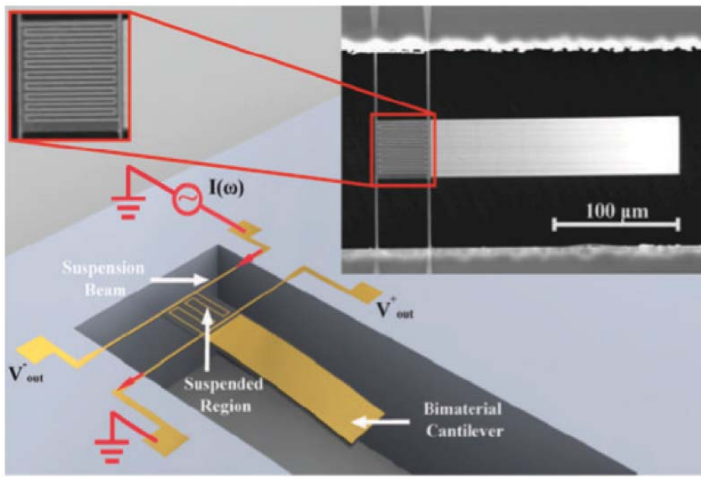

Figure 3: *Schematic of a picowatt calorimeter is shown along with a scanning electron micrograph of a microfabricated device (inset). The central area of the device is suspended by thin (~2 µm) and long (~50 µm) beams. A serpentine line that serves as a 4-probe heater/thermometer and a 200 µm long bimaterial cantilever that acts as an ultra-sensitive thermometer are integrated into the suspended region. Adapted from [7]*

the thermal conductance (G) of the beams that isolate the suspended region is ~0.5 µW/K, it is possible to resolve heat flows (q) into the suspended region with a resolution of <4 pW($G \times \Delta T$).

Future Plans

One of the major goals of this project is to understand heat transport in one-dimensional nanoscale molecular junctions. Given the advances described above to measure heat currents with picowatt resolution as well as to measure temperature fields with nanoscale resolution, we are well poised to address this challenging outstanding question ***within this year***.

In addition to probing thermal transport in 1-Dimensional systems we are also currently exploring heat dissipation in quasi-ballistic junctions. Recent studies[12] of heating in quantum point contacts suggest that heating in such quasi-ballistic contacts can be asymmetric *i.e.* when an electric current is supplied through a ballistic junction more heat is dissipated in one contact than the other.

In order to test these effects, we have recently developed an ultra-high vacuum based experimental technique that utilizes novel stiff scanning thermal microscopy (SThM) probes with integrated thermocouples. Using this technique, it is possible to create quantum point contacts, tunneling gaps, and metal-molecule-metal junctions and probe heat dissipation in such junctions. Our latest studies, using these probes, show several interesting features that unambiguously demonstrate that the key ingredient for asymmetric heating in ballistic junctions is an energy dependent transmission probability for the charge carriers. In fact, our results show that asymmetric heating is significant in tunneling barriers and molecular junctions where the transmission probability of charge carriers is strongly dependent on the energy. Further, our results show that the asymmetry in heating for Au-Au point contacts is negligible due to the negligible energy dependence of transmission in such junctions. These results, which are in excellent agreement with first principle quantum mechanical calculations performed by our collaborator (Prof. Carlos Cuevas Rodriguez), disprove recent experimental results[12]. We are currently extending this work to other molecular systems of great interest to the molecular electronics community.

References:

1. Bergfield, J.P., M.A. Solis, and C.A. Stafford, *Giant Thermoelectric Effect from Transmission Supernodes.* ACS Nano, 2010. **4**(9): p. 5314-5320.
2. Karlstrom, O., et al., *Increasing thermoelectric performance using coherent transport.* Physical Review B, 2011. **84**(11).
3. Fermi, E., J. Pasta, and S. Ulam, *Studies of non linear problems.* Los Almos Report No. LA1940 (unpublished), 1955: p. 978-988.
4. Segal, D. and A. Nitzan, *Heat rectification in molecular junctions.* Journal of Chemical Physics, 2005. **122**(19).
5. Reddy, P., et al., *Thermoelectricity in molecular junctions.* Science, 2007. **315**(5818): p. 1568-1571.
6. Tan, A., S. Sadat, and P. Reddy, *Measurement of thermopower and current-voltage characteristics of molecular junctions to identify orbital alignment.* Applied Physics Letters, 2010. **96**(1).
7. Sadat, S., et al., *Room temperature picowatt-resolution calorimetry.* Applied Physics Letters, 2011. **99**(4).
8. Tan, A., et al., *Effect of Length and Contact Chemistry on the Electronic Structure and Thermoelectric Properties of Molecular Junctions.* Journal of the American Chemical Society, 2011. **133**(23): p. 8838-8841.
9. Balachandran, J., et al., *End-Group-Induced Charge Transfer in Molecular Junctions: Effect on Electronic-Structure and Thermopower.* The Journal of Physical Chemistry Letters, 2012: p. 1962-1967.
10. Kim, K., et al., *Ultra-High Vacuum Scanning Thermal Microscopy for Nanometer Resolution Quantitative Thermometry.* ACS Nano, 2012. **6**(5): p. 4248-4257.
11. Segal, D., A. Nitzan, and P. Hanggi, *Thermal conductance through molecular wires.* Journal of Chemical Physics, 2003. **119**(13): p. 6840-6855.
12. Tsutsui, M., T. Kawai, and M. Taniguchi, *Unsymmetrical hot electron heating in quasi-ballistic nanocontacts.* Scientific Reports, 2012. **2**.

Visualization and quantification of deformation processes controlling the mechanical response of alloys in aggressive environments.

Ian M. Robertson
Department of Materials Science and Engineering
University of Illinois, 1304 West Green Street, Urbana IL 61801
ianr@illinois.edu

The objective of this program is to understand the fundamental processes governing the mechanical properties of materials exposed to different stimuli. To achieve this understanding, visualization and analysis tools to recover the through thickness information lost in a conventional electron micrographs are being developed and applied to discover the deformation response of metallic systems. Specifically, a new approach which combines *in situ* TEM deformation experiments with periodic three-dimensional snapshots acquired using diffraction contrast electron tomography is being developed.

Recent Progress: Traditional electron micrographs are two-dimensional images of the three dimensional state as projected on the electron exit surface. Electron tomography allows recovery of the through thickness information. Here we demonstrate that this technique can be applied to analysis of defect structures; the angular range, image requirement, and imaging condition associated with electron tomography can be relaxed; and it can be combined with in-situ TEM straining experiments. Recent progress is demonstrated by examples of dislocation interactions with grain boundaries in 304 stainless steel deformed at room temperature and at 400°C. The outcome is an understanding of how strain is transferred through grain boundaries by perfect and partial dislocations and how these processes are influenced by temperature. Insight into the processes responsible for ejecting partial dislocations from a grain boundary is emerging.

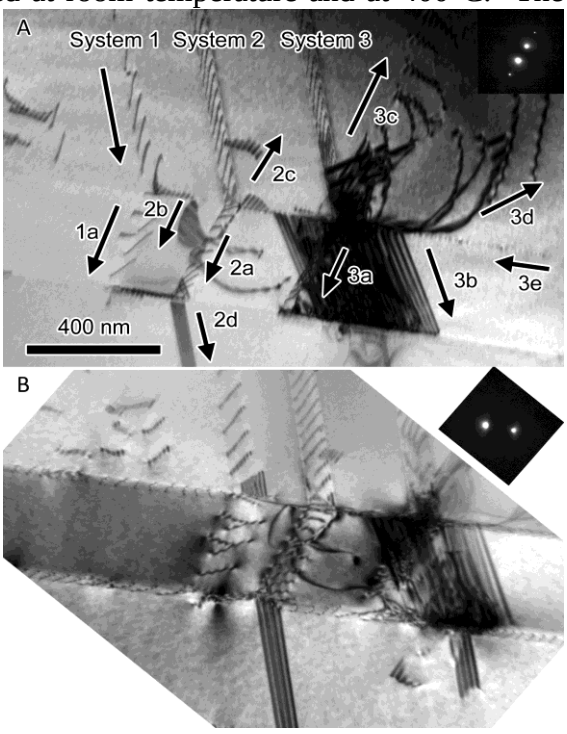

Figure 1. Bright-field TEM micrograph with associated diffraction pattern of dislocations interacting with twin boundaries. Arrows show direction of dislocation motion.

The first example shows three sets of perfect dislocations interacting with a twin boundary, Fig. 1A. Despite the interactions occurring in close proximity, each interaction unexpectedly resulted in a different transfer product being ejected into the twinned volume. These new product dislocations crossed the twinned region and intersected the other twin boundary. The resultant interactions are shown with different diffraction vectors in Fig. 1. Interestingly, there is evidence for significant dislocation activity along the twin boundary. A tilt series was collected by maintaining the tilt axis parallel to the plane normal of the twin boundaries and collecting a bright-field image every 2^{o} over an angular range of 74^{o}. The concomitant loss of resolution associated with using such a small

angular range is negated by constructing from the low resolution tomogram a three-dimensional model. Figure 2 shows snapshots taken from the model as viewed from different vantage directions and with the dislocations colored with respect to the determined Burgers vector. The real space coordinate systems, in the form of Thompson tetrahedra, are included for the matrix and twinned regions. This makes identification of the active slip system, including the nature of the dislocation, trivial. In the following, the subscripts *in* and *out* identify the frame of reference and refer to the grains containing the incoming and outgoing dislocations, respectively. The twin boundaries reside on $(\bar{1}1\bar{1})_{in}$. The incoming slip system for all three systems is $\pm\ ^{a}/_{2}[\bar{1}10]_{in}(\bar{1}\bar{1}1)_{in}$ and the line direction of the dislocation is $[112]_{in}$, making these pure edge dislocations. Each of the incoming slip systems leads to a unique transmission event. System 1 results in two sets of dislocations being emitted into the twinned region on the $\pm\ ^{a}/_{2}[101]_{out}$ $(\bar{1}\bar{1}1)_{out}$ slip system (1a), but with line directions of $[1\bar{2}\ \bar{1}]_{out}$ and near $[1\bar{3}\ \bar{2}\ ]_{out}$, making them pure edge and mixed character dislocations, respectively. A partial dislocation emerges from the boundary back into the original grain, but its character could not be determined due to its proximity to the boundary. Similarly, System 2 results in the emission of perfect dislocations into the twinned region on the slip system $\pm\ ^{a}/_{2}[101]_{out}(\bar{1}\bar{1}1)_{out}$ (2a), but in this case the dislocations have a line direction parallel to $[1\bar{2}\ \bar{1}]_{out}$, making them pure edge dislocations. Also similar to System 1, there is back emission of Shockley partial dislocations (2c). These partial dislocations are fully emitted and reside on $(1\bar{1}\bar{1})_{in}$. There is a second dislocation system emitted into the twinned region (2b); both Shockley partial and perfect dislocations are emitted in about equal numbers and reside on the $\pm\ ^{a}/_{2}[110]_{out}(\bar{1}11)_{out}$ system. The third system is complex, resulting in the emission of multiple systems into the twinned region (3a, 3b) as well as two separate dislocation systems back emitted into the original grain (3c, 3d). Due to overlapping dislocations, the dislocations in the twinned region could not be characterized. Apart from the three visible systems in the image, a large number of dislocations are mobile in the twin boundary; these migrated from interactions elsewhere on the boundary and influence the interactions involving at least system 3.

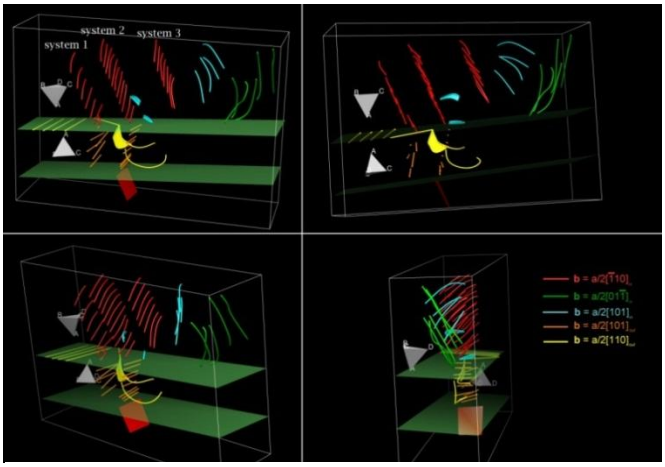

Figure 2. Three-dimensional model of interaction shown in Fig. 1.

Analysis of these interactions in terms of the slip transfer criteria proposed by Lee *et al*. [1] shows that the dominant factor controlling the interaction is the magnitude of the Burgers vector of the dislocation left in the grain boundary as a result of the transfer process. The local resolved shear just has to be sufficient to cause dislocation glide. This example illustrates the complexity of the processes and indicates the advances needed in predictive modeling to realistically treat the mechanical properties of polycrystalline systems or ones with a high density of interfaces.

The second example, demonstrates use of knowledge of dislocations and diffraction contrast theory to construct a model using images acquired over a small angular range and with no attention paid to the diffraction condition. Essentially, knowing dislocations must terminate at

free surfaces allows positioning of markers at these sites. The markers used in the alignment and reconstruction process. An example of the application of this method to dislocation interactions with a grain boundary at 400°C is presented in Figures 3 and 4. The time evolution of the interaction of incoming partial dislocations with a random high-angle grain boundary, found using electron backscatter diffraction (EBSD) to be a 36° rotation about the $[\bar{1}1\ \bar{2}2\ \bar{2}]_{in}$ are presented in Fig. 3. Images were acquired at 1° intervals over a tilt range from -29° to +28° using a single-axis tilt stage without attention to the diffraction condition. Consequently, imaging conditions vary and bend contours obscure parts of the dislocation pileup in some images, see Fig. 4. The markers indicating the intersection of the line dislocation with the free surface and select views from the reconstructed dislocation model are presented in Figure 4. The incoming dislocations reside on the $\pm{}^{a}/_{2}[10\bar{1}]_{in}(111)_{in}$ slip system and have a line direction near parallel to $[10\bar{1}]_{in}$. The back-emitted system is $\pm\ {}^{a}/_{2}[10\bar{1}]_{in}\ (1\bar{1}1)_{in}$. The dislocations were absorbed and within 0.1 s partial dislocations with an extended faulted region trailing the lead partial dislocation were emitted, see Figs. 3b and 3c. The partial dislocations were found to have a combined Burgers vector $\pm{}^{a}/_{2}[10\bar{1}]_{out}$ and to reside on $(111)_{out}$. The Burgers vector of the individual partial dislocations must be either $\pm{}^{a}/_{6}[2\bar{1}\bar{1}]_{out}$ or $\pm\ {}^{a}/_{6}[11\bar{2}]_{out}$, however, the information was insufficient to determine which was the lead partial dislocation. An additional system was emitted into the neighboring grain and remained near the boundary, preventing reliable characterization.

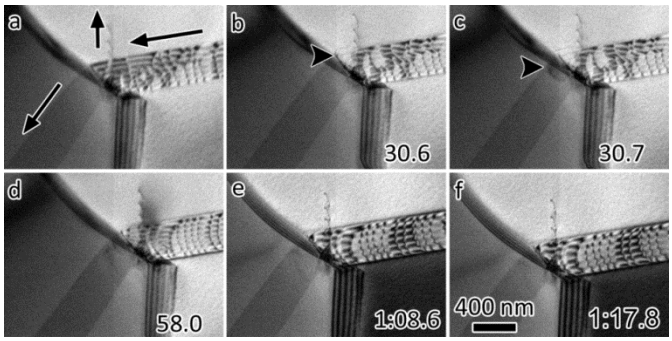

Figure 3. Frames taken from a video showing dislocations interacting with a high angle grain boundary during straining at 400°C. Video times are given in each image. Frames b and c indicate that, upon absorbing a dislocation (indicated by arrow head), a lead Shockley partial dislocation is emitted from the boundary within $1/10^{th}$ of a second.

To understand what type of dislocation is selected for emission by the grain boundary, it is necessary to consider the magnitude of the dislocation left in the boundary by the interaction. Dislocations with a Burgers vector of $\pm{}^{a}/_{2}[10\bar{1}]_{out}$, $\pm{}^{a}/_{2}[1\bar{1}0]_{out}$, or $\pm{}^{a}/_{6}[2\bar{1}\bar{1}]_{out}$ generate grain boundary dislocations with the minimum Burgers vector, $\left|b_r^{gb}\right|$. However, emission of a partial dislocation with $b=\pm{}^{a}/_{6}[2\bar{1}\bar{1}]_{out}$ increases $\left|b_r^{gb}\right|$, which accounts for the extended faulted region. Figure 5 displays a comparison of the relative resolved shear stress on the available partial dislocation systems as well as the normalized values of $\left|b_r^{gb}\right|$, associated with each system. As can be seen, the highest resolved shear stress acts on the partial dislocation with b

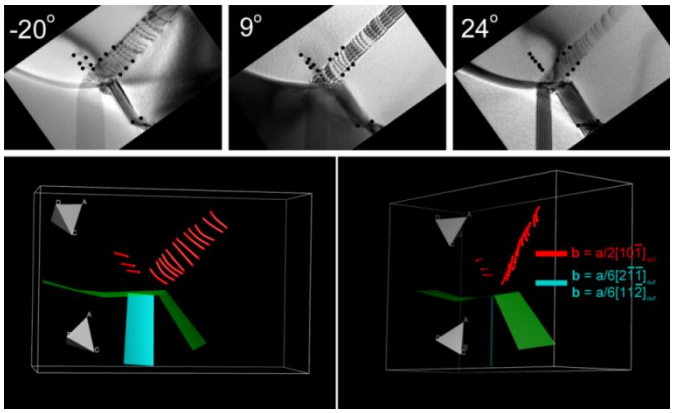

Figure 4. 3D-dislocation model of interaction shown in Figure 3 with example aligned images used in the tomogram reconstruction. Stage tilt is given in each image. The alignment markers are present in the images as black circles.

$= \pm a/6[2\bar{1}\bar{1}]_{out}$. The next two optimal systems, $\pm a/6[21\bar{1}]_{out}(111)_{out}$ and $\pm a/6[2\bar{1}1]_{out}(11\bar{1})_{out}$, have lower resolved shear stress acting on them, suggesting that the resolved shear stress acts as a deciding factor between possible dislocation systems that leave similar values of $\left|b_r^{gb}\right|$. The trailing partial dislocation emitted from the grain boundary has a significantly smaller resolved shear stress, giving an additional reason for why it is not emitted and an extended faulted region exists. However, the trailing partial was emitted occasionally suggesting perhaps an additional, but undetermined, factor is operating. This study is furthering our understanding of how partial dislocations interact with grain boundaries.

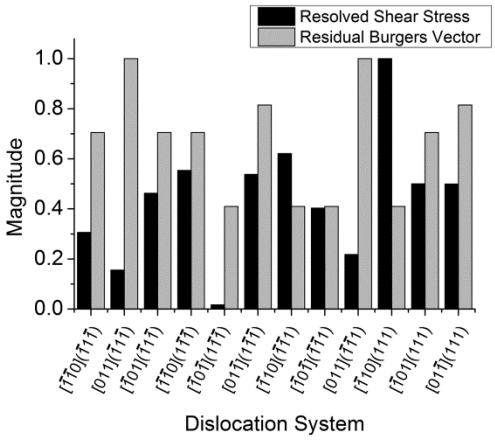

Figure 5. Relative resolved shear stress and normalized magnitude of the Burgers vector of the residual grain boundary dislocation from the interaction shown in Figure 3 on all available slip systems involving partial dislocations in the emitted grain.

Future Directions:

Future directions include extension of the three-dimensional method to the characterization of dislocation interactions in hexagonal closed packed and body centered cubic systems. A collaboration has been initiated with Jörg Wiezorek, University of Pittsburgh, to investigate the potential of using bright-field precession TEM to overcome some of the challenges facing the application of electron tomography in defect analysis. Initial experiments have shown that with careful selection of the precession angle and shape, the fluctuations in image contrast throughout a tilt series can be greatly reduced or eliminated altogether, resulting in uniform background contrast over a wide angular range. Additionally, because with precession a whole range of deviation values are being probed simultaneously, the effect of minor deviations from the specific imaging condition does not have a major effect. The reshaping of the precession path into a narrow ellipse oriented along systematic row - effectively rocking the beam - enables retention of the beams around the center and use of a smaller aperture. Further refinement of the technique is underway.

References

1. Lee, T.C., I.M. Robertson, and H.K. Birnbaum. Philos Mag A. **62** (1990) 131-153

List of Publications:

J. Kacher, G. Liu, and I.M. Robertson. Scripta Mater. **64** (2011) 677-680

J. Kacher, I.M. Robertson, M. Nowell, J. Knapp, K. Hattar. Mater Sci Eng A. **528** (2011) 1628-1635

G.S. Liu and I.M. Robertson. J Mater Res. **26**:4 (2011) 514-522

M. Tanaka, G.S. Liu, T. Kishida, K. Higashida, and I.M. Robertson. J Mater Res. **25**:12 (2010) 2292-2296.

Josh Kacher, IM Robertson, Quasi-four-dimensional analysis of dislocation interactions with grain boundaries in 304 stainless steel. Acta Materialia, accepted for publication, 2012.

Josh Kacher, Grace Liu, IM Robertson Three-dimensional characterization of dislocation-defect interactions. 3D Conference proceedings, July 2012.

Project title: Dynamical Nanoscale Electron Crystallography

Chong-Yu Ruan
Michigan State University, East Lansing, MI 48824. E-mail: ruan@pa.msu.edu

Program Scope:

Ultrafast electron crystallography (UEC) has already been proven to be useful in inspecting nanomaterials, where the strong electron scattering cross-section allows sufficient signals to be obtained close to the single particle level as the detection sensitivity generally wanes for other ultrafast probes. Ultrafast electron crystallography is also suited for the investigation of complex materials where the underlying emerging mesoscopically ordered states can be manifested in the diffraction pattern as non-Bragg features (satellites, stripes, etc.), which can be examined along with the primary Bragg reflections to report the fundamental mechanism. For example, the anisotropic electron-phonon coupling, essential to the formation of charge density waves and quasi-1 D Peierls-distorted insulator, will be present in the dynamical asymmetric responses at the momentum vector of the interaction. Because of the short-wavelength nature of electron scattering, large momentum space can be examined simultaneously, thus opening up novel access to various intriguing structurally related properties that cannot be easily examined by spectroscopic techniques. Our program seek to utilize these novel capabilities of UEC to address the fundamental problems associated with the complex phase transitions in correlated systems and to evaluate the various important plasmonics-enhanced affects associated with metallic nanoparticles. While rather different in their respective applications, a common theme exists in the two researches: enhanced functionality is enabled on the nanometer scale where selectivity and strong correlations between different degrees of freedom play a central role.

Recent Progress

I. Investigation of the space charge effects in ultrafast electron diffraction and microscopy.

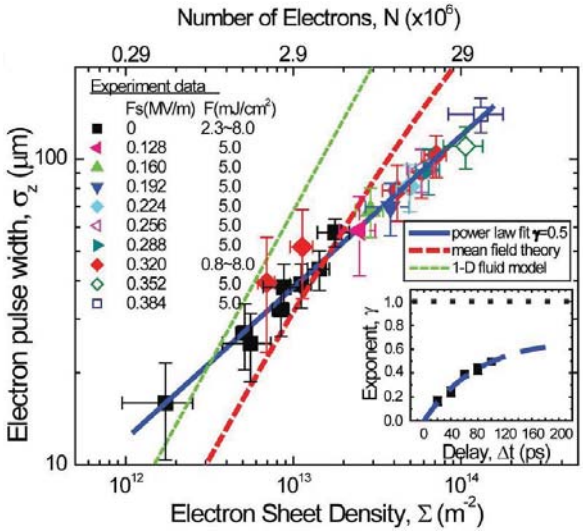

Fig. 1 Dependence of pulse length on the electron sheet density at time 100 ps for various photoexcitation fluence F and extraction field at the cathode surface F_a, showing a universal power-law increase with exponent roughly γ~0.5. Predictions based on mean-field and one-dimensional (1D) fluid models are also presented.

Realization of high-brightness ultrafast electron diffraction and imaging technology is highly challenging in that the space and time resolutions might be degraded by the space-charge effects. By employing a direct ultrafast photoelectron beam characterization based on a shadow projection imaging technique[1], the spatial and temporal evolution of a non- uniform, intense photoelectron pulse was investigated in a DC photo-gun geometry. Combined with N-particle simulations and an analytical Gaussian model, we elucidated three essential space-charge-led features: the pulse lengthening (Coulomb explosion) following a power-law scaling growth, the broadening of the initial energy distribution, and the virtual cathode threshold. The results from this investigation have been used to serve as a baseline in the design of a new RF-enabled high-brightness ultrafast electron microscope[2].

II. *Investigation of charge density waves in layered $CeTe_3$ compound.*

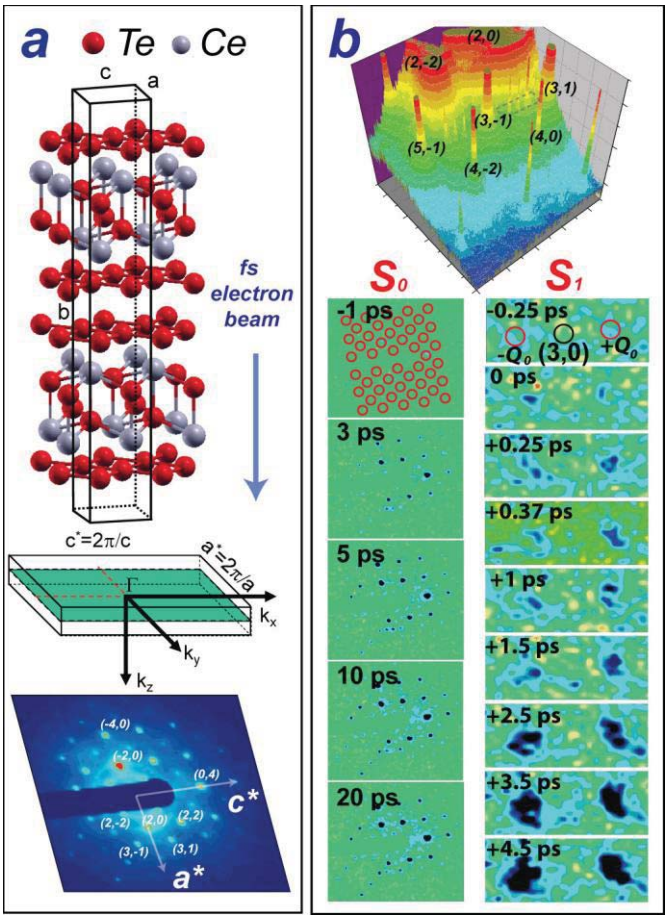

Fig. 2 (a) Crystal structure of $CeTe_3$. A charge density wave (CDW) is present within 2D Te planes, causing a periodic lattice modulation with a wave-vector $\mathbf{Q_0}$ along the crystal-c axis. (b) A scale-up 3D view of the diffraction pattern shows CDW satellite features in the region near the q=3**a***. The time-resolved crystallography examine the laser-induced melting of CDW by monitoring the satellite peak intensity (S_1) and the lattice fluctuational dynamics through Bragg reflections (S_0).

The coexistence of phases through complex couplings between different degrees of freedom (spin, charge, lattice, orbital) is a hallmark of complex materials with emerging properties such as charge density wave (CDW), superconductivity, and colossal magnetoresistivity. In particular, CDW is predicted to form in highly anisotropic systems where long- range charge ordering (CO) and periodic lattice distortion (PLD) are strongly coupled, driven by instabilities originated in either the electronic (Mott) or phononic (Peierls) subsystems. Recent femtosecond spectroscopy-based pump-probe techniques offered real-time characterizations of nonequilibrium dynamics in the different regimes of electron-phonon coupling, but their properties cannot be conclusively determined due to the observed similarity in their temporal responses representative of mostly the evolution of CO state. Using ultrafast electron crystallography, we provided a complementary view from ultrafast electron crystallography investigation of $CeTe_3$, exploiting its elegant 2D weakly correlated feature, serving as an ideal system to understand the symmetry breaking phase transition in strongly coupled electron-phonon system. We specifically examined the fluctuational dynamics using the momentum-dependent dynamical diffraction features to address the open questions. Following a strong perturbation of electron density, we observed clear evidences of nonconcerted suppressions of CDW, expressed in the ionic frame as an unexpected 2D lattice hardening and a short-lived topologically fragmented state in the long-range PLD network resulted from CO suppression, and highly nonuniform fluctuational amplitudes that are signatures of strong anisotropic electron-phonon coupling driving PLD, respectively. The nature of the transition was explained using a three-temperature model, in which the first part of the dynamics can be reconciled with the optical observations of electronic suppression; while the second part manifested in the nonadiabatic ionic responses is highly system-dependent, and informative of the electron-phonon mechanism for CDW formation.

III. Decoupling of structural and electronic phase transition in VO_2.

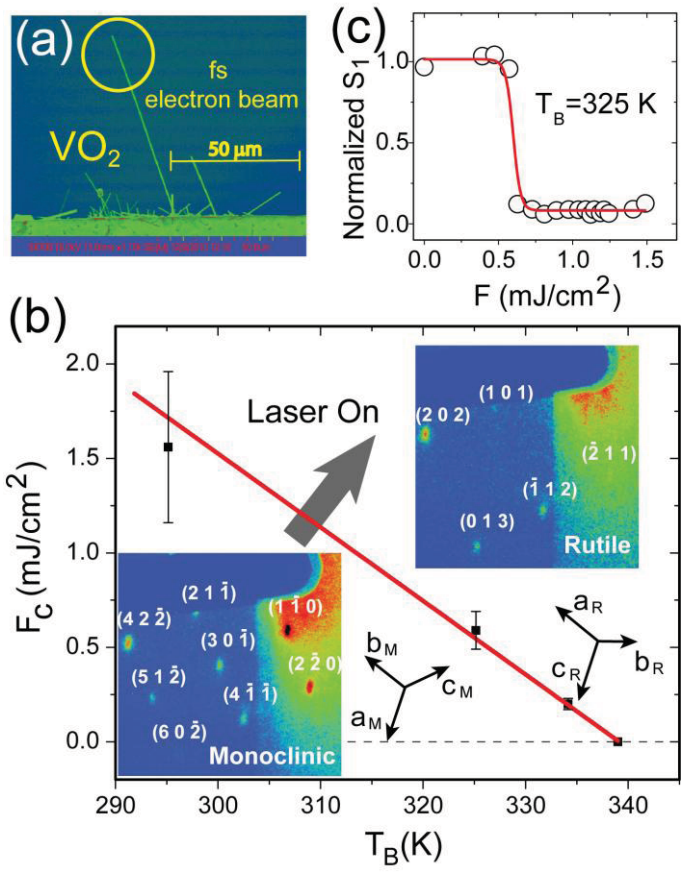

Fig. 3 (a) The SEM image of VO_2 microbeams grown on a Si substrate. (b) The critical fluence (F_c) for inducing the monoclinic-to-rutile transition as a function of base temperature T_B. The insets show the corresponding UEC patterns of the two phases. (c) The threshold behavior of laser induced phase transition, as characterized by the disappearance of the dimer reflections (S_1).

Using optical, TEM and ultrafast electron diffraction experiments we find that single crystal VO_2 microbeams gently placed on insulating substrates or metal grids exhibit different behaviors, with structural and metal-insulator transitions occurring at the same temperature for insulating substrates, while for metal substrates a new monoclinic metal phase lies between the insulating monoclinic phase and the metallic rutile phase, which we show may be stabilized by charge doping. Informed by our ultrafast single-beam measurements, the metal-insulator transition in the undoped case can be classified as Mott-driven, Peierls-limited, where the imposed cooperativity is mainly governed by the large spectral weight and the high energy scale inherent to the Peierls transition and that such stabilizing features are subjective to the strong Coulomb interaction predominant only in the insulating state without doping. We also uncover the unique delocalized nature of the interface-mediated charge doping effect that can be rationalized with an active spectral weight transfer from the unfilled band to the Peierls band in the monoclinic structure, which enhances the Peierls interaction supported by its selective effect on the structure phase transition temperature. While the results presented here are very specific, they are generally compatible with the Peierls-Mott scenario proposed by most recent theories, and amazingly reconcilable with an array of different experiments supportive of either Peierls or Mott scenarios.

Future Plans

Recently there has been a lot of progress in understanding the surface plasmon resonances (SPR) phenomena associated with metallic nanostructures[3]. By manipulating the composition, shape, and size of plasmonic nanoparticles, it is possible to design nanostructures that interact with the entire solar spectrum and beyond. The unique capacity of plasmonic nanocrystals to concentrate electromagnetic radiations in the proximity of nanocrystal surface and then covert the energy stored in the photon fields into electrical, chemical, and thermal energies is very appealing. Already, there are a surge of applications recently utilizing these features to enhance the performance of

photocatalysis, solar cells, and heat-induced selective tissue targeting, enabling a rapidly growing fields in nanoscience in the last decade. We will couple the ultrafast surface diffraction and time-of-flight mass spectrometry to provide simultaneous information on the microscopic couplings between the local plasmons and the activated electronic and phononic degrees of freedom. The key reaction coordinates to elucidate are the charge-mediated and thermally mediated channels for enhanced photoreactions. By manipulating the local morphology, we aim to control the field-enhancement and prioritize either local charge-transfer-induced or remote resonance-transfer-mediated reaction channels. Currently, there has been no consensus regarding the detailed coupling channels in plasmonics catalysis, but there is a high demand for the technology to improve its efficiency to meet the challenge of mass conversion of solar energy into chemical energy. The ultrafast electron crystallography and voltammetry methodologies offers unique capabilities to simultaneously track the electronic and structural dynamics, which are good matches to these investigations [4,5].

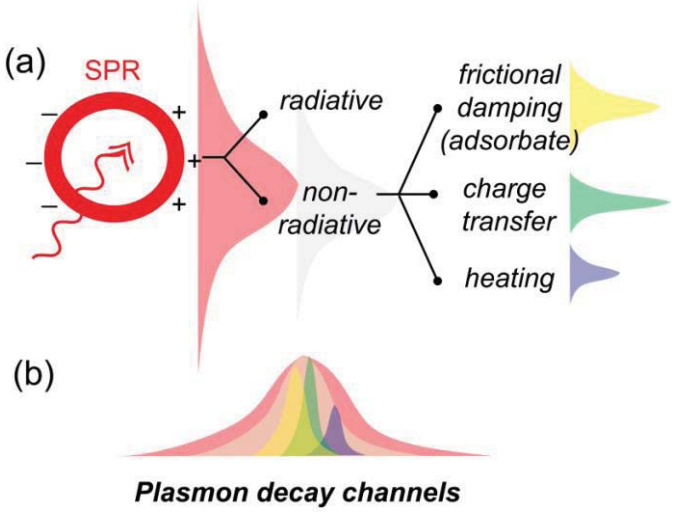

Fig. 4 (a) Various radiative and non-radiative decay channels of surface plasmons. (b) The homogeneous bandwidth at surface plasmon resonance is sustained by substituent responses from various decay channels, which can be elucidated by probes that are sensitive to the physical parameters coupled to surface plasmon decay.

Reference to DOE sponsored publications (since 2010)

1. Z. Tao, H. Zhang, P.M. Duxbury, M. Berz, C-Y. Ruan, "Space-charge effects in ultrafat electron diffraction and imaging", *J. Appl. Phys.* **111**, 044316 (2012).
2. Z. Tao, H. Zhang, R.K. Raman, T.-T. Han, K. Chang, M. Berz and C.-Y. Ruan, "Progress of Dynamical Nanomaterial imaging using ultrashort electron pulses". *Microsc. Microanal.* 16 (Suppl. 2), 498-499 (2010).
3. R.K. Raman, R.A. Murdick, R. Worhatch, Y. Murooka, S.D. Mahanti, T-R. Han, C.-Y. Ruan, "Electronically driven photo-fragmentation of silver nanocrystal revealed by ultrafast electron crystallography". *Phys. Rev. Lett.* 104, 123401 (2010).
4. K. Chang, R.A. Murdick, Z. Tao, T.-R. T. Han, C.-Y. Ruan, "Ultrafast electron diffractive voltammetry: General formalism and applications" (Review article) *Mod. Phys. Lett. B* **25**, 2099 (2011).
5. C.-Y. Ruan, Four-Dimensional Electron Nanocrystallography, Research in Optical Sciences, OSA Technical Digest (Optical Society of America, 2012), paper IT3D.5.

1. Title: ER46317: "Spin-Polarized Scanning Tunneling Microscopy Studies of Nanoscale Magnetic and Spintronic Nitride Systems"

PI: **Arthur R. Smith**

Address: **Ohio University**
Nanoscale & Quantum Phenomena Institute
Department of Physics & Astronomy
Athens, OH 45701

E-mail: **smitha2@ohio.edu**

2. Research Scope

The scope of this project is to investigate the electronic and magnetic properties of nitride-based material systems, in particular specific bi-layer systems consisting of atomic layers of magnetic materials on semiconducting nitride surfaces. The material systems include ferromagnetic binary alloys, magnetic nitrides, and dilute magnetic nitride semiconductors. Such spintronic systems are of high interest as advanced materials for future energy-related applications. In order to probe these systems, this project is focused on the use of scanning tunneling microscopy (STM) and spin-polarized STM (SP-STM). The latter is a powerful technique which can provide spin information on surfaces with atomic-scale resolution. Combining ultra-high vacuum SP-STM together with molecular beam epitaxial growth in the same system, diverse nitride material systems can be explored in a pristine state.

3. Recent Progress

- **Spin-polarized STM of antiferromagnetic manganese nitride nanopyramids**

This work recently appeared in ***Nano Letters*** – "*Three-Dimensional Spin Mapping of Antiferromagnetic Nanopyramids Having Spatially Alternating Surface Anisotropy at Room Temperature*"

We discovered by using a small applied magnetic field that the surface anisotropy alternates between different terraces. The atomic terraces in the z-direction (surface normal) have the sequence MnN-MnN-Mn-MnN-MnN-Mn-… Intervening between pairs of MnN layers is always a single layer of Mn. When imaging the surface using normal STM, these two types of terraces can be clearly distinguished structurally, but only in conductance imaging with normal tips do the adjacent MnN terraces look different. At -0.3 V applied to the sample (filled sample states), the two MnN layers have nearly the same electronic contrast. We then use magnetic tips at the same -0.3 V, and then we get magnetic contrast. This magnetic contrast is seen in Fig. 1(a). When we apply a small out-of-plane magnetic field, the contrast on the MnN layers disappears. Since our tip vector rotates in the applied field, our tip becomes insensitive to in-plane contrast. So therefore, we

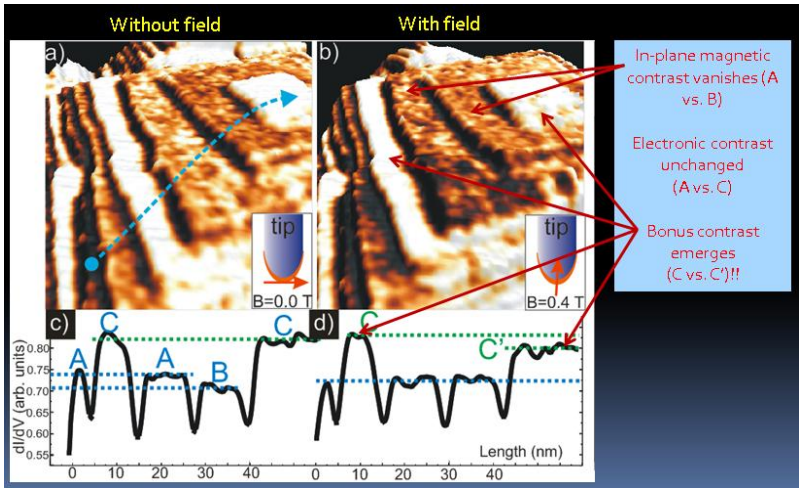

Fig. 1. SP-STM images of MnN spin pyramids with a) field OFF case; and b) field ON case. Line sections below in C) and D) illustrate the contrast between A and B layers without field and C and C' layers with field. [*Nano Letters (http://dx.doi.org/10.1021/nl204192n), (2012).***]**

verified that the 2 adjacent MnN layers have IN-plane magnetization.

We then notice that the Mn layers which normally appear bright at -0.3 V in comparison with the MnN layers, while remaining bright, now exhibit a distinguishable difference comparing consecutive Mn layers. This is faintly seen in the image of Fig. 1(b). Looking at the line sections shown in Fig. 1, the contrast between the A and B layers (MnN layers) is clear for the field OFF case, while the contrast between the C and C' layers (Mn layers) is clear for the field ON case. So therefore, we were surprised to find that the Mn layers show contrast only with field ON, which means that their magnetization is OUT-of-plane.

If you change contrast settings on the SP-STM image with field ON, it is possible to see the OUT-of-plane magnetic contrast of the C/C' (Mn) layers directly, as shown in Fig. 2.

The significance of these results is that we have been able to show the importance of detailed spin-polarized STM measurements at the nanoscale in clarifying the detailed magnetic anisotropy for more complex MBE-grown materials. It can have implications for other complex materials as well. For this result, our paper has been published in ***Nano Letters*** in January 2012.

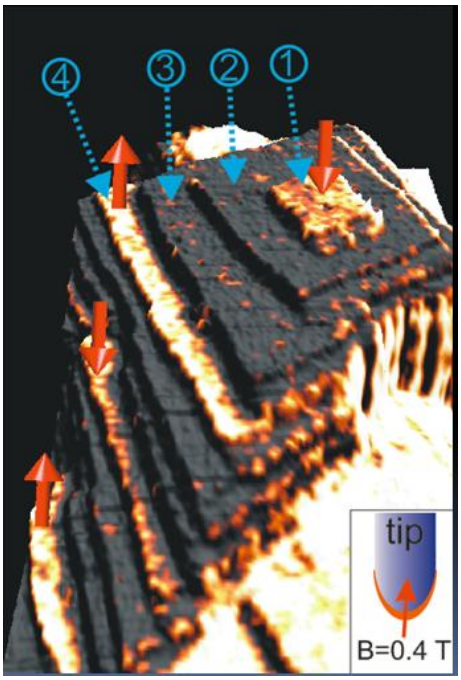

Fig. 2. SP-STM image of MnN Nano-pyramid in 3-D rendering, with contrast level suppressed, in which you can see the contrast on the C/C' layers when out-of-plane field is ON. [*Nano Letters***]**

- **Quantum size effect driven manganese gallium islands with quantum heights**

This work recently appeared in ***Applied Physics Letters***: "*Spontaneous Formation of Quantum Height Manganese Gallium Islands and Atomic Chains on N-polar Gallium Nitride(0001)*". In this paper we presented evidence for a quantum size effect driven growth mode in the manganese gallium/gallium nitride bilayer system.

The experiment begins by growing *N-polar* GaN(000$\underline{1}$) on sapphire(0001). Growth is terminated under gallium rich conditions, where the surface is expected to contain up to ~ 0.2-0.4 ML of excess Ga, some in the form of adatoms, some possibly in the form of Ga droplets. After this the sample is cooled to around 250 C, and then ~ 0.4 ML of Mn is deposited onto the Ga-rich surface.

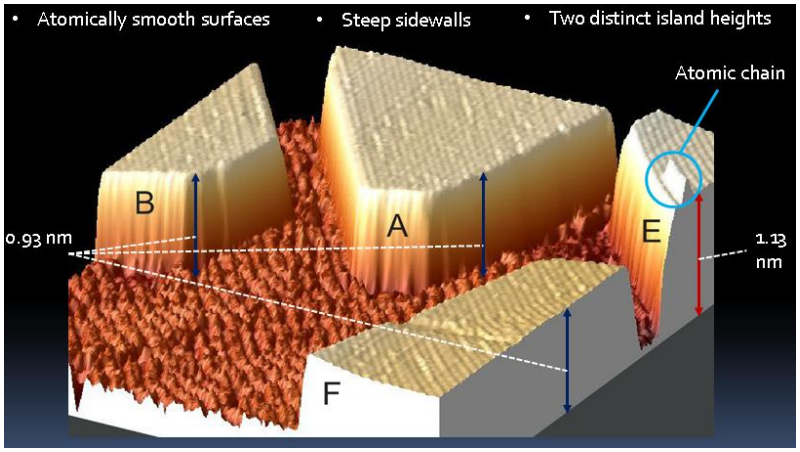

Fig. 3. 3-D rendered STM image of quantum height MnGa islands formed on GaN(000$\underline{1}$) surface. Image size is 80 nm x 87 nm, Vs = -0.87 V, It = 156 pA. Islands labeled B, A, F have the same height; the island labeled E has a different height which is higher by one atomic layer than B, A, F. [*Applied Physics Letters* *100*, 061602 (2012)**]**

Stunningly, what we find is the formation of 2-dimensional islands on the GaN surface, in which the heights of the islands are quantized, and in fact there are only 2 observed island heights. An STM image of the quantum height islands is depicted in Fig. 3. There we see that one type of island has height of 0.93 nm while the second type has a height of 1.13 nm. When the difference in height of the two types of islands is taken into account, we deduced that the two

islands are of 5 and 6 ML respectively.

While such quantum height islands have been seen before in other systems, for example Ag/GaAs(110) and Pb/Si(111),[1,2] here we have a very exciting new system to work with in which there is the possibility of a) magnetic properties of the quantum height islands; and b) tunability of the physical properties by variation of the island stoichiometry.

We have also discovered that the 5 ML height islands can spontaneously transform into 6 ML height islands which can contain atomic-width adatom chains on their surfaces. This is really just the beginning for the project on quantum height manganese gallium alloy islands. Much work remains to be done.

- **Ultra-thin manganese gallium thin films grown on *Ga-polar* GaN(0001)**

We have recently carried out a detailed study of MnGa ultra-thin films grown on GaN(0001). The thickness of these films on GaN ranges from 15-100 MLs. We obtain very high epitaxial quality, resulting in a highly ideal ferromagnet/semiconductor system. The MnGa alloy system is very interesting for future applications due to the sensitive dependence of the magnetic properties on the Mn:Ga alloy stoichiometry, going from ferromagnetic at 1:1 to partially antiferromagnetic at 3:1.[3,4]

STM images of the ultrathin MnGa films reveal the high epitaxial quality of the surfaces, in which single atomic-height steps are seen with angular facets. We are in the process of trying to understand the relationship between the structures that we see on the surface, which include a row-like structure and a hexagonal type structure, and the stoichiometry. We are very interested in understanding how the magnetic properties may vary with the surface structure and how they may be tuned.

We are currently collaborating with Professor Noboru Takeuchi and his student Reyes Garcia-Diaz, in order to carry out a theoretical study on this system. We are also closing in on spin-polarized STM measurements of the surface in order to determine the magnetic properties directly.

- **Giant spintronic response of Mn/GaN(000$\underline{1}$) to applied magnetic field measured using STM spectroscopy at room temperature**

We have developed a unique method of preparing a Mn/N-polar GaN(000$\underline{1}$) $\sqrt{3}\times\sqrt{3}$-R30° reconstructed surface. This is done by growing first GaN(000$\underline{1}$) under Ga-rich conditions then annealing to remove excess Ga adatoms. After this, 1/3 monolayer of Mn is added, and the $\sqrt{3}\times\sqrt{3}$-R30° structure forms. Theoretical calculations done by collaborators in Argentina show that this structure consists of 1 Mn per unit cell in a substitutional + T4 structure.[5]

This unique surface structure appears to have highly interesting spintronic properties. We have carried out an experiment in which we apply a magnetic field of up to 0.4 Tesla to this surface, at room temperature, while measuring I-V spectroscopy. The results, while preliminary, indicate a novel behavior when we look at the normalized conductance of this surface with field on versus with field off. In particular, we see a characteristic double peak structure around the Fermi level when plotting the % difference. Strikingly, we observe up to a 1600% increase in the normalized conductivity at Vs = +0.6 V.

The peak response may be plotted as a function of applied magnetic field. We find a rapid onset of the behavior over a small range of field less than 100 Gauss, while at higher fields it becomes saturated.

4. Future Plans

In the coming year, we will continue investigating magnetic and spintronic nitride systems and measurement of the spin structures and behaviors of the surfaces. We plan to continue to explore the Mn-containing GaN surfaces and their behavior under applied magnetic fields. We will also continue

[1] A. R. Smith, K. J. Chao, Q. Niu, and C. K. Shih, Science **273**, 226 (1996).
[2] T.-L. Chan, C. Z. Wang, M. Hupalo, M. C. Tringides, and K. M. Ho, Phys. Rev. Lett. **96**, 226102 (2006).
[3] E. Lu, D. C. Ingram, A. R. Smith, J. W. Knepper, and F. Y. Yang, Phys. Rev. Lett. **97**, 146101 (2006).
[4] W. Van Roy, H. Akinaga, and S. Miyanishi, Phys. Rev. B **63**, 184417 (2001).
[5] A. Chinchore *et al.*, manuscript in preparation.

studying Fe-containing GaN surfaces to extend current data sets. Measurements at both room temperature and cryogenic temperatures will provide highly complementary information.

Regarding the spin pyramid study, we plan to further explore how the unusual magnetic anisotropy varies with growth conditions and if we can find correlations of magnetic properties in adjacent islands.

We also plan to continue further studies on the quantum height MnGa islands occurring on the N-polar GaN surface, and to explore their electronic and magnetic properties, and the possible dependence of those properties on the quantum size effect.

With regard to the MnGa ultra-thin films grown on Ga-polar GaN, we are about to begin spin-polarized measurements on these surfaces as a function of the surface structure and growth stoichiometry. The ultimate goal is to be able to control and measure the magnetic properties down to the atomic scale.

Finally, the giant spintronic response data needs to be further confirmed. At the same time, we also plan to work with our theory colleagues to find a theoretical explanation for what we see. We also plan to attempt similar experiments using different magnetic atoms to find out if the behavior can be observed in other magnetic systems. In any case, this Mn/GaN system is very promising for nanospintronics since the observed behavior is large in magnitude and occurs at room temperature.

5. Publications of DOE sponsored research (2010-2012)

A.R. Smith's full publication list can be seen at http://www.phy.ohiou.edu/~asmith/publist.html.

70. Three-Dimensional Spin Mapping of Antiferromagnetic Nanopyramids Having Spatially Alternating Surface Anisotropy at Room Temperature, Kangkang Wang and Arthur R. Smith, Nano Letters (http://dx.doi.org/10.1021/nl204192n), (2012).
69. Spontaneous Formation of Quantum Height Manganese Gallium Islands and Atomic Chains on N-polar Gallium Nitride(000-1), Abhijit Chinchore, Kangkang Wang, Meng Shi, Yinghao Liu, and Arthur R. Smith, Applied Physics Letters **100**, 061602 (2012).
68. The effect of growth parameters on CrN thin films grown by molecular beam epitaxy, Yinghao H. Liu, Kangkang Wang, Wenzhi Lin, Abhijit Chinchore, Meng Shi, Jeongihm Pak, Arthur R. Smith, and Costel Constantin, Thin Solid Films **520**, 90 (2011), 10.1016/j.tsf.2011.06.052.
67. Efficient Kinematical Simulation of Reflection High-Energy Electron Diffraction Streak Patterns for Crystal Surfaces, Kangkang Wang and Arthur R. Smith, Computer Physics Communications **182**, 2208 (2011).
66. A Modular Designed Ultra-High-Vacuum Spin-Polarized Scanning Tunneling Microscope with Controllable Magnetic Fields for Investigating Epitaxial Thin Films, Kangkang Wang, Wenzhi Lin, Abhijit V. Chinchore, Yinghao Liu, and Arthur R. Smith, Review of Scientific Instruments **82**, 053703 (2011).
65. Structural Controlled Magnetic Anisotropy in Heusler $L1_0$-MnGa Epitaxial Thin Films, Kangkang Wang, Erdong Lu, Jacob W. Knepper, Fengyuan Yang, and Arthur R. Smith, Applied Physics Letters **98**, 162507 (2011).
64. Two-Dimensional Mn Structure on the GaN Growth Surface and Evidence for Room-Temperature Spin Ordering, Kangkang Wang, Noboru Takeuchi, Abhijit Chinchore, Wenzhi Lin, Yinghao Liu, and Arthur R. Smith, Phys. Rev. B **83**, 165407 (2011).
63. Reflection High Energy Electron Diffraction and Atomic Force Microscopy Studies of Mn_xSc_{1-x} Alloys Grown on MgO(001) Substrates by Molecular Beam Epitaxy, Costel Constantin, Abhijit Chinchore, and Arthur R. Smith, Mater. Res. Soc. Symp. Proc. (2011), **1295**: mrsf10-1295-n05-37; doi:10.1557/opl.2011.458.
62. Structural, Magnetic, and Electronic Properties of Dilute MnScN(001) Grown by RF Nitrogen Plasma Molecular Beam Epitaxy, Costel Constantin, Kangkang Wang, Abhijit Chinchore, Han-Jong Chia, John Markert and Arthur R. Smith, Mater. Res. Soc. Symp. Proc. (2011), **1290**: mrsf10-1290-i08-02; doi:10.1557/opl.2011.178.
61. Growth of Epitaxial Iron Nitride Ultrathin Film on Zinc-Blende Gallium Nitride, Jeongihm Pak, Wenzhi Lin, Kangkang Wang, Abhijit Chinchore, Meng Shi, David C. Ingram, Arthur R. Smith, Kai Sun, J. M. Lucy, A. J. Hauser, and F. Y. Yang, J. Vac. Sci. Technol. A **28(4)**, 536 (2010).
60. Lattice Parameter Variation in ScGaN Alloy Thin Films on MgO(001) Grown by RF Plasma Molecular Beam Epitaxy, Costel Constantin, Jeongihm Pak, Kangkang Wang, Abhijit Chinchore, Shi Meng, Arthur R Smith, Mater. Res. Soc. Symp. Proc. Vol. **1202**, 1202-I05-25 (2010).
59. Magnetic and Electronic Properties of Fe0.1Sc0.9N/ScN(001)/MgO(001) Films Grown by Radio-Frequency Molecular Beam Epitaxy, Costel Constantin, Kangkang Wang, Abhijit Chinchore, Han-Jong Chia, John Markert, Arthur R Smith, Mater. Res. Soc. Symp. Proc. Vol. **1198**, 1198-E07-22 (2010).

Trimodal Tapping Mode Atomic Force Microscopy: Simultaneous 4D Mapping of Conservative and Dissipative Probe-Sample Interactions of Energy-Relevant Materials

Santiago D. Solares

Department of Mechanical Engineering
University of Maryland
2181 Glenn L. Martin Hall
College Park, MD 20742
ssolares@umd.edu

The overall goal of this project is to develop a trimodal, intermittent-contact atomic force microscopy (AFM) method for the rapid and simultaneous mapping of probe-sample conservative and dissipative forces in four dimensions (three spatial dimensions plus probe velocity). This new method will be applied to characterize the time-dependent degradation of alkaline anion exchange membranes (AAEMs) as a function of temperature, moisture content and mechanical strain. The project will include experimental work as well as multi-scale simulation ranging from the atomistic to the continuum scales.

Recent developments in multifrequency and band excitation AFM have enabled the rapid mapping of the cumulative effect of conservative and dissipative interactions in two dimensions (2D). However, while these advances are significant, they still do not enable a *full* description of the elastic or viscoelastic properties of the sample, because the 2D maps they provide depend on the hardware and imaging parameters, and the acquired information can be distorted by the non-constant depth at which all contact and intermittent-contact AFM methods explore the surface. Instead, the *quantitative* acquisition of the tip-sample junction properties requires that the conservative forces be measured as a function of the 3-dimensional (3D) tip position and that the dissipative forces be mapped as a function of 4 dimensions (4D) including the three Cartesian dimensions plus the vertical velocity. This project seeks to develop such a method based on trimodal intermittent-contact atomic force microscopy (see Figure 1), whereby one of the higher cantilever modes will be operated in self-excitation to measure the conservative tip-sample interactions in 3D (see Figure 2) while a different mode will be driven through band excitation to quantify the dissipated power in 4D. Figure 1 illustrates a preliminary experimental implementation of trimodal AFM using the first three cantilever eigenmodes to characterize block co-polymer surfaces *in 2D.* The results are promising but they are still limited to the lower cantilever eigenmodes and do not yet include broadband excitation controls. Figure 2 illustrates multi-scale simulation results demonstrating that it is fundamentally possible to measure tip-sample forces in 3D using self-excited higher eigenmodes in intermittent contact AFM, although this has not yet been realized experimentally.

The new method will be coupled with mechanical elongation stages, micro-heaters and humidity controls to evaluate *in situ* the *real-time* evolution and degradation of AAEMs by quantifying the damage induced by thermomechanical and environmental stresses in terms of the

tip-sample junction's viscoelastic response. Although a variety of approaches have been employed to manufacture AAEMs with different backbones and functional groups in order to create structures through which ions can move freely from one side to the other, there is still insufficient knowledge on transport mechanisms. It is therefore essential to characterize the AAEM conducting channels at the nanoscale in order to guide the synthesis of novel polymers with the desired conductivity. Furthermore, the mechanical strength of AAEMs under compression in humidified environments (as in fuel cells) is a critical aspect with regards to durability. The current technology to evaluate the mechanical strength is to simply employ tensile tests to measure the Young's modulus. However, such tests are bulk analyses that evaluate the mechanical strength in isolation from the ion conducting properties, and can thus only reflect the intrinsic material strength in a dry, non-operational state, which is not the real case in the fuel cell. In contrast, the proposed approach will enable in-situ nanoscale coupled measurement of conductivity and mechanical strength of AAEMs.

This is a new project, so there are not yet any significant results to report.

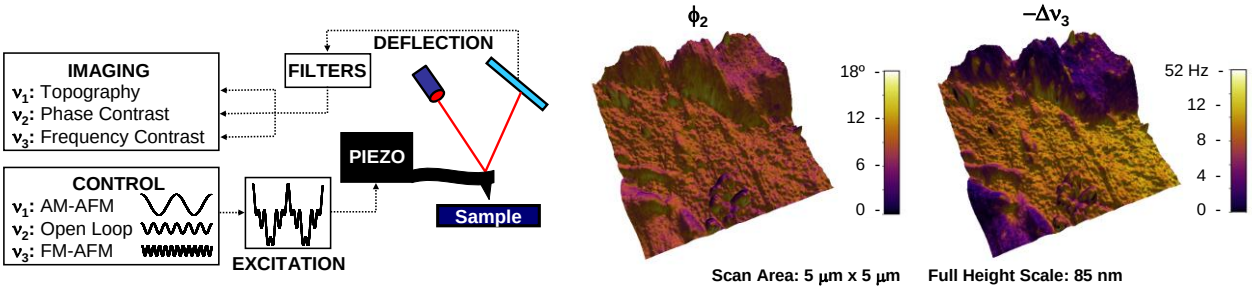

Figure 1. *Schematic of previously implemented triple-frequency intermittent-contact AFM controls scheme (left); typical images of the second eigenmode phase (ϕ_2, center) and negative of the third eigenmode frequency shift ($-\Delta\nu_3$, right) superimposed on the topography acquired with the first eigenmode for a tri-block co-polymer calibration standard. [S. D. Solares and G. Chawla, J. Appl. Phys., 108, 054901 (2010)]*

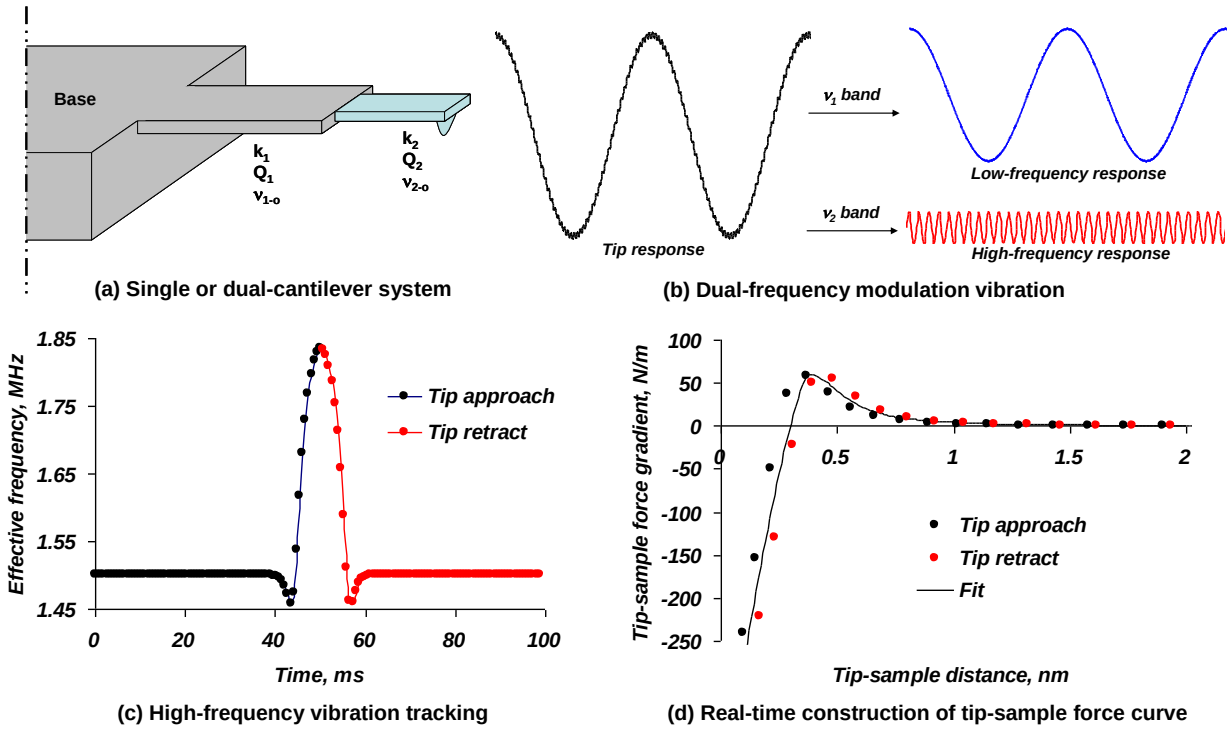

Figure 2. *Dual-frequency-modulation AFM method with a dual-cantilever system (two flexural eigenmodes of a single cantilever can also be used). The cantilever system (a) is excited such that its vibration is the superposition of two separable self-excited oscillations (b). The frequency of the higher-frequency oscillation is tracked and recorded in real time (c) and related to the tip-sample force gradient as a function of the vertical tip-sample distance, which is obtained from the lower-frequency oscillation (d). The tip-sample interaction force curve can in principle be obtained at every pixel by numerical integration of the force gradient. This procedure could enable the acquisition of 3D images of the force or force gradient through conventional raster scans. [G. Chawla and S. D. Solares, Meas. Sci. & Technol., 20, 015501 (2009)]*

Electron nanodiffraction - Seeing bonds, STEM Lithography, Oxide superlattices

John C. H. Spence and and others (1 - 12)
Arizona State University
Tempe Az. USA. 85287-1504.

DE-FG03-02ER45996

1. Scope.

This biannual report summarizes progress in our development of quantitive electron nanodiffraction to materials problems, especially devoted to atomistic processes in semiconductors and electronic oxides such as the new artificial oxide multilayers, where our microdiffraction is complemented with energy-loss spectroscopy (ELNES) and aberration-corrected STEM imaging (9). The method has also been used to map out the chemical bonds in the important GaN semiconductor (1) used for solid state lighting, and to understand the effects of stacking sequence variations and interfaces in digital oxide superlattices (8). Other projects include the development of a laser-beam Zernike phase plate for cryo-electron microscopy (5) (based on the Kapitza-Dirac effect), work on reconstruction of molecular images using the scattering from many identical molecules lying in random orientations (4), a review article on space-group determination for the International Tables on Crystallography (10), and the development of a new method of electon-beam lithography (12). We briefly summarize here the work on GaN, on oxide superlattice ELNES, and on lithography by STEM.

2 (a). Bonding in GaN.

Our paper on mapping out the chemical bonds between atoms in Galium Nitride using quantitative convergent-beam electron microdiffaction methods was finally published in late 2010 (1). GaN is an important solid-state lighting material used for energy-saving lighting applications. This project was a large undertaking over several years, in collaboration with the materials department in Cambridge UK. The significance of the work is that the polar bond in this material has now been directly observed for the first time. The redistribution of valence charge density which occurs when atoms bond to form a solid is extremely small, and has only been seen in non-centrosymmetric crystals (where phases can have any value, and cannot be measured directly by X-ray diffraction) using our method of extinction-free structure-factor phase measurement. We were able to compare the results with first-principles electronic-structure calculations, in order to test these against experiment.

2(b). Structurally induced magnetization in an $La_{2/3}Sr_{4/3}MnO_4$ superlattice.

A structural transition has been observed (11) in a digital superlattice of $La_{2/3}Sr_{4/3}MnO_4$, which is correlated to a magnetization enhancement upon cooling the sample. These artificial superlattices were grown layer-by-layer using ozone-assisted MBE Electron diffraction experiments show a phase transition below 150 K in nanopatches of the superlattice, which coincides with an enhanced magnetization starting below 110K. Atomic scale electron energy loss spectroscopy also shows changes in the Mn $L_{2,3}$ and O K edges, which are related to valence, strain, and the atomic coordination within nanopatches. Figure 1 shows typical ELNES spectra recorded using an aberration-corrected STEM instrument with 1Angstrom diameter probe. We also expect to detect the magnetic phase transition at the interface at 150 K from additional astigmatism appearing in bright-field HREM images by the Lorentz contrast mechanism.

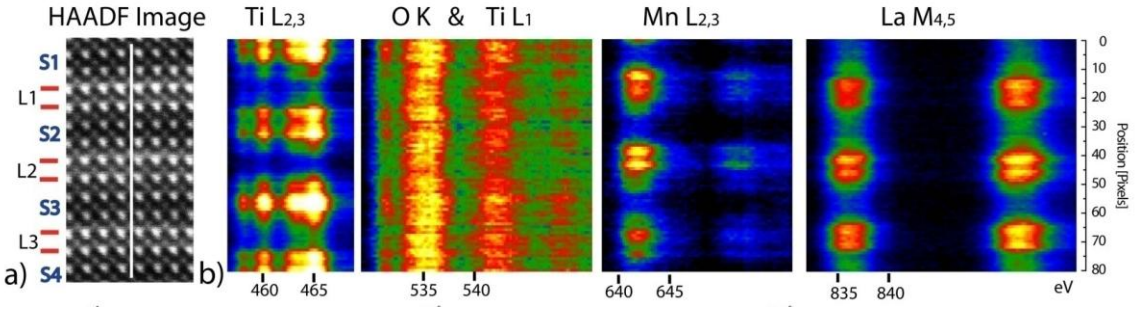

Figure 1. STEM ADF image of 2x2 LaMnO3-SrTiO3 oxide artificial superlattice, with corresponding ELNES inner-shell spectra. The vertical axis of the spectra is aligned with corresponding position in the STEM image, and the horizonal axis is energy loss at an absorption edge. Color shows intensity of inelastic scattering.

2(c). Direct-write Electron Beam Lithography on Silicate Glass using STEM.

We have described (12) a study of direct-write, one-step electron beam lithography of silicate glass resists using STEM (Scanning transmission electron microscopy). We obtained a 2.5 nm half-pitch resolution in soda-lime-silica glass resist, as shown in figure 2. For $CaSiO_3$ glass and the EELS results show that alkali- and alkaline-earth ions were driven out of the irradiated area by the electron beam, so that one writes lines of elemental silicon. The composition separation is related to selective breaks in ionic and covalent bonded components, and this local chemical re-bonding is revealed by modelling the ELNES.

3. Future plans.

As described in our renewal proposal, we plan now to study the dynamics of ion transport at the atomic level during the cycling of battery materials. More specifically, energy-loss near-edge fine structure (ELNES) and nano-diffraction will be used to monitor changes in microstructure, ion occupation and distribution under the application of high electric fields to ionic conductors. ELNES provides similar information to soft-Xray absorption spectroscopy (i.e. three-dimensional local atomic coordination and electronic structure), but on a nanometer resolution scale. New insights are expected due to the use of our unique instrumentation; specifically, the experiments will be carried out using the newly installed monochromated cold field-emission aberration-corrected Nion scanning transmission electron microscopy (Nion STEM), with its millivolt (70meV) spectral resolution and Angstrom-level spatial resolution. This work builds on our many published papers over a decade on the study of radiation damage by time-resolved ELNES in ionic materials (13). The essential idea is to use the electric field generated by the electron beam-induced charge in these insulators (where screening is absent) to mimic the electric fields within battery materials, while observing changes in local chemistry from recordings of the time-dependance of the near-edge structure and nanodiffraction patterns.

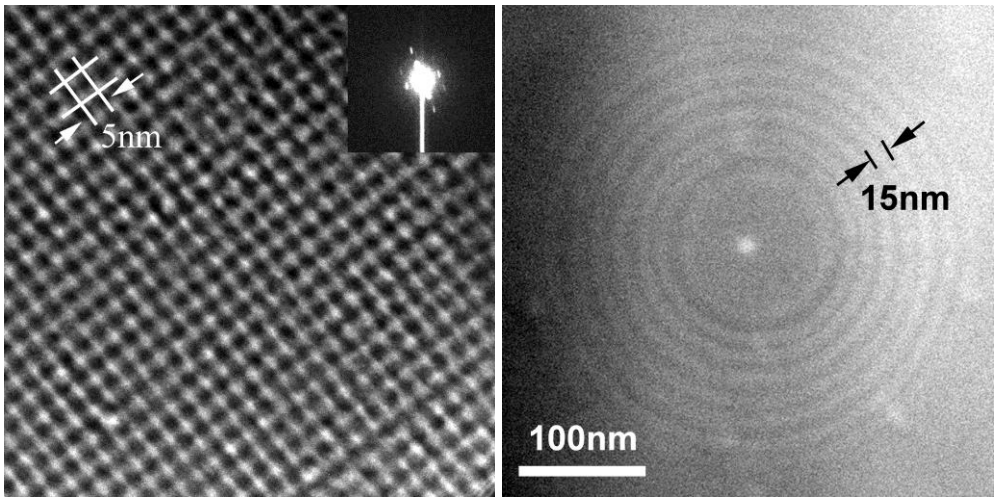

Figure 2. These patterns of elemental silicon in silicate glasses were written with a 0.2nm STEM probe, giving lines with 5nm period.

References, acknowledging DOE DE-FG03-02ER4559

1. "Combined structure factor phase measurement and theoretical calculations for mapping of chemical bonds in GaN". B. Jiang, J.Zuo, D. Holec, C. Humphreys, M. Spackman and J.Spence. Acta Cryst. A66, 446 (2010).

2. "Silicide characterization at alumina-niobium interfaces". J.T. McKeown, V.R. Radmilovic, R.Gronsky, and A.M. Glaeser. J. Mat. Sci 46, 3969 (2011).

3. "Reconstruction from a single diffraction pattern of azimuthally projected electron density of molecules aligned parallel to a single axis. D.K.Saldin, V.L. Shneerson, D. Starodub, J.C.H.Spence. Acta Cryst. A66, 32-37 (2010)

4. "Structure of a single particle from scattering by many particles randomly oriented about an axis toward structure solution without crystallization". D. Saldin, V. Shneerson, M. Howells, S. Marchesini, H. Chapman M. Bogan, D. Shapiro, R. Kirian, K. Schmidt, J. Spence. New J. of Phys. 12 p.035014 (2010).

5. "Design of TEM phase plate using a focussed continuous-wave laser" H. Muller, J. Jin, R. Danev, J. Spence, R. Glaeser. New J. Phys. (2010) 073011 .

5. "Automatic recovery of missing amplitudes and phases in tilt-limited electron crystallography of 2D crystals". B. Gipson, D. Masiel, N. Browning, J. Spence, K. Mitsuika, H. Stahlberg, Phys Rev E 84, 011916 (2011).

6 "Defects and Ionic diffusivity of Pb in β" alumina". S.D.Kim, Y.W.Kim, J.T. McKeown, M. O'Keeffe, E.E. Hellstrom, W.T. Petuskey, U. Weierstall and J.C.Spence. Proc Int Cong. Micros. Rio (2010). In press.

7. "Encapsulation-induced stabilization of dimensionallly restricted metallic alloy wires" J. Sugar, J. McKeown, V. Radmilovic, A. Glaeser, R. Gronsky. Acta Mat. 58, 5332 (2010).

8. "Diffraction from oxide superlattices - stacking sequence effects in plan view". J. Spence, A. Shah,, B.Nelson-Cheeseman A. Bhattacharya. Proc MSA 2011.

9. "Interfaces of Lanthanum and Strontium manganite superlattices". A. Shah, B. Nelson-Cheeseman, S. May, J.M.Zuo, A. Bhattacharya and J.C.H.Spence. Proc Int Union Cryt. Congress. Madrid. (2011).

10. "On methods of space group determination". Uri Shmeuli, H. Flack, J.C.H.Spence and Philip Pattison. Int. Tables Cryst. (2012). Submitted.

11. "Structural induced magnetization in a $La_{2/3}$ $Sr_{4/3}$ MnO_4 superlattice". A.B.Shah, B. Nelson-Cheeseman, P. Stadelman, A. Bhattacharya, and J. Spence. Phys Stat Sol A 209, 1322 (2012)

12. "Direct-write Electron Beam Lithography on Silicate Glass using Scanning Transmission Electron Microscopy. D. Su , N. Jiang ,*, M. Lu, and J. Spence¨ Appl Phys Letts.

13. "Electron ionization atom migration in spinel. Nucl Mater. 403, 147 (2010) and earlier papers referenced therein.

PHONONS AND ELECTRONS IN THIN COMPLEX OXIDES

Susanne Stemmer
stemmer@mrl.ucsb.edu
Materials Department, University of California, Santa Barbara, CA 93106-5050

Research Scope

The objective of this program is to develop new approaches to understand and control phase transformations in complex oxide thin films as their dimensions approach the nanoscale; in particular, to provide a fundamental understanding of how these transitions are controlled by film strain, the atomic structure of interfaces and dimensionality. Perovskite titanates are grown with high structural perfection, high purity and low intrinsic defect concentrations by oxide molecular beam epitaxy. The project builds on the unique capabilities of scanning transmission electron microscopy techniques, in particular, *quantitative* high-angle annular dark-field imaging and diffraction in STEM. The combination of macroscopic and microscopic techniques provides a wealth of information about structure-property relationships in ultrathin complex oxide films. Below we summarize several key results from this program obtained in 2010-2012, focusing on those related to the STEM experiments.

Measurements of ferroelectric polarity and octahedral tilts on the nanoscale [7, 8]

We had previously shown that a new STEM-based diffraction technique, which we termed "position averaged CBED (PACBED)" is highly sensitive to small thickness changes, and does not require changes in the optical conditions and sample orientation away from those used for STEM imaging.[1] In PACBED a zone-axis sample is illuminated with a highly convergent electron probe, as used for STEM imaging. This results in a CBED pattern containing overlapping orders of diffracted disks. These overlapping disks generate a complicated interference pattern that is highly dependent on the position of the finely focused (< 0.2 nm) electron probe within the unit cell. A PACBED pattern is formed through incoherent averaging of these CBED patterns over many probe positions. The experimental PACBED pattern is highly sensitive to the sample structure, thickness and tilt, which can be quantitatively extracted through comparison with simulated PACBED patterns. In the present project period we applied the technique to ferroelectric and strongly correlated oxide films. We showed that PACBED patterns of ferroelectric materials, such as $PbTiO_3$ and $BaTiO_3$, are sensitive to both unit cell distortion and the absolute direction of polarity within the unit cell. We showed that the polarity can be determined even in cases where real-space high-resolution transmission electron microscopy would not be capable of resolving the atomic displacements. The method was applied to determine the direction of polarization in an epitaxial $BaTiO_3$ film. As can be seen from Fig. 1, the pattern intensity is asymmetric in

[1] J. M. LeBeau, S. D. Findlay, L. J. Allen, and S. Stemmer, *Position averaged convergent beam electron diffraction: Theory and applications*, Ultramicroscopy **110**, 118 (2010).

the top and bottom lobes along 00*l*. The observed pattern asymmetry results from the non-centrosymmetricity of $BaTiO_3$ (space group *P*4*mm*). The lobe with the greater intensity and reduced contrast (bottom lobe) coincides with the direction of the polarization. PACBED patterns can thus distinguish between unit cell distortions (which affect the Bragg disk separation) *and* polarity.

We also demonstrated the utility of PACBED to determine *oxygen* octahedra tilts in ultrathin strongly correlated oxides. Many important strongly correlated oxides exhibit distorted perovskite structures, in which the TM-O octahedra show characteristic tilt patterns (TM is a transition metal ion, such as Ni). The electronic and magnetic structure of these oxides depends sensitively on the distortion of TM-O bonds. We first studied NiO_6-octahedral tilts in ultrathin $LaNiO_3$ films under biaxial tensile stress. Both the type and magnitude of the octahedral tilts were determined by comparing PACBED experiments to frozen phonon multislice simulations. Bulk $LaNiO_3$ is rhombohedral (space group *R*3*c*) with a $a^-a^-a^-$ type octahedral tilt pattern in Glazer notation and a tilt angle α = 5.2°. Simulations were carried out for a wide range of different types and amounts of octahedral rotations. For quantitative comparisons of a large number of possible tilt patterns, an automated comparison algorithm was used, which calculates the minimum χ^2 for the intensity difference between experimental and simulated PACBED patterns. Figure 2 shows such a χ^2 map of the comparison between the experimental PACBED pattern and simulated patterns of the $a^-a^-c^-$ tilt type, as a function of tilt angles α and γ. The simulated patterns were compared to the experiment as a function of thickness. The minimum of the fit function corresponded to $\alpha = 6.2 \pm 0.41°$ and $\gamma = 0.9 \pm 0.82°$. Thus the out-of-plane octahedral tilt of the epitaxial film under biaxial tensile stress increases by ~ 20%, while the in-plane rotation decreases by ~ 80%, compared to the unstrained bulk material. This shows that PACBED allows for the investigation of the local structural origins that determine the properties of nanoscale heterostructures with distorted perovskites, including Mott materials such as the rare earth nickelates or titanates.

Future Plans

We are currently applying PACBED to superlattices composed of bilayers of ultrathin $LaNiO_3$ and $SrTiO_3$. While isolated $LaNiO_3$ films of that thickness are insulating,[2] $LaNiO_3$ films in superlattice are conducting,[3] despite the fact that all films are under identical strain (coherently strained) to the substrate. PACBED of the layers comprising the superlattice will be used to investigate the origin of the different transport properties.

[2] J. Son, P. Moetakef, J. M. LeBeau, D. Ouellette, L. Balents, S. J. Allen, and S. Stemmer, *Low-dimensional Mott material: Transport in ultrathin epitaxial $LaNiO_3$ films*, Appl. Phys. Lett. **96**, 062114 (2010).

[3] J. Son, J. M. LeBeau, S. J. Allen, and S. Stemmer, *Conductivity enhancement of ultrathin $LaNiO_3$ films in superlattices*, Appl. Phys. Lett. **97**, 202109 (2010).

DOE Sponsored Publications in 2010 – 2012

[1] B. Jalan, S. Stemmer, *Large Seebeck coefficients and thermoelectric power factor of La-doped $SrTiO_3$ thin films*, Appl. Phys. Lett. 97, 042106 (2010).

[2] J. Son, P. Moetakef, B. Jalan, O. Bierwagen, N. J. Wright, R. Engel-Herbert, S. Stemmer, *Epitaxial $SrTiO_3$ films with electron mobilities exceeding 30,000 $cm^2V^{-1}s^{-1}$*, Nature Mater. 9, 482 (2010).

[3] P. Moetakef, J. Y. Zhang, A. Kozhanov, B. Jalan, R. Seshadri, S. J. Allen, and S. Stemmer, *Transport in ferromagnetic $GdTiO_3/SrTiO_3$ heterostructures*, Appl. Phys. Lett. 98, 112110 (2011).

[4] P. Moetakef, T. A. Cain, D. G. Ouellette, J. Y. Zhang, D. O. Klenov, A. Janotti, C. G. Van de Walle, S. Rajan, S. J. Allen, and S. Stemmer, *Electrostatic carrier doping of $GdTiO_3/SrTiO_3$ interfaces*, Appl. Phys. Lett. 99, 232116 (2011).

[5] P. Moetakef, J. R. Williams, D. G. Ouellette, A. P. Kajdos, D. Goldhaber-Gordon, S. J. Allen, and S. Stemmer, *Carrier-controlled ferromagnetism in $SrTiO_3$*, Phys. Rev. X 2, 021014 (2012).

[6] J. M. LeBeau, D. O. Klenov, S. Stemmer, Application to Semiconductors, in: Scanning Transmission Electron Microscopy. Imaging and Analysis. Edited by: Stephen J. Pennycook, and Peter D. Nellist (Springer, 2011), p. 523.

[7] J. M. LeBeau, A. J. D'Alfonso, N. J. Wright, L. J. Allen, S. Stemmer, *Determining ferroelectric polarity at the nanoscale*, Appl. Phys. Lett. 98, 052904 (2011).

[8] J. Hwang, J. Y. Zhang, J. Son, and S. Stemmer, *Nanoscale quantification of octahedral tilts in perovskite films*, Appl. Phys. Lett. 100, 191909 (2012).

Figures

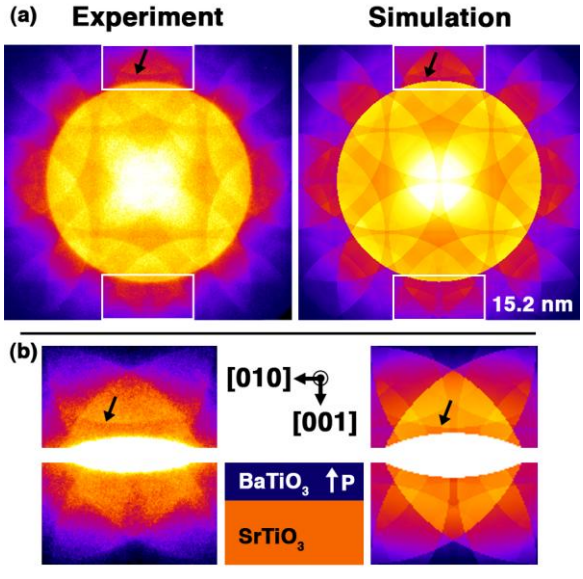

FIG. 1: Determining the ferroelectric polarization direction in a $BaTiO_3$ film. Experimental and simulated PACBED patterns of a ~ 4×4 unit cell area of a ferroelectric $BaTiO_3$ film. The bottom row shows a comparison of the top and bottom lobes (see white rectangles) in experiment and simulation. The arrows indicate features apparent only in the lobe pointing in the direction of polarization, which is due to a 4 pm off-centering of Ti atoms. From ref. [7].

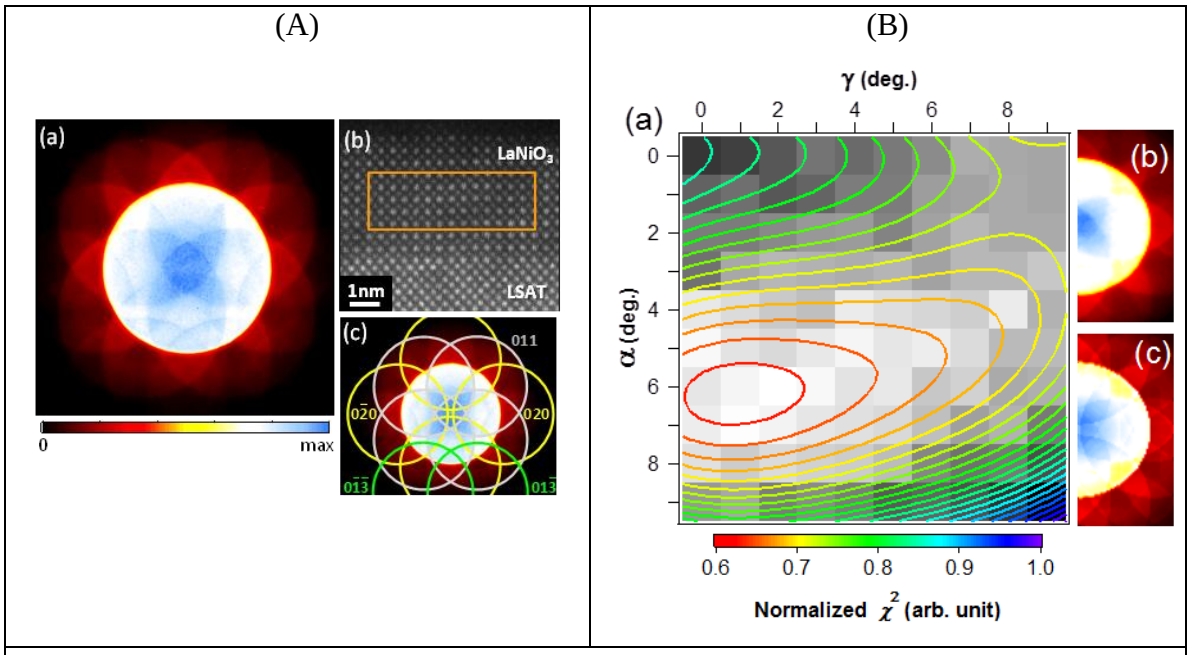

FIG. 2: **(A)** (a) Experimental PACBED pattern acquired from the area outlined by the orange box in (b). (b) HAADF-STEM image of a 5 nm thick $LaNiO_3$ film on LSAT. (c) Same as (a), with pseudocubic indices. From the distances between the disks, the ratio of in- and out-of-plane lattice parameters (0.983 ± 0.004) corresponds to that determined by x-ray diffraction, indicating that the thin TEM foil did not cause strain relaxation. **(B)** (a) χ^2 map of the comparison between the experimental PACBED pattern [shown in (b)], and simulated patterns as a function of the octahedral tilt angles, α and γ, in the simulations. The contour lines are a 2D polynomial fit to the map. The simulated pattern corresponding to the minimum χ^2 is shown in (c). From ref. [8].

Medium-range order in amorphous materials studied by fluctuation electron microscopy

Mike Treacy

Dept. of Physics, Arizona State University, PO Box 871504, Tempe AZ 85284-1504.
Email: treacy@asu.edu

Research Scope

The aim of this research is to explore how nano-scale spatial fluctuations in electron scattering from amorphous materials can be used to reveal details of structural correlations that may be present in the thinned materials. The technique, called fluctuation electron microscopy (FEM), is a hybrid imaging/diffraction-based technique that examines the fluctuations in microdiffraction patterns when a coherently focused electron probe scans a uniformly thin sample. The statistical mean and variance of the microdiffraction pattern intensities informs us about structural non-uniformities within the sample, provided the sample is of uniform thickness. Plots of the variance of intensity versus scattering angle, normalized by the square of the mean intensity, tells us which diffraction vectors in the diffraction patterns tend to be most speckled. A random specimen should have no significant peaks if the structure is truly inhomogeneous at medium-range length scales > 0.5 nm. All scattering vectors should be equally speckly, once normalized by the mean intensity. Peaks in the variance plots tell us that the material generates a lot of speckle at that diffraction vector. The presence of such peaks signifies medium-range order. Determining the structural origin of the medium-range order in any material is hard, usually relying on inspired modeling and comparison with simulations. The primary goals of this project are to:

(1) Determine the fundamentals of the scattering physics that generates the diffraction spatial variance signal.
(2) Use the discoveries in (1) above to find ways to quantify FEM.
(3) Apply the FEM method to interesting and technologically important families of amorphous materials, particularly those with important applications in energy-related processes.

Recent progress

(1) **Reverse Monte Carlo study of diffraction and FEM data from amorphous silicon**
We have shown that amorphous silicon contains a high density of paracrystalline material – that is, small regions 1 – 2 nm in diameter that contain strained cubic silicon (Fig. 1). The size and density of paracrystallites diminish when the amorphous silicon film is annealed below the recrystallization temperature, but they do not disappear entirely.

Although previous studies of amorphous silicon have indicated the presence of paracrystallites in both amorphous silicon and germanium, those results were obtained by inference; FEM data were simulated for numerous models and the paracrystallite model is found to fit the best. However, high-resolution x-ray and neutron diffraction studies have

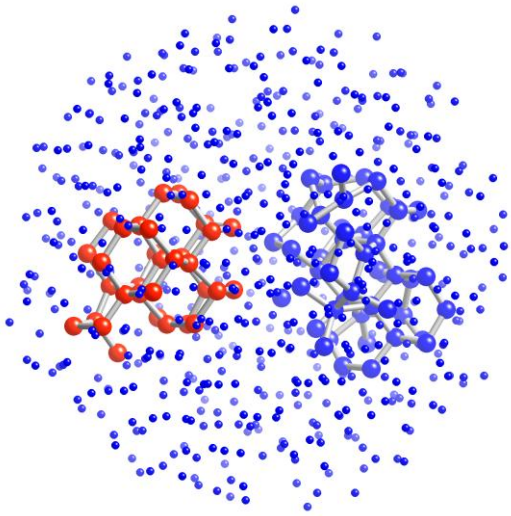

Figure 1: Paracrystalline model of amorphous silicon. The red bonded region shows a strained cubic silicon paracrystallite embedded in a matrix of disordered silicon (unbonded blue dots). The paracrystallite is viewed close to the cubic [110] direction. The region of blue bonded atoms is also disordered, and illustrates more clearly the bonding disorder.

indicated that annealed amorphous silicon is consistent with a continuous random network (CRN) model.

We obtained both selected area electron diffraction data from a wide sample area, as well as FEM data using the tilted dark-field method from four different types of amorphous silicon. A computational experimentally constrained structural relaxation (ECSR) procedure was written that took an arbitrary 1728-atom model and moved atoms (using the Metropolis algorithm) seeking an atomic configuration that fitted both the diffraction data (*i.e.* the two-body reduced density function) as well as the FEM data (*i.e.* a trace through a four-body correlation function). The Tersoff energy of the model was an additional constraint. ECSR runs took about 3 months using a computer cluster. Paracrystallite models emerged as the best fit, regardless of whether it was a crystalline, random, or polycrystalline starting model (Fig. 1). The paracrystallites are embedded in a disordered matrix, whose extent is too short to establish whether or not it is a good CRN.

The significance of this result is two-fold. First, it further legitimizes the paracrystallite model for amorphous silicon since no human bias was used to generate it. Secondly, the ECSR method shows us a way to invert the four-body FEM data. We can now use FEM data to obtain models that do not require creative guesswork.

(2) **Deeper examination of the speckle statistics in FEM.**
Although FEM is technically a quantitative experimental method, in exactly the same sense that high-resolution imaging and electron diffraction are quantitative, it has been difficult so far to come up with a straightforward analytical procedure to process the data. It is not sufficient to measure lattice spacings, or to index reflections. A physical model is needed to explain FEM data. The reverse Monte Carlo method alluded to in the previous section goes

a long way towards remedying this "blindness," but it still requires much effort and vast computational resources.

Although FEM is quantitative, some of the contributions to the speckle contrast are still poorly understood. In particular, the normalized variance is typically about one order of magnitude less than that expected from simple kinematical scattering. Important progress has been made towards understanding the origin of this speckle contrast suppression, which we refer to as *decoherence*. A detailed computational analysis of the statistics of scattering from granular materials confirms that the normalized variance $V(k,R)$, as a function of scattering vector k and resolution R obeys

$$\frac{1}{V(k,R)-1} = \frac{a}{\mathrm{L}} + \frac{b}{\mathrm{L}^3}R^2,$$

where a and b are constants. Plots of $\left[V(k,R)-1\right]^{-1}$ vs. R^2 give straight lines whose slope and intercept give L.
A model (Fig. 2) confirms that this equation is valid provided $R > \mathrm{L}$, i.e. that the microscope resolution (controlled by the objective aperture size) is greater than the characteristic length scale of the medium-range ordering. This confirms one of the more paradoxical results of FEM – that the technique works best at low resolution.

An important step forward for quantifying the effects of thickness and decoherence on the normalized variance was made by identifying the invariant quantity

$$\left[mV_m(k;t)-1\right]t = \text{constant}.$$

$V_m(k;t)$ is the normalized variance at scattering vector k for a sample thickness t, where

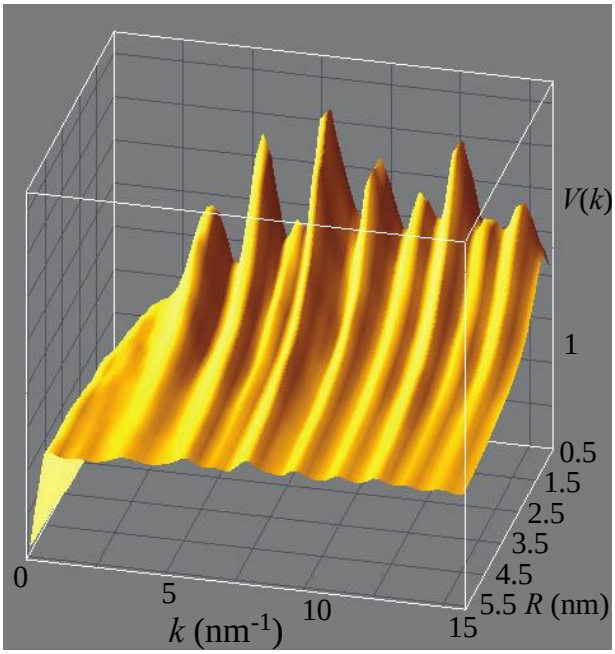

Figure 2: Three dimensional plot showing the calculated normalized variance, $V(k)$, as a function of scattering vector k and microscope resolution, R. The mean paracrystalline grain size is 1.2 nm, and the variance is a maximum near R ≈ 0.8 nm, which is the value of L for this model. For $R > \mathrm{L}$ the variance decays approximately as R^{-2}, as the model predicts for this regime. These plots do not compensate for decoherence effects, and so the baseline normalized variance equals 1.0.

$t > \mathrm{L}$. m is a parameter that characterizes the decoherence. This handy relation allows us to compute the variance for the simpler m=1 case, and thinner sample, t_1, and apply

$$V_m(k;t) = \frac{1}{m}\left(\frac{t_1}{t}\left[V_1(k;t_1) - 1\right] + 1\right).$$

The computation of $V_1(k;t_1)$ for m=1, and a much thinner model, t_1, speeds up the simulation of the desired quantity $V_m(k;t)$ considerably. Although the above equation now seems obvious to me, with hindsight, it remained elusive for over a decade. The significance of it is that this equation allows a significant speedup of variance computations for thicker samples, while correctly compensating for the effects of decoherence. The deeper significance of the parameter, m, remains somewhat elusive.

(3) Future Plans

Our near-term efforts are now focused on the application of FEM to amorphous diamond films that are being used as energy-conversion devices. The disorder depends on the level of N doping.

Our long-term efforts are aimed at ;

(i) improving the computational speed of the ECSR method for rapidly inverting FEM data.

(ii) Developing an interferometric double electron probe on the Nion aberration-corrected microscope that will arrive at ASU soon.

DOE-sponsored publications

(1) K. B. Borisenko, B. Haberl, Amelia C.Y. Liu, Y. Chen, G. Li, J. S. Williams, J. E. Bradby, D. J.H. Cockayne, M. M. J. Treacy,
Medium-range order in amorphous silicon investigated by constrained structural relaxation of two-body and four-body electron diffraction data,
Acta Materiala **60** 359–375 (2012).

(2) D. Kumar and M. M. J. Treacy,
Interferometric scanning microscopy for the study of disordered materials,
Appl. Phys. Letts. **99**, 251912 (2011).

(3) M. M. J. Treacy and D. Van Dyck,
A Surprise in the First Born Approximation for Electron Scattering,
Ultramicroscopy in press, (the corrected proof appeared online 11/2011).

(4) M. M. J. Treacy and K. B. Borisenko,
The Local Structure of Amorphous Silicon,
Science **335** 950–952 (2012).

(5) M. M. J. Treacy,
Speckles in Images and Diffraction Patterns,
Handbook of Nanoscopy, Ed. by Gustaaf van Tendeloo, Dirk van Dyck, and Stephen J. Pennycook, Ch. 12 (2012).

(6) M. M. J. Treacy and J. M. Gibson,
Examination of a polycrystalline thin-film model to explore the relation between probe size and structural correlation length in fluctuation electron microscopy.
Microscopy and Microanalysis **18** 241–253 (2012).

Imaging Point Defects with Quantitative STEM

Paul Voyles and Dane Morgan
Materials Science and Engineering, University of Wisconsin, Madison
1509 University Avenue, Madison, WI 53706, voyles@engr.wisc.edu, ddmorgan@wisc.edu

Program Scope

The state of the art in quantitative STEM imaging has advanced to the point that imaging a variety of point defects may be possible. Substitutional high-*Z* impurities were imaged a decade ago, and imaging of impurity and self-interstitials was demonstrated more recently, but imaging vacancies and low-*Z* impurities is an ongoing challenge. Our goal is to combine quantitative STEM with sub-pm precision and extremely high signal to noise with density functional theory calculations to image point defect and point defect complexes. We will apply these methods to semiconductors and to perovskite oxide materials and interfaces with fast oxygen transport and high oxygen reduction reaction catalytic activity.

Recent Progress

p-type Sb-doped ZnO Nanowires

ZnO is intrinsically *n*-type and extremely difficult to dope *p*-type. A variety of acceptor doping and co-doping schemes, including some based on Group V elements, have been investigated, but reproducible and stable *p*-type ZnO remains elusive. *p*-type ZnO would enable a variety of *p*-*n* homojunction based optoelectronic devices. Recently, Wang *et al*. synthesized Sb-doped ZnO NWs that have stable *p*-type conduction over 18 months in a single NW field effect transistor (Nanotechnology, 22, 225602, 2011).

We have used aberration-corrected Z-contrast STEM to image the Sb dopants in the *p*-type ZnO NWs.[5] Figure 1 shows HAADF STEM images revealing that all of the Sb in the NWs is incorporated into Sb-decorated basal-plane inversion domain boundaries (b-IDBs) just under the (0001) NW growth surfaces and the (0001) bottom facets of interior voids. Figure 1(a) shows a NW tip in the [11$\underline{2}$0] projection with a bright band of Sb atoms 2-3 atomic planes under the (0001) surfaces. Figure 1(b) shows a different NW tip in the [10$\underline{1}$0] projection showing that the Sb occupy only every third atomic column. Figure 1(c) shows an internal void with a Sb-decorated b-IDB on the (0001) base of the void. Voids and related IDBs occur regularly in the NWs, are the only observed defect, and incorporate all the Sb.

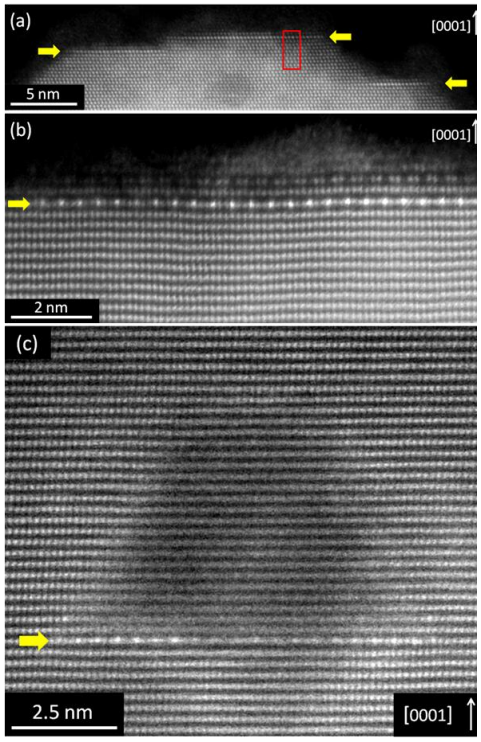

Figure 1: Z-contrast STEM images of Sb-doped ZnO NWs. (a) and (b) are images of NW tips in the [11$\underline{2}$0] and [10$\underline{1}$0] projections respectively. There are Sb-decorated H-H b-IDBs under the (0001) NW surfaces. (c) shows an internal void with a H-H b-IDB under it bottom surface. H-H b-IDBs in all the images are marked with yellow arrows. The red box in (a) shows where the lattice spacing analysis was done.

There are two types of b-IDBs in ZnO, head-to-head (H-H) and tail-to-tail (T-T), defined by the directions of the polarization vectors on either side of the boundary. Sb-decorated H-H b-IDBs contain an extra plane of O, effectively co-doping the structure with Sb and O. Sb-decorated T-T b-IDBs are a missing a plane of O. Density functional theory (DFT) calculations of the charge associated with each defect show that the extra O in the H-H IDBs act as electron acceptors, while the T-T IDBs act as electron donors. The DFT relaxed structures also reveal a much larger lattice expansion around the H-H b-IDB than the T-T b-IDBs. The experimental lattice expansion from STEM images like Figure 1(a) is consistent with H-H b-IDBs and not T-T b-IDBs. The H-H nature of the b-IDBs in our NWs is caused by the associated internal voids: the O-

polar material above the b-IDB terminates on a free surface, maintaining Zn polarity for the NW. The HAADF STEM evidence of Sb-decorated H-H b-IDBs in our ZnO NWs, combined with the DFT results, thus provides an explanation for the *p*-type conduction in our NWs. This new mechanism for *p*-type conduction in ZnO provides potential for ZnO NW based *p*-*n* homojunction devices.

We have also studied Sb-doped ZnO thin films grown by MBE, but Sb acts as a donor in those samples.[1] This is consistent with DFT calculations of the energies and electrical activity of As and Sb in ZnO, which show that defect complexes proposed to create *p*-type behavior (Limpijumnong, Phys. Rev. Lett. **9**2, 2004) actually create mid-gap states.[2,3]

Ga-doped ZnO Transparent Oxide

Ga-doped ZnO (GZ) is a potential replacement material for indium tin oxide in transparent conducting oxide applications. We have studied the defect structure and electrical properties of GZO deposited by plasma-assisted MBE on sapphire substrates and thick GaN films. The metal-to-oxygen ratio during MBE is crucial to properties of GZO thin films.[4] As-grown films grown under metal-rich conditions have resistivities $<3\times10^{-4}$ Ω·cm and optical transparency >90% in the visible. Films grown under oxygen-rich conditions have lower carrier concentration and mobility and required thermal activation. Electrical data as a function of film thickness point to a non-uniform depth distribution of free carriers in the films grown under oxygen-rich conditions.

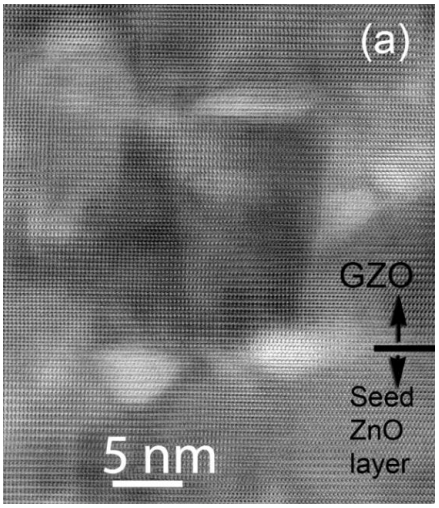

Figure 2. High resolution annular bright-field STEM image of the interface between the undoped ZnO seed layer and GZO grown under metal-rich conditions showing IDBs terminated by pores.

The microstructure of GZO also strongly depends on the metal-to-oxygen ratio during growth. When grown under metal-rich conditions, GZO films on a-sapphire have good crystal quality with slightly textured grains as large as 90 nm, but they are porous. Figure 2 shows that inside the grains, there is a mixture of domains having O- and Zn-polarity and an extremely high concentration of voids, starting from the undoped ZnO seed layer. We suggest that Ga doping of ZnO with O-polarity leads to accumulation of Ga species on the growing surface which is inhomogeneous at the nanoscale. Eventually the polarity switches locally from O to Zn, leading to a GZO layer with mixed polarity in columns.

Ga doping of ZnO grown under O-rich conditions on a-sapphire substrates leads to instability of the wurtzite (WZ) crystal structure. Figure 3 shows phase switching from WZ structure on the bottom part of GZO layer to zinc blende (ZB) structure on the top part of the layer. The grain boundaries in the top ZB layer of GZO are along the [022] direction for the ZB phase, which is tilted ~24° from the [0001] growth direction of the WZ layer. This inclination could noticeably affect the carrier scattering because an inclined grain boundary has a strong polar field in highly ionic ZnO resulting in Coulombic interaction between free carriers and grain boundaries. Al diffuses out from the sapphire substrate and accumulates on the surface.

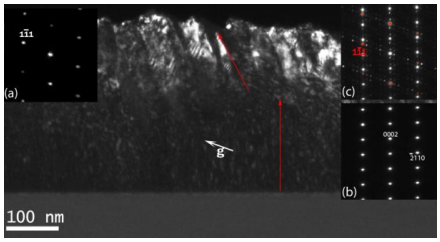

Figure 3. Dark-field image with the [111] **g** vector of the ZB structure. SAD patterns of (a) the ZB top layer, (b) the WZ bottom layer, and (c) a region with both WZ and ZB. Additional spots in (c) are caused by double diffraction and twinning in the ZB phase. The angle between the grain boundaries in the WZ and ZB corresponds to angle between $[0001]_{WZ}$ and $[2\underline{2}0]_{ZB}$.

GZO grown on GaN under similar growth conditions has Zn-polarity and does not contain voids. A network of misfit dislocations at the GZO/substrate interface relaxes most of the residual stress between the thin layers and the substrate. Ga is uniformly distributed in all our structures, which means that

GZO potentially has more predictable optical and electrical properties than Al-doped ZnO.

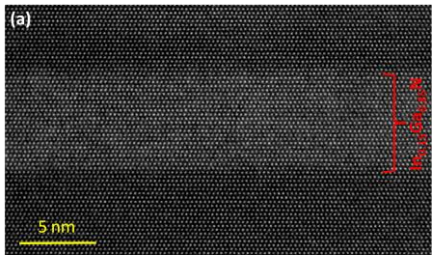

Figure 4: HAADF STEM image of the $In_{0.15}Ga_{0.85}N$ QW region in an LED. showing no signs of lateral In composition fluctuations. The image was acquired with an electron dose <1% of the reported damaging dose for InGaN at 200 kV.

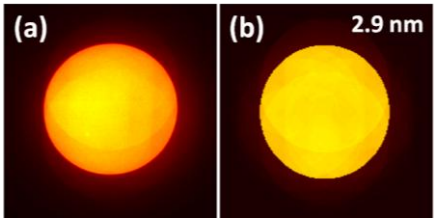

Figure 5: (a) experimental PACBED pattern from the region just below the imaged area in Figure 1(a). (b) is a simulated PACBED pattern of a 2.9 nm thick model.

<u>In Composition Fluctuations in InGaN Quantum Wells</u>

Nanoscale In clustering in InGaN quantum wells (QWs) continues to be the subject of conflicting reports. Various characterization techniques, including HRTEM, EFTEM, and EDS, have shown the presence of lateral In composition fluctuations, but Smeeton *et al* (Appl. Phys. Lett. **83**, 5419, 2003) have shown that electron beam irradiation can induce In clustering, questioning the validity of some previous work. Figure 4 shows a typical high-resolution HAADF STEM image of a $In_{0.15}Ga_{0.85}N$ QW from an LED. The regions above and below the quantum well are $In_{0.01}Ga_{0.99}N$ and $In_{0.08}Ga_{0.92}N$ respectively. The image shows some relatively weak contrast inside the quantum well, but contrast with the same length scale and intensity is also present above and below the QW. This contrast arises from oxidation or amorphization of the TEM sample, not In composition fluctuations. Figure 4 was acquired with an electron dose of 10 C/cm^2, which is <1% of the damaging dose Smeeton *et al.* reported for beam-induced composition fluctuations at 200 kV.

The images in Figure 4 were acquired from a sample thin enough to reveal the intrinsic structure of the $In_{0.15}Ga_{0.85}N$ QWs. According to the log-ratio EELS method, the sample in Figure 1(a) was 8.8 nm thick (0.08 inelastic mean free paths of 110 nm), but this is an overestimate due to surface plasmon scattering. Figure 5(a) is an experimental PACBED pattern from just below the QW in Figure 1(a). Figure 5(b) is a frozen-phonon simulation of a GaN PACBED pattern from a sample 2.9 nm thick. The match between experiment and simulation shows that the sample areas in Figure 4 is ~3 nm thick, which is thin enough to reveal small scale In composition fluctuations if they were present.

<u>High Precision STEM</u>

Precision much smaller than the resolution is routinely achievable in TEM and STEM, but STEM is at a disadvantage because the relative small signal decreases signal to noise and the serial image collection creates image distortions from sample and probe instabilities. The best reported precisions in TEM are 1-3 pm, compared to 5 pm in STEM in the best case, and more typically 10-15 pm. In collaboration with applied mathematicians Benjamin Berkels, Peter Binev, and Wolfang Dahmen, we have obtained sub-pm precision in STEM by summing together hundreds of short exposure images. They have developed a non-rigid registration scheme that averages out high-frequency instabilities and generates high signal to noise images with negligible loss of resolution. In a non-rigid registration, each pixel is assigned a translation vector from frame to frame, unlike a rigid shift in which the whole frame is assigned one translation vector. The translation vector of each pixel is determined by maximizing the normalized cross correlation between the frames, which is a badly under-constrained problem if all possible transformations are allowed. To maximize the cross correlation correctly, our collaborators adopted a regularized, multigrid, and iterative approach to solve this under-constrained problem. Once these translations are determined, they are used on the original raw data to register the image series, and then the registered images are summed without smoothing or other processing to produce the final high precision image.

Figure 6 shows results of this technique on a sample of [11$\underline{2}$0] GaN. Images were acquired on the UW Titan STEM with a 24.5 mrad convergence angle, 25 pA probe, 54 to 270 collection angle, and ~0.8 Å resolution. A series of 512, 256×256 pixel images were acquired with a 12.8 µs dwell time per pixel. Figure 6(a) is the first frame out of the series. Figure 6(b) is the average of the series after the non-rigid

registration, so the effective dwell time is 6.55 ms. We fit each of the 56 atom peaks in the averaged image to a two dimensional Gaussian to obtain the atom positions with sub-pixel accuracy, then calculated the average and standard deviation of the atom separations along *x* and *y* in the image. The standard deviation of the distances is a measure of the position precision. For this data set, the *x* precision is 0.74 pm and the *y* precision is 0.85 pm. Similar, sub-pm precision was obtained for other data sets on GaN [11$\underline{2}$0] and Si [110].

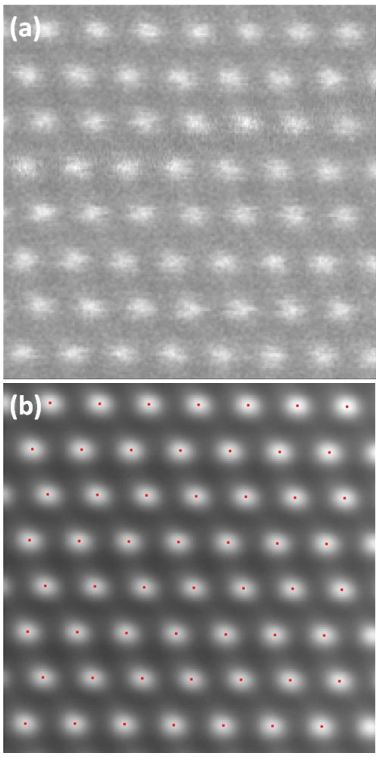

Figure 6: (a) The first of 512 frames of GaN [11$\underline{2}$0]. (b) The average of 512 frames after non-rigid registration. No other smoothing or image processing has been done. The red dots are the positions of the atomic columns determined by fitting.

Future Plans

We plan to apply the high precision STEM techniques to imaging point defects, especially vacancies. The results in Figure 6 were acquired at extremely high sample dose, so first we must explore experimentally and theoretically the effects of reduced dose on precision. We will also explore the effects of instability in lower-order aberrations. Then, we will study Si or ZnO with impurity-vacancy clusters to test imaging vacancies. Finally, we will study point defects in $La_{1-x}Sr_xMnO_{3-\delta}$ and at $La_{0.8}Sr_{0.2}CoO_{3-\delta}$ / $(La_{0.5}Sr_{0.5})_2CoO_{4-\delta}$ interfaces to understand their influence on oxygen transport and oxygen reduction reaction catalysis.

Publications Supported by this Program

1. H.Y. Liu, N. Izyumskaya, V. Avrutin, Ü. Özgür, A. B. Yankovich, A. V. Kvit, P.M. Voyles, and H. Morkoç, "Donor behavior of Sb in ZnO" J. Appl. Phys., to be published.
2. B. Puchala and D. Morgan, "Stable interstitial dopant - vacancy complexes in ZnO," Phys. Rev. B **85**, 195207 (2012)
3. B. Puchala and D. Morgan, "Atomistic Modeling of As Diffusion in ZnO," Phys. Rev. B **85**, 064106 (2012).
4. H. Y. Liu, V. Avrutin, N. Izyumskaya, Ü. Özgür, A. B. Yankovich, A.V. Kvit, P. M. Voyles, and H. Morkoç, "Electron scattering mechanisms in GZO films grown on a-sapphire substrates by plasma-enhanced molecular beam epitaxy" J. Appl. Phys. **111**, 103713 (2012).
5. A. B. Yankovich, B. Puchala, Fei Wang, Jung-Hun Seo, D. Morgan, Xudong Wang, Z. Ma, A. V. Kvit, and P. M. Voyles "Stable *p*-type conduction from Sb-decorated head-to-head basal plane inversion domain boundaries in ZnO nanowires", Nano Letters **12**, 1311 (2012).
6. A.B. Yankovich, A.V. Kvit, X. Li, F. Zhang, V. Avrutin, H.Y. Liu, N. Izyumskaya, Ü. Özgür, H. Morkoç, and P.M. Voyles "Hexagonal-Based Pyramid Void Defects in GaN and InGaN", J. Appl. Phys. **111**, 023517 (2012)
7. H.Y. Liu, X. Li, S. Liu, X. Ni, M. Wu, V. Avrutin, N. Izyumskaya, Ü. Özgür, A.B. Yankovich, A.V. Kvit, P.M. Voyles, and H. Morkoç, "InGaN based Light emitting diodes utilizing Ga doped ZnO as a highly transparent contact to p-GaN", Phys. Stat. Sol. C **8**, 1548 (2011)
8. H. Liu, V. Avrutin, N. Izyumskaya, Ü. Özgür, and H. Morkoç, "Transparent conducting oxides for electrode applications in light emitting and absorbing devices," Superlattices and Microstructures **48**, 458 (2010).
9. X. Li, H. Y. Liu, S. Liu, X. Ni, M. Wu, V. Avrutin, N. Izyumskaya, Ü. Özgür, and H. Morkoç, "InGaN based light emitting diodes with Ga doped ZnO as transparent conducting oxide," Physica Status Solidi (a) **207**, 1993, (2010).
10. H. Liu, V. Avrutin, N. Izyumskaya, M.A. Reshchikov, Ü. Özgür, and H. Morkoç, Highly conductive and optically transparent GZO films grown under metal-rich conditions by plasma-assisted molecular beam epitaxy, Physica Status Solidi: Rapid Research Letters **4**, 70 (2010).

Stability and Novel Properties of Magnetic Materials and Ferromagnet / Insulator Interfaces

Y. Austin Chang and Paul M. Voyles
Materials Science and Engineering, University of Wisconsin,
1509 University Avenue, Madison, WI 53706, voyles@engr.wisc.edu

Program Scope

Spin-dependent tunneling from a ferromagnetic metal, through an insulator, and into another ferromagnet underlies the function of various current and proposed spintronic devices. The prototypical example is a magnetic tunnel junction (MTJ), which exhibits tunneling magnetoresistance (TMR), a difference in resistance when the magnetizations of the ferromagnetic layers are parallel or antiparallel. The goal of this project is to connect the details of the atomic structure at the ferromagnet / insulator interface to the spin-dependent tunneling behavior for new materials not widely deployed in MTJs or other spintronic devices, including magnetite Fe_3O_4, Fe_4N, and the Heusler alloy Co_2MnSi. These new materials offer potential performance improvements over conventional materials and the introduction of new functions, such as negative TMR and three-state devices. However, they create significant new problems in materials synthesis and integration.

Recent Progress

(1) *Materials and Processing for Negative Spin Polarization*

An MTJ with one electrode with negative spin polarization (SP) and one electrode with positive SP will exhibit negative or inverse TMR, in which the low resistance state occurs when the electrodes have antiparallel magnetization. Achieving negative TMR requires integration of new electrode materials with negative SP into device structures. We have developed and characterized synthesis of two candidate materials, Fe_3O_4 (magnetite) and Fe_4N.

Fe_3O_4 has -100% spin polarization (SP) at room temperature and a high Curie temperature of ~850 K, making it a promising material for spintronics, including inverse TMR MTJs. Applications require smooth, low defect density, single phase Fe_3O_4 thin films, preferably on Si substrates. We fabricated Fe_3O_4 thin films meeting these requirements by selective oxidation of Fe on TiN buffered Si. Oxidation was performed using a CO_2/CO gas mixture to control the O chemical potential so that Fe_3O_4 is the equilibrium phase formed.[B] The result is Fe_3O_4 films on Si with surface roughness of 0.34 nm rms, comparable to epitaxial Fe_3O_4 grown by MBE on an MgO substrate. In comparison, sputtered Fe_3O_4 on buffered Si has 0.8 nm rms roughness.[D] The films synthesized by oxidation also reach saturation of the magnetization at much lower applied field than the sputtered films, indicating a lower concentration of anti-phase

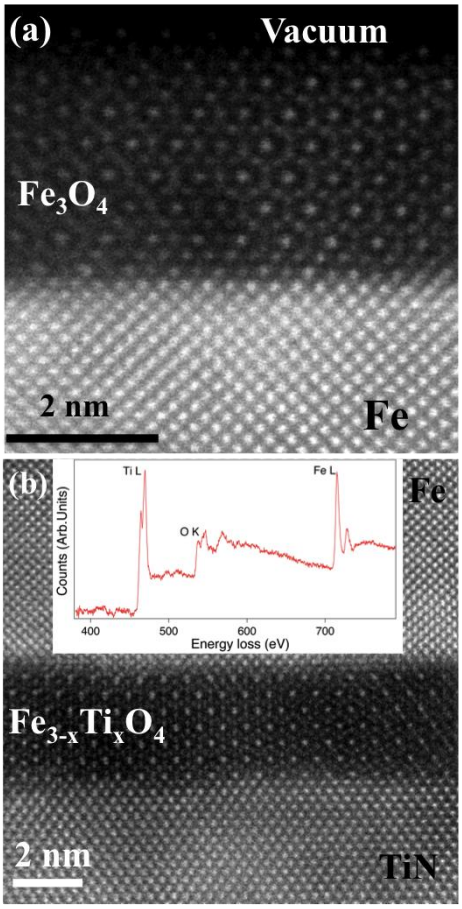

Figure 1 (a) HRSTEM image of a Fe_3O_4 film oxidized at 400 C (b) a second phase layer $Fe_{3-x}Ti_xO_4$ at the TiN/Fe interface. The inset of 2(b) is an EEL spectrum from the second phase.

boundaries.

Figure 1(a) shows an HRSTEM image of the Fe_3O_4 oxdized at 400 °C. The Fe_3O_4 quality is good, and the interface with the residual Fe is sharp. However, there is a second phase at the interface of the TiN and the residual Fe, as shown in Figure 1(b). An EEL spectrum of the second phase, shown in the inset, shows Ti L, O K and Fe L edges and EELS quantification gives an Fe/Ti atomic ratio of 2.1±0.1. Therefore, we have identified the second phase as Fe_2TiO_4, also called ulvöspinel, which has the same inverse spinel structure as Fe_3O_4. The Fe L edge of Fe_2TiO_4 shifts 0.55±0.05 eV to the lower energy compared to Fe, consistent with previous reports.[1,2] No second phase forms at the TiN/Fe interface under oxidation at 160 °C, which can be explained by the high activation energy of TiN oxidation. The growth of the Fe_3O_4 during oxidation at 160 °C follows a power law with exponent 0.26±0.02. Fabrication of nanometer thick films by this method is straightforward.

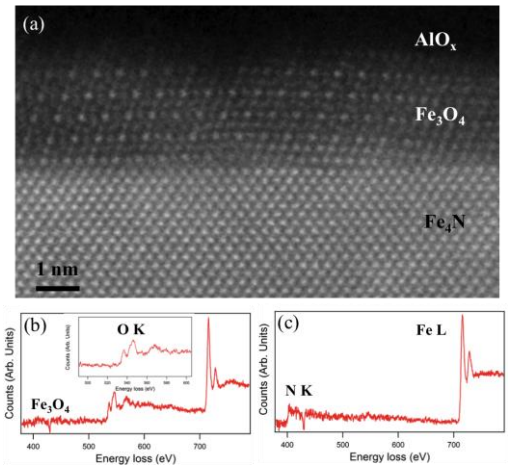

Figure 2. (a) HRSTEM image of a Fe_4N / Fe_3O_4 / AlO_x/Fe stack. (b) EEL spectrum on reaction layer. (c) EEL spectrum on the bottom Fe_4N layer.

Fe_4N is another material predicted to have nearly -100% SP at the Fermi level at room temperature.[3] We fabricated Fe_4N thin films by reactive sputtering[C] and MTJs with the structure $Fe_4N/AlO_x/Fe$. The devices exhibit negative TMR, but the magnitude is only ~8%, which is fairly small. Figure 2(a) shows the Fe_4N / AlO_x interface of the MTJ, which has a reaction layer between the Fe_4N and AlO_x. The crystal structure of the reaction layer is consistent with Fe_3O_4 along the [110] zone axis. EEL spectra extracted from a spectrum image covering the reaction layer and the bottom electrode Fe_4N are shown in Figure 2(b) and (c), respectively. In Figure 2(b), the EEL spectrum shows an O K edge with a pre-peak, the Fe L edge, but no N K edge. The O K edge pre-peak / main peak splitting agrees with our measurement on a Fe_3O_4 standard. We also observe formation of Fe_3O_4 on the surface of Fe_4N films exposed to air, so oxidation of Fe_4N seems to favor Fe_3O_4 over other iron oxides. Fe_4N may therefore provide an easy synthesis route to Fe_3O_4 junctions and inverse TMR.

(2). *Interface terminations and disorder in the Heusler alloy Co_2MnSi*

Heusler alloy Co_2MnSi (CMS) in the $L2_1$ ordered structure has +100% SP at Fermi level, suggesting potentially very high TMR. However, only the MnMn/O interface termination yields fully spin polarized tunneling in a CMS/MgO junction, and that termination is metastable.[4] The CoCo/O termination is 67% spin polarized, and the MnSi/O and SiSi/O terminations are unpolarized.[4] Previous studies by STEM have reported MnSi/O termination,[5] as have previous studies by x-ray circular magnetic dichroism.

We investigated the CMS/MgO interface in a $CoFe/MgO/Co_2Mn_{1.35}Si$ MTJ by HRSTEM. Off-stoichiometric Mn concentration was deposited to suppress Co antisite defects, which reduce the

[1] H.E. Hoefer, G.P. Brey, B. Schulz-Dobrick, R. Oberhaensli, Eur J Mineral **6**, 407–418 (1994).
[2] M. Sankararaman D. Perry, J. of Mat. Sci. **27**, 2731–2733 (1992).
[3] S. Kokado, N. Fujima, K. Harigaya, H. Shimizu, A. Sakuma, Phys. Rev. B **73**, 172410 (2006).
[4] B. Hülsen, M. Scheffler, P. Kratzer, Phys. Rev. Lett. **103**, 046802 (2009).
[5] T. Miyajima, M. Oogane, Y. Kotaka, T. Yamazaki, M. Tsukada, Y. Kataoka, H. Naganuma, Y. Ando, Appl. Phys. Exp. **2**, 093001 (2009).

SP at Fermi level.[6] This junction has quite high TMR for a CMS MTJ (1049% @ 4.2 K, 335% @ 290 K).[7] Figure 3 shows coexisting CoCo/O and MnMn/O interface terminations. The CoCo/O termination on the left hand side of the image is a simple extension of the $L2_1$ structure of the CMS. The MnMn/O termination on the right hand side is not. The line profiles in Figure 3(b) show that the interface plane has consistently higher intensity than the Si columns within the CMS, although the intensity is lower than the Mn columns due to interface strain. In other images at larger detector inner angle, the interface contrast increases towards the bulk Mn column contrast. The distance between last CMS and first MgO layers are 0.20±0.01 nm and 0.26±0.02 nm for the CoCo/O and MnMn/O terminations, respectively, in good agreements with calculations.[4] The non-equilibrium deposition by sputtering and the excess Mn in the CMS electrode may increase the MnMn/O termination in the junction.

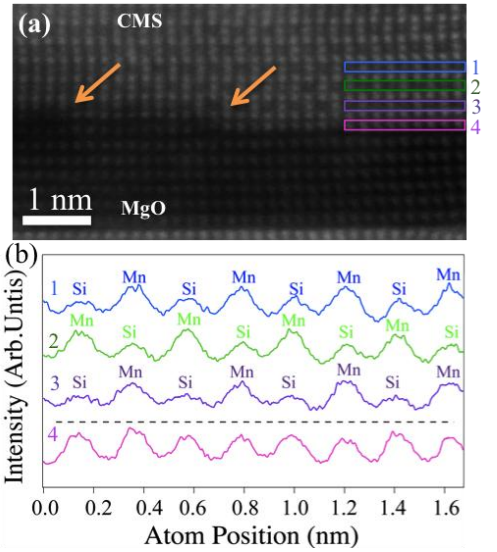

Figure 3. (a) HRSTEM image of the interface of CMS/MgO. CoCo/O and MnMn/O interface terminations are shown in the image on the left and right, respectively. Steps on the top surface of the MgO are indicated by the orange arrows. (b) Horizontal profiles taken on the MnSi planes in CMS electrode and the interface layer. The colors and the labeled numbers of the line profiles correspond to the colors of the horizontal windows in (a).

Interface roughness is another important factor determining TMR, since it disrupts the coherent tunneling of Δ_1 symmetry electrons through the MgO buffer. In Figure 3, the interface termination switches at a step in the MgO layer underneath the CMS, which is typical in this and other samples, providing another motivation to minimize the interface roughness.

(3) *Nominally symmetric CoFe/AlO$_x$/CoFe MTJs with inverse TMR*

Inverse TMR requires an asymmetric MTJ: one electrode has positive SP, one negative. Thus, the discovery of consistent, reproducible observation of inverse TMR an MTJ with the structure Si (001) / Ag (buffer) / CoFe / AlO$_x$ / CoFe / IrMn / Ag after annealed in air at 200~300 °C for 2 min, then cooled to room temperature under a 1000 Oe magnetic field was a surprise to us. STEM EELS spectrum imaging shows that a thin, discontinuous layer of Fe_3O_4 at the interface is responsible.[A] The O K edge ELNES[8] and Fe L edge core level

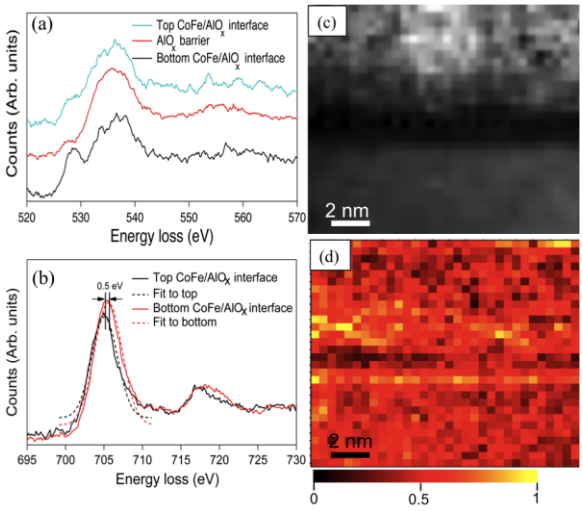

Figure 4. STEM EELS results of the inverse TMR after field cooling. (a) O K edge ELNES extracted from the barrier, top and bottom interfaces. (b) Fe L edge core level shift between upper and lower CoFe/AlOx interfaces (c) simultaneous HAADF image on the area where EEL SI was taken. (d) The intensity map of the pre peak of O K edge.

[6] M. Yamamoto, T. Ishikawa, T. Taira, G.-F. Li, K.-I. Matsuda, T. Uemura, J. Phys. Cond. Matt. **22**, 164212 (2010).

[7] H.X. Liu, Y. Honda, K. Matsuda, M. Arita, T. Uemura, M. Yamamoto, Japn. J. Appl. Phys. (to be published).

[8] C. Colliex, T. Manoubi, C. Ortiz, Phys. Rev. B **44**, 11402 (1991).

shifts[1] extracted from STEM EEL spectrum images taken at the interfaces of the inverse TMR junctions show the formation of Fe_3O_4 at the interface of CoFe/AlO_x. In Figure 4(a), the O K edge ELNES extracted from the bottom interface of CoFe/AlO_x shows a pre-peak but none was observed at the lower CoFe/AlO_x interface and the AlO_x barrier. The splitting between pre peak and main peak agrees with our measurement on a Fe_3O_4 standard. The Fe L edge core level shift shown in Figure 4(b) shows a shift of 0.5 eV to higher energy compared to FeO, consistent with Hoefer *et al*.[1] Simultaneous HAADF image is shown in Figure 4(c) and the intensity map of the pre-peak of O K edge is shown in Figure 1(d), which also indicates the Fe_3O_4 formed only at the bottom CoFe/AlO_x interface. In other junctions, Fe_3O_4 is found at the top interface, or in patches on both interfaces. Similar experiments on the MTJs with a TiN buffer and normal TMR suggest no Fe_3O_4 formed, which indicates that Fe_3O_4 is the reason for the inverse TMR. O dissolved in the Ag buffer layers is likely the source of the Fe_3O_4 layers.

Future Plans

Prof. Y. Austin Chang, the PI of this project, passed away on Aug. 2, 2011. We will therefore bring this project to its conclusion in the next year by: (1) developing a method using quantitative STEM and EELS to characterize the density and distribution of antisite defects in CMS thin films at high spatial resolution and (2) testing the hypothesis that high Mn concentration stabilizes the MnMn/O termination at the CMS/MgO interface by studying the effect of varying Mn concentration.

Publications supported by DOE between 2010 and 2012

A. F. Shi, H. Xiang, J.J. Yang, M.S. Rzchowski, Y.A. Chang, P.M. Voyles, J. Magn. Magn. Mat. **324**, 1837–1844 (2012).

B. H. Xiang, F.-Y. Shi, C. Zhang, M.S. Rzchowski, P.M. Voyles, Y.A. Chang, Scri. Mat. **65**, 739–742 (2011).

C. H. Xiang, F. Shi, M. Rzchowski, P. M. Voyles, Y. A. Chang, J. Appl. Phys. **109**, 07E126 (2011).

D. H. Xiang, F. Shi, M. Rzchowski, P. M. Voyles, Y. A. Chang, Appl. Phys. Let. **97**, 092508 (2010).

Beneath and Between: Structural, Functional, and Spectroscopic Measurements of Buried Interfaces and Interactions
DE-FG02-10ER46734
(previously Atomic-Scale Chemical, Physical and Electronic Properties of the Subsurface Hydride of Palladium)

Paul S. Weiss, Principal Investigator
California NanoSystems Institute and Departments of Chemistry & Biochemistry and of Materials Science & Engineering, UCLA, Los Angeles, CA 90095
Email: psw@cnsi.ucla.edu; Web: www.nano.ucla.edu

Collaborators:
Prof. Tomáš Baše, Czech Academy of Sciences, Institute of Inorganic Chemistry, Husinec-Rez, Czech Republic
Prof. Andrea Bertozzi, UCLA Applied Math, Los Angeles, CA
Prof. David Eisenberg, UCLA Dept. of Chemistry & Biochemistry and HHMI, Los Angeles, CA
Prof. Ken Houk, UCLA Department of Chemistry & Biochemistry, Los Angeles, CA
Prof. Chad Mirkin, Northwestern University Chemistry, Evanston, IL
Prof. Stan Osher, UCLA Math and Computer Science, Los Angeles, CA

Overall research goals have not changed: Spectroscopic imaging tools and methods, based on scanning tunneling microscopes (STMs), are being developed to examine buried layers and interfaces with ultrahigh resolution. These new methods will measure molecule-substrate bonds, buried dipoles in molecular layers, and key structural aspects of adsorbed molecules, such as tilt angles. We will develop the ability to locate lateral projections of molecular parts as a means of determining the structures of molecular layers. We will develop the ability to measure the orientation of buried functionality.

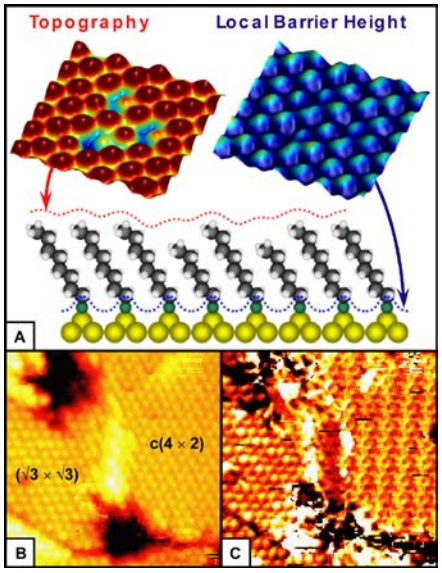

Figure 1. Simultaneous topographic and barrier-height imaging of alkanethiol mixtures self-assembled on Au{111} in a low-temperature ultrastable scanning tunneling microscope enables determination of the absolute tilt angles of molecules.

Significant achievements in 2010-2012: We appear to have observed a 2D plastic lattice in a carboranethiol monolayer by measuring the aligned dipoles of the molecules offset from the topographic maxima of the features due to the molecules in conventionally recorded STM images. We are developing algorithms to make these determinations automatically. This work was done using barrier height imaging, as previously applied to measure molecular tilt (figure 1).

We have made significant headway in identifying the positions and orientations of other molecules, such as self-assembled peptides. Further measurements seek to identify and to locate multiple bonds, heteroatoms, molecule-substrate contacts, and molecule-molecule contacts. To do this, we will use in part microwave polarizability mapping (figure 2).

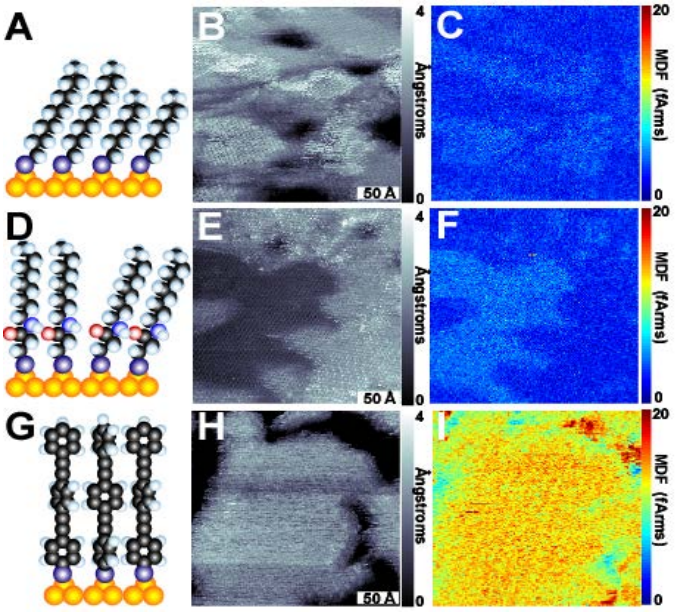

Figure 2. Simultaneous topographic and microwave polarizability mapping enables location of multiple bonds, heteroatoms, molecule-substrate contacts, and molecule-molecule contacts. This method is being used for chemical differentiation and for structural determinations.

Science objectives for 2012-2013:

- Combine STM, spectroscopic. and microwave-frequency polarizability imaging to locate buried functionality, interactions and contacts in a diverse range of systems.
- Develop routines for stacking, associating, and interpreting these multi-spectral data sets.

References to work supported by this project 2009-:

1. Heads and Tails: Simultaneous Exposed and Buried Interface Imaging of Monolayers, P. Han, A. R. Kurland, A. N. Giordano, S. U. Nanayakkara, M. M. Blake, C. M. Pochas, and P. S. Weiss, *ACS Nano* **3**, 3115-3121 (2009).
2. Identifying Reactive Intermediates in the Ullmann Coupling Reaction by Scanning Tunneling Microscopy and Spectroscopy, M. M. Blake, S. U. Nanayakkara S. A. Claridge, L. C. Fernández-Torres, E. C. H. Sykes, and P. S. Weiss, *Journal of Physical Chemistry A* **113**, 13167-13172 (2009).
3. Adsorbate-Promoted Tunneling-Electron-Induced Local Faceting of D/Pd{110}-(1x2), A. R.

Kurland, P. Han, J. C. Thomas, A. N. Giordano, and P. S. Weiss, *Journal of Physical Chemistry Letters* **1**, 2288-2294 (2010).

4. Scanning TunnelingMicroscopy and Spectroscopy of Nanoscale Assemblies, M.M. Blake, Ph.D. Thesis, Department of Chemistry, The Pennsylvania State University, University Park, PA (2010).
5. Artificial Assembly of Precise Functional Nanostructures, A. N. Giordano, M.S. Thesis, Department of Chemistry, The Pennsylvania State University, University Park, PA (2010).
6. Atomic-Scale Studies of Heterogeneous Catalysis, Substrate-Mediated Interactions, and Interface Structures" A. R. Kurland, Ph.D. Thesis, Department of Chemistry, The Pennsylvania State University, University Park, PA (2010).
7. Subtractive Patterning via Chemical Lift-Off Lithography, W.-S. Liao, S. Cheunkar, H. Cao, H. Bednar, P. S. Weiss, and A. M. Andrews, *Science* (2012), in press. DOI: 10.1126/science.1221774.

Others in preparation.

Project Title: Electron Density Determination, Bonding and Properties of Tetragonal Ferromagnetic Intermetallics

Principal Investigator: Jörg M.K. Wiezorek

Address: Department of Mechanical Engineering and Materials Science,
John A. Swanson School of Engineering,
University of Pittsburgh,
636 Benedum Hall, 3700 O'Hara Street, Pittsburgh, PA 15261.
E-mail: wiezorek@pitt.edu

Program Scope

Ordered intermetallic phases offer unique properties, often superior to those of elemental metals and compositionally equivalent solid solution alloys, rendering them suitable for various high-performance applications. The unique properties of intermetallics are directly related to their chemically ordered crystal structures and can be understood most fundamentally in terms of electron interactions and bonding. Computational materials science approaches, such as density functional theory (DFT) based calculations, have been applied successfully to develop understanding of crystal properties and structures. However, DFT calculations typically require some critical approximations, which often are empirically justified by comparison of theory predicted properties, e.g. bulk modulus, phase stability, unit cell dimensions, to experimental data for a given material. Lacking such data validation and verification of DFT predictions frequently suffers. Hence, establishing robust, accurate and facile methods for probing experimentally the electron density in crystalline solids, which is a direct result of DFT calculations, remains a high impact goal of basic science research.

This project combines transmission electron microscopy (TEM) experimentation by quantitative convergent-beam electron diffraction (QCBED) with accompanying electronic structure calculation based on DFT to study the electron density and interatomic bonding in transition metal based intermetallics. QCBED with modern field-emission gun and energy-filtering system equipped TEM instruments permits study of nano-scale volumes, thereby offering access to experimentation on a broad range of crystalline phases. The methods developed here focus on the electronic charge difference or bonding charge distribution, $\Delta\rho(r)$, as one of the quantum mechanical characteristics central for developing fundamental understanding of properties and validation of electronic structure theory in crystals. Charge difference distributions, $\Delta\rho(r)$, represent the difference between the electron density distributions measured or calculated for the crystals and those based on the independent atom model. They can be used to visualize and elucidate details of the bonding related electron density in the crystals of interest. $L1_0$-FePd and $L1_0$-FePt are selected as the primary model systems for 3d-4d/5d electron interactions in binary multifunctional intermetallics. Other isostructural and structurally related non-ferromagnetic, chemically ordered intermetallic phases, e.g. NiAl, TiAl, are used to evaluate the possible effect of ferromagnetism on the experimental QCBED methods being developed.

Key experiments use high-quality binary crystals to measure simultaneously structure (F_{hkl}) and temperature (Debye Waller, B_i) factors by QCBED. The anisotropic Debye-Waller factors (DWF's) for the different atom species and sites in chemically ordered phases can differ significantly from those known for the respective pure element crystals due to interspecies bonding effects. Therefore, they need to be measured, ideally simultaneously, together with low order structure factors to facilitate robust experimental determination of the electron density distribution and bonding studies in the chemically ordered transition metal based d-electron systems. This effort advances the state of the art in quantitative TEM experimentation, provides new experimental data uniquely suited for evaluation of computational models and enables development of improved DFT tools for reliable and ideally predictive studies of $L1_0$-FePt and $L1_0$-FePd and other intermetallics including elements with atomic numbers beyond Si.

The research team comprises the P.I., Prof. Jörg Wiezorek, a graduate student, Xiahan Sang, and a research associate, Dr. Andreas Kulovits. The project benefits from collaboration with experts in DFT, namely, Profs. Oleg Mryasov (University of Alabama) and Guofeng Wang (University of Pittsburgh).

Recent Progress (since fall 2010)

An experimental QCBED method, based on a adaptation of off-zone-axis-pattern CBED, has been established for measuring simultaneously multiple sets of structure factors and multiple anisotropic Debye Waller factors with sufficient accuracy and precision to determine experiment based electron density distributions in crystals [1-5]. High quality experimental QCBED data suitable for direct comparison with DFT results has been obtained for Cu, Ni, Fe, Cr, and equiatomic FePd and TiAl [7-11].

Furthermore, equiatomic FePt and Pd-rich $Fe_{1-x}Pd_x$, $0.5<x\leq0.58$, intermetallic alloys have been prepared by vacuum arc-melting. Initial analytical characterization indicates that thermomechanical treatments yielded an equiatomic and fully-ordered $L1_0$-FePt phase with a polytwinned microstructural morphology. Characterization of the off-stoichiometric $Fe_{1-x}Pd_x$ material is on-going. Unexpectedly, TEM sample preparation for FePt using conventional electrolytic twin-jet thinning has proven unsuccessful to date, presumably due to the excellent corrosion resistance of the chemically ordered intermetallic relative to the materials used in the commercially available equipment. Ion-beam thinning and sample preparation using thin film deposition techniques offer alternative methods and have been initiated in order to obtain TEM samples suitable for QCBED experimentation with FePt.

The structure factors with $h^2+k^2+l^2\leq16$ and the Debye Waller factors of the respective atom species have been determined from QCBED experiments for equiatomic $L1_0$-FePd and for $L1_0$-TiAl [4, 5, 8, 10, 11]. Comparisons of DFT calculated structure factors and charge difference distributions have been performed for the transition metal elements Cr, Fe, Cu and Ni, and the chemically ordered tetragonal FePd and TiAl intermetallics [e.g. 7-11]. The DFT calculations have been performed with the Wien-2K code (beyond LDA, GGA) and VASP. The comparison of QCBED experiment based and DFT calculated structure factors for the transition metal based crystals studied to date indicated that the low order structure factors with $h^2+k^2+l^2<5$ contain essentially all the details from interatomic bonding [11]. Three-dimensional charge difference maps have been constructed from the experimentally determined low-order structure factors. Figures 1 and 2 depict representative examples of charge difference maps derived from experiment and DFT calculation for equiatomic $L1_0$-TiAl and $L1_0$-FePd.

Significant differences, both qualitative and quantitative, are discernible in the three-dimensional charge difference maps obtained by DFT and by QCBED experiment for the $L1_0$-phases. DFT calculations based on VASP are not reliable beyond the second lowest structure factor, F_{110}, breaking down already for the strongly bonding affected F_{111}. In comparison to VASP the beyond-LDA Wien-2K based DFT result exhibit excellent agreement with results from the QCBED based experiments for the transition metals Cr, Fe, Cu, Ni and the ordered intermetallic $L1_0$-TiAl phase [10, 11]. However, consistently the Wien-2K DFT calculations overcompensate for delocalization of electron charge, resulting in overestimated accretion between first and second nearest neighbors of the d-electron bearing atoms, e.g. Ti atoms in TiAl and both the Fe and the Pd atoms in FePd (e.g. Figures 1 and 2, [10, 11]). The Wien-2K DFT calculations treat the bonding effects associated with the pure Al-layers in the tetragonal $L1_0$-TiAl extremely very well. Notably, Al only has p-electrons and no d-level electronic states occupied. Differences between Wien-2K DFT calculations and QCBED experiment derived charge difference maps are mostly associated with treatments of the d-electrons, i.e., regarding Ti atoms in TiAl. For FePd both Fe and Pd atoms exhibit d-electron level occupation and the discrepancy between experiment derived and DFT based charge difference maps is more pronounced than for TiAl. For instance, in FePd the DFT calculations overestimate the delocalized electron density accretion between Fe atoms along <110> and predict large bonding charge centered about the octahedral interstice at ½,½,½ in addition to that at the tetrahedral interstices, e.g. at ¼, ¼, ¼ (e.g. Figure 2, [11]). The origin(s) of the differences between the DFT based and QCEBD experiment based charge difference maps and structure factors requires further elucidation.

A systematic Bloch-wave analysis has been performed, comparing the two-beam systematic/excited row QCBED method, the symmetric zone-axis pattern QCBED method and the multi-beam off-zone axis QCBED developed during this research regarding their respective sensitivity to both Debye-Waller (DW) factors and structure factor changes and computational refinement quality. These QCBED methods have in common that they rely solely on zero-order Laue zone (ZOLZ) discs. The superior

precision and sensitivity achieved when using the multi-beam off-zone axis QCBED for simultaneous refinements of multiple DW factors and multiple structure factors correlates with an increased number and increased amplitudes of excited Bloch wave branches when compared to the other OCBED methods [12]. This enhances the contribution of dynamical interactions to the intensity variations (i.e. contrast) across the excited ZOLZ discs used for structure factor and temperature factor refinement.

Future Plans

- Continue sample preparation for the chemically ordered bulk FePt alloy materials. Ion-beam based methods and also electrolytic methods successfully established for field-ion microscopy sample preparation will be explored in order to circumvent limitations posed by designs of commercial TEM sample twin-jet electrolytic polishing instrumentation.
- Initiate QCBED experimentation to determine structure factors, Debye Waller factors and electron density in ordered FePt phase once TEM samples are obtained and compare results with calculation obtained by DFT (Wien-2K, GGA).
- Perform additional experiments and DFT calculations to probe for the origin(s) of the differences between the DFT calculation and QCEBD experiment based charge difference maps and structure factors for the transition metal based crystals.
- Initiate QCBED experimentation and DFT calculations to study of effects of off-stoichiometric compositions in Al-rich TiAl and Pd-rich FePd. Site-specific treatments of atomic properties, such as the temperature factors, are expected to become increasingly relevant. and role of substitution of excess species transition metals to the minority species sub-lattices in the $L1_0$-phases of off-stoichiometric composition can be assessed.
- Compare FePd, FePt and TiAl bonding using charge difference maps.

DOE-sponsored publications (2010-2012)

1. X. Sang, A. Kulovits, J.M.K. Wiezorek, "Quantitative Convergent Beam Electron Diffraction for simultaneous Structure Factor and Debye Waller factor Determination - Fitting Method Optimization", Microscopy and Microanalysis (2010) Vol. 16 (Suppl. 2) 938-939; *First Prize, Best Poster Award at M&M Meeting in Portland, OR, August 2010*.
2. X.H. Sang, A. Kulovits and J.M.K. Wiezorek, "Determination of Debye Waller Factor and Structure Factors for Si by Quantitative Convergent Beam Electron Diffraction using off-axis Multi-Beam Orientations", Acta Crystallographica A66, (2010) 685-693.
3. X.H. Sang, A. Kulovits and J.M.K. Wiezorek, "Simultaneous Determination of Highly Precise Debye-Waller Factors and Structure Factors for Chemically Ordered NiAl by Convergent Beam Electron Diffraction", Acta Crystallographica A66, (2010) 694-702.
4. X.H. Sang, A. Kulovits and J.M.K. Wiezorek, "Experimental Studies of Bonding Related Properties in Binary Intermetallics by Convergent Beam Electron Diffraction", MRS Symp. Proc. Vol. 1295 (2011) n05-41-46.
5. X.H. Sang, A. Kulovits and J.M.K. Wiezorek, "Simultaneous determination of highly precise Debye-Waller factors and multiple structure factors for chemically ordered tetragonal FePd", Acta Crystallographica A67 (2011) 229-239.
6. A. Kulovits, J.M.K. Wiezorek, T. LaGrange, B.W. Reed and G.H. Campbell, "Revealing the Transient States of Rapid Solidification of Aluminum Thin Films using Ultrafast In-situ Transmission Electron Microscopy", Philosophical Magazine Letters (2011) Vol.91, No.4, 287-296.
7. A. Kulovits, J.M.K. Wiezorek, T.B, LaGrange, B.W. Reed, G.H. Campbell, "Quantitative TEM delivers statistically significant data sets on materials structure with nanoscale spatial and temporal resolution", Electron Microscopy and Multiscale Modeling, EMMM 2011, Tahoe City, USA (2011) 45-46.
8. J.M.K. Wiezorek, X.H. Sang, A. Kulovits, "Quantitative Convergent-Beam Electron Diffraction with Nano-Scale TEM Probes for Electron Density Determination in Intermetallic Phases", Electron Microscopy and Multiscale Modeling, EMMM 2011, Tahoe City, USA (2011) 3-4 (Invited Extended Abstract);

9. X.H. Sang, A. Kulovits and J.M.K. Wiezorek, "On the consistency of highly accurate QCBED data refined from different zone axes for ferromagnetic tetragonal $L1_0$ FePd", Microscopy and Microanalysis Vol. 17 (Suppl. 2) (2011) 1112-1113.
10. X. Sang, A. Kulovits, G. Wang, J. Wiezorek, "High Precision Electronic Charge Density Determination for $L1_0$ ordered γ-TiAl by Quantitative Convergent Beam Electron Diffraction", Philosophical Magazine (accepted 7/2012).
11. X. Sang, PhD Dissertation, "*ELECTRON DENSITY DETERMINATION AND BONDING IN TETRAGONAL BINARY INTERMETALLICS BY CONVERGENT BEAM ELECTRON DIFFRACTION*", University of Pittsburgh, Pittsburgh, PA 15261, USA (July 2012).
12. X. Sang, A. Kulovits, J. Wiezorek, "Comparison of convergent beam electron diffraction methods for simultaneous structure and Debye Waller factor determination", Microscopy and Microanalysis (submitted 07/2012);

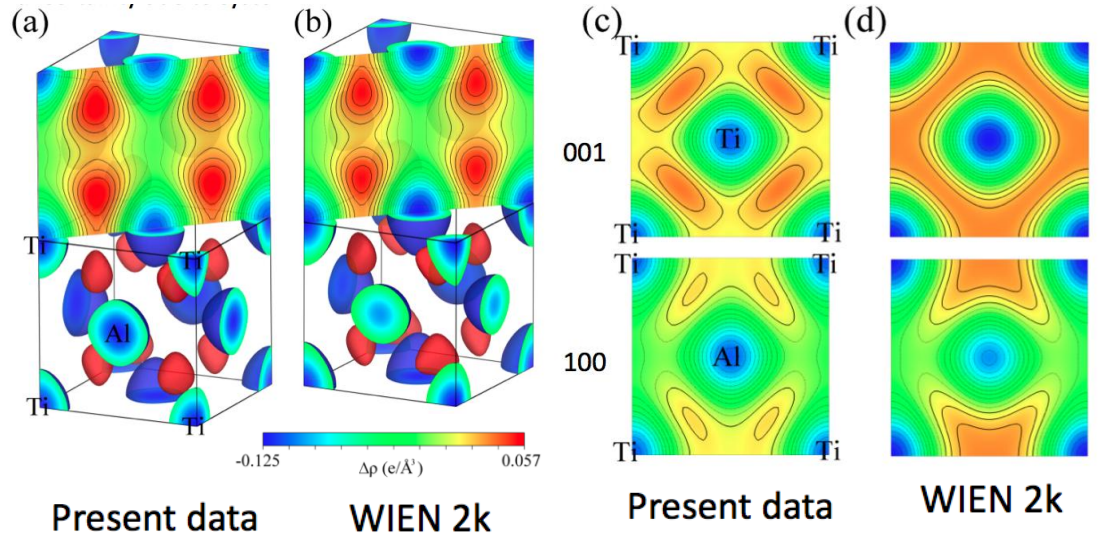

Fig. 1: Comparison of electronic charge difference maps for $L1_0$-TiAl obtained by QCBED experiment (a), (c) and DFT (GGA, Wien-2K) calculation in (b), (d). Note the bonding charge accumulation in the tetrahedral interstices (a), (b) and overestimated electron delocalization between Ti-Ti second nearest neighbors along [010], (c) vs. (d).

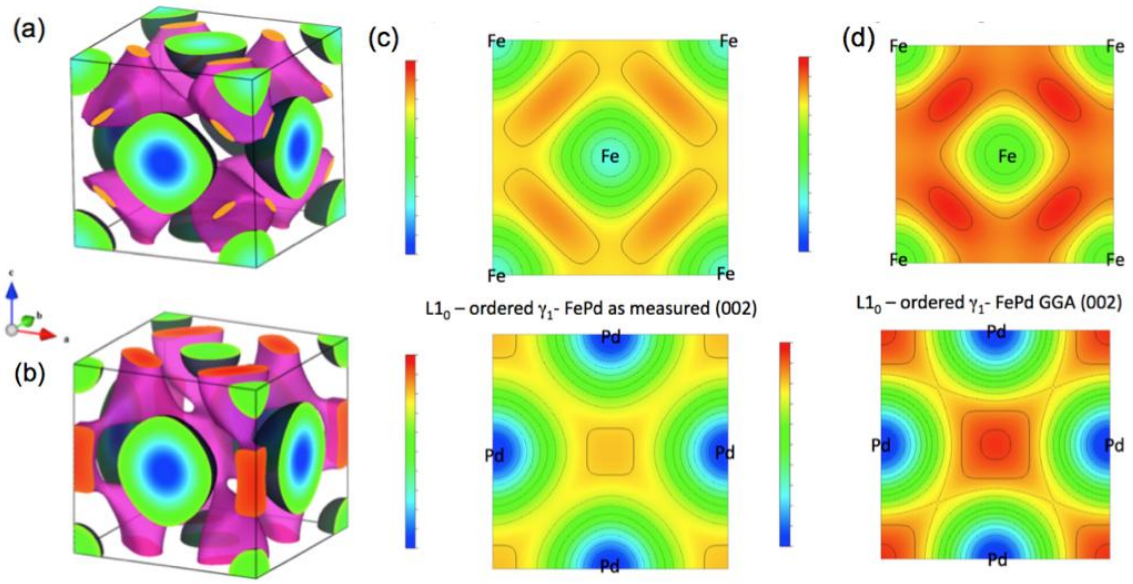

Fig. 2: Electronic charge difference for $L1_0$-FePd from QCBED measurements (a) and (c), and DFT (GGA, Wien-2K) calculation in (b) and (d). In (c) and (d) at top and bottom are shown (001) and (002) sections, respectively.

Program Title: *in situ* scanning probe microscopy studies of cross-coupled domains and domain walls

Principal Investigator: Weida Wu
Email: wdwu@physics.rutgers.edu
Rutgers Center for Emergent Materials (R-CEM)
Department of Physics and Astronomy
136 Frelinghuysen Road, Piscataway, NJ 08854, USA

Program Scope:

The objective of this project is to explore the nanoscale emergent phenomena and to understand the unconventional properties of cross-coupled domains and domain walls in multiferroics, where both ferroelectricity and magnetism coexist. The giant magnetoelectric effect due to coupled ferroic orders in multiferroics is of both fundamental and technological interest and is promising for energy-efficient multifunctional applications. The presence of domains and domain walls is a distinguishing feature of any ferroic order; their responses to external stimuli determine the macroscopic properties and the functionalities of ferroic materials. To address the challenges and to directly visualize the cross-coupled domains and domain walls and their responses to the applied electric and magnetic fields, this project will develop a unique, high-resolution and high-sensitivity *in situ* scanning force microscopy (SFM). The real space imaging of domains and domain walls by SFM aims to fundamentally understand the nature of magnetoelectric cross-coupling in representative multiferroic and magnetoelectric materials.

Program Progress:

This is a new project, recently funded under the Electron and Scanning Probe Microscopies (ESPM) program with the DOE Office of Basic Energy Sciences. Using the unique VT-MFM with *in situ* high electric/magnetic fields, the PI's group already achieved direct visualization of the magnetic net moments at ferroelectric domain walls in multiferroic hexagonal manganites [1]. In addition, significant progress on developing scanning magnetoelectric effect microscopy (SMEM) has been made during the brief initial period.

- *Magnetic moments at ferroelectric domain walls in hexagonal manganites*

Although hexagonal manganites have been known as multiferroics for a long time, the intrinsic domain structure was revealed recently by various high resolution microscopic techniques [2,3]. New topological defects, vortices of six coupled structural anti-phase and ferroelectric domain states in hexagonal manganites originate from the intriguing trimerization distortion which induced the ferroelectricity. The observation of the network of 6-state vortices has many profound impacts on condensed matter physics, ranging from 6-state clock model to graph theory. Furthermore, hexagonal manganites have been shown to be a model system for testing the cosmology model (the Kibble-Zurek mechanism of quenched topological defects) [4]. However, the magnetic properties of these intriguing topological defects have not been addressed directly. Although it has been claimed that ferroelectric domain walls always pin antiferromagnetic domain walls in millimeter size domains, whether the interlocked antiphase and ferroelectric

domain walls are coupled to antiferromagnetic domain walls at submicron scale is a burning question that needs to be addressed by high resolution probes.

Using cryogenic magnetic force microscopy (MFM) in applied magnetic fields and ambient piezo-response force microscopy (PFM) [5], the PI's group discovered that the alternating domain wall magnetizations around vortices can correlate over the entire vortex network in $ErMnO_3$. The collective nature of the domain wall magnetism appears originated from the uncompensated Er^{3+} moments at domain walls, the field-controllable spin state of antiferromagnetic domains, and the correlated organization of the vortex network. Our results demonstrate a new route for achieving nanoscale magnetoelectric coupling in single-phase multiferroics, and open the possibility of detecting spin state by harnessing domain wall magnetism. In addition, these results demonstrate that these coupled domain walls are also antiferromagnetic domain walls, i.e. they are multiferroic. To the best of our knowledge, this is the *first* direct observation of uncompensated moments at antiferromagnetic domain walls. A manuscript based on these results was submitted to Nanoletters.

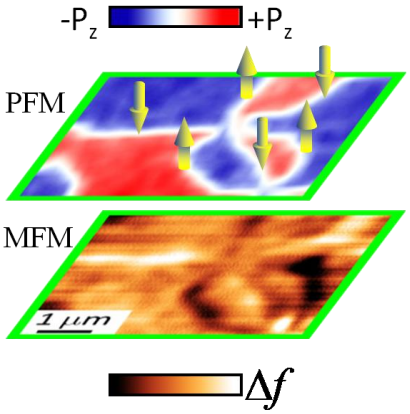

Fig. 1 | Preliminary results. RT-PFM image and MFM image (5.5 K, 0.2 T) taken at the *same* location on the (001) surface of multiferroic hexagonal $ErMnO_3$. The arrows in PFM image represent the net magnetic moments in ferroelectric domain walls. Δf = 0.8 Hz.

- *Development of scanning magnetoelectric effect microscopy (SMEM)*

ME effect was first conceived by Pierre Curie in 1894. Landau and Lifshitz provided a thermodynamic basis of such conjecture in magnetically ordered systems [6]. The same linear ME tensor (α) characterizes both magnetically induced polarization (ME_B) and electrically induced magnetization (ME_E) because they originate from the same term in the free energy expansion. Note that it is necessary to perform ME poling (or annealing) to produce single domain state for bulk ME effect measurements because of the presence of multiple ME domains. *Furthermore, ME domain structure has never been directly observed using ME response because of the weakness of ME effect in most systems.* To address these challenges, the PI will develop a scanning magnetoelectric microscopy (SMEM) using MFM, i.e. a local dynamic linear ME_E measurement with modulation lockin technique.

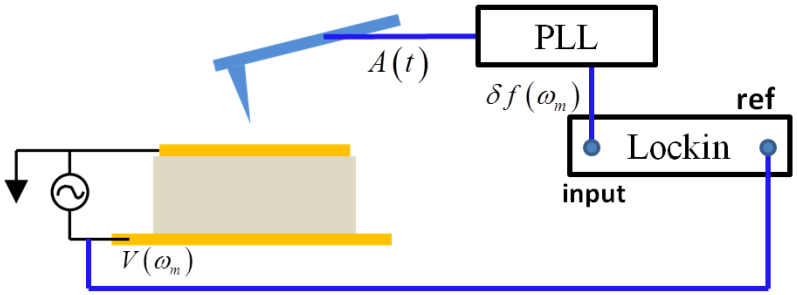

Fig. 2. Schematic of SMEM setup showing the basic principle of SMEM operation. The local moments of ME domains induced by modulated electric field produce modulated stray fields which are sensed by MFM (resonant frequency shift) and demodulated by a PLL followed by a lockin amplifier.

As shown in Figure 2, the basic principle of SMEM is a lockin detection of magnetic signal modulated by electric field. The stray field of local magnetization of ME domains induced by ME effect would be modulated at the same frequency as the applied electric field. The modulated stray field is converted to the modulated MFM signal (i.e. the resonant frequency shift) which is demodulated by a Phase Locked Loop (PLL). The output of PPL is fed to a lockin amplier to extract the ME signal. Since the applied electric field and the detected stray field are perpendicular to the sample surface, the SMEM contrast would come from diagonal ME response of opposite domains, or the head-on 180º domain walls.

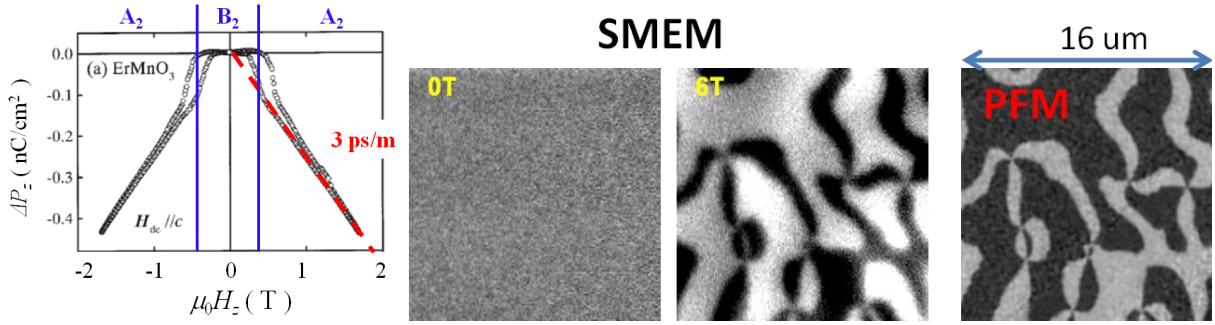

Fig. 3. $\Delta P_z(H)$ at 4.2K of $ErMnO_3$ with H // c-axis by Sugie et al. (ref. 7) Preliminary SMEM data of $ErMnO_3$ at 0 T and 6 T. RT-PFM image of the same area. V_{mod}=200 V_{rms}, f_{mod}=50 Hz.

The PI's group has overcome many technique challenges on realizing SMEM operation. First, all possible ground loops are eliminated so that no high voltage contamination is found from cantilever signal. Second, any inductive interference between high voltage lines and the electric leads of piezoelectric cantilever is eliminated by careful wiring. Third, no stray field leakage is found with 800 V_{pp} at 500 Hz on a dummy capacitor device mounted on sample stage. After optimizing the conditions of SMEM mode, we successfully observed local ME response of individual multiferroic domains in *hex*-$ErMnO_3$, as shown in Fig. 3. According to literature[7], the ME response of $ErMnO_3$ is comparable to that of Cr_2O_3 (~4 ps/m). Our preliminary results indicate that our SMEM would be able to detect ME response of most magnetoelectrics with submicron spatial resolution.

Future plans:

Magnetic imaging of multiferroic domains/walls

We will continue to investigate coupled vortex domain walls in multiferroics, e.g. hexagonal manganites using our unique VT-MFM with *in situ* high field capabilities. Observation of alternating net moments on vortex domain walls in manganites other than $ErMnO_3$ will provide a unified picture for the *hex-RE*MnO_3. We will apply this powerful technique to other multiferroics to understand the mechanism of cross-coupling between different ferroic orders.

Development and application of SMEM

We will continue the optimization of the SMEM technique for visualizing cross-coupling of domains or domain walls in mulitferroics (e.g. *hex-RE*MnO_3) and magnetoelectrics (e.g. $DyFeO_3$) with high spatial resolution.

Development of ULT-SFM with fiber-interferometer

We will develop new SFM with fiber-interferometer as deflection detection for ultra-low temperature operation. Furthermore, we will incorporate the high magnetic/electric field

capabilities in the new microscope to investigate a wide range of materials with coupled order parameters.

Reference

[1] Y. Geng, N. Lee, Y.J. Choi, S.-W. Cheong, and W. Wu, *Collective magnetism at multiferroic vortex domain walls* arXiv:1201.0694, (2012).

[2] T. Choi, Y. Horibe, H.T. Yi, Y.J. Choi, W. Wu, and S.-W. Cheong, *Insulating interlocked ferroelectric and structural antiphase domain walls in multiferroic $YMnO_3$.* Nature Materials. **9,** 253 (2010).

[3] T. Jungk, Á. Hoffmann, M. Fiebig, and E. Soergel, *Electrostatic topology of ferroelectric domains in $YMnO_3$.* Appl. Phys. Lett. **97,** 012904 (2010).

[4] S.C. Chae, N. Lee, Y. Horibe, M. Tanimura, S. Mori, B. Gao, and S.-W. Cheong, *Direct observation of the proliferation of ferroelectric dislocation loops and vortex-antivortex pairs.* Phys. Rev. Lett. **108,** 167603 (2012).

[5] S. Park *et al.*, Appl. Phys. Lett. **95**, 072508 (2009).

[6] L.D. Landau and E.M. Lifshitz, *Electrodynamics of Continuous Media*. 2nd ed. Theoretical Physics. Vol. 8. 1984, Oxford: Pergamon.

[7] H. Sugie, N. Iwata, and K. Kohn, *Magnetic Ordering of Rare Earth Ions and Magnetic-Electric Interaction of Hexagonal $RMnO_3$ (R=Ho, Er, Yb or Lu).* J. Phys. Soc. Jpn. **71,** 1558–1564 (2002).

SISGR - TRANSPORT AND IMAGING OF MESOSCOPIC PHENOMENA IN SINGLE ANDFEW LAYER GRAPHENE

Amir Yacoby, Harvard University, yacoby@physics.harvard.edu

Pablo Jarillo-Herrero, MIT, pjarillo@mit.edu

Project Scope –

The research objective of this project is to investigate novel quantum phenomena in single and few layer graphene. Special emphasis is given to the role of Coulomb interactions and to spatially varying phenomena where geometry and boundary conditions play an important role. Our experimental approach consists of both conventional transport methods as well as sophisticated local probe techniques capable of imaging the local thermodynamic and transport properties of these spatially varying quantum phenomena. We will explore both naturally occurring inhomogeneities due to intrinsic disorder as well as spatially dependent phenomena arising from patterning graphene into nanostructures, introducing inhomogeneous charge densities or magnetic fields using local electrostatic and superconducting gates, and contacting graphene with novel materials. Our focus will be on extremely high quality FLG fabricated either by suspending above a substrate or using hBN as a support structure. Such devices have very small disorder where mesoscopic and relativistic-like phenomena in the ultra-low density regime may be studied. A few examples include the investigation of the fractional quantum Hall effect and the effects of screening on such correlated phenomena, and the investigation of hybrid superconductor-graphene (S-G) devices.

Recent Progress –

In this talk we will review our recent experiments in single, bi- and twisted bilayer graphene. We will focus on transport and imaging spectroscopy in the quantum Hall regime, where novel collective many body phenomena stemming from interaction effects are most pronounced.

Screening, QHE and Landau Level Spectroscopy in Twisted BLG

The electronic properties of two stacked sheets of graphene depend crucially on their stacking orientation. The natural stacking in graphite is AB or Bernal stacking, which leads to electron dynamics described by massive chiral charge carriers. However, by introducing a relative twist angle between two graphene sheets stacked on top of each other (Fig 1a,b), the two graphene sheets can effectively decouple, retaining their linear Dirac dispersion despite their close proximity to each other. Twisted bilayer graphene at large twist angles then allows for the study of interaction effects between two FLG sheets which are separated by only a few Angstroms.

We are currently studying such twisted bilayer graphene devices, created by stacking two graphene sheets on top of each other onto an atomically-flat hexagonal boron nitride surface, resulting in a high quality twisted bilayer. The devices are dual-gated, allowing for independent control of both the total charge density in the twisted bilayer as well as the displacement field between the two layers. The effect of the two gates on the quantum Hall effect measurements of the twisted bilayer is summarized in Figures 1d,e. At zero displacement field, $D = 0$, the two graphene sheets result in an extra 2-fold degeneracy due the layer degeneracy, observed in the Hall resistance R_{xy} as steps of $8e^2/h$ in $1/R_{xy}$ instead of the usual $4e^2/h$ seen in single layer graphene (Fig 1d, black line). This 8-fold degeneracy is also observed in the longitudinal

resistance R_{xx}, as peaks at $D = 0$ are separated by total filling factor $\Delta\nu_{tot} = 8$ (Fig 1e). By applying displacement field (Fig 1d, pink line), the layer degeneracy is broken and steps of $4e^2/h$ are restored. This splitting of layer degeneracy is also seen clearly in R_{xx} (Fig 1e), where each peak in R_{xx} at $D = 0$ splits in two for $|D|>0$. As D is increased further, these peaks cross with their neighbors, indicating the crossing of Landau levels between the layers. By fitting the crossings (Fig 1e, black dots) with a full model of the inter-layer screening of the twisted bilayer

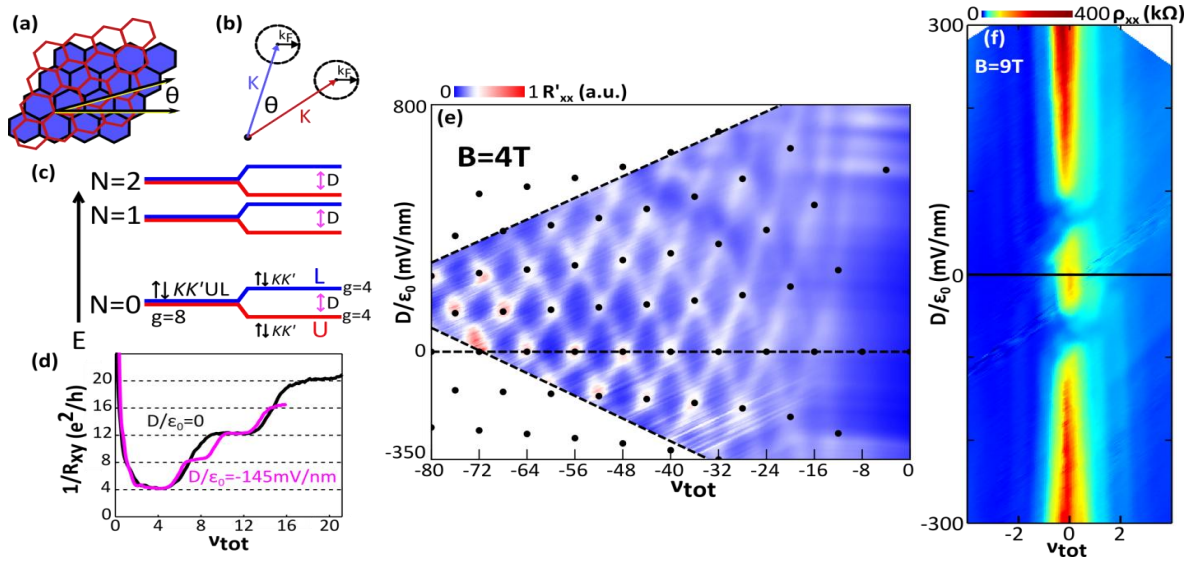

Figure 1. Quantum Hall Effect and Screening in Twisted Bilayer Graphene. (a) Twisted bilayer graphene lattice with twist angle. (b) Twist angle separates the Fermi surface of each layer in *k*-space. (c) Schematic of twisted bilayer LL spectrum. (d) $1/R_{xy}$as a function of total filling factorν_{tot} at $B = 9$T.(e) Measured longitudinal resistance $R_{xx}$with background subtracted, as a function of D and ν_{tot}at $B = 4$T. (f) Longitudinal resistivity R_{xx}as a function of D and ν_{tot}at B= 9T.

graphene, we extract the interlayer capacitance of the atomically-spaced graphene layers. We find this value to be 2-3 times larger than would be expected for two parallel plates separated by 0.34nm of vacuum, as is commonly assumed for the graphene bilayer interlayer capacitance. This is a strong indication that on such small length scales the finite thickness of the graphene atomic sheet itself must be taken into account when modeling such a system. Due to the high quality of our twisted bilayer graphene on hBN devices, we are also able to observe high magnetic field insulating states (Fig 1f) which are similar to those observed in clean SLG and BLG devices. In the twisted bilayers though, we observe an insulating state at high displacement fields which is unique to this system. The observed pattern of insulating states can be explained by the presence of counter-propagating edge modes, whereby at high displacement fields it is possible to dope the twisted bilayer graphene such that electron states exist in one layer and hole states exist in the other. Such a charge configuration would result in layer-counter-propagating edge states, and inter-layer coupling between such edge states could then lead to the observed insulating behavior. This demonstrates that a rich set of behaviors are possible in the twisted bilayer graphene, due to the extra layer degree of freedom and the possibility of coupling of charges between the layers.

Fractional quantum Hall effect in SLG

Interactions among electrons can give rise to striking collective phenomena when the kinetic energy of charge carriers is suppressed. Graphene provides a unique platform to study many-

body effects due to its massless chiral charge carriers and the fourfold degeneracy that arises from their spin and valley degrees of freedom. Recently, the fractional quantum Hall effect (FQHE) of Dirac fermions has attracted considerable attention. In graphene, the low dielectric constant and unique band structure lead to fractional quantum Hall states with energy gaps that are larger than in GaAs at the same field, particularly in the $N = 1$ Landau level. Moreover, the SU(4) symmetry of charge carriers in graphene could yield fractional quantum Hall states without analogues in GaAs. The FQHE was recently observed in graphene at all multiples of $\nu = 1/3$ up to 13/3, except at $\nu = 5/3$, but no conductance plateaus were observed at filling factors with higher denominators. It was suggested that the absence of a fractional quantum Hall state at $\nu = 5/3$ might result from low-lying excitations associated with SU(2) or SU(4) symmetry, but alternate scenarios associated with disorder could not be ruled out.

We have performed local electronic compressibility measurements of a suspended graphene flake using a scanning single-electron transistor (SET). By modulating the carrier density n and monitoring the resulting change in SET current, we measure both the local chemical potential μ and the local inverse electronic compressibility $d\mu/dn$ of the graphene flake. Our measurements reveal an unconventional sequence of incompressible fractional quantum Hall states in the lowest Landau level of graphene. Between $\nu = 0$ and 1, we observe incompressible behavior that follows the standard composite fermion sequence $\nu = p/(2p \pm 1)$ for integer $p \leq 4$ (Fig. 2a). In contrast, between $\nu = 1$ and 2, incompressible states only occur at $\nu = 4/3$, 8/5, 10/7 and 14/9 (Fig. 2b). These states correspond to a subset of the standard composite fermion sequence that includes only fractions with even numerators, suggesting a robust underlying symmetry.

Integrating inverse compressibility with respect to carrier density allows us to extract the step in chemical potential $\Delta\mu_\nu$ associated with each fractional quantum Hall state as a function of magnetic field. The steps in chemical potential are of order 1 meV at the highest available magnetic field, with $\Delta\mu_{1/3}$ the largest, reaching a maximum of about 3.5 meV at $B = 11.9$ T. At low magnetic field, $\nu = 1/3$, 2/3, 4/3 and 8/5 are the most robust, and they persist below 1.5 T. For all fractional quantum Hall states, $\Delta\mu_\nu$ can be described by a linear dependence on magnetic field, although a $B^{1/2}$ scaling cannot be ruled out for high fields. Our measurement setup also allows us to probe variations in sample behavior as a function of position. The density at which incompressible states occur varies with position, which can be explained by local density fluctuations. The magnitude of these fluctuations is similar to the width of the fractional quantum Hall states, and may explain why the FQHE has been so difficult to observe in transport studies: different regions of the sample form a given fractional quantum Hall state at different back gate voltages. The magnitudes of incompressible peaks also fluctuate substantially with position. Although some incompressible states, such as those at $\nu = 1/3$ persist at virtually all positions, others are more susceptible to disorder. Both $\nu = 2/3$ and 4/3 fully disappear in some locations, which seem to be correlated with the areas where the integer quantum Hall states are wider, a sign that local disorder is comparatively large.

Future Plans –

Our research effort for the next years will focus on the following topics:

1. Transport and imaging of ultra-high mobility in single and few layer graphene.
2. Induced superconductivity in single layer and few layer graphene.
3. Proximity effect between superconductivity and quantum Hall physics.
4. Transport and imaging of graphene in inhomogeneous magnetic fields.
5. Engineering topological phases in graphene by tuning electron-electron interactions. Such phases include quantum spin Hall and non-Abelian fractional quantum Hall states.

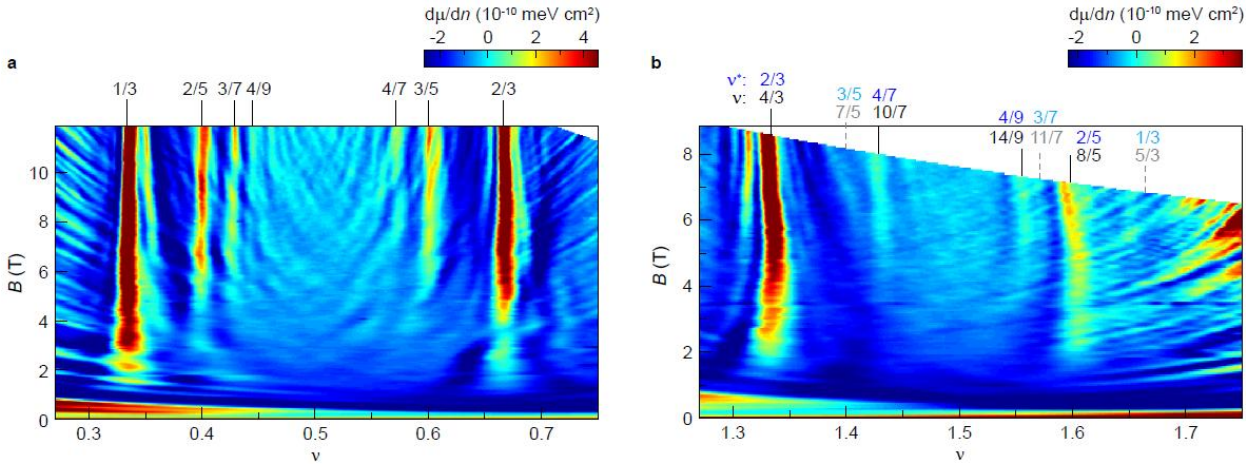

Figure 2.a, Inverse compressibility as a function of filling factor ν and magnetic field B. Incompressible states follow the standard composite fermion sequence between $\nu = 0$ and 1. b, Finer measurement of inverse compressibility between $\nu = 1$ and 2. Incompressible states occur only at filling fractions with even numerators. The incompressible behavior adheres to the sequence $\nu^* = 2 - \nu = 2p/(4p \pm 1)$ for $p \leq 2$.

Publications from DOE supported research –

1. B. E. Feldman, B. Krauss, J. H. Smet and A. Yacoby, "*Unconventional Sequence of Fractional Quantum Hall States in Suspended Graphene", **arXiv:1201.5128***, Accepted for publication in ***Science***.
2. M. Yankowitz, J. Xue, D. Cormode, J.D. Sanchez-Yamagishi, K. Watanabe, T. Taniguchi, P. Jarillo-Herrero, P. Jacquod, B.J. LeRoy, "*Emergence of Superlattice Dirac Points in Graphene on Hexagonal Boron Nitride"* ***Nature Physics* 8**, 382 (2012).
3. J. Sanchez-Yamagishi, T. Taychatanapat, K. Watanabe, T. Taniguchi, A. Yacoby, and P. Jarillo-Herrero, *"Quantum Hall Effect, Screening and Layer-Polarized Insulating States in Twisted Bilayer Graphene"*. ***Phys. Rev. Lett.*108**, 076601 (2012).
4. J. Xue, J. Sanchez-Yamagishi, K. Watanabe, T. Taniguchi, P. Jarillo-Herrero, B. J. LeRoy,*"Long wavelength local density of states oscillations near graphene step edges".* ***Phys. Rev. Lett.*108**, 016801 (2012).
5. J.Xue, J. Sanchez-Yamagishi, D. Bulmash, P. Jacquod, K. Watanabe, T. Taniguchi, P. Jarillo-Herrero and B.J. LeRoy. *"STM Spectroscopy of Ultra-Flat Graphene on HexagonalBoronNitride"*, ***Nature Materials* 10**, 282 (2011).
6. R. T. Weitz, M. T. Allen, B. E. Feldman, J. Martin and A. Yacoby, "*Broken-Symmetry States in Doubly Gated Suspended Bilayer Graphene", **Science 330***, 812 (2010).
7. J. Martin, B. E. Feldman, R. T. Weitz, M. T. Allen and A. Yacoby, "*Local Compressibility Measurements of Correlated States in Suspended Bilayer Graphene*", ***Phys. Rev. lett., 105***, 256806 (2010).

Probing Correlated Superconductors and their Phase Transitions on the Nanometer Scale

Ali Yazdani
Department of Physics
Princeton University, Princeton, NJ 08544
yazdani@princeton.edu

Program Scope:

This program is focused on understanding how correlated electronic states in materials with *d* and *f* electrons undergo phase transitions to form an unconventional metallic phase and the mechanisms by which these states become superconducting states with lowering temperature. Such phenomena are at the heart of some of the most debated issues in condensed matter physics, and their understanding is an intellectual driver for many of the DOE-BES projects for the development of novel materials and the search for higher temperature superconductivity. Our aim is to provide a microscopic view of these exotic materials and their phase transition into the superconducting state by using some of the most sophisticated scanning tunneling microscopy (STM) and spectroscopy techniques. The results of the experiments proposed here will provide important evidence that will help constrain theoretical models of unusual normal states in these complex materials and their potential mechanisms for superconductivity.

This DOE-BES program is divided into two parts. The first part focuses on examining the properties of high-T_c cuprate superconductors and specifically the high-temperature pseudogap phase of these materials. Many believe that understanding this phase is critical to determining how a Mott insulator is transformed into a high-T_c *d*-wave superconductor. Despite many efforts over the last two decades, there is currently no consensus as to what underlies this unusual electronic phase.

The second component of our program is to utilize for the first time the power of STM techniques to study the exotic normal and superconducting phases in heavy fermion compounds. The parallels between the puzzles in heavy fermions and cuprates suggest that heavy fermions might provide important clues into understanding correlated electrons and their superconductivity. Similar to the high-temperature superconducting cuprates, understanding the mechanism behind the unconventional superconductivity requires understanding the "normal state" prior to formation of superconductivity. The heavy fermions offer clean materials systems to examine issues that might be very difficult to explore in the cuprates and new Fe-based superconductors due to doping disorder in those systems. In particular, the issue of proximity to a quantum critical point and the impact of quantum phase transition on the electronic properties of material and mechanism of superconductivity can be very precisely probed in heavy fermion systems.

The two components of the proposed program provide a broad attack on some of the most important problems in the physics of correlated materials and the emergence of superconductivity in these systems. Finally, the program also supports the development of spin polarized STM measurements of correlated systems that can complement other STM measurements to directly probe the spin textures in such systems.

Recent Progress:

Detection of Incipient Stripe Order in the Pseudogap Phase of High-Temperature Superconductors (*Nature* 2010 & covered in *News and Views*) [1]

For the past several years, our group has uncovered an important aspect of the physics of high-Tc cuprates using high precision measurements of the local electronic structure of these materials with the STM (Gomes *et al., Nature* 2007, Pasupathy *et al., Science* 2008). During the last two years, the team has focused on understanding the behavior of underdoped cuprates, at light hole doping concentration, which is important to determine how superconductivity emerges from a Mott insulating state. We have

demonstrated two important findings in this area. In a series of experiments (reported by Pushp *et al*,. *Science* 2009), we showed that the pairing interaction in the underdoped samples (close to the Mott insulating ground state) became saturated in strength and demonstrated that the relative portion of the Fermi surface participating in the pairing interaction controlled the superconducting transition temperature in this region. These experiments have now been confirmed by angle-resolved photoemission spectroscopy by DOE supported group at Stanford. Furthermore, these experiments illustrated that d-wave superconductivity emerges from the electronic state in a specific part of the Fermi surface and the rest of the Fermi surface becomes unavailable, exhibiting the so-called pseudogap behavior that competes with superconductivity.

During this funding cycle, in another series of experiments (reported by Parker *et al.*, *Nature* 2010), we found that the onset of pseudogap behavior, which is precursor to superconductivity, coincided with the appearance of real space electronic modulations that exhibited the predicted characteristics of incipient short-range stripes. These experiments demonstrated that the pseudogap state is inherently unstable and results in real space patterns of spin and charge with short range order. We showed that, as expected, the strength of the stripe formation is maximal near a hole concentration of 1/8 doping, as predicted by many numerical simulations. These experiments are the first to isolate the interplay between the formation of stripes and pseudogap behavior in cuprates. This was achieved by performing experiments in the underdoped samples up to temperature T*, where the pseudogap state first forms and the real space patterns are simultaneously detected with STM spectroscopic mapping. Another important finding was that with increased underdoping (below 1/8 doping) we found the real space patterns began to fade in intensity. In this same doping region, the pseudogap energy scale continued to grow with underdoping, which suggests that while pseudogap behavior is required for stripe formation, stripes are not the cause of the pseudogap. The logical conclusion from these measurements is that pseudogap is associated with the spin gap that would be required to cause the spin patterns excepted from stripes.

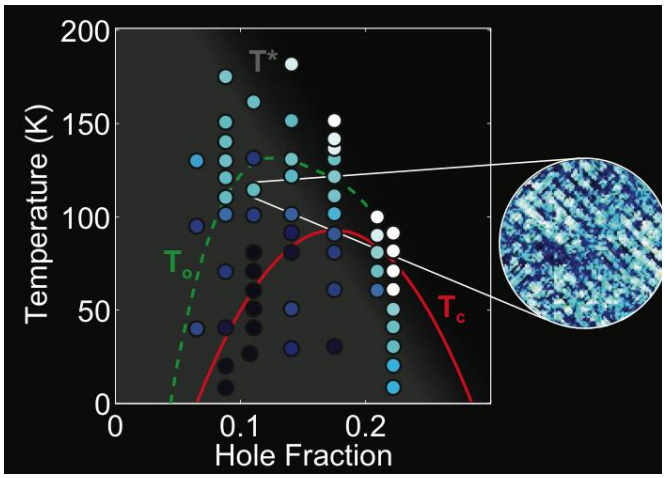

Figure 1. A phase diagram showing the strength of incipient stripes order throughout the cuprate phase diagram (Bi2212). The inset shows the ~4 atomic length patterns induced in the local density of density of states. Shown are the superconducting transition temperature, T_c, the upper boundary for the onset of superconducting fluctuations, T_o, and the pseudogap temperature T*. The incipient stripes are seen thoughout the pseudogap phase, but are strongest near a hole concentration of 1/8, as expected from various theoretical studies.

Detailed measurements & modeling of scattering of electronic states from incipient stripe order [2-3]

Following our initial measurements (reported by Parker *et. al.*, 2010) we have performed several detailed measurements and modeling studies to demonstrate that the experimental signatures of real space patterns were indeed consistent with those expected from incipient stripe order. By performing experiments both in the superconducting and non-superconducting states above Tc we established that the energy dependence of the wavelength with features in STM data in both states can be accounted for in a model of scattering of electronic states from a short-range incipient stripe order. This detailed study is the first of its kind to account for the changes in the patterns of energy dependence as the electronic system is warmed through Tc. We are continuing our efforts to understand detailed energy dependence of the incipient stripe order and other features of STM modulations as a function of doping and temperature approaching the Mott insulating state.

Visualizing Heavy Fermions Emerging in a Quantum Critical Kondo Lattice—Nature (2012) [4]

In solids containing elements with *f*-orbitals, the interaction between *f*-electron spins and those of itinerant electrons leads to the development of low-energy fermionic excitations with a large effective mass. These excitations are fundamental to the appearance of unconventional superconductivity and non-Fermi liquid behavior observed in actinide- and lanthanide-based compounds. During the last two years, our group has succeeded in applying scanning tunneling microscopy (STM) techniques to study the heavy fermion systems for the first time. Two years ago, we had a major breakthrough in the study of heavy fermion states and their phase transition into the so-called "hidden order" state in URu_2Si_2, (PNAS 2010, [5]). This year, we made an even more exciting advance in the study of heavy fermion compounds by using spectroscopic mapping with the scanning tunneling microscope to detect the emergence of heavy excitations upon lowering the temperature in a prototypical family of Ce-based heavy fermion compounds, (*Nature* 2012, [4]). The Ce-based compounds are particularly exciting to work on as they show a remarkably similar phase diagram to high-temperature cuprate superconductors. This system can be tuned between an anti-ferromagnetic ground state and an unusual high temperature non-Fermi liquid state, which when cooled exhibits unconventional superconductivity.

In this project we have demonstrated the sensitivity of the tunneling process to the composite nature of these heavy quasiparticles that arises from a quantum entanglement of itinerant conduction and *f*-electrons. Scattering and interference of the composite quasiparticles in the Ce-based 115 systems is used to resolve their energy-momentum structure and to extract their mass enhancement, which develops with decreasing temperature. This is the first time the energy-momentum structure of a generic heavy fermion state has been measured, as previous angle-resolved experiments have not had enough energy resolution to perform such studies. Such measurements provide direct evidence of change of the Fermi surface from small to large with the onset of heavy electron behavior, where *f* electrons are incorporated to form the heavy qausiparticles. Remarkably, the lifetime of the emergent heavy quasiparticles also reveals signatures of enhanced scattering and their spectral lineshape shows evidence of energy-temperature scaling. These findings demonstrate that proximity to a quantum critical point results in critical damping of the emergent heavy excitation of our Kondo lattice system. Such spectroscopic signatures are direct evidence for the breakdown of coherent fermionic excitations approaching a quantum critical point. Future expansion of our measurements to even lower temperatures will probe the interplay between quantum fluctuations and the appearance of superconductivity — an issue that continues to be one of the most debated in condensed matter physics.

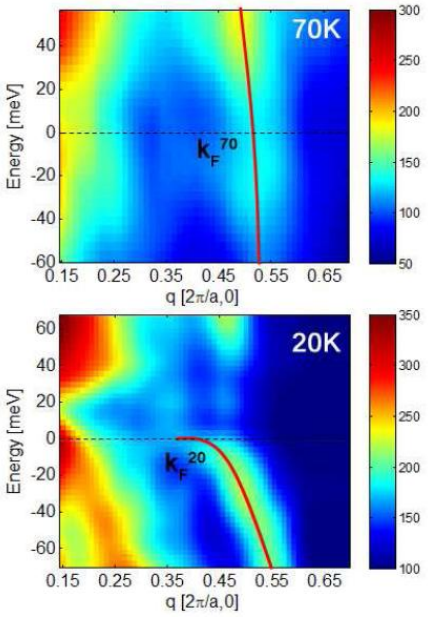

Figure 2. Transition from a small to large Fermi surface in $CeCoIn_5$ showing the development of the heavy fermion state with decreasing temperature detected by spectroscopic mapping with the STM.

Future Plans:

Development of spin polarized STM for study of correlated electronic materials

With the support of a supplementary DOE instrumentation grant, we have developed a spin-polarized STM capable of performing spin resolved experiments on correlated materials. During the last year, we completed the construction of this new instrument and started the process of testing it. We were able to prepare clean metal samples in situ and obtained the first STM images with this machine at 1.2K. In the coming months, we will installevaporators for in situ preparation of magnetic atoms, so as to prepare spin-polarized tips, and to perform the first spin-polarized STM experiments. A likely first candidate for the new machine is the study of anti-ferromagnetism in the heavy fermion 115 compounds, for which we have already obtained STM results without spin-polarized tips.

Development of ultra-low temperature high magnetic field STM for the study of correlated electronic materials

In addition to the development of an instrument dedicated to spin-polarized measurements, our group has been developing the capabilities for STM measurements at millikelvin temperature and in high magnetic fields to 14 Tesla. Our instrument is already functional and we are starting the first set of measurements on various correlated systems at very low temperatures. Such capability will be critical to study heavy electron systems as well as to probe correlated systems generically with high resolutions.

Publication Supported by the DOE-BES (2010-2012):

In addition to publications directly related to DOE-BES projects, the DOE funds that support the instrumentation in our lab have assisted other projects. The publications from these projects benefiting from DOE support are also included in the list below (marked as partially supported by DOE).

1. C. V. Parker, P. Aynajian, E. H. da Silva Neto, A. Pushp, S. Ono, J. Wen, Z. Xu, G. Gu, and A.Yazdani . "Fluctuating stripes at the onset of the pseudogap in the high-T_c superconductor $Bi_2Sr_2CaCu_2O_{8+x,}$" *Nature* **468**, 677 (2010). Fully supported by DOE.
2. E. H. da Silva Neto, C. V. Parker, P. Aynajian, A. Pushp, J. Wen, Zhijun Xu, G. Gu, and A.Yazdani, "Scattering from incipient stripe order in the high-temperature superconductor $Bi_2Sr_2CaCu_2O_{8+d,}$" *Physical Review* B **85**, 104521 (2012). Fully supported by DOE.
3. E. H. da Silva Neto, C. V. Parker, P. Aynajian, A.Pushp, J. Wen, Z. Xu, G. Gu, and A.Yazdani, "Detecting incipient stripe order in the high-temperature superconductor $Bi_2Sr_2CaCu_2O_{8+d}$," *Invited review to appear in Physica C (2012).*
4. P. Aynajian, E. H. da Silva Neto, A. Gyenis, R. E. Baumbach, J. D. Thompson, Z. Fisk, E. D. Bauer, and A.Yazdani, "Visualizing heavy fermions emerging in a quantum critical Kondo lattice," *Nature* **486**, 201 (2012). Fully supported by DOE.
5. P. Aynajian, E. H. da Silva Neto, C. V. Parker, Y. Huang, A. Pasupathy, J. Mydosh, and A. Yazdani, "Visualizing the formation of the Kondo lattice and the hidden order in URu_2Si_2" Proc. Nat'l. Acad. Sci USA **107,** 10383 (2010). Fully supported by DOE.
6. C. V. Parker, A. Pushp, A. N. Pasupathy, K. K. Gomes, J. Wen, Z. Zu, S. Ono, G. Gu, and A. Yazdani, "Nanoscale Proximity Effect in the High-Temperature Superconductor $Bi_2Sr_2Ca_2CuO_{8+\delta}$ Using a Scanning Tunneling Microscope," *Physical Review* Lett. **104,** 117001 (2010). Fully supported by DOE.
7. J. Seo, P. Roushan, H. Beidenkopf, Y. S. Hor, R. J. Cava, and A. Yazdani, "Transmission of topological surface states through surface barriers," *Nature* **466** 343 (2010). Partially supported by the DOE.
8. A. Richardella, P. Roushan, S. Mack, B. Zhou, D. Huse, D. Awschalom, and A. Yazdani "Visualizing critical spatial correlations for electronic states near the metal-insulator transition GaMnAs," *Science* **327** 665 (2010). Partially supported by the DOE.
9. H. Beidenkopf, P. Roushan, J. Seo, L. Gorman, I. Drozdov, Y. S. Hor, R. J. Cava, and A. Yazdani, "Spatial Fluctuations of Helical Dirac Fermions on the Surface of Topological Insulators," *Nature Physics* **7** 939 (2011). Partially supported by the DOE.

Local to Macroscopic Symmetry for Piezoelectric (1-x)Pb($Mg_{1/3}Nb_{2/3}$)O_3-x$PbTiO_3$ Single Crystal in the Morphotropic Phase Boundary

DE-FG02-06ER45923

Jian-Min Zuo
jianzuo@illinois.edu
Dept. of Materials Science and Engineering and Materials Research Laboratory,
University of Illinois, Urbana-Champaign, IL 61801

Program Scope

Electrons have large scattering cross sections and electron beams can be focused using magnetic lenses. However, to use the full potential of electron beams for quantitative structural determination at nanoscale, novel techniques must be developed to take advantage of electron diffraction, including newly developed ultrafast electron diffraction (UED). The scope of this proposed research is to develop quantitative and robust electron diffraction techniques for atomic structure determination for nanostructures and study their structural dynamics. The expected outcomes from the proposed research include: determination of 3D structure of selected metal and semiconductor nanoparticles, determination of the symmetry and strain in nanometer-sized ferroelectric domains in relaxor ferroelectrics, determination of domain switching dynamics.

This presentation focuses on our progress in the study of crystal symmetry in relaxor ferroelectrics, which is a new area for electron nanodiffraction. We aim to correlate the symmetry and polarization using diffraction information. The result is expected to improve our understanding of the structure of nanodomains in relaxor ferroelectrics and the expected impact is on understanding high electro-mechanical activity in these materials.

Recent Progress:

The symmetry of piezoelectric materials has been widely studied for the simple reason that symmetry controls displacements of ionic charge and position, which, in turn, determines directions of spontaneous polarization ($\mathbf{P_S}$) and spontaneous strain ($\boldsymbol{\varepsilon_S}$), and field (E)-induced orientations of ferroelectric and piezoelectric properties. The high-temperature (HT) phase of (1-x)Pb($Mg_{1/3}Nb_{2/3}$)O_3-x$PbTiO_3$ and (1-x)Pb($Zn_{1/3}Nb_{2/3}$)O_3-x$PbTiO_3$ (known as PMN-x%PT and PZN-x%PT, respectively) is cubic Pm3m with no spontaneous distortions. According to published x-T phase diagrams for PMN-xPT and PZN-xPT, the prototypic HT phase spontaneously distorts to rhombohedral (R) R3m symmetry on cooling at low x, or tetragonal (T) P4mm symmetry at higher x, in which $\mathbf{P_S}$ and $\boldsymbol{\varepsilon_S}$ are constrained to the cubic (noted by the subscript 'C') $[111]_C$ and $[001]_C$ directions for the R and T phases, respectively. The R and T phases are initially separated by a vertical boundary termed the morphotropic phase boundary (MPB), i.e., a chemically (x)-driven change in morphology. The MPB of PMN-xPT and PZN-xPT is defined in a narrow composition region where the R and T phases meet. This phase boundary composition has attracted much attention because displacements maximize as the lattice softens and transforms, giving rise to large enhancements in piezoelectric properties.

A large body of work has been reported on the structural origin of the piezoelectric properties for PMN-PT at the MPB. A new phase with monoclinic (M) symmetry was

proposed in the vicinity of MPB as identified using X-ray and neutron diffraction studies. The M phase is said to be a structural bridge that facilitates polarization rotation from the R to T phases, which is atypical of ionic displacements. Several research groups, however, have disputed whether the observed M phase truly has the monoclinic symmetry at the local (microscopic) scale. The adaptive phase model proposed by Viehland and coworkers states that the M phase found in the MPB region is not a local symmetry but an averaged symmetry obtained from twin-related domain structures.[1] Another point-of-view, put forward by Kisi et al., suggests the M phase is not a true phase but a distorted structure resulting from residual stress.[2] Thus, a determination of symmetry, from the local to macroscopic level, in the MPB region, is therefore critical to settle these disputes, and is the purpose of this investigation.

Supported by DOE, we selected a PMN-31%PT single crystal for symmetry determinations, which is an established MPB composition with reported properties.[3] PMN-xPT is known for having complex hierarchical domain structures, starting from nanodomains (of a few, to tens of nanometers,) to microdomains (of tenths, to tens of microns). The symmetry determination of nanodomains, therefore, requires a small diameter probe with nanometer resolution in order to determine the local symmetry. Considering this limitation, CBED performed in a TEM is an appropriate tool for a determination of local symmetry. Local symmetry within a few nm can be studied with a field emission gun, which can provide electron probes of ~ 2 nm in diameter or less. The symmetry over several tens of nm can be investigated with a thermionic electron source, which forms a larger probe size of tens of nm. In addition, we proposed an algorithm to quantify the symmetry recorded in the experimental CBED patterns through use of a cross-correlation coefficient.

Our results show that the symmetry of PMN-31%PT is triclinic at few nm length scales, and becomes monoclinic (M_B)-like symmetry at the length scale of few tens of nm. The macroscopic symmetry determined by XRD suggests multiple domains of different sizes in PMN-31%PT single crystal. Thus, the high piezoelectric response of PMN-31%PT single crystal at the MPB region is underlined by a structure that lacks local symmetry, which has an averaged monoclinic symmetry over tens of nanometers in some regions of the crystal. The lack of local symmetry may enhance the polarization switching behavior in this material. The monoclinic (M_B)-like symmetry at tens of nanometer scale provides the structural bridge for polar rotation that is a key to the enhancement of the piezoelectric properties under external electric field. Our result is of importance to show the missing links between the local symmetry and macroscopic symmetry.

Future Plans and Other Research Activities:

In addition to the research on symmetry and polarization of relaxor-ferroelectric materials summarized above, the funding supports the development of coherent diffraction techniques for the study of precipitates in light metals. Nanometer-sized precipitates are critical to the enhancement of the mechanical properties of light metals and their applications. The interface of precipitates and matrix is believed to play important roles to their functions. In developing coherent diffraction, we aim at direct determination of the atomic structure of precipitates including their interfaces. Success development of this technique can have a large impact on metal research. This research is being carried out in collaboration with Prof. Miyoung Kim of SNU.

The other ongoing project is to develop ultrafast electron diffraction (UED) for the study of structural dynamics of supported nanoparticles. For this activity, we have modified the UED apparatus at UIUC to introduce high temperature capabilities, which we are in the process of combining it with the laser pump probe to drive nanoparticle phase transitions and study them with the pulsed electron beam. Specifically, we are searching for experimental conditions that will allow a separation of transient electric field effect from the lattice changes induced by pulse laser illumination. Initial test has been carried out on the system of Ag on TiO_2. Figure 1 shows that the transient electric effect is confined within 500 ps after pulsed laser illumination.

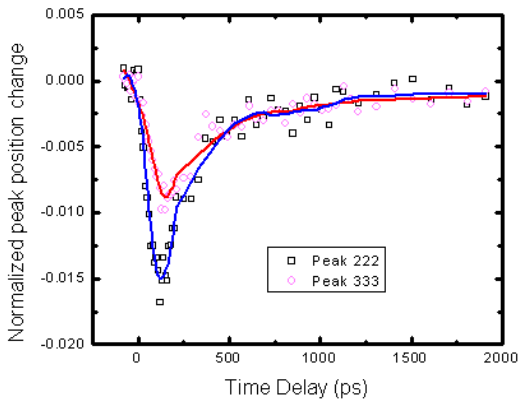

Fig.1 Ultrafast electron diffraction measurements of (222) and (333) peak positions of Ag nanocrystals supported on TiO_2 under 200 mW, 120 fs pulsed laser illumination. The peak position is normalized by length of g.

References

[1] D. Viehland, Journal of Applied Physics **88** (8), 4794 (2000).

[2] E. H. Kisi, R. O. Piltz, J. S. Forrester, and C. J. Howard, Journal of Physics-Condensed Matter **15** (21), 3631 (2003).

[3] J. Tian, P. Han, and D. A. Payne, Ieee Transactions on Ultrasonics Ferroelectrics and Frequency Control **54** (9), 1895 (2007).

DOE Sponsored Publications in 2010-2011

1) B. Jiang, J.M. Zuo, D. Holec, C.J. Humphreys, M. Spackman, J.C.H. Spence, Combined structure-factor phase measurement and theoretical calculations for mapping of chemical bonds in GaN, Acta Crystallographica Section A, 66 (2010) 446-450.

2) K.H. Kim, D.A. Payne, J.M. Zuo, Ion-beam induced domain structure in piezoelectric PMN-PT single crystal, Applied Physics Letters, 97 (2010) 261910.

3) S. Kim, J.M. Zuo, S. Kang, Effect of WC or NbC addition on lattice parameter of surrounding structure in Ti(C0.7N0.3)-Ni cermets investigated by TEM/CBED, Journal of the European Ceramic Society, 30 (2010) 2131-2138.

4) T. Kim, G. Kim, W.I. Choi, Y.K. Kwon, J.M. Zuo, Electrical transport in small bundles of single-walled carbon nanotubes: Intertube interaction and effects of tube deformation, Applied Physics Letters, 96 (2010) 173107.

5) H. Park, J.M. Zuo, Comment on "Structural Preablation Dynamics of Graphite Observed by Ultrafast Electron Crystallography", Physical Review Letters, 105 (2010) 059603.

6) S.I. Sanchez, M.W. Small, S. Sivaramakrishnan, J.G. Wen, J.M. Zuo, R.G. Nuzzo, Visualizing Materials Chemistry at Atomic Resolution, Analytical Chemistry, 82 (2010) 2599-2607.
7) J.G. Wen, J. Mabon, C.H. Lei, S. Burdin, E. Sammann, I. Petrov, A.B. Shah, V. Chobpattana, J. Zhang, K. Ran, J.M. Zuo, S. Mishina, T. Aoki, The Formation and Utility of Sub-Angstrom to Nanometer-Sized Electron Probes in the Aberration-Corrected Transmission Electron Microscope at the University of Illinois, Microscopy and Microanalysis, 16 (2010) 183-193.
8) J. Zhang, J.L. Xiao, X.H. Meng, C. Monroe, Y.G. Huang, J.M. Zuo, Free Folding of Suspended Graphene Sheets by Random Mechanical Stimulation, Physical Review Letters, 104 (2010) 166805.
9) S.W. Chee, S. Sivaramakrishnan, R. Sharma, J.M. Zuo, Electron-Beam-Induced Growth of TiO(2) Nanostructures, Microscopy and Microanalysis, 17 (2011) 274-278.
10) K. Ran, J.M. Zuo, Q. Chen, Z.J. Shi, Electron Beam Stimulated Molecular Motions, ACS Nano, 5 (2011) 3367-3372.
11) J.C. Shin, K.H. Kim, K.J. Yu, H.F. Hu, L.J. Yin, C.Z. Ning, J.A. Rogers, J.M. Zuo, X.L. Li, In(x)Ga(1-x)As Nanowires on Silicon: One-Dimensional Heterogeneous Epitaxy, Bandgap Engineering, and Photovoltaics, Nano Letters, 11 (2011) 4831-4838.
12) H. Wei, Z.D. Wang, J.O. Zhang, S. House, Y.G. Gao, L.M. Yang, H. Robinson, L.H. Tan, H. Xing, C.J. Hou, I.M. Robertson, J.M. Zuo, Y. Lu, Time-dependent, protein-directed growth of gold nanoparticles within a single crystal of lysozyme, Nature Nanotechnology, 6 (2011) 92-96.
13) J.M. Zuo, J. Zhang, W.J. Huang, K. Ran, B. Jiang, Combining Real and Reciprocal Space Information for Aberration Free Coherent Electron Diffractive Imaging Ultramicroscopy, 111 (2011) 817-823.
14) K. Ran, M Xi, Z. J. Shi, Q. Chen, Y.F. Shi, and J. M. Zuo, "Molecular Packing of Fullerenes inside Single-Walled Carbon Nanotubes," Carbon (2012), Accepted
15) K. Ran, Q. Chen, and J. M. Zuo, "Fabrication and Structure Characterization of Quasi-2-Dimensional Amorphous Carbon Structures," Acta Phys. -Chim. Sin. 28 (7), 1551-1555 (2012).

Book Chapters

J.M. Zuo, J. Tao, Scanning Electron Nanodiffraction and Diffraction Imaging, in: S. Pennycook, P. Nellist (Eds.) Scanning Transmission Electron Microscopy, Springer, New York, 2011.

J.M. Zuo, W.J. Huang, Coherent Electron Diffractive Imaging, in: G. Van Tendeloo, D. Van Dyck and S. J. Pennycook (Eds) Handbook of Nanoscopy, Wiley-VCH, Weinheim, Germany, 2012

INVITED TALKS

The Quantum and Classical Properties of Spins on Surfaces

Andreas Heinrich

IBM Research
Almaden Research Center
San Jose, CA

The scanning tunneling microscope has been an extremely successful experimental tool because of its atomic-scale spatial resolution. In recent years this has been combined with the use of low temperatures, culminating in precise atom manipulation and spectroscopy with microvolt energy resolution. In this talk I will review recent developments in investigating the electronic and magnetic properties of atoms and small clusters of atoms on surfaces. A particular focus will be on the use of magnetic materials for future device applications in the Information Technology industries.

A large enough cluster of magnetic atoms on a surface behaves similar to a macroscopic magnetic particle: it's magnetization points along an easy-axis direction in space and magnetization reversal requires sufficient thermal energy to overcome a barrier. How many atoms does it take to create such a magnet? What are the size limits of stable magnetic nanoparticles. Those are important questions for our future technologies.

When the number of atoms in a cluster becomes small quantum tunneling of magnetization can take place and hence quantum mechanics can no longer be ignored but rather takes center stage. Single atoms that are slightly decoupled from conducting substrates behave more like quantum mechanical entities. These quantum systems can be studied with inelastic tunneling spectroscopy, a technique we coined spin-excitation spectroscopy. With this approach it is possible to measure the energy eigenstates of the quantum spin Hamiltonian that describes spins on surfaces with high precision.

Frontiers of STM Manipulations: Imaging Atomic Spin to Operating Nanomachines

Saw Wai Hla

Department of Physics & Astronomy, Ohio University, OH 45701
and
Center for Nanoscale Materials, Argonne National Laboratory, IL 60439.

Development of novel energy efficient devices demands instrumentations that can be used to explore properties of materials down to atomic or even sub-atomic level. Scanning probe microscopy with its ability to image single atoms allows us not only to visualize the materials surfaces but also to probe the properties of individual atoms and molecules using local spectroscopy techniques. In recent years, manipulation of atoms and molecules with a scanning probe tip has added a whole new level of instrumentation capabilities with a great impact on our understanding of materials properties and their potential applications. This talk will highlight two vital advances achieved by using scanning tunneling microscope manipulation schemes. The first topic concerns with imaging and manipulating of atomic spins. The electron spin in an atom is a quantum mechanical property, and it has potential applications in spintronic devices with a great promise for energy efficiency. Although the electron spin has been a corner stone of physics, visualization of the spin has not been able to realize and it is usually illustrated with an arrow. Recently, by combining spin-polarized scanning tunneling microscopy and atomic manipulation, we are able to image different shapes of the atoms caused by various spin directions. Moreover, by laterally manipulating a Co atom on a spin-spiral substrate, the existence of a new frictional phenomenon originated from a spin exchange interaction is unveiled. In both cases, the atomic manipulation with a spin-polarized tip is the key for unlocking the mystery. The second part of the talk is related to energy transduction at the nanoscale. By means of inelastic electron tunneling, selective excitations of different molecular parts can be realized. Here, the electron energy transfer induces mechanical motions of the molecule. This process is used to operate a standalone molecular motor composed of multiple components: A tripod stator, a five arm rotator and, an atomic ball bearing. Strikingly, we discover that a selective tunneling into specific rotator arm can result in a controlled directional rotation of the molecular motor. Such control is achieved due to the ability of selective excitation of specific molecular orbitals thereby allowing rotation into one direction only. These experiments are innovative, and are tailored to address several critical issues covering fundamental understanding as well as demonstration of novel molecule based nanodevices on materials surfaces.

COUPLING MAGNETISM TO ELECTRICITY IN MULTIFERROIC HETEROSTRUCTURES: THE ROLE OF IMAGING AND SPECTROSCOPY

R. Ramesh
Department of Materials Science and Engineering and Department of Physics
University of California, Berkeley, CA 94720

Complex perovskite oxides exhibit a rich spectrum of functional responses, including magnetism, ferroelectricity, highly correlated electron behavior, superconductivity, etc. The basic materials physics of such materials provide the ideal playground for interdisciplinary scientific exploration. Over the past decade we have been exploring the science of such materials (for example, colossal magnetoresistance, ferroelectricity, etc) in thin film form by creating epitaxial heterostructures and nanostructures. Among the large number of materials systems, there exists a small set of materials which exhibit multiple order parameters; these are known as multiferroics. Using our work in the field of ferroelectric(FE) and ferromagnetic oxides as the background, we are now exploring such materials, as epitaxial thin films as well as nanostructures. Specifically, we are studying the role of thin film growth, heteroepitaxy and processing on the basic properties as well as magnitude of the coupling between the order parameters. In our work we are exploring the switchability of the antiferromagnetic order using this coupling.

What is the importance of this work? Antiferromagnets (AFM) are pervasive in the recording industry. They are used as exchange biasing layers in MTJ's etc. However, to date there has been no antiferomagnet that is electrically tunable. We believe that the multiferroic BiFeO3 is one compound where this can be observed at room temperature. The next step is to explore the coupling of a ferromagnet to this antiferromagnet through the exchange biasing concept. Ultimately, this will give us the opportunity to switch the magnetic state in a ferromagnet (and therefore the spin polarization direction) by simply applying an electric field to the underlying antiferromagnetic ferroelectric. In this talk, I will describe our progress to date on this exciting possibility. X-ray and electron based imaging and spectroscopy techniques are vital tools to help us understand the structural chemistry (with atomic scale resolution) as well as the various interactions at interfaces. Our work has benefited enormously through interactions with several user facilities and research teams in such national lab facilities. This talk will highlight through examples on oxide heterostuctures the role of such imaging and spectroscopy techniques.

AUTHOR INDEX AND PARTICIPANT LIST

Author Index

ESPM 2012 Principal Investigators' Meeting
Participants

Last Name	First Name	Organization	E-mail Address
Ashby	Paul	Lawrence Berkeley National Laboratory	pdashby@lbl.gov
Aynajian	Pegor	Princeton University	aynajian@princeton.edu
Balsara	Nitash	Lawrence Berkeley National Laboratory	nbalsara@berkeley.edu
Bartelt	Norman	Sandia National Laboratories, CA	bartelt@sandia.gov
Batson	Philip	Rutgers University	batson@physics.rutgers.edu
Berezovsky	Jesse	Case Western Reserve University	jab298@case.edu
Bonnell	Dawn	University of Pennsylvania	bonnell@lrsm.upenn.edu
Borisevich	Albina	Oak Ridge National Laboratory	albinab@ornl.gov
Browning	Nigel	Pacific Northwest National Laboratory	nigel.browning@pnnl.gov
Camden	Jon	University of Tennessee	jcamden@utk.edu
Campbell	Geoffrey	Lawrence Livermore National Laboratory	ghcampbell@llnl.gov
Chandrasekhar	Venkat	Northwestern University	v-chandrasekhar@northwestern.edu
Chen	Long-Qing	Pennsylvania State University	lqc3@psu.edu
Christen	Hans	Oak Ridge National Laboratory	christenhm@ornl.gov
Cobden	David	University of Washington	cobden@uw.edu
Contescu	Cristian	Oak Ridge National Laboratory	ContescuCI@ornl.gov
Crockett	Teresa	U.S. Department of Energy	teresa.crockett@science.doe.gov
Crozier	Peter	Arizona State University	crozier@asu.edu
Cumings	John	University of Maryland	cumings@umd.edu
Davis	JC Seamus	Cornell University / BNL	jcdavis@ccmr.cornell.edu
DeGraef	Marc	Carnegie Mellon University	degraef@cmu.edu
Dillon	Shen	University of Illinois, Urbana-Champaign	sdillon@illinois.edu
Dutt	Gurudev	University of Pittsburgh	gdutt@pitt.edu
Fisher	Ian	Stanford University / SLAC	irfisher@stanford.edu
Gallego	Nidia	Oak Ridge National Laboratory	gallegonc@ornl.gov
Goldhaber	David	Stanford University	goldhabergordon@gmail.com
Goldman	Rachel	University of Michigan	rsgold@umich.edu
Gozar	Adrian	Brookhaven National Laboratory	agozar@bnl.gov
Gruverman	Alexei	University of Nebraska-Lincoln	agruverman2@unl.edu
Guisinger	Nathan	Argonne National Laboratory	nguisinger@anl.gov
Hammel	P Chris	Ohio State University	hammel@physics.osu.edu
Han	Myung-Geun	Brookhaven National Laboratory	mghan@bnl.gov
Heinrich	Andreas	IBM Research	andreash@us.ibm.com
Hla	Saw Wai	Ohio University / ANL	hla@ohio.edu
Hong	Seungbum	Argonne National Laboratory	hong@anl.gov
Horton	Linda	U.S. Department of Energy	Linda.Horton@science.doe.gov
Huey	Bryan	University of Connecticut	bhuey@ims.uconn.edu
Iavarone	Maria	Temple University	iavarone@temple.edu
Idrobo	Juan Carlos	Oak Ridge National Laboratory	idrobojc@ornl.gov

Jarillo-Herrero	Pablo	Massachusetts Institute of Technology	pjarillo@mit.edu
Kalinin	Sergei	Oak Ridge National Laboratory	sergei2@ornl.gov
Kapitulnik	Aharon	SIMES / Stanford University	aharonk@stanford.edu
Kerch	Helen	U.S. Department of Energy	helen.kerch@science.doe.gov
Kiser	Lee-Ann	Oak Ridge Institute for Science and Education	lee-ann.kiser@orise.orau.gov
Koenenkamp	Rolf	Portland State University	rkoe@pdx.edu
LaGrange	Thomas	Lawrence Livermore National Laboratory	lagrange2@llnl.gov
Lev	Benjamin	Stanford University	benlev@stanford.edu
Li	An-Ping	Oak Ridge National Laboratory	apli@ornl.gov
Li	Lian	University of Wisconsin, Milwaukee	lianli@uwm.edu
Liu	Yuzi	Argonne National Laboratory	yuziliu@anl.gov
Mailhiot	Christian	Lawrence Livermore National Laboratory	mailhiot1@llnl.gov
Maksymovych	Petro	Oak Ridge National Laboratory	maksymovychp@ornl.gov
Marks	Laurence	Northwestern University	L-marks@northwestern.edu
McCartney	Martha	Arizona State University	molly.mccartney@asu.edu
McCarty	Kevin	Sandia National Laboratories, CA	mccarty@sandia.gov
Meng	Shirley	University of California, San Diego	shirleymeng@ucsd.edu
Miller	Dean	Argonne National Laboratory	miller@anl.gov
Minor	Andrew	University of California, Berkeley / LBNL	aminor@lbl.gov
Moler	Kathryn	SIMES / Stanford University	kmoler@stanford.edu
More	Karren	Oak Ridge National Laboratory	morekl1@ornl.gov
Morris	James	Oak Ridge National Laboratory	morrisj@ornl.gov
Oxley	Mark	Vanderbilt University	oxleymp@gmail.com
Pan	Minghu	Oak Ridge National Laboratory	panm@ornl.gov
Pan	Xiaoqing	University of Michigan	panx@umich.edu
Pantelides	Sokrates	Vanderbilt University	pantelides@vanderbilt.edu
Pennycook	Stephen	Oak Ridge National Laboratory	pennycooksj@ornl.gov
Petford-Long	Amanda	Argonne National Laboratory	petford.long@anl.gov
Phatak	Charudatta	Argonne National Laboratory	cd@anl.gov
Plummer	Ward	Louisiana State University	wplummer@phys.lsu.edu
Priya	Shashank	Virginia Polytechnic Institute and State University	spriya@vt.edu
Ramesh	Ramamoorthy	University of California, Berkeley	Rramesh@berkeley.edu
Raschke	Markus	University of Colorado	markus.raschke@colorado.edu
Reddy	Pramod	University of Michigan, Ann Arbor	pramodr@umich.edu
Reed	Bryan	Lawrence Livermore National Laboratory	reed12@llnl.gov
Rezikyan	Aram	Arizona State University	arezikya@asu.edu
Robertson	Ian	University of Illinois, Urbana-Champaign	ianr@illinois.edu
Ruan	Chong-Yu	Michigan State University	ruan@pa.msu.edu
Schmid	Andreas	Lawrence Berkeley National Laboratory	akschmid@lbl.gov
Schuck	P. James	The Molecular Foundry, LBNL	pjschuck@lbl.gov
Schwartz	Andrew	U.S. Department of Energy	andrew.schwartz@science.doe.gov
Smith	Arthur R.	Ohio University	smitha2@ohio.edu
Solares	Santiago	University of Maryland, College Park	ssolares@umd.edu

Spence	John	Arizona State University / LBNL	spence@asu.edu
Stemmer	Susanne	University of California, Santa Barbara	stemmer@mrl.ucsb.edu
Tao	Jing	Brookhaven National Laboratory	jtao@bnl.gov
Thurmer	Konrad	Sandia National Laboratories, CA	kthuermer@gmail.com
Treacy	Michael	Arizona State University	treacy@asu.edu
Varela	María	Oak Ridge National Laboratory	Mvarela@ornl.gov
Viehland	Dwight	Virginia Polytechnic Institute and State University	viehland@mse.vt.edu
Voyles	Paul	University of Wisconsin, Madison	voyles@engr.wisc.edu
Ward	T. Zac	Oak Ridge National Laboratory	wardtz@ornl.gov
Weiss	Paul	University of California, Los Angeles	psw@cnsi.ucla.edu
Wiezorek	Jorg	University of Pittsburgh	wiezorek@pitt.edu
Wu	Weida	Rutgers University	wdwu@physics.rutgers.edu
Yacoby	Amir	Harvard University	yacoby@physics.harvard.edu
Zheng	Haimei	Lawrence Berkeley National Laboratory	hmzheng@lbl.gov
Zhu	Jane	U.S. Department of Energy	jane.zhu@science.doe.gov
Zhu	Yimei	Brookhaven National Laboratory	zhu@bnl.gov
Zuo	Jian Min	University of Illinois, Urbana-Champaign	jianzuo@illinois.edu